

Carnegie Mellon University
MELLON COLLEGE OF SCIENCE

THESIS

SUBMITTED IN PARTIAL FULFILLMENT OF THE REQUIREMENTS
FOR THE DEGREE OF

DOCTOR OF PHILOSOPHY IN THE FIELD OF PHYSICS

TITLE: "Effective field theory of particle interactions mediated by fluid surfaces."

PRESENTED BY: Robert Haussman

ACCEPTED BY THE DEPARTMENT OF PHYSICS

| | |
|---------------------------------|---------|
| MARKUS DESERNO | 5/10/16 |
| MARKUS DESERNO, CHAIR PROFESSOR | DATE |

| | |
|---------------------------|---------|
| STEPHEN GAROFF | 5/10/16 |
| STEPHEN GAROFF, DEPT HEAD | DATE |

APPROVED BY THE COLLEGE COUNCIL

| | |
|-------------------|---------|
| FRED GILMAN | 5/10/16 |
| FRED GILMAN, DEAN | DATE |

Effective field theory of particle interactions mediated by fluid surfaces

Robert C. Haussman

May 2016

Department of Physics
Carnegie Mellon University
Pittsburgh, PA

*Submitted in partial fulfillment of the requirements
for the degree of Doctor of Philosophy*

advised by Profs. Markus Deserno and Ira Z. Rothstein

to my parents

Abstract

Fluid interfaces and membranes can mediate forces between particles bound to them. Bound objects impart local deformations of the surface geometry and modify its thermal fluctuation spectrum, the effects of which spread to distant regions where other objects can respond to it. Such surface-mediated interactions play an important role in aggregation and structure formation of both colloids at fluid interfaces, relevant for many technological applications, and protein inclusions in biological membranes, which are believed to assist in important cellular remodeling processes like endocytosis and exocytosis. While the physical characteristics of these geometric interactions are conceptually straightforward, the corresponding calculations are unfortunately far from trivial. The challenge is that one must enforce conditions at the particle–surface boundaries of finite-sized objects, which themselves may also be subject to thermal fluctuations. In this thesis we develop an Effective Field Theory (EFT) formalism which disentangles the particle boundary conditions from the calculation of the interaction free energy by constructing an equivalent point-particle description. We first motivate the intuition and key steps needed to construct an EFT through a familiar electrostatics problem, which will serve as a guiding analogy for capturing finite-size information in point-like “polarizabilities” and determining their values through a suitable “matching” procedure. We then apply the formalism to construct *complete* effective energy functionals for flat, curved, and asymmetric rigid particles bound to tension dominated and bending-elasticity dominated surfaces. The interaction potential emerges as a systematic cumulant expansion, for which we provide a powerful diagrammatic technique and derive series expansions for pairwise and multibody interactions, as well as corrections due to thermal fluctuations. In particular, we calculate to high orders—and in some cases to *all* orders—the elastic and entropic interactions between particles with various fixed and free boundary conditions, and analyze the corresponding energy landscapes to determine the preferred configurations and orientations of anisotropic and multibody systems.

Acknowledgments

This thesis punctuates an extremely long and arduous journey, both intellectually emotionally. It is not without the support and guidance of many individuals that I have been able to make it this far and, moreover, arrive in one piece. In this, the “curtain call” of my graduate career, I would like to do more than just acknowledge those who have made it all possible. I want to extend my deepest, heartfelt gratitude.

I am extremely privileged and grateful to have had Markus Deserno on my side as an advisor. In addition to his sharp intellectual proficiencies and wit, he is demonstrably a sincere and caring person. As he would likely attest, I did not make his job easy. Yet, despite all the unusual and unorthodox situations I subjected him to, he faced them with me, always accommodating my stumbles and hurdles, and ensured we would make it out. I want to thank him for going above and beyond his duties and being there for me as an ally and friend.

I also would like to thank my other dissertation committee members: Ira Rothstein, Daniel Boyanovsky, and Michael Widom. Each contributed to my development as a physicist, and I am happy that they could be a part of my examination and defense.

In the early days of my graduate studies—back when I was oriented toward particle physics—I had the fortune of working with Ira Rothstein, who helped guide and construct my foundation in field theory. In fact, his influence on me, particularly in the philosophy and methodology of effective field theory, has positively shaped how I view and approach scientific problems. Our first project led to a collaboration with Markus and fellow graduate student Cem Yolcu, and later culminated into a full-blown thesis (in fact *two*, one each for Cem and I). Although our research directions later parted ways, I feel he has equipped me with the right tools and mode of thinking to make an impact in my future pursuits.

Along the way, Daniel Boyanovsky also contributed strongly to my personal development. Through many exciting after-hours conversations in his office, he opened my eyes up to a wider world of interdisciplinary topics and encouraged me to keep an open mind and to think creatively about what physics can bring to other fields.

Outside of academics, many friends contributed either consciously or unwittingly. Two of my closest friends, Chris Crowe and Keeno Laws, were always there to lend an attentive ear and provide me with an outlet to voice my enthusiasm or concern. Additionally, they have served as constant inspiration to stay true to myself, demonstrating how fruitful life can be beyond work. At the beginning of graduate school, Feng Yu and Dao Ho made the transition not only bearable, but fun, and made living in Highland Park even more pleasant. Patrick Mende, Will Levine, and Ying Zhang provided camaraderie within and outside the office, and accommodated me during part of my *all-but-dissertation* limbo. Zach McDargh also contributed a couch more than once, and provided personal and caffeinated support

when needed. Karpur Shukla was also always there to commiserate or laugh with me as we trudged along.

I am eternally grateful to my parents, Ken and Teresa. Throughout my youth, they fostered my curiosity and encouraged me to think independently and pursue my passions, be it art, music, or academics. Their support was unwavering, even when I left home two years earlier than expected to attend a math and science boarding school. My sisters, Nicole and Amanda, have also been there to pull me back to reality when I drifted and taught me resiliency when times were tough. I am also thankful to Narsi and Shashi Rao for welcoming me into their family with open arms and providing additional encouragement and support when my spirits were down and when it came time for the final push toward completing my doctorate.

Finally, and most importantly, I wish express my sincerest thanks to my partner, Deepa Rao. I could not expect for a more loving and caring person to join me on this adventure. You pulled me up when I succumbed to shattered isolation, and showed me how to celebrate life. Throughout the ups and downs, you have made it all worth it.

Contents

| | |
|---|-----------|
| Introduction | 1 |
| 1 An invitation to Effective Field Theory | 6 |
| 1.1 An electrostatics example | 6 |
| 1.1.1 Developing a formalism | 10 |
| 1.1.2 An effective energy functional | 15 |
| 1.1.3 Interactions | 25 |
| 1.2 Effective field theory formalism | 34 |
| 1.2.1 General formalism | 35 |
| 1.2.2 Worldline EFTs | 37 |
| 2 Physics of random surfaces | 41 |
| 2.1 Mesoscopic models of interfaces and membranes | 41 |
| 2.1.1 Physical origins and considerations | 41 |
| 2.1.2 Modeling and mathematical description | 43 |
| 2.2 Surface geometry | 44 |
| 2.3 Helfrich theory | 53 |
| 2.4 Fluctuating surfaces | 57 |
| 2.4.1 Harmonic approximation | 60 |
| 2.4.2 Nonlinearities and renormalization | 66 |
| 3 Surface-mediated interactions of axisymmetric particles | 69 |
| 3.1 Surface energetics | 69 |
| 3.2 Particle boundary conditions | 72 |
| 3.2.1 Surface response to an isolated particle | 85 |
| 3.3 Effective theory | 89 |
| 3.3.1 EFT for free, flat particles: induced polarization | 90 |
| 3.3.2 EFT for constrained flat particles: induced sources | 95 |
| 3.3.3 EFT for curved particles: permanent sources | 96 |
| 3.4 Surface-mediated interactions: Preliminaries | 102 |
| 3.4.1 The diagrammatic technique | 103 |
| 3.4.2 Surface diagrammar | 110 |
| 3.5 Elastic interactions | 113 |
| 3.5.1 Pair interactions | 114 |
| 3.5.2 Multibody interactions | 117 |
| 3.5.3 The complete pair interaction for curved particles | 119 |

CONTENTS

| | | |
|----------|---|------------|
| 3.5.4 | Monopoles | 122 |
| 3.6 | Entropic interactions | 136 |
| 3.6.1 | Pair interactions | 136 |
| 3.6.2 | The complete pair interaction | 138 |
| 3.6.3 | Multibody interactions | 141 |
| 3.6.4 | Monopoles | 144 |
| 3.7 | Harmonic traps and “soft monopoles” | 154 |
| 3.7.1 | Surface response to a trapped particle | 154 |
| 3.7.2 | EFT for soft monopoles | 156 |
| 3.7.3 | Elastic interactions between trapped particles | 158 |
| 3.7.4 | Entropic interactions between trapped particles | 161 |
| 4 | Membrane-mediated interactions of axisymmetric particles | 162 |
| 4.1 | Membrane energetics | 162 |
| 4.2 | Particle boundary conditions | 164 |
| 4.2.1 | Membrane response to an isolated particle | 172 |
| 4.3 | Effective theory | 175 |
| 4.3.1 | EFT for flat particles: induced sources | 177 |
| 4.3.2 | EFT for curved particles: permanent sources | 181 |
| 4.3.3 | Some comments on the usage of point particles | 183 |
| 4.4 | Interactions diagrammar | 185 |
| 4.5 | Elastic interactions | 189 |
| 4.5.1 | Pair interactions | 189 |
| 4.5.2 | Multibody interactions | 202 |
| 4.6 | Entropic interactions | 204 |
| 5 | Particle anisotropies | 209 |
| 5.1 | Symmetry revisited | 211 |
| 5.1.1 | EFT for particles of arbitrary shape | 212 |
| 5.2 | EFT for elliptical particles | 214 |
| 5.2.1 | Effective response | 215 |
| 5.2.2 | Full-theory response | 216 |
| 5.2.3 | Matching | 219 |
| 5.2.4 | Monopoles | 220 |
| 5.3 | Entropic interactions: free particles | 224 |
| 5.3.1 | Diagrammar | 225 |
| 5.3.2 | Pair interactions | 227 |
| 5.3.3 | Multibody interactions | 231 |
| 5.4 | Entropic interactions: fixed particles | 235 |
| 5.4.1 | Leading order | 236 |
| 5.4.2 | Higher orders | 239 |

CONTENTS

| | |
|---|------------|
| Summary and conclusion | 247 |
| A Linear response and complete renormalization of polarizabilities | 251 |
| A.1 Linear response | 251 |
| A.2 Regularization and resummation | 253 |
| A.3 Matching and counterterms | 256 |
| B Soft monopoles and unpinned particles | 258 |
| B.1 Particle boundary conditions | 258 |
| B.2 Background field and response | 261 |
| B.3 Leading-order interaction energy | 262 |
| B.3.1 Elastic interactions | 262 |
| B.3.2 Entropic interactions | 262 |
| C Monopole contributions for the ellipse: asymptotics and matching | 264 |
| C.1 Asymptotics in elliptic coordinates | 264 |
| C.2 Background field and response | 266 |
| C.3 Independence of matching | 267 |
| List of Figures | 269 |
| List of Technical Notes | 270 |
| Bibliography | 271 |

Contents (detailed)

| | |
|---|-----------|
| Introduction | 1 |
| 1 An invitation to Effective Field Theory | 6 |
| 1.1 An electrostatics example | 6 |
| ▷ Case 1: Fixed charges | 7 |
| ▷ Case 2: Fixed potentials | 9 |
| 1.1.1 Developing a formalism | 10 |
| ▷ Energy principles for conducting objects | 12 |
| ◦ Fixed charges | 13 |
| ◦ Fixed potentials | 14 |
| ▷ Forces between conductors | 14 |
| 1.1.2 An effective energy functional | 15 |
| ▷ Determining Wilson coefficients via matching | 19 |
| ◦ Full theory | 19 |
| ◦ Effective theory | 20 |
| 1.1.3 Interactions | 25 |
| ▷ Electrostatic potential | 25 |
| ▷ Electrostatic energy | 27 |
| ◦ Fixed potentials | 28 |
| ◦ Fixed charges | 31 |
| 1.2 Effective field theory formalism | 34 |
| 1.2.1 General formalism | 35 |
| 1.2.2 Worldline EFTs | 37 |
| ▷ Partition function | 38 |
| ▷ Interaction potential | 40 |
| 2 Physics of random surfaces | 41 |
| 2.1 Mesoscopic models of interfaces and membranes | 41 |
| 2.1.1 Physical origins and considerations | 41 |
| 2.1.2 Modeling and mathematical description | 43 |
| 2.2 Surface geometry | 44 |
| ▷ First fundamental form (metric) | 46 |
| ▷ Second fundamental form (extrinsic curvature) | 47 |
| ▷ Covariant derivatives and intrinsic curvature | 49 |
| ▷ The <i>named</i> equations and the <i>Theorema Egregium</i> | 50 |
| ▷ Monge gauge | 51 |

| | | |
|----------|--|-----------|
| 2.3 | Helfrich theory | 53 |
| ▷ | Variations and the shape equation | 55 |
| 2.4 | Fluctuating surfaces | 57 |
| ▷ | Gauge fixing and the functional measure | 57 |
| ▷ | An additional measure factor | 60 |
| 2.4.1 | Harmonic approximation | 60 |
| ◦ | Amplitude of fluctuations | 61 |
| ◦ | Orientational order | 64 |
| 2.4.2 | Nonlinearities and renormalization | 66 |
| 3 | Surface-mediated interactions of axisymmetric particles | 69 |
| 3.1 | Surface energetics | 69 |
| ▷ | Taming the zero mode | 70 |
| ▷ | Stationary surface conditions | 71 |
| 3.2 | Particle boundary conditions | 72 |
| ▷ | Conditions for the contact line | 75 |
| ▷ | Constraint forces | 79 |
| ▷ | Pathologies | 79 |
| ▷ | Charge distributions: An electrostatics analogy | 80 |
| ▷ | Capillary charges: Attractive or repulsive? | 82 |
| 3.2.1 | Surface response to an isolated particle | 85 |
| ▷ | Flat particle | 86 |
| ▷ | Curved particle | 87 |
| ▷ | Harmonic limit | 88 |
| 3.3 | Effective theory | 89 |
| 3.3.1 | EFT for free, flat particles: induced polarization | 90 |
| ▷ | Matching | 91 |
| ▷ | Complex coordinates | 92 |
| ▷ | Some remarks on the regulator | 94 |
| 3.3.2 | EFT for constrained flat particles: induced sources | 95 |
| ◦ | (BC 2) | 95 |
| ◦ | (BC 1) | 96 |
| 3.3.3 | EFT for curved particles: permanent sources | 96 |
| ◦ | Fixed height and tilt | 97 |
| ◦ | Saddle-shaped particles | 98 |
| ◦ | General contact line | 98 |
| ▷ | Polarizabilities and preferred shape | 99 |
| ▷ | Permanent charges and force balance | 101 |
| 3.4 | Surface-mediated interactions: Preliminaries | 102 |
| 3.4.1 | The diagrammatic technique | 103 |
| ▷ | A more direct route | 107 |
| ▷ | Multiple perturbations | 108 |

| | | |
|-------|--|-----|
| | ▷ Ground state versus entropic | 109 |
| 3.4.2 | Surface diagrammar | 110 |
| | ◦ Power counting | 112 |
| | ◦ Self-interactions | 112 |
| 3.5 | Elastic interactions | 113 |
| 3.5.1 | Pair interactions | 114 |
| | ▷ Tilt freedom | 116 |
| 3.5.2 | Multibody interactions | 117 |
| 3.5.3 | The complete pair interaction for curved particles | 119 |
| | ◦ Tilt freedom | 122 |
| 3.5.4 | Monopoles | 122 |
| | ▷ Leading order interactions and resummation | 122 |
| | ◦ Two particles | 124 |
| | ◦ Three particles | 127 |
| | ▷ Higher-order corrections | 131 |
| | ◦ Two particles | 132 |
| | ◦ Three particles | 132 |
| | ▷ Curved particles | 134 |
| | ◦ Two particles | 135 |
| | ◦ Three particles | 135 |
| | ▷ Monopoles and mixed boundary conditions | 135 |
| 3.6 | Entropic interactions | 136 |
| 3.6.1 | Pair interactions | 136 |
| | ◦ Tilt freedom | 137 |
| 3.6.2 | The complete pair interaction | 138 |
| | ◦ (BC 2) | 139 |
| | ◦ (BC 3) | 140 |
| | ◦ Asymptotics and the exact solution | 140 |
| 3.6.3 | Multibody interactions | 141 |
| | ◦ Tilt freedom | 143 |
| 3.6.4 | Monopoles | 144 |
| | ▷ Leading order | 144 |
| | ◦ Two particles | 145 |
| | ◦ Three particles | 145 |
| | ▷ Higher orders | 147 |
| | ◦ Two particles | 149 |
| | ◦ Three particles | 150 |
| | ◦ Monopole screening | 152 |
| 3.7 | Harmonic traps and “soft monopoles” | 154 |
| 3.7.1 | Surface response to a trapped particle | 154 |
| 3.7.2 | EFT for soft monopoles | 156 |
| | ▷ Soft monopoles and self-capacitance | 157 |

| | | |
|----------|---|------------|
| 3.7.3 | Elastic interactions between trapped particles | 158 |
| ▷ | Comparison with the results of Ref. [LO07] | 159 |
| 3.7.4 | Entropic interactions between trapped particles | 161 |
| 4 | Membrane-mediated interactions of axisymmetric particles | 162 |
| 4.1 | Membrane energetics | 162 |
| ▷ | Stationary membrane conditions | 163 |
| 4.2 | Particle boundary conditions | 164 |
| ▷ | Constraint forces | 167 |
| ▷ | Membrane charges and pathologies | 168 |
| 4.2.1 | Membrane response to an isolated particle | 172 |
| ▷ | Flat particle | 173 |
| ▷ | Curved particle | 174 |
| 4.3 | Effective theory | 175 |
| 4.3.1 | EFT for flat particles: induced sources | 177 |
| ▷ | Matching | 178 |
| 4.3.2 | EFT for curved particles: permanent sources | 181 |
| ▷ | Matching | 182 |
| ▷ | Preferred shape | 183 |
| 4.3.3 | Some comments on the usage of point particles | 183 |
| 4.4 | Interactions diagrammar | 185 |
| 4.5 | Elastic interactions | 189 |
| 4.5.1 | Pair interactions | 189 |
| ▷ | Minimum energy configurations | 192 |
| ◦ | Up-up ($J_2 = +J$) case | 193 |
| ◦ | Up-down ($J_2 = -J$) case | 196 |
| ◦ | Attractive versus repulsive | 197 |
| ▷ | Higher orders for axisymmetric particles | 199 |
| 4.5.2 | Multibody interactions | 202 |
| 4.6 | Entropic interactions | 204 |
| ▷ | Multibody interactions | 206 |
| 5 | Particle anisotropies | 209 |
| ▷ | Model and boundary conditions | 210 |
| 5.1 | Symmetry revisited | 211 |
| 5.1.1 | EFT for particles of arbitrary shape | 212 |
| 5.2 | EFT for elliptical particles | 214 |
| 5.2.1 | Effective response | 215 |
| 5.2.2 | Full-theory response | 216 |
| ▷ | Conformal mapping | 216 |
| 5.2.3 | Matching | 219 |
| ◦ | Rotated ellipse | 219 |

| | |
|---|------------|
| ◦ Tilt freedom | 220 |
| ▷ Limiting cases: rods and disks | 220 |
| 5.2.4 Monopoles | 220 |
| ▷ Effective response | 221 |
| ▷ Full-theory response | 222 |
| ▷ Matching | 223 |
| ◦ Higher-order polarizabilities | 224 |
| ◦ Limiting cases | 224 |
| 5.3 Entropic interactions: free particles | 224 |
| 5.3.1 Diagrammar | 225 |
| 5.3.2 Pair interactions | 227 |
| ▷ Orientational dependence | 230 |
| 5.3.3 Multibody interactions | 231 |
| 5.4 Entropic interactions: fixed particles | 235 |
| 5.4.1 Leading order | 236 |
| ▷ Two particles | 237 |
| ▷ Three particles | 238 |
| 5.4.2 Higher orders | 239 |
| ▷ Two Particles | 241 |
| ▷ Three particles | 243 |
| Summary and conclusion | 247 |
| A Linear response and complete renormalization of polarizabilities | 251 |
| A.1 Linear response | 251 |
| A.2 Regularization and resummation | 253 |
| A.3 Matching and counterterms | 256 |
| B Soft monopoles and unpinned particles | 258 |
| B.1 Particle boundary conditions | 258 |
| ▷ Isolated particle | 258 |
| ▷ Particle in a harmonic trap | 260 |
| B.2 Background field and response | 261 |
| B.3 Leading-order interaction energy | 262 |
| B.3.1 Elastic interactions | 262 |
| B.3.2 Entropic interactions | 262 |
| C Monopole contributions for the ellipse: asymptotics and matching | 264 |
| C.1 Asymptotics in elliptic coordinates | 264 |
| ▷ General case | 264 |
| ▷ Asymptotics | 265 |
| C.2 Background field and response | 266 |
| C.3 Independence of matching | 267 |

Contents (detailed)

| | |
|--------------------------------|------------|
| List of Figures | 269 |
| List of Technical Notes | 270 |
| Bibliography | 271 |

Introduction

Nature exhibits a wide diversity of phenomena and structure across a multitude of scales. Yet, within Nature’s complexity, there exist fascinating patterns and commonalities. At the heart of these emergent forms and behaviors lies a concordance of influence from a tangled network of interactions, which are directed and constrained by physical laws. However, many of the associated characteristics appear universal, and may be understood by examining the underlying mathematical structure that describes them.

The modern view of particle interactions presents such a unified picture, wherein particles “communicate” with one another via the fields to which they couple. In classical field theory, the electric field mediates the Coulomb force between electric charges and the curvature of spacetime mediates forces between masses, the corresponding “charge” for gravity. In quantum field theory (QFT), field-mediated interactions appear as an exchange of quanta—quantized excitations of the field, such as photons and gravitons. The reach of this viewpoint, however, is much broader, and the analogous mathematics provides a coherent language to both describe and explain seemingly unrelated phenomena. In this thesis we will use this perspective—and the tools it offers—as a guiding theme to explore surface-mediated interactions between particles adsorbed to soft matter surfaces.

At the breakfast table, one might observe bubbles on the surface of coffee aggregating together and collecting at the walls of the mug. Similar behavior might be seen with cereal floating in milk. Perhaps as a child (or even as an adult), the reader has taken advantage of this “Cheerios effect” [VM05] to spell out their name in a bowl of alphabet soup. One may even further explore and replicate this behavior by carefully floating thumbtacks, paper clips, or segments of soda straws on a liquid surface [VM05, CFHQ02]. Humans are not the only creatures who have noticed this behavior; certain insects readily exploit this effect to pass from a water surface to land by “climbing” the meniscus at the water’s edge [HB05]. In each of these examples, the “particles” are trapped at the liquid–air interface, and the competition between gravity and surface tension deforms the surface in the vicinity of the particles’ boundaries. Positively buoyant objects like bubbles tend to move up any height gradients of the surface, such as at the liquid meniscus near the wall of a cup. Denser objects like thumbtacks, which would normally sink if not held up by surface tension, depress the surface and tend to move down height gradients. The mysterious attraction then results as like objects encounter each other’s menisci and reduce the excess area from their deformations—thereby decreasing the excess energy due to tension and gravity—during approach. In the language of the previous paragraph, the liquid surface height serves as the field and the objects source deformations in this field in much the same way as a charged conductor sources an electric field. More akin to gravity, however, in this case like “charges” attract and opposites repel.

Understanding the interactions between particles bound to soft matter surfaces of course serves more than just to explain curiosities in the dining room. It also provides insight into structure formation of colloidal particles adsorbed to fluid interfaces relevant to technological applications, and informs our understanding of protein aggregation and other structural inhomogeneities of inclusions in cellular membranes. More than a century ago, Ramsden [Ram03] and Pickering [Pic07] observed that colloidal particles may act similarly to surfactants by adsorbing to and subsequently lowering the surface tension at the interface between two normally immiscible fluids—such as oil and water—leading to particularly stable emulsions [Bin02, ABC03, MMY⁺12] (see also Ref. [NB15] for very recent theoretical and experimental treatments of particle-stabilized emulsions). This insight has found a wide range of applications, from pharmaceuticals to cosmetics to mineral processing and refining of crude oil [Bin07]. Colloidal assemblies at fluid interfaces have been utilized in the fabrication of special materials, such as macroporous ceramics—relevant to filtration and insulation technologies—and 3D photonic crystals, where colloidal crystals serve as template structures [HBS98, GYX99, SS01]. Assemblies of nanoscale colloidal metal particles have also been applied to optofluidic devices, such as tunable liquid mirrors [BKT⁺09].

Surface-mediated interactions also play an important role in biology. Fluid membranes envelope and provide basic structure to cells and their interior organelles and vesicles, but most of the biological functions are performed or controlled by their bound proteins [AJL⁺07]. Among the myriad of complex interactions between bound constituents in the “fluid mosaic” of a cellular membrane [SN72, Nic14], these objects may impart deformations on the membrane itself [MG05, ZK06], which in turn mediates interparticle forces through the overlap of its responding surface curvature. These deformations are more than incidental [VS06, PUWS09]—indeed, proteins such as clathrin, epsin, BAR domains, and various reticulons induce membrane curvature and aid in vesicle formation, endocytosis, and exocytosis [TSHDC99, BV06, Koz07, YS07, RIH⁺07, AG09, RH11], and furthermore play a role in the structural tubulation and stability of the endoplasmic reticulum and Golgi apparatus [FRT⁺01, IER⁺05, SVR06, VPS⁺06, YS07, GHV14]. Understanding how particle inclusions modify the physical properties of the membrane and how the membrane consequently mediates interparticle forces is necessary to make accurate quantitative predictions regarding the above phenomena.

Calculating these surface-mediated interactions is unfortunately far from trivial and has been met with varying degrees of success. The presence of particles creates a set of compact boundaries in the surface and therefore requires solving a rather tricky boundary value problem. Not surprisingly, such problems usually resist exact solutions, owing to the complicated shape of the intervening equilibrium surface. For particles at liquid–fluid interfaces, the one exception is the special case of two floating parallel cylinders of infinite length [GS71]; for all others, some simplifying assumptions or approximations are necessary. One common strategy, provided by Nicolson [Nic49], is to assume a superposition approximation of the particles’ respective menisci, which has been applied to flotation forces between spheres and finite cylinders [CHJW81, KPIN92, Luc92, KPD⁺93, PKDN93, KN00, KD01]. The problem with such an approach is its failure to account properly for

the modification of a particle’s local meniscus from its equilibrium shape in the absence of other particles—as well as other associated finite-size effects—much in the same way as applying Coulomb’s law to find the force between charged conducting spheres will miss polarization effects. One should at best expect it to work in the limit of infinite separation, or rather when the particle size to separation ratio is extremely small, but even in this limit the asymptotic behavior may be incorrect if the lowest-order interaction relies on a “polarization” effect. Such *point-particle approximations* must therefore be amended to preserve finite-size information if one wishes to go beyond leading order, or indeed have confidence in the leading-order result.

Gravity not generally the sole contributor to a particle’s meniscus, nor is it always significant. The contact line between the particle and the surface may be pinned in such a way as to locally deform the surface, and the resulting interparticle forces can be used to explain and engineer mesoscale 2D self-assembly processes [BTCW97, BCGW99, BWCW01, GBA⁺01, WG02, BO07, LBT⁺09]. Irregular contact lines can occur for thin but curved particles, or through differing wetting properties across a particles surface [Saf94]. For surfaces characterized by surface tension, bound particles cannot permanently impart axisymmetric height or slope deformations unless acted upon by an external force or torque. To lowest order, only anisotropic deformations of a quadrupolar shape matter (though *nonequilibrium* “dipole” configurations have been studied [RSZ13]), and lead to orientation-dependent particle interaction potentials which scale as $\sim 1/r^4$ in separation [PKDN93, BSR00, KN00, KD01, SDJ00, vNSH05, LAZY05, LYP06].

For fluid membranes in the biological context, surface tension acts weakly at small enough length scales (below 100 nm, roughly), and the surface energy is instead characterized by its curvature elasticity [Can70, Hel73, Eva74]. In this case, the surface permits contact profiles around a particle that fix the attachment slope, even axisymmetrically so. Using matched asymptotics or Green function methods, researchers have also calculated interparticle forces and torques in the weakly curved limit, and found a repulsive interaction energy that also scales as $\sim 1/r^4$, but for unconstrained isotropic particles [GBP93a, GBP93b, FD97, BF03]. More remarkably, this interaction is *not* characterized by the product of the particles’ corresponding “curvature charges,” as one finds in electrostatics or gravity, and is also nonvanishing even if the second particle imparts no curvature to the surface (a *flat* contact profile). This shows the breakdown of any superposition principle even at leading order and demonstrates that a consistent approximation strategy must be developed with care. Due to the biological importance of such interactions, many generalizations and extensions have appeared, most notably nontrivial multibody interactions [KNO98, KNO99, DF99b, CKO01, DF02, FDP03, FHP03, KCR08], relevant to the lateral distribution and configurational stability of proteins; interactions on curved membranes [GFG98], relevant when the membrane envelopes a cell or other vesicle; and corrections for nonvanishing tension [WKH98].

All the interactions discussed above are *ground state* energies, *i.e.*, in the limit of vanishing surface undulations. However, in such 2D soft matter surfaces—namely those with moduli

comparable to thermal energy—small local strain can lead to very large deformations,¹ and are thus particularly susceptible to thermal fluctuations and exhibit long-range surface correlations [LL01, BDFN95]. Even if embedded particles impart no permanent curvature, the particle attachment boundaries constrain the spectrum of thermal fluctuations, resulting in long-range fluctuation-induced forces between particles. From a physicist’s perspective, we recognize this behavior as a thermal analogue of the famed Casimir effect [Cas48, Mil01]. The Casimir effect was first theorized in 1948 to describe a force of quantum origin between neutral conducting plates due to fluctuations in the electromagnetic zero-point energy, but thirty years later Fisher and de Gennes [FdG78] placed the same ideas into a thermodynamics context. It has since been generalized to describe any fluctuation-induced interactions mediated by a field with constraining boundaries, including classical systems such as critical fluids [HHG⁺08, GMH⁺09, Gam09, SZH⁺08, NHB09] and the present work on fluctuating fluid interfaces and membranes.

Just as with the ground state forces, the calculational challenge for the fluctuating problem is in the proper handling of the nontrivial boundary conditions imposed by embedded particles. The issue is further complicated as the particles themselves may be endowed with additional fluctuating degrees of freedom, such as bobbing or tilting. A variety of strategies have been proposed and implemented to calculate such interactions [Net97, HW01, Wei01, PL96, LK91, EGJK07, EGJK08, YRD11], yielding asymptotic results for fluid interfaces [GGK96b, GGK96a, KG99, LOD06, LO07, LNO08, LNO08, NO09, YRD11, YRD12, NWZ13b, NWZ13a] and membranes [GGK96b, GGK96a, KG99, GFG98, YD12]. Pushing beyond leading order has been fraught with additional difficulty. For example, an attempt was made by Netz [Net97] to construct a point-particle representation of the membrane problem, but he did not properly account for the finite size of inclusions. Fournier and coworkers have also considered higher order corrections [DF99b, DF99a, BDF10], but conflated finite-size considerations with a specially chosen small-length cutoff. Another approach employing a scattering formalism [NWZ13b, NWZ13a] has enjoyed success; however, clarity in interpretation and intuition is obscured slightly within the resulting mathematics.

In this thesis we will take a different approach, namely that of *effective field theory* (EFT). The essence of EFT rests upon the following observation: For any system we study in science, we inevitably must ask scale-dependent questions—either implicitly or explicitly—but we also know that in certain scale regimes it is often collective or aggregate properties that are important and determine the overall behavior. That is, although the microscopic physics informs the values of the larger-scale emergent or phenomenological parameters or couplings (*e.g.*, bulk modulus, diffusion constant, conductivity), much of the microscopic detail is irrelevant. Indeed, this has been the prime reason for the success of statistical physics, but the success of “sloppy models” across other branches of science often enjoy the same feature [MCTS13, TMB⁺15]. This “coarse-graining” and scale-separation philosophy has

¹Note that large deformations due to small strains are also possible for surfaces that are *not* soft, as one might observe by bending a sheet of paper. In these cases the effect is primarily related to the reduced dimensionality, as can be understood through thin-plate theory [LL01].

undergirded much of the development of modern physics, most notably in critical phenomena and the renormalization group [Wil71a, Wil71b], and reaches maturity in EFT [Rot04] as a theory-building method. This particular incarnation of the EFT formalism was first developed in the context of general relativity and black hole physics to handle boundary conditions of massive extended objects [GR06b, GR06a, PRR11], and was subsequently applied to very different problems including finite-size corrections in the Abraham–Dirac–Lorentz radiation reaction force law in classical electrodynamics [GLR10] and the Casimir torque on cylindrical gears [Vai14]. Recently, Yolcu, Deserno, and Rothstein have adapted EFT to address surface-mediated interactions in soft matter [YRD11, YRD12, YD12]. The aim of this thesis is to both build upon and generalize the aforementioned approach, and to explore and make accessible the principles and tools of EFT beyond this specific application.

Applied to our problem, EFT exploits the separation of scales to guide the construction of an equivalent point-particle description of surface-mediated interactions in such a way that *complete* information of the short-distance physics (particle geometries, boundary conditions, and field responses) is preserved and encoded as numerical couplings. These couplings present clear physical interpretations, therefore assisting in understanding and intuition from the start. Moreover, the particle descriptions are disentangled from the rest of the problem. Particles are characterized by simpler single-particle boundary value problems, rather than by treating the particles all at once. Even if the single-particle boundary value problem is difficult, the procedure simply amounts to matching a coefficient to a number, which may be determined numerically or by experiment, or even left undetermined to give a phenomenological theory. Because of this independence, it is then easy to compute interactions between nonidentical particles of differing boundary conditions. Furthermore, by “going point-particle,” calculating multibody interactions follows almost as easily as those between pairs.

To familiarize ourselves with EFT, we begin in Chapter 1 with a discussion of an analogous field-mediated problem: the electrostatic force between conducting spheres. This textbook problem serves as a conceptual anchor to motivate and develop the EFT formalism, which we will then push to a substantial level of sophistication. After summarizing the lessons learned and discussing the general EFT philosophy and procedure, we will take an interlude in Chapter 2 to introduce the geometric theory of random surfaces and address the physical consequences for fluctuating fluid surfaces. We will then apply EFT to surface-mediated interactions between rigid, axisymmetric particles in Chapters 3 and 4, and generalize to particles of arbitrary geometry before calculating high-order results pertaining to elliptical particles in Chapter 5. We conclude with a few proposals for further investigation and close with a recap of the key results and ideas.

1 An invitation to Effective Field Theory

In this chapter, we will introduce and develop the philosophy and formalism of Effective Field Theory (EFT) through a detailed exploration of a straightforward question in classical electrostatics: *What is the force between two conducting spheres respectively held at fixed total charge or fixed potential?* Through this illustrative example, we will develop intuition about scale separation and the relationship between sources, boundary conditions, and linear response that will prove to be not only relevant, but serve as a useful guiding analogy in later chapters. Since the physics involved should be familiar to most students of physics, we will have the opportunity to introduce and clarify some of the more technical aspects of field theory within a comfortable context.

Along the way, the formalism we develop will suggest a systematic procedure for approaching similar problems of field-mediated interactions between compact objects. In the final section, we reflect on the lessons learned from the electrostatics example and summarize the steps for constructing and implementing an EFT for a more general class of problems.

1.1 An electrostatics example

Consider two (ideal) conducting spheres of radii R_1 and R_2 , separated by a distance $d \gg R_a$. Here we will explore two cases (see Fig. 1.1):

Case 1: The conductors are isolated but with fixed total charges Q_1 and Q_2 respectively.

Case 2: The conductors are respectively held at fixed potentials $\phi(\mathbf{x} \in V_1) = \Phi_1$ and $\phi(\mathbf{x} \in V_2) = \Phi_2$, with the reference potential $\Phi_\infty = 0$ at infinity, but are otherwise isolated.

This problem has a rich history, stretching back at least 170 years with William Thomson (Lord Kelvin) [Lek12c]. Maxwell himself provided a series solution (up to 22 orders!) for charged spheres in his *Treatise on Electricity and Magnetism* [Max91]. Even today, the problem of interacting spheres finds applications ranging from protein dynamics in biological systems [DY06] to electrorheological fluids in hydraulics or flexible electronics [BVS13].

Given its history, this system has been tackled by a number of mathematical methods—including zonal harmonics [Max91], method of images [SBO98], and capacitance coefficients [Lek12a, Lek12b]—each with varying levels of mathematical sophistication and physical interpretation. Here, we will provide a different perspective in which the mathematical machinery is systematic and physical intuition is manifest throughout.

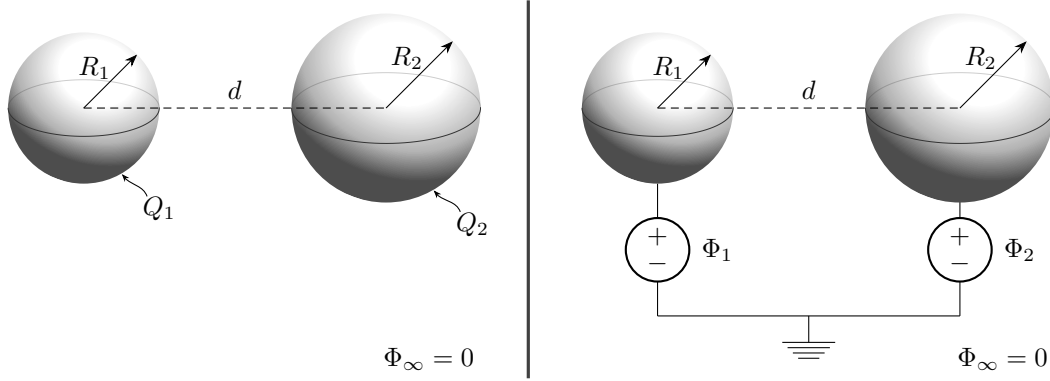


Figure 1.1: Two ideal conducting spheres of radii R_1 and R_2 are separated a distance d from their centers. In Case 1, the conductors are isolated with fixed total charges Q_1 and Q_2 respectively. In Case 2, the conductors are kept at fixed electric potentials Φ_1 and Φ_2 relative to the ground reference potential $\Phi_{\text{ground}} = \Phi_{\infty} = 0$.

Case 1: Fixed charges

At leading order, the force F_{12} that conductor 1 exerts on conductor 2 is simply given by the Coulomb force

$$F_{12} \approx F_{12}^{\text{C}} = \frac{Q_1 Q_2}{4\pi\epsilon_0 d^2}. \quad (1.1)$$

Intuitively, the electric field generated by the charge on the first conductor is of the same form as that of a point charge. At large distances, the second conductor appears as a point charge as well, giving rise to the above expression via $F_{12} \approx Q_2 E_{12}^{\text{C}}$. However, the mobile charges in a finite-sized conductor respond to an external field and will reconfigure until the net force within the conductor vanishes. At electrostatic equilibrium, the conductor's charges will no longer be uniformly distributed across the surface, but will instead create a field-dependent surface charge distribution $\sigma(\mathbf{x})$. The resulting field due to this induced charge distribution will in turn provide an additional contribution $\Delta F = F - F^{\text{C}}$ to the total force.

To quantify these finite-size effects, let us examine the response of conductor 2 due to the field generated by conductor 1. Across the spatial extent of conductor 2, the external field $E_{12} \approx E_{12}^{\text{C}}$ is approximately constant. The response ΔE_2 of the mobile charges within conductor 2 serve to completely expel the field within the volume such that $\Delta E_2^{\text{in}} = -E_{12} \approx -E_{12}^{\text{C}}$. To calculate the exterior response ΔE_2^{out} due to the resulting charge distribution σ , it will prove easier to first examine the electric potentials $\Delta\phi_2^{\text{in}}$ and $\Delta\phi_2^{\text{out}}$ since they must match along the conductor's boundary ∂V_2 .

Taking for a moment the origin to be centered on conductor 2 with the z axis passing through both centers, we can express the inner response as $\Delta\phi_2^{\text{in}} = E_{12}z = E_{12}r \cos\theta$ in spherical coordinates. Note that the inner response varies over the length scale $r \sim R_2$, so

at large distance from the conductor we should expect the potential to fall off as increasing powers of R_2/r . Outside the conductor, the potential is generated by the new charge distribution σ and can be written as the familiar multipole expansion [Zan13]

$$\Delta\phi_2^{\text{out}}(\mathbf{x}) = \frac{1}{4\pi\epsilon_0} \int_{\partial V_2} dA' \frac{\sigma(\mathbf{x}')}{|\mathbf{x} - \mathbf{x}'|} = \frac{1}{4\pi\epsilon_0} \left(\frac{q}{r} + \frac{\mathbf{p} \cdot \hat{\mathbf{x}}}{r^2} + \dots \right), \quad (1.2)$$

where

$$q := \int_{\partial V_2} dA' \sigma(\mathbf{x}'), \text{ and } \mathbf{p} := \int_{\partial V_2} dA' \sigma(\mathbf{x}') \mathbf{x}' \quad (1.3)$$

are, respectively, the total induced charge (monopole moment) and induced dipole moment of the distribution. By the angular dependence of $\Delta\phi_2^{\text{in}}$, we immediately see that $q = 0$ as expected. Furthermore, it follows from azimuthal symmetry that $\mathbf{p} \cdot \hat{\mathbf{x}} = p \cos \theta$ and therefore only the dipole moment is nonvanishing. We solve for p by imposing continuity of the potential at the boundary, $\Delta\phi_2^{\text{in}}(R_2, \theta) = \Delta\phi_2^{\text{out}}(R_2, \theta)$, which gives

$$p = 4\pi\epsilon_0 R_2^3 E_{12}. \quad (1.4)$$

We recognize the prefactor $4\pi\epsilon_0 R_2^3 =: \alpha_2$ as the (dipole) *polarizability* of the conductor. The electric field then follows from $\Delta\mathbf{E}_2^{\text{out}} = -\nabla(\Delta\phi_2^{\text{out}})$. In particular, the polarization field ΔE_{21} at the position of conductor 1 is given by

$$\Delta E_{21} = \frac{2\alpha_2 E_{12}}{4\pi\epsilon_0 d^3} = 2E_{12} \left(\frac{R_2}{d} \right)^3 \approx \frac{2Q_1 R_2^3}{4\pi\epsilon_0 d^5} \quad (1.5)$$

in the z direction. Similarly, the field of conductor 2 will polarize conductor 1, which will in turn generate a response field at conductor 2 given by

$$\Delta E_{12} = -\frac{2\alpha_1 E_{21}}{4\pi\epsilon_0 d^3} = -2E_{21} \left(\frac{R_1}{d} \right)^3 \approx -\frac{2Q_2 R_1^3}{4\pi\epsilon_0 d^5}. \quad (1.6)$$

We find that the force on conductor 2 deviates from the Coulomb force due to polarization effects, and the leading-order correction has two contributions. The first arises from the charge of conductor 2 interacting with the induced dipole field of conductor 1 and is given by $Q_2 \Delta E_{12}$. The second contribution is due to the interaction of the induced dipole moment of conductor 2 interacting with the field generated by conductor 1, which by Newton's third law can be written as $-Q_1 \Delta E_{21}$. The final result is

$$\Delta F_{12} \approx Q_2 \Delta E_{12}^{\text{C}} - Q_1 \Delta E_{21}^{\text{C}} = -2 \frac{Q_1^2 R_2^3 + Q_2^2 R_1^3}{4\pi\epsilon_0 d^5}. \quad (1.7)$$

Case 2: Fixed potentials

In contrast to isolated conductors of fixed total charge, conductors at fixed potentials require an external energy source—and therefore an external source of charges—to maintain their respective values. When a conductor is connected to such an external source (*e.g.*, a battery), charges will be drawn from the reservoir and flow until electrostatic equilibrium is reached, at which point the surface will become equipotential. This response, which occurs over the length scale of the conductor, results in a surface charge $Q = C\phi$, where C is the geometry-dependent self-capacitance of the conductor. For a spherical conductor of radius R , we see from Eq. (1.2) that a fixed potential at the boundary will induce a monopole field with charge $Q = 4\pi\epsilon_0 R\phi$, thereby revealing the self-capacitance to be $C = 4\pi\epsilon_0 R$. For our two-sphere system with fixed potentials, Coulomb's law immediately tells us that conductor 2 will experience a force by conductor 1 due to the charges induced by their respective potentials:

$$F_{12}^C = \frac{Q_1 Q_2}{4\pi\epsilon_0 d^2} = 4\pi\epsilon_0 \Phi_1 \Phi_2 \frac{R_1 R_2}{d^2}. \quad (1.8)$$

However, Coulomb's law only applies to *fixed charge* point particles. In this case, the conductors under consideration will not only present polarization effects due to their finite sizes as before, but they have a charge reservoirs that will respond to *external* electric potentials.

To account for these effects, we recall that the surface charges on each conductor generate their own spatially varying electric potentials. That is, the total electric potential at the site of a given conductor will be altered by the potential sourced from the other, and furthermore will vary across the space it occupies. This potential difference disrupts electrostatic equilibrium, so charges will be drawn from the reservoirs as before, and additionally redistribute (polarize) along the surface until an equipotential surface is reached that matches the imposed electric potential. This response again takes place over the length scale R_a of conductor a , so, keeping in mind $d \gg R_a$, we again expect the finite-size corrections to appear as increasing powers of the ratio R_a/d of the small and large length scales.

The charge $Q_1 = C\Phi_1$ on the first conductor will generate a field that alters the electric potential at the site of the second conductor by an amount $\Delta\phi_{12}^{(0)} = Q_1/4\pi\epsilon_0 d = \Phi_1 R_1/d$. The second conductor responds to the external potential by drawing from its reservoir an additional charge $\Delta Q_2^{(0)} = -C_2 \Delta\phi_{12}^{(0)}$ to restore the imposed potential. A similar process takes place for the first conductor. This results in a correction to the Coulomb force (1.8) by the interaction between charge Q_1 and the induced charge $\Delta Q_2^{(0)}$, and vice versa:

$$\Delta F_{12}^{(0)} = \frac{Q_1 \Delta Q_2^{(0)} + Q_2 \Delta Q_1^{(0)}}{4\pi\epsilon_0 d^2} = -4\pi\epsilon_0 \frac{\Phi_1^2 R_1^2 R_2 + \Phi_2^2 R_2^2 R_1}{d^3} \quad (1.9)$$

At this point we notice that higher-order corrections will appear not only from polarization effects, but also from the interactions between induced charges $\Delta Q^{(0)}$ as well as further induced charges $\Delta Q^{(1)}$ due to the induced potentials $\Delta\phi^{(0)}$ sourced from the other conductor.

From the expression of $\Delta\phi^{(0)}$, it follows that the induced monopole field response $\Delta E^{(0)} = \Delta Q^{(0)}/4\pi\epsilon_0 d^2 \sim R^2/d^3$. Furthermore, the change in potential $\Delta\phi^{(1)} = \Delta Q^{(0)}/4\pi\epsilon_0 d$ sourced by the induced charge of the opposing conductor will induce an additional charge $\Delta Q^{(1)} = C\Delta\phi^{(1)} \sim R^3/d^2$ and a monopole field response $\Delta E^{(1)} = \Delta Q^{(1)}/4\pi\epsilon_0 d^2 \sim R^3/d^4$. Therefore the next order force due to monopole induction is given by both $\Delta Q^{(0)}\Delta E^{(0)}$ and $Q\Delta E^{(1)}$, and appear at order $(R/d)^4$. However, we see from Eq. (1.7), with $Q = C\Phi \sim R$, that corrections due to polarization do not appear until order $(R/d)^5$, so the next-order contribution to the force is given solely by the interactions between charges and induced monopoles. Working out the details for conductor 2, we find

$$\begin{aligned} \Delta F_{12}^{(1)} &= \left(\Delta Q_2^{(0)} \Delta E_{12}^{(0)} - \Delta Q_1^{(0)} \Delta E_{21}^{(0)} \right) + \left(Q_2 \Delta E_{12}^{(1)} - Q_1 \Delta E_{21}^{(1)} \right) \\ &= (1 + 1 + 1 + 1) 4\pi\epsilon_0 \Phi_1 \Phi_2 \frac{R_1^2 R_2^2}{d^4} \\ &= 4\pi\epsilon_0 \Phi_1 \Phi_2 \frac{4R_1^2 R_2^2}{d^4}. \end{aligned} \tag{1.10}$$

If one wishes to press on further in this manner, it should become clear that a rather admirable amount of fortitude is required. The induced charges on one conductor generate monopole fields which subsequently induce further charges on the other conductor and so on *ad infinitum*. Moreover, these fields will polarize the opposing conductor, exciting additional multipole moments (monopole, dipole, quadrupole, *etc.*) and corresponding multipole fields. Following this logic, these higher moments will induce a staggering array of moments of the other conductor, and vice versa in an infinite regress, with each correction falling off as increasing powers of R/r . To actually *calculate* these corrections efficiently and systematically, we will need to develop a formalism better suited for this task.

1.1.1 Developing a formalism

To begin, we reframe the problem in terms of an energy-minimization principle. In general, electrostatics problems can be reduced to finding solutions which minimize—or, more generally, *extremize*—the total electrostatic energy stored in the electric field [SDJMT98],

$$U[\mathbf{E}] := \int d^3x \frac{\epsilon_0}{2} \mathbf{E}^2, \tag{1.11}$$

which are compatible with some given charge distribution and imposed boundary conditions. The electric field, however, is furthermore always required to obey Maxwell's equations. For electrostatics in particular, the equilibrium energy minimizes $U[\mathbf{E}]$ subject to the constraint imposed by Gauss's law, $\nabla \cdot \mathbf{E} = \rho/\epsilon_0$. Writing the constraint implicitly as $\mathcal{C}(\mathbf{E} | \rho) := \rho - \epsilon_0 \nabla \cdot \mathbf{E} \equiv 0$, it follows that for a fixed charge distribution ρ the electrostatic

energy $U[\rho]$ is given by the minimization problem,

$$U[\rho] := \min_{\substack{\mathbf{E} \in \mathcal{L}^2(\mathbb{R}^3) \\ \mathcal{C}(\mathbf{E} | \rho) = 0}} U[\mathbf{E}], \quad (1.12)$$

where we have indicated for completeness that the permissible vector fields $\mathbf{E}(\mathbf{x})$ must be square-integrable.

We can instead enforce the Gauss's law constraint explicitly at each point by way of a Lagrange multiplier function $\phi(\mathbf{x})$. From an energetics perspective, the idea is to augment $U[\mathbf{E}]$ by a positive energetic penalty,

$$U_{\mathcal{C}}[\mathbf{E}, \phi, | \rho] := \int d^3x \phi(\mathbf{x}) \mathcal{C}(\mathbf{E}(\mathbf{x}) | \rho(\mathbf{x})) \stackrel{!}{\geq} 0, \quad (1.13)$$

such that the Lagrange multiplier ϕ takes on as large or small a value to ensure that the constraint is satisfied. This results in the augmented functional

$$U[\mathbf{E}, \phi | \rho] := U[\mathbf{E}] + U_{\mathcal{C}}[\mathbf{E}, \phi | \rho] = \int d^3x \left[\frac{\epsilon_0}{2} \mathbf{E}^2 + \phi(\rho - \epsilon_0 \nabla \cdot \mathbf{E}) \right] \quad (1.14)$$

which, by construction, satisfies $U[\mathbf{E}] \geq U[\mathbf{E}, \phi | \rho]$. Equality of the functionals can therefore only be achieved by *maximizing* $U[\mathbf{E}, \phi | \rho]$ over ϕ . The maximization applies only to the penalty term, which gives

$$\max_{\phi} U_{\mathcal{C}}[\mathbf{E}, \phi | \rho] = \begin{cases} \infty, & \text{if } \mathcal{C}(\mathbf{E} | \rho) \neq 0 \\ 0, & \text{if } \mathcal{C}(\mathbf{E} | \rho) = 0 \end{cases} \quad (1.15)$$

and thus forces permissible minimizers \mathbf{E} to obey the constraint. The equilibrium electrostatic energy may therefore be obtained from the *unconstrained* min-max problem,

$$U[\rho] = \min_{\mathbf{E}} \max_{\phi} U[\mathbf{E}, \phi | \rho]. \quad (1.16)$$

Since the augmented functional (1.14) is convex¹ in \mathbf{E} , the order of $\min_{\mathbf{E}}$ and \max_{ϕ} can be interchanged without affecting the optimal value $U[\rho]$, providing an alternative max-min problem *dual* to Eq. (1.16). Transforming a constrained optimization problem to its dual is a common technique in convex analysis and may be rigorously justified by certain *minimax theorems* [BZ15]. Often, the dual problem results in simpler manipulations and computations as compared to the “primal” constrained problem. In our case, the minimization over \mathbf{E} is straightforward for the augmented functional. Varying the functional

¹ Convexity for functionals generalizes the standard definition for functions. For example, $U[\mathbf{E}]$ in Eq. (1.11) is convex since it satisfies $U[(\alpha - 1)\mathbf{E}_1 + \alpha\mathbf{E}_2] \leq (\alpha - 1)U[\mathbf{E}_1] + \alpha U[\mathbf{E}_2]$, where $\alpha \in [0, 1]$. Since the penalty term in Eq. (1.14) is operationally linear in \mathbf{E} , it is easy to check that the augmented functional retains its convexity: $U[(\alpha - 1)\mathbf{E}_1 + \alpha\mathbf{E}_2, \phi | \rho] \leq (\alpha - 1)U[\mathbf{E}_1, \phi | \rho] + \alpha U[\mathbf{E}_2, \phi | \rho]$, with $\alpha \in [0, 1]$.

with respect to \mathbf{E} gives

$$\begin{aligned}
 \delta_{\mathbf{E}} U[\mathbf{E}, \phi \mid \rho] &:= U[\mathbf{E} + \delta \mathbf{E}, \phi \mid \rho] - U[\mathbf{E}, \phi \mid \rho] \\
 &= \int d^3x \epsilon_0 (\delta \mathbf{E} \cdot \mathbf{E} - \phi \nabla \cdot \delta \mathbf{E}) + \int d^3x \epsilon_0 (\delta \mathbf{E})^2 \\
 &\stackrel{\text{IBP}}{=} \int d^3x \epsilon_0 \delta \mathbf{E} \cdot (\mathbf{E} + \nabla \phi) + \int d^3x \epsilon_0 (\delta \mathbf{E})^2,
 \end{aligned} \tag{1.17}$$

where the final line results from integration by parts and requiring the variation to vanish at infinity. The second-order term is positive definite, so we indeed minimize the functional with respect to \mathbf{E} by setting the first-order variation to zero. The vanishing of the first term for an arbitrary variation implies the solution $\mathbf{E} = -\nabla \phi$, revealing that we may in fact identify the Lagrange multiplier ϕ as the familiar electrostatic potential.

This relation between \mathbf{E} and ϕ provides—by insertion into Eq. (1.14) and integrating by parts—an alternative, *dual functional* in terms of the potential:

$$U[\phi \mid \rho] := \min_{\mathbf{E}} U[\mathbf{E}, \phi \mid \rho] = \int d^3x \left[-\frac{\epsilon_0}{2} (\nabla \phi)^2 + \rho \phi \right]. \tag{1.18}$$

The equilibrium energy may therefore be obtained by *maximizing* $U[\phi \mid \rho]$ with respect to the potential. Indeed, performing the ϕ variation and integrating by parts results in

$$\delta_{\phi} U[\phi \mid \rho] = \int d^3x (\epsilon_0 \nabla^2 \phi + \rho) \delta \phi - \int d^3x \epsilon_0 (\delta \nabla \phi)^2, \tag{1.19}$$

and the vanishing of the first term leaves a negative-definite remainder. The equilibrium potential $\phi[\rho]$ is therefore a solution to Poisson's equation, $-\epsilon_0 \nabla^2 \phi[\rho] = \rho$, and the energy takes the familiar form

$$\begin{aligned}
 U[\rho] &= \int d^3x \left\{ -\frac{\epsilon_0}{2} (\nabla \phi[\rho])^2 + \rho \phi[\rho] \right\} \\
 &\stackrel{\text{IBP}}{=} \int d^3x \left\{ -\frac{1}{2} \phi[\rho] (-\epsilon_0 \nabla^2 \phi[\rho]) + \rho \phi[\rho] \right\} = \frac{1}{2} \int d^3x \rho \phi[\rho].
 \end{aligned} \tag{1.20}$$

We note in passing that the *concave* functional (1.18)—perhaps equipped with additional boundary conditions—is particularly useful for analytic calculations, but for many applications involving numerical simulation or optimization, finding an energy functional that is local and globally convex in the desired dynamical degrees of freedom is often necessary (see for instance Refs. [Mag04] and [Mag12], and the more recent [SJOdIC13], including references therein).

Energy principles for conducting objects

Returning to our case study of conducting spheres, we wish to construct an energy functional that appropriately accounts for the physics at the conducting boundaries. A minimal energy

principle exists for conductors, known as Thomson's theorem [LLP84, SDJMT98, Zan13], which we will explore with Eq. (1.18) as a starting point.

Thomson's theorem states that the electrostatic energy U of a system of fixed but otherwise isolated conductors is minimized (with respect to \mathbf{E}) when the charge on each conductor distributes itself such that the electrostatic potential is constant at the surface and throughout the volume of each conductor. An analogous statement holds for a conductor at fixed potential, except the electrostatic *free energy* $\mathcal{F} := U - W_{\text{ext}}$, where W_{ext} is the external work done to maintain the potential, is instead minimized [Don03, LM08]. Mirroring the previous discussion, these statements in terms of their respective dual functionals of the electrostatic potential become instead *maximization* principles. We provide below proofs of these statements by explicit construction of the appropriate energy functionals. In what follows, the conductor shapes are arbitrary (but compact) and not tied to any spherical geometry.

Fixed charges. Consider a system of conductors with total charge Q_a and volume V_a for each conductor a . Beginning with the dual functional (1.18), we lift the fixed-charge constraint through a collection of (constant) Lagrange multipliers Φ_a . Following [FEPN11], we can break up the integration domain into the interior conductor volumes, $V_{\text{in}} = \bigcup_a V_a$; the conductor surfaces, $S = \bigcup_a S_a = \bigcup_a \partial V_a$; and the volume between and exterior to the conductors, $V_{\text{out}} = \mathbb{R}^3 \setminus \bigcup_a V_a$. Assuming an interior volume charge distribution ρ and a surface charge distribution σ , the functional can be written in the form

$$\begin{aligned} U[\phi, \Phi \mid \rho, \sigma, Q] &:= \int_{V_{\text{in}}} d^3x \left[-\frac{\epsilon_0}{2} (\nabla \phi)^2 + \rho \phi \right] - \int_{V_{\text{out}}} d^3x \frac{\epsilon_0}{2} (\nabla \phi)^2 + \int_S dA \sigma \phi \\ &\quad + \sum_a \Phi_a \left(Q_a - \int_{V_a} d^3x \rho - \int_{S_a} dA \sigma \right). \end{aligned} \quad (1.21)$$

After integrating by parts and collecting terms, the *first-order* functional variation gives

$$\begin{aligned} \delta U[\phi, \Phi \mid \rho, \sigma, Q] &= \sum_a \int_{V_a} d^3x \left[\delta \phi (\epsilon_0 \nabla^2 \phi + \rho) + \delta \rho (\phi - \Phi_a) \right] + \int_{V_{\text{out}}} d^3x \delta \phi (\epsilon_0 \nabla^2 \phi) \\ &\quad + \sum_a \int_{S_a} dA \left\{ \delta \phi [\epsilon_0 \hat{\mathbf{n}}_a \cdot (\nabla \phi_{\text{out}} - \nabla \phi_{\text{in}}) + \sigma] + \delta \sigma (\phi - \Phi_a) \right\}, \end{aligned} \quad (1.22)$$

where $\hat{\mathbf{n}}_a$ is the outward normal vector of the a^{th} conductor. Requiring this variation to vanish informs us that for each conductor a , the potential satisfies $\phi = \Phi_a$ within the conductor and at the surface. The neglected second-order term is strictly negative (*cf.* Eq. (1.19)) so the dual functional is maximized and we have completed the proof. However, the functional also provides us with additional information. In the space outside all the conductors, the potential satisfies Laplace's equation, $\nabla^2 \phi = 0$. Moreover, we find the equilibrium distribution of charge: $\rho = 0$ within the volume and $\sigma = -\epsilon_0 \hat{\mathbf{n}}_a \cdot \nabla \phi_{\text{out}}$ on the surface of each conductor a . \square

Fixed potentials. Consider now a system of conductors held at fixed potentials Φ_a . From the steps leading up to Eq. (1.22), we know that any charge will distribute on the conductors' surfaces, so we need only consider for the integration domain the regions outside and on the surfaces of each conductor. To fix the potentials, we introduce the Lagrange multiplier function $\sigma(\mathbf{x})$ at the conductor surfaces,

$$\mathcal{F}[\phi, \sigma | \Phi] := - \int_{V_{\text{out}}} d^3x \frac{\epsilon_0}{2} (\nabla \phi)^2 + \sum_a \int_{S_a} dA \sigma (\phi - \Phi_a). \quad (1.23)$$

The first-order variation is then

$$\delta \mathcal{F}[\phi, \sigma | \Phi] = \int_{V_{\text{out}}} d^3x \delta \phi (\epsilon_0 \nabla^2 \phi) + \sum_a \int_{S_a} dA \left\{ \delta \phi (\sigma + \epsilon_0 \hat{\mathbf{n}}_a \cdot \nabla \phi_{\text{out}}) + \delta \sigma (\phi - \Phi_a) \right\}, \quad (1.24)$$

where the remainder is strictly negative, as before. Thus we find the (dual) functional is maximized and the true charge distribution is given by $\sigma = -\epsilon_0 \hat{\mathbf{n}}_a \cdot \nabla \phi_{\text{out}}$ for each conductor. Notice, however, that \mathcal{F} can be decomposed into the analogue of Eq. (1.18) for a surface source,

$$\mathcal{F}[\phi, \sigma | \Phi] = U[\phi | \sigma] - \sum_a Q_a \Phi_a, \quad (1.25)$$

in which we recognize the remainder as the work W_{ext} done by the external sources to maintain the potentials.² \square

Forces between conductors

Once we have obtained an expression for the equilibrium energy of a conductor system, we may calculate the force \mathbf{F}_a exerted on each conductor a . Normally the force points down the gradient of potential energy. However, our use of two different types of energy for the fixed-charge and fixed-potential systems, Eqns. (1.21) and (1.23) respectively, requires a few comments.

For the case of fixed charges, we may calculate the energy along the same lines as Eq. (1.20), resulting in

$$U[Q] = \frac{1}{2} \sum_a Q_a \Phi_a[Q], \quad (1.26)$$

where $\Phi_a[Q]$ is the solution of the outer potential, due to the collection of conductor charges, at the surface of conductor a . We calculate a similar result for the case of fixed potentials, but the sign is reversed:

$$\mathcal{F}[\Phi] = -\frac{1}{2} \sum_a Q_a[\Phi] \Phi_a, \quad (1.27)$$

where $Q_a[\Phi] = \int_{S_a} dA \sigma[\Phi]$ is the charge on conductor a due to the fixed potentials of all

² This expression can also be interpreted as a Legendre transformation of $U[\phi | \sigma]$ that replaces fixed surface charges with fixed potentials as its natural variables [Zan13, LM08].

conductors. To find the force given the two different results, we may exploit the observation that $\mathcal{F}[\Phi]$ and $U[Q]$ differ in their natural variables (see footnote 2) and the expression (1.25) transforms between the two. Following Ref. [Zan13], adding to each conductor small amounts of charge dQ_a , and furthermore displacing their locations by $d\mathbf{x}_a$ results in a change in energy,

$$dU[Q] = \sum_a (\Phi_a dQ_a - \mathbf{F}_a \cdot d\mathbf{x}_a) \stackrel{!}{=} \sum_a \left\{ \left(\frac{\partial U}{\partial Q_a} \right) dQ_a + \left(\frac{\partial U}{\partial \mathbf{x}_a} \right) \cdot d\mathbf{x}_a \right\}, \quad (1.28)$$

where it is implicit in the partial derivatives that all other variables are held constant. This expression provides us with two relations,

$$\Phi_a = \frac{\partial U}{\partial Q_a} \text{ and } \mathbf{F}_a = -\frac{\partial U}{\partial \mathbf{x}_a} \quad (\text{fixed charge}). \quad (1.29)$$

On the other hand, by Eq. (1.25) the change in energy for fixed potentials is

$$\begin{aligned} d\mathcal{F}[\Phi] &= dU[Q] - \sum_a (Q_a d\Phi_a + \Phi_a dQ_a) \\ &= -\sum_a (Q_a d\Phi_a + \mathbf{F}_a \cdot d\mathbf{x}_a) \stackrel{!}{=} \sum_a \left\{ \left(\frac{\partial \mathcal{F}}{\partial \Phi_a} \right) d\Phi_a + \left(\frac{\partial \mathcal{F}}{\partial \mathbf{x}_a} \right) \cdot d\mathbf{x}_a \right\}, \end{aligned} \quad (1.30)$$

showing that the force in this case points down the gradient of the free energy via the resulting relations

$$Q_a = -\frac{\partial \mathcal{F}}{\partial \Phi_a} \text{ and } \mathbf{F}_a = -\frac{\partial \mathcal{F}}{\partial \mathbf{x}_a} \quad (\text{fixed potential}). \quad (1.31)$$

1.1.2 An effective energy functional

The energy principles illustrated above provide additional information and insight into the conductor problem, but actually finding the solutions to the complicated boundary value problems can be difficult or intractable for arbitrary conductor shapes. In the descriptive, yet rather heuristic solution presented in the previous section, we made progress by treating the spheres as point particles and accounting for additional induced charge and polarization effects by examining the conductors' respective responses to external fields. In order to maintain this intuitive picture, let us review two key lessons we learned from that example:

1. The setup involved two length scales, the separation distance d over which the interactions are mediated by the field, and the characteristic “particle” size R over which excitations take place. Given the scale separation $d \gg R$, higher-order corrections came equipped with increasing powers of d/R , providing a counting scheme to characterize our accuracy.

2. The response of an individual conductor to an external field was characterized by a parameter that was independent of the external field, and therefore independent of the other conductor (or even several other conductors). Indeed, a conducting sphere held at a fixed potential has a *monopole* response to a uniform electric potential that is characterized by its *monopole polarizability*, or self-capacitance $C = 4\pi\epsilon_0 R$, which depends only on its geometry and boundary conditions (for a conductor of fixed charge, the monopole response is zero). This feature persists for higher-order polarizabilities, ultimately allowing complete characterization of the conductor while keeping a point-particle prescription.

From our discussion of energy principles for conductors, there is yet another lesson that can be revealed by considering symmetry:

3. In the *absence* of external sources of charge or potentials, the energy functionals (1.11), (1.14), and (1.18) all exhibit a simultaneous discrete \mathbb{Z}_2 symmetry, under which $\mathbf{E} \rightarrow -\mathbf{E}$ and $\phi \rightarrow -\phi$. Additionally, the source-free version of Eq. (1.18) is invariant under a global shift of ϕ by a constant. These symmetries are explicitly broken by the inclusion of external sources. The implication here is that we can decompose the energetic description of a conductor into pieces which either obey or break the field symmetries—the invariant terms encode the response of the *conductor itself* to external fields, whereas the symmetry-breaking terms encode the response of the external conductor *sources* (e.g., battery or surface charges) to external fields *as mediated by the conductor*.

These lessons suggest a way to construct an *effective field theory* (EFT) of interacting conductors. In the absence of conductors, the *bulk* energy functional is given by the source-free form of Eq. (1.18),

$$U_0[\phi] = - \int_{\mathbb{R}^3} d^3x \frac{\epsilon_0}{2} (\nabla\phi)^2. \quad (1.32)$$

Lesson 2 teaches us that the conductors respond independently of each other, in the sense that they only rely on the external field at their respective locations. The inclusion of conductors therefore results in a change in energy $\Delta U_a[\phi]$ for each conductor. Hence we can construct an effective energy functional U_{eff} by including these additional local terms with U_0 :

$$U_{\text{eff}}[\phi] = U_0[\phi] + \sum_a \Delta U_a[\phi]. \quad (1.33)$$

As per lesson 1, in the large separation regime $d \gg R$ we treat the conductors as point particles and expand ΔU_a about their respective center of mass positions, or *worldlines*³ \mathbf{x}_a , resulting in a series that is polynomial in $\phi(\mathbf{x}_a)$ and its derivatives and weighted by

³The term “worldline” here is borrowed from different instances of EFT in relativistic field theory, even though the positions are stationary in our setup.

powers of R_a . Since the terms in ΔU_a must be scalars, a few possible options would be

$$c_1\phi(\mathbf{x}_a), c_2\phi^2(\mathbf{x}_a), c_3[\nabla\phi(\mathbf{x}_a)]^2, c_4\phi(\mathbf{x}_a)\nabla^2\phi(\mathbf{x}_a), \text{ etc.}$$

Since each term must ultimately have units of energy, we can apply dimensional analysis to estimate the magnitudes of their respective coefficients. Since the length scale of a given conductor is R_a and each derivative carries units of inverse length, the coefficients will scale respectively as $c_1 \sim Q_a \sim \epsilon_0 R_a \Phi_a$ (for an imposed Φ_a), $c_2 \sim \epsilon_0 R_a$, and $c_3 \sim c_4 \sim \epsilon_0 R_a^3$ for the remaining two. That is, we can order the terms by increasing numbers of derivatives to get the desired accuracy in powers of R_a .

Notice that the last term above is proportional to the variation of the particle-free bulk energy (1.32). As a consequence of the *equivalence theorem*, terms such as these play a redundant role in the description of particles [Rot04, Bur07]. In a classical field theory, observables will depend on solutions of the Euler-Lagrange equations—in this case the field must satisfy $\nabla^2\phi = 0$ (subject to boundary conditions) in the space outside the conductors—so it becomes clear that if we impose this from the start, these terms vanish and should ultimately be irrelevant. If, however, we were to retain these terms, the role they play would be limited to the formal mathematical manipulations occurring while calculating observables, but the final result would be identical to that calculated from an effective functional without those terms. From another perspective, the terms comprising the expansion form an “operator basis” in which some permissible terms may be expressed as either linear combinations of others (with perhaps more transparent properties), equivalent to others by integration by parts, or both [EW13]. It is desirable to construct a series in irreducible and nonequivalent terms to avoid redundancies—and therefore avoid unnecessary work. Although the ultimate choice of operator basis in our theory will not affect the observables—as long as it “spans” the permissible functional space—different choices may have different advantages, either in convergence or even interpretation. In our case, dropping terms containing $\nabla^2\phi$ provides what is known as an *on-shell* basis⁴ and tacitly assumes $\nabla^2\phi = 0$ outside the conductors at every stage of calculations.

In addition to the terms discussed above, the coefficients are not limited to just scalars. Indeed tensorial coefficients are permissible in general, such as a term $C_{ij}\partial_i\phi\partial_j\phi$, where $\partial_i := \partial/\partial x_i$ and summation is implied over repeated indices.⁵ However, this is where lesson 2 again simplifies matters. Since a conductor’s response is characterized by its geometry and boundary conditions, the presence of spherical symmetry will be reflected in the permissible form of the worldline terms. To make this manifest, we can restrict ΔU_a to consist of terms invariant under rotations about the point \mathbf{x}_a . Under the rotation

⁴“On-shell” is basically a fancy way saying that the Euler–Lagrange equation is satisfied. The term is appropriated from relativistic field theory in which particles satisfying the Euler-Lagrange equations of motion lie on their (hyperbolic) mass shell, $E^2 - |\mathbf{p}|^2 = m^2$ (with $c \equiv 1$ as per convention).

⁵Throughout the remainder of this chapter we will adhere to this summation convention for repeated *spatial* indices unless otherwise specified. We will treat squared terms such as $(\partial_i\phi)^2$ as equivalent to $\partial_i\phi\partial_i\phi$ so that summation is also implied. Summation over particle labels and multipole orders (to be introduced presently), however, will always be made explicit.

$\mathbf{x}' = \mathbf{R}\mathbf{x}$, it follows that $\partial_i = \partial_i x'_j \partial'_j = R_{ji} \partial'_j = (\mathbf{R}^\top)_{ij} \partial'_j$ and our example term transforms into $(R_{ik} C_{k\ell} R_{j\ell}) \partial'_i \phi \partial'_j \phi \equiv C'_{ij} \partial'_i \phi \partial'_j \phi$. Rotational invariance implies $C'_{ij} = C_{ij}$, but this can only be true if $C_{ij} \propto \delta_{ij}$ (where we have used $R_{ik} R_{jk} = (\mathbf{R} \mathbf{R}^\top)_{ij} = \delta_{ij}$). That is, the tensor coefficient itself must be rotationally invariant and our example reduces to $C \partial_i \phi \partial_i \phi = C (\nabla \phi)^2$, a term we have mentioned previously.

The end result is that ΔU_a consists of a series of rotationally-invariant terms polynomial in the electric potential ϕ and its derivatives, with the exception of any terms containing $\nabla^2 \phi$. Furthermore, based on Eqns. (1.21) and (1.23), the expansion should be truncated at quadratic order in ϕ for consistency.⁶ Finally, from lesson 3 we can decompose ΔU_a into conductor and source terms, ΔQ_a^c and ΔU_a^s respectively. Collecting terms with the same symmetries of the bulk—invariance under $\phi \rightarrow -\phi$ and $\phi \rightarrow \phi + \text{const}$ —gives the worldline conductor energy,

$$\begin{aligned} \Delta U_a^c[\phi] &= - \sum_{n>0} \frac{1}{2} C_a^{(n)} [\partial_{i_1} \cdots \partial_{i_n} \phi(\mathbf{x}_a)]^2, \\ &\equiv - \sum_{n>0} \frac{1}{2} C_a^{(n)} [\partial_I^n \phi(\mathbf{x}_a)]^2 \end{aligned} \quad (1.34)$$

where the factor of $1/2$ is inserted for later convenience, and we have introduced the more compact notation $\partial_I^n := \partial_{i_1} \cdots \partial_{i_n}$. We have also included a minus sign with the hindsight that a conductor will expel the electric field from its volume and therefore, from Eq. (1.11), lower the electrostatic energy. In the language of EFT, the prefactors $C_a^{(n)}$ are referred to as *Wilson coefficients*, and we know by dimensional analysis that they must scale as $C_a^{(n)} \sim \epsilon_0 R_a^{2n+1}$. The remaining symmetry-breaking terms constitute the worldline source energy, and can be expressed as

$$\Delta U_a^s[\phi] = -\frac{1}{2} C_a^{(0)} \phi^2(\mathbf{x}_a) + Q_a \phi(\mathbf{x}_a). \quad (1.35)$$

The first Wilson coefficient must scale as $C_a^{(0)} \sim \epsilon_0 R_a$. In the second term, we have identified the Q_a as a permanent charge [cf. Eqns. (1.18), (1.21), and (1.23)], which in the fixed-potential case is sourced by the applied potential Φ_a and therefore scales as $Q_a \sim \epsilon_0 R_a \Phi_a$. Our effective energy functional for conducting spheres can therefore finally

⁶To clarify, more complex physical considerations may suggest an additional expansion parameter that counts the nonlinearities in the field theory. For example, if the system presents some characteristic energy \mathcal{E} ($\mathcal{E} = k_B T$ at finite temperature, for example), it suggests a characteristic potential $\varphi_\epsilon = \sqrt{\mathcal{E}/\epsilon_0 R}$, indicating that nonlinearities will scale as $\phi^n \sim \varphi_\epsilon^n$. However, one may check that such a scaling implies that terms linear and quadratic in ϕ are respectively relevant and marginal, but higher orders are sufficiently *irrelevant* if the expansion parameter is small enough.

be expressed as

$$\begin{aligned}
 U_{\text{eff}}[\phi] &= U_0[\phi] + \sum_a (\Delta U_a^c[\phi] + \Delta U_a^s[\phi]) \\
 &= - \int d^3x \frac{\epsilon_0}{2} (\nabla \phi)^2 + \sum_a \left\{ - \sum_{n>0} \frac{1}{2} C_a^{(n)} [\partial_I^n \phi(\mathbf{x}_a)]^2 - \frac{1}{2} C_a^{(0)} \phi^2(\mathbf{x}_a) + Q_a \phi(\mathbf{x}_a) \right\}.
 \end{aligned} \tag{1.36}$$

Determining Wilson coefficients via matching

If we were to compute and expand observables (field responses, forces, *etc.*) from either “full-theory” functionals (1.21) or (1.23), the same observables as computed from the respective forms of the effective functional (1.36) should match up to the desired order of accuracy in powers of R/d , thereby revealing the values of the Wilson coefficients. It follows, therefore, that we have the freedom to compute and compare *any* convenient (and suitably sufficient) observables we wish in order to determine their values.

As discussed in lesson 2, the response of a conductor to an external field can be characterized by a set of field-independent parameters. These are precisely the Wilson coefficients of Eq. (1.36). Recall the steps leading up to the expressions for the electric field responses (1.5) and (1.6); along the way we introduced the dipole polarizability α , whose value was determined by a simple boundary value problem (BVP) but ultimately did not depend explicitly on the details of the field, but only the geometry of the boundary. Furthermore, the response to a linearly rising background potential was a dipole field that satisfied both continuity at the conductor boundary and vanishing at infinity. This suggests a general method to determine the Wilson coefficients:

Consider a conductor in isolation and introduce a set of background fields that excite multipole moments in its charge distribution. By Thomson’s theorem (for both fixed charge and fixed potential), the surface of the conductor will reach some constant equilibrium potential Φ_{eq} . The total electrostatic potential can then be decomposed into the background and response potentials, $\phi = \phi_{\text{bg}} + \delta\phi$, such that $\nabla^2 \phi = 0$ outside the conductor, $\delta\phi \rightarrow 0$ as $|\mathbf{x}| \rightarrow \infty$, and $\phi(\mathbf{x} \in S) = \Phi_{\text{eq}}$ at the conductor surface S . Then compute the effective response using U_{eff} and match the coefficients with the solution to the full BVP.

Full theory. For the particular case of an isolated spherical conductor sitting at the origin, it proves useful to consider the general solution to Laplace’s equation with azimuthal symmetry,

$$\phi(r, \theta) = \sum_{\ell \geq 0} \left[A_\ell r^\ell + B_\ell r^{-(\ell+1)} \right] P_\ell(\cos \theta), \tag{1.37}$$

where $P_\ell(\cos \theta)$ is the Legendre polynomial of order ℓ , and θ is the polar angle from the positive z -axis. This can be derived by separation of variables and can be found in most

standard textbooks on electrodynamics or mathematical physics. The general solution outside a sphere of radius R held at fixed potential Φ_{eq} must satisfy

$$\phi(R, \theta) = A_0 + \frac{B_0}{R} + \sum_{\ell \geq 1} \left[A_\ell R^\ell + B_\ell R^{-(\ell+1)} \right] P_\ell(\cos \theta) \stackrel{!}{=} \Phi_{\text{eq}}. \quad (1.38)$$

As a consequence of the linear independence of the Legendre polynomials, it follows that the summand must vanish for $\ell \geq 1$, and the coefficients B_ℓ can therefore be written as

$$B_\ell = \begin{cases} (\Phi_{\text{eq}} - A_0)R & \text{for } \ell = 0, \\ -A_\ell R^{2\ell+1} & \text{for } \ell \geq 1. \end{cases} \quad (1.39)$$

Put differently, if a conducting sphere at fixed potential Φ_{eq} is immersed in a background field given by

$$\phi_{\text{bg}}^{(\ell)}(r, \theta) = A_\ell r^\ell P_\ell(\cos \theta), \quad (1.40)$$

then the response $\delta\phi^{(\ell)}$ is

$$\delta\phi^{(\ell)}(r, \theta) = \frac{\Phi_{\text{eq}}^{(\ell)} R}{r} - A_\ell r^\ell P_\ell(\cos \theta) \left(\frac{R}{r} \right)^{2\ell+1}. \quad (1.41)$$

Due to the resemblance of the response to the multipole expansion, we will hereafter refer to $\phi_{\text{bg}}^{(\ell)}$ and $\delta\phi^{(\ell)}$ as an ℓ^{th} -order multipole background and response, respectively.

If an external source enforces a fixed potential Φ on the conductor, then obviously $\Phi_{\text{eq}}^{(\ell)} = \Phi$, independent of ℓ . In contrast, for an isolated conductor of fixed total charge the equilibrium potential is not fixed and depends on the external field. An isolated conductor, however, does not respond to a uniform shift in potential, so $\delta\phi^{(0)}$ consists only of the field produced by the fixed charge. This means that in the fixed-charge case $\Phi_{\text{eq}}^{(\ell)}$ is a *free parameter* whose value changes depending on external fields. If the conducting sphere has total charge Q , then the equilibrium potential in a multipole background $\phi_{\text{bg}}^{(\ell)}$ is given by $\Phi_{\text{eq}}^{(\ell)} = Q/4\pi\epsilon_0 R + A_0 \delta_{\ell,0}$.

Effective theory. To determine the effective response to a background field, we expand the functional (1.36) about the fixed background. Since the functional is quadratic in the field, the functional Taylor series truncates at second order:

$$\begin{aligned} U_{\text{eff}}[\phi_{\text{bg}} + \delta\phi] &= U_{\text{eff}}[\phi_{\text{bg}}] + \int d^3x \left. \frac{\delta U_{\text{eff}}}{\delta\phi(\mathbf{x})} \right|_{\phi_{\text{bg}}} \delta\phi(\mathbf{x}) \\ &\quad + \frac{1}{2} \int d^3x d^3y \left. \frac{\delta^2 U_{\text{eff}}}{\delta\phi(\mathbf{x}) \delta\phi(\mathbf{y})} \right|_{\phi_{\text{bg}}} \delta\phi(\mathbf{y}) \delta\phi(\mathbf{x}), \end{aligned} \quad (1.42)$$

where the integrands define the functional derivatives.⁷ Since the second term is proportional to the response, we can identify the response prefactor as an effective source ρ , which is given by the functional derivative evaluated at the fixed background field. This effective source can be broken up into two terms: the permanent charge density ρ_0 , and the induced charge density ρ_{ind} . For a single conductor at the origin, the resulting expression for the effective source is given by⁸

$$\begin{aligned}\rho(\mathbf{x} \mid \phi_{\text{bg}}) &= \left. \frac{\delta U_{\text{eff}}}{\delta \phi(\mathbf{x})} \right|_{\phi_{\text{bg}}} \\ &= \epsilon_0 \nabla^2 \phi_{\text{bg}}(\mathbf{x}) - \left(\sum_{n>0} C^{(n)} \partial_I^n \phi_{\text{bg}} (-\partial)_I^n + C^{(0)} \phi_{\text{bg}} \right) \delta(\mathbf{x}) - Q \delta(\mathbf{x}) \\ &= \epsilon_0 \nabla^2 \phi_{\text{bg}}(\mathbf{x}) + \rho_{\text{ind}}(\mathbf{x} \mid \phi_{\text{bg}}) + \rho_0(\mathbf{x}).\end{aligned}\tag{1.43}$$

Notice that the background field in general produces its own source charge, as indicated in the first term above. However, since our EFT is on shell we must require the background field to also be on shell: $\nabla^2 \phi_{\text{bg}} \equiv 0$.

The second-order functional derivative can also be broken into two pieces:

$$\frac{\delta^2 U_{\text{eff}}}{\delta \phi(\mathbf{x}) \delta \phi(\mathbf{y})} = \frac{\delta^2 U_0}{\delta \phi(\mathbf{x}) \delta \phi(\mathbf{y})} + \frac{\delta^2 \Delta U}{\delta \phi(\mathbf{x}) \delta \phi(\mathbf{y})}.\tag{1.44}$$

The bulk term results simply in

$$\frac{\delta^2 U_0}{\delta \phi(\mathbf{x}) \delta \phi(\mathbf{y})} = \epsilon_0 \nabla^2 \delta(\mathbf{y} - \mathbf{x}),\tag{1.45}$$

so that

$$\int d^3 x \, d^3 y \, \frac{\delta^2 U_0}{\delta \phi(\mathbf{x}) \delta \phi(\mathbf{y})} \delta \phi(\mathbf{y}) \delta \phi(\mathbf{x}) = \int d^3 x \, [\epsilon_0 \nabla^2 \delta \phi(\mathbf{x})] \delta \phi(\mathbf{x}).\tag{1.46}$$

⁷Functional derivatives can be defined in this way—as the integrand prefactors of the variation in a functional Taylor series—or alternatively by the (equivalent) rule

$$\frac{\delta}{\delta \phi(\mathbf{x})} \int d^3 y \, f(\mathbf{y}) \phi(\mathbf{y}) = f(\mathbf{x}),$$

for some permissible test function $f(\mathbf{x})$. Furthermore, any linear differential operators acting on ϕ will end up on $f(\mathbf{x})$ by integration by parts (in the sense of distributions), *e.g.*,

$$\frac{\delta}{\delta \phi(\mathbf{x})} \int d^3 y \, f(\mathbf{y}) \partial'_i \phi(\mathbf{y}) = -\partial_i f(\mathbf{x}).$$

⁸The object $\delta(\mathbf{x})$ here is the *three-dimensional* Dirac delta function, sometimes written as $\delta^{(3)}(\mathbf{x})$.

The second-order functional derivative can be read off similarly, giving

$$\frac{\delta^2 \Delta U}{\delta \phi(\mathbf{x}) \delta \phi(\mathbf{y})} = - \sum_{n>0} C^{(n)} \partial_I^n \delta(\mathbf{x}) \partial_I^n \delta(\mathbf{y}) - C^{(0)} \delta(\mathbf{x}) \delta(\mathbf{y}). \quad (1.47)$$

Finally, we can re-express Eq. (1.42) as

$$\tilde{U}[\delta\phi | \phi_{\text{bg}}] = U_{\text{eff}}[\phi_{\text{bg}}] + \int d^3x (\rho_0 + \rho_{\text{ind}}) \delta\phi + \int d^3x (\epsilon_0 \nabla^2 \delta\phi) \delta\phi + \mathcal{O}[(\delta\phi)^2]. \quad (1.48)$$

To solve for the effective response, we now perform the first variation $\delta\tilde{U}/\delta(\delta\phi)$ and set it to zero as usual. Neglecting the $\mathcal{O}[(\delta\phi)^2]$ terms, this results in

$$-\epsilon_0 \nabla^2 \delta\phi(\mathbf{x}) = \rho_0(\mathbf{x}) + \rho_{\text{ind}}(\mathbf{x} | \phi_{\text{bg}}). \quad (1.49)$$

At this point it is worth mentioning that we neglected the $\mathcal{O}[(\delta\phi)^2]$ terms under the assumption that the response will be small. Intuitively, linear response holds in the full theory, so we expect it to carry over in the effective theory. However, as we can see from Eq. (1.47), unphysical artifacts of the point-particle approximation will manifest as divergences in these higher-order terms. Although we will not dwell on those details at this moment, we will mention that their effects will actually vanish from a more rigorous renormalization treatment.⁹

Continuing along, we solve for the effective response from Eq. (1.49) using the method of Green functions. The *bulk Green function* here is the fundamental solution to the bulk Euler-Lagrange equation in the presence of a point source,

$$-\epsilon_0 \nabla^2 G(\mathbf{x}) = \delta(\mathbf{x}) \quad \Longleftrightarrow \quad G(\mathbf{x}) = \frac{1}{4\pi\epsilon_0 |\mathbf{x}|}, \quad (1.50)$$

which can be derived in a variety of standard ways.¹⁰ An arbitrary source ρ can be considered a “weighted sum” of point sources, $\rho(\mathbf{x}) = \int d^3x' \delta(\mathbf{x} - \mathbf{x}') \rho(\mathbf{x}')$, so by linearity

⁹The reader interested in the details may wish to glance at Appendix A, where the renormalization of similar problem in two dimensions is laid out. The formalism may be applied to the present problem with few modifications (albeit with intensified index gymnastics).

¹⁰A simple solution is to integrate both sides over a sphere of radius r . By the divergence theorem, this reduces to a surface integral of the normal derivative of G which, due to the spherical symmetry of the Laplacian, must be constant on the surface:

$$-\epsilon_0 \int_{V_r} d^3x \nabla^2 G = -\epsilon_0 \oint_{\partial V_r} dA \hat{\mathbf{r}} \cdot \nabla G = -4\pi\epsilon_0 r^2 \frac{dG}{dr} \stackrel{!}{=} 1.$$

This ordinary differential equation is then solved by integration, where we apply the boundary condition at infinity, $G(\infty) = 0$:

$$G(r) = \int_{G(\infty)=0}^{G(r)} dG = -\frac{1}{4\pi\epsilon_0} \int_{\infty}^r \frac{dr'}{r'^2} = \frac{1}{4\pi\epsilon_0 r}.$$

the response is given by the “weighted sum”, or convolution, of the point-source solution G :

$$\delta\phi(\mathbf{x}) = \int d^3x' G(\mathbf{x} - \mathbf{x}')\rho(\mathbf{x}'). \quad (1.51)$$

For the effective source (1.43), the response therefore is given by

$$\begin{aligned} \delta\phi(\mathbf{x} \mid \phi_{\text{bg}}) &= \int d^3x' G(\mathbf{x} - \mathbf{x}') [\rho(\mathbf{x}') + \rho_{\text{ind}}(\mathbf{x}' \mid \phi_{\text{bg}})] \\ &= \int d^3x' G(\mathbf{x} - \mathbf{x}') \left[Q\delta(\mathbf{x}') - \left(\sum_{n>0} C^{(n)} (\partial')_I^n \phi_{\text{bg}}(-\partial')_I^n + C^{(0)} \phi_{\text{bg}} \right) \delta(\mathbf{x}') \right] \\ &= [Q - C^{(0)} \phi_{\text{bg}}(0)] G(\mathbf{x}) - \sum_{n>0} C^{(n)} \partial_I^n \phi_{\text{bg}}(0) (-\partial)_I^n G(\mathbf{x}), \end{aligned} \quad (1.52)$$

where in the last line we used integration by parts and $(\partial')_I^n = (-\partial)_I^n$ on the Green function $G(\mathbf{x} - \mathbf{x}')$ before setting $\mathbf{x}' \rightarrow 0$. Now, we use the multipole background potential $\phi_{\text{bg}}^{(\ell)}(\mathbf{x})$ defined in Eq. (1.40). This background is especially convenient because $\partial_I^n \phi_{\text{bg}}^{(\ell)}(0)$ is only nonvanishing when $n = \ell$. It therefore follows from the expression above that a single background $\phi_{\text{bg}}^{(\ell)}$ is sufficient to determine $C^{(\ell)}$.

To proceed, we also need an expression for $(-\partial)_I^n G(\mathbf{x})$, which we construct in Technical Note 1.1. The relevant piece is

$$(-\partial)_I^n G(\mathbf{x}) = \frac{(2n-1)!!}{4\pi\epsilon_0 r^{2n+1}} x_I^n + (\dots), \quad (1.53)$$

where $x_I^n = x_{i_1} \cdots x_{i_n}$ and (\dots) represents the remaining terms containing Kronecker deltas. The Kronecker delta terms contract with the derivatives on the background, leading to terms containing $\delta_{ij} \partial_i \partial_j \phi_{\text{bg}} = \nabla^2 \phi_{\text{bg}} = 0$, so we can simply ignore them for now. The final ingredient is the observation that the multipole background fields are homogeneous polynomials, for which we can use the generalized Euler theorem [App89]:

$$x_I^n \partial_I^n h_\ell(\mathbf{x}) = \frac{\ell!}{(\ell-n)!} h_\ell(\mathbf{x}) \quad (1.54)$$

for any homogeneous polynomial $h_\ell(\mathbf{x})$ of degree $\ell \geq 0$. In our case, we have¹¹

$$x_I^n \partial_I^n \phi_{\text{bg}}^{(\ell)}(0) = \ell! \delta_{n\ell} \phi_{\text{bg}}^{(\ell)}(\mathbf{x}). \quad (1.55)$$

¹¹To clarify, since $(\partial')_I^n \phi_{\text{bg}}^{(\ell)}(\mathbf{x}')$ is evaluated at $\mathbf{x}' = \mathbf{0}$, the nonvanishing case (for which $n = \ell$) has all instances of \mathbf{x}' removed with combinations of Kronecker deltas in their stead. Since ϕ_{bg} is homogeneous, the (post-derivative) contractions with x_I^n restore the position dependence to give Eq. (1.55).

Technical Note 1.1: Derivatives of the electrostatic Green function

We can calculate the first few derivatives of $1/r$, with $r = |\mathbf{x}|$, directly without too much headache:

$$\begin{aligned} -\partial_i \frac{1}{r} &= \frac{x_i}{r^3}, \\ +\partial_i \partial_j \frac{1}{r} &= \frac{3x_i x_j - r^2 \delta_{ij}}{r^5}, \\ -\partial_i \partial_j \partial_k \frac{1}{r} &= \frac{15x_i x_j x_k - 3r^2(x_i \delta_{jk} + x_j \delta_{ki} + x_k \delta_{ij})}{r^7}. \end{aligned}$$

Higher-order derivatives result in lengthy expressions with increasing instances of Kronecker delta functions. Burgos and Bonadeo [BB81] have worked out the general expression for the n^{th} -order derivative of $1/r$, which can be written as

$$(-\partial)_I^n \frac{1}{r} = \frac{1}{r^{2n+1}} \sum_{k=0}^{\lfloor n/2 \rfloor} (-)^k (2n - 2k - 1)!! r^{2k} \mathcal{P}_I(\delta^k \mathbf{x}^{n-2k}),$$

where $\lfloor n/2 \rfloor$ is the integer part of $n/2$ and \mathcal{P}_I is the *permutation polynomial*, defined via

$$\mathcal{P}_I(\delta^k \mathbf{x}^{n-2k}) := \sum_{D(I)} \delta_{i_1 i_2} \cdots \delta_{i_{2k-1} i_{2k}} x_{i_{2k+1}} \cdots x_{i_n},$$

where the sum is over all permutations $D(I)$ of the indices which give distinct terms. Despite the proliferation of indices, the summation over k has a particularly illuminating interpretation as an operator \mathcal{T}_n that removes the traces from the totally symmetric tensor $x_I^n = x_{i_1} \cdots x_{i_n}$. That is, $(-\partial)_I^n r^{-1} = r^{-(2n+1)} (\mathcal{T}_n \mathbf{x}^n)_I$ is completely symmetric and trace-free. This *detracer* operator is used extensively in multipole analysis and its applications (see for instance Refs. [App84], [App89], [Vre05], and [GB08]).

Plugging these expressions into Eq. (1.52) and simplifying gives the multipole response,

$$\begin{aligned} \delta\phi^{(\ell)}(\mathbf{x}) &= \left(\frac{Q - C^{(0)}\delta_{0,\ell}}{4\pi\epsilon_0 r} - \sum_{n>0} C^{(n)} \frac{(2n-1)!!}{4\pi\epsilon_0 r^{2n+1}} \ell! \delta_{n\ell} \right) \phi_{\text{bg}}^{(\ell)}(\mathbf{x}) \\ &= \frac{Q}{4\pi\epsilon_0 r} - C^{(\ell)} \frac{\ell!(2\ell-1)!!}{4\pi\epsilon_0 r^{2\ell+1}} A_\ell r^\ell P_\ell(\cos\theta). \end{aligned} \quad (1.56)$$

Finally, comparing the effective response (1.56) to the full theory result (1.41) gives expressions for the coefficients. The polarizabilities, corresponding to the ($n \geq 1$) coefficients $C^{(n)}$ in $\Delta U^c[\phi]$ are revealed to be

$$C^{(n)} = \frac{4\pi\epsilon_0 R^{2n+1}}{n!(2n-1)!!} = 4\pi\epsilon_0 R \frac{2^n R^{2n}}{(2n)!} \quad (\text{for } n \geq 1), \quad (1.57)$$

where we have provided at the second equality an alternative expression using the identity

$(2n-1)!! = (2n)!/(2^n n!)$. The coefficients in $\Delta U^s[\phi]$ follow from matching the $\ell = 0$ terms. After rearranging, the matching condition reads

$$Q - C^{(0)} A_0 \stackrel{!}{=} 4\pi\epsilon_0 R \left(\Phi_{\text{eq}}^{(0)} - A_0 \right). \quad (1.58)$$

For the fixed charge case, $\Phi_{\text{eq}}^{(0)} = Q/4\pi\epsilon_0 R + A_0$ and eliminates the A_0 -dependence of the matching condition. It therefore follows that Q is the total charge as expected and, furthermore, $C^{(0)}$ must be identically zero. For the fixed potential case, $\Phi_{\text{eq}}^{(0)} = \Phi$ and therefore the induced charge $Q = 4\pi\epsilon_0 R \Phi$ and the monopole polarizability matches the self-capacitance, $C^{(0)} = 4\pi\epsilon_0 R$. In summary,

$$Q = \begin{cases} \text{total charge } Q & (\text{fixed } Q) \\ 4\pi\epsilon_0 R \Phi & (\text{fixed } \Phi) \end{cases}, \quad C^{(0)} = \begin{cases} 0 & (\text{fixed } Q) \\ 4\pi\epsilon_0 R & (\text{fixed } \Phi) \end{cases}. \quad (1.59)$$

1.1.3 Interactions

Now that we have fully determined the effective energy functional, we may calculate the forces on each conductor. We will do this in two steps. First, we will extract the stationary solution ϕ by extremizing U_{eff} . Then, we will plug this solution back into the energy functional and isolate the interaction energy part. The forces then follow from the negative gradient of the interaction energy.

Electrostatic potential

The stationary electrostatic potential must be a solution to the extremization condition $\delta U_{\text{eff}}/\delta\phi = 0$. After taking the functional derivative and rearranging, this condition reads

$$-\epsilon_0 \nabla^2 \phi(\mathbf{x}) = \sum_a Q_a \delta(\mathbf{x} - \mathbf{x}_a) - \sum_a \sum_{n \geq 0} C_a^{(n)} \partial_I^n \phi(\mathbf{x}_a) (-\partial)_I^n \delta(\mathbf{x} - \mathbf{x}_a), \quad (1.60)$$

where the value of $C_a^{(0)}$ depends on whether the a^{th} conductor's total charge or potential is held fixed. As in Eq. (1.43), we break up the right-hand side into a permanent source charge density,

$$\rho_0(\mathbf{x}) = \sum_a Q_a \delta(\mathbf{x}_a), \quad (1.61)$$

and an induced charge density,

$$\rho_{\text{ind}}(\mathbf{x} | \phi) = - \sum_a \sum_{n \geq 0} C_a^{(n)} \partial_I^n \phi(\mathbf{x}_a) (-\partial)_I^n \delta(\mathbf{x} - \mathbf{x}_a). \quad (1.62)$$

By applying the Green function method as before, we wind up with an integral equation for the electric potential,

$$\begin{aligned}
 \phi(\mathbf{x}) &= \int d^3x' G(\mathbf{x} - \mathbf{x}') \rho_0(\mathbf{x}') + \int d^3x' G(\mathbf{x} - \mathbf{x}') \rho_{\text{ind}}(\mathbf{x}' | \phi) \\
 &= \sum_a G(\mathbf{x} - \mathbf{x}_a) Q_a - \sum_a \sum_{n \geq 0} (-\partial)_I^n G(\mathbf{x} - \mathbf{x}_a) C_a^{(n)} \partial_I^n \phi(\mathbf{x}_a) \\
 &\equiv \sum_a G^{xa} Q_a - \sum_a \sum_{n \geq 0} (-\partial)_I^n G^{xa} C_a^{(n)} \partial_I^n \phi(\mathbf{x}_a),
 \end{aligned} \tag{1.63}$$

where we have introduced the abbreviated notation $G^{xa} \equiv G(\mathbf{x} - \mathbf{x}_a)$.

The above integral equation can be solved iteratively by introducing a counting parameter λ , which we will later set to unity, via

$$\phi(\mathbf{x}) = \sum_a G^{xa} Q_a - \lambda \sum_a \sum_{n \geq 0} (-\partial)_I^n G^{xa} C_a^{(n)} \partial_I^n \phi(\mathbf{x}_a), \tag{1.64}$$

and expanding ϕ as a Liouville–Neumann series,

$$\phi(\mathbf{x}) = \sum_{k \geq 0} \lambda^k \phi_k(\mathbf{x}). \tag{1.65}$$

Plugging in this expansion and comparing order by order in λ gives the recursive solution,

$$\phi_0(\mathbf{x}) = \sum_a G^{xa} Q_a, \quad \phi_{k+1}(\mathbf{x}) = - \sum_a \sum_{n \geq 0} (-\partial)_I^n G^{xa} C_a^{(n)} \partial_I^n \phi_k(\mathbf{x}_a). \tag{1.66}$$

The terms beyond ϕ_0 are:

$$\phi_1(\mathbf{x}) = - \sum_{a,b} \sum_{n \geq 0} (-\partial)_I^n G^{xa} C_a^{(n)} \partial_I^n G^{ab} Q_b, \tag{1.67a}$$

$$\phi_2(\mathbf{x}) = + \sum_{a,b,c} \sum_{n,m} (-\partial)_I^n G^{xa} C_a^{(n)} \partial_I^n (-\partial)_J^m G^{ab} C_b^{(m)} \partial_J^m G^{bc} Q_c, \tag{1.67b}$$

or more generally,

$$\phi_k(\mathbf{x}) = (-)^k \sum_{\{a\}} \sum_{\{n\}} \left[\prod_{j=1}^k (-\partial)_{I_j}^{n_j} G^{a_{j-1} a_j} C_{a_j}^{(n_j)} \partial_{I_j}^{n_j} \right] G^{a_k a_{k+1}} Q_{a_{k+1}}, \tag{1.67c}$$

where the sets $\{a\}$ and $\{n\}$ respectively indicate sums over all particle labels a_i and multipole orders n_i (both with $i \geq 1$), and $G^{a_0 a_1} = G(\mathbf{x} - \mathbf{x}_{a_1})$.

We have structured the series solution so that the k index counts the number of occurrences of the polarizability $C^{(n)}$. We can instead restructure the series to produce a truly

perturbative series in powers of R/d . The R -scaling is carried by the multipole index n , since $C^{(n)} \sim R^{2n+1}$, so we may extract the sum over $\{n\}$ from the general expression (1.67c) by writing

$$\phi_k(\mathbf{x}) =: \sum_{\{n\}} \varphi_k^{(n_1, \dots, n_k)}(\mathbf{x}), \quad (1.68)$$

and see that $\varphi_k \sim R^{2|n|+k+1}$, where $|n| := \sum_{i=1}^k n_i$. It therefore follows that the contribution scaling as R^ℓ will consist of all terms that partition ℓ into integers n_i such that $2|n|+k+1 = \ell$. Summing over ℓ —and setting $\lambda = 1$ as promised—then gives the desired form:

$$\phi(\mathbf{x}) = \sum_{\ell \geq 0} \left[\sum_k \sum_{\{n\}} \varphi_k^{(n_1, \dots, n_k)}(\mathbf{x}) \right]. \quad (1.69)$$

Electrostatic energy

We may now calculate the total electrostatic energy by plugging in the stationary solution $\phi(\mathbf{x})$ into the effective energy functional (1.36). We first use Eqns. (1.61) and (1.62) to re-express the worldline energy in terms of the external and induced charge distributions:

$$\begin{aligned} \Delta U[\phi] &= \int d^3x \left[- \sum_a \sum_{n \geq 0} \frac{1}{2} C_a^{(n)} \partial_I^n \phi(\mathbf{x}_a) (-\partial)_I^n \delta(\mathbf{x} - \mathbf{x}_a) + \sum_a Q_a \delta(\mathbf{x} - \mathbf{x}_a) \right] \phi(\mathbf{x}) \\ &= \int d^3x \left\{ \frac{1}{2} \rho_{\text{ind}}(\mathbf{x} | \phi) + \rho_0(\mathbf{x}) \right\} \phi(\mathbf{x}). \end{aligned} \quad (1.70)$$

Additionally, we integrate $U_0[\phi]$ by parts and use Eq. (1.60) to put the bulk energy in a similar form:

$$\begin{aligned} U_0[\phi] &= - \int d^3x \frac{\epsilon_0}{2} (\nabla \phi)^2 \stackrel{\text{IBP}}{=} - \int d^3x \frac{1}{2} (-\epsilon_0 \nabla^2 \phi) \phi \\ &= - \frac{1}{2} \int d^3x \left\{ \rho_{\text{ind}}(\mathbf{x} | \phi) + \rho_0(\mathbf{x}) \right\} \phi(\mathbf{x}). \end{aligned} \quad (1.71)$$

When these pieces are summed together, the ρ_{ind} terms cancel, leaving the total effective energy

$$U[\phi] = U_0[\phi] + \Delta U[\phi] = \frac{1}{2} \int d^3x \rho_0(\mathbf{x}) \phi(\mathbf{x}) = \frac{1}{2} \sum_a Q_a \phi(\mathbf{x}_a). \quad (1.72)$$

Before proceeding with the calculations, we must address the problem of *self-interactions*. The sums in the expression for $\phi(\mathbf{x})$ run over all particle labels, and consequently we encounter terms in which the Green function and its derivatives are evaluated at the same worldline position, *i.e.*, $G(\mathbf{x}_a - \mathbf{x}_b)$ with $a = b$, and are therefore divergent. These terms not only occur in the self-energy of each conductor, which we are not interested in, but also appear in the interaction energy. In hindsight, this is not a surprise—it is a technical repercussion of the point-particle prescription. By naïvely treating the conductors as singular

points, we should expect singular behavior to appear as an artifact. To determine whether there is physical information contained within the divergences, we turn to renormalization group (RG) theory [Vas04, BDFN95, Del04]. From the perspective of RG, the procedure of “integrating out” the short-scale physics necessitates a set of counterterms which, although not physically observable themselves, should appear from a careful limiting procedure and ensure that physical observables obtained from the coarse-grained, or *renormalized*, theory remain finite. Since we obtained the values of the Wilson coefficients (polarizabilities) by matching directly to physical observables, we have effectively sidestepped this issue and these couplings are in fact the renormalized versions and a series of counterterms is implicit. For our theory, all of the divergences are power-like in the sense that $\partial_l^n G(\lambda \mathbf{x} - \lambda \mathbf{x}') \sim \lambda^{-(n+1)}$ as $\lambda \rightarrow 0$, and RG tells us that there is no nontrivial running of the couplings. This means that there is no physical information contained within the divergences, and these divergent pieces will *always* be removed by pure counterterms; that is, we can completely (and safely) ignore them. In what follows, we will capture this renormalization procedure by the replacement $G(\mathbf{x}_a - \mathbf{x}_b) \rightarrow (1 - \delta_{ab})G(\mathbf{x}_a - \mathbf{x}_b)$, but otherwise keep the counterterms implicit.¹²

Fixed potentials. Previously, we found that the polarizabilities in the fixed-charge and fixed-potential cases are identical for a given conductor and only differ in their monopole terms Q and $C^{(0)}$. Since these terms are non-vanishing in the fixed-potential case, that is where we will begin our discussion.

The interaction energy \mathcal{U} is defined as the difference in energy between $U[\phi | \mathbf{x}_a, \mathbf{x}_b]$, given by Eq. (1.72), and the self-energies $U[\phi, |\mathbf{x}_a - \mathbf{x}_b| \rightarrow \infty]$. After expanding the result to $\mathcal{O}(R^9)$, dropping the self-energy and self-interaction terms, and contracting the derivatives according to the methods of Technical Note 1.1 we find¹³

$$\begin{aligned} \mathcal{U}_\Phi = \frac{1}{2} \sum_{a \neq b} & \left\{ \frac{Q_a Q_b}{4\pi\epsilon_0 d} - \frac{Q_a^2 C_b^{(0)}}{(4\pi\epsilon_0)^2 d^2} + \frac{Q_a C_b^{(0)} C_a^{(0)} Q_b}{(4\pi\epsilon_0)^3 d^3} - \frac{Q_a^2 [C_b^{(0)}]^2 C_a^{(0)}}{(4\pi\epsilon_0)^4 d^4} - \frac{Q_a^2 C_b^{(1)}}{(4\pi\epsilon_0)^2 d^4} \right. \\ & + \frac{Q_a [C_b^{(0)}]^2 [C_a^{(0)}]^2 Q_b}{(4\pi\epsilon_0)^5 d^5} + 2 \frac{Q_a C_b^{(0)} C_a^{(1)} Q_b}{(4\pi\epsilon_0)^3 d^5} - \frac{Q_a^2 [C_b^{(0)}]^3 [C_a^{(0)}]^2}{(4\pi\epsilon_0)^6 d^6} - 2 \frac{Q_a^2 C_b^{(0)} C_a^{(0)} C_b^{(1)}}{(4\pi\epsilon_0)^4 d^6} \\ & - \frac{Q_a^2 [C_b^{(0)}]^2 C_a^{(1)}}{(4\pi\epsilon_0)^4 d^6} - \frac{6 Q_a^2 C_b^{(2)}}{(4\pi\epsilon_0)^2 d^6} + \frac{Q_a [C_b^{(0)}]^3 [C_a^{(0)}]^3 Q_b}{(4\pi\epsilon_0)^7 d^7} + 2 \times 2 \frac{Q_a [C_b^{(0)}]^2 C_a^{(0)} C_a^{(1)} Q_b}{(4\pi\epsilon_0)^5 d^7} \\ & \left. + \frac{2 Q_a C_b^{(1)} C_a^{(1)} Q_b}{(4\pi\epsilon_0)^5 d^7} + 2 \frac{6 Q_a C_b^{(0)} C_a^{(2)} Q_b}{(4\pi\epsilon_0)^3 d^7} - \frac{Q_a^2 [C_b^{(0)}]^4 [C_a^{(0)}]^3}{(4\pi\epsilon_0)^8 d^8} - 3 \frac{Q_a^2 [C_b^{(0)}]^2 [C_a^{(0)}]^2 C_b^{(1)}}{(4\pi\epsilon_0)^6 d^8} \right\} \end{aligned}$$

¹²Again, the interested reader may consult Appendix A for the explicit renormalization details of a closely related problem.

¹³As a guide for those readers attempting to perform this calculation themselves, the multiplicities of each term have been set as prefactors to distinguish them from the numerical factors coming from the derivatives.

$$\begin{aligned}
& -2 \frac{Q_a^2 [C_b^{(0)}]^3 C_a^{(0)} C_a^{(1)}}{(4\pi\epsilon_0)^6 d^8} - 2 \frac{2Q_a^2 C_b^{(0)} C_a^{(1)} C_b^{(1)}}{(4\pi\epsilon_0)^4 d^8} - \frac{Q_a^2 [C_b^{(1)}]^2 C_a^{(0)}}{(4\pi\epsilon_0)^4 d^8} - 2 \frac{6Q_a^2 C_b^{(0)} C_a^{(0)} C_b^{(2)}}{(4\pi\epsilon_0)^4 d^8} \\
& - \frac{6Q_a^2 [C_b^{(0)}]^2 C_a^{(2)}}{(4\pi\epsilon_0)^4 d^8} - \frac{90Q_a^2 C_b^{(3)}}{(4\pi\epsilon_0)^2 d^8} + \mathcal{O}(d^{-9}) \Big\}, \tag{1.73}
\end{aligned}$$

where “ $a \neq b$ ” in the summation means that we sum both a and b over $\{1, 2\}$ but exclude the cases for which $a = b$ (e.g., $\sum_{a \neq b} f_{ab} = f_{12} + f_{21}$). At this point we can make a few observations:

1. By retaining the general polarizabilities, this expression is valid for the interaction energy between *any* two spherical conductors—the boundary conditions and effects of external sources are contained within the polarizabilities. In particular, setting $C^{(0)} \rightarrow 0$ immediately gives the interaction energy between two spherical conductors of fixed total charge. Furthermore, since the polarizabilities were left arbitrary, this expression also reveals the interaction behavior for two (spherical) conductors of differing boundary conditions.
2. The first term is the Coulomb energy and shows that for charges of the same sign, the energy is lowered by increasing the distance—that is, they repel—and indeed this behavior persists for large separations.
3. If one of the conductors is neutral (grounded or otherwise without a net charge), all the terms with odd powers of d vanish, including the Coulomb term. The remaining terms are all negative and show that a neutral and charged sphere are universally attracted to each other due to polarization effects.
4. The series alternates in sign and hence the interaction energy is not guaranteed to be monotonic in the separation d . Although the leading term dominates at large separation, the alternating sign suggests that the behavior may change at close approach. Indeed this is the case, as discussed in Technical Note 1.2: Two conducting spheres of like charges will repel up to some critical distance, smaller than which the effects of polarization will overcome the repulsion and the two conductors will attract with a diverging force. The only exception is if the charge ratio is the same as if the two conductors were in contact, or rather, if the two conductors are equipotential.

This behavior is revealed more explicitly by plugging in the expressions for the polarizabilities. We group the interactions into two pieces: those that appear as more “direct” interactions between the conductors, which we express as corrections to the Coulomb energy, and “indirect” interactions that we write as corrections to the conductors’ respective

Technical Note 1.2: Attraction at close approach

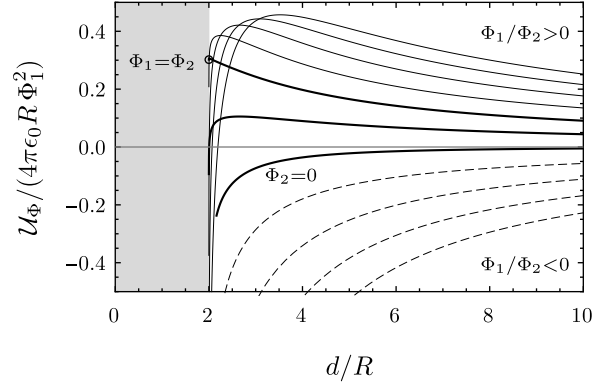
The problem of conducting spheres at fixed potentials also has a complete series solution in terms of capacitance coefficients C_{ab} [Lek12a]. The total energy stored is

$$W_\Phi = -\frac{1}{2}(C_{11}\Phi_1^2 + 2C_{12}\Phi_a\Phi_b + C_{22}\Phi_b^2),$$

where the capacitance coefficients for spheres are known and are often expressed as an infinite series in hyperbolic sine and hyperbolic cosine functions. However, applying the identity $\sinh[(n+1)\cosh^{-1}\xi] = \sqrt{\xi^2-1}U_n(\xi)$, where $U_n(\xi)$ is the Chebyshev polynomial of the second kind (apologies for the clash of notation), can put the full expression into a more compact form. In particular, for spheres of identical radii R separated by a distance d from their centers, the interaction energy—in which the self-energies are subtracted off—can be written as

$$\frac{\mathcal{U}_\Phi}{4\pi\epsilon_0 R} = -\frac{1}{2} \sum_{n=0}^{\infty} \frac{\Phi_1^2 + \Phi_2^2}{U_n(\xi) + U_{n+1}(\xi)} + \frac{R}{d} \sum_{n=0}^{\infty} \frac{\Phi_1\Phi_2}{U_n(\xi)}, \quad (1.74)$$

where $\xi := \frac{1}{2}(d/R)^2 - 1$. Shown in the plot is the behavior for opposite potentials (dashed) and like potentials (solid). Notice that for $\Phi_2/\Phi_1 \leq 0$, the spheres always attract. For $\Phi_2/\Phi_1 > 0$, the spheres repel until some critical distance; further decrease in separation leads to attraction due to polarization effects. This attractive force diverges near contact, *except* for the special case $\Phi_1 = \Phi_2$ for which the energy and force limits to a finite value (open circle) and is *always* repulsive. Analogous behavior is found between spheres with fixed total charges, where at close enough separation the spheres attract, unless they touch in which case the charges will redistribute and the spheres will subsequently repel. The special case of a (repulsive) finite limit near contact occurs for charge ratios that would remain unchanged upon contact [Lek12b].



self-energies:

$$\begin{aligned} \mathcal{U}_\Phi = 4\pi\epsilon_0\Phi_1\Phi_2 \frac{R_1R_2}{d} & \left\{ 1 + \frac{R_1R_2}{d^2} + \frac{R_1R_2(R_1^2 + R_1R_2 + R_2^2)}{d^4} \right. \\ & \left. + \frac{R_1R_2(R_1^2 + R_1R_2 + R_2^2)^2}{d^6} + \mathcal{O}(d^{-8}) \right\} \\ - \frac{1}{2} \sum_{a \neq b} 4\pi\epsilon_0 R_a \Phi_a^2 \left(\frac{R_b}{d} \right) & \left\{ \frac{R_a}{d} + \frac{R_a R_b (R_a + R_b)}{d^3} + \frac{R_a R_b (R_a^3 + R_a^2 R_b + 2R_a R_b^2 + R_b^3)}{d^5} \right. \\ & \left. + \frac{R_a R_b (R_a^5 + 2R_a^4 R_b + 5R_a^3 R_b^2 + 3R_a^2 R_b^3 + 3R_a R_b^4 + R_b^5)}{d^7} + \mathcal{O}(d^{-9}) \right\}. \end{aligned} \quad (1.75)$$

As an illustrative example, consider two spheres of equal radii R and a ratio of (independently) fixed potentials $\Phi_2/\Phi_1 =: \nu$. In this case, the interaction energy, normalized by the self-energy of sphere 1 in isolation, is given by

$$\frac{\mathcal{U}_\Phi}{4\pi\epsilon_0 R \Phi_1^2} = \nu \left(\frac{1}{\chi} + \frac{1}{\chi^3} + \frac{3}{\chi^5} + \frac{9}{\chi^7} + \dots \right) - \frac{1+\nu^2}{2} \left(\frac{1}{\chi^2} + \frac{2}{\chi^4} + \frac{5}{\chi^6} + \frac{15}{\chi^8} + \dots \right), \quad (1.76)$$

where $\chi := d/R$. The force $F_{12} = -\partial\mathcal{U}_\Phi/\partial d$ of conductor 1 on conductor 2 is given by

$$\frac{F_{12}}{4\pi\epsilon_0 \Phi_1^2} = \nu \left(\frac{1}{\chi^2} + \frac{3}{\chi^4} + \frac{15}{\chi^6} + \frac{63}{\chi^8} + \dots \right) - (1+\nu^2) \left(\frac{1}{\chi^3} + \frac{4}{\chi^5} + \frac{15}{\chi^7} + \frac{60}{\chi^9} + \dots \right). \quad (1.77)$$

In both expressions, the first term depends on the sign of the two potentials; it is repulsive for like potentials ($\nu > 0$), attractive for opposite potentials ($\nu < 0$), and vanishes when sphere 2 is grounded ($\nu = 0$). The second term exhibits universal attraction. The particular case of equipotentials ($\nu = 1$) is not captured by the expansion in large distances. Lekner [Lek12a] has explored the force at close approach up to linear order by analyzing the short-distance asymptotics of the capacitance coefficients, which we reproduce here for comparison:

$$\begin{aligned} \frac{F_{12}}{4\pi\epsilon_0 \Phi_1^2} = & -\frac{(1-\nu)^2}{8} \frac{R}{s} + \frac{(1-\nu)^2}{48} \left(\ln \frac{R}{s} + 2\gamma_E + \frac{1}{6} \right) + \frac{1+\nu^2}{48} (4\ln 2 - 1) \\ & - \frac{(1-\nu)^2}{720} \left(\ln \frac{R}{s} + 2\gamma_E - \frac{169}{40} \right) \frac{s}{R} - \frac{1+\nu^2}{720} \left(4\ln 2 + \frac{17}{4} \right) \frac{s}{R} + \dots, \end{aligned} \quad (1.78)$$

where $s = d - 2R$ is the surface to surface separation, and $\gamma_E = 0.57721566\dots$ is the Euler–Mascheroni constant. We have plotted in Fig. 1.2 the force expression (1.77) along with Lekner’s expression (1.78) for close approach and the “exact” series solution from Technical Note 1.2, demonstrating that the EFT solution, even for being derived in the limit of large separations, captures the short-range behavior remarkable well.

Fixed charges. As we mentioned earlier, the general expansion of the energy (1.73) applies to the electrostatic interaction between any two spherical conductors. The parameter Q_a refers to the monopole moment (total charge) present on conductor a if it were in isolation, and $C_a^{(0)}$ is the monopole polarizability and reflects the conductor’s coupling to a charge reservoir, pulling up additional charge in response to external fields. For free conductors, there is no such charge reservoir and hence no monopole susceptibility. Therefore, the electrostatic interaction between conductors with individually fixed charges is given by Eq. (1.73) with $C^{(0)} = 0$. Since this eliminates a number of terms, we provide a few

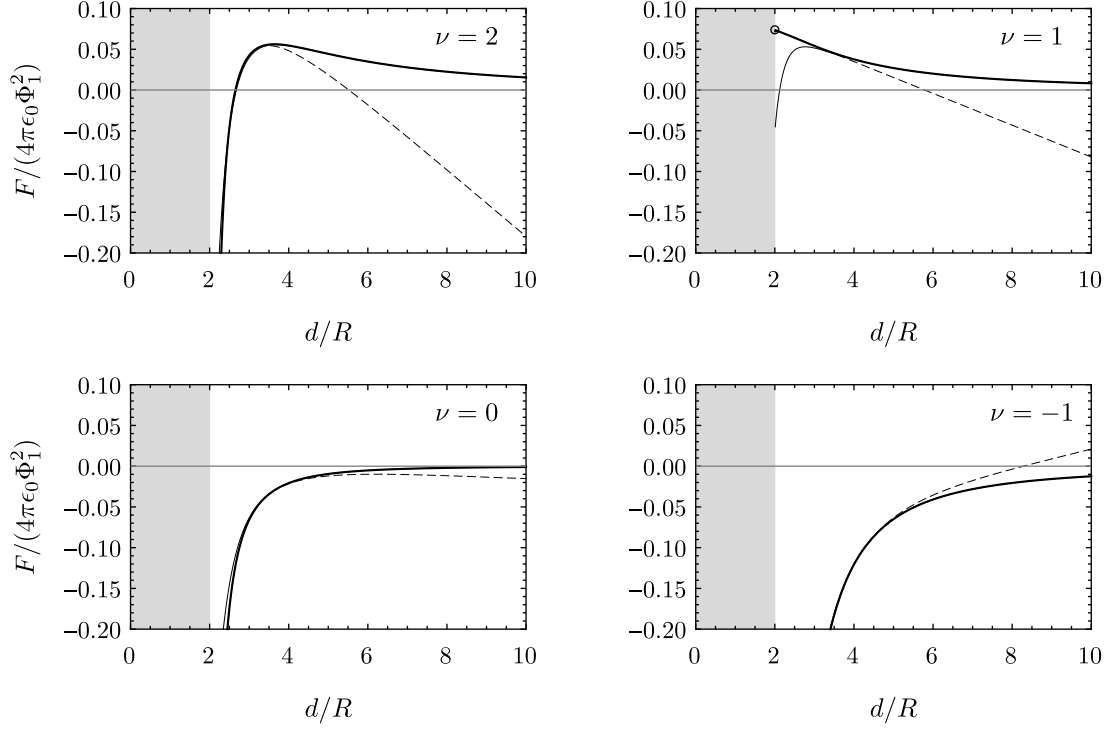


Figure 1.2: Electrostatic forces near contact for identical spheres of radii R . Plotted are the “exact” solution (solid, thick), derived from Eq. (1.74) with $n_{\max} = 49$, Lekner’s asymptotic result (1.78) (dashed) for *small separations*, and the asymptotic EFT result (1.77) for *large separations*. With $\nu := \Phi_2/\Phi_1$ as the ratio of the conductors’ respective fixed potentials, the top row presents the like-potentials $\nu = 2$ (left) and equipotentials $\nu = 1$ (right). The bottom row presents a grounded second, $\nu = 0$ (left), and opposite potentials $\nu = -1$ (right). Notice that although the EFT result was derived as an expansion in large separations, we find remarkable agreement upon close approach. Indeed, apart from the equipotential case, the thin and thick lines overlap and are difficult to distinguish.

additional orders of accuracy without too much extra effort:

$$\begin{aligned}
 \mathcal{U}_Q = \frac{1}{2} \sum_{a \neq b} \bigg\{ & \frac{Q_a Q_b}{4\pi\epsilon_0 d} - \frac{Q_a^2 C_b^{(1)}}{(4\pi\epsilon_0)^2 d^4} - \frac{6 Q_a^2 C_b^{(2)}}{(4\pi\epsilon_0)^2 d^6} + \frac{2 Q_a C_b^{(1)} C_a^{(1)} Q_b}{(4\pi\epsilon_0)^3 d^7} \\
 & - \frac{90 Q_a^2 C_b^{(3)}}{(4\pi\epsilon_0)^2 d^8} + 2 \frac{18 Q_a C_b^{(1)} C_a^{(2)} Q_b}{(4\pi\epsilon_0)^3 d^9} - \frac{4 Q_a^2 [C_b^{(1)}]^2 C_a^{(1)}}{(4\pi\epsilon_0)^4 d^{10}} - \frac{2520 Q_a^2 C_b^{(4)}}{(4\pi\epsilon_0)^2 d^{10}} \\
 & + 2 \frac{360 Q_a C_b^{(1)} C_a^{(3)} Q_b}{(4\pi\epsilon_0)^3 d^{11}} + \frac{216 Q_a C_b^{(2)} C_a^{(2)} Q_b}{(4\pi\epsilon_0)^3 d^{11}} - 2 \frac{36 Q_a^2 C_b^{(1)} C_a^{(1)} C_b^{(2)}}{(4\pi\epsilon_0)^4 d^{12}} \\
 & - \frac{54 Q_a^2 [C_b^{(1)}]^2 C_a^{(2)}}{(4\pi\epsilon_0)^4 d^{12}} - \frac{113\,400 Q_a^2 C_b^{(5)}}{(4\pi\epsilon_0)^2 d^{12}} + \frac{8 Q_a [C_b^{(1)}]^2 [C_a^{(1)}]^2 Q_b}{(4\pi\epsilon_0)^5 d^{13}} \\
 & + 2 \frac{12\,600 Q_a C_b^{(1)} C_a^{(4)} Q_b}{(4\pi\epsilon_0)^3 d^{13}} + 2 \frac{5400 Q_a C_b^{(2)} C_a^{(3)} Q_b}{(4\pi\epsilon_0)^3 d^{13}} + \mathcal{O}(d^{-14}) \bigg\} \quad (1.79)
 \end{aligned}$$

Like before, we may break up the expansion into “mutual” interactions and those in which the conductor interacts indirectly with itself via the polarization it induces in the other conductor. Plugging in for the polarizabilities, collecting terms, and simplifying results in

$$\begin{aligned}
 \mathcal{U}_Q = \frac{Q_1 Q_2}{4\pi\epsilon_0 d} \bigg\{ & 1 + \frac{2R_1^3 R_2^3}{d^6} + \frac{3R_1^3 R_2^3 (R_1^2 + R_2^2)}{d^8} + \frac{R_1^3 R_2^3 [2(R_1^2 + R_2^2)^2 - R_1^2 R_2^2]}{d^{10}} \\
 & + \frac{R_1^3 R_2^3 [5(R_1^2 + R_2^2) [(R_1^2 + R_2^2)^2 - R_1^2 R_2^2] + 8R_1^2 R_2^2]}{d^{12}} + \mathcal{O}(d^{-14}) \bigg\} \\
 & - \frac{1}{2} \sum_{a \neq b} \frac{Q_a^2}{4\pi\epsilon_0 d} \bigg\{ \frac{R_b^3}{d^3} + \frac{R_b^5}{d^5} + \frac{R_b^7}{d^7} + \frac{R_b^9 + 4R_b^6 R_a^3}{d^9} \\
 & + \frac{R_b^{11} + 12R_b^8 R_a^3 + 9R_b^6 R_a^5}{d^{11}} + \mathcal{O}(d^{-13}) \bigg\}. \quad (1.80)
 \end{aligned}$$

This expression agrees with that calculated from zonal harmonics by Maxwell [Max91, §146], who provides an expression for the energy up to $\mathcal{O}(d^{-23})$ accuracy! It is further verified by Lekner [Lek12b] who, by expanding the capacitance coefficients, reports an expression to $\mathcal{O}(d^{-10})$ accuracy. Finally, Sliško and Barito-Orta [SBO98] calculated the force between identical spheres by the method of images, and report an expression to $\mathcal{O}(d^{-21})$ accuracy, which is again in agreement.¹⁴

¹⁴For comparison and for reference, the force between two identical spheres of radii R and fixed total charges Q as calculated from Eq. (1.80) is given by

$$F = \frac{Q^2}{4\pi\epsilon_0 d^2} \left[1 - 4\chi^{-3} - 6\chi^{-5} + 14\chi^{-6} - 8\chi^{-7} + 54\chi^{-8} - 50\chi^{-9} + 154\chi^{-10} - 264\chi^{-11} + 494\chi^{-12} + \dots \right],$$

with $\chi = d/R$ as usual.

1.2 Effective field theory formalism

In the most general sense, an effective field theory is a simplified physical description at a given length or energy scale. In many cases, differing physical phenomena appear at widely separated scales, and it is this scale separation that allows us to probe and understand nature without knowing all the microscopic details. Indeed we can understand the orbits of planets without invoking quantum mechanics. Furthermore, certain physics—turbulence, for example—may only be *defined* in a certain range of scales, appearing as a high level emergent phenomena resulting from the collective behavior of its interacting constituents.

The EFT philosophy for an appropriately scale-separated problem is to provide a physical description at a chosen large scale by incorporating only the relevant degrees of freedom, while ignoring those which require details at short length scales or, equivalently, must be probed at very high energies. As we saw in the electrostatics problem, the short-distance details were irrelevant, except for determining the numerical values of the coupling constants (conductor polarizabilities). Besides those values, the *form* of our effective description was completely determined by particle and field degrees of freedom and symmetry considerations.

One way to construct an EFT is from what is referred to in the literature as a *top down* approach¹⁵ (see, for example Refs. [Geo93] or [Bai13a]). We begin with an underlying fundamental or “full” theory that is accurate all the way down to the microscopic scale. Next, through some kind of averaging or coarse-graining procedure we *eliminate*¹⁶ the short-distance degrees of freedom. That is, we take the features that are small compared to the scale of interest and shrink them down to zero in such a way that the theory is local and finite-size effects can be treated perturbatively. By doing so, we have modified the short-distance behavior and therefore introduced a bound on the range of validity of the EFT. This should of course be expected, but it is also perfectly acceptable so long as the scaling regimes are adequately disentangled. However, this limiting process of shrinking parameters to zero requires some care;¹⁷ it could be that by doing so, artificial divergences may appear, or worse, the dependence could be non-analytic in some parameter, signaling potential for phase transitions. These subtleties can be handled rather well through *renormalization*

¹⁵Unfortunately, the use of “top down” and “bottom up” is sometimes taken to have the opposite meaning. In the same *Oxford Handbook*, Batterman [Bat13] takes “top down” to mean a macroscale continuum model and “bottom up” to imply an atomistic description, whereas Bain [Bai13a] (along with other EFT authors) uses the terminology as we have above. With the exception of this section, we will avoid this language.

¹⁶By *eliminate*, we mean remove the functional dependence of the degrees of freedom from the physical description. This differs from *reducing* degrees of freedom by, for example, constraining particles to a plane $\{(x, y, z) \in \mathbb{R}^3 \mid z = 0\}$, or *restricting* degrees of freedom to, say, a range $\{(x, y, z) \in \mathbb{R}^3 \mid x^2 + y^2 + z^2 \leq r^2\}$. This distinction was emphasized in Ref. [Wil10] in the context of the philosophy of emergence and non-reductive physicalism, and further explored by Ref. [Bai13b] in the context of EFT.

¹⁷This limiting process can be studied from the point of view of *intermediate asymptotics*, which was introduced by Barenblatt [Bar79, Bar96] and later used to a great extent by Goldenfeld in the context of renormalization group theory [GMO89, Gol92]. The point is that we can express (*à la* Buckingham’s Π -theorem) some dimensionless physical quantity Π as some relation $\Pi = f(\Pi_0, \Pi_1, \dots, \Pi_n)$ of a finite set of dimensionless parameters $\{\Pi_0, \Pi_1, \dots, \Pi_n\}$. Now consider a scaling regime in which $\Pi_0 \rightarrow 0$. If f is nonsingular, then naturally $\Pi \rightarrow f(0, \Pi_1, \dots, \Pi_n)$. However, if this limit is undefined there *may* instead

group analysis [Vas04, BDFN95, Gol92], which in essence describes how the theory behaves or “flows” under coarse-graining or rescaling.

1.2.1 General formalism

For our purposes, we provide a physical description in terms of a functional $S[\phi]$, usually taken to be the energy or action, where the field ϕ characterizes some particular configuration of the system’s degrees of freedom. For convenience, let us choose $S[\phi]$ to be dimensionless. If we are interested in the macroscopic physics, we may (formally) decompose the field into short-distance and long-distance (respectively high-energy and low-energy) fields ϕ_S and ϕ_L , where ϕ_L is cut off below some small length scale ℓ , and ϕ_S is the remainder. In eliminating the short-distance degrees of freedom, the functional would become $S[\phi_L]$ plus some corrections $\Delta S[\phi_L; \ell]$. As discussed previously, we require $\Delta S[\phi_L; \ell]$ to be local, meaning it must be polynomial combinations of the field and its derivatives, all evaluated at the same point.¹⁸

From a top-down approach, we could explicitly perform the coarse-graining procedure and arrive at the ultimate form of ΔS , which would result in a derivative expansion, with each term $O_k[\phi_L]$ in the series equipped with a *Wilson coefficient* $C_k(\ell)$, which may be a multi-index object or tensor, determined by the short-distance physics. If we rescale ϕ by an appropriate parameter v so that the ratio ϕ/v is dimensionless, then the dimensions of $O_k[\phi_L/v]$ are carried by the derivatives. If $O_k[\phi_L/v]$ contains an integral, it will always be accompanied by a factor L^{-D} , where L is some length scale (possibly different from ℓ) and D is the dimension of the integral. Since ΔS is dimensionless, the Wilson coefficients $C_k(\ell)$ are therefore expected to scale generally as $L^{-D} v^{n_k} \ell^{d_k}$, where n_k is the overall power of the field in $O_k[\phi_L/v]$ and d_k counts the total number of derivatives. In this way, both v and ℓ serve as power-counting parameters that characterizes the importance of each term in the expansion. The *effective* functional can therefore be written as (dropping the “L” labels)

exist a set of real numbers $\{\alpha, \alpha_1, \dots, \alpha_n\}$ such that we have the well-defined limit

$$\lim_{\Pi_0 \rightarrow 0} \left(\frac{\Pi}{\Pi_0^\alpha} \right) = \lim_{\Pi_0 \rightarrow 0} \frac{1}{\Pi_0^\alpha} f\left(\Pi_0, \frac{\Pi_1}{\Pi_0^{\alpha_1}}, \dots, \frac{\Pi_n}{\Pi_0^{\alpha_n}}\right).$$

The α_i parameters cannot be determined from dimensional analysis, but if f obeys a partial differential equation (PDE), then in principle they can be determined by the PDE. In a field theory context, f would correspond to the renormalization group equations and the parameters α_i would be the *anomalous dimensions*, which give corrections to the naïve scaling of quantities suggested by dimensional analysis.

¹⁸In general, the coarse graining procedure could (and usually does) produce *nonlocal* interactions, *i.e.*, those that depend on more than one spatial location. However, these nonlocal interactions can be rewritten as a (functional) Taylor expansion—provided the field is suitably analytic in an open set containing each location—and the terms of the series will indeed be polynomial in the field and derivatives evaluated at a point. For example, an analytic, nonlocal interaction $\phi(x)\phi(x+a)$ could be rewritten as

$$\phi(x)\phi(x+a) = \sum_{k \geq 0} \frac{a^k}{k!} \phi(x) \partial^k \phi(x)$$

which is now a series of local terms.

$S_{\text{eff}}[\phi] = S[\phi] + \Delta S[\phi; \ell]$, where the remnants of the short-distance physics are encoded in the numerical couplings of the series expansion via

$$\Delta S[\phi; \ell] = \sum_k \mathbf{C}_k(\ell) \cdot \mathbf{O}_k[\phi] = \sum_k \frac{v^{n_k} \ell^{d_k}}{L^D} \mathbf{c}_k \cdot \mathbf{O}_k[\phi/v], \quad (1.81)$$

and where \mathbf{c}_k are dimensionless (again, possibly tensor) coefficients.

Note that there are in principle an infinite number of terms in this expansion, but only a finite number of terms contribute at any given order. By virtue of the power-counting parameter, truncating the series at some order implies our results will be accurate up to that order. So if we have a desired accuracy in mind, we need only determine a *finite* number of Wilson coefficients up to that order. Consider, for instance, a fairly general case¹⁹ for which $L \sim \ell$ and $v \propto \ell^{D/2}$. Any physics we calculate will scale as powers of (ℓ/r) , where $r \gg \ell$ is the length scale of the observable, so if we wish to construct an EFT with an accuracy of $(\ell/r)^k \gtrsim \epsilon$, we must therefore include all terms satisfying

$$k = \left(\frac{n}{2} - 1\right)D + d \lesssim \frac{\ln(1/\epsilon)}{\ln(r/\ell)}. \quad (1.82)$$

Another example, which we will run into later, is if $L = v^{2/D} \equiv \lambda$ is itself another length scale such that $\lambda \ll \ell \ll r$. Then we could to good approximation only keep terms with $n \leq 2$ powers of the field—a quadratic theory—and the remaining accuracy would be determined by the number of derivatives.

If we knew the underlying microscopic theory, and furthermore had the fortitude, we could explicitly perform the coarse-graining procedure, resulting in the series expansion above and thereby giving us the Wilson coefficients. However, we already know what form the effective functional must take, so an alternative approach—which we in essence just did—would be to construct the EFT from the *bottom up* by simply enumerating all possible products of the field and its derivatives up to the desired order. With some insight, we can actually do better. As we saw in the electrostatics problem, we can exploit symmetries to further reduce the degrees of freedom. Since the symmetries present in the system will always manifest in any physical observables, we should make the consequences of the symmetries explicit in the construction of the EFT by only including the appropriate invariants. The remaining step is to determine the Wilson coefficients. Since we require the underlying microscopic theory and large-distance effective theory to reproduce the same physics at large distances, it follows that the two theories should match all the way down to the cutoff ℓ . This suggests a way to determine the Wilson coefficients: compute convenient physical observables in both theories and match them at the larger scale (*i.e.*, above ℓ). Since only a finite number of terms appear up to a given order in the EFT expansion, only a finite number of observables are required to determine the Wilson coefficients to that order.

¹⁹This is motivated by the common appearance of $\int d^D x \frac{1}{2}(\nabla\phi)^2$ as the free action in field theory.

To summarize, the EFT philosophy consists of the following principles:

1. **Scale separation** The macroscopic (long distance, low energy) physics does not depend on most details of the microscopic (short distance, high energy) physics. The boundary between the two scaling regimes can be characterized by a small cutoff parameter.
2. **Degrees of freedom** Only the relevant macroscopic degrees of freedom are needed to describe the physics at the large scale considered. These can be further reduced by explicit symmetry considerations.
3. **Locality** Any nonlocal interactions can be exchanged by an infinite tower of local interactions. The series consists of all combinations of the fields and their derivatives that respect the symmetries, evaluated at the same point. The relative importance of each interaction is characterized by its scaling in the small cutoff parameter.
4. **Matching** Above the boundary of the scaling regimes, an effective description of the macroscopic physics should reproduce, or match to some desired precision, the observable effects due to the microscopic physics. If a microscopic theory is missing, the resulting EFT provides a predictive phenomenological model that can be fit to experiments.

1.2.2 Worldline EFTs

A worldline EFT follows the same philosophy as discussed above, but emphasizes that interacting *compact* objects with sizes below the length cutoff can be treated as particles shrunk down to points. As in the electrostatics example—and the work to follow—we are interested in field-mediated interactions between objects. The presence of such objects puts localized constraints on the field, so any effects due to the objects’ properties can be completely captured by their influence on the field’s degrees of freedom. In particular, an object’s boundary conditions and symmetries provide information about what combinations of the field degrees of freedom, such as ϕ , $\partial_i\phi$, $\partial_i\partial_j\phi$, and so forth, are relevant or permissible at the location of the object. For example, the conducting spheres of the previous section exhibit rotational symmetry, so the effective energy needed to only be constructed from rotationally invariant combinations of the field and its derivatives.

The characteristic size s of an object serves as a natural “microscopic” cutoff, so the construction of a worldline EFT for compact objects follows the EFT prescription discussed previously with $\ell = s$. Moreover, because of locality, as long as additional objects are separated by distances much larger than the particle sizes (scale separation), their descriptions completely decouple and their effects on the field can be analyzed independently. The gain is that the functional describing the physics in the larger scaling regime can be written as contributions from the particle-free field plus independent derivative expansions evaluated at the positions, or *worldlines*, of the objects:

$$S_{\text{eff}}[\phi] = S_{\text{free}}[\phi] + \sum_a \Delta S_a[\phi(\mathbf{x}_a)]. \quad (1.83)$$

Partition function

In the following chapters, we will not only be interested in “ground state” interactions mediated by the field, but those induced by thermal field fluctuations as well. Any ground state interactions require the objects to be appropriately sourced by some external agent, such as a battery or even permanent charges. Field fluctuations, however, also serve to source the objects, but this sourcing is statistical in nature rather than directly imposed.

Following the common approach in statistical physics, we wish to construct a partition function Z that captures all the thermodynamic properties of the field–particle system. However, since we are dealing with field configurations that assign numbers to every point in space, we are in a sense working with infinite degrees of freedom. The usual sum over microstates in the partition function must then be replaced by a *functional integral* over field configurations:

$$Z = \sum_i e^{-\beta E_i} \rightarrow \int \mathcal{D}\phi e^{-\beta H[\phi]}, \quad (1.84)$$

where the energy functional $H[\phi]$ serves as the Hamiltonian and the functional measure is an appropriate continuum limit of $\mathcal{D}\phi \propto \prod_{\mathbf{x}} d\phi(\mathbf{x})$. As usual, $\beta := 1/k_{\text{B}}T$.

In this context, coarse graining can be thought of as *integrating out* the microscopic degrees of freedom. In many applications, this is done according to one of two top-down approaches: real-space or Fourier-space coarse graining. The first is to discretize, or “block,” space into a lattice of points with separations on the order of the cutoff size ℓ , then in some way averaging the field over each region. We may express the average field $\bar{\phi}(\bar{\mathbf{x}})$ about each block center $\bar{\mathbf{x}}$ as (in D dimensions)

$$\bar{\phi}(\bar{\mathbf{x}}) = \int d^D x \phi(\mathbf{x}) A(\mathbf{x}, \bar{\mathbf{x}}), \quad (1.85)$$

where the integral kernel $A(\mathbf{x}, \bar{\mathbf{x}})$ is some appropriate averaging weight. For example, one might consider $A(\mathbf{x}, \bar{\mathbf{x}}) \propto \Theta(\ell - |\mathbf{x} - \bar{\mathbf{x}}|)/V_D(\ell)$, where $\Theta(\mathbf{x})$ is the Heaviside step function, which averages the field over a ball of radius ℓ centered at $\bar{\mathbf{x}}$. Alternatively, $A(\mathbf{x}, \bar{\mathbf{x}})$ may represent a smooth Gaussian weight or some more complicated distribution. The resulting coarse-grained Hamiltonian then follows from

$$e^{-\beta H_{\text{eff}}[\bar{\phi}]} \equiv \int \mathcal{D}\phi \prod_{\bar{\mathbf{x}}} \delta\left(\bar{\phi}(\bar{\mathbf{x}}) - \int d^D x \phi(\mathbf{x}) A(\mathbf{x}, \bar{\mathbf{x}})\right) e^{-\beta H[\phi]}. \quad (1.86)$$

The functional integral can then be performed, for instance, by applying the (functional) Fourier representation of the delta function and further integrating out the associated auxiliary fields.

The second, more popular procedure is to instead coarse-grain in Fourier space in which the microscopic degrees of freedom intuitively correspond to wavelengths smaller than

the small length scale ℓ . In terms of the wave number cutoff²⁰ $\Lambda \propto 2\pi/\ell$, the Fourier components are readily decomposed into small and large wavenumber contributions, $\tilde{\phi}_<$ and $\tilde{\phi}_>$ respectively, through $\tilde{\phi}(\mathbf{q}) = \tilde{\phi}_<(\mathbf{q}) + \tilde{\phi}_>(\mathbf{q})$ in which

$$\tilde{\phi}_{\gtrless}(\mathbf{q}) := \Theta(\pm(|\mathbf{q}| - \Lambda)) \tilde{\phi}(\mathbf{q}). \quad (1.87)$$

In real space, the field also decomposes linearly as $\phi(\mathbf{x}) = \phi_L(\mathbf{x}) + \phi_S(\mathbf{x})$, where ϕ_L and ϕ_S respectively encode the large and small distance degrees of freedom:

$$\phi_L(\mathbf{x}) := \int \frac{d^D q}{(2\pi)^D} \tilde{\phi}_<(\mathbf{q}) e^{i\mathbf{q}\cdot\mathbf{x}} = \int_{|\mathbf{q}| < \Lambda} \frac{d^D q}{(2\pi)^D} \tilde{\phi}(\mathbf{q}) e^{i\mathbf{q}\cdot\mathbf{x}} \quad (1.88a)$$

$$\phi_S(\mathbf{x}) := \int \frac{d^D q}{(2\pi)^D} \tilde{\phi}_>(\mathbf{q}) e^{i\mathbf{q}\cdot\mathbf{x}} = \int_{|\mathbf{q}| > \Lambda} \frac{d^D q}{(2\pi)^D} \tilde{\phi}(\mathbf{q}) e^{i\mathbf{q}\cdot\mathbf{x}} \quad (1.88b)$$

The passage between real and Fourier space is a (linear) unitary transformation, so the functional measure transforms with a unit Jacobian factor, $\mathcal{D}\phi \equiv \mathcal{D}\tilde{\phi}$, and allows for the following factorization:

$$\begin{aligned} \mathcal{D}\tilde{\phi} \propto \prod_{\mathbf{q}} d\tilde{\phi}(\mathbf{q}) &= \left(\prod_{|\mathbf{q}| < \Lambda} d\tilde{\phi}(\mathbf{q}) \right) \left(\prod_{|\mathbf{q}| > \Lambda} d\tilde{\phi}(\mathbf{q}) \right) \\ &= \left(\prod_{\mathbf{q}} d\tilde{\phi}_<(\mathbf{q}) \right) \left(\prod_{\mathbf{q}} d\tilde{\phi}_>(\mathbf{q}) \right) \\ &\equiv \left(\prod_{\mathbf{x}} d\phi_L(\mathbf{x}) \right) \left(\prod_{\mathbf{x}} d\phi_S(\mathbf{x}) \right) \propto \mathcal{D}\phi_L \mathcal{D}\phi_S. \end{aligned} \quad (1.89)$$

Like before, the effective Hamiltonian is obtained by integrating out the microscopic degrees of freedom:

$$e^{-\beta H_{\text{eff}}[\phi_L]} \equiv \int \mathcal{D}\phi_S e^{-\beta H[\phi_L + \phi_S]}. \quad (1.90)$$

In both cases, the decomposition relied on the homogeneity of space. The coarse-graining procedure is therefore more subtle (and challenging) with the introduction of spatial boundaries and their concomitant boundary conditions. However, if the inhomogeneities are compact with sizes $s \sim \ell$, the EFT prescription tells us how to bypass the complicated

²⁰Technically, one again imagines breaking space into a lattice with cell volume $v_0 = V/N = \ell^D$. Fourier modes are thus restricted to the first Brillouin zone of the reciprocal lattice, from which it follows [CL95b]:

$$\frac{1}{v_0} = \frac{N}{V} = \frac{1}{V} \sum_{\mathbf{q}} \equiv \int_{|\mathbf{q}| < \Lambda} \frac{d^D q}{(2\pi)^D} = \frac{\Omega_D}{(2\pi)^D} \frac{\Lambda^D}{D},$$

where Ω_D is the solid angle subtended by a sphere in D dimensions. The desired cutoff is therefore $\Lambda = (D/\Omega_D)^{1/D} (2\pi/\ell)$.

decomposition and integration steps. Following the steps laid out in Section 1.2.1, one constructs an effective worldline Hamiltonian,

$$H_{\text{eff}}[\phi] = H_0[\phi] + \sum_a \Delta H_a[\phi(\mathbf{x}_a)], \quad (1.91)$$

where H_0 is the defect-free Hamiltonian and ΔH_a is a series of local field operators evaluated at the locations \mathbf{x}_a of each object a . For completeness, we also note that in both coarse-graining procedures discussed above, the physics should match at the larger scale, so

$$\int \mathcal{D}\varphi e^{-\beta H_{\text{eff}}[\varphi]} \stackrel{!}{=} \int \mathcal{D}\phi e^{-\beta H[\phi]}, \quad (1.92)$$

where φ denotes either $\bar{\phi}$ or ϕ_L . In other words, to determine the associated Wilson coefficients (and thus completely determine H_{eff}), we need only calculate some convenient thermodynamic observables in the full and effective theories and match.

Interaction potential

After the EFT is fully constructed, or at least to the desired accuracy, we can then set about calculating interactions. Such interparticle interaction energies are extracted from the free energy $\mathcal{F} = -k_B T \ln Z$. Note, however, that we will never need to compute the functional integral Z directly. Instead, the interaction potential is defined as the free energy difference $\mathcal{U} := \mathcal{F} - \mathcal{F}_0$, where \mathcal{F}_0 is the free energy of the field without particles, and it follows that calculating interactions reduces to finding moments of the worldline Hamiltonian in the canonical ensemble of systems governed by the *particle-free* Hamiltonian. To clarify, we rearrange the functional integral as

$$\begin{aligned} e^{-\beta \mathcal{F}} = Z &= \int \mathcal{D}\phi e^{-\beta(H_0[\phi] + \Delta H[\phi])} = \int \mathcal{D}\phi \left(e^{-\beta \Delta H[\phi]} \right) e^{-\beta H_0[\phi]} \\ &\equiv Z_0 \left\langle e^{-\beta \Delta H[\phi]} \right\rangle_0, \end{aligned} \quad (1.93)$$

where $\langle \cdots \rangle_0$ is the expectation value weighted by the distribution $e^{-\beta H_0[\phi]}/Z_0$, and

$$Z_0 = \int \mathcal{D}\phi e^{-\beta H_0[\phi]} \equiv e^{-\beta \mathcal{F}_0}, \quad (1.94)$$

which bears no information about the particles and is often normalized to unity. Finally, using the well-known relation $\ln \langle e^X \rangle = \langle e^X \rangle_c$ between “connected averages,” or *cumulants* $\langle X \rangle_c$, and ordinary averages $\langle X \rangle$ [BDFN95], we may express the interaction potential as the cumulant expansion

$$\mathcal{U} = \mathcal{F} - \mathcal{F}_0 = -\frac{1}{\beta} \ln \left\langle e^{-\beta \Delta H[\phi]} \right\rangle_0 \equiv -\frac{1}{\beta} \sum_{q=1}^{\infty} \frac{1}{q!} \langle (-\beta \Delta H[\phi])^q \rangle_c. \quad (1.95)$$

2 Physics of random surfaces

In the previous chapter, we investigated the interaction between two conductors as mediated by the electrostatic field. We will soon turn to discuss surface-mediated interactions in soft matter, where the soft-matter surface plays the role of the deformable, fluctuating field. Many of the mathematical (and linguistic) tools will carry over from the electrostatics discussion, particularly the procedure to characterize objects by their field responses. But before we consider the additional complexity of embedded or adsorbed particles and other inhomogeneities, we must first be explicit about the mediating field. To this aim, we provide a brief overview of the physics of random surfaces and construct the requisite energy functionals.

2.1 Mesoscopic models of interfaces and membranes

2.1.1 Physical origins and considerations

In the realm of soft matter, (quasi-) two-dimensional (2D) extended objects—surfaces or membranes—typically manifest at the interface between dissimilar fluid phases (*e.g.*, liquid–vapor) or between otherwise immiscible fluids (*e.g.*, oil–water). Such an interface is not strictly a sharp discontinuity between phases, but rather a continuous transition across molecular length scales. Within the bulk of a liquid—water for example—molecules experience attractive cohesive interactions (*e.g.*, hydrogen bonds) isotropically. However, at the interface boundary, molecules necessarily experience fewer interactions or bonds from the opposing side and result in an internal pressure that contracts the boundary to some minimum area. Equivalently, the shortage of bonds at the interface entails the boundary molecules reside at higher energies compared to those in the liquid bulk. That is, the free energy of the system is concentrated across the width of the interface. Minimizing the total energy therefore requires decreasing the number of boundary molecules and thus minimizing the surface area. The free energy per unit area σ of the interface may therefore be appropriately interpreted as a *surface tension* that resists changes in the equilibrium surface area.

Technical Note 2.1 illustrates one such (simplified) instance of an interface as a semi-infinite *domain wall* between two phases described by a Ginzburg–Landau free energy functional. The bulk free energy density exhibits a smooth spike across the width of the phase profile transition and demonstrates that at *mesoscopic* length scales—*i.e.*, those for which the lateral extent and deformations of the interface are much larger than its width—the interface may be treated as an effective 2D surface with a surface tension determined by the Ginzburg–Landau expansion parameters. For more examples and details

Technical Note 2.1: Domain walls in Ginzburg–Landau theory

Consider a mixture of two fluids described by an order parameter $\phi = \rho_{\text{II}} - \rho_{\text{I}}$, where $\rho_{\text{I,II}}$ are the fluid densities, and an (Ising order) Ginzburg–Landau free energy of the form [Saf94, CL95b]

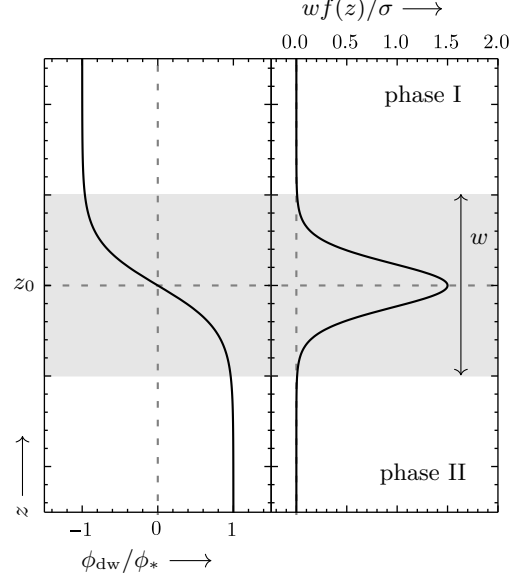
$$\mathcal{F}_{\text{GL}}[\phi] = \int d^3x \left[\frac{c}{2} (\nabla \phi)^2 + V(\phi) \right],$$

$$V(\phi) = \frac{r}{2} \phi^2 + \frac{u}{4} \phi^4,$$

with $r = r_0(T - T_c)/T_c$ and positive constants c , r_0 , and u . Alternatively, ϕ may describe the difference in concentrations of a binary fluid or the average magnetization of a spin lattice. Below the critical temperature T_c , the fluid mixture undergoes phase separation with a *domain wall*, or *interface*, between the phases $\pm\phi_*$ along the z -axis with $\phi_* = \sqrt{|r|/u}$ the degenerate minima of the mean field free energy. The interface (domain wall) profile is given by $\phi_{\text{dw}}(z) = \phi_* \tanh\left(\frac{z-z_0}{w/2}\right)$, which satisfies $\delta\mathcal{F}_{\text{LG}}/\delta\phi = 0$, where the interface has a width $w = 2\sqrt{2c/|r|}$ centered at $z = z_0$. Moreover, this phase profile “kink” concentrates the free energy within the width of the interface such that

$$\Delta\mathcal{F}_{\text{dw}} := \mathcal{F}_{\text{GL}}[\phi_{\text{dw}}] - \mathcal{F}_{\text{GL}}[\phi_*] = \int d^3x \frac{u}{2} (\phi_*^2 - \phi_{\text{dw}}^2)^2 =: A \int dz f(z) \equiv \sigma A,$$

where $f(z)$ is the free energy density (plotted above), A is the area of the interface, and $\sigma = uw\phi_*^4/3 = |r|^2 w/3u$ is the effective *surface tension* of the interface. Note that the interface is *nonfluctuating* in mean field theory, even though $\sigma \propto |T - T_c|^{3/2}$, but entropic contributions will modify the description.



on phase separation and related capillary phenomena, the reader is referred to Refs. [Saf94], [Isr11], and [RW02].

The surface energetics may be further altered by the addition of **surface-active agents**—or *surfactants*—that, when dissolved in a solvent at low concentrations, have the ability to adsorb at interfaces. For example, since there is an energetic cost to moving solvent molecules from the bulk to the surface, it follows that replacing boundary molecules with inert or otherwise insoluble molecules will lower the system’s free energy and, by extension, the surface tension. The reduction is further amplified by the increase in translational entropy of the surface-active component (the surfactant behaves like a 2D ideal gas on the surface) [Saf94].

Another important class of soft matter surfaces results from the self assembly of *amphiphiles*, such as fatty acid anions or the phospholipids of cellular membranes. Such molecules typically consist of a hydrophilic carboxyl head group and long hydrophobic hydrocarbon chains (“tails”). In an aqueous environment, the hydrophobic regions disturb the network of hydrogen bonds of nearby water molecules, which in turn forfeit translational

and rotational entropy. The resulting competition between energy and entropy favors the aggregation of amphiphiles so as to reduce the hydrophobic surface area exposed to water. This *hydrophobic effect* is responsible for the formation of monomolecular films at the water's surface [Ise92, Eas10].

In contrast to insoluble surfactants for which the number of surface molecules is fixed, the number of surface amphiphiles is determined by balancing the bulk and surface chemical potentials. If the concentration of amphiphiles is increased, then (for low concentrations) the surface tension reduces linearly, but at larger concentrations the surface saturates and it becomes more energetically favorable for amphiphiles to create new interfaces within the bulk. Beyond this *critical micelle concentration* (CMC), amphiphiles self assemble into a variety of structures that shield the hydrophobic regions from the bulk solvent (see Refs. [Saf94, Ch. 8], [Isr11, Chaps. 19, 20], [Eas10], and [Boa12, §§7.1, 7.2]).

The morphology of such structures depends on a variety of physical and chemical factors, including the length and disorder or saturation of the hydrophobic moiety, and electrostatics of the head group and solvent. However, geometric and steric considerations can provide a rough understanding of the morphology [IMN76]. Each lipid consists of a long tail of length ℓ and effective volume v , and a head group that requires an area a within an assemblage. The geometry of each lipid informs the ultimate shape of the aggregate, which can be summarized in terms of the *packing parameter* $P = v/\ell a$. For $P \lesssim 1/3$, lipids assume effective conical shapes and assemble into spherical micelles. Lipids resembling truncated cones fall in the range $1/3 \lesssim P \lesssim 1/2$ and assemble into cylindrical micelles. As the lipids shapes become more cylindrical, typical for double-chain lipids, the packing parameter falls in the range $1/2 \lesssim P \lesssim 1$ and the aggregate morphology tends toward planar bilayers. This latter category includes biologically relevant phospho- and glycolipids. For these lipid bilayers the CMC is remarkable low, around 10^{-6} – 10^{-10} M [Isr11, §20.6], and the resulting membranes are thus quite stable even with a very low surrounding lipid concentration. Moreover, at physiological temperatures, the lipid leaflets behave as 2D fluids. That is, the constituents flow and responds to changing surface shape at no cost in energy.

2.1.2 Modeling and mathematical description

To construct a phenomenological model for the above-mentioned categories of soft-matter surfaces, we take inspiration from the previous chapter on effective field theory. At sufficiently large length scales, whatever microscopic degrees of freedom conspired to form the fluid interface or surface become irrelevant. Upon coarse-graining the physical description, these degrees of freedom may leave their trace in the numerical values of the resulting emergent macroscopic parameters, but if we seek a universal description of a surface, the existence of these emergent parameters is effectively independent of the coarse-grained path that ultimately gave rise to them. By explicitly acknowledging the scale separation and any symmetry constraints, the path to a macroscopic description is in essence straightforward (though not guaranteed to be without effort).

In this thesis, we will concern ourselves with *fluid* surfaces, for which it is assumed that

the microscopic surface constituents (lipids, *etc.*) are free to move around and diffuse in the plane of the surface. The consequence of fluidity is that no point on the surface is privileged. Instead, the energy of a surface configuration only depends on its geometry and lacks any memory of previous shapes. The irrelevancies of microscopic degrees of freedom at large scales informs us the surface thus behaves as a 2D featureless elastic sheet in which there is no preferred in-plane coordinate system. That is, the mathematical description of the configuration energy should consist of coordinate-independent, or *reparametrization invariant* (RPI) quantities.

The goal then is to construct an effective energy functional out of geometric scalar invariants. The final step is to order these invariants as a series expansion in some smallness parameter. The most obvious choice is the ratio of the surface width to its radius of curvature, which as we will see soon will count the derivatives of a given scalar. To begin, we first review some relevant concepts of differential geometry. The following treatment will roughly follow the course of Ref. [Des15], with some additional insight coöpted from the general relativity literature [Che05], as well as the canonical references [Spi75, dC76].

2.2 Surface geometry

A fluid surface is appropriately modeled as a smooth, two-dimensional manifold embedded in three-dimensional Euclidean space \mathbb{R}^3 . As a geometric object, it should be completely characterized by local and global geometric quantities which naturally exist independent of any prescribed parametrization or coordinate system. However, the arbitrariness of parametrizations affords us with the choice of any representation that is most convenient for surface under consideration. So long as one is mindful of the mathematical limitations or artifacts that may be inherited from a particular parametrization, a thoughtful combination of coordinate-invariant and coordinate-explicit considerations can yield dividends when it comes to calculating interesting quantities.

Although it is not always possible to parametrize an arbitrary surface globally, we can instead cover a surface $\mathcal{S} \subset \mathbb{R}^3$ in a patchwork of submanifolds, $\bigcup_{\alpha} \mathcal{S}_{\alpha} = \mathcal{S}$, such that within each patch \mathcal{S}_{α} a local two-dimensional coordinate system is defined. As illustrated in Fig. 2.1, for each patch \mathcal{S}_{α} one constructs a *coordinate chart* that maps the pair $(u^1, u^2) \in U_{\alpha} \subset \mathbb{R}^2$ to a point on the surface by means of a three-dimensional embedding function $\mathbf{X} : U_{\alpha} \rightarrow \mathcal{S}_{\alpha}$ so that $(u^1, u^2) \mapsto \mathbf{X} = \mathbf{X}(u^1, u^2) \equiv (X^1(u^1, u^2), X^2(u^1, u^2), X^3(u^1, u^2))$. Evidently, among the “atlas” of coordinate charts, two or more associated surface patches may overlap and must satisfy appropriate continuity and differentiability conditions. Namely, for two parametrizations $\mathbf{X} : U_{\alpha} \rightarrow \mathcal{S}_{\alpha}$ and $\mathbf{Y} : U_{\beta} \rightarrow \mathcal{S}_{\beta}$ with an overlapping region $\mathcal{W} := \mathcal{S}_{\alpha} \cap \mathcal{S}_{\beta} \neq \emptyset$, the composition map $\mathbf{Y}^{-1} \circ \mathbf{X} : (\mathbf{X}^{-1}(\mathcal{W}) \subset U_{\alpha}) \rightarrow (\mathbf{Y}^{-1}(\mathcal{W}) \subset U_{\beta})$ must constitute a *diffeomorphism*¹ (*i.e.*, reparametrization), and similarly for $\mathbf{X}^{-1} \circ \mathbf{Y}$.

At each point \mathbf{X} on the surface, we can use the mapping to construct two linearly-

¹That is, the function $f := \mathbf{Y}^{-1} \circ \mathbf{X}$ defines a coordinate transformation such that $\mathbf{X} = \mathbf{Y} \circ f$ on the subset $\mathbf{X}^{-1}(\mathcal{W}) \subset U_{\alpha}$. Hence, both \mathbf{X} and \mathbf{Y} (re)parametrize the patch $\mathcal{W} \subset \mathcal{S}$.

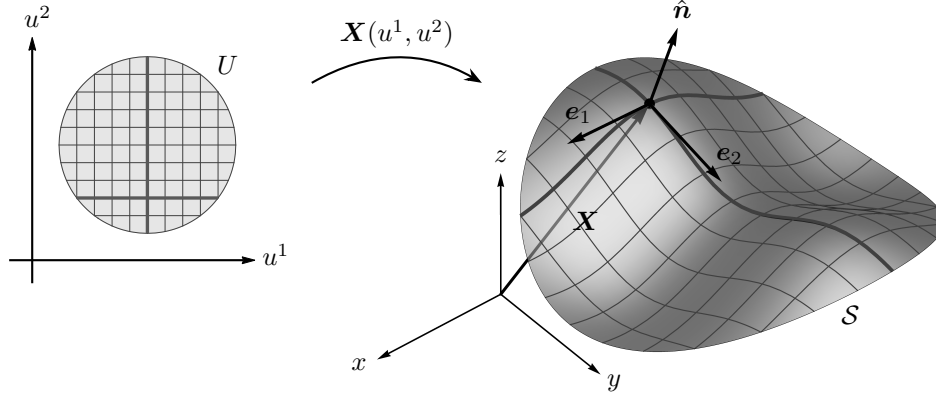


Figure 2.1: Illustration of a surface parametrization and local coordinate system. The surface $\mathcal{S} \subset \mathbb{R}^3$ consists of a single patch and is parametrized by $(u^1, u^2) \in U \subset \mathbb{R}^2$ via the embedding function $\mathbf{X} : U \rightarrow \mathcal{S}$. From the parametrization one may construct a local coordinate basis $\{\mathbf{e}_1, \mathbf{e}_2, \hat{\mathbf{n}}\}$, where $\{\mathbf{e}_1, \mathbf{e}_2\}$ spans the local tangent plane $T_{\mathbf{X}} \mathcal{S}$ and $\hat{\mathbf{n}}$ is normal to the surface. Note that it is not necessary that $\mathbf{e}_1 \cdot \mathbf{e}_2 = 0$, but $\mathbf{e}_i \cdot \hat{\mathbf{n}} = 0$ will always hold.

independent tangent vectors

$$\mathbf{e}_i := \partial_i \mathbf{X} \equiv \frac{\partial \mathbf{X}}{\partial u^i}, \quad (2.1)$$

where $i \in \{1, 2\}$, which form a basis in the corresponding tangent plane $T_{\mathbf{X}} \mathcal{S}$. Note the lower placement of the index i , as opposed to the upper indices of u^i , reminding us of its *covariant* properties under coordinate transformations (see Technical Note 2.2). The primary motivation for keeping track of covariant *vs.* contravariant components is that we ultimately wish to construct coordinate-independent scalars and the invariance of such scalars is manifest if they consist of contractions strictly between covariant and contravariant indices of proper vectors and tensors. For example, under a change of coordinates $u^i \rightarrow \tilde{u}^i$ the two vectors of the contraction² $U^i V_i$ pick up mutually compensating Jacobian factors:

$$\tilde{U}^j \tilde{V}_j = \frac{\partial \tilde{u}^j}{\partial u^k} U^k \frac{\partial u^i}{\partial \tilde{u}^j} V_i = \delta_k^i U^k V_i = U^i V_i. \quad (2.2)$$

Furthermore we construct a unit vector normal to the surface (*i.e.* normal to the tangent plane at each point) via

$$\hat{\mathbf{n}} := \frac{\mathbf{e}_1 \times \mathbf{e}_2}{|\mathbf{e}_1 \times \mathbf{e}_2|}, \quad (2.3)$$

and thereby complete a local frame (basis) $\{\mathbf{e}_1, \mathbf{e}_2, \hat{\mathbf{n}}\}$ in \mathbb{R}^3 .

²Recall that we use the Einstein summation convention in which repeated indices are summed over.

Technical Note 2.2: Covariant and contravariant components

The placement of each index serves to remind us of the “type” of component: *covariant* or *contravariant*. These names derive from the transformation properties under a smooth and invertible coordinate transformation. For example, consider a vector \mathbf{V} defined in the tangent space $T_{\mathbf{X}} \mathcal{S}$ at the point \mathbf{X} on the surface. The tangent space is spanned the basis vectors $\{\mathbf{e}_1, \mathbf{e}_2\}$, which are not generally orthogonal: $\mathbf{e}_i \cdot \mathbf{e}_j \equiv g_{ij} \neq \delta_{ij}$ (see Eq. (2.4)). There does, however, exist a dual *inverse* basis $\{\mathbf{e}^1, \mathbf{e}^2\}$, belonging to the *cotangent space* $T_{\mathbf{X}}^* \mathcal{S}$, defined such that $\mathbf{e}_i \cdot \mathbf{e}^j = \delta_i^j$. The vector \mathbf{V} can be expanded in either basis:

$$\mathbf{V} = V^i \mathbf{e}_i = V_i \mathbf{e}^i.$$

Under the coordinate transform $u^i \rightarrow \tilde{u}^i$, the basis vectors pick up a Jacobian factor

$$\tilde{\mathbf{e}}_i = \frac{\partial \mathbf{X}}{\partial \tilde{u}^i} = \frac{\partial \mathbf{X}}{\partial u^j} \frac{\partial u^j}{\partial \tilde{u}^i} = \mathbf{e}_j \frac{\partial u^j}{\partial \tilde{u}^i}. \quad (*)$$

Since vectors are coordinate-independent, $\tilde{\mathbf{V}} \equiv \mathbf{V}$ and it follows that the components V_i must *co-vary* with the change of basis:

$$\tilde{V}_i = \tilde{\mathbf{V}} \cdot \tilde{\mathbf{e}}_i \equiv \mathbf{V} \cdot \tilde{\mathbf{e}}_i = (V_j \mathbf{e}^j) \cdot \left(\mathbf{e}_k \frac{\partial u^k}{\partial \tilde{u}^i} \right) = V_j \delta_k^j \left(\frac{\partial u^k}{\partial \tilde{u}^i} \right) = V_j \frac{\partial u^j}{\partial \tilde{u}^i}. \quad (*)$$

Similarly, the components V^i must *contra-vary* so that the transformations compensate:

$$\tilde{V}^i = \tilde{\mathbf{V}} \cdot \tilde{\mathbf{e}}^i \equiv \mathbf{V} \cdot \tilde{\mathbf{e}}^i = (V^j \mathbf{e}_j) \cdot \left(\mathbf{e}^k \frac{\partial \tilde{u}^i}{\partial u^k} \right) = V^j \delta_j^k \left(\frac{\partial \tilde{u}^i}{\partial u^k} \right) = V^j \frac{\partial \tilde{u}^i}{\partial u^j}. \quad (**)$$

The “upstairs–downstairs” notation makes the transformation properties apparent: we denote *contravariant* components (those that transform like (**)) by upper indices and *covariant* components (those that transform like (*)) by lower indices.

First fundamental form (metric)

In these local coordinates, the basis vectors spanning the tangent plane are not necessarily orthogonal (nor of unit magnitude). Instead, their dot product satisfies $\mathbf{e}_i \cdot \mathbf{e}_j =: g_{ij}$, where g_{ij} is not generally proportional to δ_{ij} . The deviation from orthogonality, g_{ij} , is known as the *first fundamental form* or the (induced³) *metric tensor*. It gets its name “metric” from the important role it plays in calculating distances. Namely, the infinitesimal Euclidean distance $d\ell^2$ between two points $\mathbf{X}(u^1, u^2)$ and $\mathbf{X}(u^1 + du^1, u^2 + du^2)$ on the surface is given by

$$d\ell^2 = [\mathbf{X}(u^1 + du^1, u^2 + du^2) - \mathbf{X}(u^1, u^2)]^2 = (\mathbf{e}_i du^i) \cdot (\mathbf{e}_j du^j) \equiv g_{ij} du^i du^j. \quad (2.4)$$

³Of course the ambient embedding space may possess a nontrivial (3D) metric as well, but we take it to be Euclidean: $g_{\mu\nu} = \delta_{\mu\nu}$, where $\mu, \nu \in \{1, 2, 3\}$.

It should not be surprising that the metric also plays an important role in determining area, as seen by considering the infinitesimal area element

$$dA = |\mathbf{e}_1 du^1 \times \mathbf{e}_2 du^2| = |\mathbf{e}_1 \times \mathbf{e}_2| du^1 du^2$$

spanned by the displacement vectors $\mathbf{e}_1 du^1$ and $\mathbf{e}_2 du^2$. Using

$$\begin{aligned} |\mathbf{e}_1 \times \mathbf{e}_2|^2 &= |\mathbf{e}_1|^2 |\mathbf{e}_2|^2 \sin^2(\angle(\mathbf{e}_1, \mathbf{e}_2)) = |\mathbf{e}_1|^2 |\mathbf{e}_2|^2 [1 - \cos^2(\angle(\mathbf{e}_1, \mathbf{e}_2))] \\ &= |\mathbf{e}_1|^2 |\mathbf{e}_2|^2 - (\mathbf{e}_1 \cdot \mathbf{e}_2)^2 = g_{11}g_{22} - g_{12}g_{21} \\ &\equiv \det g_{ij} =: g, \end{aligned} \tag{2.5}$$

we see that the infinitesimal area element is related to the determinant of the metric:

$$dA = \sqrt{g} du^1 du^2. \tag{2.6}$$

Note that the positions of the metric indices in Eqs. (2.4) and (2.5) indicate covariant components. The contravariant components are given by the inverse metric g^{ij} defined through the inverse basis (see Technical Note 2.2) such that $g_{ij}g^{jk} = \delta_i^k$. By computing the Jacobians, it follows that the metric enables raising and lowering of indices, such as⁴ $g_{ij}V^j \equiv V_i$ or $T_{ijk}g^{j\ell} \equiv T_i{}^\ell{}_k$.

Second fundamental form (extrinsic curvature)

The metric alone is sufficient to describe and calculate distances and *intrinsic* curvature on the 2D surface. However, it makes no reference to the embedding space and therefore cannot describe how the surface curves *extrinsically*. Different surfaces may curve in wildly different ways in the bulk embedding space but nevertheless have identical metrics. For example, the surfaces of a cylinder and a plane are both locally Euclidean and thus share the same “flat” metric, but clearly curve differently in three dimensions.

The metric is constructed out of the local tangent vectors $\mathbf{e}_i = \partial_i \mathbf{X}$ which point in the directions of increasing u^i and characterize the “slope” of the surface at a given point. To further characterize the surface at that point, we might also consider the second derivative $\partial_i \partial_j \mathbf{X} = \partial_i \mathbf{e}_j$ as a measure of the surface’s curvature. Moreover, projecting the quantity onto the normal vector should provide the desired measure of the surface’s extrinsic curvature into the embedding space. Indeed there is another object important enough to warrant the designation *second fundamental form*, defined by⁵

$$K_{ij} = -\hat{\mathbf{n}} \cdot \partial_i \partial_j \mathbf{X} = -\hat{\mathbf{n}} \cdot \partial_j \mathbf{e}_i = \mathbf{e}_i \cdot \partial_j \hat{\mathbf{n}}, \tag{2.7}$$

⁴An explicit example: $\mathbf{V} = V^i \mathbf{e}_i = V^i \delta_i^j \mathbf{e}_j = V^i (g_{ik} g^{kj}) \mathbf{e}_j = (V^i g_{ik}) (g^{kj} \mathbf{e}_j) \equiv V_k \mathbf{e}^k = \mathbf{V}$.

⁵The inclusion of the minus sign is a matter of choice. Here, our convention assigns positive curvature to a sphere with an outward pointing normal vector. That is, the local curvature is positive if the surface bends *away* from the normal.

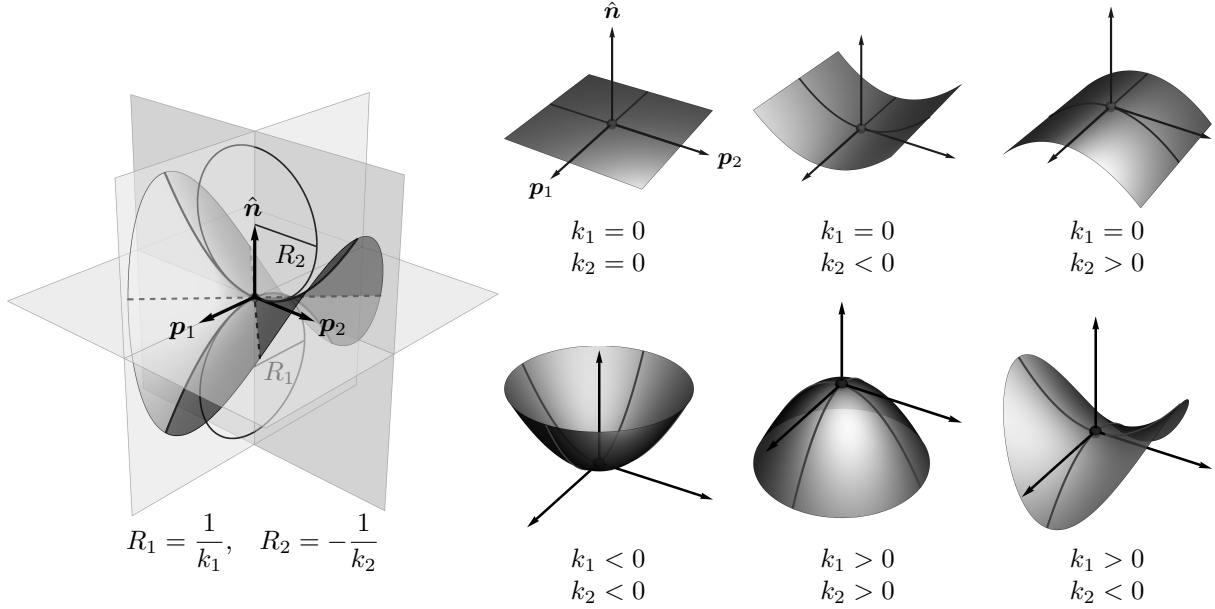


Figure 2.2: Illustration of principal curvatures. The eigenvectors \mathbf{p}_1 and \mathbf{p}_2 of the extrinsic curvature tensor K_{ij} give the *principal directions* over which the local curvature is extremal and, together with $\hat{\mathbf{n}}$, provide a local orthogonal tangent frame. As illustrated in the left figure, the local curvature at each point is characterized by the eigenvalues k_1 and k_2 , or *principal curvatures*, where each curvature k_i is the same as a tangent circle in the \mathbf{p}_i - $\hat{\mathbf{n}}$ plane of radius $R_i = |1/k_i|$. The curvature is positive if the surface curve along the principle direction locally bends away from the normal vector. Various cases are illustrated by the six figures on the right. Note that the top row present surfaces of vanishing Gaussian curvature $K_G = k_1 k_2$. The bottom right surface presents a saddle point, for which k_1 and k_2 differ in sign such that $K_G < 0$. If additionally $k_1 + k_2 = 0$, then we have a special “symmetric” saddle. Surfaces consisting exclusively of symmetric saddles are *minimal surfaces* ($K = 0$).

where the last equality follows by expanding $\partial_i(\mathbf{e}_j \cdot \hat{\mathbf{n}}) = 0$. This object, also appropriately referred to as the *extrinsic curvature tensor*, essentially characterizes the change in the surface normal over different points on the surface. The extrinsic curvature tensor K_{ij} is symmetric, as apparent from the first equality, and thus at every point on the surface can be diagonalized in an *orthogonal* frame. The associated eigenvectors define the *principal directions* over which the curvature is extremal, and their associated eigenvalues are called the *principal curvatures* (see Fig. 2.2).

The principal curvatures also find their way into two scalar invariants of the extrinsic curvature tensor. The first, called the *total extrinsic curvature* is given by the trace of K_{ij} and is hence the sum of the principal curvatures, which we denote as k_1 and k_2 :

$$K := \text{tr } K_{ij} \equiv g^{ij} K_{ij} = K_i^i = k_1 + k_2. \quad (2.8)$$

The second is called the Gaussian curvature, and is given by the determinant of the *matrix*

$K_j^i = g^{ik} K_{kj}$, which is the product of principal curvatures:

$$K_G = \det K_j^i = k_1 k_2. \quad (2.9)$$

Covariant derivatives and intrinsic curvature

Recall that our goal is to create an independent set of RPI *scalars*; any multi-index objects we construct must ultimately be contracted. We can ensure reparametrization invariance as long as these contractions occur only between true vectors and tensors. However, we quickly encounter trouble when attempting to construct important multi-index objects, particularly derivatives, since the measure of distance intervals is itself position dependent. For example, consider a (coordinate-free) vector \mathbf{V} with the expansions $\mathbf{V} = V^i \mathbf{e}_i = V_i \mathbf{e}^i$. By the product rule, and using the component projection $V^i = \mathbf{V} \cdot \mathbf{e}^i$, we observe that the derivative

$$\partial_j V^i = (\partial_j \mathbf{V}) \cdot \mathbf{e}^i + \mathbf{V} \cdot (\partial_j \mathbf{e}^i) \quad (2.10)$$

produces an extra term that depends on how the *coordinates* change with position. Although the components and the basis vectors independently transform as vectors, as does the derivative index of the object $\partial_i \mathbf{V}$ (remember, \mathbf{V} is coordinate-independent), the “moving basis” term spoils the transformation. Indeed, under a coordinate change

$$\partial_j \mathbf{e}^i \rightarrow \tilde{\partial}_j \tilde{\mathbf{e}}^i = \tilde{\partial}_j \left(\frac{\partial \tilde{u}^i}{\partial u^k} \mathbf{e}^k \right) = \frac{\partial u^\ell}{\partial \tilde{u}^j} (\partial_\ell \mathbf{e}^k) \frac{\partial \tilde{u}^i}{\partial u^k} + \frac{\partial u^\ell}{\partial \tilde{u}^j} \left(\frac{\partial^2 \tilde{u}^i}{\partial u^\ell \partial u^k} \right) \mathbf{e}^k. \quad (2.11)$$

The first term transforms properly (a Jacobian for each index), but the second term clearly does not.

To restore reparametrization invariance, we instead define a *covariant derivative* ∇_i such that invariance is again manifest. From Eq. (2.10), it is clear that the quantity $\mathbf{e}^j \cdot \partial_i \mathbf{V}$ has the required properties, so we construct the covariant derivative by simply subtracting off the misbehaving term:

$$\nabla_j V^i := \partial_j V^i + \Gamma_{jk}^i V^k, \quad (2.12)$$

where we have introduced the *Christoffel symbol of the second kind* (or *connection*) Γ_{jk}^i , defined here via $\mathbf{V} \cdot (\partial_j \mathbf{e}^i) \equiv -\Gamma_{jk}^i V^k$ or, equivalently, $\partial_j \mathbf{e}^i \equiv -\Gamma_{jk}^i \mathbf{e}^k$, with the property⁶ $\Gamma_{kj}^i = \Gamma_{jk}^i$. Performing similar calculations shows that the covariant derivative acting on a type (p, q) tensor brings about Christoffel symbols with positive signs for contravariant components and negative signs for covariant components:

$$\begin{aligned} \nabla_k T_{j_1 j_2 \dots j_q}^{i_1 i_2 \dots i_p} &= \partial_k T_{j_1 j_2 \dots j_q}^{i_1 i_2 \dots i_p} + \Gamma_{k\ell}^{i_1} T_{j_1 j_2 \dots j_q}^{\ell i_2 \dots i_p} + \Gamma_{k\ell}^{i_2} T_{j_1 j_2 \dots j_q}^{i_1 \ell \dots i_p} + \dots + \Gamma_{k\ell}^{i_p} T_{j_1 j_2 \dots j_q}^{i_1 i_2 \dots \ell} \\ &\quad - \Gamma_{kj_1}^\ell T_{\ell j_2 \dots j_q}^{i_1 i_2 \dots i_p} - \Gamma_{kj_2}^\ell T_{j_1 \ell \dots j_q}^{i_1 i_2 \dots i_p} - \dots - \Gamma_{kj_q}^\ell T_{j_1 j_2 \dots \ell}^{i_1 i_2 \dots i_p}. \end{aligned} \quad (2.13)$$

⁶This follows from taking the double covariant derivative of a scalar function ϕ and applying the definition (2.12): $\nabla_j \nabla_k \phi = \nabla_j (\partial_k \phi) = \partial_j \partial_k \phi - \Gamma_{jk}^i \partial_i \phi$. The symmetry of the derivatives therefore implies the symmetry of the lower indices.

The covariant derivative enjoys several useful properties, the first of which is that it is *metric compatible*:

$$\nabla_k g_{ij} = 0, \quad \nabla_k g^{ij} = 0, \quad \text{and} \quad \nabla_k g = 0, \quad (2.14)$$

which can be derived by expressing $g_{ij} = \mathbf{e}_i \cdot \mathbf{e}_j$ and applying $\partial_j \mathbf{e}^i = -\Gamma_{jk}^i \mathbf{e}^k$. This implies that the covariant derivative commutes with the metric and, hence, commutes with raising and lowering indices. These, together with the index symmetry of Γ_{ij}^k , also allow us to write the Christoffel symbol explicitly in terms of the metric:

$$\Gamma_{ij}^k = \frac{1}{2} g^{k\ell} (\partial_i g_{j\ell} + \partial_j g_{\ell i} - \partial_\ell g_{ij}). \quad (2.15)$$

Additionally, by virtue of the curvilinear coordinates, the covariant derivatives do not commute in general,⁷ but their commutator on vector components provides information about the surface's *intrinsic* curvature:

$$[\nabla_i, \nabla_j] V_k \equiv (\nabla_i \nabla_j - \nabla_j \nabla_i) V_k =: R_{ijk\ell} V^\ell, \quad (2.16)$$

where $R_{ijk\ell}$ is the *Riemann curvature tensor*.⁸

The *named* equations and the *Theorema Egregium*

The tools thus far now allow us to begin relating key quantities to one another. The following results are of particular importance, as signified by their appellations. First, by rewriting Eq. (2.7) so that $K_{ij} = K_i^k g_{kj} = (K_i^k \mathbf{e}_k) \cdot \mathbf{e}_j$ and using $\nabla_i \hat{\mathbf{n}} = \partial_i \hat{\mathbf{n}}$, one finds

$$\nabla_i \hat{\mathbf{n}} = K_i^j \mathbf{e}_j. \quad \text{Weingarten} \quad (2.17)$$

Similarly, one can obtain

$$\nabla_i \mathbf{e}_j = -K_{ij} \hat{\mathbf{n}}. \quad \text{Gauss} \quad (2.18)$$

Furthermore, from the *integrability condition* $\partial_i \partial_j \mathbf{e}_k = \partial_j \partial_i \mathbf{e}_k$ follow two additional equations. Namely, expanding the above condition and collecting the components in the $\hat{\mathbf{n}}$ direction gives

$$\nabla_i K_{jk} - \nabla_j K_{ik} = 0, \quad \text{Codazzi–Mainardi} \quad (2.19)$$

whereas the tangential component yields

$$K_{ik} K_{j\ell} - K_{i\ell} K_{jk} = R_{ijk\ell}. \quad \text{Gauss} \quad (2.20)$$

Note that the final equation also provides us with an explicit representation of the Riemann

⁷They do, however, *always* commute when acting on scalars since $\nabla_i \phi \equiv \partial_i \phi$.

⁸Note that since ∇_i and V_k both transform properly as vectors, $R_{ijk\ell}$ is also a proper tensor.

tensor in terms of Christoffel symbols,

$$R_{ijkl} = \partial_k \Gamma_{jli} - \partial_\ell \Gamma_{jki} + \Gamma_{jk}^m \Gamma_{ilm} - \Gamma_{jl}^m \Gamma_{ikm}. \quad (2.21)$$

Equation (2.20) is perhaps the most important of the above four named equations, quietly revealing a deep mathematical truth. The Riemann tensor R_{ijkl} , by way of the Christoffel representation above, is seen to be to be completely determined by the induced metric. That is, it is an *intrinsic* quantity that is invariant under isometric deformations—bending without stretching—and, moreover, independent of any embedding. On the other hand, the curvature tensor K_{ij} is by definition *extrinsic* since it references the ambient embedding space (\mathbb{R}^3) via \hat{n} . Yet, there is a direct relationship between the two. A perhaps more remarkable finding appears once we begin contracting the indices of R_{ijkl} . First, we construct the Ricci tensor,

$$R_{k\ell} := g^{ik} R_{ijkl} = K K_{j\ell} - K_{ji} K_\ell^i. \quad (2.22)$$

Then, performing the remaining trace give the Ricci scalar,

$$\mathcal{R} := g^{j\ell} R_{j\ell} = K^2 - K_i^j K_j^i = 2K_G, \quad (2.23)$$

where we have recognized the middle combination as the determinant of K_i^j , and thus as the Gaussian curvature. Hence, we arrive at the remarkable conclusion that the Gaussian curvature, originally defined via extrinsic quantities, is revealed to be entirely *intrinsic*. This is Gauss’s *Theorema Egregium*.

Finally, there is an additional simplification worth noting that is particular to two-dimensions. Namely,

$$R_{ijkl} = K_G (g_{ik} g_{j\ell} - g_{i\ell} g_{jk}), \quad (2.24)$$

$$R_{ij} = \frac{1}{2} \mathcal{R} g_{ij} = K_G g_{ij}, \quad (2.25)$$

showing that the Gaussian curvature is in fact the only independent component of the Riemann tensor.⁹

Monge gauge

At this point, we have determined all that is needed to construct an effective theory of fluctuating surfaces. However, before proceeding we must discuss a particular surface parametrization that we will use heavily throughout this thesis. The most common manifestation of a surface we will encounter will be that which only deviates and deforms weakly—with no overhangs or bubbles—about a flat plane. In this case, it suffices to

⁹In general relativity, the quantity $G_{\mu\nu} := R_{\mu\nu} - \frac{1}{2} \mathcal{R} g_{\mu\nu}$, known as the *Einstein tensor*, is identified as proportional to the energy–momentum tensor $T_{\mu\nu}$. In two dimensions, $G_{\mu\nu} \equiv 0$ as per Eq. (2.25). In this sense, 2D gravity—or or rather (1 + 1)D gravity—is often referred to as “trivial.”

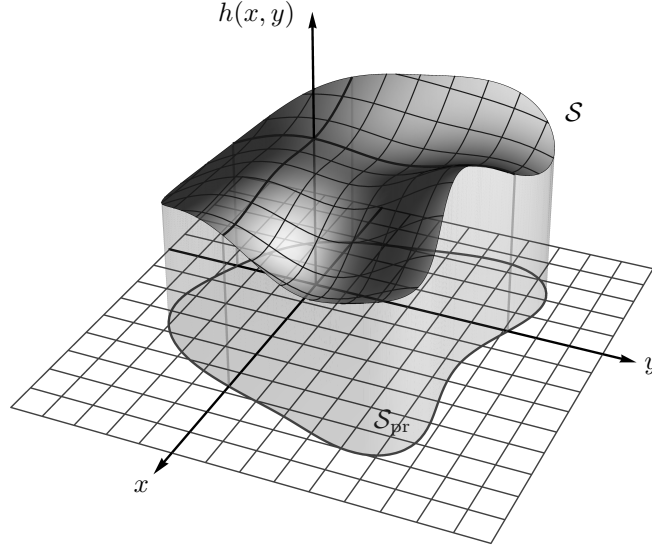


Figure 2.3: A surface \mathcal{S} parametrized in the Monge gauge. The embedding $\mathbf{X} : \mathcal{S}_{\text{pr}} \rightarrow \mathcal{S}$ describes each point on the surface by its height $h(x, y)$ above the point (x, y) in the base plane $\mathcal{S}_{\text{pr}} \subset \mathbb{R}^2$.

describe the surface by a height profile $h(x, y)$ above some flat reference plane parametrized by x and y .

In this so-called *Monge gauge*, illustrated in Fig. 2.3, we express each point \mathbf{X} on the surface \mathcal{S} by the embedding graph $\mathbf{X} = \mathbf{X}(x, y) := (x, y, h(x, y))$, where the coordinates (x, y) lie within the region $\mathcal{S}_{\text{pr}} \subset \mathbb{R}^2$ defined by the projection of the surface onto the reference base plane. It is straightforward to see that in this parametrization, or *gauge*, the local tangent vectors are given by $\mathbf{e}_x = (1, 0, \partial_x h)$ and $\mathbf{e}_y = (0, 1, \partial_y h)$, and hence the metric is

$$g_{ij} = \delta_{ij} + \partial_i h \partial_j h = \begin{pmatrix} 1 + (\partial_x h)^2 & \partial_x h \partial_y h \\ \partial_x h \partial_y h & 1 + (\partial_y h)^2 \end{pmatrix}. \quad (2.26)$$

Accordingly, the metric determinant and invariant area element are given respectively by

$$g = \det g_{ij} = 1 + (\nabla h)^2, \quad (2.27)$$

$$dA = \sqrt{1 + (\nabla h)^2} dx dy, \quad (2.28)$$

where $\nabla \equiv (\partial_x, \partial_y)$ is the usual gradient operator in Euclidean space (\mathbb{R}^2). Continuing along, we apply Eq. (2.3) with Eq. (2.5) to give the normal vector,

$$\hat{\mathbf{n}} = \frac{\mathbf{e}_x \times \mathbf{e}_y}{\sqrt{g}} = \frac{-\nabla h + \hat{\mathbf{e}}_z}{\sqrt{1 + (\nabla h)^2}}, \quad (2.29)$$

which generates the curvature tensor via Eq. (2.7):

$$K_{ij} = -\frac{\partial_i \partial_j h}{\sqrt{1 + (\nabla h)^2}}. \quad (2.30)$$

Finally, we take the trace and determinant to obtain the total extrinsic and Gaussian curvatures respectively,

$$K = -\nabla \cdot \left(\frac{\nabla h}{\sqrt{1 + (\nabla h)^2}} \right), \quad (2.31)$$

$$K_G = \frac{\det[\partial_i \partial_j h]}{[1 + (\nabla h)^2]^2}. \quad (2.32)$$

If the surface deformations are sufficiently weak, meaning that the surface gradients $|\nabla h| \ll 1$, then we may expand and truncate the above equations in small gradients. In this *linearized Monge gauge*—which will prove valid in many of our applications—the determinant factor in the area element becomes a squared gradient,

$$\sqrt{g} \approx 1 + \frac{1}{2}(\nabla h)^2, \quad (2.33a)$$

and the curvatures reduce to

$$K \approx -\text{tr}[\partial_i \partial_j h] = -\nabla^2 h, \quad (2.33b)$$

$$K_G \approx \det[\partial_i \partial_j h]. \quad (2.33c)$$

2.3 Helfrich theory

As we mentioned early on, at the mesoscopic scale much of the local, microscopic physics disentangles from the aggregate behavior of the whole surface or membrane. The physical and chemical confluence of interactions among the constituents that make up the surface are not always resolvable, nor do their microscopic descriptions necessarily provide useful information or insight into the larger-scale collective phenomena. Instead, their collective effects dictate the emergence of patterns and structure, and ultimately determine the values of the associated—and more universal—material parameters. From this perspective, and in the spirit of the previous chapter, we will study the fluctuating surface system from the top down rather than bottom up. That is, we will attempt from the beginning to capture emergent properties from phenomenological considerations and symmetry principles. A particularly insightful construction that adheres to this philosophy is provided by Deserno in Ref. [Des15], which we will follow closely.

We begin with a reminder of our primary physical consideration: Fluidity of the surface implies that its energetic description cannot depend on internal degrees of freedom and, moreover, that the surface cannot retain memory of previous shape configurations. The corresponding mathematical statement is that the surface's (free) energy must be invariant

under reparametrizations (diffeomorphisms) of its internal coordinates and, furthermore, depend only on the current geometry. Hence, our challenge is to construct an effective energy functional that consists of only geometric invariants.

Luckily, in the previous section we discovered that all RPI scalars can be constructed out of combinations and of the total extrinsic curvature K , the (intrinsic) Gaussian curvature K_G , and covariant derivatives ∇_i acting on the two curvatures. However, to determine the relevancy of any given combination, we also need account for dimensionality and scaling. From the definitions (2.7), (2.8), and (2.9), it is clear that the two curvatures scale as $[K] \sim L^{-1}$ and $[K_G] \sim L^{-2}$. Additionally, each additional derivative contributes another factor of L^{-1} . We make the assumption that the curvatures, and by extension the derivatives of the curvatures, are small so that the length scales over which the surface varies are relatively large. In this sense, we may construct an energy functional as a power series in inverse length. As per the EFT formalism (see for instance Section 1.2), this series is to be constructed from a complete “operator basis” in which redundancies are eliminated. Since many terms that can be constructed from K , K_G , and their (covariant) derivatives are related or equivalent up to boundary terms via integration by parts, the challenge is to first find a complete, *independent* set of scalars. Such a task has been completed by Capovilla *et al.* [CGS03] up to L^{-4} (where they use \mathcal{R} instead of K_G), and hence the most general effective Hamiltonian for a surface \mathcal{S} follows as [Des15]

$$\begin{aligned} \mathcal{H}[\mathcal{S}] = \int_{\mathcal{S}} dA \Big\{ & C^{(0)} + C^{(1)}K + C_1^{(2)}K^2 + C_2^{(2)}K_G + C_1^{(3)}K^3 + C_2^{(3)}KK_G \\ & + C_1^{(4)}K^4 + C_2^{(4)}K^2K_G + C_3^{(4)}K_G^2 + C_4^{(4)}(\nabla_i K)(\nabla^i K) + \mathcal{O}(L^{-5}) \Big\}, \end{aligned} \quad (2.34)$$

where the index n in each coefficient $C^{(n)}$ indicates the term’s overall scaling L^{-n} .

Note that since the area element also introduces a scaling factor L^2 , the first energy term will also scale as $\sim L^2$ and is therefore very relevant. Similarly, the second energy term will scale as $\sim L$, but the next two are *marginal* ($\sim L^0$). Higher-order energy terms scale as higher powers of inverse length, so they become less relevant under coarse graining so they may be neglected to good approximation. Finally, we make one further alteration by relabeling the coefficients via

$$\begin{aligned} C^{(0)} &= \sigma + \frac{1}{2}\kappa K_0^2 & C^{(1)} &= -\kappa K_0 \\ C_1^{(2)} &= \frac{1}{2}\kappa & C_2^{(2)} &= \bar{\kappa}, \end{aligned} \quad (2.35)$$

which puts the functional into the form of the celebrated Helfrich Hamiltonian [Hel73],

$$\mathcal{H}[\mathcal{S}] = \int_{\mathcal{S}} dA \left[\sigma + \frac{\kappa}{2}(K - K_0)^2 + \bar{\kappa}K_G \right], \quad (2.36)$$

where σ is the *surface tension*, K_0 is the *spontaneous curvature*, and the two curvature

moduli κ and $\bar{\kappa}$ are known respectively as the *bending rigidity* and the *Gaussian modulus* (or *saddle splay modulus*).

Surface tension. The first phenomenological parameter σ in the Helfrich Hamiltonian is the *surface tension* and characterizes the dominant free-energy cost per area of creating the fluid surface or interface. The natural interpretation of σ is a (constant) material parameter conjugate to the area, as is appropriate for fluid–fluid interfaces, but it may alternatively be interpreted as a Lagrange multiplier fixing the total area (*i.e.*, a type of boundary condition). The proper interpretation for fluid lipid membranes is more subtle, depending on, for example, whether the area per lipid is held fixed, and does not necessarily correspond the expansion modulus of the membrane (see Refs. [Des15] and [Saf94, Ch. 6]).

Spontaneous curvature. The second parameter K_0 is the *spontaneous curvature* and, as its name suggests, it indicates a preferred global curvature of the surface and breaks the $\hat{n} \rightarrow -\hat{n}$ symmetry that would be required for a surface with indistinguishable sides. This could arise, for example, from an unbalanced curvature tendency between lipid bilayer leaflets, or adsorption of flexible polymers on one side. Note also that, as per $C^{(0)}$ in Eq. (2.35), K_0 further contributes a “spontaneous tension” [Lip13, Lip14].

Curvature moduli. The remaining curvature terms are multiplied by the *bending rigidity* κ and the *Gaussian curvature modulus* $\bar{\kappa}$ (also referred to as the *saddle splay modulus*). These two curvature moduli are not entirely independent, as the positive definiteness of the energy functional requires the inequality $-2\kappa \leq \bar{\kappa} \leq 0$ to hold [Des15].¹⁰ The bending rigidity characterizes the energy penalty for deviations from the preferred curvature K_0 . Similarly, $\bar{\kappa}$ characterizes the energy cost of nonzero Gaussian curvature. However, the term involving the Gaussian curvature, by virtue of the Gauss–Bonnet theorem (see Technical Note 2.3) actually integrates to a topological invariant and a boundary term and, except for extreme events such membrane fission and fusion, is typically a constant and thus has no influence.

Variations and the shape equation

A functional variation of the Helfrich Hamiltonian (2.36) leads to the associated Euler–Lagrange equation, or *shape equation*, whose solutions describe the ground state (zero undulations) surface shapes. The variation is performed as an infinitesimal change in the embedding function,

$$\mathbf{X} \rightarrow \mathbf{X} + \delta\mathbf{X}, \quad (2.37)$$

where the variation $\delta\mathbf{X}$ can be decomposed into components normal and tangential to the surface:

$$\delta\mathbf{X} = \nu\hat{n} + \varepsilon^i\mathbf{e}_i. \quad (2.38)$$

¹⁰This argument is also presented by Safran [Saf94, §6.3], but his final result is incorrect.

Technical Note 2.3: Gauss–Bonnet theorem

The Gauss–Bonnet theorem states that for a multiply connected surface patch \mathcal{S} with boundaries $\partial\mathcal{S}$,

$$\int_{\mathcal{S}} dA K_G = 2\pi\chi(\mathcal{S}) - \oint_{\partial\mathcal{S}} dA k_g,$$

where K_G is the Gaussian curvature, k_g is the *geodesic curvature* of the boundary curves $\partial\mathcal{S}$, and $\chi(\mathcal{S})$ is the *Euler characteristic* of the surface patch [Spi75, Kok06]. The Euler characteristic $\chi(\mathcal{S}) = 2 - 2g(\mathcal{S})$ is a topological invariant, depending only on the genus $g(\mathcal{S})$ (number of “handles”) of the surface patch. The geodesic curvature k_g of a point on the boundary curve $\partial\mathcal{S}$ is defined as the curvature of $\partial\mathcal{S}$ as projected onto the surface’s tangent plane at that point. It essentially quantifies how far off the curve is from a *geodesic*—the generalization of a straight line on a curved surface. In this thesis, we will only consider surfaces with fixed topology and, furthermore, with boundaries that are either rigid or infinitely far away. Under these circumstances, the integral over the Gaussian curvature is constant and thus has no influence over the surface energetics.

To first order, the tangential variation is equivalent to a reparametrization of the surface’s local coordinates, which we have already required to be a manifest symmetry. That is, the tangential variation will provide no additional information regarding the bulk of the surface; however, its inclusion will generate boundary terms (if there exists surface boundaries) and thus provide information regarding natural boundary conditions. The normal component, on the other hand, is a more useful variation.

In many cases, for instance when dealing with vesicles, one might also include a Lagrange multiplier term $-PV$ to fix the volume, similar to how σ can be interpreted as fixing the area. With this term included, one may perform the rather tedious process of passing the variation through the various scalars, and ultimately arrive at the fourth-order nonlinear partial differential *shape equation* [ZcH89, CGS03, Des15]

$$\kappa \left\{ -\Delta K + \frac{1}{2}(K - K_0)[(K - K_0)K - 2K(K - 2K_G)] \right\} + \sigma K = P, \quad (2.39)$$

where $\Delta \equiv \nabla^i \nabla_i$ is the covariant Laplace operator. Uncovering the subtle physics hidden in the shape equation has been a major research thrust for many years [Lip91, Sei97, OYLXYZ99]. Note that the “brute force” approach to the surface variation is not the only route to the shape equation. An alternative is to enforce all the geometric constraints by a set of Lagrange multiplier terms \mathcal{H}_c [Guv04],

$$\begin{aligned} \mathcal{H}_c = \int_{\mathcal{S}} dA \Big[& \mathbf{f}^i \cdot (\mathbf{e}_i - \nabla_i \mathbf{X}) + \lambda_{\perp}^i (\mathbf{e}_i \cdot \hat{\mathbf{n}}) + \lambda_n (\hat{\mathbf{n}}^2 - 1) \\ & + \lambda^{ij} (g_{ij} - \mathbf{e}_i \cdot \mathbf{e}_j) + \Lambda^{ij} (K_{ij} - \mathbf{e}_i \cdot \nabla_j \hat{\mathbf{n}}) \Big], \end{aligned} \quad (2.40)$$

so that all quantities can be varied independently. This leads to the elegant stress and torque tensor formalism [Guv04, Mül07, Des15].

2.4 Fluctuating surfaces

For fluid surfaces in the zero temperature limit, the equilibrium surface shapes are governed by the shape equation (2.39). At finite temperature, however, the fluid surface can exchange energy with its environment and therefore explore a larger configuration space that includes more energetically costly deformations. The statistical properties of a fluctuating fluid surface at thermodynamic equilibrium is encoded in the partition function which is given *formally* by the sum over all spatial configurations \mathcal{S} of the surface:

$$Z = \sum_{\mathcal{S}} e^{-\beta \mathcal{H}[\mathcal{S}]}, \quad (2.41)$$

where $\beta = 1/k_B T$ as usual. Although we spent effort constructing the surface Hamiltonian to be coordinate-free, to actually perform the partition sum we must choose a parametrization. Note, however, that any given surface configuration possesses several (*infinitely* many) possible parametrizations, and a naïve sum over all possible surfaces would be (infinitely) redundant and problematic. Therefore we must instead ensure that the sum only runs over all possible *distinct* surfaces. To do so, we re-express the partition sum as a functional integral over surface embeddings,

$$Z = \mathcal{N} \int \mathcal{D}[\mathbf{X}] e^{-\beta \mathcal{H}[\mathbf{X}]}, \quad (2.42)$$

where \mathcal{N} is some normalization, and place restrictions on the *functional measure* $\mathcal{D}[\mathbf{X}]$.

Gauge fixing and the functional measure

The functional measure should satisfy a few natural conditions, the first being reparametrization invariance. We also require that it be local (*i.e.*, widely separated deformations should be independent), for otherwise, large-distance correlations would necessitate the inclusion of additional degrees of freedom and would therefore correspond to a different physical problem [Dav]. Furthermore, there must be a short-distance cutoff to account for the breakdown of the geometric continuum theory at small scales. Finally, we have the above-mentioned requirement that only distinct surfaces be considered.

To handle the latter condition, we follow the same approach as used in the functional quantization of gauge theories [Dav, IZ05]: Treat the measure $\mathcal{D}[\mathbf{X}]$ as reparametrization invariant and sum over *all* configurations. Pick out a “gauge slice” through some *gauge-fixing condition* and transform the partition sum as an integral over the gauge slice in which each representative configuration is weighted by the volume of its equivalence class.

Throughout the remainder of this thesis, we will work in the Monge gauge, which is a special case of the slightly more general *normal gauge* [CLNP94, Dav] in which surface configurations $\mathbf{X}(u)$ are expressed as deviations from some *fixed* reference surface $\mathbf{X}_0(u)$:

$$\mathbf{X}(u) = \mathbf{X}_0(u) + h(u) \hat{\mathbf{n}}_0(u), \quad (2.43)$$

where $u \equiv (u^1, u^2)$ are the local coordinates of the reference surface. The corresponding gauge-fixing condition is expressed as

$$F_i(\mathbf{X}(u)) = \mathbf{e}_{i,0}(u) \cdot [\mathbf{X}(u) - \mathbf{X}_0(u)]. \quad (2.44)$$

To enforce reparametrization invariance, we note that the *infinitesimal* change of coordinates $u^i \rightarrow \tilde{u}^i = u^i + \varepsilon^i(u)$ has the effect of translating $\mathbf{X}(u)$ tangentially along the surface,

$$\mathbf{X}(u) \rightarrow \mathbf{X}_\varepsilon(u) = \mathbf{X}(u) + \varepsilon^i(u) \partial_i \mathbf{X}(u) = \mathbf{X}(u) + \varepsilon^i(u) \mathbf{e}_i(u). \quad (2.45)$$

This change, however, is simply a reordering of points along the surface without changing the shape (a diffeomorphism) and, hence, should not be counted separately.

The infinitesimal vectors $\varepsilon^i(u)$ are the generators of diffeomorphisms and therefore characterize the equivalence class of our chosen gauge slice. The (infinite) “volume” of this equivalence class can be expressed formally as

$$V_{\text{Diff}} = \int \mathcal{D}[\varepsilon] \equiv \int \left(\prod_u \sqrt{g(u)} \, d^2 \varepsilon(u) \right), \quad (2.46)$$

where the appearance of $\sqrt{g(u)}$ ensures the covariance of the measure, and the product is thought of as being taken over a grid of mass points on the surface such that each grid cell size occupies equal area in the bulk 3D space. Note that the grid cells in *coordinate space* are not generally going to be of equal area. We will return to this complication shortly. In what follows, we will let the u dependence of each term be implied without always explicitly notating it.

With the above details in place, we may now carry out the gauge-fixing procedure. Following Cai *et al.* [CLNP94], we define the *Faddeev-Popov determinant* $\mathcal{J}_f[\mathbf{X}]$ as the formal resolution of the identity:

$$1 \equiv \mathcal{J}_f[\mathbf{X}] \int \mathcal{D}[\varepsilon] \delta[F_i(\mathbf{X}_\varepsilon)], \quad \mathcal{J}_f[\mathbf{X}] = \det \left(\left. \frac{\delta F_i(\mathbf{X}_\varepsilon)}{\delta \varepsilon^j} \right|_{\varepsilon=0} \right), \quad (2.47)$$

where the delta functional enforces the gauge constraint.¹¹ We now plug this into the functional integral (2.42) and find

$$\begin{aligned} Z &= \mathcal{N} \int \mathcal{D}[\varepsilon] \int \mathcal{D}[\mathbf{X}] e^{-\beta \mathcal{H}[\mathbf{X}]} \mathcal{J}_f[\mathbf{X}] \delta[F_i(\mathbf{X}_\varepsilon)] \\ &= \left(\mathcal{N} \int \mathcal{D}[\varepsilon] \right) \int \mathcal{D}[\mathbf{X}] e^{-\beta \mathcal{H}[\mathbf{X}]} \mathcal{J}_f[\mathbf{X}] \delta[F_i(\mathbf{X})] \\ &= N \int \mathcal{D}[\mathbf{X}] e^{-\beta \mathcal{H}[\mathbf{X}]} \mathcal{J}_f[\mathbf{X}] \delta[F_i(\mathbf{X}_\varepsilon)]. \end{aligned} \quad (2.48)$$

¹¹The idea here is to generalize the familiar 1D identity $1 = |f'(x_0)| \int dx \delta(f(x))$, where $f(x_0) = 0$.

Between the first and second lines, we used the reparametrization invariance of the measure, Hamiltonian, and determinant and transformed $\mathbf{X} \rightarrow \mathbf{X}_\varepsilon$. Since all the functional arguments are dummy variables with respect to the functional integration, we then simply relabeled back to \mathbf{X} . The third line follows from Eq. (2.46) and absorbing the constant volume into the normalization.

Instead of attempting to directly compute the functional determinant of Eq. (2.47), we may instead employ Eq. (2.46) and use the composition property of the delta function:

$$\frac{1}{\mathcal{J}_f[\mathbf{X}]} = \int \left(\prod_u \sqrt{g} \, d^2\varepsilon \right) \delta[F_i(\mathbf{X}_\varepsilon)] = \int \left(\prod_u \sqrt{g} \, d^2\varepsilon \right) \frac{\delta^{(2)}(\varepsilon)}{\det(J_{ij})}, \quad (2.49)$$

where J_{ij} is the Jacobian in the normal gauge,

$$J_{ij} = \left. \frac{\partial F_i(\mathbf{X}_\varepsilon)}{\partial \varepsilon^j} \right|_{\varepsilon=0} = \mathbf{e}_{i,0} \cdot \mathbf{e}_j. \quad (2.50)$$

The Faddeev–Popov determinant is therefore

$$\mathcal{J}_f[\mathbf{X}] = \prod_u \frac{\det(\mathbf{e}_{i,0} \cdot \mathbf{e}_j)}{\sqrt{g}}. \quad (2.51)$$

Finally, we wish to integrate out components tangential to the surface and leave the partition sum as a functional integral over only the height function $h(u)$. To this aim, we express an arbitrary point \mathbf{X} from the reference surface as

$$\mathbf{X}(u) = \mathbf{X}_0(u) + h(u)\hat{\mathbf{n}}_0(u) + v^i(u)\mathbf{e}_{i,0}(u), \quad (2.52)$$

where v^i is a tangential *displacement* and not a reparametrization. In this case, the gauge constraint (2.44) becomes $F_i(\mathbf{X}) = \mathbf{e}_{i,0} \cdot \mathbf{e}_{j,0} v^j = 0$. Similar to Eq. (2.46), we use the reference metric to enforce the covariance of the measure $\mathcal{D}[\mathbf{X}]$. Applying it to Eq. (2.48) results in

$$\begin{aligned} Z &= N \int \left(\prod_u \sqrt{g_0} \, d^2v \, dh \right) \mathcal{J}_f[\mathbf{X}] \delta[\mathbf{e}_{i,0} \cdot \mathbf{e}_{j,0} v^j] e^{-\beta \mathcal{H}[\mathbf{X}]} \\ &= N \int \left(\prod_u \sqrt{g_0} \, d^2v \, dh \right) \left(\prod_{u'} \frac{\det(\mathbf{e}_{i,0} \cdot \mathbf{e}_j)}{\sqrt{g}} \right) \frac{\delta^{(2)}(v)}{\det(\mathbf{e}_{i,0} \cdot \mathbf{e}_{j,0})} e^{-\beta \mathcal{H}[h]} \\ &= \int \left(N \prod_u dh \right) \left(\prod_{u'} \hat{\mathbf{n}} \cdot \hat{\mathbf{n}}_0 \right) e^{-\beta \mathcal{H}[h]}, \\ &= \int \mathcal{D}h \left(\prod_u \hat{\mathbf{n}} \cdot \hat{\mathbf{n}}_0 \right) e^{-\beta \mathcal{H}[h]}, \end{aligned} \quad (2.53)$$

where we used $\det(\mathbf{e}_{i,0} \cdot \mathbf{e}_j) = (\mathbf{e}_{1,0} \times \mathbf{e}_{2,0}) \cdot (\mathbf{e}_1 \times \mathbf{e}_2) = \sqrt{g_0} \hat{\mathbf{n}}_0 \cdot \sqrt{g} \hat{\mathbf{n}}$. Note that in the Monge gauge, $\hat{\mathbf{n}}_0 = \hat{\mathbf{e}}_z$ so the corresponding measure factor is $\hat{\mathbf{n}} \cdot \hat{\mathbf{n}}_0 = g^{-1/2}$.

An additional measure factor

The Faddeev–Popov contribution can alternatively be expressed as an energetic contribution to the Hamiltonian via $\prod_u g^{-1/2}(u) = e^{-\beta \mathcal{H}_{\text{FP}}}$, where

$$\mathcal{H}_{\text{FP}} = \frac{1}{2\beta} \sum_u \ln g(u) \quad (2.54)$$

and the sum is assumed to be taken over surface grid cells with equal area in the embedding space. However, in normal gauges the physical surface area is generally larger than the surface area of the reference, unless the two coincide. Hence, the grid of the reference surface must change as the physical surface fluctuates so as to maintain fixed grid cell area of the physical surface. Alternatively, if we were to compensate for the fluctuating grid cell area, we could fix the reference grid. This is often more desirable, since a fixed grid allows for efficient calculational techniques such as Fourier transforms. One accounts for the missing reference area by including an additional measure factor $e^{-\beta \Delta \mathcal{H}}$, which is analogous to the Liouville correction in string theory [För86, Dav88, DK89, CLNP94].

It is worth emphasizing that fixing the reference grid essentially amounts to *integrating out* the local fluctuating degrees of freedom. This is reminiscent of the previous chapter in which we “integrated out” the local degrees of freedom at the boundary of a conductor by subsuming their effects as a correction ΔU to the conductor-free energy functional. From the EFT perspective, we (further) coarse grain the description of a fluctuating surface by writing the energy functional with respect to a fixed reference grid and account for the fluctuation contribution *of the grid* through the correction $\Delta \mathcal{H}$. The functional form of $\Delta \mathcal{H}$ can be constructed via symmetry arguments, and the concomitant Wilson coefficients may be matched via appropriate renormalization conditions. Indeed, this is the essence of how the measure correction was dealt with in Ref. [CLNP94].

2.4.1 Harmonic approximation

As we alluded to previously, we will primarily work in the linearized Monge gauge, in which the energy is truncated to leading order in a small-gradient expansion. Since we will consider fluctuations about a flat surface, the spontaneous curvature $K_0 = 0$. Furthermore, we do not wish to consider topological changes, so the Gaussian curvature term can be ignored. With this specialization in mind, and taking $(x, y, h(x, y)) \equiv (\mathbf{x}, h(\mathbf{x}))$, we apply the small gradient expansion via Eqs. (2.33) to put the Helfrich Hamiltonian (2.36) into the form

$$\mathcal{H}_0[h] = \sigma A + \frac{1}{2} \int d^2x [\sigma (\nabla h)^2 + \kappa (\nabla^2 h)^2], \quad (2.55)$$

where A is the area of the reference plane. We will refer to the above form as the *harmonic approximation* since, similar to a harmonic oscillator, the energy is quadratic in h . This form allows for a rather simple treatment of thermal fluctuations, as we shall see.

To begin, we first make a few observations about the functional (2.55). First, what one measures should actually be the energy difference $E[h] := \mathcal{H}_0[h] - \sigma A$ from the flat configuration. Second, the functional enjoys both rotational symmetry in the plane and translation symmetry in the vertical direction. This latter symmetry, $h \rightarrow h + \text{const.}$, is of particular importance. In particular, by choosing the position of the base plane, we technically break the (continuous) translation symmetry. However, the residual symmetry inherent in Eq. (2.55) indicates that long-wavelength fluctuations will cost vanishingly small energy and hence may build up without bound and potentially spoil long-range order (*i.e.*, flatness).

To study the effects of thermal fluctuations, it helps to first put the energy into a more convenient form. Assume for a moment that the base plane spans a frame of size $L \times L$ and, for convenience, that the boundaries are periodic. Following Ref. [Des], we decompose the height function as a sum over Fourier modes:

$$h(\mathbf{x}) = \sum_{\mathbf{q}} h_{\mathbf{q}} e^{i\mathbf{q} \cdot \mathbf{x}}, \quad \mathbf{q} = \frac{2\pi}{L} \begin{pmatrix} n_x \\ n_y \end{pmatrix} \quad (2.56)$$

for integers n_x and n_y . The complex basis satisfies the completeness relation

$$\int d^2x e^{-i(\mathbf{q}-\mathbf{q}') \cdot \mathbf{x}} = L^2 \delta_{\mathbf{q}, \mathbf{q}'}. \quad (2.57)$$

As usual, since $h(\mathbf{x})$ is real, it follows that $h_{-\mathbf{q}} = h_{\mathbf{q}}^*$.

We now apply the Fourier transform to the energy functional. The various derivatives simply bring down factors of \mathbf{q} via $\nabla(e^{i\mathbf{q} \cdot \mathbf{x}}) = i\mathbf{q} e^{i\mathbf{q} \cdot \mathbf{x}}$. After recognizing that the spatial integral produces $\delta_{\mathbf{q}, -\mathbf{q}'}$ by the completeness relation, we ultimately find that the energy decouples into a sum over modes,

$$E = \frac{L^2}{2} \sum_{\mathbf{q}} |h_{\mathbf{q}}|^2 (\sigma q^2 + \kappa q^4) =: \sum_{\mathbf{q}} E_{\mathbf{q}}. \quad (2.58)$$

This means each fluctuating degree of freedom may be treated independently. In particular, the equipartition theorem informs us that the energy of each *harmonic* mode $\langle E_{\mathbf{q}} \rangle = k_B T/2$. We solve for the fluctuation spectrum by rearrangement, giving

$$\langle |h_{\mathbf{q}}|^2 \rangle = \frac{k_B T}{L^2 (\sigma q^2 + \kappa q^4)}. \quad (2.59)$$

Amplitude of fluctuations. Equipped with the fluctuation spectrum (2.59), we may now quantify global fluctuation properties of the surface. First, on a mode per mode basis,

Eq. (2.59) informs us that the quantity $\sqrt{\sigma/\kappa} =: q_c$ defines a crossover wave vector such that modes $q \ll q_c$ are dominated by surface tension and modes $q \gg q_c$ are dominated by bending energy. From a real-space perspective, the quantity $L_c := \sqrt{\kappa/\sigma}$ defines a crossover length scale. Length scales smaller than L_c (large q) are dominated by bending energy, whereas larger length scales (small q) are dominated by tension. We will consider surfaces in these three limits: (i) general (finite σ and κ), (ii) tension dominated ($\kappa \rightarrow 0$), which is applicable to capillary-type surfaces,¹² and (iii) bending-dominated ($\sigma \rightarrow 0$), which applies to typical fluid lipid membranes.

Let us now compute the average fluctuation amplitude across the entire surface. The expectation value has two ingredients: the positional average within each configuration, and the thermal average over all permissible configurations. The in-plane positional average per configuration is the straightforward weighted integral

$$\overline{h^2} := \frac{1}{L^2} \int d^2x h^2(\mathbf{x}). \quad (2.60)$$

It has the Fourier expansion

$$\overline{h^2} = \frac{1}{L^2} \int d^2x \sum_{\mathbf{q}, \mathbf{q}'} h_{\mathbf{q}} h_{\mathbf{q}'} e^{i(\mathbf{q}+\mathbf{q}') \cdot \mathbf{x}} = \frac{1}{L^2} \sum_{\mathbf{q}, \mathbf{q}'} h_{\mathbf{q}} h_{\mathbf{q}'} L^2 \delta_{\mathbf{q}, -\mathbf{q}} = \sum_{\mathbf{q}} |h_{\mathbf{q}}|^2, \quad (2.61)$$

where we have again applied the completeness relation (2.57). Notice that because of the translation invariance of the integral, the Fourier modes again decouple. The subsequent thermal average can therefore be written in terms of the fluctuation spectrum (2.59), giving

$$\langle \overline{h^2} \rangle = \sum_{\mathbf{q}} \langle |h_{\mathbf{q}}|^2 \rangle = \sum_{\mathbf{q}} \frac{k_B T}{L^2 (\sigma q^2 + \kappa q^4)}. \quad (2.62)$$

Finally, we approximate the mode summation by taking the the continuum limit $\sum_{\mathbf{q}} \rightarrow (L/2\pi)^2 \int d^2q$. We cut off the long wavelength modes according to the system size, $q_{\max} = 2\pi/L$. Furthermore, we introduce a small wavelength cutoff $q_{\min} = 2\pi/a$, where a is comparable to the molecular length scale and relates to the surface thickness. Performing

¹² This also applies to the domain wall solution of Technical Note 2.1. To see this, consider a small deviation $h(\mathbf{x}_{\parallel})$ above each point $\mathbf{x}_{\parallel} = (x, y)$ of the flat interface so that $\phi_{\text{dw}}(z) \rightarrow \phi_{\text{dw}}(z - h)$. In this case the gradient term of the (mean field) free energy expands as $[\nabla \phi_{\text{dw}}(z - h)]^2 = [\phi'_{\text{dw}}(z - h)]^2 [1 + (\nabla_{\parallel} h)^2]$. The translation by h leaves the z -integral unaffected and it follows that the energy difference reduces to the harmonic form:

$$\begin{aligned} \Delta \mathcal{F}_{\text{dw}}[\phi_{\text{dw}}(z - h)] - \sigma A &= \int d^2 \mathbf{x}_{\parallel} \frac{c}{2} (\nabla_{\parallel} h)^2 \int_{-\infty}^{\infty} dz \left[\frac{d\phi_{\text{dw}}(z - h)}{dz} \right]^2 = \int d^2 \mathbf{x}_{\parallel} \frac{c}{2} (\nabla_{\parallel} h)^2 \frac{w\phi_*^2}{3c} \\ &= \int d^2 \mathbf{x}_{\parallel} \frac{1}{2} (\nabla_{\parallel} h)^2 \left(\frac{uw}{3} \phi_*^4 \right) = \int d^2 \mathbf{x}_{\parallel} \frac{\sigma}{2} (\nabla_{\parallel} h)^2. \end{aligned}$$

the integration gives

$$\begin{aligned}\langle \overline{h^2} \rangle &\approx \int \frac{d^2q}{(2\pi)^2} \frac{k_B T}{(\sigma q^2 + \kappa q^4)} = \int_{2\pi/L}^{2\pi/a} \frac{dq}{2\pi} \frac{k_B T}{q(\sigma + \kappa q^2)} \\ &= \frac{k_B T}{4\pi\sigma} \ln \left(\frac{4\pi^2 \kappa + \sigma L^2}{4\pi^2 \kappa + \sigma a^2} \right).\end{aligned}\quad (2.63)$$

We now specialize to the three limits. For the general case, the above expression can be simplified further by expanding for $a/L \ll 1$ and retaining only the dominant term. The other two limits must be applied to Eq. (2.63) directly. After the required manipulations, we obtain

$$\langle \overline{h^2} \rangle \approx \begin{cases} \frac{k_B T}{2\pi\sigma} \ln \left(\frac{L}{2\pi} \sqrt{\frac{\sigma}{\kappa}} \right), & \text{general } (a/L \ll 1) \\ \frac{k_B T}{2\pi\sigma} \ln(L/a), & \text{tension dom. } (\kappa = 0) \\ \frac{k_B T}{16\pi^3 \kappa} (L^2 - a^2), & \text{bending dom. } (\sigma = 0) \end{cases}$$

$$(2.64a)$$

$$(2.64b)$$

$$(2.64c)$$

The above expressions reveal several significant consequences, the most profound being that in all three cases, the amplitude of undulations *increases* with system size. That is, for increasing system size, there is *no long-range positional order*; the average position of the surface becomes less and less well defined. This finding is a manifestation of a more general principle known as the *Mermin–Wagner–Hohenberg theorem* [MW66, Hoh67], which states that no spontaneous breaking of a continuous symmetry occurs for systems with short-range interactions in dimensions $d \leq 2$. An important corollary, however, is that in the lower critical dimension $d_c = 2$, a phase transitions can occur in special cases—such as the formation of a fluid interface—but at the expense of dispensing with true long-range order [Kar07].

Although we demonstrated that asymptotically flat surfaces appear not to exist in three dimensions, let us put the results (2.64) into perspective. At least in the first two cases, the average undulation amplitude increases without bound, but it does so *very slowly* and hence exceptionally large surfaces are required to detect appreciable fluctuations. On the other hand, fluctuations are considerable for bending-dominated surfaces (*e.g.*, fluid lipid membranes). For example, at $T = 20^\circ\text{C}$ the thermal energy is $k_B T \approx 4 \text{ pN} \cdot \text{nm}$. The surface tension of typical capillary surfaces (liquid–air interfaces) ranges between $\sigma \approx 20\text{--}80 \text{ mN/m}$ (see Ref. [Jas72] for a comprehensive list), and a typical fluid lipid membrane possesses a bending modulus of $\kappa \approx 20 k_B T$ [Nag13]. Substituting these values into Eq. (2.64) and taking the square root provides us with the root mean square (rms) fluctuation amplitudes,

$$h_{\text{rms}} \sim \begin{cases} (1.8\text{--}0.9 \text{ \AA}) \sqrt{\ln(L/a)}, & \text{tension dom. } (\sigma \approx 20\text{--}80 \text{ mN/m}, \kappa = 0) \\ L/100, & \text{bending dom. } (\sigma = 0, \kappa \approx 20 k_B T) \end{cases}\quad (2.65)$$

For tension dominated surfaces, we see that the interface is *exceedingly* flat. For instance, taking a system size of $L \approx 10$ cm and a cutoff of $a \approx 1$ nm yields an rms value of only $h_{\text{rms}} \sim 3.8\text{--}7.7$ Å! On the other hand, the rms amplitude for a bending dominated surface is always about 1% of the system size which, although relatively smooth, is not indiscernible. Typical membranes with lateral extents on the order of $10\text{ }\mu\text{m}$ will have $h_{\text{rms}} \sim 100$ nm and indeed can be seen to “flicker” [BL75, FN91].

Orientalional order. Apart from long range positional order of a fluid surface, we may also ask how thermal fluctuations affect long range *orientational* order. Accordingly, we examine the average deviation of the surface normal from the vertical defined by the base plane. This will in a sense provide a measure of the surface *roughness*.

To begin, we compute the general deviation from vertical, which for small gradients reduces to

$$\hat{\mathbf{n}}(\mathbf{x}) \cdot \hat{\mathbf{e}}_z = \frac{1}{\sqrt{1 + (\nabla h)^2}} \approx 1 - \frac{1}{2}(\nabla h)^2. \quad (2.66)$$

The expansion in Fourier modes follows just as before, with the positional average of the gradient term given by

$$\overline{(\nabla h)^2} = \frac{1}{L^2} \int d^2x \sum_{\mathbf{q}, \mathbf{q}'} (-\mathbf{q} \cdot \mathbf{q}') h_{\mathbf{q}} h_{\mathbf{q}'} e^{i(\mathbf{q} + \mathbf{q}') \cdot \mathbf{x}} = \sum_{\mathbf{q}} q^2 |h_{\mathbf{q}}|^2. \quad (2.67)$$

Applying the equipartition theorem to the Fourier amplitudes via Eq. (2.59) and passing to the continuum limit, we find the average deviation to be

$$\begin{aligned} 1 - \langle \hat{\mathbf{n}}(\mathbf{x}) \cdot \hat{\mathbf{e}}_z \rangle &\approx \frac{1}{2} \sum_{\mathbf{q}} q^2 \langle |h_{\mathbf{q}}|^2 \rangle \approx \frac{1}{2} \int \frac{d^2q}{(2\pi)^2} \frac{k_B T}{\sigma + \kappa q^2} \\ &= \frac{1}{2} \int_{2\pi/L}^{2\pi/a} \frac{dq}{2\pi} \frac{q k_B T}{\sigma + \kappa q^2} = \frac{k_B T}{8\pi\kappa} \ln \left[\left(\frac{L}{a} \right)^2 \left(\frac{4\pi^2\kappa + \sigma a^2}{4\pi^2\kappa + \sigma L^2} \right) \right]. \end{aligned} \quad (2.68)$$

Finally, we specialize to three limits:

$$1 - \langle \hat{\mathbf{n}}(\mathbf{x}) \cdot \hat{\mathbf{e}}_z \rangle \approx \begin{cases} \frac{k_B T}{4\pi\kappa} \ln \left(\frac{2\pi}{a} \sqrt{\frac{\kappa}{\sigma}} \right), & (a/L \ll 1) & (2.69a) \\ \frac{\pi}{2} \frac{k_B T}{\sigma a^2} [1 - (a/L)^2], & (\kappa = 0) & (2.69b) \\ \frac{k_B T}{4\pi\kappa} \ln(L/a), & (\sigma = 0) & (2.69c) \end{cases}$$

In the first two cases, we observe that the orientational deviations quickly approach *fixed* values. Provided the constants evaluate to appreciably less than one—which is also required for the validity of the small gradient expansion—this implies that both surface types possess long range orientation order. For a bending dominated surface, the deviations increase with

system size, but logarithmically so. This technically means the surface does *not* possess long range orientational order, but only past a certain size. The lateral extent past which the assumption of a flat surface with no overhangs breaks down is known as the *persistence length* ξ_p . Here, we estimate

$$\xi_p \sim a e^{4\pi\kappa/k_B T}. \quad (2.70)$$

Interestingly, from a different approach Helfrich [Hel85] calculated maximum excess area due to undulations area before which bending energy loses out over entropy, and the square root of his result matches Eq. (2.70).

A somewhat better measure of surface flatness comes not from the deviations from vertical, but rather the orientation angle between distant points, given by $\hat{\mathbf{n}}(\mathbf{x}) \cdot \hat{\mathbf{n}}(\mathbf{x}') = \cos \theta$. After a slightly more involved calculation [Boa12, §8.3], one finds *twice* the values of Eq. (2.69) (also with the replacement $L = |\mathbf{x} - \mathbf{x}'|$). Allowing the correlation to vanish gives the de Gennes–Taupin [dGT82] persistence length

$$\xi_p \sim a e^{2\pi\kappa/k_B T}. \quad (\text{de Gennes–Taupin}) \quad (2.71)$$

Using a more detailed renormalization group approach, Peliti and Leibler [PL85] obtained a result that amounts to *three* times Eq. (2.69c) (see also the next section):

$$\xi_p \sim a e^{4\pi\kappa/3k_B T}. \quad (\text{Peliti–Leibler}) \quad (2.72)$$

Note that the expressions (2.69) also provide a measure for (twice) the squared gradient, $\langle (\nabla h)^2 \rangle$, and hence reveal the validity of the small gradient expansion. However, all the values depend on the cutoff a , and hence may provide questionable quantitative information. For example, the surface tension of a water–air interface at 20 °C is $\sigma \approx 73 \text{ mN/m}$ and, together with the thermal energy $k_B T$, defines a length scale $\sqrt{k_B T / \sigma} \sim 2 \text{ \AA}$ which obviously competes with the cutoff. Instead of fixing the cutoff, we may instead ask how the gradient varies when the cutoff is altered. If we increase the cutoff by $a \rightarrow \lambda a$, and correspondingly “integrate out” the smaller scale physics, the surface description essentially becomes “grainier.” To restore the description’s original resolution, we must now rescale all the physical lengths via $L \rightarrow \lambda L$, $\mathbf{x} \rightarrow \lambda \mathbf{x}$, and $h \rightarrow \lambda h$. Applying this “coarse-graining and rescaling” procedure¹³ to Eqs. (2.69), we see that the (squared) gradient of a tension dominated surface *decreases* under coarse-graining as $\sim 1/\lambda^2$. That is, the small gradient expansion becomes more accurate. Similarly, for a surface with finite σ and κ , the squared gradient also decreases, though very slowly and *additively*, by $-(k_B T / 2\pi\kappa) \ln \lambda$. Finally, for a bending dominated surface, the gradient is seen to be *invariant* under coarse graining—its roughness is self-similar or fractal.

¹³A third step would be to notice that rescaling alters the fluctuation spectrum and hence the “contrast.” To restore contrast, one then introduces a multiplicative factor to absorb the discrepancy and thereby *renormalize* the quantity. This conceptual description of the renormalization group procedure is outlined in Kardar’s excellent book [Kar07, Ch. 4].

2.4.2 Nonlinearities and renormalization

We conclude this chapter with a brief discussion of the nonlinear corrections to the harmonic approximation, and the renormalization of the tension and bending moduli due to thermal fluctuations. In the previous discussion, we observed that for a bending dominated surface (membrane), upon increasing scale fluctuations compound and wrinkle the surface up to a certain scale (the persistence length), after which the concept of surface flatness breaks down. Physically, bending the membrane costs energy—which is characterized by κ —and for large enough membranes the overall energy of thermal fluctuations wins out over the energetic cost of bending [dGT82]. In this sense, the membrane can be thought of as *softening* at larger scales (or higher temperatures). From an alternate perspective, one may posit that the entropic energy may be absorbed into the membrane description as a negative surface energy. In particular, due to the manner in which the entropic energy emerges mathematically, it may be absorbed into the definition of the bending modulus κ . That is, $\kappa \rightarrow \kappa(T, L, a)$ gets *renormalized* according to thermal and spatial scales.

One may regard the renormalization procedure as *integrating out* the thermal fluctuations from the energetic description of the surface. It is not clear *a priori*, however, that the resulting entropic contributions can be absorbed into the couplings. Indeed, the previous heuristic argument was based on the harmonic approximation, but the elastic moduli of the Helfrich Hamiltonian multiply quantities that are highly nonlinear in h and its derivatives. Moreover, the large scale softening is an inherently long wavelength phenomena, but it is modified by short wavelength fluctuations. Nonlinearities must be integral to this effect, as Fourier modes decouple in the harmonic approximation. The situation is further complicated by the amendments introduced by the functional measure.

Owing much to these subtle issues, there has been an interesting disagreement in the literature as to how the moduli renormalize. Following Ref. [Hel87], we summarize the results for the bending rigidity as

$$\kappa(T, L, a) = \kappa - \alpha \frac{k_B T}{4\pi} \ln(L/a), \quad (2.73)$$

with a being inversely proportional to the short wavelength (“ultraviolet”) cutoff. The parameter α accounts for the differing results among various authors. Helfrich [Hel85, Hel87], and later Förster [För87], derived Eq. (2.73) with $\alpha = 1$. Other authors found $\alpha = 3$, including Peliti and Leibler [PL85], Förster [För86], and Kleinert [Kle86, Kle89]. This result was further verified by a variety of techniques [CLNP94, GK96, BKS99, SZ05]. In contrast, Helfrich and Pinnow [Hel98, PH00] also obtained $\alpha = -1$ (meaning the membrane *stiffens*) by constructing an alternative functional in which the local mean curvature is promoted to the fundamental integration measure with the aim of respecting in-plane incompressibility.¹⁴

Similarly, several authors have considered the renormalization of the surface tension σ in the presence of nonzero bending rigidity. It turns out that the surface tension does not

¹⁴It should be noted that this restriction may be problematic. For example, Cai and Lubensky [CL95a] found that a membrane can never be considered as incompressible at long length scales.

alter the renormalization of κ , but the curvature renormalization *does* induce a surface energy even if one begins with $\sigma = 0$ before integrating out fluctuations. Indeed, from the measure factor (2.54) in the gradient expansion, it should be apparent that a tension-like term should develop. Like before, we may summarize the results as

$$\sigma(T, L, a) = \sigma + \alpha' \frac{k_B T}{4\pi} \frac{\sigma}{\kappa} \ln(L/a), \quad (2.74)$$

where the parameter value $\alpha' = 1$ was obtained by Refs. [För86, DL91, CLNP94, BKS99, SZ05], and $\alpha' = 3$ by Refs. [PL85, Kle86]. As pointed out in Ref. [BKS99], the differences found in Refs. [PL85, Kle86] can be attributed to beginning with a tensionless membrane, only to have a tension develop due to thermal fluctuations.

We close by speculating that this issue, though worthy of further investigation, is somewhat illusory and misleading—a sentiment also put forth in the closely related context of quantum gravity (see, for instance, [Ham09, § 2.4]). The primary difficulty appears to stem from attempting to properly handle the short-distance cutoff in a covariant way. For example, the continuum limit of the Faddeev–Popov contribution Eq. (2.54) becomes the integral

$$\mathcal{H}_{\text{FP}} \rightarrow \frac{\rho}{2\beta} \int d^2u \ln g(u), \quad (2.75)$$

where the factor ρ essentially represents the density “ N_{dof}/A ” of degrees of freedom per area. For a discretized grid, N_{dof} counts the number of permissible wavevectors per cell and may be approximated by replacing the grid Brillouin zone by a circular zone of equal area [CL95b, §5.8]

$$\rho = \frac{1}{A} \sum_{\mathbf{q} \in \text{B.Z.}} \approx \int_0^\Lambda \frac{d^2q}{(2\pi)^2}, \quad (2.76)$$

where $\Lambda \propto 1/a$ is some ultraviolet cutoff. As discussed in Section 2.4 (page 60), one must account for the fluctuating area of the grid cells to avoid a mismatch of degrees of freedom in the surface description. By going to the continuum limit, this constraint must be nontrivially enforced by the cutoff Λ or, alternatively, be accounted for by an appropriate counterterm (*i.e.*, the Liouville correction).

Based on our remarks in the previous section, it seems the most appropriate route is via the EFT formalism. For instance, one writes down all possible covariant operators that respect any additional imposed symmetries, and then matches the coefficients to physical observables. Indeed, this is what was essentially done in Ref. [CLNP94]: The authors fixed the gauge through the Faddeev–Popov determinant, which was then transformed to an exponent as a contribution to the energy. Then they introduced a series of *counterterms* which were intended to account for additional nonlinearities to restore covariance that was broken by the cutoff. Ultimately, all terms were fixed by matching to the (observable) frame tension which, in essence, is akin to enforcing a renormalization condition. For alternative renormalization schemes, the path to the final result may be more straightforward. For

example, Borelli, Kleinert, and Schakel [BKS99] calculated the renormalization in full nonlinear glory by way of the derivative expansion technique and dimensional regularization, which has the benefit of setting to zero many of the controversial terms (including the measure factor (2.54)).

3 Surface-mediated interactions of axisymmetric particles

In this chapter we examine the interactions between particles bound to a fluid surface characterized by its surface tension. Surfaces of this type are found in a variety of physical systems, perhaps the most well known being soap films [Ise92] and fluid–fluid interfaces, such as between microemulsions or the surface of water [RW02, dGBWQ04]. As discussed in the introduction, understanding such colloidal systems or assemblies is key to a variety of industrial applications, including microfabrication and separation technologies. Here we will restrict our attention to a more idealized class of rigid particles and study surface-mediated interactions among a small but diffuse collection.

3.1 Surface energetics

The energy functional¹ for a tension-dominated fluid surface \mathcal{S} is given in covariant form by

$$\mathcal{H} = \sigma \int_{\mathcal{S}} dA, \quad (3.1)$$

where σ is the surface tension. Since we will be interested in deviations about a flat equilibrium ground-state surface, we will work in the Monge gauge in which the surface is described by its orthogonal displacement $z = h(\mathbf{x})$ from a base plane parametrized by $\mathbf{x} = (x, y)$. This representation is appropriate with the additional assumption that thermal fluctuations are small and without bubbles or overhangs. Taking the base plane to coincide with the flat ground state (*i.e.*, $h = 0$), we can then write the energy cost associated with surface deformations as the Hamiltonian

$$\mathcal{H} = \sigma(\mathcal{A}_{\mathcal{S}} - \mathcal{A}_{\mathcal{S}_{\text{pr}}}) = \sigma \int_{\mathcal{S}_{\text{pr}}} d^2x \left[\sqrt{1 + (\nabla h)^2} - 1 \right] =: \mathcal{H}[h], \quad (3.2)$$

where $\mathcal{A}_{\mathcal{S}}$ and $\mathcal{A}_{\mathcal{S}_{\text{pr}}}$ are respectively the areas of the surface \mathcal{S} and its projection \mathcal{S}_{pr} onto the base plane. Assuming the deformations are gentle enough so that $|\nabla h| \ll 1$, we can instead work in the *linearized* Monge gauge by performing a gradient expansion and keeping

¹For many systems, including fluid phase interfaces, it would technically be more correct to refer to this as a *free energy*. This is because the microscopic degrees of freedom that allow for the surface fluidity are necessarily temperature dependent, and this dependence leaves its trace in the phenomenological parameters of the coarse-grained theory. For example, the domain wall solution in Ginzburg–Landau theory gives $\sigma \propto |T - T_c|^{3/2}$, where T_c is the critical temperature (see Technical Note 2.1).

the leading term:

$$\mathcal{H}[h] \approx \sigma \int_{\mathcal{S}_{\text{pr}}} d^2x \frac{1}{2} (\nabla h)^2. \quad (3.3)$$

To justify dropping the higher order terms, we can look at the average gradient size using the Fourier methods of the last chapter, for which we find

$$\langle (\nabla h)^2 \rangle = \sum_{\mathbf{q}} q^2 \langle |h_{\mathbf{q}}|^2 \rangle \approx \pi \frac{k_{\text{B}} T}{\sigma a^2} \equiv \pi \frac{\ell_{\text{m}}^2}{a^2},$$

where a is a small length cutoff. In the last equality we introduced the thermal *molecular* length scale $\ell_{\text{m}} = \sqrt{k_{\text{B}} T / \sigma}$. This length scale is very small for many fluid systems. For example, water at room temperature has a surface tension of about 73 mN/m, so the length scale $\ell_{\text{m}} \approx 2 \text{ \AA}$, which is comparable to the size of a water molecule. Since both ℓ_{m} and a are small, one might question which dominates and whether the gradients are actually small. The resolution is due to the rescaling argument given previously—upon sufficient coarse-graining (*i.e.*, increasing the size of the cutoff a beyond the molecular scale ℓ_{m}), $\langle (\nabla h)^2 \rangle$ indeed gets smaller and the gradient expansion becomes more accurate.

From a different perspective, the appearance of ℓ_{m} as an appropriate measure of the fluctuation amplitude suggests we compare the energy with the typical thermal energy $k_{\text{B}} T$ and recast the Hamiltonian in terms of the dimensionless height function $\phi = h / \ell_{\text{m}}$:

$$\begin{aligned} \frac{\mathcal{H}[\phi]}{k_{\text{B}} T} &= \frac{1}{\ell_{\text{m}}^2} \int_{\mathcal{S}_{\text{pr}}} d^2x \left[\sqrt{1 + \ell_{\text{m}}^2 (\nabla \phi)^2} - 1 \right] \\ &= \frac{1}{\ell_{\text{m}}^2} \int_{\mathcal{S}_{\text{pr}}} d^2x \left\{ \frac{\ell_{\text{m}}^2}{2} (\nabla \phi)^2 - \frac{\ell_{\text{m}}^4}{8} [(\nabla \phi)^2]^2 + \dots \right\} \\ &= \int_{\mathcal{S}_{\text{pr}}} d^2x \frac{1}{2} (\nabla \phi)^2 + \mathcal{O}(\ell_{\text{m}}^2). \end{aligned} \quad (3.4)$$

We see, then, that the length scale ℓ_{m} becomes useful as a small power-counting parameter, showing that the higher order gradients provide negligible corrections on the order of ℓ_{m}^2 . We are therefore justified in retaining only the leading-order term.

Taming the zero mode

Recall from the previous chapter that the existence of an interface breaks translation symmetry in the z direction. In accordance with the Mermin–Wagner theorem, this allows the buildup of long-wavelength fluctuations and an ultimate loss of long-range positional order—implying the surface cannot be asymptotically flat. However, we know that height-difference correlations only diverge logarithmically (see Eq. (2.64b)), so the flatness issue is relatively minor. In contrast, when we later calculate interactions this problem may resurface, so we need a method to dampen (or *regulate*) the fluctuations. The most obvious physical option is to include a gravitational energy cost to Eq. (3.2). For an interface

between two fluids with a density difference $\Delta\rho$, any deviations $h(\mathbf{x})$ from equilibrium increases the system's potential energy by an amount

$$\mathcal{H}_g[h] = \int_0^h dh' \int_{\mathcal{S}_{\text{pr}}} d^2x \Delta\rho g h' = \int_{\mathcal{S}_{\text{pr}}} d^2x \frac{1}{2} \Delta\rho g h^2 \equiv \sigma \int_{\mathcal{S}_{\text{pr}}} d^2x \frac{1}{2} \ell_c^{-2} h^2, \quad (3.5)$$

where we have introduced the *capillary length* $\ell_c = \sqrt{\sigma/|\Delta\rho|g}$. The interpretation of the capillary length becomes especially clear if we examine the Fourier modes of the surface energy. Following Section 2.4.1, the free energy of a surface of size $L \times L$ is given by the mode summation (Fourier transform of the quantity Eq. (3.2) + Eq. (3.5))

$$E = \frac{\sigma(L/\ell_c)^2}{2} \sum_{\mathbf{q}} |h_{\mathbf{q}}|^2 [(\ell_c \mathbf{q})^2 + 1]. \quad (3.6)$$

The terms within brackets imply that wavelengths much *larger* than the capillary length ($1/q \gg \ell_c$) are suppressed by the gravitational energy. Conversely, for length scales much smaller than ℓ_c , gravity is negligible. Typical values for ℓ_c are on the order of millimeters for room temperature water and other simple liquids [dGBWQ04], but may be much larger for immiscible fluids of comparable densities. The capillary length will be the largest length scale in any system we will consider, and will therefore serve to regulate any large distance divergences. As such, we will work in the asymptotic $\ell_c \rightarrow \infty$ limit, for which Eq. (3.2) is usually satisfactory, but, as we will see in Sections 3.5.4 and 3.6.4, some care will be needed in taking the limit properly.

Stationary surface conditions

We wish to look for surface profiles $h(\mathbf{x})$ for which the energy functional is stationary under small variations $h \rightarrow h + \delta h$. In the linearized Monge gauge, the energy variation becomes (to leading order)

$$\begin{aligned} \delta\mathcal{H}[h] &= \sigma \int_{\mathcal{S}_{\text{pr}}} d^2x \nabla h \cdot \nabla \delta h \\ &\stackrel{\text{IBP}}{=} \sigma \int_{\mathcal{S}_{\text{pr}}} d^2x (-\nabla^2 h) \delta h + \sigma \oint_{\partial\mathcal{S}_{\text{pr}}} ds (\hat{\ell} \cdot \nabla h) \delta h, \end{aligned} \quad (3.7)$$

where the second line follows from integration by parts (*à la* the divergence theorem). In the boundary integral, $\hat{\ell}$ is the outward unit normal (in the base plane) from the projected surface boundary $\partial\mathcal{S}_{\text{pr}}$. Note that for an *exterior* problem in which \mathcal{S}_{pr} is the region outside a compact domain \mathcal{A} , $\hat{\ell}$ will point *into* \mathcal{A} . Setting the above variation to zero provides the stationary conditions for the surface. Moreover, the second-order term we neglected in Eq. (3.7) is an integral over $(\nabla \delta h)^2$ and is therefore positive-definite, so setting $\delta\mathcal{H} = 0$ provides conditions that minimize the energy. Since, the variation δh is arbitrary, each contribution to $\delta\mathcal{H}$ must generally vanish independently. Setting the surface integral to zero

tells us the minimum energy surface configuration $h(\mathbf{x})$ must satisfy Laplace's equation,

$$-\nabla^2 h(\mathbf{x}) = 0 \text{ for } \mathbf{x} \in \mathcal{S}_{\text{pr}}. \quad (3.8)$$

This is the usual Euler–Lagrange equation for the above energy functional. On the other hand, the boundary integral suggests some naturally appropriate boundary conditions: either δh must vanish on the boundary, implying $h|_{\partial\mathcal{S}_{\text{pr}}}$ is fixed (Dirichlet boundary conditions), or the normal gradient $(\hat{\ell} \cdot \nabla h)|_{\partial\mathcal{S}_{\text{pr}}}$ must vanish (Neumann boundary conditions).

If we were to include the gravitational potential energy, the variational problem would be similar but with the following modification to the Euler–Lagrange equation:

$$(-\nabla^2 + \ell_c^{-2})h(\mathbf{x}) = 0 \text{ for } \mathbf{x} \in \mathcal{S}_{\text{pr}}. \quad (3.9)$$

The boundary conditions would remain unchanged.

3.2 Particle boundary conditions

The surface acts as a medium for “communication” between embedded particles; it is only through the surface constraints imposed by the particles that the particles can (indirectly) interact with one another. In this sense, any relevant description of the particles must be posited in the language of surface degrees of freedom in the neighborhood of the particles. In this thesis, we will consider only compact rigid particles in which the surface is attached (or *pinned*) to a particular fixed contact line around each particle boundary (see Fig. 3.1). This can be enforced, for instance, by engineering so-called *Janus particles* with wetting properties that favor opposing fluid phases. Since the only direct interaction between a particle and the surface is through pinning at the boundary, particles with the same contact line profiles (and the same allowed motions) will fall into an equivalence class. According to the surface, a flat, circular disk and a (symmetric) Janus sphere are the same.

Note that the attachment requirement is a boundary condition of the Dirichlet type. For a particle with a projected region \mathcal{A} in the base plane, the height function must assume the contact profile $h(\mathbf{x})|_{\partial\mathcal{A}} = h^{\text{ct}}(\mathbf{x})|_{\partial\mathcal{A}}$ at the (projected) particle boundary $\partial\mathcal{A}$. That is, the surface may be extended into the particle domain, but since the contact slope cannot be consistently fixed along with the position, this continuation cannot generally be done smoothly and we should not worry about kinks at contact. This is analogous to electrostatics, in which the potential is continuous across the boundary, but the electric field may be discontinuous due to the presence of surface charges. Alternative boundary conditions are of course possible and indeed correspond to other interesting problems. Neumann boundary conditions are relevant for non-rigid surface holes, as considered in [Rot12]. A particular combination of the two conditions appear in the study of smooth, partially-wetting spheres trapped at a fluid–fluid interface (for instance, see [LO07]). However, in this thesis we will only consider the Dirichlet conditions.

We can express an arbitrary contact profile $h^{\text{ct}}(\mathbf{x})$ as a series expansion about the particle's

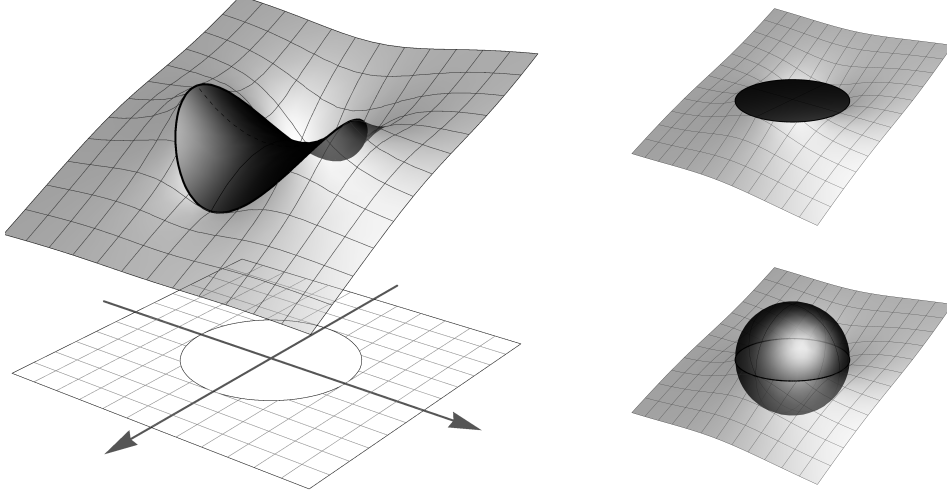


Figure 3.1: Illustration of bound particles with circular contact line projections in the base plane. The surface attaches to a particle along fixed contact lines whose height profile is parametrized by its projected boundary. So long as the allowed rigid-body motions are the same, any particles with equivalent contact line profiles—such as the disk and Janus sphere to the right—are considered equivalent.

center. As per the previous discussion, the particle may not actually take this physical shape, but since the surface only encounters the particle’s boundary, we may choose any functional representation that is most convenient. For $\mathbf{x} \in \partial\mathcal{A}$, we may therefore express the contact line in the general form

$$\begin{aligned} h^{\text{ct}}(\mathbf{x}) &= h^{\text{ct}}(0) + x_i \partial_i h^{\text{ct}}(0) + \frac{1}{2} x_i x_j \partial_i \partial_j h^{\text{ct}}(0) + \cdots \\ &=: h_0 + \mathbf{s} \cdot \mathbf{x} - \frac{1}{2} \eta_{ij} x_i x_j + \cdots, \end{aligned} \tag{3.10}$$

where we sum over repeated indices as usual.² In the second line, we define the parameters h_0 , \mathbf{s} , and η_{ij} which each have an intuitive interpretation. Consider for a moment a particle with a *flat* contact line. That is, the contact line is fixed to a flat, imaginary plane. If the particle were to undergo any rigid-body motions, namely changing height or tilt with respect to the base plane, so must this particle reference plane. Returning to Eq. (3.10), we notice that the height at the center of this particle representation is given by $h^{\text{ct}}(0) = h_0$. Similarly, if the particle were tilted in the $x_i z$ -plane by an angle θ_i , the particle reference plane would be as well, with a slope given by $s_i = \tan \theta_i = \partial_i h^{\text{ct}}(0)$. We see then that the

²Recall that in the Monge gauge, the base plane is Euclidean so there is no need to distinguish between up and down indices.

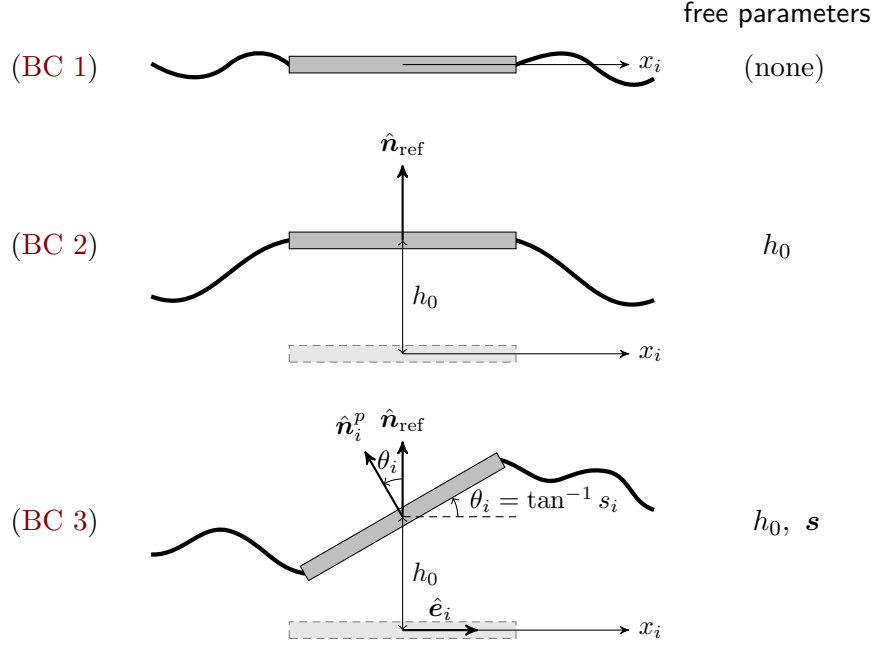


Figure 3.2: Illustration of the three boundary conditions for a flat particle. The freedom of the particle to fluctuate in height and tilt is parametrized by h_0 and s respectively, measured from the equilibrium base plane. The component s_i gives the slope of the particle's rim in the $x_i z$ -plane and is given by $s_i = \tan \theta_i$, where θ_i is the angle from the horizontal. The slope can also be expressed as the ratio of vertical and horizontal projections of the particle normal vector \hat{n}_i^p (in the $x_i z$ -plane): $s_i = -(\hat{n}_i^p \cdot \hat{e}_i) / (\hat{n}_i^p \cdot \hat{n}_{\text{ref}})$, where \hat{e}_i and \hat{n}_{ref} are respectively the x_i unit vector and base plane normal vector.

two first terms of Eq. (3.10) parametrize the height and tilt of a flat contact line:

$$h_{\text{flat}}(\mathbf{x}) = h_0 + \mathbf{s} \cdot \mathbf{x}. \quad (3.11)$$

Any remaining tensor coefficients must therefore parametrize permanent vertical deviations from a flat (though potentially tilted) contact line. In this chapter, we will only consider the lowest-order term and write

$$h_{\text{perm}}(\mathbf{x}) = -\frac{1}{2} \eta_{ij} x_i x_j. \quad (3.12)$$

Note that $\eta_{ij} = -\partial_i \partial_j h^{\text{ct}}(0)$, and hence represents the extrinsic curvature tensor of the contact line parametrization in the small gradient expansion (*cf.* Eq. (2.30)).

For the rigid particles we will consider, any deviations from a flat contact line must be fixed—they are *intrinsic* properties of the particle. Whether h_0 and \mathbf{s} are fixed or may fluctuate, however, depends on what *extrinsic* conditions are imposed. Following the

categorization of Ref. [L007], we will consider three types of boundary conditions (see Fig. 3.2):

(BC 1) The position and tilt are fixed.

(BC 2) The vertical position is allowed to fluctuate but the tilt is fixed.

(BC 3) The vertical position and tilt are both allowed to fluctuate.

In terms of the contact line parameters, the first condition (BC 1) “freezes” the particle in place by fixing both the height h_0 and tilt \mathbf{s} through some external mechanism. In the second condition (BC 2), the tilt is fixed, but the height is unconstrained. That is, h_0 is a *free parameter* that can fluctuate freely with the surface without an energy cost. Similarly, in (BC 3) the particle height and tilt may fluctuate with the surface, so both h_0 and \mathbf{s} are free parameters.

Conditions for the contact line

Previously, we discussed the energy costs of out-of-plane surface deformations for a general surface \mathcal{S} . To account for particle inclusions, we need to make their presence explicit in the surface domain. Since we will consider particles that are much smaller than the surface, we can take the projected surface region to be infinite; *i.e.*, it will span \mathbb{R}^2 . If we include particles, their boundaries will effectively cut holes into the plane. For a collection of N particles, the full projected surface is then $\mathcal{S}_{\text{pr}} = \mathbb{R}^2 \setminus \bigcup_{a=1}^N \mathcal{A}_a$ where \mathcal{A}_a is the area of the a th particle projected onto the base plane. The boundary conditions above are then applied at the boundaries $\partial\mathcal{A}_a$. However, in the case of (BC 3) the tilt degree of freedom means that the projected area \mathcal{A} may fluctuate from its equilibrium area. That is, we must account for a projected boundary that fluctuates. To illuminate and resolve this complication, let us reconsider the particle inclusions from an alternative perspective.

Consider the surface to be continuous ($\mathcal{S}_{\text{pr}} = \mathbb{R}^2$). We can then deal with the energy costs $\Delta\mathcal{H}$ of particle inclusions directly in the Hamiltonian. The general form for a single particle is

$$\Delta\mathcal{H} = \Delta\mathcal{H}_{\text{ex}} + \Delta\mathcal{H}_g + \Delta\mathcal{H}_{\text{ct}}, \quad (3.13)$$

where $\Delta\mathcal{H}_{\text{ex}}$ accounts for the energy associated with the surface patch excluded by the particle, $\Delta\mathcal{H}_g$ corrects the gravitational energy cost above the patch, and $\Delta\mathcal{H}_{\text{ct}}$ accounts for any energies required to enforce the contact line (such as wetting properties). The first term accounts for the surface patch exclusion by cutting the region \mathcal{A} from the surface as well as the region \mathcal{A}_{eq} from the equilibrium surface (see Fig. 3.3). The energy cost is therefore given as the difference from equilibrium,

$$\Delta\mathcal{H}_{\text{ex}} = -\sigma \left(\int_{\mathcal{A}} d^2x \sqrt{1 + (\nabla h)^2} - \mathcal{A}_{\text{eq}} \right). \quad (3.14)$$

The particle also alters the gravitational energy over the region \mathcal{A} , which we can account for by removing the gravitational energy of the excluded surface patch and replacing it with

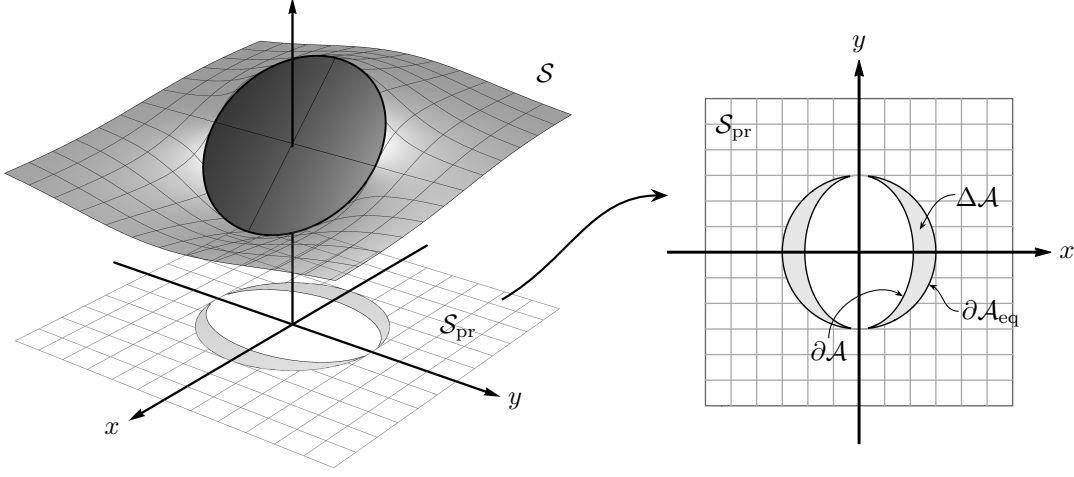


Figure 3.3: Illustration of an example particle's projection \mathcal{A} onto the base plane as compared to its equilibrium projection \mathcal{A}_{eq} . The particle's tilt results in an excess (projected) area $\Delta\mathcal{A} = \mathcal{A}_{\text{eq}} - \mathcal{A}$.

the potential energy at the particle's center of mass height h_{cm} . This correction then takes the form

$$\begin{aligned}\Delta\mathcal{H}_g &= -\frac{1}{2}\Delta\rho g \int_{\mathcal{A}} d^2x h^2 + \frac{1}{2}\Delta\rho g h_{\text{cm}}^2 \mathcal{A} \\ &= -\sigma \int_{\mathcal{A}} d^2x \frac{1}{2} \left(\frac{h}{\ell_c} \right)^2 + \frac{1}{2} \left(\frac{h_{\text{cm}}}{\ell_c} \right)^2 \sigma \mathcal{A}.\end{aligned}\tag{3.15}$$

To enforce the contact line, $\Delta\mathcal{H}_{\text{ct}}$ must encode an energy penalty for deviations from h^{ct} at the boundary. For particles at a fluid–fluid interface, the third term could be written

$$\Delta\mathcal{H}_{\text{ct}} = \sigma_{\text{I}}\Delta\mathcal{A}_{\text{I}}^{\text{ct}} + \sigma_{\text{II}}\Delta\mathcal{A}_{\text{II}}^{\text{ct}} = (\sigma_{\text{I}} - \sigma_{\text{II}})\Delta\mathcal{A}_{\text{I}}^{\text{ct}},\tag{3.16}$$

where $\sigma_{\text{I,II}}$ are the contact tensions between the particle and the upper and lower fluid phases (I and II respectively) and $\Delta\mathcal{A}_{\text{I,II}}^{\text{ct}}$ are the changes in respective contact area from the equilibrium configuration. In the second step, we used that the sum $\mathcal{A}_{\text{I}}^{\text{ct}} + \mathcal{A}_{\text{II}}^{\text{ct}}$ is the total particle area, so $\Delta\mathcal{A}_{\text{II}}^{\text{ct}} = -\Delta\mathcal{A}_{\text{I}}^{\text{ct}}$. This term would be particularly relevant for particles without fixed contact lines, such as smooth spheres trapped but not pinned to an interface. However, for the pinned particles we will consider, the surface is permanently attached to the contact line, so $\Delta\mathcal{A}^{\text{ct}} = 0$ always. To enforce this condition, we could instead include a term in which deviations from h^{ct} on the boundary would cost an “infinite” energy (provided by the intrinsic particle properties), which we will examine shortly.

Let us now focus on the exclusion energy $\Delta\mathcal{H}_{\text{ex}}$ in the small gradient expansion:

$$\begin{aligned}\Delta\mathcal{H}_{\text{ex}} &\approx -\frac{\sigma}{2} \int_{\mathcal{A}} d^2x (\nabla h)^2 + \sigma(\mathcal{A}_{\text{eq}} - \mathcal{A}) \\ &= -\frac{\sigma}{2} \int_{\mathcal{A}} d^2x (-\nabla^2 h)h - \frac{\sigma}{2} \oint_{\partial\mathcal{A}} ds (\hat{\mathbf{n}}_{\mathcal{A}} \cdot \nabla h)h + \sigma(\mathcal{A}_{\text{eq}} - \mathcal{A}),\end{aligned}\tag{3.17}$$

where the second line follows by integration by parts, and $\hat{\mathbf{n}}_{\mathcal{A}}$ is the outward normal vector of the projected particle boundary $\partial\mathcal{A}$ in the base plane. We also dropped the boundary term at infinity, which is justified by the assumption that the surface returns to its flat equilibrium shape at infinity:³ $h(r \rightarrow \infty) \rightarrow 0$. The last term above gives energy cost when the projected particle area differs from its equilibrium value. However, since the particle is rigid, the true area defined by the contact line representation h^{ct} must be unchanged, giving the equal-area condition

$$\int_{\mathcal{A}} d^2x \sqrt{1 + (\nabla h^{\text{ct}})^2} = \mathcal{A}_{\text{eq}}.\tag{3.18}$$

The small gradient expansion then provides the approximate area difference, which after integration by parts becomes

$$\mathcal{A}_{\text{eq}} - \mathcal{A} = \frac{1}{2} \int_{\mathcal{A}} d^2x (-\nabla^2 h^{\text{ct}})h^{\text{ct}} + \frac{1}{2} \oint_{\partial\mathcal{A}} ds (\hat{\mathbf{n}}_{\mathcal{A}} \cdot \nabla h^{\text{ct}})h^{\text{ct}}.\tag{3.19}$$

Plugging this result into Eq. (3.17), and noting that $h = h^{\text{ct}}$ on the boundary, we find that the boundary terms cancel, leaving

$$\Delta\mathcal{H}_{\text{ex}} = -\frac{\sigma}{2} \int_{\mathcal{A}} d^2x (-\nabla^2 h)h + \frac{\sigma}{2} \int_{\mathcal{A}} d^2x (-\nabla^2 h^{\text{ct}})h^{\text{ct}}.\tag{3.20}$$

The first term simply corrects the continuous particle-free surface Hamiltonian by removing the patch \mathcal{A} from $\mathcal{S}_{\text{pr}} = \mathbb{R}^2$ so that $\mathcal{S}_{\text{pr}} \rightarrow \mathbb{R}^2 \setminus \mathcal{A}$. The second term gives the energy cost of the tilted contact line, which we can make vanish by continuing the contact line within the particle domain such that it satisfies Laplace's equation, $-\nabla^2 h^{\text{ct}} = 0$ for $\mathbf{x} \in \mathcal{A}$.

The condition on the extended contact line, $-\nabla^2 h^{\text{ct}} = 0$, provides insight into the equivalence classes of particle shapes. Recall that η_{ij} from Eq. (3.12) is the curvature tensor for $h^{\text{ct}}(\mathbf{x})$, and the total curvature is given by $\text{tr}[\eta_{ij}] = -\text{tr}[\partial_i \partial_j h^{\text{ct}}(0)] = -\nabla^2 h^{\text{ct}}(0)$. Equation (3.20) therefore implies that any total curvature imposed on the surface by a particle must cost external energy. To clarify, the contact slope at the boundary cannot be fixed—a particle imparting nonzero total curvature will feel a force from the surface and will ultimately reach equilibrium where the curvature vanishes unless acted on by some other counterforcing mechanism (whose energy will show up in $\Delta\mathcal{H}_{\text{ct}}$). Nonzero *Gaussian*

³An alternative justifying assumption is that the surface is *asymptotically flat*; i.e., $\partial_r h(r \rightarrow \infty) \rightarrow 0$. In most cases, both assumptions are satisfied.

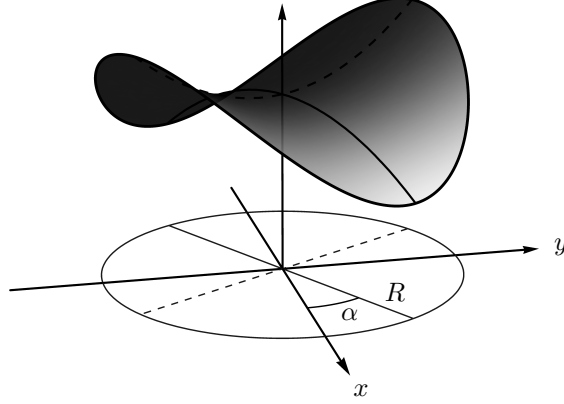


Figure 3.4: Illustration of a saddle-shaped particle with Gaussian curvature $-S^2$. The principal directions are highlighted with a solid line for positive curvature (curves down) and a dashed line for negative curvature (curves up). The principal axis of positive curvature lies at an angle α from the x -axis.

curvature $\det[\eta_{ij}]$, however, is not forbidden. With this information, we are now ready to provide an explicit expression for η_{ij} and hence $h_{\text{perm}}(\mathbf{x})$.

Since η_{ij} is necessarily real and symmetric, it may be parametrized by two independent variables, the most convenient choice being the basis-invariant trace and determinant, which respectively correspond to the total and Gaussian curvatures. Since we require $\text{tr}[\eta_{ij}] = 0$, η_{ij} must be symmetric and *trace-free*, and have the following representation in its diagonal basis:

$$\eta_{ij} \doteq S \mathbf{M} = S \begin{pmatrix} 1 & 0 \\ 0 & -1 \end{pmatrix}. \quad (3.21)$$

The Gaussian curvature $\det[\eta_{ij}] = -S^2$ shows that the two principal curvatures are $+S$ in the x direction and $-S$ in the y direction and hence η_{ij} defines a *saddle* shape. Since the curvature is an invariant, we can rotate the basis of \mathbf{M} via

$$\mathbf{M} \rightarrow \mathbf{R}(\alpha) \mathbf{M} \mathbf{R}^T(\alpha) = \begin{pmatrix} \cos 2\alpha & \sin 2\alpha \\ \sin 2\alpha & -\cos 2\alpha \end{pmatrix}, \quad (3.22)$$

to give a saddle rotated by an angle α from the x -axis. The final expression for $h_{\text{perm}}(\mathbf{x})$ then simplifies in polar coordinates (r, φ) :

$$h_{\text{perm}}(\mathbf{x}) = -\frac{1}{2} \mathbf{x}^T (S \mathbf{R} \mathbf{M} \mathbf{R}^T) \mathbf{x} = -\frac{1}{2} S r^2 \cos(2\varphi - 2\alpha). \quad (3.23)$$

The corresponding shape is illustrated in Fig. 3.4.

Constraint forces

Let us now return to our discussion of $\Delta\mathcal{H}_{\text{ct}}$, the energy costs of enforcing the contact line. With the now modified integration domain $\mathcal{S}_{\text{pr}} = \mathbb{R}^2 \setminus \mathcal{A}$, we may enforce the contact line at the boundary $\partial\mathcal{A}$ with a Lagrange multiplier $\lambda(\mathbf{x} \in \partial\mathcal{A})$ to give the unconstrained energy functional

$$\begin{aligned}\mathcal{H}[h, \lambda \mid h^{\text{ct}}] &= \mathcal{H}[h \mid \mathcal{S}_{\text{pr}}] + \Delta\mathcal{H}_{\text{ct}}[h, \lambda \mid h^{\text{ct}}] \\ &= \frac{\sigma}{2} \int_{\mathcal{S}_{\text{pr}}} d^2x (\nabla h)^2 - \oint_{\partial\mathcal{A}} ds \lambda (h - h^{\text{ct}}).\end{aligned}\quad (3.24)$$

In this construction, the boundary term is (minus) the external work required to maintain the contact line. Accordingly, we interpret the Lagrange multiplier λ as a linear force density acting on the surface in the neighborhood of the boundary. That is, λ is as large as required to enforce the contact line and therefore formally provides an infinite energy penalty for any deviations from $h = h^{\text{ct}}$ on the boundary. The original constrained energy is therefore given by $\mathcal{H}[h, h^{\text{ct}}] = \max_{\lambda} \mathcal{H}[h, \lambda \mid h^{\text{ct}}]$.

The first-order variation is, after integrating by parts and dropping the infinite boundary term,

$$\delta\mathcal{H}[h, \lambda \mid h^{\text{ct}}] = \sigma \int_{\mathcal{S}_{\text{pr}}} d^2x (-\nabla^2 h) \delta h - \oint_{\partial\mathcal{A}} ds \left[(\sigma \hat{\mathbf{n}}_{\mathcal{A}} \cdot \nabla h + \lambda) \delta h + (h - h^{\text{ct}}) \delta \lambda \right]. \quad (3.25)$$

The second-order variation integrates over $(\nabla \delta h)^2$ and is therefore positive-definite, so the energy is minimized when the above variation vanishes. Setting the first term to zero gives Laplace's equation $-\nabla^2 h = 0$ on the surface outside the particle as usual. The last term simply enforces the contact line $h = h^{\text{ct}}$ on the boundary, but the second term provides something new. At equilibrium, the force density is given by⁴

$$\lambda = -\sigma \hat{\mathbf{n}}_{\mathcal{A}} \cdot \nabla h, \quad (3.26)$$

where h is the exterior solution to $-\nabla^2 h = 0$ with the boundary condition $h(\partial\mathcal{A}) = h^{\text{ct}}(\partial\mathcal{A})$. Note that the above analysis generalizes quite simply for finite ℓ_c , by replacing $-\nabla^2 h = 0$ with $(-\nabla^2 + \ell_c^{-2})h = 0$, and to multiple particles via $\mathcal{A} \rightarrow \bigcup_a \mathcal{A}_a$, $\partial\mathcal{A} \rightarrow \bigcup_a \partial\mathcal{A}_a$, and $\lambda \rightarrow \lambda_a$.

Pathologies

Recall that the undamped ($\ell_c \rightarrow \infty$) Hamiltonian Eq. (3.2) suffers from divergences due to the buildup of long-wavelength fluctuations, the origin of which is the broken translation symmetry in the direction orthogonal to the surface. As hinted at previously, this problem may reappear once particles are included. If the boundary conditions imposed by a particle also break invariance of the Hamiltonian under translation $h \rightarrow h + \text{const.}$, such as in (BC 1), it is not guaranteed that the surface response to the particle is well-behaved or

⁴Recall that $\hat{\mathbf{n}}_{\mathcal{A}}$ is defined as the normal vector in the base plane pointing out from the region \mathcal{A} .

physical, even in the absence of fluctuations. To be more precise, let us examine a general stationary solution $h(\mathbf{x})$ to the Euler–Lagrange equation (3.8) in polar coordinates (r, φ) :

$$h(\mathbf{x}) = a \ln br + \sum_{n \geq 1} [c_n r^n \cos(n\varphi - n\alpha_n) + r^{-n} d_n \cos(n\varphi - n\beta_n)], \quad (3.27)$$

with undetermined parameters a, b, c_n, d_n, α_n , and β_n . Acceptable (*i.e.*, physical) exterior solutions are those proportional to r^{-n} , whereas acceptable interior solutions are those proportional to r^n . Notice that the first term, $a \ln br$, was excluded from both; it is divergent for both large and short distances. This term is therefore a *pathological* solution which we must avoid when dealing with physics in either the interior or exterior domains.

By adding a damping term, namely the gravitational potential (3.5), the pathologies disappear. With this modification, the Euler–Lagrange equation is instead given by Eq. (3.9) and has a general stationary solution

$$h(\mathbf{x}) = \sum_{n \geq 0} [A_n I_n(r/\ell_c) \cos(n\varphi - n\vartheta_n) + B_n K_n(r/\ell_c) \cos(n\varphi - n\psi_n)], \quad (3.28)$$

where $I_n(x)$ and $K_n(x)$ are the modified Bessel functions of the first and second kind respectively, and A_n, B_n, ϑ_n , and ψ_n are undetermined coefficients and phases. For large distances, $K_n \rightarrow 0$, whereas $I_n \rightarrow 0$ for short distances. That is, for finite ℓ_c there are no longer pathological solutions. At the end of the day, however, we wish to take the asymptotic limit $\ell_c \rightarrow \infty$. As we will see, for (BC 2) and (BC 3) we can safely take the limit from the beginning and use the solutions (3.27) without problems. However, we will need to be more careful with (BC 1).

Charge distributions: An electrostatics analogy

To further understand the various terms in Eqs. (3.27) and (3.28), we draw an analogy to electrostatics. In the linearized Monge gauge, the Hamiltonian (3.3) is equivalent to the source-free ($\rho = 0$) electrostatics energy functional (1.18), but with one fewer dimension and an additional minus sign. We will discuss the significance of the minus sign shortly. In this analogy, h serves as the electrostatic potential, and $-\nabla h$ serves as the electric field. With this in mind, consider the two-dimensional version of Gauss’s Law:

$$\nabla \cdot (-\nabla h) = -\nabla^2 h =: \frac{1}{\sigma} \rho(\mathbf{x}) \iff Q := \int_{\mathcal{A}} d^2x \rho(\mathbf{x}) = \oint_{\partial\mathcal{A}} ds \sigma \hat{\mathbf{n}}_{\mathcal{A}} \cdot (-\nabla h), \quad (3.29)$$

where we have defined the *capillary charge distribution* $\rho(\mathbf{x})$ and the total *capillary charge* Q within the domain \mathcal{A} . Comparing with the expression (3.26) for the force density λ , we see that a “charge” in the surface context corresponds to the strength of a point force acting on the surface. Similarly, ρ has units of pressure, so it may also be understood as a distribution of “pressure points” acting on the surface.

Now consider Eq. (3.27) within a circular region of radius R , for which $\hat{\mathbf{n}}_{\mathcal{A}} \cdot \nabla = \partial_r$.

Applying Gauss's Law and using

$$\int_0^{2\pi} d\varphi \cos n\varphi = 0, \quad \forall n \in \mathbb{Z}, \quad (3.30)$$

we find that most terms vanish. The only nonzero term is in fact the first one:

$$\int_0^{2\pi} R d\varphi [-\partial_r(a \ln br)] = -2\pi a \equiv Q/\sigma. \quad (3.31)$$

One way to interpret this result is that the first term, $a \ln br$, is a *monopole* potential of charge $Q = -2\pi\sigma a$. The remaining terms correspond to higher-order *multipole* potentials which, of course, have no net charge. These higher-order multipole potentials instead provide information about how the surface domain “polarizes.”

If we instead calculate the boundary integral using Eq. (3.28), we also find that only the $n = 0$ terms are nonvanishing. Furthermore, in the $\ell_c \rightarrow \infty$ limit, only one of the two terms survives:

$$\partial_r I_0(r/\ell_c) = \frac{I_1(r/\ell_c)}{\ell_c} \rightarrow 0, \quad (3.32)$$

$$\partial_r K_0(r/\ell_c) = -\frac{K_1(r/\ell_c)}{\ell_c} \rightarrow -\frac{1}{r}. \quad (3.33)$$

Since the integral yields an additional factor of $2\pi R$, we see that the term $B_0 K_0(r/\ell_c)$ corresponds to a monopole potential of charge $Q = 2\pi\sigma B_0$ in the $\ell_c \rightarrow \infty$ limit. The difference here, however, is that the monopole potential is suitably regularized at large distances by the ℓ_c cutoff:

$$K_0(r/\ell_c) \stackrel{\ell_c \rightarrow \infty}{\sim} \ln\left(\frac{2\ell_c}{\gamma_e r}\right), \quad (3.34)$$

where $\gamma_e = e^{\gamma_E}$ and $\gamma_E = 0.57721\dots$ is the Euler–Mascheroni constant.

The benefit of this electrostatics analogy is that we can apply some of the insight gained from the conducting spheres problem from Chapter 1. In particular, we can reinterpret the contact line profile (3.10) in terms of charges: h_0 corresponds to a fixed potential and thus for a particle of finite size, it is proportional to the total charge (monopole moment), with the proportionality constant depending only on the boundary geometry. Similarly, the tilt parameter \mathbf{s} is proportional to the dipole moment, and the higher-order coefficients correspond to higher-order multipole moments. However, recall that allowing the particle to tilt entails a changing boundary in the base plane. This implies that once fluctuations are included, the interpretation of the terms as multipole moments is only valid for small fluctuations in which the change in the projected boundary is negligible. Fortunately, as seen previously, the circumstances in which the linearized Monge gauge is justified ensures that this is indeed true as long as $-\nabla^2 h^{\text{ct}} = 0$, which we restrict to in this chapter, and the interpretation is appropriate.

The particle boundary conditions may also be viewed from this perspective. The first two conditions have the following electrostatics analogues:

$$(\text{BC 1}) \iff \text{conductor held at a fixed potential}$$

$$(\text{BC 2}) \iff \text{free conductor}$$

In the correspondence above, each conductor may also contain permanent internal charge configurations that do not respond to an external field. Interpreting (BC 3), however, is a little strange in that it would behave as a free conductor except that it will not respond to a linear electric potential (it has no dipole susceptibility). Notice that in (BC 2) and (BC 3), the particles are invariant under global changes in constant height. But in (BC 1), this shift would be met with an induced monopole charge (external force) in order to hold the particle at a fixed height. That is, (BC 1) is the only one of the boundary conditions that is sensitive to the pathological monopole solution of Eq. (3.27). As such, it is the only one that will require the use of the ℓ_c regulator.

Capillary charges: Attractive or repulsive?

Let us now return to the minus sign difference in the analogy. In one regard, it appears to make no difference since in both the electrostatics and surface (with $\ell_c \rightarrow \infty$) problems, the corresponding scalar fields satisfy Poisson's equation. However, recall that the electric potential ϕ appeared in the energy functional as a Lagrange multiplier to enforce Gauss's law—the fundamental field is the vector \mathbf{E} , not the scalar field ϕ . Indeed, it is the condition $\delta\mathcal{H}/\delta\mathbf{E} = 0$ that minimizes the energy, whereas $\delta\mathcal{H}/\delta\phi = 0$ instead maximizes it. The difference in the sign of the energy functional, then, is really a manifestation of the difference between vector field and scalar field theories.⁵

To see how the minus sign changes the physics, consider a collection of capillary point charges (forces) $\rho(\mathbf{x}) = \sum_a f_a \delta(\mathbf{x} - \mathbf{x}_a)$ in the surface. The energy functional is then modified in the usual way

$$\mathcal{H}[h | \rho] = \int d^2x \left\{ \frac{\sigma}{2} [(\nabla h)^2 + \ell_c^{-2} h^2] - \rho h \right\}, \quad (3.35)$$

appearing similar to the electrostatics functional (1.18) when $\ell_c \rightarrow \infty$, but with the opposite

⁵The origin of the minus sign difference can be explained more definitively once dynamics are considered. In the relativistic Lagrangian formulation, the kinetic term $\propto (\partial_t \phi)^2$ of a scalar field theory must appear with a positive sign in order for the corresponding energy to be bounded from below, and thus the gradient appears with a minus sign via $\partial_\mu \phi \partial^\mu \phi = (\partial_t \phi/c)^2 - (\nabla \phi)^2$. To get the Hamiltonian, one applies the usual Legendre transformation which ultimately flips the sign of $(\nabla \phi)^2$ and results in the same form as Eq. (3.3). In electrodynamics, the “kinetic” term instead applies to the vector potential A^μ so that $(\partial_t \mathbf{A})^2$ appears with a positive sign. The scalar potential A_0 actually does not appear with any time derivatives, and indeed can be interpreted again as a Lagrange multiplier that enforces Maxwell's equations. More details on the differences between scalar, vector, and tensor fields—and their implications in relativistic and quantum field theories—can be found in Refs. [Des05], [Zee03], and [Pad10].

sign. The minimum-energy solution must satisfy $(-\nabla^2 + \ell_c^{-2})h = \rho/\sigma$, as follows from setting the functional variation to zero. This may be solved by the method of Green functions to give

$$h(\mathbf{x} \mid \rho) = \frac{1}{\sigma} \int d^2x' G(\mathbf{x} - \mathbf{x}') \rho(\mathbf{x}') = \sum_a \frac{f_a}{\sigma} G(\mathbf{x} - \mathbf{x}_a), \quad (3.36)$$

where the Green function comes from the $n = 0$ term in Eq. (3.28):⁶

$$G(\mathbf{x}) = \frac{1}{2\pi} K_0(r/\ell_c). \quad (3.37)$$

In the harmonic limit $\ell_c \rightarrow \infty$, the Green function takes the asymptotic form,

$$G_H(\mathbf{x}) = \frac{1}{2\pi} \ln\left(\frac{2\ell_c}{\gamma_e r}\right). \quad (3.38)$$

We can now plug this solution back into the functional (3.35) to find the energy, but it first helps to rewrite the functional in the form (*cf.* Eq. (1.20)),

$$\mathcal{H}[\rho] = -\frac{1}{2} \int d^2x \rho(\mathbf{x}) h(\mathbf{x} \mid \rho) = -\frac{1}{2\sigma} \int d^2x d^2x' \rho(\mathbf{x}) G(\mathbf{x} - \mathbf{x}') \rho(\mathbf{x}'). \quad (3.39)$$

The first part of the above expression results from integration by parts and applying the stationary condition $(-\nabla^2 + \ell_c^{-2})h = \rho/\sigma$. In doing so, we have dropped the boundary term at infinity, which is acceptable since both $K_0(r/\ell_c)$ and $\partial_r K_0(r/\ell_c)$ vanish as $r \rightarrow \infty$. In the harmonic limit, this is also valid since $\partial_r \ln(2\ell_c/\gamma_e r) = -1/r \rightarrow 0$ as $r \rightarrow \infty$ (*i.e.*, $h[\rho]$ is asymptotically flat), but additionally since the regularization condition $r \ll \ell_c$ implies we replace the infinite distance limit with the (noncommuting) nested limits

$$\lim_{\ell_c \rightarrow \infty} \left[\lim_{r \rightarrow \ell_c} \ln\left(\frac{2\ell_c}{\gamma_e r}\right) \right],$$

which indeed vanishes.

The energy for a collection of point forces therefore follows by plugging in the expression

⁶The factor of $1/2\pi$ may be checked by integrating both sides of $(-\nabla^2 + \ell_c^{-2})B_0 K_0(r/\ell_c) = \delta(\mathbf{x})$ over a disc D of radius r and applying the divergence theorem:

$$\begin{aligned} B_0 \int_D (-\nabla^2 + \ell_c^{-2}) K_0(r/\ell_c) &= -2\pi r B_0 \partial_r K_0(r/\ell_c) + \frac{B_0}{\ell_c^2} \int_D d^2x K_0(r/\ell_c) \\ &= -2\pi r B_0 [-K_1(r/\ell_c)/\ell_c] + \frac{2\pi B_0}{\ell_c^2} [\ell_c^2 - \ell_c r K_1(r/\ell_c)] \stackrel{!}{=} 1 \end{aligned}$$

After canceling terms, it follows that $B_0 = 1/2\pi$.

for ρ into Eq. (3.39), giving

$$\mathcal{H}[f_a] = -\frac{1}{2\sigma} \sum_{a,b} f_a f_b G(\mathbf{x}_a - \mathbf{x}_b) = -\sum_a \frac{f_a^2}{2\sigma} G(0) - \sum_{a < b} \frac{f_a f_b}{\sigma} G(\mathbf{x}_a - \mathbf{x}_b). \quad (3.40)$$

The first term on the right side ($\propto G(0)$) corresponds to the self-energy of each of these “charges,” and, as familiar in electrostatics, it diverges for point charges. The last term corresponds to the interaction energy between pairs of point sources indexed by a and b , and unfortunately also appears to diverge in the $\ell_c \rightarrow \infty$ limit. However, in both cases these divergences in energy are inconsequential as physical observables depend on overall differences in energy, and the dependence on ℓ_c can be seen to no longer be singular. For example, the force between two point sources is finite:

$$F = -\frac{\partial}{\partial r} \left[-\frac{f_1 f_2}{2\pi\sigma} K_0(r/\ell_c) \right] = -\frac{f_1 f_2}{2\pi\sigma\ell_c} K_1(r/\ell_c) \xrightarrow{\ell_c \rightarrow \infty} -\frac{f_1 f_2}{2\pi\sigma r}. \quad (3.41)$$

Note the sign in the above force equation. If the two “charges” are of like sign, then the force is *attractive*. Likewise, with opposite signs the force is repulsive. This is in contrast to electrostatics, in which like charges repel and opposites attract. This significant difference in behavior is in fact a universal feature in field theory: Like charges always attract in scalar field theories, repel in vector field theories, attract in rank-2 tensor field theories (*e.g.*, gravity), and so on [Zee03, Pad10].

Let us end the discussion by circling back to the *Cheerios effect* mentioned in the introduction. If the point forces are due to small objects floating on a liquid surface, then Eq. (3.41) at finite capillary length becomes the leading-order attractive flotation force. A more detailed calculation [VM05] shows that a floating sphere of radius R , density ρ_s , and contact angle θ with the liquid has an effective weight $f = 2\pi\sigma R \text{Bo} \Sigma(\theta)$, where $\text{Bo} = R^2/\ell_c^2$ is the particle *Bond number* and

$$\Sigma(\theta) = \frac{2(\rho_s/\rho) - 1}{3} - \frac{1}{2} \cos \theta + \frac{1}{6} \cos^3 \theta.$$

Substituting this into Eq. (3.41) for finite ℓ_c reproduces the force at large separation between identical spheres calculated in Refs. [CHJW81, VM05],

$$F = -2\pi\sigma R \text{Bo}^{5/2} \Sigma^2(\theta) K_1(r/\ell_c). \quad (3.42)$$

As a final comment, in the absence of gravity, the effective weight of each particle vanishes and therefore so does the interparticle flotation force. Hence, at vanishing Bond number—and in the absence of other external forces—there are no surface-mediated forces in the ground state unless at least one particle imparts an irregular contact line on the surface. We will explore how that changes the leading-order force law in Section 3.5.

Having discussed particle responses qualitatively, let us now examine the quantitative implications of the imposed boundary conditions on our finite-sized particles.

3.2.1 Surface response to an isolated particle

In the spirit of Sections 1.1 and 1.2, we characterize each embedded particle by examining its response δh to an imposed stationary background surface deformation (background field) h_{bg} . The total field $h_{\text{bg}} + \delta h$ must then satisfy the attachment condition at the particle contact line. Furthermore, as discussed in the previous chapter, a given particle may be characterized completely by its surface responses alone and therefore we need only consider the full-theory boundary value problem for particles in isolation. In this chapter, we will specialize to the case of axisymmetric particles, which we will define as those whose projected equilibrium contact lines are circles in the base plane.

For one such disk-like particle of radius R , the attachment condition in polar coordinates states

$$h(R, \varphi) = h_{\text{bg}}(R, \varphi) + \delta h(R, \varphi) \stackrel{!}{=} h^{\text{ct}}(R, \varphi). \quad (3.43)$$

This condition must hold for any background field, so we are free to choose h_{bg} so that the boundary value problem is as simple as possible. One approach is to take advantage of the circular symmetry of the boundary and apply the general solutions (3.27) and (3.28). Physically, we expect the surface response due to the particle to die off at infinity, so we should impose the additional condition $\delta h(r \rightarrow \infty) \rightarrow 0$. Consider now the expansion (3.28). The functions $I_n(r/\ell_c)$ are regular at $r = 0$ but monotonically increasing, whereas the functions $K_n(r/\ell_c)$ are singular at $r = 0$ but monotonically decreasing and regular as $r \rightarrow \infty$ (or rather, as $r \rightarrow \ell_c$). With this in mind, permissible response fields must take the form

$$\delta h(\mathbf{x}) = \sum_{n \geq 0} B_n K_n(r/\ell_c) \cos(n\varphi - n\vartheta_n). \quad (3.44)$$

Likewise, we will ultimately want to treat particles as points, so permissible background fields should be well behaved at the particle centers. The background fields should therefore take the form

$$h_{\text{bg}}(\mathbf{x}) = \sum_{n \geq 0} A_n I_n(r/\ell_c) \cos(n\varphi - n\vartheta_n). \quad (3.45)$$

Note that although the above expression diverges at infinity, it does not mean that background fields cost infinite energy. Instead, we assume that background deformations are, for instance, externally sourced at the far away (but *finite* distance) surface boundary so that the particle-free surface takes on the profile given by Eq. (3.45).

Since both expansions are solutions to $(-\nabla^2 + \ell_c^{-2})h = 0$ by construction, a convenient boundary value problem *and solution* presents itself:

$$\begin{cases} (-\nabla^2 + \ell_c^{-2})h(\mathbf{x}) = 0, & |\mathbf{x}| > R, \\ \delta h(R, \varphi) = h^{\text{ct}}(R, \varphi) - h_{\text{bg}}(R, \varphi), \end{cases} \quad (3.46)$$

where δh and h_{bg} are given by Eqs. (3.44) and (3.45). For simplicity, we will set $\vartheta_n = 0$ in the background field (3.45). What remains is to solve for the coefficients B_n in terms of A_n .

Flat particle

Earlier, we explored the various terms that contribute to a particle's contact line h^{ct} and decomposed its series expansion into terms describing rigid-body motions, h_{flat} , and those encoding permanent deformations, h_{perm} . The boundary condition in Eq. (3.46) then consists of three terms, $h_{\text{flat}} + h_{\text{perm}} - h_{\text{bg}}$, which the response must match at the boundary $r = R$. By linearity, the solution δh can also be decomposed as

$$\delta h = \delta h_{\text{ind}} + \delta h_{\text{flat}} + \delta h_{\text{perm}}, \quad (3.47)$$

where the responses have the following interpretations:

δh_{ind} : Induced response to the background field for a particle contact line both flat and fixed in the equilibrium base plane (*i.e.*, the contact line coincides with its projection so that $h_0 = 0$ and $\mathbf{s} = \mathbf{0}$).

δh_{flat} : Permanent response, independent of the background, for a particle with a flat contact line and fixed h_0 and \mathbf{s} .

δh_{perm} : Permanent response, independent of the background, for a particle fixed in the equilibrium base plane with $h_0 = 0$ and $\mathbf{s} = \mathbf{0}$ and fixed contact line curvature.

The background field response δh_{ind} is analogous to the induced polarization potential of a conductor in an external field, whereas the two permanent responses account for permanent multipole potentials. Depending on the particle degrees of freedom—that is, whether h_0 and \mathbf{s} are fixed or free—the response δh_{flat} will serve different purposes. Namely, when both parameters are fixed, δh_{flat} simply gives the permanent surface deformation imparted by the particle. But if h_0 and \mathbf{s} are free parameters, their values will change to balance the forces and torques generated by the background field response, canceling any nonzero height and tilt.

With $h_{\text{perm}} = 0$, the response consists of just the first two terms, $\delta h = \delta h_{\text{ind}} + \delta h_{\text{flat}}$, and corresponds to particles with a flat contact line. The solution follows quickly from the expansions (3.44), (3.45), and (3.11) matched at the boundary:

$$\delta h_{\text{ind}}(R, \varphi) = \sum_{n \geq 0} B_n K_n(R/\ell_c) \cos n\varphi \stackrel{!}{=} - \sum_{n \geq 0} A_n I_n(R/\ell_c) \cos n\varphi \quad (3.48a)$$

$$\begin{aligned} \delta h_{\text{flat}}(R, \varphi) &= C_0 K_0(R/\ell_c) + K_1(R/\ell_c) (C_1 \cos \varphi + C'_1 \sin \varphi) \\ &\stackrel{!}{=} h_0 + s_x R \cos \varphi + s_y R \sin \varphi \end{aligned} \quad (3.48b)$$

The final result is

$$\delta h_{\text{ind}}(\mathbf{x}) = - \sum_{n \geq 0} A_n \frac{I_n(R/\ell_c)}{K_n(R/\ell_c)} K_n(r/\ell_c) \cos n\varphi, \quad (3.49)$$

$$\delta h_{\text{flat}}(\mathbf{x}) = h_0 \frac{K_0(r/\ell_c)}{K_0(R/\ell_c)} + (\mathbf{s} \cdot R\hat{\mathbf{r}}) \frac{K_1(r/\ell_c)}{K_1(R/\ell_c)}. \quad (3.50)$$

Now let us examine what happens when h_0 and \mathbf{s} are promoted to free parameters. If h_0 is free, as in (BC 2), the particle will respond by changing its height to $h_0 = A_0 I_0(R/\ell_c)$, canceling the $n = 0$ term of δh_{ind} . Similarly, if \mathbf{s} is free, the particle will respond by tilting with a slope $\mathbf{s} = (A_1/R) I_1(R/\ell_c) \hat{\mathbf{e}}_x$, which then cancels the $n = 1$ term of δh_{ind} . To summarize, we present the full flat-particle responses for the three boundary conditions:

$$\text{(BC 1): } \delta h(\mathbf{x}) = h_0 \frac{K_0(r/\ell_c)}{K_0(R/\ell_c)} + (\mathbf{s} \cdot R\hat{\mathbf{r}}) \frac{K_1(r/\ell_c)}{K_1(R/\ell_c)} - \sum_{n \geq 0} A_n \frac{I_n(R/\ell_c)}{K_n(R/\ell_c)} K_n(r/\ell_c) \cos n\varphi \quad (3.51)$$

$$\text{(BC 2): } \delta h(\mathbf{x}) = (\mathbf{s} \cdot R\hat{\mathbf{r}}) \frac{K_1(r/\ell_c)}{K_1(R/\ell_c)} - \sum_{n \geq 1} A_n \frac{I_n(R/\ell_c)}{K_n(R/\ell_c)} K_n(r/\ell_c) \cos n\varphi \quad (3.52)$$

$$\text{(BC 3): } \delta h(\mathbf{x}) = - \sum_{n \geq 2} A_n \frac{I_n(R/\ell_c)}{K_n(R/\ell_c)} K_n(r/\ell_c) \cos n\varphi \quad (3.53)$$

Note that in the applications we will discuss, we will usually choose $h_0 = 0$ and $\mathbf{s} = \mathbf{0}$.

Curved particle

For particles with irregular contact lines, the curvature imparted on the nearby boundary will be encoded in the surface response δh_{perm} . By linearity, this will simply add to the total field $h_{\text{bg}} + \delta h$ and can therefore be analyzed independently. For a general permanent contact line h_{perm} , we may calculate the corresponding response field by first decomposing it into Fourier components on the boundary,

$$h_{\text{perm}}(R, \varphi) = \sum_{n \geq 2} (a_n \cos n\varphi + b_n \sin n\varphi) \quad (3.54a)$$

with

$$\begin{Bmatrix} a_n \\ b_n \end{Bmatrix} = \frac{1}{\pi} \int_{-\pi}^{\pi} d\varphi h_{\text{perm}}(R, \varphi) \begin{Bmatrix} \cos n\varphi \\ \sin n\varphi \end{Bmatrix}, \quad (3.54b)$$

and matching coefficients to the solution (3.44). Here we will restrict ourselves to the case of saddle shapes, where h_{perm} is given by Eq. (3.23) and already appears in the desired form. Matching on the boundary $r = R$ yields the condition

$$\delta h_{\text{perm}}(R, \varphi) = B_2 K_2(R/\ell_c) \cos(2\varphi - 2\alpha) \stackrel{!}{=} -\frac{1}{2} S R^2 \cos(2\varphi - 2\alpha) \quad (3.55)$$

and, after solving for B_2 , the permanent surface deformation becomes

$$\delta h_{\text{perm}}(\mathbf{x}) = -\frac{1}{2}SR^2 \frac{K_2(r/\ell_c)}{K_2(R/\ell_c)} \cos(2\varphi - 2\alpha). \quad (3.56)$$

Harmonic limit

In this chapter, we will primarily restrict our discussion to the case of vanishing Bond number, which corresponds to the limit $\ell_c \rightarrow \infty$ and associated solutions that obey Laplace's equation $-\sigma \nabla^2 h = 0$. But in doing so, we will retain the capillary length ℓ_c as a regulator such that $r \ll \ell_c$. Accordingly we must be careful about taking the $\ell_c \rightarrow \infty$ limit. In general, one should avoid taking the limit until the end of the calculation of an observable. The consequence of taking the limit prematurely is that singularities will be encountered which otherwise would have been regulated by ℓ_c , and furthermore may undesirably set many other terms to zero which could have an implicit ℓ_c -dependence in the coefficients. For example, we know the general solution (3.28) should reduce to the Laplace equation solution (3.27) when $\ell_c \rightarrow \infty$, but naïvely taking the limit would annihilate all I_n terms for $n > 0$ and cause all K_n terms to diverge. This is seen by looking at their asymptotic forms [DLMF],

$$I_n(r/\ell_c) \sim \frac{1}{n!} \left(\frac{r}{2\ell_c} \right)^n, \quad (3.57)$$

$$K_0(r/\ell_c) \sim \ln \left(\frac{2\ell_c}{r\gamma_e} \right), \quad (3.58)$$

$$K_{n>0}(r/\ell_c) \sim \frac{(n-1)!}{2} \left(\frac{2\ell_c}{r} \right)^n. \quad (3.59)$$

The solution to Laplace's equation in polar coordinates indeed has the same r -dependence, so for the limit to reproduce the correct series (3.27), the coefficients A_n and B_n in Eq. (3.28) must have implicit ℓ_c -dependencies. Keeping this in mind, we may now present the properly regularized background and response solutions in the harmonic limit:

$$h_{\text{bg}}(\mathbf{x}) = a_0 + \sum_{n \geq 1} a_n r^n \cos n\varphi \quad (3.60)$$

$$\delta h_{\text{perm}}(\mathbf{x}) = -\frac{1}{2}S \frac{R^4}{r^2} \cos(2\varphi - 2\alpha) \quad (3.61)$$

$$(\text{BC 1}): \quad \delta h(\mathbf{x}) = (h_0 - a_0) \frac{\ln\left(\frac{2\ell_c}{r\gamma_e}\right)}{\ln\left(\frac{2\ell_c}{R\gamma_e}\right)} + (\mathbf{s} \cdot \hat{\mathbf{r}} - a_1 \cos \varphi) \frac{R^2}{r} - \sum_{n \geq 2} a_n \frac{R^{2n}}{r^n} \cos n\varphi \quad (3.62)$$

$$(\text{BC 2}): \quad \delta h(\mathbf{x}) = (\mathbf{s} \cdot \hat{\mathbf{r}} - a_1 \cos \varphi) \frac{R^2}{r} - \sum_{n \geq 2} a_n \frac{R^{2n}}{r^n} \cos n\varphi \quad (3.63)$$

$$\text{(BC 3):} \quad \delta h(\mathbf{x}) = - \sum_{n \geq 2} a_n \frac{R^{2n}}{r^n} \cos n\varphi \quad (3.64)$$

The above equations take the form of two-dimensional multipole expansions, which should not be surprising given the similarity between the surface and electrostatics governing equations. As such, we will use the term *multipole order* when referring to the numbers n in the above sums.⁷ We remark in passing that the recognition and use of the multipole formalism has been exploited before, namely by Kralchevsky and coworkers [KDD01, DKNB05, DK10] who also treat the given ground state problem in terms of “capillary multipoles.”

3.3 Effective theory

Instead of calculating physical observables in the full theory, where the multiple boundaries pose a significant challenge, we will take a step back and reformulate the problem in a way that takes advantage of the system’s scale separation. The largest and smallest length scales of the problem are of course the spatial extent of the surface, which we take to be infinite, and the molecular length scale for which the effective geometric theory breaks down. Besides those we have the capillary length ℓ_c , which characterizes the size of the *flat* surface, and the characteristic particle sizes $R_a \ll \ell_c$, which is still much larger than the molecular length scale. In this chapter, we will be interested in the interactions between particles that are widely separated. The length scale at which we calculate observables is thus characterized by the separation r , generating the scaling hierarchy $R \ll r \ll \ell_c$. Given the large separation of the particles relative to their sizes, the effects of their neighbors will appear as coming from localized sources. Accordingly, we will construct an effective point-particle Hamiltonian for which the physics at the particle length scale manifests as a series of point sources and interactions:

$$\mathcal{H}_{\text{eff}}[h] = \mathcal{H}_0[h] + \Delta\mathcal{H}[h], \quad (3.65)$$

where $\mathcal{H}_0[h]$ is the particle-free—or *bulk*—surface Hamiltonian,

$$\mathcal{H}_0[h] = \frac{\sigma}{2} \int_{\mathbb{R}^2} d^2x [(\nabla h)^2 + \ell_c^{-2} h^2], \quad (3.66)$$

and $\Delta\mathcal{H}[h]$ is the *worldline* Hamiltonian and accounts for the energetic contributions of bound particles. The task then is to determine the additional contributions $\Delta\mathcal{H}[h]$ from the inclusion of particles.

⁷Just a note on language: A perhaps better name for the multipole order n would be the “derivative order”—which we will use interchangeably—since n counts the number of derivatives required in the multipole expansion. However, the terms *monopole*, *dipole*, *quadrupole*, *octopole*, *etc.*, linguistically count the number of poles (the “pluses” and “minuses”) and a general multipole of order n should be called a 2^n -pole.

In general, to construct $\Delta\mathcal{H}$ we must write down all possible local scalar terms $\mathcal{C}^{(k)} \cdot \mathcal{O}_k[h]$, or *operators* in the EFT language, that obey the symmetries of the surface and the particles. The prefactors (Wilson coefficients) $\mathcal{C}^{(k)}$ encode the short distance particle information and will be determined later by a matching procedure. By locality, the operators $\mathcal{O}_k[h]$ must be polynomial in the field h and its derivatives, and, since we have shrunk the particle boundaries to points, each operator will be localized to individual particles and evaluated at their respective positions (*worldlines*) $\mathbf{x} = \mathbf{x}_a$. The impact of a given operator can be estimated by dimensional analysis, and hence the sum of operators can be organized to form a power series in each of the physical scales, thereby allowing us to truncate the series to any desired order of accuracy in a consistent and controlled way.

Let us first consider the bulk Hamiltonian (3.66) in the absence of gravity ($\ell_c \rightarrow \infty$). Then there are three relevant field transformations that leave the energy invariant:

T₁. Reflection ($h \rightarrow -h$) across the base plane.

T₂. Transformations of the field of the form $h \rightarrow h + h_0$, where h_0 is a constant.

T₃. Rotations around a vertical axis centered at *any* point in the base plane.

The inclusion of a particle may either break or preserve these symmetries, and the corresponding particle descriptions can thus be decomposed and categorized as such. The contribution of a single particle clearly breaks the in-plane translation symmetry implicit in **T₃** by selecting a preferred origin, but rotational symmetry will still apply about the center of a flat, circular particle. The transformation symmetry **T₂** is preserved in (BC 2) and (BC 3), as the particle height is a free parameter in both cases, but it is broken for (BC 1). The reflection symmetry **T₁** also holds for flat particles but may be broken for particles that are curved or fixed at nonzero heights or tilts. Just as in the electrostatics problem (see Section 1.1.2), the terms in $\Delta\mathcal{H}$ can be grouped into those which respect the symmetries, and hence correspond to induced polarization responses, and those which break them and correspond to external surface “charges” or forces. We will examine each case separately.

3.3.1 EFT for free, flat particles: induced polarization

We will first consider particles with the most degrees of freedom, and hence respect the most bulk symmetries: flat particles with the freedom to bob and tilt. This corresponds to the case (BC 3). As laid out previously in the discussion of δh_{ind} , induced and permanent surface deformations combine linearly. Hence, any further conditions that break the symmetries will appear as additional terms. In fact the worldline Hamiltonian for free, flat particles will apply to all boundary conditions we consider, and encodes the induced surface deformation response to any impinging background field. Once again, we may draw an analogy to electrostatics—the total amount and distribution of *permanent* charges on a conductor does not affect its capacitance or polarizabilities and thus does not affect its response to an external field.

Since the bulk Hamiltonian (3.66) results from a small-gradient expansion and is truncated at quadratic order in the field h , the worldline Hamiltonian must be at most quadratic in h . The reflection symmetry \mathbf{T}_1 rules out any operators with odd powers of h , so terms linear in h will not appear. As per our discussion at the end of Section 3.2.1, free particles with flat contact lines respond to changes in height and slope without costing energy, and furthermore, at quadratic order the changes in the projected boundary are negligible. Hence, we require that transformations of the type $h \rightarrow h + h_0 + \mathbf{s} \cdot \mathbf{x}$ do not alter the *worldline energy*, so all terms with less than two derivatives acting on each occurrence of h are ruled out. Because of the circular symmetry of the projected particle boundary (see the remarks at the end of Section 3.2.1), the \mathbf{T}_3 symmetry—without translation—is respected and requires that all derivatives must be contracted amongst themselves; *i.e.*, any tensorial Wilson coefficients must be proportional to the identity (see the discussion in Section 1.1.2). Finally, physical observables will always depend on solutions to the bulk Euler–Lagrange equation, $-\nabla^2 h = 0$, so we choose an *on-shell* operator basis that enforces this from the start by setting to zero all terms with at least two derivative indices contracted on the same field instance. Together, these rules dramatically simplify the form and enumeration of possible terms, and the worldline Hamiltonian for all *free*, *flat*, and *circular particles* takes the compact form

$$\Delta\mathcal{H}_f[h] = \sum_a \sum_{n \geq 2} \frac{1}{2} c_a^{(n)} [\partial_I^n h(\mathbf{x}_a)]^2, \quad (3.67)$$

where the particles and their respective positions are labeled by “ a ” and we have used the compact notation $\partial_I^n := \partial_{i_1} \cdots \partial_{i_n}$, with repeated indices summed over as usual. Each Wilson coefficient $c_a^{(n)}$ multiplies a term with $2n$ derivatives and therefore scales as $c_a^{(n)} \sim \sigma R_a^{2n}$ by dimensional analysis. Note the similarity to the worldline Hamiltonian (1.34) for conductors. There we interpreted the coefficients as generalized polarizabilities. An analogous interpretation is appropriate here, so we will also refer to the coefficients $c_a^{(n)}$ in the surface context as *polarizabilities* of the particle a .

Matching

To determine the polarizabilities, we again compute the response to the background field (3.60), but this time using the effective Hamiltonian $\mathcal{H}_{\text{eff}} = \mathcal{H}_0 + \Delta\mathcal{H}_f$. As the background field meets the particle boundaries, the surface and particles respond to obey the boundary conditions, thereby generating a distribution of point sources localized in the neighborhood of the boundary. Indeed, setting $h \rightarrow h_{\text{bg}} + \delta h$ in the Hamiltonian and expanding generates a term linear in δh , appearing as the expected induced source (*cf.* Eq. (3.35)). Picking out

this source term gives⁸

$$\begin{aligned}\rho(\mathbf{x} \mid h_{\text{bg}}) &= -\frac{\delta\Delta\mathcal{H}_f}{\delta h(\mathbf{x})}\Big|_{h=h_{\text{bg}}} \\ &= -\sum_a \sum_{n \geq 2} \left[c_a^{(n)} \partial_I^n h_{\text{bg}}(\mathbf{x}_a) (-\partial)_I^n \right] \delta(\mathbf{x} - \mathbf{x}_a).\end{aligned}\tag{3.68}$$

Restricting now to the case of a single particle at the origin, the resulting response field is calculated in the standard way as the convolution with the bulk Green function,

$$\begin{aligned}\delta h_f^{\text{eff}}(\mathbf{x} \mid h_{\text{bg}}) &= \frac{1}{\sigma} \int d^2x' G(\mathbf{x} - \mathbf{x}') \rho(\mathbf{x}' \mid h_{\text{bg}}) \\ &= -\sum_{n \geq 2} c^{(n)} \partial_I^n h_{\text{bg}}(0) (-\partial)_I^n G(\mathbf{x}),\end{aligned}\tag{3.69}$$

where $G(\mathbf{x})$ is given by Eq. (3.38) and we have dropped the particle label for convenience.⁹ To proceed, we will need an expression for $(-\partial)_I^n G(\mathbf{x})$ so that we may perform the required index contractions. In the previous chapter, we did so via the *detracer* operator from Technical Note 1.1. However, here we can do better by a change of variables.

Complex coordinates

A particular luxury of two dimensions is that points and vectors in the Euclidean plane may alternatively be described in terms of complex numbers. With this description come the elegant results of complex analysis, which will significantly simplify our work compared to the three dimensional system studied in Chapter 1. In particular, the field h satisfies Laplace's equation $-\nabla^2 h = 0$, and can therefore always be broken up into holomorphic and antiholomorphic functions. This provides motivation to work directly in *complex coordinates* $\mathbf{z} = (z, \bar{z})$ with $z = x + iy$ and $\bar{z} = z^* = x - iy$. Under this change of variables, the \mathbf{x} -derivatives are replaced by the complex *Wirtinger derivatives* [Kre09], $\partial := \partial_z = (\partial_x - i\partial_y)/2$ and $\bar{\partial} := \partial_{\bar{z}} = (\partial_x + i\partial_y)/2$, according to

$$\frac{\partial}{\partial x_i} = T_{ij} \frac{\partial}{\partial z_j} \text{ with } T_{ij} \doteq \begin{pmatrix} 1 & 1 \\ i & -i \end{pmatrix}.\tag{3.70}$$

Laplace's equation then takes the form $-4\partial\bar{\partial}h = 0$, so one of the immediate benefits of this coordinate transformation is that mixed derivatives acting on on-shell fields will always

⁸Note that an additional source term could appear from the bulk Hamiltonian via $(\delta\mathcal{H}_0/\delta h)|_{h_{\text{bg}}}$, but we have chosen to consider only on-shell background field for which this term vanishes. If h_{bg} did not satisfy the bulk Euler–Lagrange equation, then the aforementioned term would give the source necessary to maintain the background.

⁹As a reminder, the negative signs multiplying the Green function derivatives in Eq. (3.69) result from integration by parts in \mathbf{x}' and using $(\partial')_I^n = (-\partial)_I^n$ before setting $\mathbf{x}' = \mathbf{x}_a = \mathbf{0}$.

vanish. That is, in our derivative expansion only exclusively ∂ or $\bar{\partial}$ derivatives will appear on each instance of the field.¹⁰

Applying this to the worldline Hamiltonian (3.67) puts it in the form

$$\Delta\mathcal{H}_f[h] = \sum_a \sum_{n \geq 2} C_a^{(n)} [\partial^n h \bar{\partial}^n h] \Big|_{z=z_a}. \quad (3.71)$$

Since the coefficients have yet to be determined, the relation between the new and old polarizabilities $C_a^{(n)}$ and $c_a^{(n)}$ is irrelevant, but for completeness we mention that they differ only by a factor of $2^n \times 2$, where the extra factor of two is due to the term being its own complex conjugate. Similarly, applying the transformation to the single-particle response (3.69) gives

$$\delta h_f^{\text{eff}}(z | h_{\text{bg}}) = -\frac{1}{\sigma} \sum_{n \geq 2} C^{(n)} \bar{\partial}^n h_{\text{bg}}(0) (-\partial)^n G(z) + \text{c.c.}, \quad (3.72)$$

where “c.c.” denotes complex conjugation of the preceding terms. As promised, the multi-index contractions between G and h_{bg} have reduced to a much simpler task of multiplication. Furthermore, the (harmonic) Green function rewritten in complex coordinates becomes

$$G(z) = \frac{1}{4\pi} \ln \left(\frac{4\ell_c^2}{z\bar{z}\gamma_e^2} \right) = \frac{1}{4\pi} \ln \left(\frac{2\ell_c}{z\gamma_e} \right) + \frac{1}{4\pi} \ln \left(\frac{2\ell_c}{\bar{z}\gamma_e} \right), \quad (3.73)$$

for which performing the ∂ and $\bar{\partial}$ derivatives is simple:

$$(-\partial)^n G(z) = \frac{(n-1)!}{4\pi z^n}, \quad (3.74)$$

and similar for the complex conjugate. Applying this to the response (3.72) finally gives

$$\delta h_f^{\text{eff}}(z | h_{\text{bg}}) = -\sum_{n \geq 2} \frac{(n-1)! C^{(n)}}{4\pi \sigma z^n} \bar{\partial}^n h_{\text{bg}}(0) + \text{c.c.} \quad (3.75)$$

Note also the way in which h_{bg} appears in Eqs. (3.72) and (3.75), with its derivatives evaluated at $z = 0$. This suggests that the most convenient form the background field could take would be proportional to z^n (plus the complex conjugate) since only n^{th} -order derivatives would survive when evaluated at zero. Of course, for these backgrounds to apply, we require them to satisfy Laplace’s equation $-4\partial\bar{\partial}h_{\text{bg}} = 0$, which indeed any function of exclusively z or \bar{z} satisfies. Let us return to the background field (3.60). Rewriting in

¹⁰Strictly speaking, z and z^* are not independent. However, the formal manipulations can be justified by promoting x and y to complex numbers so that $(z, \bar{z}) \in \mathbb{C}^2$. The ∂ and $\bar{\partial}$ derivatives then follow the standard derivative rules of calculus. After performing computations we can restrict the results to the “real surface,” $\{(z, \bar{z}) \in \mathbb{C}^2 \mid \bar{z} = z^*\}$.

complex coordinates shows that it happens to appear in this convenient form,

$$h_{\text{bg}}(\mathbf{z}) = a_0 + \sum_{n \geq 1} \frac{a_n}{2} (z^n + \bar{z}^n). \quad (3.76)$$

The corresponding full-theory response (3.64) also appears in an elegant form:

$$\delta h(\mathbf{z}) = - \sum_{n \geq 2} \frac{a_n}{2} R^{2n} (z^{-n} + \bar{z}^{-n}). \quad (3.77)$$

Let us finally put everything together. The background field satisfies $\partial^n h_{\text{bg}}(0) = n!a_n/2$, singling out only the n^{th} multipole order. This fits our expectations about multipole fields and symmetry—a multipole background field of order n impinging on a circular boundary with vanishing Dirichlet conditions (*e.g.*, a perfect conductor) will produce a strictly n^{th} -order multipole response. This indeed is the case according to Eq. (3.75). Matching the full and effective responses can therefore be performed order-by-order without mixing, and the matching condition $\delta h(\mathbf{z}) \stackrel{!}{=} \delta h_{\text{f}}^{\text{eff}}(\mathbf{z})$ becomes

$$- \frac{(n-1)!C^{(n)}}{4\pi\sigma} \frac{n!a_n}{2} \stackrel{!}{=} - \frac{a_n}{2} R^{2n}. \quad (3.78)$$

Thus we find the set of polarizabilities for free, flat particles:

$$C_a^{(n)} = \frac{4\pi\sigma R_a^{2n}}{n!(n-1)!} \quad (n \geq 2). \quad (3.79)$$

Some remarks on the regulator

Before proceeding, a few comments are in order regarding the capillary length. When ℓ_c is finite, we include the gravitational term $\ell_c^{-2}h^2$ in the Hamiltonian, and the bulk Euler-Lagrange equation is modified to $(-\nabla^2 + \ell_c^{-2})h = 0$. That is, $\nabla^2 h = \ell_c^{-2}h \neq 0$, so the attentive reader might question the validity of dropping Laplacian terms in the effective worldline Hamiltonian (3.67). The reason this is still permissible is that the *complete* effective Hamiltonian is constructed out of *all* possible terms, so we may indeed apply the bulk Euler-Lagrange equations to replace $\nabla^2 h$ with $\ell_c^{-2}h$, but in doing so we will ultimately reproduce terms that already appear. Since the Wilson coefficients were yet undetermined, we can simply absorb the ℓ_c^{-2} contributions into the coefficients and end up with the same form for the effective Hamiltonian, but with the knowledge that they have implicit ℓ_c -dependencies. Now, since the bulk symmetries are slightly different, namely the transformation \mathbf{T}_2 no longer leaves the bulk Hamiltonian invariant, we find that terms linear in h , as well as a quadratic h^2 term (without derivatives), are now generally permissible. This is actually not undesirable, since our particle degrees of freedom may break those symmetries anyway. In fact, this is precisely why we wished to include the gravity term in the first place; for (BC 1) particles, fixing the height breaks vertical translation symmetry

and excites the ill-defined and divergent zero modes of the bulk Hamiltonian. Breaking the symmetry in the bulk allows the divergences to be tamed, with ℓ_c acting as a regulator.

Now, we still wish to work in the regime of vanishing Bond number, so the gravitational term appears as a *bulk perturbation*. This necessarily breaks the bulk symmetries, but they are restored when $\ell_c \rightarrow \infty$. If we were to keep ℓ_c finite, we could still do the matching using Eqs. (3.53) and (3.69) (or even Eq. (3.72)), but the higher-order derivatives would be significantly more tricky thanks to the Bessel functions. We would find that the polarizabilities would depend on ℓ_c , but in such a way that they are regular for $\ell_c \rightarrow \infty$ and ultimately reproduce Eq. (3.79) in the limit. The terms that break vertical height translation symmetry will also have a dependence on ℓ_c , but instead of decaying as ℓ_c^{-p} for some power p , they would do so with a logarithmic correction, similar to the $(h_0 - a_0)$ term in Eq. (3.62). As we will see later, this logarithmic behavior is important in properly capturing interactions with surface monopoles that are finite and nonzero, even with $\ell_c \rightarrow \infty$.

3.3.2 EFT for constrained flat particles: induced sources

The induced polarization effects of the previous section also apply to the two remaining boundary condition types, (BC 1) and (BC 2). However, fixing the height and tilt of a particle requires external forces that may change in response to those imposed by a background field. This is analogous to a conductor maintained at a fixed electrostatic potential: it must be connected to some reservoir of charge (*e.g.*, a battery) so that charge may flow to and from the conductor surface to make up for the potential difference. We will discuss now how to incorporate these effects into the worldline Hamiltonian for flat particle. Just as before, we need only discuss fixing the height and tilt for flat particles in the equilibrium configuration, $h_0 = 0$ and $\mathbf{s} = \mathbf{0}$, as enforcing nonzero values must be handled by additional terms that can be treated separately.

(BC 2). First consider the case (BC 2) in which the particle slope \mathbf{s} is fixed to zero, but is free to bob in the vertical direction. That is, $h \rightarrow h + h_0$ is still a symmetry for $\Delta\mathcal{H}$, but $h \rightarrow h + \mathbf{s} \cdot \mathbf{x}$ is not. This means an additional term proportional to $(\nabla h)^2$ is now permissible, so in addition to Eq. (3.67), such particles provide the additional $n = 1$ contribution:

$$\Delta\mathcal{H}_f[h] = \sum_a \sum_{n \geq 1} \frac{1}{2} c_a^{(n)} [\partial_I^n h(\mathbf{x}_a)]^2 \quad (3.80a)$$

$$= \sum_a \sum_{n \geq 1} C_a^{(n)} [\partial^n h \bar{\partial}^n h] \Big|_{z=z_a}, \quad (3.80b)$$

where we have gone ahead and rewritten the expression in complex coordinates. Since the polarizabilities for $n \geq 2$ have already been determined, we need only match $C_a^{(1)}$. Using the same background field (3.76) and $\mathbf{s} = \mathbf{0}$, the full-theory response is given by

Eq. (3.77) but with the $n = 1$ term included in the sum. Hence, the expression (3.79) for the polarizabilities holds also for $n = 1$ and $C_a^{(1)} = 4\pi\sigma R^2$.

(BC 1). Now consider particles with both height and tilt fixed such that $h_0 = 0$ and $\mathbf{s} = \mathbf{0}$. This is the notorious case which breaks the bulk $h \rightarrow h + h_0$ symmetry. In addition to Eq. (3.80), this case allows for one more symmetry-breaking contribution which is proportional to h^2 . Given its significance, we will isolate the contribution and write

$$\Delta\mathcal{H}_f^m[h] = \frac{1}{2} \sum_a M_a^{(0)} h^2(\mathbf{x}_a), \quad (3.81)$$

where “m” stands for “monopole.” By dimensional analysis, we see that $M^{(0)} \sim \sigma$ and thus cannot be treated perturbatively in R . This will add a few subtleties later on when calculating interactions. Finding its value, however, is simple. An imposed background field h_{bg} will induce a monopole response, sourced by the external constraint forces—akin to a conductor drawing charge from a battery—which for a single particle at the origin takes the form

$$\delta h_m^{\text{eff}}(\mathbf{x} | h_{\text{bg}}) = -M^{(0)} h_{\text{bg}}(0) G(\mathbf{x}) = -\frac{M^{(0)}}{2\pi} h_{\text{bg}}(0) \ln\left(\frac{2\ell_c}{r\gamma_e}\right). \quad (3.82)$$

The only multipole background that excites this response is a constant shift in height, $h_{\text{bg}}(0) = a_0$, for which the full-theory response is given by the first term in Eq. (3.62) (with $h_0 = 0$). Matching coefficients therefore gives the monopole polarizability,

$$M_a^{(0)} = \frac{2\pi\sigma}{\ln\left(\frac{2\ell_c}{R_a\gamma_e}\right)}. \quad (3.83)$$

Note that among all polarizabilities, this is the only one that explicitly depends on the capillary length. Hence, we might expect that later taking the $\ell_c \rightarrow \infty$ limit may be tricky.

3.3.3 EFT for curved particles: permanent sources

So far, we have constructed an effective Hamiltonian that reproduces the particle-surface responses induced by an external background field. As we mentioned before, a particle may also impart permanent deformations in the surface either due to the curvature of the contact line, or due to fixing the particle’s height or tilt away from its equilibrium position. In both cases, these deformations cost energy which either must be supplied by the material properties of the particle, or via external forcing mechanisms. In the previous section we discussed how the force “reservoirs” respond to match and cancel any imposed height differences at the particle’s boundary due to external fields. Fixing any height deviations from equilibrium, then, will be accounted for by *permanent* sources, independent of the background. To clarify, it is the permanent sources which force fixed surface deformations in the ground state, but the induction terms are responsible for maintaining the particle position and contact line against background deformations. In the language of the functional,

these permanent sources must necessarily persist even when $h_{\text{bg}} = 0$ and are given by $(\delta\Delta\mathcal{H}/\delta h)|_{h=0}$. That is, they must appear as terms *linear* in (derivatives of) h , evaluated at the particle position. The permanent distribution of charges at the boundaries does not need to respect rotational symmetry, so the most general worldline source Hamiltonian takes the form

$$\Delta\mathcal{H}_{\text{p}}[h] = - \sum_a \sum_{n \geq 0} (\mathcal{Q}_a^{(n)})_{i_1 \dots i_n} \partial_{i_1} \dots \partial_{i_n} h(\mathbf{x}_a) \quad (3.84a)$$

$$= - \sum_a \left\{ Q_a^{(0)} h + \sum_{n \geq 1} \left[Q_a^{(n)} \partial^n h(\mathbf{z}_a) + \bar{Q}_a^{(n)} \bar{\partial}^n h(\mathbf{z}_a) \right] \right\}, \quad (3.84b)$$

where in the first line the tensors $\mathcal{Q}_I^{(n)}$ are completely (pairwise) traceless to remove any Laplacians on h , and in the second line we have transformed to complex coordinates, with $\bar{Q}^{(n)} = [Q^{(n)}]^*$ so that $\Delta\mathcal{H}_{\text{p}}$ is real. In the rest of this chapter we will work primarily in complex coordinates, so the relationship between $\mathcal{Q}_I^{(n)}$ and $Q^{(n)}$ is unimportant. The resulting permanent source for a single particle at the origin is therefore

$$\rho_{\text{p}}(\mathbf{z}) = Q^{(0)} \delta(\mathbf{z}) + \sum_{n \geq 1} \left[Q^{(n)} (-\partial)^n + \bar{Q}^{(n)} (-\bar{\partial})^n \right] \delta(\mathbf{z}), \quad (3.85)$$

and convolving this with the Green function gives the permanent response,

$$\begin{aligned} \delta h_{\text{p}}^{\text{eff}}(\mathbf{z}) &= \frac{1}{\sigma} Q^{(0)} G(\mathbf{z}) + \frac{1}{\sigma} \sum_{n \geq 1} \left[Q^{(n)} (-\partial)^n G(\mathbf{z}) + \bar{Q}^{(n)} (-\bar{\partial})^n G(\mathbf{z}) \right] \\ &= \frac{Q^{(0)}}{2\pi\sigma} \ln\left(\frac{2\ell_{\text{c}}}{r\gamma_{\text{e}}}\right) + \sum_{n \geq 1} \frac{(n-1)!}{4\pi\sigma} \left(\frac{Q^{(n)}}{z^n} + \frac{\bar{Q}^{(n)}}{\bar{z}^n} \right) \end{aligned} \quad (3.86)$$

Fixed height and tilt. As we found in Eq. (3.62), fixing the particle height h_0 and tilt \mathbf{s} entails a permanent field response,

$$\delta h(\mathbf{x} \mid h_0, \mathbf{s}) = h_0 \frac{\ln\left(\frac{2\ell_{\text{c}}}{r\gamma_{\text{e}}}\right)}{\ln\left(\frac{2\ell_{\text{c}}}{R\gamma_{\text{e}}}\right)} + (\mathbf{s} \cdot \hat{\mathbf{r}}) \frac{R^2}{r}. \quad (3.87)$$

To compare with Eq. (3.86), we first rewrite the above expression with the second term in complex coordinates:

$$\delta h(\mathbf{z} \mid h_0, \mathbf{s}) = h_0 \frac{\ln\left(\frac{2\ell_{\text{c}}}{r\gamma_{\text{e}}}\right)}{\ln\left(\frac{2\ell_{\text{c}}}{R\gamma_{\text{e}}}\right)} + \frac{\vartheta R^2}{2} \left(\frac{e^{i\theta}}{z} + \frac{e^{-i\theta}}{\bar{z}} \right), \quad (3.88)$$

where ϑ and θ are defined via $s_x + is_y = \vartheta e^{i\theta}$ and represent a rising vertical slope of magnitude ϑ oriented the direction an angle θ from the x -axis in the base plane.¹¹ Finally, setting $\delta h_p^{\text{eff}}(z) \stackrel{!}{=} \delta h(z | h_0, \mathbf{s})$ solves for the two nonvanishing charges,

$$Q_a^{(0)} = h_0 \frac{2\pi\sigma}{\ln\left(\frac{2\ell_c}{R\gamma_e}\right)} \quad (3.89)$$

and

$$Q^{(1)} = 2\pi\sigma \vartheta R^2 e^{i\theta}. \quad (3.90)$$

Observe that the monopole charge satisfies $Q^{(0)} = M^{(0)} h_0$, with $M^{(0)}$ given in Eq. (3.83), analogous to the capacitance equation $Q = C\Phi$ in electrostatics.

Saddle-shaped particles. The remaining terms with $n \geq 2$ in Eq. (3.86) correspond to sources that fix the permanent curvature at the contact line. We have already calculated the permanent surface response for a saddle-shaped particle in Eq. (3.61). We re-express the solution in complex coordinates and find

$$\delta h(z | S, \alpha) = -\frac{1}{4} S R^4 \left(\frac{e^{2i\alpha}}{z^2} + \frac{e^{-2i\alpha}}{\bar{z}^2} \right). \quad (3.91)$$

Matching with Eq. (3.86) then selects the permanent charge

$$Q^{(2)} = -\pi\sigma S R^4 e^{2i\alpha}. \quad (3.92)$$

General contact line. We mentioned earlier, that the contact line profile $h^{\text{ct}}(\mathbf{x})$ of any generic, compact particle could be described by decomposing its representation at the boundary into Fourier modes via Eqs. (3.54) and (3.44). For completeness, we will briefly discuss this procedure and the corresponding EFT description.

Recall from Eq. (3.10) that an arbitrary contact line h^{ct} can be represented by its Taylor series about the particle origin, which we will reproduce here for convenience in the compact form

$$h^{\text{ct}}(\mathbf{x}) = \sum_{n \geq 0} \frac{1}{n!} x_I^n \partial_I^n h^{\text{ct}}(0). \quad (3.93)$$

We discussed the interpretation of such terms: $n = 0$ corresponds to height, $n = 1$ gives the tilt, and $n \geq 2$ describes the permanent curvature. We selected the first such curvature term and found it corresponded to a *quadrupole* moment or saddle shape. Part of this

¹¹This form result from rewriting $(\mathbf{s} \cdot \hat{\mathbf{r}})/r$ in complex coordinates using $1/z = (\cos \varphi - i \sin \varphi)/r$. Rearranging terms yields the form

$$\frac{(\mathbf{s} \cdot \hat{\mathbf{r}})}{r} = \frac{1}{2} \left(\frac{s_x + is_y}{z} + \frac{s_x - is_y}{\bar{z}} \right).$$

Defining the complex number $\vartheta e^{i\theta} = s_x + is_y$ then leads to the result (3.88).

interpretation relies on the information revealed by discussing surface energetics: the surface is insensitive to a particle's *total curvature* unless acted upon by an external force. That is, in our representation of the contact line, we should choose $\nabla^2 h^{\text{ct}} = 0$ to avoid unnecessary or redundant information. This is actually a bonus for our analysis, because h^{ct} is therefore a real harmonic function and in complex coordinates decomposes into $h^{\text{ct}}(z, \bar{z}) = f(z) + \bar{f}(\bar{z})$ for some function f . Applying the transformation (3.70) and using $\partial\bar{\partial}h^{\text{ct}} = 0$ puts Eq. (3.93) into the form

$$h^{\text{ct}}(z) = h^{\text{ct}}(0) + \sum_{n \geq 1} \frac{1}{n!} [z^n \partial^n h^{\text{ct}}(0) + \bar{z}^n \bar{\partial}^n h^{\text{ct}}(0)]. \quad (3.94)$$

On the particle boundary $\partial\mathcal{A}$, $z = R e^{i\varphi}$ and the contact line indeed becomes a Fourier series,

$$h^{\text{ct}}(\varphi | \partial\mathcal{A}) = h^{\text{ct}}(0) + \sum_{n \geq 1} \frac{R^n}{n!} [\partial^n h^{\text{ct}}(0) e^{in\varphi} + \bar{\partial}^n h^{\text{ct}}(0) e^{-in\varphi}], \quad (3.95)$$

with Fourier modes $a_n = \partial^n h^{\text{ct}}(0) R^n / n!$ (and complex conjugate). The permanent response then follows by matching coefficients to a general exterior solution, giving

$$\delta h(z | h^{\text{ct}}) = h^{\text{ct}}(0) \frac{\ln(\frac{2\ell_c}{r\gamma_e})}{\ln(\frac{2\ell_c}{R\gamma_e})} + \sum_{n \geq 1} \frac{R^{2n}}{n!} \left(\frac{\bar{\partial}^n h^{\text{ct}}(0)}{z^n} + \frac{\partial^n h^{\text{ct}}(0)}{\bar{z}^n} \right). \quad (3.96)$$

Finally, we match this solution to the EFT result (3.86) and find the complete set,¹²

$$Q_a^{(0)} = \frac{2\pi\sigma}{\ln(\frac{2\ell_c}{R_a\gamma_e})} h_a^{\text{ct}}(0), \quad (3.97a)$$

$$Q_a^{(n)} = \frac{4\pi\sigma R_a^{2n}}{n!(n-1)!} \bar{\partial}^n h_a^{\text{ct}}(0) \quad (n \geq 1), \quad (3.97b)$$

where we have reinstated the particle label a . The special cases we have considered can be verified by substitution, and directly reproduce the expressions (3.89), (3.90), and (3.92).

Polarizabilities and preferred shape

In light of the previous discussion, let us remark on an additional conceptualization of the particle polarizabilities. Looking back on the expressions (3.97a) and (3.97b), we observe that the prefactors precisely match the expressions for the polarizabilities (3.83) and (3.79); *i.e.*,

$$Q_a^{(0)} = M_a^{(0)} h_a^{\text{ct}}(0) \quad \text{and} \quad Q_a^{(n \geq 1)} = C_a^{(n)} \bar{\partial}^n h_a^{\text{ct}}(0). \quad (3.98)$$

¹²If the particle is not centered on the origin, we simply translate the argument of $h_a^{\text{ct}}(\mathbf{x})$ via $h_a^{\text{ct}}(\mathbf{x} - \mathbf{x}_a)$ so that when evaluated at the particle position $\mathbf{x} = \mathbf{x}_a$, it still gives the *same values* $h_a^{\text{ct}}(0)$. Higher-order derivatives should be interpreted similarly in these expressions.

Written in this form, the interpretation of $M^{(0)}$ and $C^{(n)}$ respectively as the self-capacitance and n^{th} -order polarizability¹³ is even more clearly appropriate: Given the source fields $\bar{\partial}^n h^{\text{ct}}(0)$ due to particle properties or external mechanisms, the permanently induced charge (*force*) distributions $Q^{(n)}$ are characterized by the self-capacitance and polarizabilities.

Substituting the above expressions into Eq. (3.84) leads to an interesting simplification. Comparing the resulting terms with those in Eqs. (3.80) and (3.81) shows that one may complete the square in the following way:

$$\begin{aligned}
 & \frac{1}{2} M_a^{(0)} h^2(\mathbf{x}_a) + \sum_{n \geq 1} C_a^{(n)} |\partial^n h(\mathbf{z}_a)|^2 - Q_a^{(0)} h - \sum_{n \geq 1} \left[Q_a^{(n)} \partial^n h(\mathbf{z}_a) + \bar{Q}_a^{(n)} \bar{\partial}^n h(\mathbf{z}_a) \right] \\
 &= \frac{1}{2} M_a^{(0)} \left(h(\mathbf{z}_a) - \frac{Q_a^{(0)}}{M_a^{(0)}} \right)^2 + \sum_{n \geq 1} C_a^{(n)} \left| \partial^n h(\mathbf{z}_a) - \frac{\bar{Q}_a^{(n)}}{C_a^{(n)}} \right|^2 - \frac{1}{2} \frac{[Q_a^{(0)}]^2}{M_a^{(0)}} - \sum_{n \geq 1} \frac{|Q_a^{(n)}|^2}{C_a^{(n)}} \\
 &= \frac{1}{2} M_a^{(0)} [h(\mathbf{z}_a) - h_a^{\text{ct}}(0)]^2 + \sum_{n \geq 1} C_a^{(n)} |\partial^n h(\mathbf{z}_a) - \partial^n h_a^{\text{ct}}(0)|^2 \\
 &\quad - \frac{1}{2} M_a^{(0)} [h_a^{\text{ct}}(0)]^2 - \sum_{n \geq 1} C_a^{(n)} |\partial^n h_a^{\text{ct}}(0)|^2
 \end{aligned} \tag{3.99}$$

Notice the way in which the contact line appears. We may understand this in two ways. First, the worldline energy as expressed above appears with h^{ct} behaving as an external background field. To make this evident, let us express the *source-free* ($Q^{(n)} = 0$) worldline terms as

$$\Delta \mathcal{H}^{\text{f}}[h] = \sum_a \int d^2 x \Delta \mathcal{H}_a^{\text{f}}[h(\mathbf{x})] \delta(\mathbf{x} - \mathbf{x}_a), \tag{3.100}$$

where the δ -function serves to evaluate the terms at the particle positions. Then, the inclusion of external sources that fix the contact line is handled by including h^{ct} as a background field via

$$\Delta \mathcal{H}_a^{\text{f}}[h(\mathbf{x})] \rightarrow \Delta \mathcal{H}_a^{\text{f}}[h(\mathbf{x}) - h_a^{\text{ct}}(\mathbf{x} - \mathbf{x}_a)] - \Delta \mathcal{H}_a^{\text{f}}[h^{\text{ct}}(\mathbf{x} - \mathbf{x}_a)], \tag{3.101}$$

where the argument of h^{ct} evaluates to the particle positions as per footnote 12. The second term above gives the (negative) external work done to maintain the contact line. We note in passing that the monopole term of Eq. (3.99)—the first term after the last equality—is reminiscent of the way in which Lehle and Oettel include a harmonic potential to model laser tweezers acting on a colloid [LO07]. We will return to this in Section 3.7.

The inclusion of sources via (3.99) and (3.101) is also similar to the way in which spontaneous curvature is included in the Helfrich energy (*cf.* Eq. (2.36)), and provides an alternative interpretation. For each possible permanent deformation implicitly sourced via h^{ct} , there exists a *preferred background field* $h_p^{(n)}$ such that it satisfies the boundary conditions and $\partial^n h_p^{(n)}(\mathbf{z}_a) = \partial^n h_a^{\text{ct}}(0)$, and thus no $2n$ -pole excitation occurs. Likewise, we

¹³*i.e.*, a $2n$ -pole polarizability

may interpret h^{ct} as the *preferred shape* for a particle in a given background field if its permanent deformation conforms exactly to that of the background field. We have used this idea implicitly when discussing the responses to generic particle shapes. Namely, the saddle shaped particles impart a permanent quadrupolar deformation in the surface, and thus there exists a preferred quadrupolar background that directly counters and conforms to this deformation.

Permanent charges and force balance

We conclude this section with a short discussion of the relationship between permanent sources and polarizabilities. The relationships expressed in Eq. (3.98) are not mere coincidence, but reflect the force balance at the particle contact line. To understand this, let us reconsider fixing the contact line explicitly in the energy functional. The remarks leading up to Eq. (3.101) motivate thinking of the external sources as imposing a background field h^{ct} centered at the particle position. However, the resulting forces must be balanced for there to exist an equilibrium solution for an unperturbed particle. Any permissible field configurations h beyond h^{ct} should be governed by the energy difference $\mathcal{H}[h + h^{\text{ct}}] - \mathcal{H}[h^{\text{ct}}]$, but with the restriction that the net *permanent* source (force distributions) vanish. We can extract an explicit consistency condition by expanding the energy functional and identifying the quantity coupling linearly to h as the total force distribution ρ_{tot} and setting it to zero:

$$\begin{aligned} \mathcal{H}[h + h^{\text{ct}}] - \mathcal{H}[h^{\text{ct}}] &= \int d^2x \left. \frac{\delta \mathcal{H}}{\delta h} \right|_{h^{\text{ct}}} h(\mathbf{x}) + \frac{1}{2} \int d^2x d^2x' \left. \frac{\delta^2 \mathcal{H}}{\delta h(\mathbf{x}) \delta h(\mathbf{x}')} \right|_{h^{\text{ct}}} h(\mathbf{x}) h(\mathbf{x}') \\ &\equiv - \int d^2x \rho_{\text{tot}}(\mathbf{x} | h^{\text{ct}}) h(\mathbf{x}) + (\mathcal{H}_0[h] + \mathcal{H}_f[h]), \end{aligned} \quad (3.102)$$

where on the right side the integral reproduces the purely quadratic terms and \mathcal{H}_f includes the monopole term (3.81). Force balance therefore requires that

$$\begin{aligned} \rho_{\text{tot}}(\mathbf{x} | h^{\text{ct}}) &= - \left. \frac{\delta \mathcal{H}_0}{\delta h} \right|_{h^{\text{ct}}} - \left. \frac{\delta \Delta \mathcal{H}_f}{\delta h} \right|_{h^{\text{ct}}} - \left. \frac{\delta \Delta \mathcal{H}_p}{\delta h} \right|_{h^{\text{ct}}} \\ &= 0 + \rho_f(\mathbf{x} | h^{\text{ct}}) + \rho_p(\mathbf{x} | h^{\text{ct}}) \stackrel{!}{=} 0, \end{aligned} \quad (3.103)$$

where the vanishing of the bulk derivative follows from $-\sigma \nabla^2 h^{\text{ct}} = 0$ (see Section 3.2).¹⁴ Applying this condition not only verifies the consistency of our matching procedure, but

¹⁴Equation (3.103) is somewhat similar to the *average-force cancellation* condition of Ref. [BLDW07]. There, the condition arises as a necessary (but not sufficient) requirement for there to exist a global solution for a fluid surface of constant mean curvature when in the absence of gravity. Namely, if one appends to the surface energy both the energy costs of a pressure difference, $-\int_{\Omega} d^2x \Delta p h(\mathbf{x})$, and the forces at the outer boundary, $-\oint_{\partial\Omega} ds \tilde{\sigma}(s) h(\mathbf{x})$, the condition reads

$$Q := \Delta p \times \text{Area}(\Omega) + \oint_{\partial\Omega} ds \tilde{\sigma}(s) \stackrel{!}{=} 0.$$

also provides the permanent sources *for free*:

$$\begin{aligned}
 \rho_f(\mathbf{z} | h^{\text{ct}}) + \rho_p(\mathbf{z} | h^{\text{ct}}) &= -M^{(0)}h^{\text{ct}}(0)\delta(\mathbf{z}) - \sum_{n \geq 1} C^{(n)} [(-\partial)^n \delta(\mathbf{z}) \bar{\partial}^n h^{\text{ct}}(0) + \text{c.c.}] \\
 &\quad + Q^{(0)}\delta(\mathbf{z}) + \sum_{n \geq 1} [Q^{(n)}(-\partial)^n \delta(\mathbf{z}) + \text{c.c.}] \\
 &= [Q^{(0)} - M^{(0)}h^{\text{ct}}(0)]\delta(\mathbf{z}) \\
 &\quad + \sum_{n \geq 1} \left\{ [Q^{(n)} - C^{(n)}\bar{\partial}^n h^{\text{ct}}(0)](-\partial)^n \delta(\mathbf{z}) + \text{c.c.} \right\} \quad (3.104)
 \end{aligned}$$

Setting the above equation to zero therefore reproduces the matched expressions in Eq. (3.98).

By now we have completely rewritten and restructured the original problem in a point-particle EFT framework. The Hamiltonian for the surface or interface is simply that of a particle-free gradient-squared theory with a gravitational perturbation serving to regulate divergences, Eq. (3.66). The structure of the originally finite-sized particles is recaptured in a local derivative expansion, which encodes particle polarizabilities, Eqs. (3.80) and (3.81), and possible finite deformations due to the shape and conditions on the particle contact lines, Eq. (3.84). The complete sets of Wilson coefficients for both expansions have also been determined—respectively Eqs. (3.79) (including $n = 1$) and (3.83), and Eqs. (3.97) and (3.98), with special cases for height, tilt, and saddle shapes: Eqs. (3.89), (3.90), and (3.92). Since it has been a rather lengthy journey with important results scattered along the way, we summarize the complete effective Hamiltonian in Technical Note 3.1.

3.4 Surface-mediated interactions: Preliminaries

We are now in the position to calculate surface-mediated interactions between bound particles. Such interactions arise from the free energy difference with respect to the particle-free surface, and depend on the spatial arrangements—and possibly the orientations—of the bound particles. In what follows we will not only be interested in ground state interactions, which necessarily must be sourced by permanent deformations or external forces, but also those induced by thermal fluctuations of the surface. As we discussed formally in Section 1.2.2 of the previous chapter, the relevant physics is completely captured in the thermodynamic partition function Z , and the corresponding interaction potentials may be extracted from the free energy difference $\mathcal{U} = \mathcal{F} - \mathcal{F}_0 = -k_B T \ln(Z/Z_0)$, where the subscript “0” refers to the particle-free system. By expanding the Hamiltonian as $\mathcal{H}_{\text{eff}} = \mathcal{H}_0 + \Delta\mathcal{H}$, we may treat the effects of particle inclusions perturbatively via Eq. (1.95), so finding \mathcal{U} amounts to calculating a series of cumulants $\propto \langle (\Delta\mathcal{H}[h])^q \rangle_c$. However, the the worldline Hamiltonian $\Delta\mathcal{H}$ itself contains many terms, so the number of terms in the cumulant

Technical Note 3.1: The complete EFT for circular particles

For convenience and reference, we present the complete effective Hamiltonian for circular particles on a tension-dominated surface (with the understanding $\ell_c \rightarrow \infty$):

$$\begin{aligned}\mathcal{H}_{\text{eff}}[h] &= \mathcal{H}_0[h] + \Delta\mathcal{H}_{\text{f}}[h] + \Delta\mathcal{H}_{\text{p}}[h] \\ &= \frac{\sigma}{2} \int_{\mathbb{R}^2} d^2x h(-\nabla^2 + \ell_c^{-2})h + \sum_a \left[\frac{1}{2} M_a^{(0)} h^2(\mathbf{z}_a) + \sum_{n \geq 1} C_a^{(n)} \partial^n h(\mathbf{z}_a) \bar{\partial}^n h(\mathbf{z}_a) \right] \\ &\quad - \sum_a \left\{ Q_a^{(0)} h(\mathbf{z}_a) + \sum_{n \geq 1} \left[Q_a^{(n)} \partial^n h(\mathbf{z}_a) + \bar{Q}_a^{(n)} \bar{\partial}^n h(\mathbf{z}_a) \right] \right\}.\end{aligned}$$

The values of the polarizabilities $C^{(n)}$ and $M^{(0)}$, and the permanent sources $Q^{(n)}$ depend on the particle's out-of-plane contact line curvature and fluctuation degrees of freedom:

$$\begin{aligned}\text{Polarizabilities:} &\quad \left\{ \begin{array}{ll} \text{(BC 1):} & M_a^{(0)} = \frac{2\pi\sigma}{\ln(\frac{2\ell_c}{R_a\gamma_e})}, \quad C_a^{(n)} = \frac{4\pi\sigma R_a^{2n}}{n!(n-1)!} \quad (n \geq 1) \\ \text{(BC 2):} & M_a^{(0)} = 0, \quad C_a^{(n)} = \frac{4\pi\sigma R_a^{2n}}{n!(n-1)!} \quad (n \geq 1) \\ \text{(BC 3):} & M_a^{(0)} = 0, \quad C_a^{(1)} = 0, \quad C_a^{(n)} = \frac{4\pi\sigma R_a^{2n}}{n!(n-1)!} \quad (n \geq 2) \end{array} \right. \\ \text{Permanent charges:} &\quad Q_a^{(0)} = M_a^{(0)} h_a^{\text{ct}}(0), \quad Q_a^{(n)} = C_a^{(n)} \bar{\partial}^n h_a^{\text{ct}}(0) \quad (n \geq 1) \\ \text{Special cases:} &\quad \left\{ \begin{array}{ll} \text{height:} & h_a^{\text{ct}}(0) = h_{0,a}, \quad Q_a^{(0)} = \frac{2\pi\sigma}{\ln(\frac{2\ell_c}{R_a\gamma_e})} h_{0,a} \\ \text{tilt:} & \bar{\partial} h_a^{\text{ct}}(0) = \frac{\vartheta_a}{2} e^{i\theta_a}, \quad Q_a^{(1)} = 2\pi\sigma \vartheta_a R_a^2 e^{i\theta_a} \\ \text{curvature:} & \bar{\partial}^2 h_a^{\text{ct}}(0) = -\frac{1}{2} S_a e^{2i\alpha_a}, \quad Q_a^{(2)} = -\pi\sigma S_a R_a^4 e^{2i\alpha_a} \end{array} \right.\end{aligned}$$

expansion quickly proliferates and requires a transparent bookkeeping system. Fortunately, there exists a standard tool from quantum and statistical field theory that provides such a system: Feynman diagrams.

3.4.1 The diagrammatic technique

To standardize our treatment, we will briefly review the technique of Feynman diagrams as it pertains to our quadratic theory. More elaborate and detailed discussions can of course be found in standard books (for examples, Refs. [NO88, BDFN95, ZJ02, Zee03, Vas04]).

Consider the following functional integral with a real symmetric and positive-definite kernel function $K(\mathbf{x}, \mathbf{x}')$

$$Z_0 = \int \mathcal{D}h e^{-\frac{1}{2} \mathbf{h}^\top \mathbf{K} \mathbf{h}}, \quad (3.105)$$

where we have used the abbreviated notation

$$\mathbf{h}^\top \mathbf{K} \mathbf{h} \equiv \int d^2x d^2x' h(\mathbf{x}) K(\mathbf{x}, \mathbf{x}') h(\mathbf{x}'). \quad (3.106)$$

The reason for the font choice and transpose symbol is to make manifest the connection to linear algebra, where the indices are instead continuous and the inner product corresponds to spatial integration.¹⁵ For many applications, including ours, the kernel represents some differential operator $D(\partial)$ and can be expressed as $K(\mathbf{x}, \mathbf{x}') = D(\partial_x) \delta(\mathbf{x} - \mathbf{x}')$. The meaning of the transpose then relates to integration by parts such that for every derivative $\partial^\top = -\partial$.

If the indices were discrete so that $\mathbf{K} \mathbf{h} = K_{ij} h_j$ and $\mathcal{D}h = \prod_i dh_i$, the answer could be directly calculated. To do so, one could diagonalize \mathbf{K} by an orthogonal transformation, thereby decoupling the integral into a product of single-variable Gaussian integrals. The result would then contain a product of all eigenvalues of \mathbf{K} , which is identified with the determinant, finally giving

$$Z_0 = \left(\det \frac{\mathbf{K}}{2\pi} \right)^{-1/2}. \quad (3.107)$$

The functional integral (3.105) is the continuum generalization of the above result, and indeed the functional determinant can be formally defined by the above expression [Vas04]. Note that in passing to the continuum limit, there are many mathematical subtleties in rigorously defining and regularizing such functional determinants (see, for instance Ref. [Dun08]), but for our purposes it will suffice to proceed formally.

Now consider adding linear (source) and quadratic perturbations,

$$Z = \int \mathcal{D}h e^{-\frac{1}{2} \mathbf{h}^\top \mathbf{K} \mathbf{h} - \frac{1}{2} \mathbf{h}^\top \mathbf{V} \mathbf{h} + \mathbf{J}^\top \mathbf{h}}. \quad (3.108)$$

This is the same form as in our effective theory with the identifications

$$K(\mathbf{x}, \mathbf{x}') = \frac{\delta^2(\beta \mathcal{H}_0)}{\delta h(\mathbf{x}) \delta h(\mathbf{x}')} \quad (3.109a)$$

$$V(\mathbf{x}, \mathbf{x}') = \frac{\delta^2(\beta \Delta \mathcal{H}_f)}{\delta h(\mathbf{x}) \delta h(\mathbf{x}')}, \quad (3.109b)$$

$$J(\mathbf{x}) = -\frac{\delta(\beta \Delta \mathcal{H}_p)}{\delta h(\mathbf{x})}, \quad (3.109c)$$

with \mathcal{H}_0 , $\Delta \mathcal{H}_f$, and $\Delta \mathcal{H}_p$ given in Technical Note 3.1. Using the functional identity

$$\frac{\delta}{\delta J(\mathbf{x})} e^{\mathbf{J}^\top \mathbf{h}} = h(\mathbf{x}) e^{\mathbf{J}^\top \mathbf{h}}, \quad (3.110)$$

¹⁵This connection is precisely what Dirac's *bra-ket* notation was invented for, but we wish to avoid a confusing clash between inner products and thermal averages.

we may replace instances of h with functional derivatives of the source J . In particular, we may pull the quadratic perturbation (V) outside the functional integral:

$$Z = \sum_{k \geq 0} \frac{1}{k!} \left(-\frac{1}{2} \frac{\delta^\top}{\delta \mathbf{J}} \mathbf{V} \frac{\delta}{\delta \mathbf{J}} \right)^k \int \mathcal{D}h e^{-\frac{1}{2} \mathbf{h}^\top \mathbf{K} \mathbf{h} + \mathbf{J}^\top \mathbf{h}}, \quad (3.111)$$

where the functional operator is shorthand for

$$\frac{\delta^\top}{\delta \mathbf{J}} \mathbf{V} \frac{\delta}{\delta \mathbf{J}} = \int d^2x d^2x' \frac{\delta}{\delta J(\mathbf{x})} V(\mathbf{x}, \mathbf{x}') \frac{\delta}{\delta J(\mathbf{x}')} \quad (3.112)$$

and the integrals and derivatives act on everything to the right.¹⁶ The functional integral can then be calculated by “completing the square” in the exponent, which may be accomplished by simply shifting the field via $\mathbf{h} \rightarrow \mathbf{h} + \mathbf{K}^{-1} \mathbf{J}$, where \mathbf{K}^{-1} is the inverse of the kernel $K(\mathbf{x}, \mathbf{x}')$ and satisfies

$$\mathbf{K}^{-1} \mathbf{K} = \mathbf{1} \iff \int d^2x'' K^{-1}(\mathbf{x}, \mathbf{x}'') K(\mathbf{x}'', \mathbf{x}') = \delta(\mathbf{x} - \mathbf{x}'). \quad (3.113)$$

For differential operators, the inverse corresponds to the Green function, and in our problem

$$K^{-1}(\mathbf{x}, \mathbf{x}') = (\beta\sigma)^{-1} G(\mathbf{x} - \mathbf{x}') \quad (3.114)$$

with G given by Eq. (3.38) (or equivalently Eq. (3.73)). With this in mind, we will use the notation $\mathbf{G} = \mathbf{K}^{-1}$. The inverse \mathbf{G} is also symmetric, a property inherited from \mathbf{K} . After substituting in the shifted field and expanding, we use this to simplify the terms in the exponent and find that the residual h -dependence factors out into the form (3.105), resulting in

$$Z = Z_0 \sum_{k \geq 0} \frac{1}{k!} \left(\frac{\delta^\top}{\delta \mathbf{J}} \mathbf{V} \frac{\delta}{\delta \mathbf{J}} \right)^k e^{\frac{1}{2} \mathbf{J}^\top \mathbf{G} \mathbf{J}}. \quad (3.115)$$

At this point, we can begin performing the functional derivatives, which bring down factors of \mathbf{G} and \mathbf{J} but otherwise leave the exponential intact. In this sense, the above expression generates a perturbative expansion for the partition function, where the index k counts how many times \mathbf{V} occurs in a given term. Writing

$$Z/Z_0 = e^{\frac{1}{2} \mathbf{J}^\top \mathbf{G} \mathbf{J}} \sum_{k \geq 0} \zeta^{(k)}, \quad (3.116)$$

¹⁶Note, however, that $V(\mathbf{x}, \mathbf{x}')$ does not depend on J , so the functional derivative passes through it.

we find the first couple of terms to be¹⁷ ($\zeta^{(0)} = 1$ trivially),

$$\zeta^{(1)} = -\frac{1}{2} \left[\text{tr} \mathbf{V} \mathbf{G} + \mathbf{J}^\top \mathbf{G} \mathbf{V} \mathbf{G} \mathbf{J} \right] \quad (3.117)$$

$$\begin{aligned} \zeta^{(2)} = \frac{1}{8} & \left[4 \mathbf{J}^\top \mathbf{G} \mathbf{V} \mathbf{G} \mathbf{V} \mathbf{G} \mathbf{J} + 2 \text{tr} \mathbf{V} \mathbf{G} \mathbf{V} \mathbf{G} + (\text{tr} \mathbf{V} \mathbf{G})^2 \right. \\ & \left. + 2(\text{tr} \mathbf{V} \mathbf{G})(\mathbf{J}^\top \mathbf{G} \mathbf{V} \mathbf{G} \mathbf{J}) + (\mathbf{J}^\top \mathbf{G} \mathbf{V} \mathbf{G} \mathbf{J})^2 \right], \end{aligned} \quad (3.118)$$

where the functional trace acting on some \mathbf{A} is defined via

$$\text{tr} \mathbf{A} \equiv \int d^2x A(\mathbf{x}, \mathbf{x}). \quad (3.119)$$

The form in which the factors contract with one another suggests the following graphical representation in terms of Feynman diagrams,

$$\zeta^{(1)} = \text{loop} + \text{line} \quad (3.120)$$

$$\begin{aligned} \zeta^{(2)} = & \text{line-line} + \text{loop-loop} + \frac{1}{2} \left[\text{loop} \right]^2 \\ & + \text{line-loop} + \frac{1}{2} \left[\text{line-line} \right]^2 \end{aligned} \quad (3.121)$$

In the above diagrams, each two-legged vertex represents a factor of $-\mathbf{V}$, each end node represents a factor of \mathbf{J} , and each connecting line represents a *propagator* \mathbf{G} . Additionally, each diagram is endowed with a combinatorial factor that relates to the symmetry of the diagram. We will return to this shortly. Taking a step back to Eq. (3.116), the associated free energy difference has the expansion (ordered according to the number of vertices)

$$\begin{aligned} -\beta \mathcal{U} = \ln(Z/Z_0) &= \frac{1}{2} \mathbf{J}^\top \mathbf{G} \mathbf{J} + \ln \left(1 + \sum_{k \geq 1} \zeta^{(k)} \right) \\ &= \frac{1}{2} \mathbf{J}^\top \mathbf{G} \mathbf{J} + \zeta^{(1)} + \left(\zeta^{(2)} - \frac{1}{2} [\zeta^{(1)}]^2 \right) + \dots \end{aligned} \quad (3.122)$$

¹⁷ To produce these expressions, one could revert to index notation

$$\frac{\delta}{\delta \mathbf{J}} (\mathbf{J}^\top \mathbf{G} \mathbf{J}) \implies \frac{\delta}{\delta J_i} (J_k G_{k\ell} J_\ell) = G_{i\ell} J_\ell + J_k G_{ki} \iff \mathbf{G} \mathbf{J} + \mathbf{G}^\top \mathbf{J} = 2 \mathbf{G} \mathbf{J}.$$

A similar calculation shows $\frac{\delta}{\delta \mathbf{J}} \mathbf{J}^\top \mathbf{V} \mathbf{G} \mathbf{J} = \text{tr} \mathbf{V} \mathbf{G}$. Alternatively, one could use $\frac{\delta}{\delta \mathbf{J}} \mathbf{J}^\top \mathbf{V} \frac{\delta}{\delta \mathbf{J}} = \text{tr} \mathbf{V} \frac{\delta}{\delta \mathbf{J}} \frac{\delta}{\delta \mathbf{J}}^\top$, where the trace and derivative operators act on everything to the right.

If one notices the disconnected part $\zeta^{(2)}$ —*i.e.*, the last three terms of Eq. (3.121)—combine to give $[\zeta^{(1)}]^2/2$, it is seen that these disconnected diagrams cancel out in the calculation of the free energy above. This property actually holds to all orders, with the conclusion that the free energy is given by the sum of all *connected* diagrams. This is nothing but the relation between cumulants and ordinary averages, but in diagrammatic form.

Since we only have one- and two-legged vertices (only linear and quadratic terms appear in \mathcal{H}), the only completely connected diagrams possible here are of linear and ring types. Hence the diagrammatic expansion of the free energy difference is given by

$$-\beta\mathcal{U} = \sum_{k \geq 0} \text{Diagram}_k + \sum_{k \geq 1} \text{Diagram}_k \quad (3.123)$$

Finally, let us track down all the numerical factors that end up as an overall combinatorial weight. For each diagram with k \mathbf{V} -vertices, we have a factor $(-1)^k/(k!2^k)$ simply coming from the Taylor expansion of the exponential factor (see Eqs. (3.111) and (3.115)). Now, in constructing the diagrams, there are $k!$ ways in which to order the \mathbf{V} -vertices, and a further 2^k ways of connecting them for each ordering, achieved by swapping the vertex legs. Hence, all the numerical factors cancel, except $(-1)^k$. However, this possibly overcounts the number of ways to construct the diagram by a factor S , which is called the *symmetry factor*. The reason for the overcounting is that some of the reordering and relinking mentioned above treat connections that can be rotated or reflected into one another as if they are distinct. Therefore, the symmetry factor counts the number of transformations that can be performed on the diagram that preserve its connectivity.¹⁸ The numerical factors for each diagram is then $(-1)^k/S$, correcting for the overcounting. For the linear diagrams, we can either do nothing (the identity) or reverse the vertex ordering, *i.e.*, perform one reflection, so $S = 2$. For the ring diagrams, the symmetry group consists of the identity plus rotations and reflections, *i.e.*, the dihedral group D_k , and thus $S = 2k$.

A more direct route

The previous discussion is a fairly standard treatment for (perturbatively) calculating the partition function and free energy. If the theory had instead some generic interactions $\mathcal{V}[h]$ which include perhaps higher-order terms beyond quadratic, the functional derivative identity (3.110) would allow for the replacement $\mathcal{V}[h] \rightarrow \mathcal{V}[\delta/\delta J]$ and result in an expression similar to Eq. (3.115), but with the terms in parentheses replaced by $-\mathcal{V}[\delta/\delta J]$. This would then generate the required perturbative expansion.

With a quadratic theory, however, we may arrive at the result (3.123) in a more direct manner by exploiting Eq. (3.107). We do so by first treating \mathbf{K} and \mathbf{V} on an equal footing and, instead of expanding as in Eq. (3.111), jump directly to “completing the

¹⁸That is, $S_\Gamma = |\text{Aut } \Gamma|$ is the order of the group of graph automorphisms for the given diagram Γ .

square” in the exponent. This is accomplished again by shifting the field, but this time via $\mathbf{h} \rightarrow \mathbf{h} + (\mathbf{K} + \mathbf{V})^{-1} \mathbf{J}$. After simplifying the exponent, we may apply Eq. (3.107) to find

$$Z/Z_0 = e^{\frac{1}{2} \mathbf{J}^\top (\mathbf{K} + \mathbf{V})^{-1} \mathbf{J}} \left[\frac{\det(\frac{\mathbf{K} + \mathbf{V}}{2\pi})}{\det(\frac{\mathbf{K}}{2\pi})} \right]^{-1/2}. \quad (3.124)$$

Next, we rewrite the operator sum as¹⁹ $\mathbf{K} + \mathbf{V} = \mathbf{K}(\mathbf{1} + \mathbf{K}^{-1} \mathbf{V})$. The determinant of a product is the product of determinants, so the $\det(\mathbf{K}/2\pi)$ terms cancel. Using the notation $\mathbf{G} = \mathbf{K}^{-1}$ as before, this leaves

$$Z/Z_0 = e^{\frac{1}{2} \mathbf{J}^\top (\mathbf{1} + \mathbf{G} \mathbf{V})^{-1} \mathbf{G} \mathbf{J}} [\det(\mathbf{1} + \mathbf{G} \mathbf{V})]^{-1/2}, \quad (3.125)$$

and hence the free energy difference becomes

$$-\beta \mathcal{U} = \ln(Z/Z_0) = \frac{1}{2} \mathbf{J}^\top (\mathbf{1} + \mathbf{G} \mathbf{V})^{-1} \mathbf{G} \mathbf{J} - \frac{1}{2} \ln \det(\mathbf{1} + \mathbf{G} \mathbf{V}). \quad (3.126)$$

Finally, we use the operator identity $\ln \det \mathbf{A} = \text{tr} \ln \mathbf{A}$, and the two expansions

$$(\mathbf{1} + \mathbf{A})^{-1} = \sum_{k \geq 0} (-\mathbf{A})^k, \quad (3.127)$$

$$\ln(\mathbf{1} + \mathbf{A}) = - \sum_{k \geq 1} \frac{1}{k} (-\mathbf{A})^k, \quad (3.128)$$

to rewrite the free energy as

$$-\beta \mathcal{U} = \sum_{k \geq 0} \frac{1}{2} \mathbf{J}^\top (-\mathbf{G} \mathbf{V})^k \mathbf{G} \mathbf{J} + \sum_{k \geq 1} \frac{1}{2k} \text{tr}(-\mathbf{G} \mathbf{V})^k, \quad (3.129)$$

which exactly reproduces the diagrammatic expansion (3.123), including the symmetry factors $1/2$ and $1/2k$.

Multiple perturbations

The above analysis is not limited to a single interaction vertex \mathbf{V} . Indeed, the linear and quadratic worldline terms \mathcal{H}_p and \mathcal{H}_f each consist of a whole series of differential operators. To see how that affects the diagrammar, consider the replacement $\mathbf{V} \rightarrow \mathbf{V}_1 + \mathbf{V}_2$ in Eq. (3.129). Both sums then require expanding $(\mathbf{G} \mathbf{V}_1 + \mathbf{G} \mathbf{V}_2)^k$, but since $\mathbf{G} \mathbf{V}_1$ and $\mathbf{G} \mathbf{V}_2$

¹⁹In its full glory, this expression reads:

$$K(\mathbf{x}, \mathbf{x}') + V(\mathbf{x}, \mathbf{x}') = \int d^2 x'' K(\mathbf{x}, \mathbf{x}'') \left[\delta(\mathbf{x}'' - \mathbf{x}') + \int d^2 y K^{-1}(\mathbf{x}'', \mathbf{y}) V(\mathbf{y}, \mathbf{x}') \right].$$

do not necessarily commute we cannot use a simple binomial expansion. Instead, we write

$$(\mathbf{G}\mathbf{V}_1 + \mathbf{G}\mathbf{V}_2)^k = \sum_{\ell=0}^k \mathcal{P} \left[(\mathbf{G}\mathbf{V}_1)^\ell (\mathbf{G}\mathbf{V}_2)^{k-\ell} \right], \quad (3.130)$$

where $\mathcal{P}[\dots]$ is the sum of all possible permutations of ℓ instances of $\mathbf{G}\mathbf{V}_1$ and $k-\ell$ instances of $\mathbf{G}\mathbf{V}_2$. Many of the permutations produce identical terms, as does the cyclic property of the trace, so we could alternatively re-express the sum in terms of distinct permutations weighted by their multiplicities. In terms of diagrams, the inclusion of nonidentical vertices may break the rotation or reflection symmetries and hence alter the symmetry factors. This is often the case, and the new symmetry factor for a given diagram can be found by dividing the old symmetry factor by the new diagram's multiplicity, or *equivalently* by directly counting the symmetries of the new diagram. For the linear diagrams, this is very simple: $S = 2$ if the diagram is palindromic, otherwise $S = 1$. For the ring diagrams, one must count the rotations and reflections case by case.

Ground state versus entropic

Let us return to the correspondence between our problem and the generic quadratic “action” in the exponent of Eq. (3.108). We originally wrote the action without any factors of β —this was simply to avoid clutter—but the action is to be identified with $\beta\mathcal{H}$. There is some physical insight to be gained by examining the temperature dependence of the perturbative expansion, so let us restore β in Eq. (3.108) by the replacements $\mathbf{K} \rightarrow \beta\mathbf{K}$, $\mathbf{V} \rightarrow \beta\mathbf{V}$, and $\mathbf{J} \rightarrow \beta\mathbf{J}$. Accordingly, the propagator (Green function) must be replaced via $\mathbf{G} \rightarrow \frac{1}{\beta}\mathbf{G}$. With these replacements, the β -dependence drops out of the product $\mathbf{G}\mathbf{V}$, and the free energy expansion (3.129) ultimately simplifies to

$$\mathcal{U} = - \sum_{k \geq 0} \frac{1}{2} \mathbf{J}^\top (-\mathbf{G}\mathbf{V})^k \mathbf{G}\mathbf{J} - k_B T \sum_{k \geq 1} \frac{1}{2k} \text{tr}(-\mathbf{G}\mathbf{V})^k. \quad (3.131)$$

In general, the interaction free energy can be broken up into two terms: $\mathcal{U} = E - TS$, where E is the (difference in) internal or *ground state* energy, and S is the (difference in) entropy. With the temperature dependence restored in Eq. (3.131), it becomes clear that the first sum alone accounts for the ground state ($T = 0$) interactions. On the other hand, the second sum is linear in temperature and thus accounts for purely entropic, or fluctuation-induced, interactions. To distinguish these different types of interactions, we will use the symbols E and $U := -TS$ respectively for the ground state and entropic interaction energies so that $\mathcal{U} = E + U$. In terms of diagrams, it follows from Eq. (3.123) that ground state interactions are strictly of the linear-type and entropic interactions are strictly of the ring-type.

Regarding the ground state energy, the expansion could also be generated without the use of the partition function. It is, after all, unrelated to thermodynamic fluctuations. Instead,

one may consider the “classical solution” \mathbf{h}_c to the Euler–Lagrange equation $(\mathbf{K} + \mathbf{V}) \mathbf{h} = \mathbf{J}$. This may be solved using the *full Green function* $\mathcal{G} = (\mathbf{K} + \mathbf{V})^{-1}$ so that

$$\mathbf{h}_c = \mathcal{G} \mathbf{J} = \sum_{k \geq 0} (-\mathbf{G} \mathbf{V})^k \mathbf{G} \mathbf{J}. \quad (3.132)$$

The interaction energy follows from Eq. (3.39) to give

$$E = -\frac{1}{2} \mathbf{J}^\top \mathbf{h}_c = -\sum_{k \geq 0} \frac{1}{2} \mathbf{J}^\top (-\mathbf{G} \mathbf{V})^k \mathbf{G} \mathbf{J}, \quad (3.133)$$

which reproduces the ground state terms in Eq. (3.131). This type of series expansion was actually performed in the previous chapter—though with less brevity—under the guise of a *Liouville–Neuman series*, resulting in Eq. (1.67) and later Eq. (1.72). Were we so inclined, we could have alternatively generated those solutions through a diagrammatic expansion.

3.4.2 Surface diagrammar

Having developed the diagrammatic formalism, let us now apply these techniques to our problem of surface-bound particles. We have identified the appropriate correspondence between the generic action and our problem in Eq. (3.109), showing that the vertex and source factors are generated by functional derivatives. For the moment, we will delay the discussion of the monopole terms (those proportional to $Q^{(0)}$ and $M^{(0)}$) since these terms will require additional comments and consideration regarding proper handling of the regulator. Instead, we will write $\mathbf{V} \rightarrow \mathbf{V}_m + \mathbf{V}$ and $\mathbf{J} \rightarrow \mathbf{J}_m + \mathbf{J}$ to single out the monopole contributions and later handle them according to the discussion surrounding Eq. (3.130). Performing the required calculation gives (in complex coordinates)

$$J(\mathbf{z}) = \sum_a \sum_{n \geq 1} \left[\beta Q_a^{(n)} (-\partial)^n \delta_a^z + \beta \bar{Q}_a^{(n)} (-\bar{\partial})^n \delta_a^z \right], \quad (3.134)$$

$$V(\mathbf{z}, \mathbf{z}') = \sum_a \sum_{n \geq 1} \beta C_a^{(n)} \left[(-\partial)^n \delta_a^z (-\bar{\partial})^n \delta_a^{z'} + (z \leftrightarrow z') \right], \quad (3.135)$$

where we have used the abbreviated notation $\delta_a^z := \delta(\mathbf{z} - \mathbf{z}_a)$.

When the above factors appear in the free energy expansion, the derivatives acting on delta functions get transferred onto the propagators upon integration. Moreover, due to these delta functions, the propagators will always “propagate” between two particle positions, so we will encounter factors such as $\partial^n \bar{\partial}^m G(\mathbf{z}_a - \mathbf{z}_b)$. It follows from the Euler–Lagrange equation that any terms in which a Laplacian ($\nabla^2 = 4\partial\bar{\partial}$) acts on a propagator $G(\mathbf{z}_a - \mathbf{z}_b)$ will vanish, provided $\mathbf{z}_a \neq \mathbf{z}_b$ (we will consider self-interactions in a moment). That is, only *strictly* ∂ - or $\bar{\partial}$ -derivatives may act on a given propagator. Our aim, then, is to make this property manifest in the diagrams, which we accomplish by representing propagators receiving ∂ -derivatives by a single line, and propagators receiving $\bar{\partial}$ -derivatives by a double

line. For additional clarity, we will represent propagators receiving no derivatives with a dashed line. The benefit here should be clear, that single, double, and dashed lines connecting two vertices must share the same flavor of derivatives (∂ or $\bar{\partial}$) coming from the two vertex factors. Complex conjugation then simply swaps single lines for double lines and vice versa (and leaves the dashed line unaffected). The visual correspondence is therefore,

$$z \text{ --- } z' = (\beta\sigma)^{-1}G(z - z') \rightarrow \begin{cases} z \text{ ---} z' & \text{no derivatives} \\ z \text{ ---} z' & \partial\text{-derivatives} \\ z \text{ == } z' & \bar{\partial}\text{-derivatives} \end{cases} \quad (3.136)$$

where the solid dots at the ends do not represent interaction vertices, but rather indicate that the propagator links between two spatial points.

Similarly, the expansions (3.134) and (3.135) can be represented diagrammatically via

$$\textcircled{J} \text{ --- } z = J(z) = \textcircled{\circ} \text{ --- } z + \textcircled{=} z \quad (3.137a)$$

$$= \sum_a \sum_{n \geq 1} \left[z_a \cdots \textcircled{\circ}^{(n)} \text{ --- } z + z_a \cdots \textcircled{=}^{(n)} z \right], \quad (3.137b)$$

and

$$\textcircled{V} \begin{matrix} \nearrow z \\ \searrow z' \end{matrix} = -V(z, z') = \begin{matrix} \nearrow z \\ \searrow z' \end{matrix} + \begin{matrix} \nearrow z \\ \searrow z' \end{matrix} \quad (3.138a)$$

$$= \sum_a \sum_{n \geq 1} \left(z_a \cdots \textcircled{\circ}^{(n)} \begin{matrix} \nearrow z \\ \searrow z' \end{matrix} + z_a \cdots \textcircled{=}^{(n)} \begin{matrix} \nearrow z \\ \searrow z' \end{matrix} \right), \quad (3.138b)$$

where we have dropped the monopole terms for now. The dotted lines connecting the vertices to the particle worldlines do not represent propagators, but instead remind us that both z and z' will be contracted to z_a upon integration. Additionally, the reason for the capped ends in the above diagrams is to remind us that the lines emanating from the vertex do not *yet* represent propagators, but rather that they must connect—like a ball and socket—to the appropriate single- or double-lined propagator from Eq. (3.136).²⁰ In the first line of each diagram expansion, we have implicitly included the sum over particle labels and derivative order in the vertices, and made them explicit in the respective second lines. The explicit operators corresponding to these vertices are as follows:

$$z_a \cdots \textcircled{\circ}^{(n)} \text{ --- } z = \beta Q_a^{(n)} (-\partial)^n \delta_a^z \quad (3.139a)$$

$$z_a \cdots \textcircled{=}^{(n)} z = \beta \bar{Q}_a^{(n)} (-\bar{\partial})^n \delta_a^z \quad (3.139b)$$

²⁰The “balls and sockets” are here just as a visual aide, but once a vertex is connected to a propagator the “joint” should disappear. For example: $\textcircled{\circ} \text{ --- } \textcircled{\circ} \rightarrow \textcircled{\circ} \text{ --- } \textcircled{\circ}$

$$z_a \cdots \text{---} \bullet \begin{matrix} \nearrow z \\ \searrow z' \end{matrix} = -\beta C_a^{(n)} (-\partial)^n \delta_a^z (-\bar{\partial})^n \delta_a^{z'} \quad (3.139c)$$

Power counting. Since one of our goals is to express the interaction energy as a perturbative expansion in the interparticle separation r , it helps to determine which diagrams contribute to a given order. This may be achieved through a simple power-counting argument. The Green function G has a logarithmic dependence on r , but is otherwise unitless. As we found in Eq. (3.74), derivatives of the Green function scale as $\partial^n G \sim r^{-n}$, with $r = |z|$. These derivatives originate from the sources and interaction vertices, where a charge $Q^{(n)}$ contributes n derivatives, and a polarizability $C^{(n)}$ contribute $2n$ derivatives. A linear diagram consisting of N_V vertices (and hence $N_V + 1$ propagators) in a chain capped on both ends by sources will therefore scales as $\sim r^{-p}$ with

$$p = \sum_{i=1}^{N_V} 2n_i^V + n_1^J + n_2^J, \quad (3.140)$$

$$p = \sum_{i=1}^{N_V} 2n_i^V. \quad (3.141)$$

$$p = \sum_{i=1}^{N_V} 2n_i^V. \quad (3.141)$$

Self-interactions. For interactions that occur on the same particle worldline, we will encounter terms such as $\partial^n \bar{\partial}^m G(\mathbf{z}_a - \mathbf{z}_a) = \partial^n \bar{\partial}^m G(0)$, which are divergent. Such terms arise in two particular ways. The first is through pure self-interactions—those involving interactions solely on and between a single particle worldline, such as the first diagram in Eq. (3.120). These divergences occur at every order in the perturbative expansion, but since they do not reference the other particles or their relative positions, they do not contribute to the interaction energy. As such, these pure self-interactions can be removed by a redefinition of the interaction free energy: $\mathcal{U}(\{\mathbf{x}_a\}) \rightarrow \mathcal{U}(\{\mathbf{x}_a\}) - \mathcal{U}(\{\mathbf{x}_a\} \mid r_{ab} \rightarrow \infty)$ where $r_{ab} = |\mathbf{x}_b - \mathbf{x}_a|$ and $a \neq b$.

112

in coarse-graining the Hamiltonian, we have in effect reduced the particle structure—and corresponding (uncountably infinite) field degrees of freedom—to infinitesimal points. It should not be surprising, then, that divergences should appear as an artifact. The resolution is that proper coarse-graining should be accompanied by an appropriate renormalization of the couplings. In fact, for a sensible finite theory the *bare* parameters of the Hamiltonian must also suffer from similar but compensating divergences. If we wish to express the Hamiltonian in terms of the renormalized parameters—that is, those which will factor into observables—we may, for example, write the bare polarizability as a series in the renormalized (physical) polarizabilities and make the substitution

$$C_b^{(n)} = C_r^{(n)} + (C_b^{(n)} - C_r^{(n)}) =: C_r^{(n)} + \delta C^{(n)}, \quad (3.142)$$

where $\delta C^{(n)}$ is a series of *counterterms* that subtract off the divergences. In doing so, the renormalized parameters may depend on a renormalization scale, but this is precisely set by our matching procedure. Indeed, the matching procedure we applied earlier provides the renormalized (and thus observable) polarizabilities, but in doing so we implicitly assumed that a proper renormalization procedure would eliminate the self-interactions we neglected by dropping the $\delta^2(\Delta\mathcal{H})/\delta\phi^2$ terms in the linear response problem. This is in fact the case, and the details are provided in Appendix A. Here we will summarize the key points.

For the quadratic Hamiltonian we consider, the renormalization and identification of counterterms is straightforward and accomplished with the following observations. First, the bulk Green function is isotropic and so any derivatives of the Green function evaluated at the origin must inherit that property. In complex coordinates, this implies $\partial^n \bar{\partial}^m G(0) = \delta_{nm}(\partial\bar{\partial})^n G(0)$ and hence an appropriate regularization method should yield $\partial^n G(0) = 0$, and similarly for the complex conjugate. This implies our claim, that only exclusively ∂ - or $\bar{\partial}$ -derivatives should act on a propagator, only applies for propagation between different particles. Propagators between the same particle worldline must have paired $\partial\bar{\partial}$ derivatives and, consequently, only self-interactions of the same polarizability orders can possibly contribute. If we were to include the self-interacting terms in the matching procedure, we would generate the relationship between the bare and renormalized parameters, and thus identify the full set of counterterms. These counterterms can then be seen to subtract off, order by order, all self-interactions for every observable. Instead of including the tower of counterterms, it is instead more economical to simply exclude all diagrams that include self-interactions, or alternatively, redefine the Green function via $G(\mathbf{z}_a - \mathbf{z}_b) \rightarrow (1 - \delta_{ab})G(\mathbf{z}_a - \mathbf{z}_b)$ (no sum) for all particle labels a and b .

3.5 Elastic interactions

In the previous section we observed that the ground state ($T = 0$) interactions between particles, for which we will use the symbol E , is given by a sum of linear diagrams capped off by the permanent sources. Earlier, we found that the permanent sources and the polarizabilities are all proportional to the surface tension σ , whereas the propagator is

proportional to $1/\sigma$. A generic interaction will scale as $\sim \sigma^{N_J+N_V-N_G}$, but for the linear diagrams $N_J = 2$ and $N_G = N_V + 1$ and therefore they each scale as $\sim \sigma$. That is, interaction strength is set by the elastic modulus σ , and as such we will refer to them as *elastic interactions*. Returning again to our thematic analogy to electrostatics, note that with the one-legged vertices interpreted as permanent charges as usual, and with ϵ_0 as some electrostatic “elasticity” of the vacuum, the elastic interactions are completely analogous to the interactions of Chapter 1: the permanent sources interact directly as well as through respective induced polarizations, mediated by the deformations on the field. As discussed earlier, the only difference is in the overall sign of the energy.

We will begin by examining the interactions between two particles, and consider multi-particle interactions shortly after.

3.5.1 Pair interactions

According to our summary in Technical Note 3.1, the difference between our three categories of boundary conditions is whether the first two polarizabilities vanish. Given that the monopole interactions require some additional discussion, we first consider saddle-type particles (permanent quadrupoles) with the freedom to bob, *i.e.*, (BC 2). The same interaction expansion applies when we permit the freedom to tilt, (BC 3), but with $C^{(1)} = 0$. On the other hand, (BC 1) will provide additional monopole corrections to these same results.

According to our power-counting formula (3.140), the leading-order interaction between permanent quadrupoles occurs for $N_V = 0$ and $n_a^J = 2$ and scales as $\sim r^{-4}$. This corresponds to a single propagator between two quadrupole sources,

$$-\beta E^{(4)} = \overset{(2)}{\circ} \text{---} \overset{(2)}{\circ} + \overset{(2)}{\circ} \text{=}\text{=} \overset{(2)}{\circ} = 2 \operatorname{Re} \left[\overset{(2)}{\circ} \text{---} \overset{(2)}{\circ} \right]. \quad (3.143)$$

The superscript refers to the expected power of r^{-1} , and the second equality follows by recalling that swapping single for double lines in the propagators corresponds to complex conjugation. Following the diagrammatic rules laid out earlier, these diagrams evaluate to

$$-\beta E^{(4)} = 2 \operatorname{Re} \left[\frac{1}{2} \sum_{a \neq b} \beta Q_a^{(2)} \frac{\partial^4 G^{ab}}{\beta \sigma} \beta Q_b^{(2)} \right], \quad (3.144)$$

where the factor of $1/2$ is included due to the reflection symmetry of the diagram, and the constraint $a \neq b$ is included in the sum to prevent self-interactions. Plugging in for the sources and Green function derivatives gives

$$E^{(4)} = - \sum_{a \neq b} \operatorname{Re} \left[\sigma \pi^2 S_a R_a^4 e^{2i\alpha_a} \frac{3!}{4\pi z_{ab}^4} S_b R_b^4 e^{2i\alpha_b} \right], \quad (3.145)$$

where $z_{ab} = z_b - z_a$, and the angles are measured from the line joining the particle centers.

As the diagram clearly indicates, this interaction involves a maximum of two particles and thus encodes only pair interactions. Thus the resulting interaction between two particles, labeled 1 and 2, separated by a distance r is found to be

$$E_{\{1,2\}}^{(4)} = -3\pi\sigma \frac{R_1^4 R_2^4}{r^4} S_1 S_2 \cos(2\alpha_1 + 2\alpha_2). \quad (3.146)$$

This is the same interaction energy found by Stamou *et al.* [SDJ00], also discussed in Refs. [FG02] and [DKNB05], and calculated with the same EFT formalism in Ref. [YRD12].²¹ At leading order, it therefore follows that the interaction implies a nonzero vertical torque between the particles, and the orientation-dependent force can either be attractive or repulsive. Maximal attraction occurs for a full range of orientations such that $\alpha_1 + \alpha_2 \equiv 0 \pmod{\pi}$, which included the tip-to-tip configurations for which like-curvatures are aligned. Similarly, maximal repulsion occurs for a range of orientations satisfying $\alpha_1 + \alpha_2 \equiv \pi/2 \pmod{\pi}$, including configurations for which opposite curvatures are aligned.

This angular degeneracy of maximal attraction or repulsion in fact holds to all orders, the reason being that the angular dependence only comes from the sources, of which there can only be two in a given linear diagram. In particular, the angular dependence can only occur when the sources come from different particles, for which a factor of $\cos(2\alpha_1 + 2\alpha_2)$ will always appear. However, if the sources are from the same particle, no angular dependence occurs. This conclusion follows simply from a diagrammatic argument: For pair interactions, the linear diagrams must adhere to structure ab , aba , $abab$, $ababa$, and so on. That is, sources with the same particle label can only occur for diagrams with an odd number of vertices. Since each vertex is paired to single- and double-line propagators, the end sources must therefore be conjugates of each other. Since $Q_a^{(2)} \bar{Q}_a^{(2)} \propto e^{2i\alpha_a} e^{-2i\alpha_a}$, the dependence on angles disappears.

To find the corrections to the interaction energy, we recall that for (BC 2), the monopole polarizability is zero. Hence the next contribution must stem from the sources interacting with the dipole moments they have respectively induced in the other particle. In the diagrammatic expansion, this interaction comes from the single term

$$-\beta E^{(6)} = \text{Diagram: } \textcircled{(2)} \text{---} \textcircled{(1)} \text{---} \textcircled{(2)}, \quad (3.147)$$

which evaluates to

$$\begin{aligned} -\beta E^{(6)} &= -\frac{\beta}{\sigma^2} \sum'_{abc} Q_a^{(2)} \partial_a^2 \partial_b G^{ab} C_b^{(1)} \bar{\partial}_b \bar{\partial}_c^2 G^{bc} \bar{Q}_c^{(2)} \\ &= +\frac{\beta}{\sigma^2} \sum'_{abc} Q_a^{(2)} \partial^3 G^{ab} C_b^{(1)} \bar{\partial}^3 G^{bc} \bar{Q}_c^{(2)}, \end{aligned} \quad (3.148)$$

²¹Note that in Refs. [SDJ00, FG02, DKNB05], the corresponding “curvature charge” used by the authors was the undulation amplitude H with values half that of the saddle curvature, so their interaction energy has a prefactor of $12H_1 H_2$ rather than $3S_1 S_2$.

where the prime on the summation reminds us to exclude self-interactions.²² Since we are at the moment only considering pair interactions, we sift out the contribution

$$\begin{aligned} E_{\{1,2\}}^{(6)} &= -\frac{1}{\sigma^2} \sum_{a \neq b} |Q_a^{(2)}|^2 C_b^{(1)} \partial^3 G^{ab} \bar{\partial}^3 G^{ba} = \frac{1}{\sigma^2} \sum_{a \neq b} |Q_a^{(2)}|^2 C_b^{(1)} \left| \frac{2!}{4\pi z_{ab}^3} \right|^2 \\ &= \sum_{a \neq b} \pi \sigma \frac{R_a^2 R_b^2}{r^6} S_a^2 R_a^6 = \pi \sigma \frac{R_1^2 R_2^2}{r^6} (S_1^2 R_1^6 + S_2^2 R_2^6). \end{aligned} \quad (3.149)$$

This contribution is purely repulsive and, as predicted in the previous discussion, has no orientational dependence. Observe that in the above interaction, we encounter the first breakdown of the superposition principle—a given source interacts purely through the polarization it induces in the other particle. Such an interaction can occur even if one of the two particles is “uncharged.” In Ref. [YRD12], it was claimed that the leading-order correction occurs at $\mathcal{O}(r^{-8})$; however, the authors only considered particles that were free to tilt, for which the dipole polarizability vanishes and hence this contribution vanishes as well.

Let us now calculate the $\mathcal{O}(r^{-8})$ correction, where we first encounter the quadrupole polarizability. The relevant diagrams are

$$-\beta E^{(8)} = \text{Diagram 1} + 2 \operatorname{Re} \left[\text{Diagram 2} \right], \quad (3.150)$$

(Diagram 1: A horizontal line with four vertices. The first and fourth vertices are open circles with a (2) above them. The second and third vertices are solid black circles with a (2) above them. A double line connects the second and third vertices.)
 (Diagram 2: A horizontal line with four vertices. The first and fourth vertices are open circles with a (2) above them. The second and third vertices are solid black circles with a (1) above them. A double line connects the second and third vertices.)

which for pairs evaluates to

$$E_{\{1,2\}}^{(8)} = \sum_{a \neq b} \left\{ \frac{1}{\sigma^2} |Q_a^{(2)}|^2 C_b^{(2)} |\partial^4 G^{ab}|^2 - \frac{2}{\sigma^3} \operatorname{Re} \left[\frac{1}{2} Q_a^{(2)} C_b^{(1)} C_a^{(1)} Q_b^{(2)} \partial^3 G^{ab} \bar{\partial}^2 G^{ba} \partial^3 G^{ab} \right] \right\}. \quad (3.151)$$

We omit the intermediate details of the calculation, and instead quote the final result:

$$E_{\{1,2\}}^{(8)} = \frac{9}{2} \pi \sigma \frac{R_1^4 R_2^4}{r^8} (S_1^2 R_1^4 + S_2^2 R_2^4) - 2 \pi \sigma \frac{R_1^6 R_2^6}{r^8} S_1 S_2 \cos(2\alpha_1 + 2\alpha_2). \quad (3.152)$$

Tilt freedom

If we now consider (BC 3) by allowing the particles the freedom to tilt, then the dipole polarizability $C^{(1)}$ vanishes. As we mentioned before, the corresponding interaction energy follows from the same calculations as above, but with the appropriate diagrams dropped. In particular, the leading order contribution comes solely from the first diagram in Eq. (3.150),

²²An attempt was also made to explicitly track the minus signs, which can sometimes be a frustrating game. If in doubt, note that a propagator from vertex $C_a^{(n)}$ to vertex $C_b^{(m)}$ will appear with derivatives as $\partial_a^n \partial_b^m G^{ab}$ (or the conjugate). Transforming the derivatives to the entire Green function argument picks up minus signs from ∂_b , giving $(-)^m \partial^{n+m} G^{ab}$. We could also write this as $(-)^n (-\partial)^{n+m} G^{ab}$ so that we may directly apply Eq. (3.74).

and thus

$$E_{\{1,2\}}^{(8)} = \frac{9}{2}\pi\sigma \frac{R_1^4 R_2^4}{r^8} (S_1^2 R_1^4 + S_2^2 R_2^4) \quad (3.153)$$

for pairs. This reproduces the finding in Ref. [YRD12].

3.5.2 Multibody interactions

For more than two particles, the interaction energy can also depend on the geometric configuration of the entire collection. In the previous calculations, the single-vertex diagrams corresponded exclusively to pair interactions. For multiple particles, those contributions would yield a pairwise sum over the complete set. The first true multibody interaction—that is, an interaction that cannot be decomposed into pairwise contributions—is the *triplet* interaction, and at leading order results from the diagram in Eq. (3.147). Summing over the three particle labels then yields the triplet interaction,

$$\begin{aligned} E_{\text{tri}}^{(6)} &= -\sum'_{abc} \pi^2 \sigma S_a R_a^4 e^{2i\alpha_a} (4\pi R_b^2) S_c R_c^4 e^{-2i\alpha_c} \left(\frac{2}{4\pi z_{ab}^3} \right) \left(\frac{2}{4\pi \bar{z}_{bc}^3} \right) \\ &= -\pi\sigma \sum'_{abc} S_a R_a^4 R_b^2 R_c^4 S_c e^{2i(\alpha_a - \alpha_c)} \frac{e^{-3i(\varphi_{ab} - \varphi_{bc})}}{r_{ab}^3 r_{bc}^3}. \end{aligned} \quad (3.154)$$

At this point a few comments on notation are in order. The complex coordinate $z_{ab} = z_b - z_a$ represents a position vector that points from the center of particle a to the center of particle b , and can alternatively be written in polar form as $z_{ab} = r_{ab} e^{i\varphi_{ab}}$, where r_{ab} is the separation distance and φ_{ab} is the angle z_{ab} makes as measured from the x -axis. Since the choice of coordinate system is arbitrary, it is better to consider a coordinate-free grouping of the terms. To do so, we denote by φ_{ac}^b the angle the vector z_{bc} makes with the (oriented) line parallel to z_{ab} . As illustrated in Fig. 3.5, this *exterior angle* is found to be $\varphi_{ac}^b = -\varphi_{ab} + \varphi_{bc}$. Similarly, we wish to relate the orientation of the particles' principle axes to the interparticle joining lines. To that aim, we define $\theta_{bc}^{(b)} := \alpha_b - \varphi_{bc}$ which gives the angle the principle axis of particle b makes with the line parallel to z_{bc} . Note that the exterior angle is antisymmetric in the lower indices, $\varphi_{ca}^b = -\varphi_{ac}^b$. On the other hand, the quadrupole source is invariant (or rather, equivalent) under rotations by integer multiples of π , so given that $\varphi_{cb} \equiv \varphi_{bc} \pmod{\pi}$, the particle angle $\theta_{cb}^{(b)} \equiv \theta_{bc}^{(b)} \pmod{\pi}$ and is therefore effectively symmetric in the lower indices for our particles.

Applying these definitions, the angles in Eq. (3.154) can be regrouped as $2(\alpha_a - \varphi_{ab}) - 2(\alpha_c - \varphi_{bc}) - \varphi_{ab} + \varphi_{bc}$ so that

$$E_{\text{tri}}^{(6)} = -\pi\sigma \sum'_{a,b,c} S_a R_a^4 R_b^2 R_c^4 S_c \frac{e^{i[\varphi_{ac}^b + 2\theta_{ab}^{(a)} - 2\theta_{bc}^{(c)}]}}{r_{ab}^3 r_{bc}^3}. \quad (3.155)$$

By the symmetries of the indices, the sum of angles in the complex exponent is completely antisymmetric under the exchange $a \leftrightarrow c$, implying this exchange gives the complex

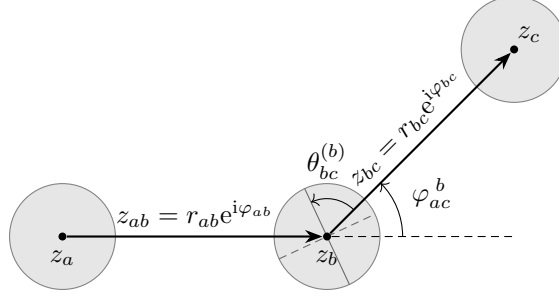


Figure 3.5: Illustration of the parameter definitions in a multibody configuration involving three particles situated at the coordinates z_a , z_b , and z_c with $z_{ab} = z_b - z_a$ and similar. The exterior angle φ_{ac}^b is measured from the line parallel to z_{ab} . The orientation angle $\theta_{bc}^{(b)}$ of particle b is measured from the line joining particles b and c to the principle axis of positive “saddle” curvature of the particle contact line.

conjugate of the interaction. Then, we use the identity

$$\sum_{a,b,c}^{\text{perm.}\{1,2,3\}} f(a,b,c) \rightarrow \sum_{a,b,c}^{\text{cyc.}\{1,2,3\}} [f(a,b,c) + f(c,a,b)] \quad (3.156)$$

relating the sum over total permutations to the sum over *cyclic* permutations for any summand $f(a,b,c)$, noting that in this case $f(c,a,b) = f^*(a,b,c)$, to express the interaction energy in its real form,

$$E_{\text{tri}}^{(6)} = -2\pi\sigma \sum_{a,b,c}^{\text{cyc.}\{1,2,3\}} \frac{S_a R_a^4 R_b^2 R_c^4 S_c}{r_{ab}^3 r_{bc}^3} \cos(\varphi_{ac}^b + 2\theta_{ab}^{(a)} - 2\theta_{bc}^{(c)}). \quad (3.157)$$

The triplet interaction can be collectively attractive or repulsive depending on the geometry of the triangle formed by the particle positions as well as the orientations of the particles’ principle axes with respect to the triangle edges. Consider, for example, a “bisector configuration” in which like curvature axes are aligned with the bisector at each triangle vertex; *i.e.*, the particle curvature axes all point to the triangle centroid. The particle orientations can then be expressed in terms of the exterior angles via $\theta_{ab}^{(a)} = (\pi - \varphi_{cb}^a)/2$ and $\theta_{bc}^{(c)} = (\pi - \varphi_{ba}^c)/2 + \varphi_{ba}^c = (\pi + \varphi_{ba}^c)/2$. The exterior angles must sum to 2π , which reduces the argument of the cosine to

$$\varphi_{ac}^b + 2\theta_{ab}^{(a)} - 2\theta_{bc}^{(c)} = 2\varphi_{ac}^b - 2\pi.$$

Plugging this into the triplet interaction then yields

$$E_{\text{tri,bis}}^{(6)} = -2\pi\sigma \sum_{a,b,c}^{\text{cyc.}\{1,2,3\}} R_a^2 R_b^2 R_c^2 \frac{S_a R_a^2 R_c^2 S_c}{r_{ab}^3 r_{bc}^3} \cos 2\varphi_{ac}^b, \quad (3.158)$$

which for the special case of an equilateral configuration ($\varphi_{ac}^b = 2\pi/3$ at each vertex) gives an overall repulsive interaction,

$$E_{\text{tri,bis}}^{(6)}(\triangle) = \pi\sigma R_1^2 R_2^2 R_3^2 \left(\frac{S_1 R_1^2 R_3^2 S_3}{r_{12}^3 r_{23}^3} + \frac{S_2 R_2^2 R_1^2 S_1}{r_{23}^3 r_{31}^3} + \frac{S_3 R_3^2 R_1^2 S_1}{r_{31}^3 r_{12}^3} \right). \quad (3.159)$$

In the limit that the bisector configuration lies along a line, the two particles at the ends will be oriented parallel to one another, whereas the middle particle will be oriented perpendicular to both. In this case $2\varphi_{ac}^b \equiv 0 \pmod{2\pi}$ and, from Eq. (3.158), the triplet interaction is seen to be *attractive*. This, however, is not the true preferred configuration. The pair interactions up to $\mathcal{O}(r^{-6})$ (Eqs. (3.146) and (3.149)) suggest the preferred angles should satisfy $\alpha_a \equiv -\alpha_c \pmod{\pi}$ for each $a \neq c \in \{1, 2, 3\}$ and imply that the configuration suggested by the triplet interaction is frustrated. Three saddle-shaped particles are therefore likely to aggregate into zigzag chains.

3.5.3 The complete pair interaction for curved particles

The relative simplicity of the diagrammatic expansion allows us to push further and express the complete interaction energy for two particles.²³ One way to accomplish this is to first express the expansion in worldline-form with the particle labels specified explicitly:

$$\begin{aligned} -\beta E_{\{1,2\}} = 2 \operatorname{Re} & \left[\begin{array}{c} \text{Diagram 1: } z_1 \text{ to } z_2 \text{ (vertical)} \\ \text{Diagram 2: } z_1 \text{ to } z_2 \text{ (diagonal)} \\ \text{Diagram 3: } z_1 \text{ to } z_2 \text{ (diagonal)} \end{array} + \dots \right] \\ + \operatorname{Re} & \left[\begin{array}{c} \text{Diagram 4: } z_1 \text{ to } z_2 \text{ (diagonal)} \\ \text{Diagram 5: } z_1 \text{ to } z_2 \text{ (diagonal)} \\ \text{Diagram 6: } z_1 \text{ to } z_2 \text{ (diagonal)} \end{array} + \dots + \updownarrow \right], \end{aligned} \quad (3.160)$$

where we have organized the terms based on whether the interactions start and end on the same particle. For diagrams that are reflection-symmetric across the middle—those in the first line—the sum over worldlines cancels the symmetry factor. Adding the complex conjugates equates to twice the real part of the diagrams above. The remaining diagrams are their own complex conjugates, and hence real, which we will have indicated explicitly.

Evidently, the organization of the terms above also groups the terms according to whether the number of interaction vertices is even or odd. In accordance, we will express the energy

²³One could do the same for additional particles, but the cluttered form will not likely aid in additional understanding.

as a sum indexed by the number of (two-legged) interaction vertices and decompose it into even and odd indices,

$$E_{\{1,2\}} = \sum_{k \geq 0} E_k = \sum_{k \geq 0} (E_{2k} + E_{2k+1}). \quad (3.161)$$

What remains is to translate the diagrams into mathematics.

Perhaps surprisingly, it is actually more straightforward to first consider two particles with *arbitrary* contact lines $h_a^{\text{ct}}(\mathbf{x} - \mathbf{x}_a)$, though still with the restriction that they project to circles in the base plane. This is because we found earlier that the sources can be expressed in terms of the polarizabilities via $Q_a^{(n)} = C_a^{(n)} \bar{\partial}^n h_a^{\text{ct}}(0)$ (see the discussion surrounding Eq. (3.98)), so every vertex—including the source terms—will bring down a factor of $-4\pi R_a^{2n} / [n_a!(n_a - 1)!]$. We begin by first considering E_{2k} , which corresponds to the first line of Eq. (3.160), and denote the polarizability orders of the two sources as n_0 and n_{2k+1} respectively. Each propagator will give a factor $(n + m - 1)! / 4\pi r^{n+m}$, where n and m are the polarizability orders of the vertices it connects, and r is the separation. Note that all the minus signs due to the propagators ultimately cancel one another,²⁴ and their factors of 4π cancel all but one from the product of polarizabilities. Putting everything together therefore yields

$$E_{2k} = -8\pi\sigma \sum_{\{n\}} \frac{\text{Re}[\bar{\partial}^{n_0} h_1^{\text{ct}}(0) \bar{\partial}^{n_{2k+1}} h_2^{\text{ct}}(0)]}{n_0!(n_{2k+1} - 1)!} \frac{R_1^{2(n_0+n_2+\dots+n_{2k})} R_2^{2(n_1+n_3+\dots+n_{2k+1})}}{r^{n_0} r^{2(n_1+n_2+n_3+\dots+n_{2k})} r^{n_{2k+1}}} \times \frac{(n_0 + n_1 - 1)! (n_1 + n_2 - 1)! \dots (n_{2k} + n_{2k+1} - 1)!}{n_1!(n_0 - 1)! n_2!(n_1 - 1)! \dots n_{2k+1}!(n_{2k} - 1)!}, \quad (3.162)$$

where we have taken the liberty of shifting around the factorials so that they appear in the form of binomial coefficients. To somewhat simplify the above expression, we observe that R_1 occurs with powers indexed by even terms, whereas R_2 occurs with odd indices, and define the sums $N_e = \sum_{j=1}^k n_{2j}$ and $N_o = \sum_{j=0}^{k-1} n_{2j+1}$, finally arriving at the expression

$$E_{2k} = -8\pi\sigma \sum_{\{n\}} \frac{\text{Re}[\bar{\partial}^{n_0} h_1^{\text{ct}}(0) \bar{\partial}^{n_{2k+1}} h_2^{\text{ct}}(0)]}{n_0!(n_{2k+1} - 1)!} \frac{R_1^{2(n_0+N_e)} R_2^{2(N_o+n_{2k+1})}}{r^{n_0+2(N_o+N_e)+n_{2k+1}}} \prod_{i=0}^{2k} \binom{n_i + n_{i+1} - 1}{n_{i+1}}. \quad (3.163)$$

The interactions that start and end on the same particle worldline are found in the same

²⁴To see this, consider $\partial_a^n \partial_b^m G^{ab} \bar{\partial}_b^m \bar{\partial}_a^\ell G^{ba}$. Transforming the derivatives so that they act on the full argument leads to $\partial_a^n \partial_b^m G^{ab} = (-)^m \partial^{n+m} G^{ab}$ and $\bar{\partial}_b^m \bar{\partial}_a^\ell G^{ba} = (-)^\ell \bar{\partial}^{m+\ell} G^{ba} = (-)^m \bar{\partial}^{m+\ell} G^{ab}$. The product, $\partial^{n+m} G^{ab} \bar{\partial}^{m+\ell} G^{ab}$, is therefore positive and depends on powers of $z_{ab} = z_b - z_a$ (and the complex conjugate).

way. Denoting the source polarizability orders as n_0 and n_{2k+2} respectively, we find

$$E_{2k+1} = 4\pi\sigma \sum_{\{n\}} \frac{\text{Re}[\bar{\partial}^{n_0} h_1^{\text{ct}}(0) \partial^{n_{2k+2}} h_1^{\text{ct}}(0)]}{n_0!(n_{2k+2}-1)!} \times \frac{R_1^{2(n_0+N_e+n_{2k+2})} R_2^{2N_o}}{r^{n_0+2(N_o+N_e)+n_{2k+2}}} \prod_{i=0}^{2k+1} \binom{n_i+n_{i+1}-1}{n_{i+1}} + (1 \leftrightarrow 2), \quad (3.164)$$

where the overall minus sign is canceled by the odd number of $-C^{(n_i)}$ factors.

In both contributions, (3.163) and (3.164), the sum over $\{n\}$ implies the sums over all polarizabilities n_0, n_1, n_2, \dots . The first and last sums refer to the sources (that is, the sums over n_0 and either n_{2k+1} or n_{2k+2}), but in all cases the sums are taken over $n_a \geq 1$ for (BC 2) or $n_a \geq 2$ for (BC 3). Before specializing to the case of saddles, we should emphasize that the above expression is the *complete* ground state interaction energy for any two (circular) particles with undulating contact lines $h_a^{\text{ct}}(\mathbf{x} - \mathbf{x}_a)$. It is interesting to compare these results with those of Refs. [DKNB05] and [DK10], where the authors calculate the (ground state) pair interactions between general capillary multipoles using bipolar coordinates. Presented there are specific multipole–multipole interaction energies, but a systematic series expansion is missing.

For saddle-shaped particles, the sources are given by quadrupole moments and $\bar{\partial}^n h_a^{\text{ct}}(0) = -(S_a/2)e^{2i\alpha_a} \delta_{n2}$ (see Technical Note 3.1). This picks off the terms for which $n_0 = n_{2k+1} = 2$ in the expression for E_{2k} and $n_0 = n_{2k+2} = 2$ for E_{2k+1} . These two contributions then take the following forms:

$$E_{2k} = -\pi\sigma \sum_{\{n\}} \frac{S_1 R_1^{2(N_e+2)} R_2^{2(N_o+2)} S_2}{r^{2(N_o+N_e+2)}} \cos(2\alpha_1 + 2\alpha_2) \times \binom{n_1+1}{n_1} \binom{n_{2k}+1}{2} \prod_{i=1}^{2k-1} \binom{n_i+n_{i+1}-1}{n_{i+1}}, \quad (3.165)$$

$$E_{2k+1} = \frac{\pi\sigma}{2} \sum_{\{n\}} \frac{S_1^2 R_1^{2(N_e+4)} R_2^{2N_o} + S_2^2 R_2^{2(N_e+4)} R_1^{2N_o}}{r^{2(N_o+N_e+2)}} \times \binom{n_1+1}{n_1} \binom{n_{2k+1}+1}{2} \prod_{i=1}^{2k} \binom{n_i+n_{i+1}-1}{n_{i+1}}, \quad (3.166)$$

where it is understood that the n_1 binomial factor is absent from E_{2k} when $k = 0$.

It is now a straightforward matter to expand out the two series to gives the asymptotic expansions of the interaction energy. Since the expressions are lengthy and cluttered, we will instead—for brevity's sake—quote the high-order expansions for two identical saddles. With $S_1 = S_2 = S$ and $R_1 = R_2 = R$, the expansions form a power series in the dimensionless separation distance $\chi := r/R$. For (BC 2) where the particles are free to bob, but not tilt,

we find

$$\begin{aligned} \frac{E_{\{1,2\}}}{\pi\sigma S^2 R^4} = & - \left\{ \frac{3}{\chi^4} + \frac{2}{\chi^8} + \frac{12}{\chi^{10}} + \frac{53}{\chi^{12}} + \frac{204}{\chi^{14}} + \frac{728}{\chi^{16}} + \frac{2496}{\chi^{18}} + \frac{8427}{\chi^{20}} + \dots \right\} \cos(2\alpha_1 + 2\alpha_2) \\ & + \left\{ \frac{2}{\chi^6} + \frac{9}{\chi^8} + \frac{26}{\chi^{10}} + \frac{66}{\chi^{12}} + \frac{176}{\chi^{14}} + \frac{540}{\chi^{16}} + \frac{1872}{\chi^{18}} + \frac{6882}{\chi^{20}} + \dots \right\}, \end{aligned} \quad (3.167)$$

where “ \dots ” are terms of $\mathcal{O}(\chi^{-22})$.

Tilt freedom For (BC 3), where the particles are free to both bob and tilt, the complete pair interaction is still provided by Eqs. (3.163) and (3.164), but with the polarizability sums taken over $n_i \geq 2$. The asymptotic series begins at $\mathcal{O}(r^{-8})$, and for identical particles becomes

$$\begin{aligned} \frac{E_{\{1,2\}}}{\pi\sigma S^2 R^4} = & \left\{ \frac{9}{\chi^8} + \frac{24}{\chi^{10}} + \frac{50}{\chi^{12}} + \frac{90}{\chi^{14}} + \frac{228}{\chi^{16}} + \frac{872}{\chi^{18}} + \frac{3690}{\chi^{20}} + \frac{14880}{\chi^{22}} + \frac{56943}{\chi^{24}} + \dots \right\} \\ & - \cos(2\alpha_1 + 2\alpha_2) \left\{ \frac{27}{\chi^{12}} + \frac{144}{\chi^{14}} + \frac{540}{\chi^{16}} + \frac{1794}{\chi^{18}} + \frac{5791}{\chi^{20}} + \frac{18948}{\chi^{22}} + \frac{63702}{\chi^{24}} + \dots \right\}, \end{aligned} \quad (3.168)$$

where the remaining terms are $\mathcal{O}(\chi^{-26})$.

3.5.4 Monopoles

As we have alluded to multiple times, computing interactions that include monopole vertices requires some care. Recall that the monopole polarizabilities $M^{(0)}$ are proportional to the surface tension, but are otherwise dimensionless. Hence in order to express the interactions in a proper series in increasing powers of particle size, or rather in powers of inverse separation, we must sum up *all possible* $M^{(0)}$ insertions into each diagram. At first glance this seems daunting, requiring a systematic way to categorize all possible ways to place and permute particle labels on arbitrarily large diagrams while avoiding self-interactions. However, we can save ourselves from intimidating combinatorial gymnastics with a little mathematical rephrasing: For a collection of N particles, monopole interactions between particles a and b can be thought of as the ab^{th} element of an $N \times N$ matrix \mathcal{M} . The sum of all possible $M^{(0)}$ insertions then appears as a *summable* series in powers of \mathcal{M} . This approach is particularly manageable for strictly monopole interactions, so we first focus on the leading-order interaction energy to discuss the general resummation principles.

Leading order interactions and resummation

For the case of (BC 1) in which the particles are fixed at specified heights from the base plane, the interaction energies find contributions from both the monopole sources and monopole polarizabilities. Just as in Eqs. (3.134) and (3.135), the source and interaction vertices follow from functional derivatives of the field. We represent these interactions

diagrammatically with the following correspondence:

$$z_a \cdots \textcircled{\circ} \cdots z = \beta Q_a^{(0)} \delta_a^z \quad (3.169a)$$

$$z_a \cdots \textcircled{\otimes} \cdots \begin{array}{l} \nearrow z \\ \searrow z' \end{array} = -\beta M_a^{(0)} \delta_a^z \delta_a^{z'} \quad (3.169b)$$

where the dashed lines indicate that the vertices do not place derivatives on the propagator.

The leading-order interaction energy comes from the complete series,

$$-\beta E^{(0)} = \textcircled{\circ} \cdots \textcircled{\circ} + \textcircled{\circ} \cdots \textcircled{\otimes} \cdots \textcircled{\circ} + \textcircled{\circ} \cdots \textcircled{\otimes} \cdots \textcircled{\otimes} \cdots \textcircled{\circ} + \textcircled{\circ} \cdots \textcircled{\otimes} \cdots \textcircled{\otimes} \cdots \textcircled{\otimes} \cdots \textcircled{\circ} + \cdots \quad (3.170)$$

The first term in the series is the point-source interaction from Eq. (3.40). This term embodies a strict superposition principle, but the remaining contributions correct for this by accounting for the particles' finite sizes. At first glance, every term appears to vanish in the limit $\ell_c \rightarrow \infty$. This follows from the observation that in each diagram with k internal monopole vertices, there is a product $\sim [M^{(0)}]^{k+2} [G]^{k+1}$ (recall $Q^{(0)} = M^{(0)} h_0$). In the asymptotic limit, the product $M^{(0)} G / \sigma \rightarrow 1$, leaving behind in each diagram a single factor of $M^{(0)}$ which vanishes as $\ell_c \rightarrow \infty$. This line of reasoning, however, is flawed and instead demonstrates the noncommutativity of these infinite limits.²⁵ Consistency requires that we treat ℓ_c as large but *finite* throughout our calculations and only take the limit at the very end. This means that we should instead view each term above as being very small, but nonzero. It remains, however, to see whether a residual nonvanishing contribution appears after the limit is taken correctly.²⁶

To proceed, we will focus on the induced interactions (everything but the first term in Eq. (3.170)) and perform the following manipulations:

$$\begin{aligned} & \textcircled{\circ} \cdots \textcircled{\otimes} \cdots \textcircled{\circ} + \textcircled{\circ} \cdots \textcircled{\otimes} \cdots \textcircled{\otimes} \cdots \textcircled{\circ} + \textcircled{\circ} \cdots \textcircled{\otimes} \cdots \textcircled{\otimes} \cdots \textcircled{\otimes} \cdots \textcircled{\circ} + \cdots \\ &= \textcircled{\circ} \cdots \bullet \left(\nearrow \textcircled{\otimes} \searrow + \nearrow \textcircled{\otimes} \searrow \textcircled{\otimes} \searrow + \nearrow \textcircled{\otimes} \searrow \textcircled{\otimes} \searrow \textcircled{\otimes} \searrow + \cdots \right) \bullet \cdots \textcircled{\circ} \\ &= \textcircled{\circ} \cdots \bullet \left[\nearrow \textcircled{\otimes} \searrow \left(\bullet \cdots \searrow + \bullet \cdots \textcircled{\otimes} \searrow + \bullet \cdots \textcircled{\otimes} \searrow \textcircled{\otimes} \searrow + \cdots \right) \right] \bullet \cdots \textcircled{\circ} \\ &= \textcircled{\circ} \cdots \bullet \left[\nearrow \textcircled{\otimes} \searrow \sum_{k=0}^{\infty} \left(\bullet \cdots \textcircled{\otimes} \searrow \right)^k \right] \bullet \cdots \textcircled{\circ} \\ &\stackrel{*}{=} \textcircled{\circ} \cdots \bullet \left[\nearrow \textcircled{\otimes} \searrow \left(\bullet \cdots \searrow - \bullet \cdots \textcircled{\otimes} \searrow \right)^{-1} \right] \bullet \cdots \textcircled{\circ} \\ &= \textcircled{\circ} \cdots \bullet \left[\nearrow \textcircled{\otimes} \searrow (\mathbf{1} + \mathbf{G} \mathbf{M})^{-1} \right] \bullet \cdots \textcircled{\circ} \end{aligned} \quad (3.171)$$

²⁵Moreover, this line of reasoning has also lead to some inaccurate claims in the published literature. We will address these in the next section on entropic interactions.

²⁶Spoiler: It does.

The starred equality follows from completing the geometric sum. In the last line, we have identified the sum as the inverse of the matrix

$$(\mathbf{1} + \mathbf{GM})_j^i = \delta_j^i + \frac{1}{\sigma} \sum_a G^{ia} M_a^{(0)} \delta_j^a (1 - \delta_a^i) = \delta_j^i + \frac{1}{\sigma} G^{ij} M_j^{(0)} (1 - \delta_j^i), \quad (3.172)$$

where the indices run over all particle labels, and the factor of $(1 - \delta_j^i)$ makes explicit the absence of self-interactions. Note also the change in sign after the starred equality. Recall that the diagrammatic rules dictate that each vertex brings with it a negative sign so, when expanded, it cancels the negative sign from the geometric sum. We therefore see that for a collection of N particles, resumming the monopole interactions reduces to finding the inverse of the following matrix:

$$\mathbf{1} + \mathbf{GM} = \begin{pmatrix} 1 & \frac{1}{\sigma} G^{12} M_2^{(0)} & \dots & \frac{1}{\sigma} G^{1N} M_N^{(0)} \\ \frac{1}{\sigma} G^{21} M_1^{(0)} & 1 & \dots & \frac{1}{\sigma} G^{2N} M_N^{(0)} \\ \vdots & \vdots & \ddots & \vdots \\ \frac{1}{\sigma} G^{N1} M_1^{(0)} & \frac{1}{\sigma} G^{N2} M_2^{(0)} & \dots & 1 \end{pmatrix}. \quad (3.173)$$

This is the matrix \mathcal{M} that was promised earlier. If the number of particles is not too large, one can explicitly write down the inverse without much trouble. We will demonstrate by examining the leading-order interaction energy for pairs and for three particles.

Two particles. By way of the Cayley–Hamilton theorem (see Technical Note 3.2), it follows that the inverse will contain an overall factor of $1/\det(\mathbf{1} + \mathbf{GM})$ and up to $N - 1$ powers of \mathbf{GM} and their traces. For two particles, the matrix is 2×2 and its inverse takes the simple form

$$(\mathbf{1} + \mathbf{GM})^{-1} = \frac{\mathbf{1} - \mathbf{GM}}{\det(\mathbf{1} + \mathbf{GM})}. \quad (3.174)$$

Now, we combine this with the monopole vertex and observe the following decomposition:

$$\begin{aligned} \left[\text{---}\bigotimes\text{---} (\mathbf{1} + \mathbf{GM})^{-1} \right]_j^i &= -\beta \sum_a M_a^{(0)} \delta_a^i \left[\frac{\delta_j^a - \frac{1}{\sigma} \sum_b G^{ab} (1 - \delta_b^a) M_b^{(0)} \delta_j^b}{\det(\mathbf{1} + \mathbf{GM})} \right] \\ &= -\sum_a \delta_a^i \frac{M_a^{(0)}}{\det(\mathbf{1} + \mathbf{GM})} \delta_j^a + \sum_{a,b} \delta_a^i \frac{\frac{1}{\sigma} M_a^{(0)} G^{ab} (1 - \delta_b^a) M_b^{(0)}}{\det(\mathbf{1} + \mathbf{GM})} \delta_j^b \\ &\equiv i \text{---}\bigotimes\text{---} j + i \text{---}\bigotimes\text{---}\bigotimes\text{---} j \end{aligned} \quad (3.175)$$

We interpret these expressions in the following way. The first term corresponds to diagonal elements and accounts for the full series of monopole interactions that begin and end on the same particle worldline. The second term corresponds to the off-diagonal elements and accounts for the complete remainder of interactions that begin and end on different particle

Technical Note 3.2: The Cayley–Hamilton theorem and matrix inverse

In broad strokes, the Cayley–Hamilton theorem states that an $n \times n$ invertible matrix \mathcal{M} satisfies its own characteristic polynomial. More precisely, the characteristic polynomial $p(\lambda)$ is defined as $p(\lambda) = \det(\lambda \mathbf{1} - \mathcal{M})$, and the theorem states $p(\mathcal{M}) = \mathbf{0}$, where $\mathbf{0}$ is the zero matrix. A useful application of the theorem is that it enables one to express the matrix inverse as a trace identity. Writing

$$p(\mathcal{M}) = \mathcal{M}^n + c_{n-1} \mathcal{M}^{n-1} + \cdots + c_1 \mathcal{M} + (-)^n \mathbf{1} \det \mathcal{M} = \mathbf{0},$$

one multiplies through by \mathcal{M}^{-1} and rearranges to find

$$\mathcal{M}^{-1} = \frac{(-)^{n-1}}{\det \mathcal{M}} (\mathcal{M}^{n-1} + c_{n-1} \mathcal{M}^{n-2} + \cdots + c_1 \mathbf{1}).$$

The coefficients can be found in a variety of ways, including an application of Newton’s identities or successive differentiation of the corresponding Mercator series, and can be written compactly as

$$c_{n-m} = \frac{(-)^m}{m!} \begin{vmatrix} \text{tr } \mathcal{M} & m-1 & 0 & \cdots \\ \text{tr } \mathcal{M}^2 & \text{tr } \mathcal{M} & m-2 & \cdots \\ \vdots & \vdots & \vdots & \ddots \\ \text{tr } \mathcal{M}^{m-1} & \text{tr } \mathcal{M}^{m-2} & \cdots & \cdots & 1 \\ \text{tr } \mathcal{M}^m & \text{tr } \mathcal{M}^{m-1} & \cdots & \cdots & \text{tr } \mathcal{M} \end{vmatrix}.$$

Applied to the matrix $\mathbf{1} + \mathbf{G} \mathbf{M}$, one finds for $n = 2$ and $n = 3$:

$$(\mathbf{1} + \mathbf{G} \mathbf{M})_{2 \times 2}^{-1} = \frac{\mathbf{1} - \mathbf{G} \mathbf{M}}{\det(\mathbf{1} + \mathbf{G} \mathbf{M})}, \quad (\mathbf{1} + \mathbf{G} \mathbf{M})_{3 \times 3}^{-1} = \frac{[1 - \frac{1}{2} \text{tr}(\mathbf{G} \mathbf{M})^2] \mathbf{1} - \mathbf{G} \mathbf{M} + (\mathbf{G} \mathbf{M})^2}{\det(\mathbf{1} + \mathbf{G} \mathbf{M})}.$$

worldlines. Diagrammatically, we represent these terms by the two effective monopole vertices in the final line of Eq. (3.175).

We may simplify our analysis further by expanding out the determinant. For this 2×2 matrix, we write

$$\det(\mathbf{1} + \mathbf{G} \mathbf{M}) = 1 - \frac{1}{\sigma^2} G^{12} M_2^{(0)} G^{21} M_1^{(0)} \equiv 1 - g_{12}^2, \quad (3.176)$$

where for brevity, and with a nod to the authors of Ref. [NWZ13a], we have defined the notation

$$g_{ij}^2 := \frac{1}{\sigma^2} G^{ij} M_j^{(0)} G^{ji} M_i^{(0)} = \frac{\ln^2\left(\frac{2\ell_c}{r_{ij}\gamma_e}\right)}{\ln\left(\frac{2\ell_c}{R_1\gamma_e}\right) \ln\left(\frac{2\ell_c}{R_2\gamma_e}\right)}. \quad (3.177)$$

Additionally, we would like to separate out the $\ell_c \rightarrow \infty$ asymptotics, so to this aim we define the parameter

$$\Lambda_{ij} = \ln\left(\frac{2\ell_c}{\sqrt{R_i R_j} \gamma_e}\right). \quad (3.178)$$

Applying this definition to g_{ij} to extract out the asymptotics, we massage the expression to

the form²⁷

$$g_{ij}^2 = \frac{\left[\Lambda_{ij} - \ln\left(\frac{r_{ij}}{\sqrt{R_i R_j}}\right) \right]^2}{\Lambda_{ij}^2 - \ln^2 \sqrt{R_i/R_j}}, \quad (3.179)$$

which will prove incredibly useful for the remainder of the chapter. In particular, we may expand the determinant factors of Eqs. (3.174) and (3.175) for large Λ_{ij} to isolate the asymptotics from the interparticle separation:

$$\frac{1}{1 - g_{12}^2} = \frac{\Lambda_{12}}{2 \ln\left(\frac{r}{\sqrt{R_1 R_2}}\right)} + \frac{\ln^2\left(\frac{r}{\sqrt{R_1 R_2}}\right) + \ln^2 \sqrt{\frac{R_1}{R_2}}}{4 \ln^2\left(\frac{r}{\sqrt{R_1 R_2}}\right)} + \frac{\left[\ln^2\left(\frac{r}{\sqrt{R_1 R_2}}\right) - \ln^2 \sqrt{\frac{R_1}{R_2}} \right]^2}{8 \Lambda_{12} \ln^2\left(\frac{r}{\sqrt{R_1 R_2}}\right)} + \mathcal{O}(\Lambda_{12}^{-2}). \quad (3.180)$$

At last, we may use the above results to sift out the leading-order pair interactions from Eq. (3.170):

$$\begin{aligned} -\beta E_{\{1,2\}}^{(0)} &= \begin{array}{c} \text{(0)} \quad \text{(0)} \\ \text{---} \quad \text{---} \end{array} + \begin{array}{c} \text{(0)} \quad \text{(0)} \\ \text{---} \quad \text{---} \end{array} + \begin{array}{c} \text{(0)} \quad \text{(0)} \\ \text{---} \quad \text{---} \end{array} \\ &= \frac{\beta}{2} \sum_{a \neq b} Q_a^{(0)} \frac{G^{ab}}{\sigma} Q_b^{(0)} - \frac{\beta}{2} \sum_{a \neq b} Q_a^{(0)} \frac{G^{ab}}{\sigma} \left(\frac{M_b^{(0)}}{1 - g_{12}^2} \right) \frac{G^{ba}}{\sigma} Q_a^{(0)} \\ &\quad + \frac{\beta}{2} \sum_{a \neq b} Q_a^{(0)} \frac{G^{ab}}{\sigma} \left(\frac{\frac{1}{\sigma} M_b^{(0)} G^{ba} M_a^{(0)}}{1 - g_{12}^2} \right) \frac{G^{ab}}{\sigma} Q_b^{(0)}. \end{aligned} \quad (3.181)$$

Plugging in the source “capacitance equation” $Q^{(0)} = M^{(0)} h$ and performing the particle sum simplifies the interaction energy to

$$E_{\{1,2\}}^{(0)} = -\frac{h_1 h_2}{\sigma} M_1^{(0)} G^{12} M_2^{(0)} + \frac{1}{2} \left(M_1^{(0)} h_1^2 + M_2^{(0)} h_2^2 - 2 h_1 h_2 M_1^{(0)} \frac{G^{12}}{\sigma} M_2^{(0)} \right) \frac{g_{12}^2}{1 - g_{12}^2}. \quad (3.182)$$

To conclude, we extract the asymptotics from the above expression using Eq. (3.178) and find that the terms complete a square in the particle height difference:

$$E_{\{1,2\}}^{(0)} = \pi \sigma \frac{(h_1 - h_2)^2}{2 \ln\left(\frac{r}{\sqrt{R_1 R_2}}\right)} + \mathcal{O}(\Lambda_{12}^{-1}). \quad (3.183)$$

This result reveals several interesting features. As mentioned earlier, the first term in Eq. (3.181) corresponds to representing the two particles as points and applying superposition, but it vanishes in the limit $\ell_c \rightarrow \infty$ (i.e., $\Lambda \rightarrow \infty$). The remaining terms correct for the particles’ finite sizes and yield nonvanishing contributions even at vanishing Bond

²⁷Through straightforward manipulations, one may obtain $\Lambda_{ij} = \frac{1}{2} \left[2 \ln\left(\frac{2\ell_c}{R_i \gamma_e}\right) + \ln \frac{R_i}{R_j} \right]$. Rearrangement shows $\ln\left(\frac{2\ell_c}{R_i \gamma_e}\right) = \Lambda_{ij} - \ln \sqrt{R_i/R_j}$ and $\ln\left(\frac{2\ell_c}{R_j \gamma_e}\right) = \Lambda_{ij} + \ln \sqrt{R_i/R_j}$. Equation (3.179) follows by applying these identities to g_{ij} .

number. The interparticle force is therefore seen to be strictly *repulsive*,

$$F_{\{1,2\}}^{(0)} = -\frac{\partial E_{\{1,2\}}^{(0)}}{\partial r} = \pi\sigma \frac{(h_1 - h_2)^2}{2r \ln^2\left(\frac{r}{\sqrt{R_1 R_2}}\right)}, \quad (3.184)$$

with a strength governed by the difference in particle heights. One may interpret this as the restoration of vertical translation symmetry of the full surface in the limit $\ell_c \rightarrow \infty$: The surface is free to equilibrate in such a way that minimizes the overall surface deformations due to the particles. If the particles are fixed to the same height, the surface translates to meet their vertical positions, eliminating both the surface deformations and the interparticle forces. If the particles are at different heights, the surface translates between their respective heights so as to minimize the deformations and equilibrates such that the particles are respectively positioned above and below the surface position. This interpretation may be checked by calculating the interaction between two particles vertically separated by a distance $h_1 - h_2$. The calculation proceed similarly, but with the permanent sources modified by $h_1 \rightarrow (h_1 - h_2)/2$ and $h_2 \rightarrow -(h_1 - h_2)/2$. Equation (3.183) is then shown to be invariant under this replacement by plugging in and simplifying.

In the electrostatics analogy (see Fig. 3.6), it is the electric potential differences that determine the physics, and this equilibrium configuration corresponds to connecting two conductors' voltage sources so that a fixed potential difference is held between them. This leads to opposite induced charges, irrespective of the signs or values of h_1 and h_2 , which for surface-mediated interactions is universally repulsive. Moreover, this repulsive force has the same $1/r$ power law as the attractive (but vanishing) point-particle term, but with a squared logarithmic correction.^{28,29} It is worth emphasizing again that this force does not appear in mechanical isolation; external forces (and torques) on the particles are still required to fix their positions, just like an external voltage source is required to fix the potential difference between conductors.

Three particles. Since the problem has been re-expressed in terms of matrix algebra, the extension to several particles is relatively straightforward, or at least systematic. To demonstrate, we will consider a system of three particles. The monopole interactions form a geometric series in the interaction vertices, which we have shown sums to an inverse matrix. Again, by way of the Cayley–Hamilton theorem, we express the 3×3 matrix inverse as the

²⁸To the best of my knowledge, this force law—as well as the following results of this section—does not appear elsewhere in the published literature. A near exception, however, is found in Ref. [LO07], where the authors calculate the pair interaction between particles constrained by harmonic “traps.” We will explore this further in Section 3.7.

²⁹Multiplicative logarithmic corrections should actually not be surprising since marginal perturbations at the critical dimension (monopole perturbations, in our case) are known to generically produce logarithmic corrections to scaling [Ken12]. Similar log-dependencies on finite particle sizes have also been observed in the context of electromagnetic Casimir interactions [REJK08].

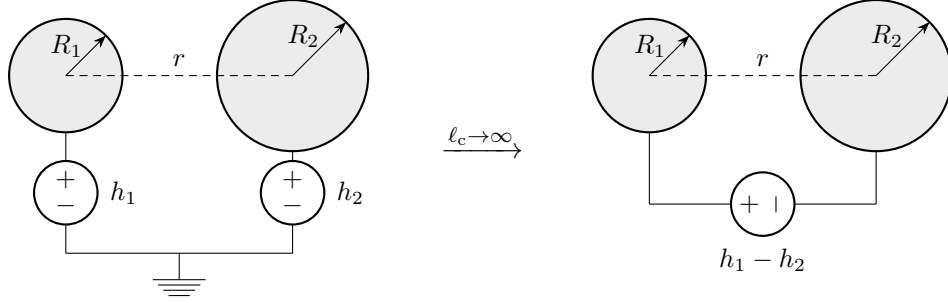


Figure 3.6: Illustration of the electrostatics analogy applied to monopoles at vanishing Bond number. The fixed heights h_1 and h_2 correspond to fixed potentials from some reference. Taking $\ell_c \rightarrow \infty$ relaxes the constraint that $h(\infty) = 0$, instead allowing the surface to vertically translate to equilibrium so that $\partial_i h(\infty) = 0$ (asymptotic flatness). In the electrostatics language, this corresponds to holding the conductors at a fixed potential difference, but leaving the ground voltage unconstrained.

useful trace identity (valid *only* for 3×3 invertible matrices),

$$(\mathbf{1} + \mathbf{GM})^{-1} = \frac{[1 - \frac{1}{2} \text{tr}(\mathbf{GM})^2] \mathbf{1} - \mathbf{GM} + (\mathbf{GM})^2}{\det(\mathbf{1} + \mathbf{GM})}. \quad (3.185)$$

As before, the matrix elements encode the complete monopole interactions which either start and end on the same particle (diagonal) or end on a different particle (off-diagonal), which we represent diagrammatically with the effective monopole vertices,

$$[\text{---} \otimes \text{---} (\mathbf{1} + \mathbf{GM})^{-1}]_j^i = i \text{---} \otimes \text{---} j + i \text{---} \otimes \text{---} \otimes \text{---} j. \quad (3.186)$$

The values of the vertices follow by expanding the traces and determinant. Using the definition (3.177), the first effective vertex reduces to

$$i \text{---} \otimes \text{---} j = -\beta \sum_a \delta_a^i \frac{M_a^{(0)} [1 - (g_{12}^2 + g_{23}^2 + g_{31}^2) + \sum_k g_{ak}^2 (1 - \delta_k^a)]}{1 - (g_{12}^2 + g_{23}^2 + g_{31}^2 - 2g_{12}g_{23}g_{31})} \delta_j^a. \quad (3.187)$$

Written as it is, the above expression appears rather complicated, but a simple pattern emerges once the particle label a is given explicitly. For example, taking $a = 1$ eliminates most of the terms in the numerator, leaving behind $M_1^{(0)}(1 - g_{23}^2)$. For $a = 2$ or $a = 3$, the numerator simplifies similarly, with the indices of g given by the two particle labels not equal to a (*i.e.*, g_{31} and g_{12} respectively).

The second effective vertex is a bit more involved, but can ultimately be expressed in the

form

$$i \text{---} \textcircled{\otimes} \text{---} j = \beta \sum_{a,b} \delta_a^i \frac{M_a^{(0)} \left[\frac{G^{ab}}{\sigma} - \sum_k \frac{G^{ak}}{\sigma} M_k^{(0)} \frac{G^{kb}}{\sigma} (1 - \delta_k^a)(1 - \delta_b^k) \right] (1 - \delta_b^a) M_b^{(0)}}{1 - (g_{12}^2 + g_{23}^2 + g_{31}^2 - 2g_{12}g_{23}g_{31})} \delta_j^b. \quad (3.188)$$

The numerator is rather complex, but the Kronecker deltas only appear to prevent self-interactions. Again, setting a and b to explicit values reveals a simple pattern. The sum over k will, because of the Kronecker deltas, produce only one term indexed by the remaining label not picked out by a and b . For example, choosing $(a, b) = (1, 2)$ forces the sum to choose $k = 3$.

At this point, we will skip a few steps and immediately consider the asymptotic limit. Many logarithmic terms will soon appear, so we will define the following parameter for space-saving convenience:

$$\varrho_{ij} = (1 - \delta_{ij}) \ln \left(\frac{r_{ij}}{\sqrt{R_i R_j}} \right), \quad (3.189)$$

where the Kronecker delta enforces $i \neq j$. Using this definition along with Eq. (3.178), it follows that $g_{ij}^2 \rightarrow 1 + 2\varrho_{ij}/\Lambda_{ij} + \mathcal{O}(\Lambda^{-2})$. Furthermore, we expand the determinant and find that it vanishes as $\sim \Lambda^{-2}$,

$$\det(\mathbf{1} + \mathbf{GM}) = \sum_{i,j,k}^{\text{cyc.} \{1,2,3\}} \frac{2\Lambda_{12}\Lambda_{23}\Lambda_{31}\Lambda_{ki}\varrho_{ij}\varrho_{jk} - \Lambda_{jk}^2\Lambda_{ki}^2\varrho_{ij}^2}{\Lambda_{12}^2\Lambda_{23}^2\Lambda_{31}^2} + \mathcal{O}(\Lambda^{-3}), \quad (3.190)$$

implying that it contributes a multiplicative $\sim \Lambda^2$ divergence when it is in the denominator. For the first effective monopole vertex, the numerator vanishes as $\sim \Lambda^{-2}$, so the vertex leaves behind a finite (and nonzero) contribution in the limit. For the second effective monopole vertex, the numerator appears to only vanish as fast as $\sim \Lambda^{-1}$, but both terms are actually identical to leading order so their difference cancels. This leaves behind a leading-order contribution that vanishes as $\sim \Lambda^{-2}$ and cancels off the divergence from the determinant. The limit is therefore also finite and nonvanishing. The end result for both vertices is

$$i \text{---} \textcircled{\otimes} \text{---} j = -\beta \sum_a 2\pi\sigma \delta_a^i \frac{2 \sum_{\text{cyc.}} (\varrho_{kl} - \varrho_{al})}{\sum_{\text{cyc.}} (2\varrho_{kl}\varrho_{lm} - \varrho_{kl}^2)} \delta_j^a + \mathcal{O}(\Lambda^{-1}), \quad (3.191)$$

$$i \text{---} \textcircled{\otimes} \text{---} j = \beta \sum_{a,b} 2\pi\sigma \delta_a^i \frac{(\sum_{\text{cyc.}} \varrho_{kl}) - 2\varrho_{ab}}{\sum_{\text{cyc.}} (2\varrho_{kl}\varrho_{lm} - \varrho_{kl}^2)} (1 - \delta_b^a) \delta_j^b + \mathcal{O}(\Lambda^{-1}), \quad (3.192)$$

where the “cyc.” notation of the sums refer to summing the nearby indices k , ℓ , and m cyclically over the labels $\{1, 2, 3\}$. In this asymptotic version, the numerator still enjoys a simplifying pattern when the outer summation indices are explicitly given. Namely, the numerator’s cyclic sum in first term will sift out the two labels not chosen by a and reduce

to $2\varrho_{k\ell}$, where $k \neq a$ and $\ell \neq a$ (and $k \neq \ell$). In the second term, the numerator reduces to $\varrho_{ak} + \varrho_{kb} - \varrho_{ab}$ where k is the remaining label not picked out by a or b .

We may now calculate the leading-order interaction energy for three particles. The diagrammatic expansion is the same as in Eq. (3.181), but with the effective monopole vertices having the values above. As before, the first term vanishes for $\ell_c \rightarrow \infty$, but the remaining two diagrams have nonvanishing contributions. After translating the diagrams into their corresponding mathematics, we find that the terms combine and simplify to the following expression:

$$E_{\{1,2,3\}}^{(0)} = 2\pi\sigma \frac{\sum_{\text{cyc.}} (h_a - h_b) \varrho_{bc} (h_a - h_c)}{\sum_{\text{cyc.}} (2\varrho_{ij} \varrho_{jk} - \varrho_{ij}^2)} + \mathcal{O}(\Lambda^{-1}). \quad (3.193)$$

Similar to the pair interaction, the strength is governed by the differences in the fixed particle heights. Furthermore, one may check that the total multibody force is inversely proportional to the separation(s) with a squared logarithmic correction. The numerator sum is always positive if at least one particle is at a different height than the other two, and the total force is collectively repulsive (or zero if all particles are at the same height). This repulsion can again be understood as a consequence of the surface's restored vertical translation symmetry: the surface translates to minimize deformations and equilibrates with an imbalance on either side of the surface. One of the three particles must always end up on the opposite side of the surface than the other two, effectively producing opposite charges which are universally repulsive.

Just to emphasize, the above result is the *complete* three-body interaction potential at leading order. The pair and triplet contributions are not so straightforwardly extracted from the above equation. Instead, one may sum the two-body interaction (3.183) over pairs selected from the set $\{1, 2, 3\}$ to get the pair contribution, and extract the triplet contribution by subtracting off that result from Eq. (3.193):

$$E_{\text{tri}}^{(0)} = E_{\{1,2,3\}}^{(0)} - \left(E_{\{1,2\}}^{(0)} + E_{\{2,3\}}^{(0)} + E_{\{3,1\}}^{(0)} \right). \quad (3.194)$$

The resulting expression is not particularly transparent, so we will examine two example three-body configurations. For simplicity, we will take all particles to have the same radius R .

First, consider an arrangement such that the particles are, as viewed from above, respectively positioned at the vertices of an equilateral triangle with side length d . Furthermore, without loss of generality, let particles 1 and 3 be fixed at the lowest and highest positions respectively, and particle 2 fixed between them at a height $h_2 - h_1 = \alpha(h_3 - h_1)$ with $0 \leq \alpha \leq 1$. Subtracting the pair interactions from Eq. (3.193) and simplifying gives the pure triplet interaction,

$$E_{\text{tri},\Delta}^{(0)} = -\pi\sigma \frac{1 - \alpha(1 - \alpha)}{3 \ln(d/R)} (h_3 - h_1)^2. \quad (3.195)$$

The numerator is strictly positive (for *all* α) and gives a minimum value of $3/4$ at $\alpha = 1/2$, for which the equilibrium surface meets the position of the second particle. The minus sign and d -dependence therefore shows that the pure triplet interaction *lowers* the energy upon bringing the particles closer together. That is, the triplet interaction is collectively attractive, but not enough so to overcome the repulsive pair interactions.

Next, consider an evenly-spaced collinear arrangement such that $r_{12} = r_{23} = d$ and $r_{31} = 2d$ (*i.e.*, particle 2 is in the middle). By a similar calculation, and some creativity in simplifying the logarithms, we find the pure triplet interaction

$$E_{\text{tri,lin}}^{(0)} = -\frac{\pi\sigma}{2} \frac{(\Delta h_{31})^2 \ln \frac{d}{R} + [(\Delta h_{12})^2 + (\Delta h_{23})^2] (\ln \frac{d}{R} - \ln 2)}{\ln(\frac{d}{R}) (3 \ln \frac{d}{R} - \ln 2)}, \quad (3.196)$$

where we have used the shorthand $\Delta h_{ab} := h_a - h_b$. Since $d \geq 2R$, otherwise the particles would overlap, it is clear both the numerator and denominator are strictly positive, and the triplet interaction is again seen to be collectively attractive, but does not overcome the pairwise repulsion.

In both cases we observe an interesting three-body effect: the pure triplet interaction energy is collectively *attractive*, and diminishes the pairwise repulsion. A natural set of questions then arises. Is there always competition between the pairwise and multibody interactions and, if so, does the pairwise repulsion always beat out the triplet attraction order by order? We will address this line of inquiry by examining the leading-order two-body and three-body corrections to the interaction energy.

Higher-order corrections

At higher orders, the other polarizabilities begin to play a role. With regards to performing the calculations, the effect of the monopoles is that the diagrammatic expansion of the elastic interaction energy is modified by all possible insertions of the effective monopole vertices between the higher-order multipole vertices. Consistency requires that the two effective monopole vertices never connect to each other (or themselves), so the modification can be accomplished by replacing each propagator with the sum

$$\bullet \cdots \bullet \rightarrow \bullet \cdots \bullet + \bullet \cdots \otimes \cdots \bullet + \bullet \cdots \otimes \cdots \otimes \cdots \bullet. \quad (3.197)$$

Since we will only consider the asymptotic limit $\ell_c \rightarrow \infty$, a few simplifications already appear. In the limit, the product $M_a^{(0)} G^{ab} / \sigma \rightarrow 1$, implying that a nonvanishing contribution must have all monopole polarizabilities balanced by the same number of derivative-free propagators. Since every higher-order polarizability vertex places derivatives on the neighboring propagators, this rules out all interactions except those in which both monopole sources are directly connected to effective monopole vertices. The nonvanishing leading-order

corrections to the interaction energy therefore consist of the diagrams,

$$\begin{aligned}
 -\beta E^{(2)} = & \text{Diagram 1} + 2 \operatorname{Re} \left[\text{Diagram 2} \right] \\
 & + \text{Diagram 3}.
 \end{aligned} \tag{3.198}$$

The diagrams are represented as follows: Diagram 1 is a chain of three circles labeled (0), (1), and (0) from left to right. The first and second circles are connected by a dashed line, and the second and third circles are connected by a solid line. Diagram 2 is a chain of three circles labeled (0), (1), and (0) from left to right. The first and second circles are connected by a dashed line, and the second and third circles are connected by a solid line. Diagram 3 is a chain of three circles labeled (0), (1), and (0) from left to right. The first and second circles are connected by a dashed line, and the second and third circles are connected by a solid line.

This diagrammatic representation holds for any N -body system, but with the effective monopole vertices taking the appropriate N -body forms.

Two particles. For two particles, the effective monopole vertices are given in the decomposition (3.175), and may be readily expanded for $\Lambda_{12} \rightarrow \infty$. The straightforward calculation yields the pair interaction,

$$\begin{aligned}
 E_{\{1,2\}}^{(2)} &= \pi\sigma \frac{h_1^2 R_1^2 + h_2^2 R_2^2}{4r^2 \ln^2\left(\frac{r}{\sqrt{R_1 R_2}}\right)} - \pi\sigma \frac{2h_1 h_2 (R_1^2 + R_2^2)}{4r^2 \ln^2\left(\frac{r}{\sqrt{R_1 R_2}}\right)} + \pi\sigma \frac{h_1^2 R_2^2 + h_2^2 R_1^2}{4r^2 \ln^2\left(\frac{r}{\sqrt{R_1 R_2}}\right)} \\
 &= \pi\sigma \frac{(h_1 - h_2)^2 (R_1^2 + R_2^2)}{4r^2 \ln^2\left(\frac{r}{\sqrt{R_1 R_2}}\right)},
 \end{aligned} \tag{3.199}$$

where the three terms in the first line correspond to the evaluation of the three diagrams of Eq. (3.198). The strength is again governed by the difference in particle heights, and the corresponding force is

$$F_{\{1,2\}}^{(2)} = \pi\sigma (h_1 - h_2)^2 (R_1^2 + R_2^2) \left[\frac{1 + \ln\left(\frac{r}{\sqrt{R_1 R_2}}\right)}{2r^3 \ln^3\left(\frac{r}{\sqrt{R_1 R_2}}\right)} \right], \tag{3.200}$$

a power law with logarithmic corrections which strengthens the repulsion of the leading-order contribution.

Three particles. For three particles, the evaluation of the diagrams in Eq. (3.198) is again straightforward, but somewhat tedious to simplify. Guided by the insight that the strength should be governed by the interparticle height differences, one may check that all height terms indeed organize into differences $\Delta h_{ab} = h_a - h_b$. In the end, the complete

leading-order correction may be expressed as the sum

$$E_{\{1,2,3\}}^{(2)} = \pi\sigma \sum_{a,b,c}^{\text{cyc.}} \left\{ - \frac{R_a^2 [(\varrho_{ab} - \varrho_{bc})\Delta h_{ca} + (\Delta h_{ab} - \Delta h_{bc})\varrho_{ca}]^2 + R_b^2 [(\varrho_{ca} - \varrho_{ab})\Delta h_{bc} + (\Delta h_{ca} - \Delta h_{ab})\varrho_{bc}]^2}{r_{ab}^2 \left[\sum_{\text{cyc.}} (2\varrho_{ij}\varrho_{jk} - \varrho_{ij}^2) \right]^2} + 2R_b^2 \cos \varphi_{ac}^b \frac{[(\varrho_{bc} - \varrho_{ca})\Delta h_{ab} + (\Delta h_{bc} - \Delta h_{ca})\varrho_{ab}] \times [(\varrho_{ca} - \varrho_{ab})\Delta h_{bc} + (\Delta h_{ca} - \Delta h_{ab})\varrho_{bc}]}{r_{ab}r_{bc} \left[\sum_{\text{cyc.}} (2\varrho_{ij}\varrho_{jk} - \varrho_{ij}^2) \right]^2} \right\}. \quad (3.201)$$

At this order we also observe the first complete dependence on the particles' geometric configuration, which is encoded by the exterior angles φ_{ac}^b of the triangle formed by the three particles. The magnitude of the first term is greater than or equal to the magnitude of the second term, with a discrepancy further amplified by the cosine factor (since $|\cos \varphi_{ac}^b| \leq 1$). The exterior angles cannot all simultaneously equal zero (mod 2π), so the full sum must be overall negative. Moreover, if all the distances are rescaled by factor λ , the overall result scales as $-\ln^2 \lambda / (\lambda^2 \ln^4 \lambda)$, and therefore the energy is lowered if the particles are brought closer together. Thus, we observe a more interesting three-body effect: the above interaction energy is collectively *attractive*, and diminishes the leading-order repulsion. This implies that the pure three-body interaction overcomes the pairwise (two-body) repulsive interactions derived from Eq. (3.199). Such deviations due to three-body effects have also been discovered before in a slightly different context, namely for the case of fluctuation-induced forces between fixed colloids, first noted by Noruzifar *et al.* [NWZ13b, NWZ13a] and later generalized and extended by the present author in Ref. [HD14]. We will revisit those findings in the next section.

As we did for the leading-order case, we substantiate this collective attraction by examining two example three-body configurations. For simplicity, we will again take all particles to have the same radius R . First, consider the particles arranged so that they are respectively positioned at the vertices of an equilateral triangle of side lengths d (as viewed from above). The exterior angles all equal $2\pi/3$ and the interaction energy simplifies to

$$E_{\{1,2,3\}}^{(2)}(\Delta) = -\pi\sigma R^2 \frac{\Delta h_{12}\Delta h_{13} + \Delta h_{23}\Delta h_{21} + \Delta h_{31}\Delta h_{32}}{d^2 \ln^2(d/R)}. \quad (3.202)$$

The numerator can be seen to be overall positive by following the same analysis as before. Without loss of generality, let particles 1 and 3 be respectively fixed at the lowest and highest positions ($\Delta h_{31} > 0$), and particle 2 fixed between them at a height $\Delta h_{21} = \alpha \Delta h_{31}$ with $0 \leq \alpha \leq 1$. The above energy then reduces to

$$\frac{E_{\{1,2,3\}}^{(2)}(\Delta)}{\pi\sigma(\Delta h_{31})^2} = - \frac{1 - \alpha(1 - \alpha)}{(d/R)^2 \ln^2(d/R)}. \quad (3.203)$$

The numerator is identical to that of Eq. (3.195) and is positive definite. The minus sign combined with the d -dependence therefore shows the interaction to be collectively attractive for all α . We will not go through the steps of extracting out the pure triplet energy, but it suffices to re-emphasize that the repulsive pairwise interaction sum derived from Eq. (3.199) is overcome by the triplet energy to give the ultimately attractive contribution above.

Next, consider a collinear configuration of three particles such that $r_{12} = r_{23} = d$ and $r_{31} = 2d$. The exterior angles then satisfy $\varphi_{13}^2 = 0$ and $\varphi_{21}^3 = \varphi_{32}^1 = \pi$. After some time with scratch paper, we find that the total interaction energy correction eventually simplifies to

$$E_{\text{lin}}^{(2)} = -\frac{\pi\sigma R^2}{4d^2 \ln^2\left(\frac{2d}{R}\right) \left(3 \ln \frac{d}{R} - \ln 2\right)^2} \left\{ \left[3\Delta h_{12} \ln \frac{d}{R} - (2\Delta h_{23} - \Delta h_{12}) \ln 2 \right]^2 + 4(\Delta h_{31})^2 \left(3 \ln \frac{d}{R} - \ln 2 \right)^2 + \left[3\Delta h_{23} \ln \frac{d}{R} - (2\Delta h_{12} - \Delta h_{23}) \ln 2 \right]^2 \right\}. \quad (3.204)$$

The quantity within braces is clearly positive, as it is a sum of squares, and the d -dependence shows the energy is lowered by decreasing the particles separations. As in the previous example, this energy is minimum when the second particle is vertically positioned halfway between the other two, and hence at the equilibrium surface.

Curved particles

So far we have explored the interaction energy associated with flat particles at fixed heights. However, our detailed discussion in the previous sections revealed that a particle's curvature is accounted for by higher-order permanent sources, and provide contributions that simply add to the *flat*-particle interaction energy. Hence, the monopole interaction energies for two particles, given by Eqs. (3.183) and (3.199), and for three particles, given by Eqs. (3.193) and (3.201), all contribute to the total interaction energy between curved particles at fixed heights. For particles with permanent quadrupole sources, these combine with the previous results, derived by the pairwise interactions (3.146) and (3.149) (and so on), and the triplet interaction (3.157). Finally, there are additional contributions due to the interactions between the permanent monopole sources with the permanent quadrupole sources. These curvature-corrections begin at $\mathcal{O}(r^{-2})$, and are given by the diagrams

$$-\beta E_{\text{curv.}}^{(2)} = 2 \text{Re} \left[\textcircled{\circ}^{(0)} - \textcircled{\otimes}^{(2)} - \textcircled{\circ}^{(2)} + \textcircled{\circ}^{(0)} - \textcircled{\otimes}^{(2)} - \textcircled{\otimes}^{(2)} - \textcircled{\circ}^{(2)} \right], \quad (3.205)$$

where the effective monopole vertices take the appropriate multibody forms depending on the number of particles in the system.

Two particles. For two particles, the diagrams evaluate to give the energy

$$E_{\text{curv.}}^{(2)} = -\pi\sigma \frac{(h_1 - h_2)}{2r^2 \ln\left(\frac{r}{\sqrt{R_1 R_2}}\right)} [S_1 R_1^4 \cos 2\alpha_1 - S_2 R_2^4 \cos 2\alpha_2]. \quad (3.206)$$

This contribution has the same power law as the monopole–monopole interaction (3.199), but with one fewer power in the logarithm correction. Observe that the interaction also depends on the relative orientations of the particles’ saddles curvatures, showing the effects of particle anisotropy appear at a lower order than if the particles were not fixed in place. Interestingly, the monopole–quadrupole interaction suggests that the preferred configuration (energy minimum) is attractive and occurs when the particles’ curvature axes are aligned perpendicularly, or, more specifically, when the higher particle’s saddle-curvature slopes down toward the lower particle and the lower particle’s saddle-curvature slopes up toward the higher particle (*e.g.*, $\alpha_1 = 0$ and $\alpha_2 = \pi/2$ for $h_1 > h_2$). This should not be surprising, however, since this configuration minimizes the surface deformation between the particles.

Three particles. For three particles, the diagrams evaluate to give the complete (two- and three-body) interaction energy

$$E_{\text{curv.}}^{(2)} = -\pi\sigma \sum_{a,b,c}^{\text{cyc.}} \left\{ \frac{S_a R_a^4 [(\varrho_{ab} - \varrho_{bc})\Delta h_{ca} + (\Delta h_{ab} - \Delta h_{bc})\varrho_{ca}]^2 + S_b R_b^4 [(\varrho_{ca} - \varrho_{ab})\Delta h_{bc} + (\Delta h_{ca} - \Delta h_{ab})\varrho_{bc}]^2}{r_{ab}^2 \sum_{\text{cyc.}} (2\varrho_{ij}\varrho_{jk} - \varrho_{ij}^2)} \cos 2\theta_{ab}^{(a)} \right\}. \quad (3.207)$$

Here, the geometry of the particle arrangement plays a role, as does the particles’ relative curvature orientations. Just as the two-body case, the power law is the same as the monopole interaction (*cf.* Eq. (3.201)) but with one fewer power of the logarithmic correction.

Monopoles and mixed boundary conditions

We have noted earlier that the limit $\ell_c \rightarrow \infty$ should be interpreted as restoring the vertical translation symmetry of the surface. The interaction between particles with fixed monopole sources then must be interpreted in light of this fact: the surface will translate freely until it reaches an equilibrium state that balances the deformation forces with the external mechanical forces required to fix the particles’ (relative) vertical positions. If there is only one particle with a fixed height, it stands to reason that the surface should equilibrate to meet that particle’s position and the particle’s height relative to the surface should vanish. Hence, if we examined the interaction between a fixed particle with another particle (or many) with the freedom to translate vertically, both the surface and the other particle(s) should meet at the same vertical position as the fixed particle. That is, any effects of the fixed monopole source will disappear.

This line of reasoning serves as a conceptual consistency check for EFT method. First,

we recall that the enforcement of the monopole constraint is encoded in the monopole polarizability $M^{(0)}$. We emphasize this particular role of $M^{(0)}$ to clarify the meaning of a vanishing monopole source $Q^{(0)}$. Indeed $Q^{(0)} = 0$ means one of two things depending on the context: If the particle height is fixed, then an external source is required to hold this position and $M^{(0)} \neq 0$, so the vanishing of $Q^{(0)}$ means nothing more than the particle position is fixed at the same height as the *reference* plane, *i.e.*, $h = 0$, not necessarily at the position of the surface. If the particle is vertically unconstrained, then $M^{(0)} = 0$ so $Q^{(0)}$ *necessarily* vanishes since $Q^{(0)} \propto M^{(0)}$. This means that setting $h_a = 0$ for one of the particles in the previous interaction energy expressions, such as Eq. (3.206), is not equivalent to relaxing the vertical constraint of a particle.

If we look at a (BC 1)–(BC 2) pair interaction, we must recall that the effective monopole vertices were constructed by considering all possible insertions of monopole vertices in each propagator. For (BC 2), there is no monopole vertex, meaning that no two monopole vertices can be linked, otherwise it would give a self-interaction. Hence, no resummation is possible and the statement that every diagram containing monopoles vanishes is now consistently valid. The only other possibility for a nonvanishing monopole interaction is to balance each occurrence of $M^{(0)}$ with a derivative-free propagator. This is *only* possible if a monopole source links directly to a monopole vertex; however, this is ruled out if only one particle is fixed because both the source and vertex would lie on the same worldline, again giving a self-interaction. Hence, no monopole effects can be observed in the $\ell_c \rightarrow \infty$ limit, other than the translation of the equilibrium surface, unless more than one particle has a fixed position.

3.6 Entropic interactions

We now explore interaction that arise from thermal fluctuations. The intuitive picture is that a compact object bound to a surface necessarily imposes some boundary conditions on the surface in the neighborhood of the surface-particle contact line. These conditions in turn affect the fluctuation spectrum, and hence the associated entropy and surface free energy. With more than one bound object, the fluctuation spectrum will be affected in a way that depends generally on the objects' relative positions and geometric arrangement.

As discussed in Section 3.4.1 (namely, pages 109–110), the entropic contribution U to the interaction free energy is given by the sum of ring-type diagrams. Moreover, the elastic and entropic contributions separate completely, so the results that follow will apply to both flat particles and those with permanent multipole moments. By the same logic as the previous section, we will first consider interactions between (BC 2) particles, since (BC 3) follows by setting $C^{(1)} = 0$ and (BC 1) gives additional contributions.

3.6.1 Pair interactions

At leading order, the entropic pair energy is given by an induced dipole–dipole interaction, and by the power-counting formula (3.141) scales as r^{-4} . Performing the calculation yields

the well known result, first calculated by Lehle *et al.* in Refs. [LOD06] and [LO07]:

$$\begin{aligned}
 -\beta U^{(4)} = -\beta U_{\text{dip-dip}} &= \text{Diagram: a circle with two vertices, each labeled (1)} = \frac{1}{2} \sum_{a \neq b} C_a^{(1)} \frac{\partial_a \partial_b G^{ab}}{\sigma} C_b^{(1)} \frac{\bar{\partial}_b \bar{\partial}_a G^{ba}}{\sigma} \\
 \Rightarrow \beta U_{\{1,2\}}^{(4)} &= -\frac{C_1^{(1)} C_2^{(1)}}{(4\pi\sigma)^2 r^4} = -\frac{R_1^2 R_2^2}{r^4}.
 \end{aligned} \tag{3.208}$$

Just as a reminder, the factor of 1/2 is due to the diagram's symmetry factor. The leading-order correction stems from the induced dipole–quadrupole interaction, and is calculated similarly:

$$\begin{aligned}
 -\beta U^{(6)} = -\beta U_{\text{dip-quad}} &= \text{Diagram: a circle with two vertices, labeled (1) and (2)} = \sum_{a \neq b} C_a^{(1)} \frac{\partial_a \partial_b^2 G^{ab}}{\sigma} C_b^{(2)} \frac{\bar{\partial}_b^2 \bar{\partial}_a G^{ba}}{\sigma} \\
 \Rightarrow \beta U_{\{1,2\}}^{(6)} &= -4 \frac{C_1^{(1)} C_2^{(2)} + C_1^{(2)} C_2^{(1)}}{(4\pi\sigma)^2 r^6} = -2 \frac{R_1^2 R_2^4 + R_1^4 R_2^2}{r^6},
 \end{aligned} \tag{3.209}$$

in agreement with Ref. [YRD11]. At the next order, the number of diagrams increases and consists of dipole–hexapole and quadrupole–quadrupole interactions, and a longer chain of multiple dipole interactions:

$$-\beta U^{(8)} = \text{Diagram: circle with vertices (1), (3)} + \text{Diagram: circle with vertices (2), (2)} + \text{Diagram: circle with vertices (1), (1), (1), (1)}. \tag{3.210}$$

The symmetry factors for the three diagrams are respectively 1, 2, and 4, and the the sum evaluates to

$$\begin{aligned}
 \beta U_{\{1,2\}}^{(8)} &= -(3!)^2 \frac{C_1^{(1)} C_1^{(3)} + C_1^{(3)} C_2^{(1)}}{(4\pi\sigma)^2 r^8} - \frac{(3!)^2}{2} \frac{2 C_1^{(2)} C_1^{(2)}}{(4\pi\sigma)^2 r^8} - \frac{1}{4} \frac{2 [C_1^{(1)}]^2 [C_2^{(1)}]^2}{(4\pi\sigma)^4 r^8} \\
 &= -3 \frac{R_1^2 R_2^6 + R_1^6 R_2^2}{r^8} - 9 \frac{R_1^4 R_2^4}{r^8} - \frac{1}{2} \frac{R_1^4 R_2^4}{r^8} \\
 &= -\frac{6 R_1^2 R_2^6 + 19 R_1^4 R_2^4 + 6 R_1^6 R_2^2}{2 r^8},
 \end{aligned} \tag{3.211}$$

again, in agreement with Ref. [YRD11].

Tilt freedom. If one is interested in the interaction between two particles with the freedom to tilt, or with differing boundary conditions, the physics can also be extracted from the

above expressions. For example, if the tilt constraint is relaxed for only particle 2, then $C_2^{(1)} = 0$ and we obtain

$$\beta U_{\{1,2\}} = -2 \frac{R_1^2 R_2^4}{r^6} - 3 \frac{R_1^2 R_2^6 + 3 R_1^4 R_2^4}{r^8} + \mathcal{O}(r^{-10}). \quad (3.212)$$

The leading-order term was first found in Ref. [LO07]. If instead both particles are allowed to tilt freely, both $C_1^{(1)} = C_2^{(1)} = 0$ and the interaction energy reduces to the leading-order expression

$$\beta U_{\{1,2\}} = -9 \frac{R_1^4 R_2^4}{r^8} + \mathcal{O}(r^{-10}), \quad (3.213)$$

also found first in Refs. [LOD06, LO07].

3.6.2 The complete pair interaction

For two particles, the simplicity of the ring diagrams allows us to write down the complete entropic pair interaction like we did for elastic interactions. One may proceed in two ways, either diagrammatically or through the explicit trace form extracted from Eq. (3.131) (and applying Eq. (3.135)). Here, we will apply the diagrammatic technique.

Since each interaction vertex has both single- and double-line legs, each ring diagram must alternate single- and double-line edges and it follows that there must be an even number of vertices in each diagram. This is true even in the multibody case, but for pairs this is reinforced since the worldline labels must also alternate. The diagrammatic expansion therefore takes the form

$$-\beta U = \sum_{k \geq 1} \text{Diagram with } 2k \text{ vertices}, \quad (3.214)$$

where the sum over k corresponds to all diagrams with $2k$ vertices. Note that the presence of the double-line edges changes the symmetry factor, but it does so in a fairly simple way. One way to work out the new symmetry factor is to think of the double-line edge as a vertex so that the diagram is isomorphic to a ring with k vertices (and k identical edges). Then, we find that the order of the symmetry group is reduced by half and $S = 2k$.

We now plug in the values of the polarizabilities and Green function derivatives. A general diagram with $2k$ vertices evaluates to the cyclic product

$$\begin{aligned} \text{Diagram with } 2k \text{ vertices} &= \frac{1}{2k} \sum_{a \neq b} \sum_{\{n\}} \prod_{i=1}^k C_a^{(n_{2i-1})} \frac{\partial_a^{n_{2i-1}} \partial_b^{n_{2i}} G^{ab}}{\sigma} C_b^{(n_{2i})} \frac{\bar{\partial}_b^{n_{2i}} \bar{\partial}_a^{n_{2i+1}} G^{ba}}{\sigma} \\ &= \frac{2}{2k} \sum_{\{n\}} \prod_{i=1}^k \frac{(n_{2i-1} + n_{2i} - 1)!(n_{2i} + n_{2i+1} - 1)!}{n_{2i-1}!(n_{2i-1} - 1)!n_{2i}!(n_{2i} - 1)!} \frac{R_1^{2n_{2i-1}} R_2^{2n_{2i}}}{z^{n_{2i-1}} r^{2n_{2i}} \bar{z}^{n_{2i+1}}}, \end{aligned} \quad (3.215)$$

where $n_{2k+1} \equiv n_1$ and $\sum_{\{n\}} \equiv \sum_{n_1, \dots, n_{2k}}$. In the second line, we used that the diagram

is invariant (equivalent) under the exchange $a \leftrightarrow b$. The cyclic product can of course be simplified further by rearranging factors. In particular, we may shift the factors of z and \bar{z} so that the denominator is more obviously real. Furthermore, we may rearrange the factorials so that they can be recognized as a product of binomial coefficients. Finally, our choice of derivative-order labels assigns all the odd labels to R_1 and the even labels to R_2 , so, as we did previously, we define the sums $N_o = \sum_{j=1}^k n_{2j-1}$ and $N_e = \sum_{j=1}^k n_{2j}$. After the appropriate manipulations, we obtain the complete pair interaction,

$$\beta U_{\{1,2\}} = - \sum_{k \geq 1} \frac{1}{k} \sum_{\{n\}} \frac{R_1^{2N_o} R_2^{2N_e}}{r^{2(N_o+N_e)}} \prod_{i=1}^{2k} \binom{n_i + n_{i+1} - 1}{n_{i+1}}, \quad (3.216)$$

in agreement with Ref. [YRD12] (though derived in a slightly different way).

The above expression is relatively straightforward to expand to very high orders, either by hand or using algebraic manipulation software (such as MATHEMATICA). If one is interested in accuracy up to and including r^{-p} , the power-counting formula (3.141) proves useful once again, relating the expansion order with the derivative orders via $n_1 + n_2 + \dots + n_{N_V} = p/2$, where $N_V = 2k$ for some k . In particular, if we only consider (BC 2) particles, then $n_i \geq 1$ and all diagrams up to $N_V = p/2$ vertices must be included, so the sum in Eq. (3.216) must run over all $k = 1, 2, \dots, \lfloor p/4 \rfloor$. To find how high the sum over polarizabilities must extend, we assign to all but one vertex a derivative order $n_i = 1$, leaving the final vertex to take on the remainder, $p/2 - (N_V - 1) = p/2 - (2k - 1)$. That is, the polarizability sums must run over the range $1 \leq n_i \leq p/2 - (2k - 1)$ for every k and vertex i . Similarly, for (BC 3) particles, $n_i \geq 2$ so one must consider all diagrams with up to $\lfloor p/4 \rfloor$ vertices, or up to $k = \lfloor p/8 \rfloor$. For each vertex i , the polarizabilities must be summed over the range $2 \leq n_i \leq p/2 - 2(2k - 1)$ for every k .

(BC 2). As an example, we will expand out the energy to $p = 22$ for two identical particles ($R_1 = R_2 = R$) whose respective heights are free to fluctuate. With $p = 22$, it follows from the previous discussion that all diagrams with up to 11 vertices will contribute (actually 10 since N_V must be even), which translates into $k_{\max} = \lfloor 22/4 \rfloor = 5$. For each k , the polarizabilities must sum over (at least) the range $1 \leq n_i \leq 11 - (2k - 1)$. For example $k = 1$ corresponds to a two-vertex diagram with a sum that must contain the ranges $1 \leq n_i \leq 10$, whereas $k = 5$ corresponds to a 10-vertex diagram with a sum that must contain the range $1 \leq n_i \leq 2$. Applying these conditions to Eq. (3.216) results in the expansion

$$-\beta U_{\{1,2\}} = \frac{1}{\chi^4} + \frac{4}{\chi^6} + \frac{31}{2\chi^8} + \frac{60}{\chi^{10}} + \frac{697}{3\chi^{12}} + \frac{900}{\chi^{14}} + \frac{13\,955}{4\chi^{16}} + \frac{40\,612}{3\chi^{18}} + \frac{262\,966}{5\chi^{20}} + \frac{204\,600}{\chi^{22}} + \mathcal{O}(\chi^{-24}), \quad (3.217)$$

where $\chi = r/R$ is the usual dimensionless distance. This expansion was also generated in Ref. [YRD12] up to r^{-12} , and of course we find perfect agreement.

(BC 3). We may similarly expand out the energy for two identical particles whose respective heights and tilts are free to fluctuate. The difference from the previous example is that the polarizability sums instead start at two since $C^{(1)} = 0$. Let us expand out to $p = 24$, for which the earlier analysis tells us that all diagrams with up to $N_V = 24/4 = 6$ vertices would contribute, or equivalently $k_{\max} = 3$ in Eq. (3.216). The polarizability sums must cover at least the range $2 \leq n_i \leq 12 - 2(2k - 1)$ for every k and vertex i (e.g., $k = 1$ gives $2 \leq n_i \leq 10$ and $k = 3$ implies all $n_i = 2$). Applying these conditions results in the expansion,

$$-\beta U_{\{1,2\}} = \frac{9}{\chi^8} + \frac{48}{\chi^{10}} + \frac{200}{\chi^{12}} + \frac{780}{\chi^{14}} + \frac{6059}{2\chi^{16}} + \frac{11\,856}{\chi^{18}} + \frac{46\,656}{\chi^{20}} + \frac{183\,960}{\chi^{32}} + \frac{725\,353}{\chi^{24}} + \mathcal{O}(\chi^{-26}). \quad (3.218)$$

The first three terms appear as a limiting case in Ref. [HD14], but the remaining terms are otherwise not found elsewhere.³⁰

Asymptotics and the exact solution. Although we will not rederive the findings here, Yolcu *et al.* [YRD12] have examined the compact expression (3.216) in detail and found useful results regarding the validity of the asymptotics. First, the authors compared high-order expansions of Eq. (3.216) with numerical results to determine an empirical heuristic for the expansions accuracy. In particular, they found that for some fixed edge-to-edge separation $d = r - 2R$, the power p for which the series may be truncated and still achieve less than 5% error obeys the asymptotic relationship $p \sim 8.2(d/R)^{-1}$. Furthermore, Yolcu demonstrated that although Eq. (3.216) is an asymptotic series in inverse powers of separation, its completeness allows it to be massaged in such a way that the *proximity* asymptotics can also be extracted. He was able to isolate the leading-order divergence $\beta U \sim -\pi^2/24\sqrt{d}$, where d is the edge-to-edge separation, which agrees with results obtained by the Derjaguin proximity approximation [LO07].

Since the asymptotic series (3.216) is complete, one might wonder if there is an analytic continuation in terms of special functions. This was done to an extent in Ref. [YRD12], as mentioned above, but a similar system has also been studied via conformal field theory (CFT) techniques, for which exact results have been obtained. In particular, Rothstein [Rot12] has calculated the free energy of a bosonic field on a plane with two circular holes satisfying Neumann boundary conditions, which was later generalized by Bimonte *et al.* [BEK13]. Strictly speaking, the Neumann problem is not entirely isomorphic to ours (to correct the claim in Ref. [YRD12]), but the change in boundary conditions—Dirichlet with a free parameter to Neumann—only manifests as a change in sign of the Wilson coefficients (see Ref. [Rot12]). For pair interactions, there is always an even power of Wilson coefficients, so the resulting (interaction) free energy turns out to be identical. Bimonte *et al.* provide the exact solution for identical holes in terms of the Dedekind η -function,³¹ which with our

³⁰Of course the tools to generate this expansion are set up in Ref. [YRD12], but the authors restricted their discussion to particles of the type (BC 2).

³¹The common definition is $\eta(\tau) = e^{i\pi\tau/12} \prod_{n=1}^{\infty} (1 - e^{2\pi i n \tau})$, for $\text{Im } \tau > 0$ [DLMF, 27.14(iv)].

usual notation $\chi = r/R$ expands as [Rot12]

$$\begin{aligned}\beta U_{\{1,2\}} &= \frac{\pi}{6C} + \ln \eta \left(\frac{2i}{C} \right) \\ &= \sum_{k \geq 1} \ln \left(1 - \left[\frac{1}{2} (\chi^2 - \chi \sqrt{\chi^2 - 4} - 2) \right]^{2k} \right),\end{aligned}\tag{3.219}$$

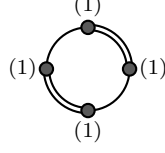
where $C = 2\pi / \cosh^{-1}(\frac{1}{2}\chi^2 - 1)$ is the “mutual capacitance” between two identical disks of radii R . The first line enables an expansion in small separation ($\chi \approx 2$), as there exists many convenient representations of η , and doing so indeed reproduces the divergence mentioned above. Both the first and second lines are useful for expanding in large separations ($\chi \gg 2$), and easily reproduce the series (3.217).³² The power of the CFT method clearly lies in the ability to produce exact expressions for all separations via Eq. (3.219); however, the dirty work is in constructing the two-body mutual capacitance C , which is nontrivial for arbitrarily-shaped objects (a hybrid EFT/CFT approach could prove useful). Furthermore, it does not directly extend to multibody interactions. For example, the pair interaction corresponds to a CFT on a cylinder with boundaries (which maps to an annulus), but a three-body system corresponds to a CFT on a genus-2 “pair of pants” with boundaries and necessitates some complicated multiply-connected mappings. Of course, it also requires conformal symmetry of the field theory, so it does not apply to non-conformal systems like the biharmonic membrane of the next chapter.

3.6.3 Multibody interactions

With more than two particles in the system, multibody interactions will amend the pairwise summation. For three (BC 2)-type particles, power counting suggests that the leading-order triplet interaction would be of a dipole–dipole–dipole type and thus scale as $r_{12}^2 r_{23}^2 r_{31}^2$. However, the prefactor of this term is identically zero [YRD12]. To see this, we once again recall that interaction vertices have two legs—one single-lined and the other double-lined—so they may only be connected to form a ring if there is an even number of vertices (and hence an alternating pattern of single- and double-line propagators). Therefore, it follows from the diagram components that a dipole–dipole–dipole interaction diagram cannot be constructed, which is equivalent to the statement that such an interaction would place a Laplacian on one of the propagators (between nonidentical points) and thus vanish. The leading-order triplet interaction must therefore be contained within the tetravalent interaction diagram,

³²Evidently, comparing the two series (3.216) and (3.219) provides the (likely unknown) summation identity

$$-\frac{1}{k} \sum_{\{n_j \geq 1\}} \prod_{j=1}^{2k} \chi^{-n_j} \binom{n_j + n_{j+1} - 1}{n_{j+1}} = \ln \left(1 - \left[\frac{1}{2} (\chi^2 - \chi \sqrt{\chi^2 - 4} - 2) \right]^{2k} \right).$$



which, incidentally, is where the quadruplet interaction begins as well.

In the above diagram, a sum over particle labels is implied at each vertex. For three particles, two *nonadjacent* vertices must be placed on the same worldline, which can be done in two ways. The resulting sum over label permutations may also be reduced to twice a cyclic sum, since an interchange of the nonrepeated labels returns an equivalent diagram. That is, representing the worldline-labeled evaluation of the diagram by $f(a, b, c, d)$, the diagram symmetries allow for the summation reduction,

$$\sum'_{a,b,c,d} f(a, b, c, d) \rightarrow 2 \sum_{a,b,c}^{\text{perm. } \{1,2,3\}} f(a, b, c, b) \rightarrow 4 \sum_{a,b,c}^{\text{cyc. } \{1,2,3\}} f(a, b, c, b).$$

The concluding factor of four cancels the diagram's symmetry factor, and we find the leading-order triplet interaction,

$$\begin{aligned} \beta U_{\text{tri}}^{(8)} &= -4 \sum_{a,b,c}^{\text{cyc. } \{1,2,3\}} \frac{1}{4} C_a^{(1)} [C_b^{(1)}]^2 C_c^{(1)} \frac{\partial_a \partial_b G^{ab}}{\sigma} \frac{\bar{\partial}_b \bar{\partial}_c G^{bc}}{\sigma} \frac{\partial_c \partial_b G^{cb}}{\sigma} \frac{\bar{\partial}_b \bar{\partial}_a G^{ba}}{\sigma} \\ &= - \left(\frac{R_1^2 R_2^4 R_3^2}{r_{12}^4 r_{23}^4} + \frac{R_1^2 R_2^2 R_3^4}{r_{23}^4 r_{31}^4} + \frac{R_1^4 R_2^2 R_3^2}{r_{31}^4 r_{12}^4} \right), \end{aligned} \quad (3.220)$$

in agreement with Ref. [YRD12], and recently derived through a scattering approach in Refs. [NWZ13b, NWZ13a]. The interaction is purely attractive and does not explicitly depend on the triangle angles of the three-particle system (though the three lengths *are* sufficient to uniquely determine the triangle).

The leading-order quadruplet interaction is also contained within the same diagram, but the summation is instead given over all permutations of the label set $\{1, 2, 3, 4\}$. The diagram symmetries again reduce the summation, but this time the interchange of nonadjacent labels produces the diagram's complex conjugate. The product of Green function derivatives results in many angles, which may be combined in several equivalent coordinate-free ways. We first choose the convention that reproduces the result in Ref. [YRD12]:

$$\begin{aligned} \beta U_{\text{quad}}^{(8)} &= - \frac{C_1^{(1)} C_2^{(1)} C_3^{(1)} C_4^{(1)}}{\sigma^4} 2 \text{Re} \left(\partial^2 G^{12} \bar{\partial}^2 G^{23} \partial^2 G^{34} \bar{\partial}^2 G^{41} \right. \\ &\quad \left. + \partial^2 G^{13} \bar{\partial}^2 G^{32} \partial^2 G^{24} \bar{\partial}^2 G^{41} \right. \\ &\quad \left. + \partial^2 G^{13} \bar{\partial}^2 G^{34} \partial^2 G^{42} \bar{\partial}^2 G^{21} \right) \end{aligned}$$

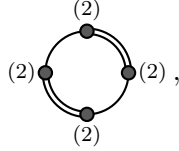
$$\begin{aligned}
 = -2R_1^2 R_2^2 R_3^2 R_4^2 & \left[\frac{\cos(\varphi_{13}^2 - \varphi_{24}^3 + \varphi_{31}^4 - \varphi_{42}^1)}{r_{12}^2 r_{23}^2 r_{34}^2 r_{41}^2} \right. \\
 & + \frac{\cos(\varphi_{14}^2 - \varphi_{23}^4 + \varphi_{41}^3 - \varphi_{32}^1)}{r_{12}^2 r_{24}^2 r_{43}^2 r_{31}^2} \\
 & \left. + \frac{\cos(\varphi_{12}^3 - \varphi_{34}^2 + \varphi_{21}^4 - \varphi_{43}^1)}{r_{13}^2 r_{32}^2 r_{24}^2 r_{41}^2} \right]. \quad (3.221)
 \end{aligned}$$

This expression depends on six distances and twelve angles, reflecting the four different triangles that can be formed between the four particle positions. However, many of these parameters are not independent. A fact from planar trigonometry is that any polygon with n vertices may be uniquely determined by $2n - 3$ parameters (sides and angles), at least $n - 2$ of which must be side lengths [Hob57]. For $n = 4$, this means the irreducible set contains five parameters, at least two of which must be lengths. Hence, the energy expression above is actually highly overdetermined and most of the lengths and angles could be re-expressed in terms of a set of five parameters. The form expressed, however, is perhaps preferable to one containing additional trigonometric relationships. An alternative (but still overdetermined) expression is also suggested by the Green function derivatives and reduces the angular-dependence by half:

$$\beta U_{\text{quad}}^{(8)} = -2R_1^2 R_2^2 R_3^2 R_4^2 \left[\frac{\cos(2\varphi_{13}^2 + 2\varphi_{31}^4)}{r_{12}^2 r_{23}^2 r_{34}^2 r_{41}^2} + \frac{\cos(2\varphi_{14}^2 + 2\varphi_{41}^3)}{r_{12}^2 r_{24}^2 r_{43}^2 r_{31}^2} + \frac{\cos(2\varphi_{12}^3 + 2\varphi_{21}^4)}{r_{13}^2 r_{32}^2 r_{24}^2 r_{41}^2} \right]. \quad (3.222)$$

Although the number of particles has somewhat increased the geometric complexity, we observe that angular configurations which maximize the cosines will minimize the energy and lead to a collective four-body attraction. One may check that this occurs for both rectangular and collinear particle arrangements, where the cosine arguments *all* vanish (mod 2π).

Tilt freedom. For particles with the freedom to tilt as well as fluctuate vertically, the dipole polarizabilities vanish, so the leading-order triplet contribution must stem from induced quadrupoles. By the same argument as before, this contribution must come from a tetravalent interaction diagram,



for which power-counting reveals the scaling dependence $\sim \text{distance}^{-16}$. As before, the consideration of the diagram's symmetries shows that distributing the three particle labels on the four vertices such that no self-interactions occur can be done in three unique ways, each of which has a multiplicity of four which cancels the symmetry factor of the original

diagram. The interaction energy then appears as the cyclic sum,

$$\begin{aligned}\beta U_{\text{tri}}^{(16)} &= - \sum_{a,b,c}^{\text{cyc. } \{1,2,3\}} \frac{C_a^{(2)} [C_b^{(2)}]^2 C_c^{(2)}}{\sigma^4} \partial^4 G^{ab} \bar{\partial}^4 G^{bc} \partial^4 G^{cb} \partial^4 G^{ba} \\ &= -81 \left(\frac{R_1^4 R_2^8 R_3^4}{r_{12}^8 r_{23}^8} + \frac{R_1^4 R_2^4 R_3^8}{r_{23}^8 r_{31}^8} + \frac{R_1^8 R_2^4 R_3^4}{r_{31}^8 r_{12}^8} \right),\end{aligned}\quad (3.223)$$

which agrees with Ref. [NWZ13a], wherein the authors derived the above result via scattering methods.

3.6.4 Monopoles³³

For particles frozen in position, monopole polarizabilities will contribute to their entropic interactions. Just as before, the entropic interactions are independent of the particles' permanent sources, so without losing generality we may treat the particles as flat and positioned in the reference plane ($h = 0$). Our treatment of monopoles for elastic interactions carries over to entropic interactions, but applies to subleading and higher-order contributions to the interaction energy. At leading order, the fluctuation-induced interactions between monopoles is much simpler.

Leading order

The relevant diagrams at leading order must be built from only monopole vertices, and consistency in the perturbative expansion dictates that this infinite set of such monopole rings be summed completely. Previously, this resummation was achieved by considering all possible monopole insertions into each propagator and identifying and completing the resulting geometric series. At leading order, however, the resummation essentially reverses the derivation from diagrams to the trace expression in Eq. (3.129) to the determinant form in Eq. (3.126):

$$\begin{aligned}-\beta U^{(0)} &= \sum_{k=1}^{\infty} \text{diagram}_k = \sum_{k=1}^{\infty} \frac{1}{2k} \text{tr} \left(\text{diagram}_k \right) = \frac{1}{2} \text{tr} \sum_{k=1}^{\infty} \frac{(-\mathbf{GM})^k}{k} \\ &= -\frac{1}{2} \text{tr} \ln(\mathbf{1} + \mathbf{GM}) = -\frac{1}{2} \ln \det(\mathbf{1} + \mathbf{GM}),\end{aligned}\quad (3.224)$$

where the matrix is given in Eqs. (3.172) and (3.173). We have purposely set the sum to run over all $k \geq 1$ so that the Taylor series of the logarithm is apparent, and kept the exclusion of self-interactions implicit (it is contained within the expression for $\mathbf{1} + \mathbf{GM}$). By

³³The content and development of this section closely follow Section V. of Ref. [HD14], but specialized to the case of circular particles.

replacing continuous operators with finite matrices, the calculation for N particles reduces to computing the standard determinant of an $N \times N$ matrix. We demonstrate this for two- and three-particle systems below.

Two particles. We have already calculated the determinant for two particles in Eq. (3.176); applying the result to Eq. (3.224) reveals the leading-order entropic interaction energy to be

$$\beta U_{\{1,2\}}^{(0)} = \frac{1}{2} \ln(1 - g_{12}^2). \quad (3.225)$$

As we discussed previously, the argument of the logarithm vanishes as $\sim \Lambda^{-1}$ in the $\ell_c \rightarrow \infty$ limit (*cf.* Eq. (3.180)), so the interaction energy diverges. This divergence can be factorized, however, and can be separated from the interaction energy as an infinite but *irrelevant* constant. To see this, we expand the energy in powers of Λ_{12} to find

$$\beta U_{\{1,2\}}^{(0)} = -\frac{1}{2} \ln \Lambda_{12} + \frac{1}{2} \ln \left[2 \ln \left(\frac{r}{\sqrt{R_1 R_2}} \right) \right] + \mathcal{O}(\Lambda^{-1}). \quad (3.226)$$

The corresponding attractive force is long-ranged and slightly suppressed by a logarithmic correction:

$$F_{\{1,2\}}^{(0)} = -\frac{k_B T}{2r \ln \left(\frac{r}{\sqrt{R_1 R_2}} \right)} + \mathcal{O}(\Lambda^{-1}). \quad (3.227)$$

Up to irrelevant constants, the above energy expression agrees with the literature, namely Ref. [LO07], where the result first appears, Ref. [YRD12], where the result is calculated via EFT methods similar to here, Refs. [NWZ13b, NWZ13a], where the result is obtained using a scattering formalism, and Ref. [BEK13], where the exact expression is calculated via CFT methods and the above term matches the large-distance expansion to leading order. The last reference is of note because, unlike the Neumann problem mentioned earlier, the Dirichlet problem maps exactly onto the frozen-particle system considered here. We will return to this when we discuss higher-order corrections.

Three particles. Similarly, we calculate the *complete* leading-order interaction energy for a three-particle system and find

$$\beta U_{\{1,2,3\}}^{(0)} = \frac{1}{2} \ln [1 - (g_{12}^2 + g_{23}^2 + g_{31}^2 - 2g_{12}g_{23}g_{31})]. \quad (3.228)$$

Contained within this result are both the triplet and pairwise interactions. The decomposition is not readily apparent, but we may do as before and subtract off the pairwise sum using Eq. (3.225) to obtain an expression for the triplet interaction:

$$U_{\text{tri}}^{(0)} = U_{\{1,2,3\}}^{(0)} - \left(U_{\{1,2\}}^{(0)} + U_{\{2,3\}}^{(0)} + U_{\{3,1\}}^{(0)} \right). \quad (3.229)$$

The logarithms combine, and we find the pure triplet interaction energy at leading order,

$$\beta U_{\text{tri}}^{(0)} = \frac{1}{2} \ln \left[\frac{1 - (g_{12}^2 + g_{23}^2 + g_{31}^2 - 2g_{12}g_{23}g_{31})}{(1 - g_{12}^2)(1 - g_{23}^2)(1 - g_{31}^2)} \right]. \quad (3.230)$$

The expression above reproduces the findings of Refs. [NWZ13b, NWZ13a], obtained through a scattering matrix expansion.³⁴

To understand the three-particle behavior, we may again expand the result for $\ell_c \rightarrow \infty$ using Eqs. (3.190) and (3.226). After some simplification, the total three-body interaction energy (3.228) becomes³⁵

$$\beta U_{\{1,2,3\}}^{(0)} = -\frac{1}{3} \ln(\Lambda_{12}\Lambda_{23}\Lambda_{31}) + \beta \mathcal{E}_{\text{tot}} + \mathcal{O}(\Lambda^{-1}), \quad (3.231)$$

with

$$\beta \mathcal{E}_{\text{tot}} = \frac{1}{2} \ln \left[\sum_{\text{cyc.}} (2\varrho_{ab}\varrho_{bc} - \varrho_{ab}^2) \right], \quad (3.232)$$

where as usual the sum is over cyclic permutations of the label set $\{1, 2, 3\}$. Observe that the divergences again separate as an irrelevant constant, and the distance dependence is contained within \mathcal{E}_{tot} . As an aside, we note that the above equation may alternatively be expressed as

$$\beta \mathcal{E}_{\text{tot}} = \frac{1}{2} \ln \left(\sum_{\text{cyc.}} \left[\varrho_{ab}^2 - (\varrho_{ab} - \varrho_{bc})^2 \right] \right). \quad (3.233)$$

The three-body entropic energy is collectively attractive. To see this, we can examine the behavior under the distance rescaling $r_{ab} \rightarrow \lambda r_{ab}$:

$$-\frac{\partial(\beta \mathcal{E}_{\text{tot}})}{\partial \lambda} = -\frac{1}{\lambda} \frac{\varrho_{12} + \varrho_{23} + \varrho_{31}}{\sum_{\text{cyc.}} (2\varrho_{ab}\varrho_{bc} - \varrho_{ab}^2)} = -\frac{1}{\lambda} \frac{\ln(\lambda^3 \frac{r_{12}r_{23}r_{31}}{R_1 R_2 R_3})}{\sum_{\text{cyc.}} (2\varrho_{ab}\varrho_{bc} - \varrho_{ab}^2)}, \quad (3.234)$$

where the rescaling is implied in the ϱ_{ab} terms. According to the above equation, decreasing the interparticle separation lowers the energy, and thus the interaction is collectively attractive. It is interesting to see how the pure triplet interaction contributes to the attraction, so we compute it by subtracting off the pairwise energy sum,³⁶

$$\beta \mathcal{E}_{\text{p}} = \frac{1}{2} \ln(8\varrho_{12}\varrho_{23}\varrho_{31}), \quad (3.235)$$

³⁴ There is, however, a discrepancy with the published versions of Refs. [NWZ13b, NWZ13a]: The g^3 term has the opposite sign. I have communicated with the authors and verified that this is a typographical error, and our results do indeed agree.

³⁵ There are many ways to manipulate terms, but they all inevitably rely on the limit $\Lambda_{ab}/\Lambda_{cd} \rightarrow 1$. To arrive at the clean form in Eq. (3.231), one may express the denominator of Eq. (3.190) as $[(\Lambda_{12}\Lambda_{23}\Lambda_{31})^{1/3}]^4 (\Lambda_{12}\Lambda_{23}\Lambda_{31})^{2/3}$ and take the ratio limit of the Λ^4 terms in the numerator and denominator.

³⁶ Of course, one could alternatively just expand Eq. (3.230).

to give the triplet energy

$$\beta\mathcal{E}_{\text{tri}} = \beta(\mathcal{E}_{\text{tot}} - \mathcal{E}_{\text{p}}) = -\frac{1}{2} \ln \left[\frac{8\varrho_{12}\varrho_{23}\varrho_{31}}{\sum_{\text{cyc.}} (2\varrho_{ab}\varrho_{bc} - \varrho_{ab}^2)} \right]. \quad (3.236)$$

The numerator contains an additional power of ϱ compared with the denominator, so the argument of the logarithm is greater than one. Moreover, this additional power in the numerator suggests that under distance rescaling by λ the energy behaves like $-\ln \ln \lambda$ and is therefore collectively *repulsive*.

We check this repulsive behavior with our usual three-body example configurations of identical particles ($R_a = R$). For an equilateral triangle arrangement ($r_{12} = r_{23} = r_{31} = d$), the triplet interaction energy reduces dramatically to

$$\beta\mathcal{E}_{\text{tri},\Delta} = -\frac{1}{2} \ln \left[\frac{8}{3} \ln \left(\frac{d}{R} \right) \right], \quad (3.237)$$

for which the repulsion is indeed clear. For the collinear arrangement ($r_{12} = r_{23} = r_{31}/2 = d$), the triplet energy reduces to

$$\beta\mathcal{E}_{\text{tri},\text{lin}} = -\frac{1}{2} \ln \left[\frac{8 \ln^2(d/R)}{3 \ln(d/R) - \ln 2} \right]. \quad (3.238)$$

To demonstrate more clearly that this is attractive, we look at how the energy changes under rescaling the energy by λ :

$$-\frac{\partial(\beta\mathcal{E}_{\text{tri},\text{lin}})}{\partial\lambda} = \frac{1}{2\lambda} \frac{3 \ln(\frac{\lambda d}{R}) - 2 \ln 2}{\ln(\frac{\lambda d}{R}) [3 \ln(\frac{\lambda d}{R}) - \ln 2]}. \quad (3.239)$$

Since we require $\lambda d \geq 2R$, it follows that the right side is positive and hence the triplet interaction is collectively repulsive.

Similar to our findings regarding elastic interactions, we observe another interesting three-body effect. When the particles are all free to fluctuate in height, or fluctuate in height *and* tilt, the triplet contribution reinforces the collective attraction. However, when the positions of the particles are fixed, the triplet interaction reduces the overall attraction. This reproduces the observations in Refs. [NWZ13b, NWZ13a].

Higher orders

Luckily, during our discussion of monopole contributions to elastic interactions, we have completely laid out the tools required to calculate higher-order corrections to the entropic interaction energies. We will not rederive them here, but instead summarize the formalism and results.

For a system of N particles with fixed positions, (BC 1), the interparticle interaction energy is given by the pairwise and multibody diagrammatic expansion (3.214) applicable

to (BC 2) (*i.e.*, $C^{(1)} \neq 0$)—where the vertices sum over *all* particle positions—modified by all possible monopole insertions on each propagator (including zero insertions). As we found previously, the monopole insertions on any given propagator can be resummed as a geometric series and results in three terms: the identity which leaves the propagator unaffected, an effective monopole vertex which starts and ends on the same particle worldline, and an effective monopole vertex which starts and ends on different particle worldlines. In both cases, the effective monopole vertices depend on the total number of particles in the system, and in this sense are complete. That is, only the N -body effective monopole vertices for a system of N particles are used, and consistency dictates that the effective $N - 1$, $N - 2$, *etc.* monopole vertices are not needed. Although this provides the complete monopole contributions at each order rather efficiently, we note that to determine the *explicit* pair, triplet, quadruplet, *etc.* contributions, one would still need to determine the effective ($n < N$)-body monopole vertices and apply the appropriate subtraction like we did above.

Here we will apply the formalism to both two- and three-body particle systems. For ease of reference, we provide the effective monopole vertices in the $\ell_c \rightarrow \infty$ limit below:

$$N = 2 : \begin{cases} i \text{---} \otimes \text{---} j = -\beta \sum_a 2\pi\sigma \delta_a^i \left(\frac{1}{2\varrho_{12}} \right) \delta_j^a \\ i \text{---} \otimes \text{---} \otimes \text{---} j = \beta \sum_{a,b} 2\pi\sigma \delta_a^i \left(\frac{1 - \delta_b^a}{2\varrho_{12}} \right) \delta_j^b \end{cases} \quad (3.240)$$

$$N = 3 : \begin{cases} i \text{---} \otimes \text{---} j = -\beta \sum_a 2\pi\sigma \delta_a^i \frac{2 \sum_{\text{cyc.}} (\varrho_{kl} - \varrho_{al})}{\sum_{\text{cyc.}} (2\varrho_{kl}\varrho_{lm} - \varrho_{kl}^2)} \delta_j^a \\ i \text{---} \otimes \text{---} \otimes \text{---} j = \beta \sum_{a,b} 2\pi\sigma \delta_a^i \frac{(\sum_{\text{cyc.}} \varrho_{kl}) - 2\varrho_{ab}}{\sum_{\text{cyc.}} (2\varrho_{kl}\varrho_{lm} - \varrho_{kl}^2)} (1 - \delta_b^a) \delta_j^b \end{cases} \quad (3.241)$$

Incorporating these vertices into the expansion follows from the discussion of multiple perturbations surrounding Eq. (3.130). The fluctuation-induced interaction energy then consists of all ring diagrams with distinct permutations of effective monopole insertions:

$$\begin{aligned} -\beta U = & \sum_{k=1}^{\infty} \text{diagram}_k + \sum_{k \geq 1} \text{diagram}_{2k} + \text{diagram}_1 + \text{diagram}_2 \\ & + 2 \text{Re} \left[\text{diagram}_1 + \text{diagram}_2 \right] + \text{diagram}_1 + \text{diagram}_2 \\ & + \text{diagram}_1 + 2 \text{Re} \left[\text{diagram}_1 \right] + \text{diagram}_1 + \text{diagram}_2 + \dots \end{aligned} \quad (3.242)$$

Two particles. The subleading contribution to the pair interaction energy comes from the single dipole–monopole diagram,

$$-\beta U_{\text{BC1}}^{(2)} = \text{diagram}, \quad (3.243)$$

and is easily evaluated, giving

$$\beta U_{\text{BC1}}^{(2)} = -\frac{R_1^2 + R_2^2}{4r^2 \varrho_{12}}. \quad (3.244)$$

We have dropped the usual $\{1, 2\}$ label on U in favor of “BC1” to distinguish it from the (BC 2) contributions.

The next order finds contributions from the (BC 2) dipole–dipole interaction, expressed in Eq. (3.208), as well as the interactions between two induced dipoles and two (effective) monopoles, and between monopoles and an induced quadrupole. These are represented by the expansion,

$$\begin{aligned} -\beta U_{\text{BC1}}^{(4)} = & -\beta U_{\text{BC2}}^{(4)} + \text{diagram} + 2 \operatorname{Re} \left[\text{diagram} \right] \\ & + \text{diagram} + \text{diagram} + \text{diagram} + \text{diagram}. \end{aligned} \quad (3.245)$$

As usual for pair interactions, only diagrams with an even number of vertices contribute since an odd number would entail self-interactions. The evaluation of the diagrams is again fairly straightforward; one needs to just be careful to include the correct symmetry factors. The diagram in brackets has a symmetry factor of two due to one reflection. The first and third diagrams in the second line have the same diagram symmetry, a single rotation of 180° , and thus they share the same symmetry factor of two. Similarly, the second and fourth diagrams in the second line share the same symmetry factor of two due to a single reflection across the horizontal midline. After evaluating and simplifying—and completing the square in two terms—we arrive at the expression

$$\beta U_{\text{BC1}}^{(4)} = \beta U_{\text{BC2}}^{(4)} - \frac{(R_1^2 + R_2^2)^2 + 2R_1^2 R_2^2}{8r^4 \varrho_{12}} - [\beta U_{\text{BC1}}^{(2)}]^2. \quad (3.246)$$

The final term comes from the last line of Eq. (3.245) and its identification with the square of the subleading energy is unique to two-particle systems since the one- and two-vertex effective monopole vertices furnish the same factors of $\pi\sigma/\varrho_{12}$. This interesting regrouping

can be seen by decomposing the diagrams, rearranging factors, and reconnecting the links:

$$\begin{aligned}
 & \text{Diagram 1} + \text{Diagram 2} + \text{Diagram 3} + \text{Diagram 4} \\
 &= \sum_{a \neq b}^2 \left(\frac{2\pi\sigma}{2\varrho_{12}} \right)^2 \left\{ \frac{1}{2} \times 2 \left(\begin{array}{c} b \quad a \quad b \\ \vdots \quad \vdots \quad \vdots \\ \bullet \text{---} \bullet \\ (1) \end{array} \right)^2 + \frac{1}{2} \times 2 \left(\begin{array}{c} b \quad a \quad b \\ \vdots \quad \vdots \quad \vdots \\ \bullet \text{---} \bullet \\ (1) \end{array} \right) \left(\begin{array}{c} a \quad b \quad a \\ \vdots \quad \vdots \quad \vdots \\ \bullet \text{---} \bullet \\ (1) \end{array} \right) \right\} \\
 &= \left[\sum_{a \neq b}^2 \left(\frac{2\pi\sigma}{2\varrho_{12}} \right) \left(\begin{array}{c} b \quad a \quad b \\ \vdots \quad \vdots \quad \vdots \\ \bullet \text{---} \bullet \\ (1) \end{array} \right) \right]^2 = \left[\text{Diagram 5} \right]^2.
 \end{aligned} \tag{3.247}$$

As we mentioned earlier, the exact free energy for two particles was obtained in Ref. [BEK13], and the Dirichlet-Dirichlet case corresponds exactly to the present system. Their result reads,

$$\beta U_{\text{BC1}} = \frac{\pi}{6C} + \frac{1}{2} \ln \left(\frac{2\pi}{C} \right) + \ln \eta \left(\frac{2i}{C} \right), \tag{3.248}$$

where η is the Dedekind eta function and C is the mutual capacitance between the two objects. For the case of identical disks of radii R , the capacitance is given by $C = 2\pi / \cosh^{-1}(\frac{1}{2}\chi^2 - 1)$, where $\chi = r/R$ as usual. The expansion for large separations generates the first few terms,

$$\beta U_{\text{BC1}} = \frac{1}{2} \ln(2 \ln \chi) - \frac{1}{2\chi^2 \ln \chi} - \frac{1}{\chi^2} \left(1 + \frac{3}{4 \ln \chi} + \frac{1}{4 \ln^2 \chi} \right) - \dots \tag{3.249}$$

Combining our own results, namely Eqs. (3.226), (3.244), and (3.246), we find (up to the irrelevant constant)

$$\beta U_{\text{BC1}} = \frac{1}{2} \ln(2\varrho_{12}) - \frac{R_1^2 + R_2^2}{4r^2 \varrho_{12}} - \frac{1}{r^4} \left[R_1^2 R_2^2 + \frac{(R_1^2 + R_2^2)^2 + 2R_1^2 R_2^2}{8\varrho_{12}} + \frac{(R_1^2 + R_2^2)^2}{16\varrho_{12}^2} \right] - \dots, \tag{3.250}$$

which we see for $R_1 = R_2 = R$ indeed agrees with the expansion (3.249).

Three particles. For a system of three particles, diagrams with odd numbers of vertices now appear and the subleading contribution to the interaction energy is given by the two

diagrams,

$$-\beta U_{\text{BC1}}^{(2)} = \text{Diagram 1} + \text{Diagram 2}. \quad (3.251)$$

We evaluate the diagrams in the standard way, being careful about minus signs in the second diagram, and find

$$\beta U_{\text{BC1}}^{(2)} = - \sum_{a,b,c}^{\text{cyc.}} \left[\frac{\varrho_{ca} R_a^2 + R_b^2 \varrho_{bc}}{r_{ab}^2 \sum_{\text{cyc.}} (2\varrho_{kl} \varrho_{lm} - \varrho_{kl}^2)} + \frac{(\varrho_{ca} + \varrho_{ab} - \varrho_{bc})}{\sum_{\text{cyc.}} (2\varrho_{kl} \varrho_{lm} - \varrho_{kl}^2)} \frac{R_a^2}{r_{ca} r_{ab}} \cos \varphi_{cb}^a \right]. \quad (3.252)$$

In contrast to the leading-order correction of three-body elastic energy, Eq. (3.201), the above expression reinforces the leading-order fluctuation-induced attraction. Moreover, the pure triplet interaction is also in harmony and appears attractive. We demonstrate this through our usual example configurations. For three identical particles ($R_a = R$) arranged at the vertices of an equilateral triangle of side lengths $r_{ab} = d$, the above interaction energy reduces quite dramatically to

$$\beta U_{\text{tot},\Delta}^{(2)} = - \frac{3R^2}{2d^2 \ln(d/R)}. \quad (3.253)$$

We compare this to the pairwise sum generated by Eq. (3.244), which simplifies to

$$\beta U_{\text{p},\Delta}^{(2)} = - \frac{3R^2}{2d^2 \ln(d/R)}, \quad (3.254)$$

and find the surprising result that the pure triplet interaction vanishes completely for this configuration. For a collinear arrangement in which $r_{12} = r_{23} = r_{31}/2 = d$, and the exterior angles satisfy $\varphi_{13}^2 = 0$ and $\varphi_{21}^3 = \varphi_{32}^1 = \pi$, the three-body interaction energy becomes

$$\beta U_{\text{tot,lin}}^{(2)} = - \frac{9R^2 \ln(d/R)}{2d^2 \ln(d/R) (3 \ln(d/R) - \ln 2)}, \quad (3.255)$$

which we see is collectively attractive. We now compare this to the pairwise sum, given by

$$\beta U_{\text{p,lin}}^{(2)} = - \frac{R^2}{d^2} \left(\frac{1}{\ln(d/R)} + \frac{1}{8 \ln(2d/R)} \right). \quad (3.256)$$

Subtracting from Eq. (3.255) yields the pure triplet energy. Admittedly, there are many different ways to simplify the logarithms, but for demonstration purposes we present one such regrouping that isolates the overall minus sign and keeps both the numerator and

denominator clearly positive:

$$\beta U_{\text{tri,lin}}^{(2)} = \beta \left(U_{\text{tot,lin}}^{(2)} - U_{\text{p,lin}}^{(2)} \right) = - \frac{8 \ln^2 \left(\frac{d}{2R} \right) + \ln \left(\frac{d}{R} \right) \ln \left(\frac{2d}{R} \right)}{8 \left(\frac{d}{R} \right)^2 \ln \left(\frac{d}{R} \right) \ln \left(\frac{2d}{R} \right) [3 \ln \left(\frac{d}{R} \right) - \ln 2]}. \quad (3.257)$$

In this form, the attractive nature becomes transparent.

Monopole screening. We close this section with an alternative interpretation of the effective monopole polarizabilities. In Section 3.5.4, we made it clear that the $\ell_c \rightarrow \infty$ limit corresponded to the restoration of the surface’s vertical translation symmetry, analogous to connecting two conductors to a voltage source so that the potential difference is maintained, but the ground voltage is unconstrained. This has the effect that elastic interactions between vertically constrained particles only depend on their respective height differences. From this perspective, the effective monopoles in the expansion (3.181) account for the work done by the external sources to maintain the height differences.

The picture is not much different in the entropic case, except that the effective monopoles also account for the work done by the external sources to maintain the particles’ positions against vertical fluctuations. That is, once fluctuations are included, the effective monopoles serve two purposes: to fix the particle positions relative to their respective neighbors (elastic) and to counter surface height fluctuations (entropic). This motivates the following reinterpretation of the effective monopole contributions and logarithmic factors ϱ_{ij} .³⁷

At leading order, the entropic interaction energy is governed by Eq. (3.226), which we will write as $\beta \mathcal{E}_{ij} = \frac{1}{2} \ln(2\varrho_{ij})$ by dropping the irrelevant constant. This energy is due in part to the attachment constraints at the particle–surface boundary, but also the external sources that fix the vertical positions. The effective monopoles account for the latter, and are governed by the expressions in Eq. (3.240) for a two-particle system. These contain only the factor $1/\varrho_{12}$, which we may re-express according to the leading-order interaction energy,

$$\frac{1}{2\varrho_{ij}} = e^{-2\beta \mathcal{E}_{ij}}, \quad (3.258)$$

which is of pure monopole origin. This form suggests that the multiplicative logarithmic corrections be interpreted as a type of monopole *screening*.³⁸ Indeed, the external sources

³⁷This discussion expands somewhat on the interpretation I suggested in Ref. [HD14].

³⁸The term “screening” is also suggestive of its similarity to Debey–Hückel theory which, describes the screening of the electrostatic potential ϕ in polarizable medium of effective permittivity ϵ via

$$-\epsilon \nabla^2 \phi(\mathbf{x}) = \rho_{\text{ext}}(\mathbf{x}) - \lambda_D^{-2} \phi(\mathbf{x}),$$

where ρ_{ext} is a distribution of charges immersed in the medium and λ_D is the Debye screening length. A similar governing equation follows from Eqs. (3.66), (3.81), and (3.85), but with the analogue of λ_D augmented by a distribution:

$$-\sigma \nabla^2 h(\mathbf{x}) = \rho_p(\mathbf{x}) - \left[\ell_c^{-2} + \sum_a M_a^{(0)} \delta(\mathbf{x} - \mathbf{x}_a) \right] h(\mathbf{x}).$$

perform work suppressing height fluctuations, and the suppression of fluctuations near the particle boundaries effectively shields the particles from one another, or rather, it screens the interactions between monopoles and induced higher-order multipole moments. For example, an entropic monopole–dipole interaction should scale as $1/r^2$ by dimensional analysis, but as we see by rewriting Eq. (3.244), the monopoles screen this interaction through the entropic monopole–monopole energy:

$$\beta U_{\text{BC1}}^{(2)} = -e^{-2\beta\mathcal{E}_{12}} \left(\frac{R_1^2 + R_2^2}{2r^2} \right). \quad (3.259)$$

This interpretation of course extends to three particles. Using Eq. (3.232), we rewrite the total three-body monopole interaction energy as

$$e^{2\beta\mathcal{E}_{\text{tot}}} = \sum_{\text{cyc.}} \left[\varrho_{ab}^2 - (\varrho_{ab} - \varrho_{bc})^2 \right] = e^{2\beta(\mathcal{E}_{\text{tri}} + \mathcal{E}_{12} + \mathcal{E}_{23} + \mathcal{E}_{31})}, \quad (3.260)$$

where in the last equality we decomposed the energy into the triplet energy and the pairwise sum. A similar decomposition is achieved for the effective monopole vertices in Eq. (3.241):

$$i \text{---} \textcircled{\otimes} \text{---} j = -\beta \sum_a 2\pi\sigma \delta_a^i e^{-2\beta(\mathcal{E}_{\text{tri}} + \mathcal{E}_{ka} + \mathcal{E}_{a\ell})} \delta_j^a \quad (3.261a)$$

$$\begin{aligned} i \text{---} \textcircled{\otimes} \text{---} \textcircled{\otimes} \text{---} j &= \beta \sum_{a,b} 2\pi\sigma \delta_a^i \frac{1}{2} e^{-2\beta(\mathcal{E}_{\text{tri}} + \mathcal{E}_{ab})} \\ &\times \left[e^{-2\beta\mathcal{E}_{ak}} + e^{-2\beta\mathcal{E}_{kb}} - e^{-2\beta(\mathcal{E}_{ak} + \mathcal{E}_{kb} - \mathcal{E}_{ab})} \right] \delta_j^b, \end{aligned} \quad (3.261b)$$

where for the first vertex, the indices k and ℓ ($k \neq \ell$) are the two other particle labels not picked out by a , and for the second vertex, the index k is the remaining particle label not picked out by a and b . One benefit of expressing the vertices in this form is that it makes the reduction to two particles clear. That is, the three-body vertices are consistent with the two-body result: In a two-particle system, both the triplet $\mathcal{E}_{\text{tri}} = 0$ and the pairs $\mathcal{E}_{23} = \mathcal{E}_{31} = 0$, so the above expressions reduce to those in Eq. (3.240).

The vertices in Eq. (3.261) show that the entropic interactions between monopoles and higher-order multipole moments are again suppressed, or screened, by the pairwise monopole interactions, but it also appears the triplet energy suppresses interactions as well. However, recall that the triplet energy is negative (see Eq. (3.236)), so the triplet actually amplifies the interactions slightly. The pairwise interactions outcompete the triplet energy, so we again find an overall screening effect. We illustrate by rewriting Eq. (3.252), the entropic

three-body interaction energy between monopoles and dipoles:

$$\beta U_{\text{BC1}}^{(2)} = -\frac{1}{2} \sum_{a,b,c}^{\text{cyc.}\{1,2,3\}} e^{-2\beta(\mathcal{E}_{\text{tri}})} \left[e^{-2\beta\mathcal{E}_{ab}} \frac{e^{-2\beta\mathcal{E}_{bc}} R_a^2 + e^{-2\beta\mathcal{E}_{ca}} R_b^2}{r_{ab}^2} + e^{-2\beta\mathcal{E}_{bc}} \frac{e^{-2\beta\mathcal{E}_{ca}} + e^{-2\beta\mathcal{E}_{ab}} - e^{-2\beta(\mathcal{E}_{ca}+\mathcal{E}_{ab}-\mathcal{E}_{bc})}}{r_{ca}r_{ab}} R_a^2 \cos \varphi_{cb}^a \right]. \quad (3.262)$$

The “screening” behavior due to the leading-order pair and multibody energies will persist for more numerous collections of particles. Since, by way of the Cayley–Hamilton theorem, the effective vertices will always carry with them the factor $\det(\mathbf{1} + \mathbf{GM})$, it follows that all monopole interactions will be exponentially suppressed by the total leading-order multibody monopole energy (*cf.* Eq. (3.224)). As this suppression will always contain multibody energies specific to the total number of particles, these interactions are not just simply sums over partitions (pairwise, tripletwise, and so on) of the collection of particles, but they mix the multibody effects in various ways like in the above examples.

3.7 Harmonic traps and “soft monopoles”

Throughout this chapter we have only considered *idealized* particle constraints—the fluid surface or interface is perfectly pinned to the particle, the contact line is perfectly rigid, and the rigid-body motions are, apart from the surface coupling, either perfectly fixed or completely free. The most restricted case in which a particle is fixed in place might be realized, for instance, by engineering a Janus cylinder and arranging it perpendicular to the surface with the cylinder ends clamped. In this example, the surface pins to the cylinder’s material dividing line, which serves as the effective “particle.” However, a perhaps more realistic experimental setup might instead involve constraining a colloid’s position by optical tweezers, such as in Ref. [PF11].

In this final section, we will consider such a modified “monopole” system in which each particle’s position is not perfectly fixed, but rather trapped in an external potential well. This affords each particle a vertical degree of freedom, but with an energy cost for deviations from the potential minimum. Correspondingly, we will refer to the associated surface moment as a *soft monopole* since the external potential can only provide a *finite* restoring force and hence small height deviations can occur. Soft monopoles will therefore give rise to interparticle elastic and entropic forces that are similar to the perfect monopoles of the previous sections, but with modifications due to the somewhat relaxed vertical constraint.

3.7.1 Surface response to a trapped particle

For simplicity—and generality—we will neglect the physical mechanisms of the particle trap and model it as an external Hookean potential that provides a linear restoring force to counter height deviations from the bottom of the potential well. The energy of a particle in

the trap may thus be expressed as the harmonic potential

$$V(h_{\text{cm}}) = \frac{1}{2}k(h_{\text{cm}} - h_0)^2, \quad (3.263)$$

where h_{cm} is the center-of-mass height of the particle, h_0 is the position of the trap minimum, and k is the trap stiffness or “spring constant.” As we remarked in Section 3.3.3, Lehle and Oettel [LO07] have also used this external potential to model optical tweezers acting on colloids, and their results will serve as a useful comparison.

To determine the effects the trap ultimately has on the surface profile, we incorporate the trap as contact-line constraints in much the same way as in Section 3.2. There we related the surface field h to the particle constraints (and degrees of freedom) encoded in h^{ct} by requiring them to match at the particle–surface boundary. At the monopole level, the relevant parameter for soft monopoles is the contact line height, which we may alternatively express as the boundary average,

$$h_{\text{cm}} = \oint_{\partial\mathcal{A}} ds \frac{h}{L(\partial\mathcal{A})}, \quad (3.264)$$

where $L(\partial\mathcal{A})$ is the perimeter length of the boundary $\partial\mathcal{A}$. The energy functional then consists of the surface Hamiltonian plus the trap potential (3.263) with the above constraint enforced by a Lagrange multiplier f :

$$\begin{aligned} \mathcal{H}[h, f \mid h_{\text{cm}}] &= \mathcal{H}_0[h \mid \mathcal{S}_{\text{pr}}] + V(h_{\text{cm}}) + \Delta\mathcal{H}_{\text{ct}}[h, f \mid h_{\text{cm}}] \\ &= \frac{\sigma}{2} \int_{\mathcal{S}_{\text{pr}}} d^2x [(\nabla h)^2 + \ell_c^{-2} h^2] + \frac{1}{2}k(h_{\text{cm}} - h_0)^2 + f \left(h_{\text{cm}} - \oint_{\partial\mathcal{A}} ds \frac{h}{L(\partial\mathcal{A})} \right). \end{aligned} \quad (3.265)$$

It is worth mentioning that the Lagrange-multiplier term in the above functional is equivalent to the constraint term in Eq. (3.24) at the monopole level, with the obvious relationship $\lambda_{\text{m}} = f/L(\partial\mathcal{A})$ between the constraint force f and (monopole) force density λ_{m} . Note that this formulation assumes both a *pinned* contact line as usual and, furthermore, that the particle’s center of mass is at the same point as the contact-line center (*cf.* Section 3.2). If the center of mass height is different, it can be incorporated by the simple modification in the constraint term $h \rightarrow h - h_{\text{ref}}$, where h_{ref} is the height difference between the pinned contact line center and the particle’s true center of mass. Note also that the functional (3.265) refers to a single particle at the origin, but the generalization to several particles should be clear (quantities inherit a particle label a , which is summed over all particles).

The stationary-surface conditions are revealed by setting the (linear) variations to zero, giving the following:

$$\delta_h \mathcal{H} : \quad \begin{cases} (-\nabla^2 + \ell_c^{-2})h = 0, & \mathbf{x} \in \mathcal{S}_{\text{pr}} \\ -\sigma \hat{\mathbf{n}}_{\mathcal{A}} \cdot \nabla h = \frac{f}{L(\partial\mathcal{A})}, & \mathbf{x} \in \partial\mathcal{A} \end{cases} \quad (3.266a)$$

$$\delta_{h_{\text{cm}}} \mathcal{H} : \quad f = -k(h_{\text{cm}} - h_0) \quad (3.266b)$$

$$\delta_f \mathcal{H} : \quad h_{\text{cm}} = \frac{1}{L(\partial\mathcal{A})} \oint_{\partial\mathcal{A}} ds h \quad (3.266c)$$

The first set of equations reproduces the BVP mentioned above (*cf.* Eq. (3.26)) with the constraint force density $f/L(\partial\mathcal{A})$. Equation (3.266b) shows that the trap provides a uniform, linear restoring force at the particle–surface boundary. The final equality of course just restates the constraint. For a circular particle of radius R , these together give the surface boundary condition

$$\left. \frac{\partial h}{\partial r} \right|_{r=R} = \frac{k}{2\pi\sigma R} \left(\frac{1}{2\pi} \int_0^{2\pi} d\varphi h(R, \varphi) - h_0 \right). \quad (3.267)$$

The boundary condition (3.267) dictates the particle–surface response to a background surface deformation. To determine the response, we mirror Section 3.2.1 and decompose the field as a superposition of the background field h_{bg} and response δh , where the original BVP, Eq. (3.46), now has the modified boundary condition (3.267). Outside the particle boundary, the equations governing the surface are unaltered, so we may still apply the convenient background field, Eq. (3.45), and know that the response will take the form of Eq. (3.44). Since only the monopole polarizability is altered, we need only consider $h_{\text{bg}} = A_0 I_0(r/\ell_c)$, which leads to the response $\delta h = B_0 K_0(r/\ell_c)$. Substituting into Eq. (3.267) yields

$$\begin{aligned} \frac{A_0}{\ell_c} I_1(R/\ell_c) - \frac{B_0}{\ell_c} K_1(R/\ell_c) &= \frac{k}{2\pi\sigma R} [A_0 I_0(R/\ell_c) + B_0 K_0(R/\ell_c) - h_0] \\ \Rightarrow B_0 &= - \frac{A_0 [I_0(R/\ell_c) - \frac{2\pi\sigma}{k} \frac{R}{\ell_c} I_1(R/\ell_c)] - h_0}{K_0(R/\ell_c) + \frac{2\pi\sigma}{k} \frac{R}{\ell_c} K_1(R/\ell_c)} \\ &\xrightarrow{\ell_c \rightarrow \infty} - \frac{A_0 - h_0}{\frac{2\pi\sigma}{k} + \ln\left(\frac{2\ell_c}{R\gamma_e}\right)} \end{aligned} \quad (3.268)$$

and therefore shows the “full theory” response (for large ℓ_c) to be

$$\delta h(\mathbf{x}) = - \left[\frac{A_0 - h_0}{\frac{2\pi\sigma}{k} + \ln\left(\frac{2\ell_c}{R\gamma_e}\right)} \right] \ln\left(\frac{2\ell_c}{r\gamma_e}\right). \quad (3.269)$$

3.7.2 EFT for soft monopoles

The appearance of the trap energy, Eq. (3.263), is similar to the monopole contribution to the effective Hamiltonian, Eq. (3.81). However, this similarity is somewhat misleading; indeed, the worldline energy $\Delta\mathcal{H}_f^{\text{m}}[h]$ is vanishing in the $\ell_c \rightarrow \infty$ limit but, on the other hand, the trap strength k is independent of the surface properties and becomes infinite for a perfectly rigid trap. To see how soft monopoles relate to pure monopoles, we construct the effective Hamiltonian just as before by adding to the particle-free Hamiltonian the worldline

monopole and permanent source terms,

$$\Delta\mathcal{H}_m[h] = \frac{1}{2}\tilde{M}^{(0)}h^2(0) - \tilde{Q}^{(0)}h(0), \quad (3.270)$$

where the tilde decorations are just to distinguish the coefficients from the pure versions, Eqs. (3.83) and (3.89).

We match coefficients by decomposing the field and calculating the effective response to the background field. The background induces an effective source,

$$\rho_m(\mathbf{x} \mid h_{\text{bg}}) = -[\tilde{M}^{(0)}A_0 + \tilde{Q}^{(0)}]\delta(\mathbf{x}), \quad (3.271)$$

which generates the induced response

$$\delta h_m^{\text{eff}}(\mathbf{x} \mid h_{\text{bg}}) = -\frac{(A_0\tilde{M}^{(0)} - \tilde{Q}^{(0)})}{2\pi\sigma} \ln\left(\frac{2\ell_c}{r\gamma_e}\right). \quad (3.272)$$

Comparison with Eq. (3.269) yields the values of the monopole polarizability and permanent charge. Again, the force-balance condition (3.103) is upheld:

$$\tilde{M}^{(0)} = \frac{2\pi\sigma}{\frac{2\pi\sigma}{k} + \ln\left(\frac{2\ell_c}{R\gamma_e}\right)} \quad (3.273)$$

$$\tilde{Q}^{(0)} = \tilde{M}^{(0)}h_0 \quad (3.274)$$

Perfect monopoles are, of course, recovered in the limit of infinite trap strength; *i.e.*, $M^{(0)} = \lim_{k \rightarrow \infty} \tilde{M}^{(0)}$.

Soft monopoles and self-capacitance

In Section 3.5.4 we discussed how the $\ell_c \rightarrow \infty$ limit is analogous to the electrostatics system illustrated in Fig. 3.6. The monopole polarizability $M^{(0)}$ corresponds to the “self-capacitance” of the particle, and the external mechanism enforcing the fixed position is analogous to a battery or other voltage source maintaining the electric potential. From this perspective, it is appropriate to speak of the particle trap as having a capacitance k , and the new monopole polarizability $\tilde{M}^{(0)}$ as being the equivalent capacitance of the particle–trap system. The analogous electrostatics system for a trapped particle is illustrated in Fig. 3.7.

It seems appropriate, then, that the equivalent “capacitance” of a particle in a trap should follow the reciprocal addition rules for combining capacitors in series. In the electrostatics case, such an arrangement implies the total charge is conserved between the capacitor plate and the conductor so that charge of equal magnitude but opposite sign resides on each.

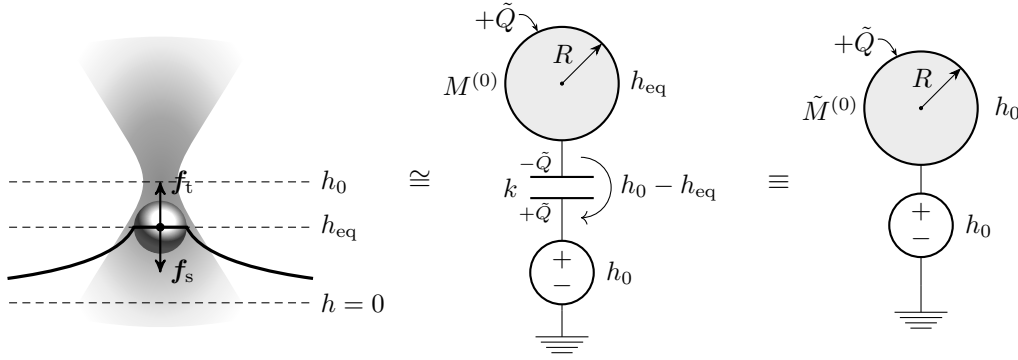


Figure 3.7: Trapped particle and its electrostatics analogy. The left figure illustrates a surface-bound particle in an (ideal) optical trap. The trap provides a restoring force f_t to the particle for deviations from the trap height h_0 , whereas the surface provides a force $f_s = -f_t$ for deviations from $h = 0$. At equilibrium, the particle settles to a height h_{eq} . In the right figure, a grounded voltage source fixes the potential of a conductor system. The particle trap maps onto such a source with a mediating capacitor. At equilibrium, charge $+\tilde{Q}$ provided by the voltage source is balanced by charge $-\tilde{Q}$ on the opposite side of the capacitor by pushing charge $+\tilde{Q}$ onto the conductor. This charge balance sets up a potential difference across the capacitor and thereby alters the equilibrium potential of end conductor.

The electric potential is additive, and the capacitance adds “upside-down:”

$$\begin{aligned}
 h_{eq} + (h_0 - h_{eq}) &= h_0 \Leftrightarrow \frac{\tilde{Q}}{M^{(0)}} + \frac{\tilde{Q}}{k} \equiv \frac{\tilde{Q}}{\tilde{M}^{(0)}} \\
 \Rightarrow \frac{1}{\tilde{M}^{(0)}} &= \frac{1}{k} + \frac{1}{M^{(0)}}
 \end{aligned} \tag{3.275}$$

Plugging in the value for $M^{(0)}$ and rearranging reproduces Eq. (3.273). The soft monopole polarizability also follows from the force (“charge”) balance, $f_s = f_t$, where the restoring force of the trap is $f_t = k(h_0 - h_{eq})$ and the force from the surface is $f_s = M^{(0)}h_{eq}$. By definition, the equivalent soft monopole characterizes the force in terms of the external field h_0 so that $f = \tilde{M}^{(0)}h_0$. Force balance therefore implies that the above result also solves the equivalent double equality

$$M^{(0)}h_{eq} = k(h_0 - h_{eq}) = \tilde{M}^{(0)}h_0. \tag{3.276}$$

3.7.3 Elastic interactions between trapped particles

Calculating interactions between trapped particles proceeds just as before with the only change being the replacements $M^{(0)} \rightarrow \tilde{M}^{(0)}$ and $Q^{(0)} \rightarrow \tilde{Q}^{(0)}$. The elastic interaction between two trapped particles is given by Eq. (3.181) with the required replacements and

simplifies to

$$E_{\{1,2\}}^{(0)} = -h_{0,1}\tilde{M}_1^{(0)}\frac{G^{12}}{\sigma}\tilde{M}_2^{(0)}h_{0,2} + \frac{1}{2}\left(\tilde{M}_1^{(0)}h_{0,1}^2 + \tilde{M}_2^{(0)}h_{0,2}^2 - 2h_{0,1}\tilde{M}_1^{(0)}\frac{G^{12}}{\sigma}\tilde{M}_2^{(0)}h_{0,2}\right)\frac{\tilde{g}_{12}^2}{1-\tilde{g}_{12}^2}. \quad (3.277)$$

Note that here $h_{0,a}$ refers to the height of particle a 's trap potential minimum and *not* the true position of particle a in general.

Similar to before, if both particles experience identical trap potentials—that is, $h_{0,1} = h_{0,2} \equiv h_0$ —then the elastic interaction energy vanishes in the limit $\ell_c \rightarrow \infty$. Again, this is understood as a restoration of vertical translation symmetry in the absence of a surface dampening force (*e.g.*, gravity); the surface translates to a new equilibrium position that meets the shared height of the particle traps. For identical particles, expanding and simplifying Eq. (3.277) gives the leading-order interaction energy for large ℓ_c ,

$$E_{\{1,2\}}^{(0)} = -\frac{h_0^2[\tilde{M}^{(0)}]^2(G^{12}/\sigma)^2}{1 + \tilde{M}^{(0)}(G^{12}/\sigma)} = -\frac{2\pi\sigma h_0^2 2\pi G^{12}}{(2\pi\sigma/\tilde{M}^{(0)})[(2\pi\sigma/\tilde{M}^{(0)}) + 2\pi G^{12}]} \\ = -\frac{2\pi\sigma h_0^2 \ln(\frac{2\ell_c}{r\gamma_e})}{\left[\frac{2\pi\sigma}{k} + \ln(\frac{2\ell_c}{R\gamma_e})\right]\left[\frac{2\pi\sigma}{k} + \ln(\frac{4\ell_c^2}{rR\gamma_e^2})\right]}. \quad (3.278)$$

If the trap potentials of the two particles are not identical, then a nonzero result survives the $\ell_c \rightarrow \infty$ limit and depends on the trap height difference:

$$E_{\{1,2\}}^{(0)} = \frac{-h_{0,1}h_{0,2}\tilde{M}_1^{(0)}\tilde{M}_2^{(0)}(G^{12}/\sigma) + \frac{1}{2}\left(\tilde{M}_1^{(0)}h_{0,1}^2 + \tilde{M}_2^{(0)}h_{0,2}^2\right)\tilde{M}_1^{(0)}\tilde{M}_2^{(0)}(G^{12}/\sigma)^2}{1 - \tilde{M}_1^{(0)}\tilde{M}_2^{(0)}(G^{12}/\sigma)^2} \\ \xrightarrow{\ell_c \rightarrow \infty} \frac{(\pi\sigma/2)(h_{0,1} - h_{0,2})^2}{\frac{\pi\sigma}{k_1} + \frac{\pi\sigma}{k_2} + \ln\left(\frac{r}{\sqrt{R_1 R_2}}\right)}. \quad (3.279)$$

As expected, for traps of infinite strength ($k_a \rightarrow \infty$), the particles become frozen at the trap heights and the energy limits to the pure monopole result (3.183).

Comparison with the results of Ref. [LO07]

Part of the motivation for considering soft monopoles is to make sense of the results presented by Lehle and Oettel in Ref. [LO07]. There, the authors consider external harmonic potentials on spherical colloids of equal (effective) radii R_0 and calculate the resulting interaction energy between two particles. In particular, they obtain similar expressions to Eqs. (3.278) and (3.279), namely Eqs. (61) and (62) of Ref. [LO07], but with important differences. For convenience, we reproduce their two results below in our own notation. First, for equal external potentials, the interaction energy—which they express as the meniscus energy

V_{men} —vanishes in the $\ell_c \rightarrow \infty$ limit but with a leading-order term³⁹

$$V_{\text{men}} \approx - \frac{4\pi\sigma h_0^2 \ln\left(\frac{2\ell_c}{r\gamma_e}\right)}{\left[\frac{2\pi\sigma}{k} + \ln\left(\frac{2\ell_c}{R_0\gamma_e}\right)\right] \left[\frac{2\pi\sigma}{k} + \ln\left(\frac{4\ell_c^2}{rR_0\gamma_e}\right)\right]}. \quad (3.280)$$

Additionally, they calculate the nonvanishing contribution for nonidentical potentials and find

$$V_{\text{men}} \xrightarrow{\ell_c \rightarrow \infty} \frac{\pi\sigma(h_{0,1} - h_{0,2})^2}{1 + \pi\sigma(1/k_1 + 1/k_2) + \ln r/R_0}. \quad (3.281)$$

Some additional comments are in order. First, in their paper the authors consider a variety of boundary conditions, including the case of *unpinned* contact lines. They did not explicitly state whether pinned or unpinned particles were assumed in the calculations leading to the above results, but it seems that unpinned particles are implied.⁴⁰ However, their first result, Eq. (3.280) above, matches our own result, Eq. (3.278), for *pinned* particles. The only discrepancy is an additional factor of two, which is possibly due to a double-counting error on their end. For nonidentical external potentials, their result, Eq. (3.281) above, differs less trivially from our pinned contact line result, Eq. (3.279). In addition to another factor of two discrepancy, the denominator includes an additive constant of one. Since this difference may be due to the unpinned degrees of freedom of the contact line, we repeat our EFT construction in Appendix B for unpinned particles. We indeed reproduce Eq. (3.281) (*cf.* Eq. (B.16)) and also find the correct *unpinned* version of Eq. (3.280) (*cf.* Eq. (B.15)), though in both cases the same factor of two discrepancy remains. In the process we also uncover and clarify some subtleties hidden in the above expression. First, the effective radius $R_0 \leq R$ refers to the projected radius of the three-phase contact line in the single-particle equilibrium configuration, wherein the surface is flat and the particle's center of mass lies below the contact line with a position governed by Young's law. Second, we find that the parameters $h_{0,a}$ should in general refer not to the position of the external potential's energy minimum, but rather the height difference between the minimum and the equilibrium center of mass position of the particle *in isolation* (*i.e.*, in the absence of the external potential or other particles). For identical particles, however, the reference equilibrium heights will be the same and hence cancel in the difference. To summarize, we reproduce (and generalize to nonidentical particles) the two results of Lehle and Oettel up to a factor of two and, furthermore, discover that Eq. (3.280) is applicable only for *pinned* contact lines, whereas Eq. (3.281) is only applicable for *unpinned* contact lines. More details on the unpinned EFT construction and results can be found in Appendix B.

³⁹We have flipped the arguments of the logarithms so that the logs are manifestly positive. Additionally, we have corrected a typo in the rightmost logarithm in the denominator (replacing γ_e by γ_e^2).

⁴⁰The authors base part of their analysis on Ref. [ODD05], wherein only unpinned colloids are considered. In particular, the boundary condition they report, Eq. (58) of Ref. [LO07], is pulled from Ref. [ODD05].

3.7.4 Entropic interactions between trapped particles

For completion, we present the leading-order entropic interaction between trapped particles (with pinned contact lines). From Eq. (3.225) with the replacement $M^{(0)} \rightarrow \tilde{M}^{(0)}$, we find

$$\begin{aligned}\beta U_{\{1,2\}}^{(0)} &= \frac{1}{2} \ln(1 - \tilde{g}_{12}^2) \\ &= -\frac{1}{2} \ln \Lambda_{12} + \frac{1}{2} \ln \left[\frac{2\pi\sigma}{k_1} + \frac{2\pi\sigma}{k_2} + 2 \ln \left(\frac{r}{\sqrt{R_1 R_2}} \right) \right] + \mathcal{O}(\Lambda^{-1}).\end{aligned}\quad (3.282)$$

The corresponding interparticle force in the $\ell_c \rightarrow \infty$ limit is

$$F_{\{1,2\}}^{(0)} = -\frac{\partial U_{\{1,2\}}^{(0)}}{\partial r} = -\frac{k_B T}{2r \left[\frac{\pi\sigma}{k_1} + \frac{\pi\sigma}{k_2} + \ln \left(\frac{r}{\sqrt{R_1 R_2}} \right) \right]} + \mathcal{O}(\Lambda^{-1}).\quad (3.283)$$

We can also compare with the results of Ref. [LO07]. There, the authors calculate the fluctuation and mean-field contributions to the entropic force separately, Eqs. (23) and (63) in their paper, but they combine to give (for identical particles)

$$\begin{aligned}F = F_{\text{fluc}} + F_{\text{mf}} &= -\frac{k_B T}{2} \frac{1}{r \ln(r/\tilde{R})} + \frac{k_B T}{2} \frac{1}{r \ln(r/\tilde{R})} \frac{1}{1 + \frac{o_1 o_2 \ln(r/\tilde{R})}{o_1 + o_2}} \\ &= -\frac{k_B T}{2r [1/o_1 + 1/o_2 + \ln(r/\tilde{R})]},\end{aligned}\quad (3.284)$$

where

$$o_i = \begin{cases} k_i/(\pi\sigma), & \text{pinned contact line} \\ 2/(1 + 2\pi\sigma/k_i), & \text{unpinned contact line} \end{cases}\quad (3.285)$$

and \tilde{R} refers here to the effective radius of the particle—either the pinned radius or the equilibrium contact line radius for an unpinned particle. This is in agreement with Eq. (3.283). We also calculate the entropic force for the unpinned case in Appendix B.3.2 (see Eq. (B.18)) and again find agreement.

4 Membrane-mediated interactions of axisymmetric particles

In this chapter, we shift our focus to investigate particle interactions mediated by a surface characterized solely by its bending elasticity. Such surfaces model the class of soft-matter interfaces discussed in Chapter 2 that arise from the self assembly of surfactant molecules within a bulk aqueous environment. One notable incarnation is the fluid lipid bilayer membrane, which provides critically important structure and protection for cells and their organelles, as well as hosts and regulates many of the cell’s biological functions [AJL⁺83, Boa12].

Mesoscopically, the energetics of membranes are well captured by the Helfrich theory of two-dimensional fluid surfaces. However, in biological systems, proteins and other macromolecules constitute more than half of the surface area and comprise roughly 70% of the total mass of typical membranes, and diffuse and aggregate to form highly heterogeneous and dynamic structure [LS95, PKT09]. Among the biophysical and biochemical factors influencing the collective behavior and lateral distribution of particles are curvature and fluctuation-induced forces mediated by the membrane itself. Here we will model finite-size membrane inclusions by rigid particles classified by their boundary conditions at the particle–membrane boundary. Mirroring the previous chapter, we will begin with a general discussion on membrane energetics and permissible boundary conditions before moving on to construct an effective theory that incorporates the constraints and energetic costs of finite-size membrane inclusions. We will then adapt the EFT formalism developed in Chapter 3 to calculate elastic and entropic particle interactions.

4.1 Membrane energetics

The starting point for our discussion of membrane-mediated interactions is the Helfrich energy functional from Chapter 2:

$$\mathcal{H}[\mathcal{S}] = \int_{\mathcal{S}} dA \left[\sigma + \frac{\kappa}{2}(K - K_0)^2 + \bar{\kappa}K_G \right], \quad (4.1)$$

where K , K_0 , and K_G respectively denote the total extrinsic curvature, spontaneous curvature, and Gaussian curvature of the membrane surface \mathcal{S} , and the parameters σ , κ , and $\bar{\kappa}$ respectively measure the surface tension, bending rigidity, and Gaussian modulus. For the class of membranes we will consider in this chapter, we will assume the bending-dominated limit in which the crossover length $\sqrt{\kappa/\sigma}$ is larger than the system size or,

equivalently $\sigma \rightarrow 0$ (see Section 2.4.1). Furthermore, we will assume an up–down symmetry such that the ground state surface is flat with no spontaneous curvature ($K_0 = 0$). Finally, we will assume a fixed topology of the system which, by virtue of the Gauss–Bonnet theorem (see Technical Note 2.3), entails the final term is constant and can be safely ignored.¹

Finally, for membranes that deform and fluctuate weakly from a flat plane, it is convenient to perform calculations in the Monge gauge and, furthermore, work to leading order in the small gradient expansion,

$$\mathcal{H}[h] = \frac{\kappa}{2} \int_{\mathcal{S}_{\text{pr}}} d^2x \left[(\nabla^2 h)^2 - \frac{1}{2} (\nabla^2 h)^2 (\nabla h)^2 - 2 \nabla^2 h \partial_i h \partial_i \partial_j h \partial_j h + \mathcal{O}(h^6) \right], \quad (4.2)$$

where \mathcal{S}_{pr} is the projected surface domain in the reference base plane. To justify the validity of the expansion, we note that the bending modulus and thermal energy together provide a relevant power-counting parameter $\delta := k_{\text{B}}T/\kappa$. For typical membranes at biological temperatures, $\kappa \approx 20k_{\text{B}}T$ and $\delta \approx 0.05$ which is indeed small. Let us now define a rescaled field $\phi(\mathbf{x}) = h(\mathbf{x})/\sqrt{\delta}$. The exponent in the canonical partition function will then become

$$\beta \mathcal{H}[h] = \frac{1}{2} \int_{\mathcal{S}_{\text{pr}}} d^2x \left\{ (\nabla^2 \phi)^2 - \delta \left[\frac{1}{2} (\nabla^2 \phi)^2 (\nabla \phi)^2 - 2 \nabla^2 \phi \partial_i \phi \partial_i \partial_j \phi \partial_j \phi \right] + \mathcal{O}(\delta^2 \phi^6) \right\}, \quad (4.3)$$

which shows that terms which are of order h^n scale as $\sim \delta^{n/2-1}$. It is therefore acceptable to retain only the marginal $\mathcal{O}(\delta^0)$ term since higher orders are all suppressed by increasing powers of δ . With the stated conditions and assumptions in place, the Helfrich energy functional reduces to the harmonic approximation,

$$\mathcal{H}[h] = \frac{\kappa}{2} \int_{\mathcal{S}_{\text{pr}}} d^2x (\nabla^2 h)^2. \quad (4.4)$$

Stationary membrane conditions

As usual, we look for equilibrium membrane profiles for which the energy functional is stationary under small variations. With $h \rightarrow h + \delta h$ in the linearized Monge gauge, we have to first order

$$\begin{aligned} \delta \mathcal{H}[h] &= \kappa \int_{\mathcal{S}_{\text{pr}}} d^2x \nabla^2 h \nabla^2 \delta h \\ &\stackrel{\text{IBP}}{=} -\kappa \int_{\mathcal{S}_{\text{pr}}} d^2x \nabla (\nabla^2 h) \cdot \nabla \delta h + \kappa \oint_{\partial \mathcal{S}_{\text{pr}}} ds \nabla^2 h (\hat{\ell} \cdot \nabla \delta h) \end{aligned}$$

¹Note that beyond topological changes, there are boundary conditions for which the Gaussian term matters. For example, if the particle boundary is flexible, then it is possible the corresponding geodesic curvature of the rim may fluctuate, necessitating further considerations of the Gaussian term. Another example is provided by Brannigan and Brown, who discuss a scenario in which the Gaussian modulus of lipid monolayers—by way of “hydrophobic mismatch” considerations of the inclusion—may leave a trace in membrane-mediated interactions [BB07].

$$\stackrel{\text{IBP}}{=} \kappa \int_{\mathcal{S}_{\text{pr}}} d^2x \nabla^4 h \delta h - \kappa \oint_{\partial \mathcal{S}_{\text{pr}}} ds \left[\hat{\ell} \cdot \nabla (\nabla^2 h) \right] \delta h + \kappa \oint_{\partial \mathcal{S}_{\text{pr}}} ds \nabla^2 h \left(\hat{\ell} \cdot \nabla \delta h \right), \quad (4.5)$$

where $\hat{\ell}$ is the outward unit normal on the (projected) surface boundary $\partial \mathcal{S}_{\text{pr}}$. The neglected second-order term is positive definite, so the energy is minimized if the first-order variation vanishes. Since the height variation δh is arbitrary, the vanishing of the surface integral informs us that our desired membrane profile $h(\mathbf{x})$ satisfies the biharmonic equation,

$$\kappa \nabla^4 h(\mathbf{x}) = 0 \text{ for } \mathbf{x} \in \mathcal{S}_{\text{pr}}. \quad (4.6)$$

The vanishing of the two boundary terms suggests a couple of natural options for boundary conditions. One is to require that the height function is always harmonic on the boundary, *i.e.*, $\nabla^2 h(\partial \mathcal{S}_{\text{pr}}) = 0$. In the linearized Monge gauge, this corresponds to the total extrinsic curvature vanishing in the neighborhood of the boundary. An alternative is to fix both the height and the slope at the boundary so that both $\delta h = 0$ and $\hat{\ell} \cdot \nabla \delta h = 0$ respectively. These latter two conditions are particularly appropriate for membrane surfaces that are asymptotically flat at the far (infinite) outer boundary.

4.2 Particle boundary conditions

Based on the above observations, we will consider particle inclusions such that the membrane surface is pinned to the particle boundary at a fixed (and rigid) contact line and, furthermore, at a fixed slope in the neighborhood of the boundary. Since we will only consider interactions mediated by the membrane surface, these two parameters—together with allowed rigid body motions—are all that are required from the perspective of the surface to fully characterize a given particle. In this sense, we can choose a convenient representative particle shape for each equivalency class.² If we express the contact line height profile as $h^{\text{ct}}(\mathbf{x})$ and the contact slope profile as $S^{\text{ct}}(\mathbf{x})$, the corresponding mathematical statement for a particle with a projected area boundary $\partial \mathcal{A}$ in the base plane is

$$(h, \hat{\mathbf{n}}_{\mathcal{A}} \cdot \nabla h)|_{\partial \mathcal{A}} = (h^{\text{ct}}, S^{\text{ct}})|_{\partial \mathcal{A}}, \quad (4.7)$$

where $\hat{\mathbf{n}}_{\mathcal{A}}$ is the *outward* pointing unit vector normal to $\partial \mathcal{A}$ in the base plane.

As we illustrate in Fig. 4.1, one simple class of representative *curved* particles can be generated by analytically continuing the surface such that the height function and its normal derivative are both continuous across the boundary. Although this condition does not exhaust the possible particle-types to consider, in this chapter we will only focus on particles for which $S^{\text{ct}} = \hat{\mathbf{n}}_{\mathcal{A}} \cdot \nabla h^{\text{ct}}$. That is, the parametrization h^{ct} defines both the contact height and slope profiles at the boundary. Furthermore, we will only consider particles with a

²Other characterizations, such as a pressure difference from asymmetric exposure on either side of the membrane, may be accounted for as external forces in the energy. These forces, however, still amount to placing conditions on the contact line and angle, so we are not losing any generality.

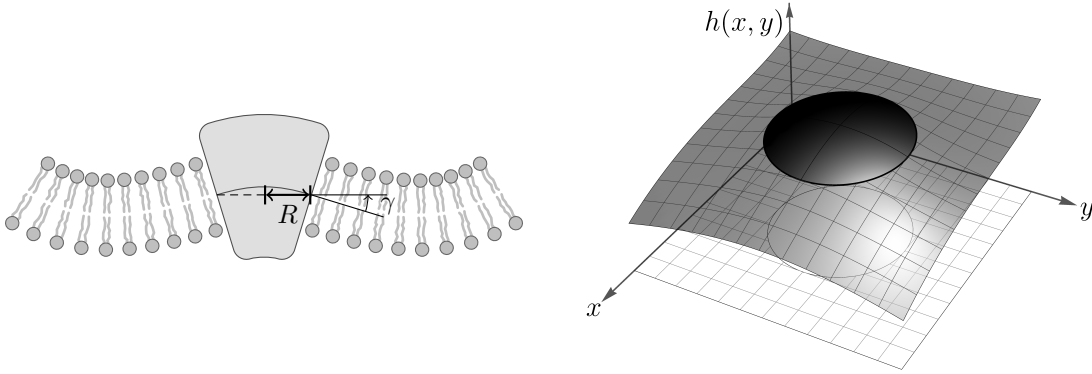


Figure 4.1: The left graphic illustrates a closer look at the cross section of a conical-wedge particle inclusion in a lipid bilayer membrane. At the particle boundary, the membrane attaches at a fixed contact angle $-\gamma$ from the horizontal. In the surface continuum limit, an embedded particle is characterized by its contact line and slope, so we can describe an equivalence class of particles by a convenient representative particle. One such option is to analytically continue the surface across the boundary, which we will take here as the attachment at the membrane's neutral surface, and use the corresponding parametrization of the contact line as the particle shape. The curve within the wedge is one such continuation, giving a paraboloidal cap with a circular imprint of radius R . The graphic on the right shows this representation from the perspective of our geometric theory.

circular footprint in the base plane. With these (self-imposed) restrictions in mind, the appropriate boundary conditions are then

$$(h, \partial_r h)|_{r=R} = (h^{\text{ct}}, \partial_r h^{\text{ct}})|_{r=R} \quad (4.8)$$

for a projected circular boundary of radius R positioned at the origin.

Just as in Chapter 3, we may express an arbitrary contact line profile $h^{\text{ct}}(\mathbf{x})$ as a series expansion,

$$h^{\text{ct}}(\mathbf{x}) = h_0 + \mathbf{s} \cdot \mathbf{x} - \frac{1}{2} \eta_{ij} x_i x_j + \cdots \quad (4.9)$$

where, as before, h_0 and \mathbf{s} respectively parametrize the height and tilt of the particle. That is, the combination

$$h_{\text{flat}}(\mathbf{x}) = h_0 + \mathbf{s} \cdot \mathbf{x} \quad (4.10)$$

defines the particle reference plane, as illustrated in Fig. 4.2, with s_i as the slope of the plane with respect to the (horizontal) x_i direction. As in the previous chapter, we will assume that $|\mathbf{s}|$ is small so that the deviations in the projected area are negligible, second-order effects. The permanent out-of-plane deviations of the contact line, which we will write as $h_{\text{perm}}(\mathbf{x})$, are encoded in the higher-order terms and contribute to the contact slope an amount $\hat{\mathbf{n}}_{\mathcal{A}} \cdot \nabla h_{\text{perm}}$ for this class of particles. For ease of discussion, we will extend $h^{\text{ct}}(\mathbf{x})$ within the particle and use it as the representative shape like we do in Fig. 4.1 (*e.g.*,

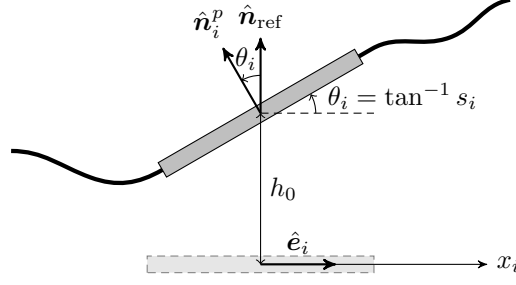


Figure 4.2: Illustration of the particle isometries (rigid displacements). We may define a particle reference plane from the flat part of the contact line expression, $h_{\text{flat}}(\mathbf{x}) = h_0 + \mathbf{s} \cdot \mathbf{x}$. The height h_0 is measured from the (equilibrium) base plane. The component $s_i = \tan \theta_i$ of the tilt parameter give the slope, and consequently the angle θ_i of the plane from the x_i direction. Alternatively, s_i can be expressed as the ratio $s_i = -(\hat{\mathbf{n}}_i^p \cdot \hat{\mathbf{e}}_i) / (\hat{\mathbf{n}}_i^p \cdot \hat{\mathbf{n}}_{\text{ref}})$ of the projections of the particle plane normal vector $\hat{\mathbf{n}}_i^p$ (in the $x_i h$ -plane) onto the base plane unit vector $\hat{\mathbf{e}}_i$ and normal vector $\hat{\mathbf{n}}_{\text{ref}}$.

“paraboloidal cap” instead of “conical wedge”). In this representation, $\eta_{ij} = -\partial_i \partial_j h^{\text{ct}}(0)$ therefore defines the extrinsic curvature tensor (in the linearized Monge gauge) at the center of the particle. If h^{ct} truncates at quadratic order, then η_{ij} gives the whole particle shape.

Unlike in the previous chapter, where caps and disks were equivalent from the perspective of the surface energetics (we could not simultaneously fix both the contact height *and* slope), kinks in the membrane surface are energetically forbidden and so the surface will respond differently to each. Accordingly, we will in this chapter study particles that combine the different disk, cap, and saddle shapes. To do so, we will first need an explicit parametrization of h_{perm} .

The particle curvature tensor η_{ij} is real and symmetric, so we can parametrize it with two (independent) variables. For instance, we can decompose it into the trace and a symmetric, trace-free part,

$$\eta_{ij} \doteq J \mathbf{1} + S \mathbf{M} = J \begin{pmatrix} 1 & 0 \\ 0 & 1 \end{pmatrix} + S \begin{pmatrix} 1 & 0 \\ 0 & -1 \end{pmatrix}, \quad (4.11)$$

where we have written η_{ij} in a diagonal basis. In this case, $-\nabla^2 h^{\text{ct}} = \text{tr}[\eta_{ij}] = 2J$ and shows that J is the mean curvature. If $J = 0$, then the Gaussian curvature $\det[\partial_i \partial_j h^{\text{ct}}] = \det[\eta_{ij}] = -S^2$. That is, $\pm S$ are the principal curvatures ($+S$ along the x direction and $-S$ along the y direction) and characterize the “saddleness” of the particle.³ With J included, the Gaussian curvature is $J^2 - S^2$. If we instead want the principal directions to be rotated by an angle α from the x -axis, we can rotate the basis of \mathbf{M} without altering the (invariant)

³Recall that in our convention a positive curvature bends *away* from the normal vector. Hence a particle with $J > 0$ bends downward, as does the saddle axis with $S > 0$ (see Fig. 4.3). Note that this convention is opposite that of Ref. [YHD14].

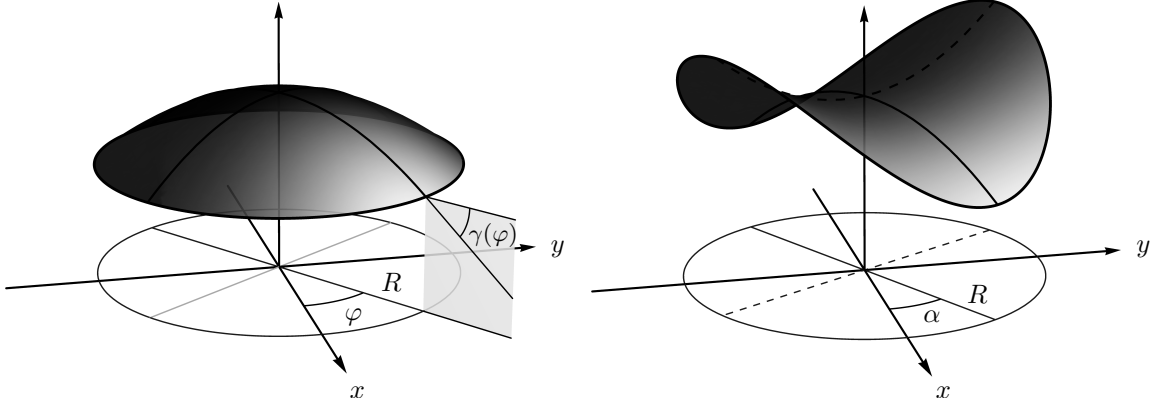


Figure 4.3: The left graphic shows a paraboloidal cap with mean and Gaussian curvatures J and J^2 respectively. This cap-shape represents any particle that enforces a contact angle of $-\gamma = RJ$ from the horizontal, such as in Fig. 4.1. The right graphic illustrates a saddle-shaped particle with Gaussian curvature $-S^2$ and vanishing mean curvature ($J = 0$). The principal directions are highlighted with a solid line for positive curvature (curves down) and a dashed line for negative curvature (curves up). The principal axis of positive curvature lies at an angle α from the x -axis. The shape implied by the contact line in Eq. (4.13) is a linear superposition of these two shapes.

curvatures:

$$\mathbf{M} \rightarrow \mathbf{R}(\alpha) \mathbf{M} \mathbf{R}^T(\alpha) = \begin{pmatrix} \cos 2\alpha & \sin 2\alpha \\ \sin 2\alpha & -\cos 2\alpha \end{pmatrix}. \quad (4.12)$$

With this parametrization, we can now express the contact line deformation as a superposition of paraboloidal and saddle shapes:

$$h_{\text{perm}}(\mathbf{x}) = -\frac{1}{2} \mathbf{x}^T (J \mathbf{1} + S \mathbf{R} \mathbf{M} \mathbf{R}^T) \mathbf{x} = -\frac{1}{2} J r^2 - \frac{1}{2} S r^2 \cos(2\varphi - 2\alpha) \quad (4.13)$$

in polar coordinates. We illustrate these shapes in Fig. 4.3.

Constraint forces

We account for the particles in the energy by modifying the integration domain and including external sources to fix the boundary conditions. With the inclusion of a particle with projected domain area \mathcal{A} in the base plane, the projected membrane surface becomes $\mathcal{S}_{\text{pr}} = \mathbb{R}^2 \setminus \mathcal{A}$. Introducing the Lagrange multipliers $\lambda(\mathbf{x})$ and $f(\mathbf{x})$ to fix the boundary to the contact line, we can express the energy functional as

$$\mathcal{H}[h, \lambda, f | h^{\text{ct}}, S^{\text{ct}}] = \frac{\kappa}{2} \int_{\mathcal{S}_{\text{pr}}} d^2x (\nabla^2 h)^2 - \oint_{\partial \mathcal{A}} ds [\lambda (h - h^{\text{ct}}) + f (\partial_{\perp} h - S^{\text{ct}})], \quad (4.14)$$

where $\partial_\perp = \hat{\mathbf{n}}_\mathcal{A} \cdot \nabla$ is the outward (from \mathcal{A}) normal derivative in the base plane. The original constrained energy is then $\mathcal{H}[h] = \max_{\lambda, f} \mathcal{H}[h, \lambda, f | h^{\text{ct}}, S^{\text{ct}}]$. The above boundary term is (minus) the external work required to maintain the contact line, so λ and f can be interpreted respectively as the required linear force density and force acting on the membrane in the neighborhood of the boundary. For a pinned particle, this term acts as an infinite energy penalty for deviations from h^{ct} or S^{ct} .

We can learn a bit more by examining the energy functional's stationarity conditions. The first-order variation is

$$\begin{aligned} \delta \mathcal{H}[h, \lambda, f | h^{\text{ct}}, S^{\text{ct}}] = & \kappa \int_{S_{\text{pr}}} d^2x \nabla^4 h \delta h + \oint_{\partial \mathcal{A}} ds \left\{ [\partial_\perp (\kappa \nabla^2 h) - \lambda] \delta h - (\kappa \nabla^2 h + f) \partial_\perp \delta h \right\} \\ & - \oint_{\partial \mathcal{A}} ds \left[(h - h^{\text{ct}}) \delta \lambda + (\partial_\perp h - S^{\text{ct}}) \delta f \right], \end{aligned} \quad (4.15)$$

where we have dropped the boundary term at infinity since we require the membrane to be asymptotically flat. The second-order variation is positive ($\sim [\nabla^2 \delta h]^2$), showing that the energy is minimized when the first-order variation vanishes. The first term implies h satisfies the biharmonic equation $\kappa \nabla^4 h = 0$ outside the particle boundary. The terms in the second line simply enforce the constraints we imposed. The boundary term on the first line, however, tells us something new. Namely, the force required to enforce the contact angle is proportional to the curvature: $f = -\kappa \nabla^2 h$. Additionally, the linear force density keeping the contact line fixed is proportional to the gradient of the curvature—and hence the gradient of f —normal to the boundary in the base plane: $\lambda = \partial_\perp (\kappa \nabla^2 h) = -\partial_\perp f$.

For the class of curved particles we will consider, in which $S^{\text{ct}} = \partial_\perp h^{\text{ct}}$ with $h^{\text{ct}} = h_{\text{flat}} + h_{\text{perm}}$ and h_{perm} given by Eq. (4.13), the constraint force *at equilibrium*, $f = 2\kappa J$, is constant and the force gradient λ vanishes. Out of equilibrium, the energy is governed by the functional

$$\mathcal{H}[h, f | h^{\text{ct}}] = \frac{\kappa}{2} \int_{S_{\text{pr}}} d^2x (\nabla^2 h)^2 - \oint_{\partial \mathcal{A}} ds [f \partial_\perp (h - h^{\text{ct}}) - \partial_\perp f (h - h^{\text{ct}})], \quad (4.16)$$

where we have traded λ for its on-shell value.

Membrane charges and pathologies

Let us now examine more explicitly the energetic cost of particle inclusions. As we saw in the previous chapter, one must be careful when dealing with zero modes of the surface energy. An ideal membrane satisfies the biharmonic equation $\nabla^4 h = 0$, and the corresponding zero modes reflect the bulk symmetries. One symmetry is translation in height, $h \rightarrow h + h_0$, like in the previous chapter. Ideal membranes additionally enjoy a linear displacement symmetry, $h \rightarrow h + \mathbf{s} \cdot \mathbf{x}$. The rigid body displacements discussed previously fall into these categories, so it is prudent to understand the consequences of constraining these particle degrees of freedom which explicitly break the bulk symmetries.

A first natural step is to consider what happens if we include a set of point forces,⁴ $\rho = \sum_a f_a \delta(\mathbf{x} - \mathbf{x}_a)$, in the membrane. This is accounted for in the usual way, via

$$\mathcal{H}[h | \rho] = \int d^2x \left[\frac{\kappa}{2} (\nabla^2 h)^2 - \rho h \right]. \quad (4.17)$$

The stationary solution must satisfy the sourced biharmonic equation, $\kappa \nabla^4 h = \rho$. We solve this as usual by the method of Green functions, giving

$$h(\mathbf{x} | \rho) = \frac{1}{\kappa} \int d^2x' G(\mathbf{x} - \mathbf{x}') \rho(\mathbf{x}'). \quad (4.18)$$

The biharmonic Green function is

$$G(\mathbf{x} - \mathbf{x}') = \frac{L^2 - (\mathbf{x} - \mathbf{x}')^2}{16\pi} - \frac{(\mathbf{x} - \mathbf{x}')^2}{16\pi} \ln \left[\frac{L^2}{(\mathbf{x} - \mathbf{x}')^2} \right], \quad (4.19)$$

where L is a large-distance cutoff representing the radial extent of the membrane, and is required to satisfy asymptotic flatness. The details of its derivation are presented in Technical Note 4.1. For a single point force at the origin, the solution reads

$$h(\mathbf{x}) = \frac{f}{16\pi\kappa} \left\{ L^2 - r^2 [1 + 2 \ln(L/r)] \right\}. \quad (4.20)$$

It immediately follows that the external force holds the membrane up at an equilibrium height of $h(0) = fL^2/16\pi\kappa$ at the source point. Put differently, to fix a point on the membrane to a height h_0 requires a force $f = 16\pi\kappa h_0/L^2$. We can make sense of the L -dependence by recalling that our ideal membrane only suffers energy costs from bending. A larger membrane will allow a smaller overall curvature between the point source and the boundary, so a smaller force is required to overcome the bending energy and to reach the same height. For an infinite membrane, it follows that an infinitesimal force will lead to an infinite translation in height.

Perhaps more troubling is the resulting membrane energy. Plugging this solution back into the Hamiltonian leads to

$$\mathcal{H}[\rho] = -\frac{1}{2} \int d^2x \rho(\mathbf{x}) h(\mathbf{x} | \rho) = -\frac{1}{2\kappa} \int d^2x d^2x' \rho(\mathbf{x}) G(\mathbf{x} - \mathbf{x}') \rho(\mathbf{x}'), \quad (4.21)$$

To arrive at the above expression, we have integrated by parts and dropped the boundary term at infinity, which may appear suspect. However, if we take the boundary to be at the finite cutoff L , then the boundary terms manifestly vanish as $r \rightarrow L$ by virtue of the Green function.⁵ In this form, the integral is trivial due to the delta functions and we immediately

⁴These membrane “charges” f have units of force and ρ has units of pressure, so one may think of ρ as a set of “pressure points.”

⁵One could also compute the Hamiltonian’s original integrals directly and find the same result.

Technical Note 4.1: The biharmonic Green function

The biharmonic Green function is the particular solution to the biharmonic equation with a point source,

$$\nabla^4 G(\mathbf{x}) = \nabla^2 (\nabla^2 G(\mathbf{x})) = \delta(\mathbf{x}).$$

From the above equation, we observe that $\nabla^2 G$ must itself be harmonic, so we can write $\nabla^2 G = a + b \ln(r/L)$, where we have introduced a scale L to make the argument of the logarithm dimensionless. From Chapter 3 we know that $\nabla^2 \ln(r/L) = 2\pi\delta(\mathbf{x})$. Applying the Laplace operator to $\nabla^2 G$ therefore gives $\nabla^4 G = 2\pi b \delta(\mathbf{x})$, and it follows that $b = 1/2\pi$. Next, we integrate both sides of $\nabla^2 G = a + b \ln(r/L)$ over a disk of radius r and use the divergence theorem to give a differential equation for G . The left side leads to

$$\int_D d^2x \nabla \cdot \nabla G = \oint_{\partial D} ds \partial_r G = 2\pi r \frac{dG}{dr},$$

where we have used the circular symmetry of G . After integrating the right side, we find the ODE,

$$\frac{dG}{dr} = \frac{ar}{2} + \frac{r}{8\pi} [2 \ln(r/L) - 1].$$

We wish now to apply the asymptotic flatness condition, $\partial_r G(r \rightarrow \infty) \rightarrow 0$, but the above expression obviously diverges. At this point we must suspend the notion of an unbounded membrane and introduce a large-distance cutoff to rescue our boundary conditions. If we interpret $L > r$ as the radial extent of the membrane, we can instead enforce the condition $\partial_r G(L) = 0$. This condition then leads to $a = 1/4\pi$ and

$$\frac{dG}{dr} = -\frac{r}{4\pi} \ln(L/r).$$

Integrating both sides over $[0, r]$ yields $G(r) = G(0) - \frac{r^2}{16\pi} [1 + 2 \ln(L/r)]$. Finally, we can enforce the final boundary condition $G(L) = 0$, which informs us that $G(0) = L^2/16\pi$. The appropriate biharmonic Green function is therefore

$$G(r) = \frac{1}{16\pi} (L^2 - r^2) - \frac{1}{8\pi} r^2 \ln(L/r).$$

find

$$\mathcal{H} = -\frac{f^2}{2\kappa} G(0) = -\frac{f^2}{32\pi\kappa} L^2. \quad (4.22)$$

That is, the surface energy diverges as the square of the membrane size.

In electrostatics, we are familiar with the self-energy of a point charge diverging, but interactions *between* point charges nonetheless remaining finite. To check if this also holds for our membrane “charges,” consider two point forces separated by a distance r . Plugging in $\rho = \sum_{a=1}^2 f_a \delta(\mathbf{x} - \mathbf{x}_a)$ and dropping the self-energy terms gives the interaction energy,

$$\mathcal{U} = -\frac{f_1 f_2}{16\pi\kappa} \left\{ L^2 - r^2 [1 + 2 \ln(L/r)] \right\}. \quad (4.23)$$

We find that for point forces of the same sign, the energy is lowered by decreasing the particles’ separation—like “membrane charges” attract while opposites repel. This behavior

is verified in the force expression

$$F = -\frac{\partial \mathcal{U}}{\partial r} = -\frac{f_1 f_2}{4\pi\kappa} r \ln(L/r), \quad (4.24)$$

from which it is also apparent the force drops to zero at close approach.

Unfortunately both the energy and force expressions above depend on the cutoff and, moreover, diverge for an unbounded membrane.⁶ That is, attempting to fix the positions of particle inclusions leads to unbounded energies and forces. A similar argument applies to fixing particle orientations from the horizontal, though the divergence in the energy is less severe and the force appears finite, but long ranged (see Technical Note 4.2).

So what is going wrong? Let us return to the particle-free version of the Hamiltonian (4.4). Physical systems must have finite energy, but for an extended (infinite) membrane there exist families of solutions that satisfy the biharmonic equation but nonetheless lead to an infinite energy. In particular, there are solutions for which $\nabla^2 h$ is not square integrable. The problem with the zero modes is that constraining their parameters leads precisely to these problematic membrane responses. We made an attempt to mend this by introducing a cutoff, but the divergences persisted. This will also lead to trouble once we include fluctuations. As we learned in Chapter 2, long-wavelength fluctuations build up and spoil any positional order on the membrane, and similarly for orientational order but to a lesser degree. The origin of this catastrophe lies again with the zero modes, for which the dimensionality of the surface is not enough to dampen the low-energy excitations.⁷

For the particle inclusions we wish to consider, even the simple act of fixing a particle's position and orientation to match the *flat* equilibrium surface is sufficient to cause havoc. The fluctuating membrane will explore its full configuration space, with the lowest-energy excitations being the most probable. So a gentle undulation will inevitably meet resistance from the constrained particle and induce a pathological response.

In the previous chapter we made great headway because the inclusion of gravitational forces proved sufficient to regulate the theory. This was possible because the divergent interaction energies were in a sense only *marginally* infinite; the resulting forces were finite, albeit very long ranged. We find that a similar treatment is possible as well for point dipoles in our membrane theory, but inadequate for point forces. Rather than pushing into this technical and potentially thorny territory, we will instead be content to allow the zero mode parameters to be free as they are wont to be. We will allow the particles to conform or

⁶Note that if we were to include some nonlinear terms, we learned from Chapter 2 that fluctuations would act to soften the membrane and lead to an effective *renormalized* bending rigidity, $\tilde{\kappa} = \kappa - (3k_B T/4\pi) \ln(\Lambda L)$. Using this renormalized value, the force become finite, though temperature dependent:

$$F = -\frac{f_1 f_2}{4\pi} \frac{r \ln(L/r)}{\tilde{\kappa} + \frac{3k_B T}{4\pi} \ln(\Lambda L)} \xrightarrow{L \rightarrow \infty} -\frac{f_1 f_2}{3k_B T} r.$$

We see that particles with like charges interact with a Hooke-like attraction with an effective spring constant $k = f_1 f_2 / 3k_B T$. However, this does not rescue the ground state forces as it still diverges in the zero-temperature limit.

⁷Mermin–Wagner strikes again!

Technical Note 4.2: Membrane point dipoles

To see the effects of fixing a particle's orientation from the horizontal, we include an external point-dipole source, $\rho = -\mathbf{p} \cdot \nabla \delta(\mathbf{x})$. The stationary solution is given by the convolution of the Green function and source as usual, and we find $h(\mathbf{x}) = -\frac{1}{\kappa} \mathbf{p} \cdot \nabla G(\mathbf{x})$. This corresponds to fixing the slope $s = (\mathbf{p}/4\pi\kappa) [\ln(L/\epsilon) - 1]$ in the neighborhood ϵ of the source point. The associated self-energy then follows from Eq. (4.21), giving $\mathcal{H} = (1/2\kappa) p_i p_j \partial_i \partial_j G(0)$. The Green function derivatives are

$$\partial_i G(r) = -\frac{1}{4\pi} x_i \ln(L/r), \quad \partial_i \partial_j G(r) = \frac{1}{4\pi} \left[\frac{x_i x_j}{r^2} - \delta_{ij} \ln(L/r) \right],$$

so the self-energy evidently suffers from long-scale as well as the more familiar short-scale divergences. The interparticle energies also suffer divergences for large membranes. For example, consider a point force (monopole) and a point dipole with a separation vector \mathbf{r} pointing from the monopole to dipole. The interaction energy is $\mathcal{U}_{\text{m-d}} = -(f/\kappa) \mathbf{p} \cdot \nabla G(\mathbf{r})$. The energy and force then simplify to

$$\mathcal{U}_{\text{m-d}} = \frac{f(\mathbf{p} \cdot \mathbf{r})}{4\pi\kappa} \ln(L/r) = \frac{f p r \cos \theta}{4\pi\kappa} \ln(L/r), \quad \text{and} \quad F_{\text{m-d}} = \frac{f p \cos \theta}{4\pi\kappa} [\ln(L/r) - 1],$$

where θ is the angle \mathbf{p} makes from the joining line. This is attractive when f and p are of the same sign and the dipole points to the monopole, which is to be expected since that entails like “charges” are infinitesimally closer. Note that the force is still divergent. Now consider the interaction energy between two dipoles, $\mathcal{U}_{\text{d-d}} = \frac{1}{\kappa} p_{1,i} p_{2,j} \partial_i \partial_j G(\mathbf{r})$. After taking the dot products and applying the product-sum trig identity, we find for the energy and force,

$$\mathcal{U}_{\text{d-d}} = \frac{p_1 p_1}{8\pi\kappa} \left\{ \cos(\theta_1 + \theta_2) + [1 - 2 \ln(L/r)] \cos(\theta_2 - \theta_1) \right\}, \quad \text{and} \quad F_{\text{d-d}} = -\frac{p_1 p_2}{4\pi\kappa r} \cos(\theta_2 - \theta_1).$$

This interaction is attractive for parallel dipoles, and repulsive for antiparallel. The physical reason is that the dipoles are free to shift vertically: Parallel dipoles will displace vertically so that membrane follows the slope and minimizes bending between the particles. The membrane between antiparallel dipoles must always have a local extremum since the slope must switch sign, hence the bending cost increases for closer particles. Note that the forces now are finite, but long ranged.

fluctuate freely in response to any vertical rigid-body translation or tilt above the base plane. The relevant “charges,” therefore, will be due solely to nonvanishing, permissible membrane curvature $-\partial_i \partial_j h$ localized around the particle contact line.

4.2.1 Membrane response to an isolated particle

Having settled on the allowable particle degrees of freedom, we may now investigate the response of an isolated particle to an imposed background deformation. This entails solving the biharmonic equation, $\nabla^4 h = 0$, outside the circle at $r = R$. Since we are interested in those solutions which are eventually fields of localized sources, we want the solution to flatten and be well-behaved infinitely far away. The most general solution obeying

$\nabla h(r \rightarrow \infty) \rightarrow \mathbf{0}$ in polar coordinates is

$$h(\mathbf{x}) = a_0 \ln er + a_1 r^{-1} \cos(\varphi - \alpha_1) + \sum_{n \geq 2} \left[a_n r^{-n} \cos(n\varphi - n\alpha_n) + a'_n r^{-n+2} \cos(n\varphi - n\alpha'_n) \right] \quad (4.25)$$

up to an irrelevant constant. Since rigid body displacements are allowed, it follows that the prefactor in the argument of the logarithm can be chosen arbitrarily. We have adjusted it to make the following mathematical expressions more aesthetically clean. In particular we include Euler's number so that the biharmonic Green function may take a much nicer form that presented in Eq. (4.19). Starting with $\nabla^2 G(\mathbf{x}) = (1/2\pi) \ln er$, we follow the same steps as in Technical Note 4.1, but arrive at a more compact form,

$$G(\mathbf{x}) = \frac{1}{8\pi} r^2 \ln r, \quad (4.26)$$

where we have fully exploited the height translation and tilt freedom to remove the constants and (now irrelevant) cutoff.⁸

Similarly, we may write down the biharmonic solutions that diverge at infinity. We select from them a subset that is well-behaved at the origin, but omit those that are constant or linear as per the particle degrees of freedom. This subset will make up the list of useful, on-shell background fields. These solution families fall into two categories, those strictly harmonic and those strictly not harmonic. Accordingly, we will separate them into two different background profiles to highlight the difference, grouping the solutions under h_{bg} if they are strictly harmonic, or under \tilde{h}_{bg} if otherwise:

$$h_{\text{bg}}(\mathbf{x}) = \sum_{n \geq 2} b_n r^n \cos n\varphi, \quad (4.27)$$

$$\tilde{h}_{\text{bg}}(\mathbf{x}) = \sum_{n \geq 0} \tilde{b}_n r^{n+2} \cos n\varphi. \quad (4.28)$$

Flat particle

When a background h_{bg} is applied, the presence of the particle contributes a response δh so that the total field is $\delta h + h_{\text{bg}}$. Therefore, in the boundary condition (4.8), we substitute $\delta h + h_{\text{bg}}$ for h , to obtain $\delta h(R) = h_{\text{flat}}(R) - h_{\text{bg}}(R)$ and $\partial_r \delta h(R) = \partial_r h_{\text{flat}}(R) - \partial_r h_{\text{bg}}(R)$. Starting with the harmonic background, we use the expansion (4.25) for δh and determine the coefficients by plugging in h_{bg} from Eq. (4.27). By linearity, the total response will consist of two additive contributions, one from h_{flat} and the other from the background. Since the parameters in h_{flat} are all free, it suffices to mention that they will always take on

⁸Technically, some length parameter should be introduced to ensure that the arguments of the logarithms are dimensionless. However, it will always disappear by the end the calculation of an observable, so we will simply omit it from the beginning.

values to conform to any overall height and slope that are introduced from the background deformations. Since this behavior is not present in our harmonic background choice, we may ignore it in the response calculation. We note in passing that we *could* proceed assuming fixed values of h_0 and s , but that approach is not without difficulty (see Technical Note 4.3).

Since the overall height and slope of h_{bg} are zero, it immediately follows that a_0 and a_1 vanish. For the rest, we plug h_{bg} into the boundary conditions to obtain the following pair of equations:

$$\begin{aligned} a_n + a'_n R^2 &= -b_n R^{2n}, \\ na_n R^{-1} + (n-2)a'_n R &= nb_n R^{2n-1}. \end{aligned} \quad (4.29)$$

We solve to find the coefficients, $a_n = (n-1)b_n R^{2n}$ and $a'_n = b_n R^{2n-2}$, and therefore the induced response,

$$\delta h(\mathbf{x}) = \sum_{n \geq 2} b_n [(n-1)R^{2n}r^{-n} - nR^{2n-2}r^{-n+2}] \cos n\varphi. \quad (4.30)$$

We proceed similarly for the response to the nonharmonic background \tilde{h}_{bg} . In this case, there is a nonzero height and slope of the background, so h_{flat} makes an appearance. A system of equations for the coefficients then follows from the boundary conditions:

$$\begin{aligned} a_0 \ln eR &= h_0 - \tilde{b}_0 R^2 \\ a_0 R^{-1} &= -2\tilde{b}_0 R & na_n R^{-1} + (n-2)a'_n R &= (n+2)\tilde{b}_n R^{2n+1} \\ a_1 R^{-1} &= sR - \tilde{b}_1 R^3 & a_n + a'_n R^2 &= -\tilde{b}_n R^{2n+2} \\ -a_1 R^{-2} &= s - 3\tilde{b}_1 R^2 \end{aligned} \quad (4.31)$$

As a consequence of the height and tilt freedom, the particle will rise by an amount $h_0 = -\tilde{b}_0 R^2(2 \ln eR - 1)$ and tilt with a slope of $s = 2\tilde{b}_1 R^2$ to meet the imposed background deformation. The resulting response field is

$$\begin{aligned} \delta \tilde{h}(\mathbf{x}) &= -2\tilde{b}_0 R^2 \ln er + \tilde{b}_1 R^4 r^{-1} \cos \varphi \\ &+ \sum_{n \geq 2} \tilde{b}_n R^{2n} [nR^2 r^{-n} - (n+1)r^{-n+2}] \cos n\varphi. \end{aligned} \quad (4.32)$$

Curved particle

The response δh to a *curved* particle in a background field can be decomposed into two contributions, δh_{perm} from the particle curvature itself and δh_{ind} induced from the background field. Indeed, at the boundary we require $\delta h_{\text{perm}} + \delta h_{\text{ind}} = h_{\text{flat}} + h_{\text{perm}} - h_{\text{bg}}$ and similarly for the derivatives. Just previously, we computed the induced response δh_{ind} , so that takes care of a portion of $h_{\text{flat}} - h_{\text{bg}}$ on the right side of the equation. What is left is the field due to the particle's permanent deformation of the contact line, together with

any additional displacements resulting from h_{perm} . The solution can later be superimposed with the induced response from some nontrivial background.

The contact profile appears as $h_{\text{flat}} + h_{\text{perm}}$, with h_{perm} given by Eq. (4.13), which we will repeat here for convenience:

$$h^{\text{ct}}(\mathbf{x}) = h_0 - \frac{1}{2}Jr^2 - \frac{1}{2}Sr^2 \cos(2\varphi - 2\alpha). \quad (4.33)$$

We included the constant term from h_{flat} since h_{perm} is nonzero at the particle boundary, but $\mathbf{s} = \mathbf{0}$ trivially. The parameters h_0 and \mathbf{s} encode rigid-body displacements, and one could imagine fixing those as well. This would, as we have discussed, lead to pathological problems for an unbounded domain, but we could nonetheless make progress by considering a large, but finite surface. We illustrate a few of the details in Technical Note 4.3, but we will not pursue this further.

We proceed now exactly as we did for a flat particle. Comparing the form of h^{ct} with the expansion (4.25), we see that only the coefficients a_0 , a_2 , and a'_2 will be nonzero. Plugging the fields into the boundary conditions therefore gives a simpler system of coefficient equations than previously:

$$\begin{aligned} a_0 \ln eR &= h_0 - \frac{1}{2}JR^2 & a_2 R^{-2} + a'_2 &= -\frac{1}{2}SR^2 \\ a_0 R^{-1} &= -JR & -2a_2 R^{-3} &= -SR \end{aligned} \quad (4.34)$$

We conclude that the permanent response is therefore

$$\delta h_{\text{perm}}(\mathbf{x}) = -JR^2 \ln er + \frac{1}{2}SR^2(R^2 r^{-2} - 2) \cos(2\varphi - 2\alpha), \quad (4.35)$$

where the particle has shifted by an amount $h_0 = -1/2JR^2 \ln R$ to meet with the equilibrium ($h = 0$) base plane.

4.3 Effective theory

We now turn our focus to an effective point-particle formulation of membrane-mediated interactions. As usual, we take advantage of the scale separation between the generic particle size ($\sim R$) and the interparticle distance ($\sim r$). Accordingly, we integrate out the short distance physics in favor of a coarse-grained model that subsumes the finite-size particle information and (nontrivial) boundary conditions into a series of point sources and interactions. Shrinking the finite particle boundaries into points therefore results in an effective Hamiltonian,

$$\mathcal{H}_{\text{eff}}[h] = \mathcal{H}_0[h] + \Delta\mathcal{H}[h], \quad (4.36)$$

Technical Note 4.3: Biharmonic solution on an annulus

No biharmonic solution exists that both fixes a particle's height and tilt *and* satisfies asymptotic flatness. However, a workaround is to introduce a cutoff $L \gg r > R$ so that the response obeys $\delta h(L) = 0$ and $\partial_r \delta h(L) = 0$. The boundary value problem now is well-posed in an annular domain $(r, \varphi) \in [R, L] \times [0, 2\pi)$. The contact line profile for a flat, circular particle is $h_{\text{flat}} = h_0 + sr \cos(\varphi - \vartheta)$ in polar coordinates, where $s = |s|$ and ϑ is the angle s makes with the x -axis. This is then matched with the response expansion,

$$\delta h(r, \varphi) = c_0 + c_1 \ln r + c_2 r^2 + c_3 r^2 \ln r + \left(\frac{d_0}{r} + d_1 r + d_2 r \ln r + d_3 r^3 \right) \cos(\varphi - \vartheta)$$

at the inner and outer boundaries. We omit the details, but after comparing coefficients and cleverly applying properties of logarithms, we find (after a few cups of coffee),

$$\begin{aligned} \delta h_{\text{flat}}(r, \varphi) = h_0 & \frac{(L^2 - R^2)(L^2 - r^2) - 2L^2 R^2 \ln(\frac{L}{r}) [2 \ln(\frac{L}{r}) - 1] - 2r^2 [L^2 \ln(\frac{L}{r}) + R^2 \ln(\frac{r}{R})]}{(L^2 - R^2) - 4L^2 R^2 \ln^2(\frac{L}{R})} \\ & + \frac{s}{2r} \frac{(L^2 - r^2)(r^2 + R^2) - 2r^2(L^2 + R^2) \ln(\frac{L}{r})}{(L^2 - R^2) - (L^2 + R^2) \ln(\frac{L}{R})} \cos(\varphi - \vartheta). \end{aligned}$$

As this solution is an observable, we expect to be able now to safely take the $L \rightarrow \infty$ limit. Indeed we can and obtain

$$\delta h_{\text{flat}}(r, \theta) \xrightarrow{L \rightarrow \infty} h_0 + sr \cos(\varphi - \vartheta),$$

which simply returns the contact profile. If this solution is used, however, one must keep in mind its regime of validity.

where $\mathcal{H}_0[h]$ is the particle-free—or *bulk*—membrane Hamiltonian,

$$\mathcal{H}_0[h] = \frac{\kappa}{2} \int_{\mathbb{R}^2} d^2x (\nabla^2 h)^2, \quad (4.37)$$

and $\Delta \mathcal{H}[h]$ is a derivative expansion localized on the particle worldlines.

Our pragmatic approach for constructing the derivative expansion $\Delta \mathcal{H}[h]$ is to simply include all possible scalars expressible as localized derivatives of the field, up to quadratic order (consistent with the bulk Hamiltonian (4.37)) and respecting the symmetries of the problem. There are three transformations under which the bulk Hamiltonian is invariant:

- T₁.** Reflection ($h \rightarrow -h$) across the base plane.
- T₂.** Transformations of the field of the form $h \rightarrow h + h_{\text{flat}}$, where h_{flat} is given by Eq. (4.10).
- T₃.** Rotations around a vertical axis centered at *any* point in the base plane.

The contribution of a single particle to the effective theory, then, can be categorized as either symmetry-respecting or symmetry breaking. Of course the inclusion of a particle

already breaks the in-plane translation symmetry of \mathbf{T}_3 by selecting a preferred origin. However, for a flat,⁹ circular particle, rotational symmetry is retained about the particle center. Furthermore, we agreed in the previous section to restrict our attention to particles with the freedom to bob and tilt, so \mathbf{T}_2 will always be respected. Finally, \mathbf{T}_1 will remain a symmetry for flat particles. On the other hand, curved particles may break each one of these symmetries, and consequently must serve as an external source of “curvature charge.”

4.3.1 EFT for flat particles: induced sources

We first consider flat particles, *i.e.*, those that force the boundary into a planar shape in the vicinity of their boundary. Recall that the boundary condition that the surface needs to satisfy at the circumference of a particle is as follows: the surface has to attach to the rim of the particle, and do so at an angle which makes the slope continuous normally across the boundary. These boundary conditions are in harmony with the bulk symmetries \mathbf{T}_1 , \mathbf{T}_2 , and \mathbf{T}_3 (without translation), so we may begin enumerating the admissible worldline terms for flat particles, which we will denote by $\Delta\mathcal{H}_f[h]$.

The first of the bulk symmetries rules out terms linear in (derivatives of) h in the construction of $\Delta\mathcal{H}_f$. The second forbids the usage of the zeroth and first derivatives of the field. Hence, $\partial_i\partial_j h$ is the field occurrence with the least number of derivatives allowed in the derivative expansion $\Delta\mathcal{H}_f$. The third symmetry—rotational invariance—requires that no derivatives are left uncontracted between the field factors. Although these properties are sufficient to write out the derivative expansion, we have one final simplification. We wish to eliminate the redundant terms that will vanish when the field h is on-shell. That is, we restrict the fields h to satisfy the bulk Euler-Lagrange equation, $\nabla^4 h = 0$, so at most *one* instance of a Laplacian can act on a given field instance. The effective theory is then constructed by writing all terms obeying these rules, for all particles a :

$$\Delta\mathcal{H}_f[h] = \sum_a \sum_{n \geq 2} \left[\frac{1}{2} c_a^{(n)} (\partial_I^n h)^2 + \dot{c}_a^{(n)} \partial_I^{n-1} \nabla^2 h \partial_I^{n-1} h + \frac{1}{2} \ddot{c}_a^{(n)} (\partial_I^{n-2} \nabla^2 h)^2 \right] \Big|_{x=x_a}, \quad (4.38)$$

where $\partial_I^n = \partial_{i_1} \partial_{i_2} \cdots \partial_{i_n}$. Each Wilson coefficient labeled by derivative order n multiplies a term that possesses a total of $2n$ derivatives, and the accents on them indicate the number of ∇^2 's among the derivatives.¹⁰ Accordingly, each coefficient must scale as κR^{2n-2} by dimensional analysis. Note that the term $\dot{c}_a^{(2)} \partial_i \nabla^2 h \partial_i h$ violates the \mathbf{T}_2 symmetry, so $\dot{c}_a^{(2)} = 0$ for flat particles.

⁹Recall that “flatness” here refers only to the boundary conditions at the particle rim; the true shape of the particle is irrelevant beyond the pinned membrane height and angle along the contact line. A flat particle is defined as having a contact line that lies completely within a plane and a contact slope that is everywhere tangent to that plane in the neighborhood of the boundary.

¹⁰Thanks to Cem Yolcu for this delightful ornamentation. The relevance of the ring notation will become apparent in Section 4.4.

Matching

To determine the values of the coefficients, we use $\mathcal{H}_{\text{eff}}[h]$ to compute the effective responses to the background fields (4.27) and (4.28). The background fields are disrupted by the particles, and subsequently excite a distribution of “curvature charges” near the particle boundaries. This induced curvature source is computed with Eq. (4.17) as inspiration, leading to the distribution,

$$\begin{aligned} \rho(\mathbf{x} \mid h_{\text{bg}}) &= -\frac{\delta\mathcal{H}}{\delta h(\mathbf{x})} \Big|_{h=h_{\text{bg}}} \\ &= -\sum_a \sum_{n \geq 2} \left[c_a^{(n)} \partial_I^n h_{\text{bg}} (-\partial)_I^n \right. \\ &\quad + \dot{c}_a^{(n)} \partial_I^{n-1} \nabla^2 h_{\text{bg}} (-\partial)_I^{n-1} \\ &\quad + \ddot{c}_a^{(n)} \partial_I^{n-1} h_{\text{bg}} (-\partial)_I^{n-1} \nabla^2 \\ &\quad \left. + \ddot{\ddot{c}}_a^{(n)} \partial_I^{n-2} \nabla^2 h_{\text{bg}} (-\partial)_I^{n-2} \nabla^2 \right] \delta(\mathbf{x} - \mathbf{x}_a). \end{aligned} \quad (4.39)$$

This has the expected form of a collection of point sources whose magnitudes are proportional to (derivatives of) the field incident upon them. It is therefore appropriate to refer to all these Wilson coefficients again as *polarizabilities*. We will further abuse this analogy occasionally by using the term *multipole* order interchangeably with *derivative* order when referring to the numbers n .

The response field δh emanating from the particles is given by the convolution of the induced source distribution and the bulk Green function as in Eq. (4.18), where now the Green function

$$G(\mathbf{x} - \mathbf{x}') = \frac{1}{16\pi} (\mathbf{x} - \mathbf{x}')^2 \ln(\mathbf{x} - \mathbf{x}')^2. \quad (4.40)$$

Due to the locality of the Hamiltonian, we may consider each particle separately, and we find the induced response of a single particle a centered at the origin,

$$\begin{aligned} \delta h_{\text{f}}^{\text{eff}}(\mathbf{x} \mid h_{\text{bg}}) &= -\frac{1}{\kappa} \sum_{n \geq 2} \left[c^{(n)} \partial_I^n h_{\text{bg}}(0) (-\partial)_I^n G(\mathbf{x}) \right. \\ &\quad + \dot{c}^{(n)} \partial_I^{n-1} \nabla^2 h_{\text{bg}}(0) (-\partial)_I^{n-1} G(\mathbf{x}) \\ &\quad + \ddot{c}^{(n)} \partial_I^{n-1} h_{\text{bg}}(0) (-\partial)_I^{n-1} \nabla^2 G(\mathbf{x}) \\ &\quad \left. + \ddot{\ddot{c}}^{(n)} \partial_I^{n-2} \nabla^2 h_{\text{bg}}(0) (-\partial)_I^{n-2} \nabla^2 G(\mathbf{x}) \right], \end{aligned} \quad (4.41)$$

where the label a was dropped from the polarizabilities for convenience.

The tensors $\partial_I^n G$ and $\partial_I^n h_{\text{bg}}$, and their various contractions, pose a bit of a technical challenge. Instead of continuing along this path we will take a lesson from the previous chapter and switch over to complex coordinates $\mathbf{z} = (z, \bar{z})$. The Green function then takes on the form,

$$G(\mathbf{z} - \mathbf{z}') = \frac{1}{16\pi} (z - z')(\bar{z} - \bar{z}') \ln(z - z')(\bar{z} - \bar{z}') \quad (4.42)$$

To convert the worldline Hamiltonian, we could perform the required transformations directly. Instead we recall that a given rotationally symmetric terms must have an equal number of ∂ and $\bar{\partial}$ derivatives,¹¹ and $\nabla^2 = 4\partial\bar{\partial}$. It is straightforward, then, to re-express the derivative expansion in complex coordinates:

$$\Delta\mathcal{H}_f[h] = \sum_a \sum_{n \geq 2} \left[C_a^{(n)} \partial^n h \bar{\partial}^n h + \mathring{C}_a^{(n)} \partial^{n-1} \partial \bar{\partial} h \bar{\partial}^{n-1} h + \mathring{\mathring{C}}_a^{(n)} \partial^{n-1} h \bar{\partial}^{n-1} \partial \bar{\partial} h + \mathring{\mathring{\mathring{C}}}_a^{(n)} \partial^{n-2} \partial \bar{\partial} h \bar{\partial}^{n-2} \partial \bar{\partial} h \right] \Big|_{z=z_a}, \quad (4.43)$$

The relation between the coefficients in Eq. (4.38) and (4.43) is irrelevant since they are yet to be determined, but the number of accents still indicate the number of Laplacians in their respective terms acting on the field. Due to the rigid body symmetry \mathbf{T}_2 , we still have $\mathring{C}^{(2)} = 0$.

With the worldline Hamiltonian rewritten as above, the corresponding response (4.41) of a single particle in a background field becomes

$$\begin{aligned} \delta h_f^{\text{eff}}(z | h_{\text{bg}}) = & -\frac{1}{\kappa} \sum_{n \geq 2} (-)^n \left[C^{(n)} \partial^n h_{\text{bg}}(0) \bar{\partial}^n G(z) \right. \\ & - \mathring{C}^{(n)} \partial^{n-1} \partial \bar{\partial} h_{\text{bg}}(0) \bar{\partial}^{n-1} G(z) \\ & - \mathring{\mathring{C}}^{(n)} \partial^{n-1} h_{\text{bg}}(0) \bar{\partial}^{n-1} \partial \bar{\partial} G(z) \\ & \left. + \mathring{\mathring{\mathring{C}}}^{(n)} \partial^{n-2} \partial \bar{\partial} h_{\text{bg}}(0) \bar{\partial}^{n-2} \partial \bar{\partial} G(z) \right] + \text{c.c.} \end{aligned} \quad (4.44)$$

The way $h_{\text{bg}}(z)$ appears in the above terms with its derivatives evaluated at $z = 0$ immediately suggests the most convenient form to use for the backgrounds: z^n and $z^n z \bar{z}$ (plus their complex conjugates) for positive integers n .¹² The background fields (4.27) and (4.28) are seen to be precisely of this form when re-expressed in complex coordinates:

$$h_{\text{bg}}(z) = \frac{1}{2} \sum_{n \geq 2} b_n (z^n + \bar{z}^n), \quad (4.45)$$

$$\tilde{h}_{\text{bg}}(z) = \frac{1}{2} \sum_{n \geq 0} \tilde{b}_n z \bar{z} (z^n + \bar{z}^n). \quad (4.46)$$

Let us impose the two forms separately and calculate the effective response they induce. When the harmonic background $h_{\text{bg}}(z)$ is applied, we find the response (refer to Technical

¹¹We remind the reader that $\partial = \partial/\partial z$ and $\bar{\partial} = \partial/\partial \bar{z}$. For other relations and properties, see Section 3.3.1.

¹²Of course, convenience is not the only criterion here. We have mentioned earlier that we write our effective theory on-shell, *i.e.*, without any terms involving $\nabla^4 h$ owing to the Euler-Lagrange equation $\nabla^4 h = 0$. Accordingly, we must match on-shell as well, using backgrounds that obey $\nabla^4 h_{\text{bg}} = 16\partial^2 \bar{\partial}^2 h_{\text{bg}} = 0$, which these backgrounds do.

Note 4.4 for the Green function derivatives) to be

$$\delta h_{\text{f}}^{\text{eff}}(z) = -\frac{1}{2} \sum_{n \geq 2} b_n \left[\frac{C^{(n)}}{16\pi\kappa} n! (n-2)! \frac{z}{\bar{z}^{n-1}} - \frac{\mathring{C}^{(n+1)}}{16\pi\kappa} n! (n-1)! \frac{1}{\bar{z}^n} \right] + \text{c.c.} \quad (4.47)$$

Similarly, the nonharmonic background $\tilde{h}_{\text{bg}}(z)$ induces the effective response

$$\begin{aligned} \delta \tilde{h}_{\text{f}}^{\text{eff}}(z) = & -\tilde{b}_0 \frac{\mathring{C}^{(2)}}{16\pi\kappa} \ln(e^2 z \bar{z}) + \tilde{b}_1 \frac{\mathring{C}^{(3)}}{16\pi\kappa} \frac{1}{\bar{z}} \\ & - \frac{1}{2} \sum_{n \geq 2} \tilde{b}_n \left[\frac{\mathring{C}^{(n+1)}}{16\pi\kappa} (n+1)! (n-2)! \frac{z}{\bar{z}^{n-1}} - \frac{\mathring{C}^{(n+2)}}{16\pi\kappa} (n+1)! (n-1)! \frac{1}{\bar{z}^n} \right] + \text{c.c.} \end{aligned} \quad (4.48)$$

We now wish to compare with the full-theory responses (4.30) and (4.32). In complex coordinates, these solutions appear as

$$\delta h_{\text{f}}^{\text{full}}(z) = -\frac{1}{2} \sum_{n \geq 2} b_n R^{2n} \left[n R^{-2} \frac{z}{\bar{z}^{n-1}} - (n-1) \frac{1}{\bar{z}^n} \right] + \text{c.c.}, \quad (4.49)$$

$$\begin{aligned} \delta \tilde{h}_{\text{f}}^{\text{full}}(z) = & -\frac{1}{2} \tilde{b}_0 R^2 \ln(e^2 z \bar{z}) + \frac{1}{2} \tilde{b}_1 R^4 \frac{1}{\bar{z}} \\ & - \frac{1}{2} \sum_{n \geq 2} \tilde{b}_n R^{2n} \left[(n+1) \frac{z}{\bar{z}^{n-1}} - n R^2 \frac{1}{\bar{z}^n} \right] + \text{c.c.} \end{aligned} \quad (4.50)$$

In this form we can easily match coefficients via $\delta h_{\text{f}}^{\text{eff}} = \delta h_{\text{f}}^{\text{full}}$ and $\delta \tilde{h}_{\text{f}}^{\text{eff}} = \delta \tilde{h}_{\text{f}}^{\text{full}}$, and therefore find the complete set of polarizabilities:

$$C^{(n)} = \frac{16\pi\kappa R^{2n-2}}{(n-1)! (n-2)!}, \quad (4.51a)$$

$$\mathring{C}^{(n)} = (n-2) C^{(n)}, \quad (4.51b)$$

$$\mathring{\mathring{C}}^{(n)} = (n-2)^2 C^{(n)}, \quad (4.51c)$$

for $n \geq 2$, with the exception of the coefficient for pure laplacians: $\mathring{\mathring{C}}^{(2)} = C^{(2)}/2$. It is perhaps surprising that $\mathring{\mathring{C}}^{(2)}$ and $C^{(2)}$ are so similar; the latter only parametrizes (part of) the local Gaussian curvature, whereas the former additionally accounts for the square of the total curvature.¹³ However, a factor of 1/2 is to be expected regardless. By convention, we usually include a factor of $1/n!$ for terms that contain n powers of an identical field operator because of their exchange symmetry, and indeed $\mathring{\mathring{C}}^{(2)}$ multiplies $(\partial\bar{\partial}h)^2$ so normally we would include a 1/2 prefactor on this term. We refrained from doing so in the worldline

¹³In complex coordinates, the total curvature takes the form $K = -\nabla^2 h = -4\partial\bar{\partial}h$ and the Gaussian curvature is $K_G = \det[\partial^2 h] = 4(\partial^2 h \bar{\partial}^2 h - \partial\bar{\partial}h \partial\bar{\partial}h)$.

Technical Note 4.4: Derivatives of the biharmonic Green function

We summarize here for reference the derivatives of the biharmonic Green function (4.42) in complex coordinates:

$$\begin{aligned} G(z) &= \frac{1}{16\pi} z\bar{z} \ln z\bar{z}, \\ \partial\bar{\partial}G(z) &= \frac{1}{16\pi} \ln(e^2 z\bar{z}), \\ \partial^n G(z) &= (-)^n \frac{(n-2)!}{16\pi} \frac{\bar{z}}{z^{n-1}} \quad (n \geq 2), \\ \partial^{n-2} \partial\bar{\partial}G(z) &= (-)^{n-1} \frac{(n-3)!}{16\pi} \frac{1}{z^{n-2}} \quad (n \geq 3). \end{aligned}$$

We will always rewrite the derivatives so that they act on the full argument of the Green function and hence appear in the forms above. For example, $\partial_a^n G(z_b - z_a) = (-)^n \partial^n G(z_{ab})$ with $z_{ab} = z_b - z_a$.

Hamiltonian to keep the sum relatively compact, but the exceptional factor of two will reappear when we discuss interactions.

4.3.2 EFT for curved particles: permanent sources

Curved particles impart and enforce permanent deformations on the membrane surface without the need for a background field or fluctuations to induce them. In the EFT, these deformations appear as permanent sources, $\delta\Delta\mathcal{H}/\delta h \neq 0$ with $h = 0$, and augment the Hamiltonian by local worldline terms that explicitly break the field symmetries. Of the three field symmetries discussed on page 176, we wish to retain the rigid-body displacements \mathbf{T}_2 , but break the both vertical reflection \mathbf{T}_1 and rotational symmetry \mathbf{T}_3 of the membrane about the particle's center. The breaking of vertical reflection symmetry subject to \mathbf{T}_1 suggests including derivative expansion linear in h but with derivative order of at least two. The breaking of point rotational symmetry tells us we do not need to ensure each term is rotation invariant. Recalling that more than one $\partial\bar{\partial} \sim \nabla^4$ in the effective theory is redundant, the most general linear term we can add to the worldline Hamiltonian $\Delta\mathcal{H}$ to capture permanent sources is

$$\Delta\mathcal{H}_p[h] = - \sum_a \sum_{n \geq 2} \left[Q_a^{(n)} \partial^n h(z_a) + \mathring{Q}_a^{(n)} \partial^{n-2} \partial\bar{\partial} h(z_a) \right] + \text{c.c.} \quad (4.52)$$

The worldline terms quadratic in h do not contribute to a source deformation in the absence of an incident field; they account for only *induced* polarization.¹⁴ The breaking of rotational symmetry in the quadratic terms, therefore, is not the result of a permanent source, but rather a consequence of a particle with a noncircular projected boundary. In other words, the quadratic terms account for induced deformations and any anisotropy of

¹⁴This is analogous to the statement in electrostatics that the actual amount of charge on a conductor does not affect its capacitance or polarizabilities.

the particle boundary, whereas the linear terms account for permanent deformations and any anisotropy in the contact curvature. Thus the quadratic worldline terms $\Delta\mathcal{H}_f$ require no modification for our class of particles, and there is no need to re-match the polarizabilities; the series (4.52) fully captures the permanent particle curvature, and $\Delta\mathcal{H} = \Delta\mathcal{H}_f + \Delta\mathcal{H}_p$ is the complete set of worldline terms.

Matching

To determine the “curvature charges” $Q^{(n)}$ and $\mathring{Q}^{(n)}$, we first calculate the permanent field response due to $\Delta\mathcal{H}_p[h]$. At zero incident field ($h_{\text{bg}} = 0$), we find the permanent source for a single particle,

$$\rho_p(z) = -\frac{\delta\mathcal{H}[h]}{\delta h(z)}\Big|_{h=0} = \sum_{n \geq 2} \left[Q^{(n)}(-\partial)^n + \mathring{Q}^{(n)}(-\partial)^{n-2}\partial\bar{\partial} \right] \delta(z) + \text{c.c.}, \quad (4.53)$$

and its corresponding field response,

$$\delta h_p^{\text{eff}}(z) = \frac{1}{\kappa} \sum_{n \geq 2} (-)^n \left[Q^{(n)} \partial^n G(z) + \mathring{Q}^{(n)} \partial^{n-2} \partial \bar{\partial} G(z) \right] + \text{c.c.} \quad (4.54)$$

We now compare this to the full-theory response (4.35), which in complex coordinates reads

$$\delta h_p^{\text{full}}(z) = -\frac{1}{4} J R^2 \ln e^2 z \bar{z} + \frac{1}{4} S e^{2i\alpha} \frac{R^2}{z^2} (R^2 - 2z\bar{z}) + \text{c.c.} \quad (4.55)$$

To further simplify the matching, we refer to Technical Note 4.4 and rewrite the expression in terms of the Green function:

$$\delta h_p^{\text{full}}(z) = -8\pi J R^2 \partial \bar{\partial} G(z) - 4\pi S e^{2i\alpha} R^2 [R^2 \partial^2 \partial \bar{\partial} G(z) + 2\partial^2 G(z)] + \text{c.c.} \quad (4.56)$$

In this form, the requisite matching condition $\delta h_p^{\text{eff}} = \delta h_p^{\text{full}}$ shows that all the Wilson coefficients are zero except for the following three (and their complex conjugates):

$$Q^{(2)} = -8\pi\kappa S e^{2i\alpha} R^2, \quad (4.57a)$$

$$\mathring{Q}^{(2)} = -4\pi\kappa J R^2, \quad (4.57b)$$

$$\mathring{Q}^{(4)} = -4\pi\kappa S e^{2i\alpha} R^4, \quad (4.57c)$$

and hence the worldline source Hamiltonian is

$$\Delta\mathcal{H}_p[h] = -\sum_a \left[Q_a^{(2)} \partial^2 h(z_a) + \mathring{Q}_a^{(2)} \partial \bar{\partial} h(z_a) + Q_a^{(4)} \partial^2 \partial \bar{\partial} h(z_a) \right] + \text{c.c.} \quad (4.58)$$

As an additional word of caution, both $\dot{Q}^{(2)}$ and $\partial\bar{\partial}h$ are real, so the middle term actually occurs twice due to the addition of the complex conjugate. This will be another source of exceptional factors of two to keep in mind.

Preferred shape

Let us briefly comment on a useful way to conceptualize the permanent sources, namely, as a “preferred shape” for the surface at the location of the particles. The easiest way to see this is to consider, for instance, the “quadrupole” terms

$$C^{(2)}\partial^2h\bar{\partial}^2h - Q^{(2)}\partial^2h - \bar{Q}^{(2)}\bar{\partial}^2h$$

from the worldline Hamiltonian. Collecting terms, this becomes

$$\frac{1}{2}C^{(2)}\bar{\partial}^2h\left[\partial^2h - 2\frac{\bar{Q}^{(2)}}{C^{(2)}}\right] + \text{c.c.},$$

which is of the same form as the Lagrange multiplier terms of the full-theory Hamiltonian (4.14) and appropriately relates the Wilson coefficients to the contact line and constraint forces. Not surprisingly, this view is reminiscent of the way Dommersnes and Fournier [DF99a, DF99b] enforced a preferred form K_{ij} on the curvature tensor $-\partial_i\partial_jh$ of the surface, through the usage of a factor $\delta(\partial_i\partial_jh + K_{ij})$ in the integration measure, to account for the curvature of the particles.

Alternatively, one can easily check that, up to an irrelevant numerical constant, these terms can be rewritten as $C^{(2)}|\partial^2h - \bar{Q}^{(2)}/C^{(2)}|^2$. That is, when the surface shape obeys $\partial^2h = \bar{Q}^{(2)}/C^{(2)}$, no excitation occurs. Viewed in this manner, these permanent sources appear as a local *spontaneous curvature* as imposed by the particle. More generally, one could impose a desired shape by including analogous “spontaneous curvature” terms in the appropriate worldline terms, providing an alternative construction of the effective Hamiltonian.

4.3.3 Some comments on the usage of point particles

The EFT formalism replaces the finite-sized particles by points with suitable additional local properties. As mentioned in the introduction, other strategies have been employed which involve, either effectively or directly, point-like particles. Before moving on to computing mediated forces using the effective theory we have constructed, we wish to briefly discuss these other approaches in the membrane context and explain how they differ from EFT.

The route followed by Netz [Net97] as well as Marchenko and Misbah [MM02] also utilizes localized quadratic and linear terms in the Hamiltonian in order to account for the particles, and points out the role of the quadratic terms in allowing interactions that a superposition approximation would not capture. Neither of these works, however, recognized (or at least exploited) the ability of such a strategy to handle finite-sized particles. This is also reflected

in the fact that the quadratic terms were kept at lowest derivative order. Netz [Net97] did capitalize on how amenable the form of such a theory is to a standard statistical field theory framework, but he missed a second set of quadratic operators¹⁵ while setting up the problem and later neglected to apply derivatives to the correlation functions. Also, he interprets the polarizabilities as coupling constants and then claims that infinite values for them correspond to rigid particles. This is not the right interpretation, though, as Sec. 4.3.1 shows.

Marchenko and Misbah [MM02] similarly exploited the convenience of point particles, and illuminated the form of the lowest order mediated interaction based on the symmetry the particles possess. However, in their treatment the particles impact the membrane in a very different way: Rather than rigidly enforcing a particular *shape*, they impose a localized *force distribution*, such as a point quadrupole. Since the response of the membrane to a given force becomes weaker if the membrane gets stiffer, their interaction energies scale *inversely* with the bending rigidity. The same philosophy was followed by Evans *et al.* [ETS03], who generalized the treatment to arbitrary force densities. Bartolo and Fournier showed that this different scaling indeed only results from a different way in which the particle-membrane interaction is treated [BF03].

Dommersnes and Fournier [DF99a, DF99b] also employed a point particle method where they fixed the local curvature of the membrane by a delta function. To our knowledge, their work for the first time attempted to calculate higher order terms in the asymptotic expansion of mediated interactions in terms of inverse distance, thanks to the simplicity of the point particle assumption. However, in that case, the only way the particle affects the surface is by constraining the curvature (*i.e.*, the second derivative of the field) at a point, by assumption. In relation to the EFT framework, this corresponds to truncating the world line Hamiltonian right after the coefficients of derivative order 2. One can imagine adding delta function constraints for higher order derivatives, then, in order to remove the “point curvature defect” assumption and incorporate the rest of the boundary conditions around a finite sized particle. However, this does not suffice to recover the otherwise ignored features of the boundary in a quantitative way. The reason is that in such a treatment there is no systematic means of linking the properties of the point particle to those of the original particle before it was coarse grained into a point. Another related matter is the ambiguity in the magnitudes of physical observables (*e.g.*, forces) in the form of a cutoff dependence. The cutoff is afterwards reinterpreted as the size of the particle, arguing that what counts as a point should be of size comparable to the cutoff wavelength beyond which the continuum description is unreliable. Consequently, this approach cannot be considered a suitable strategy for treating particles of arbitrary size *effectively* as if they were point-like. Also, the cutoff regularization is an operation which eventually has to do with the field, and not the particles. Hence, particles of different size cannot be dealt with. More importantly,

¹⁵Stated in the terminology developed in Sec. 4.3.1, his version of Eq. (4.38) only consists of the one term proportional to the polarizability $\hat{C}^{(2)}$. This is inconsistent, since the term proportional to $C^{(2)}$ contributes at the same derivative order. Indeed, as Eqns. (4.71), (4.72) and (4.110) below will show, both terms contribute to the leading order (axisymmetric) elastic and entropic interaction, respectively.

though, the cutoff is innately an ambiguous quantity no matter what kind of regularization it achieves on the theory, and therefore by construction cannot be *equated* to anything observable.

The following are not point particle approaches *per se*, but can be considered as such to the extent that EFT can be considered a point particle approach. The scattering formalism adopted by Lin *et al.* [LZMP11], and the somewhat closely related method incorporating δ -functions to constrain the partition sum [GBP93a, GBP93b, GKG96a, GKG96b], treat the particles “fully”, as we do. The particle information then ends up in a collection of numbers, to arbitrary accuracy, similar to EFT. In fact, there is an equivalence between these approaches and the EFT formalism *on the quadratic level*, where the former is valid, and this can be shown using Hubbard-Stratonovich transformations. Lin *et al.* [LZMP11] have recently treated the problem of membrane mediated Casimir interactions within the scattering framework, even under finite surface tension, and evaluated the pair interaction numerically as a function of distance.

4.4 Interactions diagrammar

Now that we have recaptured the finite-size particle data in the EFT framework, we are set to calculate the interparticle forces. As a reminder, our goal is the calculate the interaction potential \mathcal{U} defined by

$$\mathcal{U} = -\frac{1}{\beta} \ln \left[\sum_{k \geq 0} \frac{1}{k!} \langle (-\beta \Delta \mathcal{H}[h])^k \rangle_0 \right], \quad (4.59)$$

where $\langle \dots \rangle_0$ is the expectation value weighted by the particle-free distribution $e^{-\beta \mathcal{H}_0[h]} / Z_0$. As we learned in the previous chapter, this free energy difference can be expressed graphically as a sum of linear and ring diagrams for a quadratic theory:

$$-\beta \mathcal{U} = \sum_{k \geq 0} \text{Diagram}_k + \sum_{k \geq 1} \text{Diagram}_k, \quad (4.60)$$

where the source and interaction vertices are given by the functional derivatives on the worldline,

$$\begin{aligned} \text{Diagram}_k &= - \left[\frac{\delta(\beta \Delta \mathcal{H})}{\delta h(z)} \right]_{h=0} \\ &= \beta \sum_a \left[Q_a^{(2)} \partial^2 + \dot{Q}_a^{(2)} \partial \bar{\partial} + \dot{Q}_a^{(4)} \partial^2 \partial \bar{\partial} \right] \delta_a^z + \text{c.c.}, \end{aligned} \quad (4.61a)$$

$$\begin{aligned}
 \text{Diagram: } \text{a vertex } V \text{ with two outgoing lines labeled } z \text{ and } z' &= - \left[\frac{\delta^2(\beta \Delta \mathcal{H})}{\delta h(z) \delta h(z')} \right]_{h=0} \\
 &= -\beta \sum_a \sum_{n \geq 2} \left[C_a^{(n)} \partial^n \delta_a^z \bar{\partial}^n \delta_a^{z'} + \mathring{C}_a^{(n)} \partial^{n-1} \partial \bar{\partial} \delta_a^z \bar{\partial}^{n-1} \delta_a^{z'} \right. \\
 &\quad \left. + \mathring{C}_a^{(n)} \partial^{n-1} \delta_a^z \bar{\partial}^{n-1} \partial \bar{\partial} \delta_a^{z'} + \mathring{\mathring{C}}_a^{(n)} \partial^{n-2} \partial \bar{\partial} \delta_a^z \bar{\partial}^{n-2} \partial \bar{\partial} \delta_a^{z'} \right] + (z \leftrightarrow z'),
 \end{aligned} \tag{4.61b}$$

where $\delta_a^z := \delta(z - z_a)$. The propagator—the edges connecting these vertices in the complete diagrams—is proportional to the Green function:

$$z \bullet \text{-----} \bullet z' = (\beta \kappa)^{-1} G(z - z'). \tag{4.62}$$

The linear and quadratic vertices appear as a tower of derivatives acting on delta functions, which will then be thrown onto the propagators upon integration. If we encounter a term in which a bi-Laplacian ($\nabla^4 = 16\partial^2\bar{\partial}^2$) acts on the propagator, it will vanish; *i.e.*, for $z_a \neq z_b$, $\partial^n \bar{\partial}^m G(z_a - z_b) = 0$ when $n, m \geq 2$. We make this property manifest diagrammatically by representing propagators receiving at least two ∂ -derivatives by a single line and propagators receiving at least two $\bar{\partial}$ -derivatives by a double line. Additionally, propagators receiving a single Laplacian ($\nabla^2 = 4\partial\bar{\partial}$) will be indicated by a small circle along the usual single or double line, which explains the motivation for the ring-accent notation of the Wilson coefficients. Complex conjugation will simply swap single lines for double lines and vice-versa. With this in mind, we assign new diagrams to each term in the source and vertex expansions above. For general permanent source terms, we write:

$$\begin{aligned}
 z_a \cdots \overset{(n)}{\circ} \text{---} z &= \beta Q_a^{(n)} (-\partial)^n \delta_a^z & z_a \cdots \overset{(n)}{\circ} \text{---} z &\stackrel{*}{=} \beta \mathring{Q}_a^{(n)} (-\partial)^{n-2} \partial \bar{\partial} \delta_a^z \\
 z_a \cdots \overset{(n)}{\circ} \text{=}= z &= \beta \bar{Q}_a^{(n)} (-\bar{\partial})^n \delta_a^z & z_a \cdots \overset{(n)}{\circ} \text{=}= z &\stackrel{*}{=} \beta \mathring{\bar{Q}}_a^{(n)} (-\bar{\partial})^{n-2} \partial \bar{\partial} \delta_a^z
 \end{aligned} \tag{4.63a}$$

The starred equality “ $\stackrel{*}{=}$ ” in the right column is there to remind us that the $\mathring{Q}^{(2)}$ term appears twice in the source expansion (4.61a) and should therefore include a factor of two when $n = 2$. Moreover, the $\mathring{Q}_a^{(2)}$ term will serve diagrammatically as either a single or double line, depending on what other vertices it links to.

For the interaction vertices, we write:

$$\begin{aligned}
 z_a \cdots \text{---} \text{---} \text{---} \begin{array}{c} (n) \\ \diagup \quad \diagdown \\ z \quad z' \end{array} &= -\beta C_a^{(n)} \partial^n \delta_a^z \bar{\partial}^n \delta_a^{z'} & z_a \cdots \text{---} \text{---} \text{---} \begin{array}{c} (n) \\ \diagup \quad \diagdown \\ z \quad z' \end{array} &\stackrel{*}{=} -\beta \overset{\circ}{C}_a^{(n)} \partial^{n-1} \bar{\partial} \delta_a^z \bar{\partial}^{n-1} \partial \delta_a^{z'} \\
 z_a \cdots \text{---} \text{---} \text{---} \begin{array}{c} (n) \\ \diagup \quad \diagdown \\ z \quad z' \end{array} &= -\beta \overset{\circ}{C}_a^{(n)} \partial^n \bar{\partial} \delta_a^z \bar{\partial}^{n-1} \delta_a^{z'} & z_a \cdots \text{---} \text{---} \text{---} \begin{array}{c} (2) \\ \diagup \quad \diagdown \\ z \quad z' \end{array} &= -2\beta \overset{\circ}{C}_a^{(2)} \partial \bar{\partial} \delta_a^z \partial \bar{\partial} \delta_a^{z'} \\
 z_a \cdots \text{---} \text{---} \text{---} \begin{array}{c} (n) \\ \diagup \quad \diagdown \\ z \quad z' \end{array} &= -\beta \overset{\circ}{C}_a^{(n)} \partial^{n-1} \delta_a^z \bar{\partial}^n \partial \delta_a^{z'} & z_a \cdots \text{---} \text{---} \text{---} \begin{array}{c} (2) \\ \diagup \quad \diagdown \\ z \quad z' \end{array} &= -2\beta \overset{\circ}{C}_a^{(2)} \partial \bar{\partial} \delta_a^z \partial \bar{\partial} \delta_a^{z'}
 \end{aligned} \tag{4.63b}$$

We have singled out the $\overset{\circ}{C}^{(2)}$ vertex since it may behave as any of the three diagrams in the right column depending on what other vertices it links to. As hinted at previously, since $\overset{\circ}{C}^{(2)}$ multiplies the square of a field operator, $(\partial \bar{\partial} h)^2$, it corresponds to a vertex with two identical legs and so is always accompanied by an additional factor of two due to the freedom to swap the legs.¹⁶ This is explicitly included in the two bottom right vertices, and the starred equality “ $\stackrel{*}{=}$ ” after the top right vertex is there to remind us that the factor of two should be included when $n = 2$.

For both the permanent source and interaction vertices we have explicitly included the particle worldline position z_a . When convenient—which is most of the time—we will drop the label (and dotted line) and let the vertex imply a sum over all particles.

As is hopefully apparent, the single versus double lines govern the connectivity of the vertices. In addition, we claim that no two legs labeled with circles shall be connected—these edge accents denote Laplacians, and two Laplacians on a link make it vanish. This is in accordance with our on-shell Hamiltonian and demonstrates why the exclusion of any worldline terms carrying the Euler-Lagrange derivative ∇^4 does not affect the partition function; the bi-Laplacian would nullify any link it appears on.

The usual Feynman rules include a numerical weight $1/S$ that accounts for the multiplicity and symmetries of each diagram. This *symmetry factor* S is simple for the linear and ring diagrams of Eq. (4.60): 2 and $2k$ respectively. The expansion into the various types of vertices (4.63) will reduce the symmetry of resulting diagrams, but the symmetry factors are still found in the same straightforward way: count and add together the number N_{refl} of reflections and the number N_{rot} of rotations under which the diagram is invariant. For linear diagrams, $S = 2$ if the diagram is invariant under reflection across the middle, otherwise $S = 1$. For ring diagrams, $S = 1 + N_{\text{refl}} + N_{\text{rot}}$.

Notice that each diagram will result in an overall factor of $\beta^{N_V + N_J - N_G}$, where N_V , N_J , and N_G are respectively the numbers of interaction (two-leg) vertices, source (one-leg) vertices, and propagators. The first two stem from the power in the Taylor expansion in Eq. (4.59), whereas the last is due to the propagator (4.62). For the linear diagrams, $N_G = N_V + 1$ and $N_J = 2$, resulting in an overall factor of β which cancels that from $-\beta \mathcal{U}$. This reminds us—and verifies—that the linear diagrams represent temperature-independent

¹⁶We mentioned on page 181 that this term would conventionally be accompanied by a factor of $1/2!$ for precisely this reason. The price we pay for keeping the $\Delta \mathcal{H}$ expansion compact is that we must be vigilant about the factors of two floating around.

ground state interactions. For the ring diagrams, $N_V = N_G$ and $N_J = 0$, resulting in an overall factor of β^0 for $-\beta\mathcal{U}$. That is, these contributions to the free energy are proportional to $k_B T$ and represent entropic, Casimir-type interactions.

To determine which diagrams contribute at a given order in inter-particle distance we can perform simple power counting of the diagram ingredients. Referring back to the list of Green function derivatives in Technical Note 4.4, we see that $\partial\bar{\partial}G$ is unitless, but both $\partial^n G$ and $\partial^{n-2}\partial\bar{\partial}G$ scale as $\sim r^{-(n-2)}$, with $r = |z|$. Since G itself scales as $\sim r^2$, the power-counting scheme follows: each link gives a power of 2 and each derivative reduces the power by one. Therefore, a given linear diagram will scale as $\sim r^{-p}$ with

$$p = \sum_{i=1}^{N_V} 2n_i^V + n_1^J + n_2^J - 2(N_V + 1), \quad (4.64)$$

where n^V and n^J are the derivative orders corresponding to a given interaction or source vertex, respectively. Similarly for ring diagrams,

$$p = \sum_{i=1}^{N_V} 2n_i^V - 2N_V. \quad (4.65)$$

Before proceeding with the calculations, we must address the problem of self-interactions—diagrams in which propagators begin and end on vertices on the same particle worldline. Similar to the previous chapter, we look at how self-interactions diverge and see that they are all power-like in the sense that $\partial^{n>2}G(\lambda\mathbf{x} - \lambda\mathbf{x}') \sim \lambda^{2-n}$ as $\lambda \rightarrow 0$, and therefore the RG flow is trivial and the divergences contain no physical information. These divergent contributions will always be removed by pure counterterms, so we can save ourselves the hassle and effectively ignore them. Diagrammatically this means we can safely drop *any* diagrams that contain self-interactions.

To summarize, computing interactions reduces down to drawing all relevant diagrams and evaluating them. The rules for evaluating the diagrams are straightforward: Every two-legged vertex labeled by a derivative order n , unless otherwise stated, affords a sum over all particles of the appropriate polarizability for the vertex (one of $C_a^{(n)}$, $\check{C}_a^{(n)}$, or $\check{\check{C}}_a^{(n)}$)—see Eqs. (4.63). Similarly, one-legged vertices contribute permanent charges $Q_a^{(n)}$ or $\check{Q}_a^{(n)}$ (or their complex conjugates) summed over all particles. Possible numerical factors are the (reciprocal) symmetry factor $1/S$, and the factors of 2 that accompany each occurrence of $\check{Q}^{(2)}$ and $\check{\check{C}}^{(2)}$, as explained following Eqs. (4.63a) and (4.63b). Each propagator is placed to link together the legs from two different vertices, and inherits their respective summation labels in its argument. From each leg, the propagator receives derivatives acting at the position variable of the associated vertex. The number of derivatives is equal to the derivative order n of the vertex if it is of types $C^{(n)}$, $\check{C}^{(n)}$, $Q^{(n)}$, or $\check{Q}^{(n)}$. If, however, it is of type $\check{\check{C}}^{(n)}$, the leg with the Laplacian (circle) has $n + 1$ derivatives and the other $n - 1$. If there is no Laplacian on the leg, all derivatives are either ∂ or $\bar{\partial}$ depending, respectively, on whether the link is plain or double. If there is a Laplacian on the leg, there is one $\bar{\partial}$ among

∂s , or vice versa. Finally, the sum over the particle labels must be done with the stipulation that no single propagator begins and ends on the same particle. One then extracts the terms from the sum in pairwise, tripletwise, *etc.*, fashion.

4.5 Elastic interactions

The interaction free energy \mathcal{U} consists of two parts, one proportional to $k_B T$ and the other to κ , stemming respectively from ring and linear diagrams. In this section, we will be concerned with terms of the latter type, and, since the interaction strength is set by the elastic modulus κ , we refer to them as *elastic* interactions. Note that with these interactions having *no* temperature dependence (at the scale where the Helfrich Hamiltonian is valid, that is), and the rest being linear in temperature, the elastic part constitutes the ground state ($T = 0$) energy E in $\mathcal{U} = E - TS$. Therefore we will use the symbol E for these interactions. We will begin with a discussion of particle pairs and then examine multibody effects.

4.5.1 Pair interactions

Recall that due to the freedom of the particles to move vertically and tilt, we do not have any field occurrence with less than 2 derivatives in $\Delta\mathcal{H}_f$ or $\Delta\mathcal{H}_p$. Equivalently, no vertex leg exists in our diagrams which differentiates the propagator less than twice, and since a propagator is differentiated at both ends, the least number of derivatives on a propagator is four. Hence, the lowest possible order in the interaction is achieved by a single propagator between two source vertices of derivative order 2 and, by Eq. (4.64), will scale as $\sim r^{-(2+2-2)} = r^{-2}$. The elastic interaction energy is therefore

$$-\beta E^{(2)} = 2 \operatorname{Re} \left[\overset{(2)}{\circ} \text{---} \overset{(2)}{\circ} + \overset{(2)}{\circ} \text{---} \overset{(2)}{\circ} \right], \quad (4.66)$$

where the Re operator appears since the complex conjugate of each diagram contributes as well. The superscript on the symbol E indicates the power of r^{-1} that is expected. Following the diagrammatic rules laid out earlier, these diagrams evaluate as

$$E^{(2)} = -\frac{2}{\beta} \sum'_{a,b} \operatorname{Re} \left[\frac{1}{2} \beta^2 Q_a^{(2)} Q_b^{(2)} \frac{\partial^4 G_{ab}}{\beta \kappa} + 2 \beta^2 \dot{Q}_a^{(2)} Q_b^{(2)} \frac{\partial^3 \bar{\partial} G_{ab}}{\beta \kappa} \right]. \quad (4.67)$$

The prime on the summation enforces $a \neq b$, since self-interaction terms are unphysical. In the above expression $G_{ab} \equiv G(\mathbf{z}_a - \mathbf{z}_b)$ and we have dropped the argument-dependence of the derivatives by transforming their variables to the full Green function argument. Following the diagrammatic rules, a factor of $1/2$ is included in the first term due to the reflection symmetry of its diagram, and a factor of 2 accompanying $\dot{Q}^{(2)}$ is also included.

After substitution of the Wilson coefficients and the Green function derivatives, we have

$$E_{\{1,2\}}^{(2)} = - \sum_{a \neq b} 2 \operatorname{Re} \left[\frac{1}{2} \kappa (8\pi)^2 S_a e^{2i\alpha_a} R_a^2 S_b e^{2i\alpha_b} R_b^2 \frac{2! \bar{z}}{16\pi z^3} + 2\kappa 8\pi J_a R_a^2 4\pi S_b e^{2i\alpha_b} R_b^2 \frac{-1! \bar{z}}{16\pi z^2} \right]. \quad (4.68)$$

This interaction involves only a maximum of two particles at once, as the diagrams clearly indicate, and therefore encodes only *pair* interactions. The resulting pair interaction between some arbitrarily chosen pair of particles, 1 and 2, is then sifted out from the above summation:

$$E_{\{1,2\}}^{(2)} = -8\pi\kappa \frac{R_1^2 R_2^2}{r^2} \left[2S_1 S_2 \cos(2\alpha_1 + 2\alpha_2) - S_1 J_2 \cos 2\alpha_1 - J_1 S_2 \cos 2\alpha_2 \right]. \quad (4.69)$$

This result was also worked out in Ref. [YD12], and earlier in Ref. [DF99b] up to explicit dependence on particle size and a differing angle convention.

Several physical insights can be gained by examining the angular and curvature dependencies of Eq. (4.69). When the mean curvatures J_a are of the same sign, the particles tend to align their principal axes of smallest curvature with the joining line between the particles (*i.e.*, $\alpha_a = \pi/2$ for $J_a > 0$, and $\alpha_a = 0$ for $J_a < 0$) and attract. To clarify the picture, each particle enforces a contact angle at the rim of $\gamma(\varphi) = -JR - SR \cos(2\varphi - 2\alpha)$ from the horizontal. For $J > 0$, the magnitude of this contact angle is greatest at $\varphi = \alpha$ (the direction of downward curvature) and smallest in the perpendicular direction. The above expression tells us that the lowest energy state occurs when the axes of smallest contact curvature line up. This makes sense energetically because this configuration minimizes the magnitude of interparticle membrane curvature. If J_a vanishes, as in the case of two perfect saddles, the particles are maximally attractive across the full range of orientations satisfying $\alpha_1 + \alpha_2 = 0 \pmod{\pi}$, at least to this order.

Notice that every term includes at least one factor of S -type. This implies that if both particles are curved, but axisymmetrically so, they will exert *no* force upon each other at this order. The $1/r^2$ interaction hinges entirely on the broken axisymmetry in particle curvature, which was pointed out earlier by Marchenko and Misbah [MM02]. We may understand this directly from our effective Hamiltonian: With axisymmetry, the term $Q^{(2)} \partial^2 h$ drops from the world line when $S_a = 0$, leaving only the rotationally invariant term, $\dot{Q}^{(2)} \partial \bar{\partial} h$ (recall $\nabla^2 \sim \partial \bar{\partial}$). The field therefore receives a Laplacian as it spreads out from one curvature-charge distribution, and then receives another when it interacts with the other particle, yielding an interaction proportional to $\nabla^2 \nabla^2 G(\mathbf{x}_a - \mathbf{x}_b) = 0$.

At the next order, the elastic energy takes the form

$$\begin{aligned}
 -\beta E^{(4)} = & \text{diagram 1} + \text{diagram 2} + \text{diagram 3} \\
 & + 2 \operatorname{Re} \left[\text{diagram 4} + \text{diagram 5} \right] + 2 \operatorname{Re} \left[\text{diagram 6} \right].
 \end{aligned} \tag{4.70}$$

Notice that since $\mathring{C}^{(2)} = 0$ there are no diagrams with a single circle on the quadratic vertex. Evaluating the diagrams (recall that both $\mathring{Q}^{(2)}$ and $\mathring{C}^{(2)}$ always come with a factor of two) gives the sum over particle worldlines

$$\begin{aligned}
 E^{(4)} = & \frac{1}{\kappa^2} \sum'_{a,b,c} \left\{ Q_a^{(2)} C_b^{(2)} \bar{Q}_c^{(2)} \partial^4 G_{ab} \bar{\partial}^4 G_{bc} \right. \\
 & + 2^2 \mathring{Q}_a^{(2)} C_b^{(2)} \mathring{Q}_c^{(2)} \partial^3 \bar{\partial} G_{ab} \partial^3 \bar{\partial} G_{bc} + 2 Q_a^{(2)} \mathring{C}_b^{(2)} \bar{Q}_c^{(2)} \partial^3 \bar{\partial} G_{ab} \bar{\partial}^3 \partial G_{bc} \\
 & + 2 \operatorname{Re} \left[2 \mathring{Q}_a^{(2)} C_b^{(2)} \bar{Q}_c^{(2)} \partial^3 \bar{\partial} G_{ab} \bar{\partial}^4 G_{bc} + \frac{1}{2} \times 2 Q_a^{(2)} \mathring{C}_b^{(2)} Q_c^{(2)} \partial^3 \bar{\partial} G_{ab} \partial^3 \bar{\partial} G_{bc} \right] \Big\} \\
 & - \frac{1}{\kappa} \sum'_{a,b} 2 \operatorname{Re} \left[Q_a^{(2)} \mathring{Q}_b^{(4)} \partial^5 \bar{\partial} G_{ab} \right],
 \end{aligned} \tag{4.71}$$

where the primes on the sums remind us that we exclude all self-interaction terms. Notice that the first sum contains not only pairwise interactions, but triplet interactions as well—the latter we will consider in the next section. Taking the terms that involve only a *pair* of particles, labeled 1 and 2, we obtain the first correction to the pair interaction. After a short calculation, which involves plugging in for the sources and polarizabilities, expanding the Green function derivatives using the lookup table in Technical Note 4.4, and simplifying, gives [YD12]

$$\begin{aligned}
 E_{\{1,2\}}^{(4)} = & 4\pi\kappa \frac{R_1^2 R_2^2}{r^4} \left[R_1^2 J_1^2 + R_2^2 J_2^2 + -4R_1^2 J_1 S_1 \cos 2\alpha_1 - 4R_2^2 J_2 S_2 \cos 2\alpha_2 \right. \\
 & + 5R_1^2 S_1^2 + 5R_2^2 S_2^2 + R_1^2 S_1^2 \cos 4\alpha_1 + R_2^2 S_2^2 \cos 4\alpha_2 \\
 & \left. + 6(R_1^2 + R_2^2) S_1 S_2 \cos(2\alpha_1 + 2\alpha_2) \right].
 \end{aligned} \tag{4.72}$$

As we mentioned previously, if the particles are axisymmetric, then both S_a vanish as well as the entire $\mathcal{O}(r^{-2})$ term. The interaction above therefore reduces to the lowest order interaction for axisymmetric particles, and, recalling that $\gamma_a = R_a J_a$ (no summation) are the detachment angles, can be expressed as

$$E_{\{1,2\}}^{(4)} = 4\pi\kappa (\gamma_1^2 + \gamma_2^2) \frac{R_1^2 R_2^2}{r^4}. \tag{4.73}$$

The calculation of the above interaction, Eq. (4.72), was also attempted in Ref. [DF99b];

however, the last term was missed. This term originates from the interaction between $Q^{(2)}$ and $\tilde{Q}^{(4)}$, the latter of which is not encoded if one treats a particle as a point curvature defect. This term turns out to be significant in determining the overall behavior of the interaction. The richness of the energy landscape—even at this order—is not adequately represented in the published literature where it appears (namely [YD12] and [YHD14]) so we will take an excursion to examine the preferred particle configurations in detail.

Minimum energy configurations

To simplify the discussion, we will consider identical particles such that $R_1 = R_2 = R$, $S_1 = S_2 = S$, and $|J_1| = |J_2| = J$. Since an inverted saddle ($S \rightarrow -S$) is equivalent to a saddle rotated by $\pi/2$ we will keep S positive without loss of generality. However, inverting one of the cap shapes ($J \rightarrow -J$) is qualitatively different, so we will consider each case separately with $J > 0$, $J_1 = J$, and $J_2 = \pm J$. To clean up the expressions, we define $\chi = r/R$ like before, and also define $\gamma_0 = RJ$ and $\eta = S/J$. The expression for γ_0 is the contact angle for an axisymmetric cap ($S = 0$), and η is the ratio of saddle to cap curvature. We may then write the interaction energy as

$$\frac{E_{\pm}}{4\pi\kappa\gamma_0^2} =: \tilde{E}_{\pm} = \tilde{E}_{\pm}^{(2)} + \tilde{E}_{\pm}^{(4)} + \mathcal{O}(\chi^{-6}), \quad (4.74)$$

where the \pm subscript corresponds to the sign of J_2 relative to J_1 , and the two contributions may be expressed as

$$\tilde{E}_{\pm}^{(2)} \chi^2 = 2\eta(\pm \cos 2\alpha_1 + \cos 2\alpha_2) - 4\eta^2 \cos(2\alpha_1 + 2\alpha_2), \quad (4.75)$$

$$\tilde{E}_{\pm}^{(4)} \chi^4 = 2 - 4\eta(\cos 2\alpha_1 \pm \cos 2\alpha_2) + \eta^2[10 + \cos 4\alpha_1 + \cos 4\alpha_2 + 12 \cos(2\alpha_1 + 2\alpha_2)]. \quad (4.76)$$

To begin, let us consider just the $\tilde{E}^{(4)}$ contribution. If the final term $\propto \cos(2\alpha_1 + 2\alpha_2)$ is missed as in Ref. [DF99b], then this contribution is always positive and therefore always repulsive, regardless of the sign of J_2 . Just to emphasize, without this term there is no possibility for this contribution to be attractive. Now, with the term included, the $\tilde{E}^{(4)}$ contribution is still always repulsive when $J_2 > 0$, but it can be attractive if $J_2 < 0$. In particular, if $J_2 < 0$ and $\eta > 1/4$, then the preferred configuration suggested by this contribution—that is, the minimum energy configuration of $\tilde{E}^{(4)}$ alone—is attractive. Furthermore, this preferred configuration occurs for $\alpha_1 = 0$ and $\alpha_2 = \pi/2$, but only until a critical ratio $\eta_c = 1$, after which it bifurcates into *two* degenerate minima:

$$\left. \begin{aligned} \alpha_1 &\equiv \pm \frac{1}{2} \cos^{-1} \frac{1}{\eta} \pmod{\pi} \\ \alpha_2 &\equiv \frac{\pi}{2} - \alpha_1 \pmod{\pi} \end{aligned} \right\}, \quad \eta \geq \eta_c = 1. \quad (4.77)$$

The energetic behavior of the $\tilde{E}^{(4)}$ contribution alone, however, does not present the full

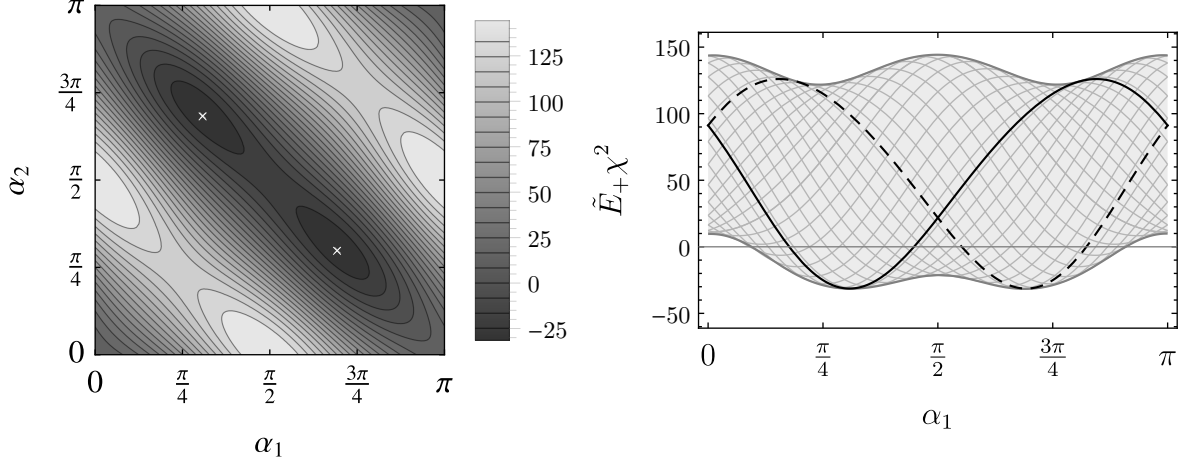


Figure 4.4: Visual representations of the interaction energy landscape, plotted as $\tilde{E}_+ \chi^2$, for the values $\chi = r/R = 2.5$ and $\eta = S/J = 6$. The two white crosses on the contour plot (left) show the points of minimum energy, which occur for $(\alpha_1, \alpha_2) \approx (0.3076, 0.6924)\pi$ and $(0.6924, 0.3076)\pi$. Notice that the energy exhibits reflection symmetry about the two lines $\alpha_2 = \alpha_1$ and $\alpha_2 = \pi - \alpha_1$. An alternative view of the energy is presented on the right by plotting the family of energy curves as a function of α_1 for fixed α_2 . The corresponding envelope provides information about the energy extremes. The global minimum gives the preferred angle α_1 , and α_2 follows from the curve which touches the minimum point.

story as it competes with the $\tilde{E}^{(2)}$ contribution. An analysis of both terms together is therefore prudent. We will consider the two cases $J_2 = \pm J$ separately.

Up-up ($J_2 = +J$) case. The energy landscape is determined by calculating the energy \tilde{E}_+ for various configurations of α_1 and α_2 . We present this visually as a contour plot in Fig. 4.4, where the preferred configurations are located at the minimum energy points. As an alternative representation, we may consider slicing up the $\alpha_1\alpha_2$ -plane and plotting the family of energy curves as a function of α_1 for various fixed values of α_2 . The global minimum of the envelope of these curves then yields the preferred angle α_1 , and α_2 comes from the curve that touches this minimum. One could of course proceed to find the energy minima numerically, but the functional form is tractable enough to examine the behavior completely analytically.

A useful starting point is to consider and exploit any symmetries the energy function exhibits. An obvious symmetry is the interchange of the two angles, $\alpha_1 \leftrightarrow \alpha_2$, which one may also observe from the contour plot in Fig. 4.4. More generally, we may look for reflection symmetry across a line $\alpha_2 = s\alpha_1 + \beta$, where s is the slope and β is the α_2 -intercept. The exchange symmetry is one such invariance with $s = 1$ and $\beta = 0$. To see how reflection across the line transforms the angle coordinates, we refer to Technical Note 4.5 with the identifications $y_0 \rightarrow \alpha_2$, $x_0 \rightarrow \alpha_1$, $m \rightarrow s$, and $b \rightarrow \beta$. Due to the particle symmetry and periodicity, we only need to consider (α_1, α_2) in the fundamental domain $[0, \pi)^2$ and keep

Technical Note 4.5: Point reflections across a line

Consider the point (x_0, y_0) reflected across the line $y = mx + b$. The new reflected point (x'_0, y'_0) is found by inverting the normal vector between the line and the point (x_0, y_0) . The construction is as follows: Translate the coordinate system so that the y -intercept occurs at the origin and let $\mathbf{v} = (x_0, y_0 - b)$ be the position vector from this new origin. Next, construct a unit vector $\hat{\mathbf{u}} = (1, m)/\sqrt{1 + m^2}$ that points along the reflection line, from which we then construct a unit normal vector to the line, $\hat{\mathbf{n}} = (-m, 1)/\sqrt{1 + m^2}$. The vector projection of \mathbf{v} in this normal direction is given by $\mathbf{v}_\perp = (\mathbf{v} \cdot \hat{\mathbf{n}})\hat{\mathbf{n}} = D\hat{\mathbf{n}}$ and therefore the vector reflection $\mathbf{v}' = \mathbf{v} - 2\mathbf{v}_\perp$. Translating back up by b then gives the reflected point

$$\begin{pmatrix} x'_0 \\ y'_0 \end{pmatrix} = \begin{pmatrix} x_0 + 2Dm/\sqrt{1 + m^2} \\ y_0 - 2D/\sqrt{1 + m^2} \end{pmatrix}, \quad D = \frac{-mx + (y - b)}{\sqrt{1 + m^2}}.$$

all angle results modulo π (the “angle space” defines a torus). Plugging the transformation into (4.74) shows that there are two reflection lines of symmetry, $\alpha_2 = \alpha_1$ and $\alpha_2 = \pi - \alpha_1$. Again, both lines of symmetry are apparent in Fig. 4.4.

The benefit of considering such reflection symmetries is that they provide hints about (or outright reveal) the locations of the maxima and minima. An application of either reflection transformation must preserve both numbers of global maxima and minima,¹⁷ otherwise it would contradict the invariance. Hence, if there is only one global minimum it *must* occur at the intersection of the two lines. Note that there are in fact *two* such intersections: There is the obvious intersection at $(\pi/2, \pi/2)$, but also one at $(0, 0)$ due to periodicity and our choice of fundamental domain. If there are two degenerate minima, then both points must either lie on one of the reflection lines *or* they must occur on the boundary, for which one or the other angle vanishes.¹⁸ We could of course generalize to a higher number of degenerate global minima; however, the energy function does not contain terms higher than doubly-periodic in this domain, so we expect *at most* two such solutions.

With this in mind, let us consider the energy along the line $\alpha_2 = \pi - \alpha_1$. If a minimum exists along this line, it must satisfy

$$\frac{\partial}{\partial \alpha_1} \tilde{E}_+(\alpha_1, \pi - \alpha_1) = -\frac{8\eta}{\chi^4} \sin 2\alpha_1 (\chi^2 - 2 + 2\eta \cos 2\alpha_1) = 0, \quad (4.78)$$

where we have simplified the expression using $\sin 4\alpha_1 = 2 \sin 2\alpha_1 \cos 2\alpha_1$. Along this line, this expression vanishes when either $\sin 2\alpha_1 = 0$ or the terms in parentheses sum to zero. The first solution gives $\alpha_1 = \alpha_2 = \pi/2$ along the line. Setting the terms in parentheses to zero gives the solution

$$\cos 2\alpha_1 = -\frac{\chi^2 - 2}{2\eta}, \quad (4.79)$$

¹⁷It must in fact preserve the number of *all* critical points, including saddles points.

¹⁸Recall that the fundamental domain identifies 0 and π , so having solutions on the boundary does not double the number of critical points as it appears to suggest in the contour plot of Fig. 4.4.

which in the fundamental domain corresponds to the two angle solutions

$$\alpha_1 = \frac{\pi}{2} \pm \frac{1}{2} \cos^{-1} \left(\frac{\chi^2 - 2}{2\eta} \right) \quad (4.80)$$

with $\alpha_2 = \pi - \alpha_1$ for each. Since $\eta \geq 0$ and $\chi \geq 2$ by definition (the particles overlap when $\chi < 2$), this solution is only valid when $-1 \leq (\chi^2 - 2)/2\eta \leq 1$. That is, for the fixed curvature ratio η , this solution only applies up to a critical separation distance: $2 \leq \chi \leq \chi_c$ with $\chi_c := \sqrt{2(\eta + 1)}$. We could instead consider a fixed distance χ , for which the solution applies when the curvature ratio is larger than a critical value $\eta_c := (\chi^2 - 2)/2$.

For the plots in Fig. 4.4 we used $\eta = 6$ and $\chi = 5/2$. The corresponding critical values are $\eta_c = 17/8 = 2.125$ and $\chi_c = \sqrt{14} \approx 3.742$, so the plots are indeed in the two-minima regime. To check that these points indeed correspond to energy minima, we check the second derivative:

$$\frac{\partial^2}{\partial \alpha_1^2} \tilde{E}_+(\alpha_1, \pi - \alpha_1) = -\frac{32\eta^2}{\chi^4} \left[\frac{(\chi^2 - 2)}{2\eta} \cos 2\alpha_1 + (2 \cos^2 2\alpha_1 - 1) \right]. \quad (4.81)$$

Using $(\chi^2 - 2)/2\eta = \eta_c/\eta$, we find for the value $\alpha_1 = \pi/2$ that

$$\frac{\partial^2}{\partial \alpha_1^2} \tilde{E}_+(\alpha_1, \pi - \alpha_1) = -\frac{32\eta}{\chi^4} (\eta - \eta_c). \quad (4.82)$$

This point can only be a minimum if the second derivative is positive, so this tells us that $\alpha_1 = \pi/2$ corresponds to an energy minimum only when $\eta < \eta_c$. For the other solution, we use the simplified expression $\cos 2\alpha_1 = -\eta_c/\eta$ which gives for the second derivative

$$\frac{\partial^2}{\partial \alpha_1^2} \tilde{E}_+(\alpha_1, \pi - \alpha_1) = \frac{32}{\chi^4} (\eta^2 - \eta_c^2), \quad (4.83)$$

showing that this corresponds to a minimum when $\eta > \eta_c$, which indeed matches the condition for which this solution applies. For the plots in Fig. 4.4, the minima occur for the angles

$$\alpha_1 = \frac{\pi}{2} \pm \frac{1}{2} \cos^{-1} \left(\frac{17}{48} \right) \approx \frac{\pi}{2} \pm 0.6044 \quad (4.84)$$

and therefore occur for the configurations $(\alpha_1, \alpha_2) \approx (0.6924, 0.3076)\pi$ and $(0.3076, 0.6924)\pi$.

To summarize, up to $\mathcal{O}(\chi^{-6})$ corrections $E_+(\alpha_1, \alpha_2)$ is minimized for

$$\alpha_1 = \begin{cases} \frac{\pi}{2} \pm \frac{1}{2} \cos^{-1} \left(\frac{\chi^2 - 2}{2\eta} \right) & \text{if } 2 \leq \chi \leq \sqrt{2(\eta + 1)} \\ \frac{\pi}{2} & \text{if } \chi \geq \sqrt{2(\eta + 1)} \end{cases}, \text{ and } \alpha_2 = \pi - \alpha_1. \quad (4.85)$$

This behavior is illustrated in Fig. 4.5. For a fixed curvature ratio η , there are two degenerate

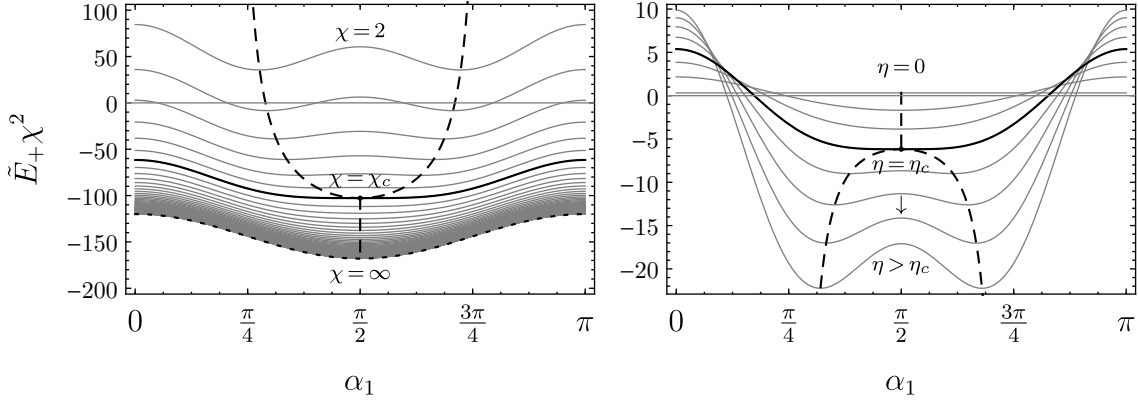


Figure 4.5: Illustration of the minimum-energy bifurcation behavior along the line $\alpha_2 = \pi - \alpha_1$. The left plot is for a fixed curvature ratio $\eta = 6$ and shows the “binodal” lines (dashed) which trace out the energy minima. Observe that as the scaled separation χ is increased, the minima merge into one solution at a critical distance χ_c . Note that the particles overlap for $\chi < 2$, so the configurations at contact are curvature dependent and occur in the open interval $\frac{\pi}{4} < \alpha_1 < \frac{3\pi}{4}$ and are symmetric about $\alpha_1 = \pi/2$. The right plot is for a fixed separation $\chi = 2.5$ and shows the bifurcation of the energy minima beyond a critical curvature ratio η_c . The solutions asymptote to $\alpha_1 = \pi/2 \pm \pi/4$.

minimum energy configurations which, as the particle separation is increased, ultimately merge into one configuration $(\pi/2, \pi/2)$ at and after a critical separation $\chi_c = \sqrt{2(\eta + 1)}$. Analogously, at a fixed (scaled) distance χ , we may consider increasing the curvature ratio η from zero and find one minimum at $(\pi/2, \pi/2)$ up to a critical ratio $\eta_c = (\chi^2 - 2)/2$ at which point it bifurcates into two degenerate energy minima that asymptote to $(3\pi/4, \pi/4)$ and $(\pi/4, 3\pi/4)$.

Up-down ($J_2 = -J$) case. For the case in which the “cap” nature of the two particles is anti-aligned ($J_2 = -J_1 = -J$), we may apply the same analysis. Applying the reflection transformation from Technical Note 4.5, we find the energy E_- is symmetric across the two lines $\alpha_2 = \alpha_1 - \pi/2$ and $\alpha_2 = \pi/2 - \alpha_1$, each modulo π . In this case, the most convenient choice of fundamental domain is to shift α_1 by a phase: $(\alpha_1, \alpha_2) \in (-\frac{\pi}{2}, \frac{\pi}{2}] \times [0, \pi)$.

Within this domain, consider the energy along the line $\alpha_2 = \alpha_1 + \pi/2$. The extreme values along this line must satisfy

$$\frac{\partial}{\partial \alpha_1} \tilde{E}_+(\alpha_1, \alpha_1 + \pi/2) = \frac{8\eta}{\chi^4} \sin 2\alpha_1 [\chi^2 + 2 - 2\eta(2\chi^2 - 5) \cos 2\alpha_1] = 0. \quad (4.86)$$

One may check using the same procedure as before that the solutions to the above equation correspond to energy minima and exhibit a similar bifurcation behavior as in the E_+ case.

The minimum energy configurations are therefore given by

$$\alpha_1 = \begin{cases} \pm \frac{1}{2} \cos^{-1} \left[\frac{\chi^2 + 2}{2\eta(2\chi^2 - 5)} \right] & \text{if } \chi^2 + 2 \leq 2\eta(2\chi^2 - 5), \text{ and } \alpha_2 = \alpha_1 + \frac{\pi}{2}. \\ 0 & \text{if } \chi^2 + 2 \geq 2\eta(2\chi^2 - 5) \end{cases} \quad (4.87)$$

The bifurcation picture in this case is a bit more subtle. For a fixed separation χ , there is a single energy minimum at $(0, \pi/2)$ as η is increased from zero until a critical ratio $\eta_c = (\chi^2 + 2)/[2(2\chi^2 - 5)]$, after which there are two minima. For a fixed curvature ratio η we the picture is as follows: If $0 \leq \eta \leq \frac{1}{4}$, there is the single solution for all separations $\chi \geq 2$. If $\frac{1}{4} < \eta \leq 1$, then there is the single solution until a critical separation $\chi_c^2 = 2(5\eta + 1)/(4\eta - 1)$, after which it bifurcates into two degenerate energy minima. When the curvature ratio $\eta > 1$, there are always two degenerate minima.

Attractive versus repulsive. The energy considerations above may alternatively be interpreted as describing a “phase transition” from one ground state configuration to two degenerate configurations. From this perspective we may construct a phase diagram in the $\chi\eta$ -plane, wherein the regions of one versus two minima are separated by a critical line. This critical line depends on the sign of J_2 relative to J_1 and may be expressed as either

$$\chi_c(\eta) = \begin{cases} \sqrt{2(\eta + 1)} & \text{if } J_2 = +J_1 \\ \sqrt{\frac{2(5\eta + 1)}{4\eta - 1}} & \text{if } J_2 = -J_1 \end{cases} \quad (4.88)$$

or

$$\eta_c(\chi) = \begin{cases} \frac{1}{2}(\chi^2 - 2) & \text{if } J_2 = +J_1 \\ \frac{\chi^2 + 2}{2(2\chi^2 - 5)} & \text{if } J_2 = -J_1 \end{cases}. \quad (4.89)$$

Note that for $J_2 = -J_1$, the critical line only occurs in the interval $\frac{1}{4} < \eta \leq 1$ since $\chi \geq 2$ and $\eta > 0$.

Missing from this discussion is whether the preferred configurations are attractive or repulsive. We have looked at the angular configurations that minimize the energy, but the force depends on the spatial gradient of the energy. Since the two contributions (4.75) and (4.76) differ in powers of χ , the sign of the forces is not necessarily in agreement with the sign of the energy in the preferred angular configurations.

To proceed, we examine the dimensionless force

$$\tilde{F} := \frac{R}{4\pi\kappa\gamma_0^2} F = -\frac{\partial}{\partial\chi} \tilde{E} = \frac{2}{\chi^3} \tilde{E}^{(2)} + \frac{4}{\chi^5} \tilde{E}^{(4)} + \mathcal{O}(\chi^{-7}) \quad (4.90)$$

evaluated at the minimum energy configurations. The phase diagram will then consist of two regions in the $\chi\eta$ -plane divided by the critical line $\chi_c(\eta)$, each of which will be further divided into attractive and repulsive subregions depending on the sign of the force for the minimum energy configurations. Thus, there are four cases to study:

1. $J_2 = +J_1$, $\chi \geq \chi_c$. The preferred configuration is $\alpha_1 = \alpha_2 = \pi/2$, and the corresponding force $\tilde{F}_{>}^+$ is

$$\tilde{F}_{\chi \geq \chi_c}^+ = \frac{8}{\chi^5} [1 + 4\eta(3\eta + 1) - \chi^2\eta(\eta + 1)]. \quad (4.91)$$

The force vanishes along the curve

$$\chi_{>}^+(\eta) = \sqrt{\frac{1 + 4\eta(3\eta + 1)}{\eta(\eta + 1)}} \quad (4.92)$$

which divides the region $\chi \geq \chi_c(\eta)$ into an attractive ($F < 0$) region when $\chi > \chi_{>}^+(\eta)$ and a repulsive ($F > 0$) region when $\chi < \chi_{>}^+(\eta)$.

2. $J_2 = +J_1$, $\chi \leq \chi_c$. The preferred configuration is given by Eq. (4.85), which fed into the force expression gives

$$\tilde{F}_{\chi \leq \chi_c}^+ = \frac{8}{\chi^5} [\chi^2 - 1 + \eta^2(10 - \chi^2)]. \quad (4.93)$$

The region $\chi \leq \chi_c(\eta)$ is therefore divided by the curve

$$\chi_{<}^+(\eta) = \sqrt{\frac{10\eta^2 - 1}{\eta^2 - 1}} \quad (4.94)$$

into an attractive region when $\chi > \chi_{<}^+(\eta)$ and a repulsive region when $\chi < \chi_{<}^+(\eta)$. Note that all critical curves meet at the same point (χ_c^*, η_c^*) , where a short calculation shows

$$\eta_c^* = \frac{1}{6} \left[8 + \left(710 + 18\sqrt{201} \right)^{1/3} + \left(710 - 18\sqrt{201} \right)^{1/3} \right] \approx 4.26215, \quad (4.95a)$$

$$\chi_c^* = \sqrt{2(\eta_c^* + 1)} \approx 3.24412. \quad (4.95b)$$

3. $J_2 = -J_1$, $\eta \leq \eta_c$. In this case there is one preferred configuration of $(\alpha_1, \alpha_2) = (0, \pi/2)$ with the corresponding force

$$\tilde{F}_{\eta \leq \eta_c}^- = \frac{8}{\chi^5} [1 - 4\eta + \chi^2\eta(\eta - 1)]. \quad (4.96)$$

The region $\eta \leq \eta_c(\chi)$ is therefore divided by the curve

$$\chi^-(\eta \leq \eta_c) = \sqrt{\frac{4\eta - 1}{\eta(\eta - 1)}} \iff \eta_{<}^-(\chi) = \frac{1}{2\chi^2} \left(\chi^2 + 4 - \sqrt{\chi^4 + 4\chi^2 + 16} \right) \quad (4.97)$$

into an attractive region $\eta > \eta_{<}^-(\chi)$ and a repulsive region $\eta < \eta_{<}^-(\chi)$.

4. $J_2 = -J_1$, $\eta \geq \eta_c$. Here there are two preferred angular configurations given by Eq. (4.87). The corresponding force is given by

$$\tilde{F}_{\eta \geq \eta_c}^- = -\frac{4}{\chi^2(2\chi^2 - 5)^2} \left[\chi^6 + 42\chi^2 - 70 - 2\eta^2(2\chi^2 - 5)^2(10 - \chi^2) \right]. \quad (4.98)$$

The region $\eta \geq \eta_c(\chi)$ is therefore divided by the curve

$$\eta_{>}^-(\chi) = \sqrt{\frac{\chi^6 + 42\chi^2 - 70}{2(10 - \chi^2)(2\chi^2 - 5)^2}} \quad (4.99)$$

into an attractive region $\eta < \eta_{>}^-(\chi)$ and a repulsive region $\eta > \eta_{>}^-(\chi)$.

The final phase portraits in the $\chi\eta$ -plane are presented and summarized in Fig. 4.6

Higher orders for axisymmetric particles

If we wish to calculate higher-order corrections, we simply follow the machinery laid out by the Feynman rules. To demonstrate, let us consider axisymmetric particles ($S_a = 0$) to keep the number of terms reasonable. Then, the only source vertex is of the type $\hat{Q}^{(2)}$, which carries a Laplacian and has a strength given by Eq. (4.57b). For axisymmetric particles there is no interaction of r^{-2} dependence—the leading-order interaction is given by Eq. (4.72) with $S_a = 0$. The first correction therefore involves six powers of inverse distance, and will be given by the diagrams

$$-\beta E^{(6)} = 2 \operatorname{Re} \left[\text{diagram 1} + \text{diagram 2} \right]. \quad (4.100)$$

Many-body interactions involving two, three, and four particles at once can be extracted from this interaction, as the number of vertices in the diagrams suggest, but we will limit ourselves to pair interaction for the moment. Extracting, as usual, the pair interaction between particles 1 and 2, one has [YD12]

$$\begin{aligned} E_{\{1,2\}}^{(6)} &= -16\pi\kappa J_1 J_2 \frac{R_1^4 R_2^4}{r^6} + 8\pi\kappa (J_1^2 + J_2^2) \frac{R_1^4 R_2^4}{r^6} \\ &= 8\pi\kappa (J_1 - J_2)^2 \frac{R_1^4 R_2^4}{r^6}, \end{aligned} \quad (4.101)$$

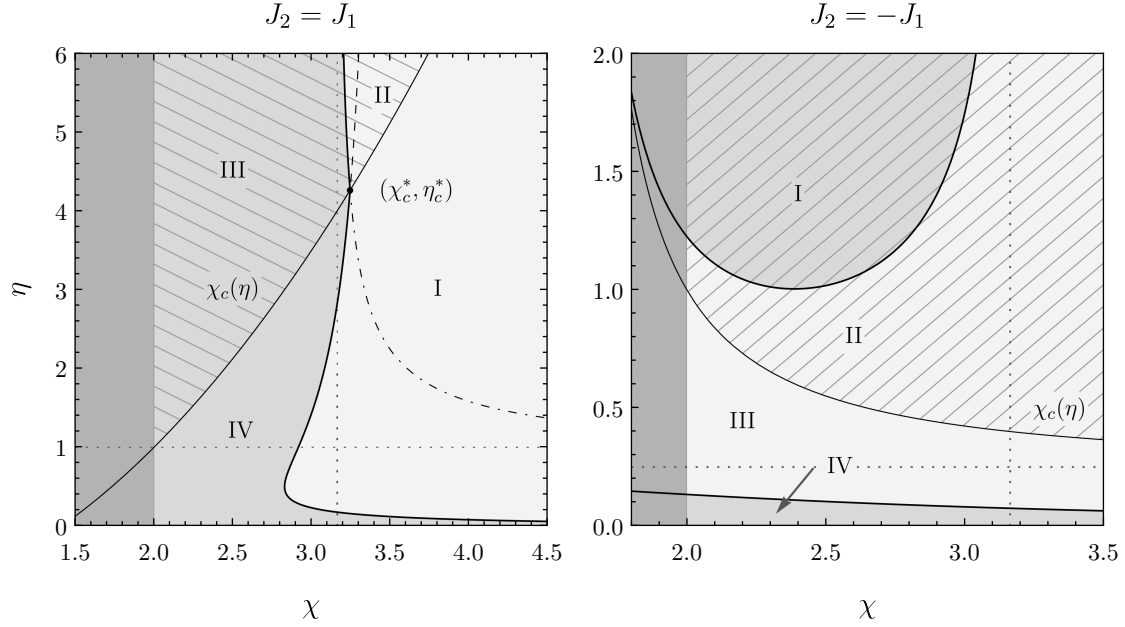


Figure 4.6: Illustrations of the phase portraits in the up-up (left plot) and up-down (right plot) cases. Each portrait in the $\chi\eta$ -plane is divided by a critical curve $\chi_c(\eta)$ into two regions with either one or two preferred (minimum energy) angular configurations. The two-minima regions are denoted by hatch lines. These regions are further subdivided into subregions for which the preferred configurations are either attractive (light gray) or repulsive (darker gray). The darkest regions for $\chi < 2$ are forbidden and correspond to the particles overlapping. The vanishing force lines (solid lines)—presented in the text—are extended (dashed and dot-dashed lines) beyond their corresponding regions for clarity. The dotted lines indicate asymptotes. In the left plot, the regions correspond to I: one attractive minimum, II: two attractive minima, III: two repulsive minima, and IV: one repulsive minimum. Observe that all lines meet at a special point $(\chi_c^*, \eta_c^*) \approx (3.24412, 4.26215)$ [see Eqs. (4.95)]. In the right plot, the regions correspond to I: two repulsive minima, II: two attractive minima, III: one attractive minimum, and IV: one repulsive minimum. Note that in both plots, as $\eta \rightarrow 0$ (*i.e.*, for axisymmetrically curved particles) the preferred configurations become repulsive for all separations (at least to this order), but at larger separations any small anisotropy in curvature ($S \neq 0$) will change the behavior from repulsive to attractive.

where the two separate terms in the first line originate from the two diagrams in Eq. (4.100), respectively. The calculation of this order was attempted in Ref. [DF99a], but due to the point curvature defect assumption the second term could not be calculated. Again, the neglect of this term leads to an interaction which seems to be attractive or repulsive depending on the signs of J_a . However, the two terms complete a square $\sim (J_1 - J_2)^2$ so the correct interaction is strictly repulsive, and it vanishes if the two curvatures are equal.

Continuing to higher orders is not conceptually difficult—one needs to just follow the recipe and pay attention to power counting (and factors of two). From Eq. (4.64) it follows that an order r^{-2p} diagram with k vertices of multipole orders n_i must satisfy $\sum_{i=1}^k n_i = p + k - 1$, resulting in the following expansion for the next two orders:

$$\begin{aligned}
 -\beta E^{(8)} = & \text{Diagram 1} + 2 \operatorname{Re} \left[\text{Diagram 2} + \text{Diagram 3} \right] \\
 & + \text{Diagram 4} + \text{Diagram 5} \\
 & + 2 \operatorname{Re} \left[\text{Diagram 6} \right]
 \end{aligned} \tag{4.102}$$

$$\begin{aligned}
 -\beta E^{(10)} = & \text{Diagram 1} + 2 \operatorname{Re} \left[\text{Diagram 2} + \text{Diagram 3} \right] \\
 & + 2 \operatorname{Re} \left[\text{Diagram 4} + \text{Diagram 5} \right] \\
 & + \text{Diagram 6} + 2 \operatorname{Re} \left[\text{Diagram 7} \right] \\
 & + \text{Diagram 8} + \text{Diagram 9} \\
 & + \text{Diagram 10} + 2 \operatorname{Re} \left[\text{Diagram 11} \right] \\
 & + \text{Diagram 12} + 2 \operatorname{Re} \left[\text{Diagram 13} \right] \\
 & + \text{Diagram 14} + \text{Diagram 15}
 \end{aligned} \tag{4.103}$$

We may then extract the pair interactions as usual and simplify. The resulting expressions enjoy similar simplification and show that the interaction is still strictly repulsive:

$$E_{\{1,2\}}^{(8)} = 12\pi\kappa \frac{R_1^4 R_2^4}{r^8} \left[J_1^2 R_1^2 + J_2^2 R_2^2 + (J_1 - J_2)^2 (R_1^2 + R_2^2) \right] \tag{4.104}$$

$$E_{\{1,2\}}^{(10)} = 16\pi\kappa \frac{R_1^4 R_2^4}{r^{10}} \left[(J_1 R_1^2 + J_2 R_2^2)^2 + (J_1 - J_2)^2 (R_1^4 + R_2^4 + 5R_1^2 R_2^2) \right] \tag{4.105}$$

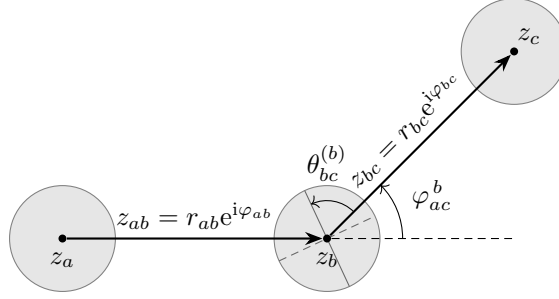


Figure 4.7: Illustration of the parameter definitions in a multibody configuration involving three particles situated at the coordinates z_a , z_b , and z_c with $z_{ab} = z_b - z_a$ and similar. The exterior angle φ_{ac}^b is measured from the joining line between particles a and b . The orientation angle $\theta_{bc}^{(b)}$ of particle b is measured from the line joining particles b and c to the principle axis of positive “saddle” curvature of the particle contact line.

4.5.2 Multibody interactions

The leading order triplet interactions come from the first sum in Eq. (4.71), where a maximum of three particle labels can be mixed. These interactions depend on the (three) separations between each pair of particles, as well as the orientations of their principal axes, in a way that cannot be decomposed as a sum over pairs. Since these interactions now mix the particle coordinates, it is useful to define $z_{ab} := z_b - z_a =: r_{ab} e^{i\varphi_{ab}}$ as well as the exterior vertex angle $\varphi_{ac}^b := -\varphi_{ab} + \varphi_{bc}$ between three particles situated at positions z_a , z_b , and z_c (see Fig. 4.7). Similarly, define the angle which the principal axis of a particle at position z_a makes with the joining line z_{ab} as $\theta_{ab}^{(a)} := \alpha_a - \varphi_{ab}$. With these variables we can write the final result in a coordinate-free manner.

As a consequence of dropping the self-interaction terms, the sum over the three particles’ worldlines can be written as the sum over all permutations of particle labels $\{1, 2, 3\}$. For terms symmetric in the two endpoint worldline labels, the sum can be instead written as twice the sum over only *cyclic* permutations:

$$\sum_{a,b,c}^{\text{perm.}} \rightarrow 2 \sum_{a,b,c}^{\text{cyc.}} \quad (\text{if symmetric under } a \leftrightarrow c)$$

The final result is¹⁹

$$\begin{aligned}
 E_{\{1,2,3\}}^{(4)} = & 8\pi\kappa \sum_{a,b,c}^{\text{cyc.}} \frac{R_a^2 R_b^2 R_c^2}{r_{ab}^2 r_{bc}^2} \left[S_a S_c \cos(2\theta_{ab}^{(a)} - 2\theta_{bc}^{(c)}) \right. \\
 & + 4S_a S_c \cos(2\varphi_{ac}^b + 2\theta_{ab}^{(a)} - 2\theta_{bc}^{(c)}) \\
 & + S_a S_c \cos(2\theta_{ab}^{(a)} + 2\theta_{bc}^{(c)}) + J_a J_c \cos 2\varphi_{ac}^b \Big] \\
 & - 16\pi\kappa \sum_{a,b,c}^{\text{perm.}} \frac{J_a R_a^2 R_b^2 R_c^2 S_c}{r_{ab}^2 r_{bc}^2} \cos(2\varphi_{ac}^b - 2\theta_{bc}^{(c)}). \tag{4.106}
 \end{aligned}$$

In the case of axisymmetric particles ($S_a = 0$), this reduces to the simple form [YD12]

$$E_{\{1,2,3\}}^{(4)} = 8\pi\kappa \sum_{a,b,c}^{\text{cyc.}} \frac{R_a^2 R_b^2 R_c^2}{r_{ab}^2 r_{bc}^2} J_a J_c \cos 2\varphi_{ac}^b, \quad (S_a = 0). \tag{4.107}$$

Notice that this triplet term has the same order (distance⁻⁴) as the pair force (4.72). Indeed, the pair force originates with a curvature charge polarizing a second particle, which then interacts back with the first charge. In this triplet term the polarized second particle instead interacts with the curvature charge of a third particle. Still, both cases involve two curvature charges and a quadrupole polarizability. Because of this kinship, it is actually possible to express the lowest order (axisymmetric) pair and triplet term in a single formula. Defining $\gamma_a = R_a J_a$ (no summation) and $\zeta_{ab} = z_{ab}/\sqrt{R_a R_b}$, the sum of all pair- and triplet-interactions between N axisymmetric particles can be written as

$$\begin{aligned}
 E^{(4)} &= 4\pi\kappa \sum_{a=1}^N \left(\sum_{b \neq a} \frac{\gamma_b^2}{\zeta_{ab}^2 \bar{\zeta}_{ab}^2} + \sum_{\substack{c \neq b \neq a \\ c \neq a}} \frac{\gamma_c \gamma_b}{\zeta_{ca}^2 \bar{\zeta}_{ab}^2} \right) \\
 &= 4\pi\kappa \sum_{a=1}^N \left| \sum_{b \neq a} \frac{\gamma_b}{\zeta_{ab}^2} \right|^2. \tag{4.108}
 \end{aligned}$$

This elegant formula was first derived by Kim *et al.* [KNO98] using rather different techniques. These authors apply it to explore the interactions between N particles in special arrangements. For instance, they prove that five identical particles placed at the corners of a regular pentagon and subject to the potential energy (4.108) are “geometrically stable” (*i.e.*, (only) affine deformations of the plane leave the energy invariant). However, this result

¹⁹The angles defined have the properties $\varphi_{ca}^b = -\varphi_{ac}^b$ and $\theta_{ac}^{(c)} = \theta_{ca}^{(c)}$. Since cosine is even, it follows then that all the terms in summation over cyclic permutations are indeed symmetric under $a \leftrightarrow c$.

actually holds only approximately, since five particles will also be subject to quadruplet and quintuplet interactions: even though Eq. (4.108) involves the coordinates of N particles, it is *not actually* an N -body potential; it only contains the pair and triplet contributions to the full N -body potential. Quadruplet and quintuplet interactions begin to appear at orders distance $^{-6}$ and distance $^{-8}$ respectively, along with further pair and triplet interactions. Although we will not explore it here, it is possible that these contributions may disrupt the proposed geometric stability.

We leave higher order (in multibody as well as in terms of distance dependence) terms at this point, and move on to interactions that arise from thermal fluctuations.

4.6 Entropic interactions

We have seen above how permanent deformations on the particles propagate to other particles and initiate interactions. The strength of these interactions were set by the elastic modulus associated with the intervening medium. In addition to these permanent curvature charges, however, thermal fluctuations induce fluctuating charges due to the boundary conditions around the particles. Interactions initiated by these induced fluctuating charges are akin to Casimir interactions from electrodynamics. To the quadratic order we have written our theory, we have stated several times that the free energy of interaction \mathcal{U} is made up of two parts, one proportional to κ and the other proportional to $k_B T$. These Casimir-like interactions are the latter, and we refer to them as *entropic* since they constitute the $-TS =: U$ in the free energy $E - TS$. As mentioned previously, these interactions are contained within all the ring diagrams of Eq. (4.60). The leading order contribution comes from a diagram with two links, each differentiated twice at every leg, hence scaling as $(R/r)^{-4}$, and is given by the two induced quadrupolar interactions

$$-\beta U^{(4)} = \text{Diagram 1} + \text{Diagram 2} . \quad (4.109)$$

Evaluating the diagrams gives the well known result for pairs [GBP93a, GBP93b, GGK96b, GGK96a, PL96, DF99a, DF99b, HW01, YRD11, YD12]

$$\begin{aligned} \beta U_{\{1,2\}}^{(4)} &= - \sum_{a \neq b} \left[\frac{1}{2} C_a^{(2)} C_b^{(2)} \frac{\partial^4 G_{ab}}{\kappa} \frac{\bar{\partial}^4 G_{ba}}{\kappa} + 2 \bar{C}_a^{(2)} C_b^{(2)} \frac{\partial^3 \bar{\partial} G_{ab}}{\kappa} \frac{\bar{\partial}^3 \partial G_{ba}}{\kappa} \right] \\ &= -(4+2) \frac{R_1^2 R_2^2}{r^4} = -6 \frac{R_1^2 R_2^2}{r^4} . \end{aligned} \quad (4.110)$$

In the above calculation, the factor of $1/2$ comes from the reflection symmetry of the first diagram across the horizontal, and as before each $\bar{C}^{(2)}$ comes with a factor of two.

We had quite a few examples on how to apply the Fenyman rules to obtain algebraic

the result in Ref. [YD12],

$$\begin{aligned}
 \beta U_{\{1,2\}}^{(8)} &= - \sum_{a \neq b} \left\{ \left(\frac{48 \cdot 2}{2} - 2 \cdot 24 + 0 + (12 + 3) \right) \frac{R_a^6 R_b^2}{r^8} \right. \\
 &\quad \left. + \left(\frac{576}{2} - 2 \cdot 144 - \frac{36}{2} + 36 \right) \frac{R_a^4 R_b^4}{r^8} + \left(\frac{16}{4} + 4 + \frac{1}{2} + \frac{1}{2} \right) \frac{R_a^4 R_b^4}{r^8} \right\} \\
 &= - \frac{15 R_1^2 R_2^6 + 54 R_1^4 R_2^4 + 15 R_1^6 R_2^2}{r^8}.
 \end{aligned} \tag{4.114}$$

In the above calculation, the first term in parentheses corresponds to the quadrupole–hexadecapole two-vertex diagrams, the second term corresponds to the octupole–octupole two-vertex diagrams, and the third line corresponds to the four-vertex diagrams of quadrupole vertices. The symmetry factors were also kept explicit for clarity.

It is clear that cranking out higher-order contributions to any desired order is a straightforward task, albeit cumbersome, given how the number of diagrams begins to proliferate. However, the formalism is amenable to implementation in symbolic algebra software such as MATHEMATICA. This was also done up to $\mathcal{O}(R^{20}/r^{20})$ in Ref. [YD12] and we quote the result

$$\begin{aligned}
 \beta U_{\{1,2\}} &= - \frac{6}{\chi^4} - \frac{20}{\chi^6} - \frac{84}{\chi^8} - \frac{344}{\chi^{10}} - \frac{1\,388}{\chi^{12}} - \frac{5\,472}{\chi^{14}} \\
 &\quad - \frac{21\,370}{\chi^{16}} - \frac{249\,968}{3\chi^{18}} - \frac{1\,628\,876}{5\chi^{20}} - \dots,
 \end{aligned} \tag{4.115}$$

where it was assumed that $R_1 = R_2 = R$ and $\chi = r/R$, for the sake of a compact expression.

Multibody interactions

Let us now consider multibody entropic interactions. The leading-order is a *triplet* interaction given by

$$\begin{aligned}
 -\beta U_{\{1,2,3\}}^{(6)} &= 2 \operatorname{Re} \left(\text{Diagram} \right) \\
 &= -\frac{1}{2} \sum_{a,b,c}^{\text{perm. } \{1,2,3\}} \frac{2}{\kappa^3} \operatorname{Re} \left[2 \bar{C}_a^{(2)} C_b^{(2)} C_c^{(2)} \partial^3 \bar{\partial} G_{ab} \bar{\partial}^4 G_{bc} \partial^3 \bar{\partial} G_{ca} \right],
 \end{aligned} \tag{4.116}$$

where the factor of $1/2$ is due to reflection symmetry of the diagram across the vertical. Since this expression is invariant under $b \leftrightarrow c$, we can evaluate this as twice the sum over cyclic permutations. Recalling the exterior angle definition $\varphi_{ac}^b := -\varphi_{ab} + \varphi_{bc}$, we arrive at

the final result [YD12]

$$\beta U_{\{1,2,3\}}^{(6)} = 4 \frac{R_a^2 R_b^2 R_c^2}{r_{ab}^2 r_{bc}^2 r_{ca}^2} \sum_{a,b,c}^{\text{cyc.}} \cos(2\varphi_{ac}^b - 2\varphi_{ba}^c). \quad (4.117)$$

This interaction can be attractive or repulsive, depending on the angles. However, one may have to be more specific about what is meant by attractive (or repulsive) when there are more than two distances involved: The distance dependence is contained in the fraction above. If it is multiplied by a negative (or positive) quantity, then the free energy of interaction decreases when *all* distances are *scaled down* (or *scaled up*) at once. Under such an interpretation, this triplet interaction can definitely be repulsive for appropriate relative placings of the three particles (*i.e.*, angles φ_{ac}^b). As such, particles converging in on each other is not *necessarily* favorable energetically (or entropically, since these are entropic forces). Therefore, the common conceptualization of entropic forces as arising from a desire to free up more space for the field to fluctuate must be taken with a grain of salt.

Let us more precisely investigate the magnitude of the triplet interaction. The joining lines between the three particles form a triangle, with the exterior angles always summing to 2π . Following similar logic as our previous discussions of multibody configurations, we observe that repulsion is maximal for equilateral configurations as well as evenly spaced collinear arrangements. Similarly, we find that maximal attraction occurs when the set $\{\varphi_{13}^2, \varphi_{21}^3, \varphi_{32}^1\}$ is equal to $\{0, \pi/3, 2\pi/3\}$. The triangle formed by these angles is one in which two of the particles are on top of each other (or the distance between them is infinitely smaller than their distance to the other, to be precise). This is interesting, because it suggests that the triplet interaction is becoming more and more attractive as the spatial configuration of particles grows more and more (practically) similar to a pair of particles. We take this as a hint that perhaps the attractiveness of the force has to do with to what degree the sources can be localized into *two* regions.

To finish off, let us demonstrate the effectiveness of the EFT technique by considering the leading order *quadruplet* interaction. This interaction simply arises from the last four diagrams of Eq. (4.113):

$$-\beta U_{\{1,2,3,4\}}^{(8)} = \text{(diagram 1)} + \text{(diagram 2)} + \text{(diagram 3)} + \text{(diagram 4)}. \quad (4.118)$$

Applying the usual diagrammar, we find

$$\beta U_{\{1,2,3,4\}}^{(8)} = -\frac{1}{2} \sum_{a,b,c,d}^{\text{perm.}} \frac{R_a^2 R_b^2 R_c^2 R_d^2}{r_{ab}^2 r_{bc}^2 r_{cd}^2 r_{da}^2} \left[8 \cos(4\varphi_{ac}^b + 4\varphi_{ca}^d) + 8 \cos(4\varphi_{ac}^b + 2\varphi_{ca}^d) \right. \\ \left. + \cos(2\varphi_{ac}^b + 2\varphi_{ca}^d) + \cos(2\varphi_{ac}^b - 2\varphi_{ca}^d) \right]. \quad (4.119)$$

This result has not been derived previously, as far as we know.²⁰ It admittedly looks awfully complicated, but given how many angles and distances are involved, this ought not to be too terribly surprising. It may be a slight relief, however, that one only requires $2 \times 4 - 3 = 5$ parameters to uniquely determine the geometry (see page 143), so much of the apparent complexity is redundant. Perhaps the most important take home message is not the specific form of this interactions, but rather the fact that it can be derived in a straightforward (albeit not effortless) way.

²⁰Except, of course, for the article [YHD14] on which this chapter is based and which it extends.

5 Particle anisotropies

Up to this point we have only considered ideal particle models in which the particle boundaries project circular footprints onto the base plane. Although the particle footprints were restricted to be axisymmetric, we have also generalized slightly to *nonflat* particles. Specifically, we considered a particular case of particle anisotropy in which vertical undulations $h^{\text{ct}}(\partial\mathcal{A})$ of the contact line at the boundary $\partial\mathcal{A}$ were allowed—or, more accurately, permanent multipole moments were imposed—but the particle footprint was nonetheless still circular. This type of contact line asymmetry is important to elastic interactions between particles, but plays no additional role when it comes to fluctuation-induced (entropic) interactions. Entropic interactions instead depend on the *projected* boundary shapes $\partial\mathcal{A}$, but, with the exception of the conditions placed on the particles’ rigid body motions (bobbing and tilting), is independent of h^{ct} .

Symmetry breaking at the particle contact line, due either to the boundary shape or out-of-plane curvature, has the potential to significantly alter the behavior of particle interactions. For example, in Chapter 4 we found that anisotropic curvature alters the leading-order elastic interactions from $\sim 1/r^4$ for axisymmetric cap or wedge shapes, *cf.* Eq. (4.69), to $\sim 1/r^2$ for particles with quadrupolar (saddle) curvature, *cf.* Eq. (4.72). The two results manifest in the interactions between the (isotropic) mean curvature charges $\dot{Q}_i^{(2)} \propto J_i R_i^2$ and the (anisotropic) Gaussian saddle-curvature charges $Q_i^{(2)} \propto S_i R_i^2$ (which also leaves a trace in $Q_i^{(4)} \propto S_i R_i^4$). More specifically, two anisotropic $Q^{(2)}$ charges interact directly to produce an energy difference that scales as $\sim \kappa S_1 S_2 R_1^2 R_2^2 / r^2$, whereas two $\dot{Q}^{(2)}$ charges may only interact indirectly through an induced $C^{(2)}$ -polarization, giving a higher-order, isotropic result $\sim \kappa J_i^2 R_i^2 R_1^2 R_2^2 / r^4$ (which, incidentally, also breaks superposition). For fluid surfaces characterized by surface tension—the model of Chapter 3—no such difference can occur since the surface is agnostic to mean curvature (in that there is no way to impose a mean curvature that “spreads out” from the place of imposition) and, hence, anisotropic curvatures are required for elastic interactions to exist (see Section 3.5.1).

It is conceivable, however, that anisotropies of the particle boundaries may alter the leading-order *entropic* interactions. Indeed, such interactions are influenced by the symmetries of the curvature-response spectrum (*i.e.*, polarizabilities), which inherit the symmetries of the particle boundaries. This question was addressed in part by Oettel and coworkers [LNO08, NO09] by studying ellipses, and they found that anisotropic effects do not change the order, but instead append orientation-dependent corrections to the leading-order asymptotics, *except* in the case of particles with fixed heights, for which the leading-order result remains isotropic and long ranged (double logarithmic). Their results follow from a particularly involved calculation in which the functional integral is entangled with an elliptic multipole expansion in a way that obfuscates a generalization to arbitrary geometries.

In contrast, the EFT formalism disentangles the boundary expansion from the partition function as a much simpler matching problem, so the behavior can be determined from the form of the effective Hamiltonian alone.

A question not addressed is how anisotropies apply to multibody interactions. In Chapter 3, the pure triplet interaction was found to begin at $1/r_{ij}^4 r_{jk}^4$, rather than the expected $\sim 1/r_{12}^2 r_{23}^2 r_{31}^2$ from dimensional analysis (the vanishing of this term is understood most succinctly by the diagrammatic argument in Section 3.6.3). Boundary anisotropies are expected to violate this special case and allow for the lower-order contributions. We will see in Section 5.3.3 that this is indeed the case.

In this chapter we will explore the consequences of relaxing isotropy of the particle boundaries and calculate the anisotropic contributions to particle interactions. To make connection with previous studies, we will consider the simplest case of broken symmetry: particles with elliptic boundaries. This choice has the added advantage of smoothly interpolating from disk-like objects, for which we may directly compare with the results of Chapter 3, and rod- or needle-like objects, which represent the most extreme asymmetry. Unlike the previous chapters, we will forgo a discussion of elastic interactions in favor of a focus on entropic interactions. This is because the broken symmetry of the (projected) boundary shapes is encoded in the particle polarizabilities, which govern each particle's response to external fields and hence completely dictate fluctuation-induced interactions. Although permanent sources necessarily break rotational symmetry as well, we have already considered them in their most general form and little further insight is to be gained.

Model and boundary conditions

Fluid surfaces characterized by surface tension were the primary focus of Chapter 3, so instead of repeating the discussion of energetics here, we refer the reader the early sections of that chapter. Here we will summarize the necessary ingredients.

We describe the fluid surface in the Monge gauge through a height function $h(\mathbf{x})$ with respect to an appropriate reference base plane, which we take to be the equilibrium surface in the absence of fluctuations. At a finite temperature, entropic contributions are characterized by the energy $k_B T$, which when compared with the surface energy $\sigma \ell^2$ defines a length scale $\ell_m = \sqrt{k_B T / \sigma}$ characterizing the amplitude of fluctuations. As discussed in Chapter 3, this length scale is extraordinarily small and comparable to the molecular length scale ($\ell_m \sim 10^{-10}$ m for an air–water interface at room temperature). To avoid factors of σ and $\beta = 1/k_B T$ from floating around—which can be a distracting nuisance—in this chapter we will work with the dimensionless height function $\phi := h/\ell_m$.

The behavior of the fluid surface is described through the energy functional, or *bulk* Hamiltonian,

$$\begin{aligned} \beta \mathcal{H}_0[\phi] &= \frac{1}{\ell_m^2} \int_{\mathcal{S}_{\text{pr}}} d^2x \left[\sqrt{1 + \ell_m^2 (\nabla \phi)^2} - 1 \right] \\ &= \int_{\mathcal{S}_{\text{pr}}} d^2x \frac{1}{2} (\nabla \phi)^2 + \mathcal{O}(\ell_m^2), \end{aligned} \tag{5.1}$$

where \mathcal{S}_{pr} is the region defined by the projection of the surface onto the base plane. In the second line we applied the small-gradient approximation, which is valid for small deviations from flatness and justified by the negligible $\mathcal{O}(\ell_{\text{m}}^2)$ corrections. In cases that break the vertical translation symmetry of the bulk surface energy, long-wavelength fluctuations will build up, leading to divergences and pathologies. In these circumstances, we will tame them by including a gravitational potential,

$$\beta\mathcal{H}_{\text{g}}[\phi] = \int_{\mathcal{S}_{\text{pr}}} d^2x \frac{1}{2} \frac{\phi^2}{\ell_{\text{c}}^2}, \quad (5.2)$$

where $\ell_{\text{c}} = \sqrt{\sigma/|\Delta\rho|g}$ is the capillary length and will serve as a large-distance regulator. After calculating observables, we will take the limit $\ell_{\text{c}} \rightarrow \infty$. This will restore the bulk translation symmetry, but allow the intermediate steps to be well-posed.

Finally, the inclusion of particles has the effect of removing compact domains from the surface (and its projection). We take the surface to be infinite, so for a collection of N particles, each with projected areas \mathcal{A}_{α} , the integration domain can be written as $\mathcal{S}_{\text{pr}} = \mathbb{R}^2 \setminus \bigcup_{\alpha=1}^N \mathcal{A}_{\alpha}$. As usual, we will take the surface to be pinned to the boundary of each particle α with some contact line profile $\phi_{\alpha}^{\text{ct}}(\mathbf{x})$ where $\mathbf{x} \in \partial\mathcal{A}_{\alpha}$. We will not consider permanent sources of surface deformation, so each contact line will be taken as *flat* and therefore completely parametrized by the allowable rigid-body motions of the corresponding particle, *i.e.*, vertical bobbing and out-of-plane tilt (the reader is referred to Fig. 3.2 for an illustration). As in Chapter 3, we will consider the following three types of particle boundary conditions:

(BC 1) The position and tilt are fixed: $\phi(\partial\mathcal{A}_{\alpha}) = 0$.

(BC 2) The vertical position may fluctuate freely but the tilt is fixed: $\phi(\partial\mathcal{A}_{\alpha}) = \phi_{0,\alpha}$.

(BC 3) The vertical position and tilt may both fluctuate freely:
 $\phi(\partial\mathcal{A}_{\alpha}) = (\phi_{0,\alpha} + \mathbf{s}_{\alpha} \cdot \mathbf{x})|_{\partial\mathcal{A}_{\alpha}}$.

In the above enumeration, $\phi_{0,\alpha}$ and \mathbf{s}_{α} respectively parametrize the height and tilt of particle α with respect to the base plane, and may fluctuate with the surface without costing any energy. Given the subtleties associated with fixing the height, we will first discuss (BC 2) and (BC 3), and defer the discussion of (BC 1) to Section 5.2.4.

5.1 Symmetry revisited

The gravity-free, small-gradient surface Hamiltonian (5.1), with $\mathcal{S}_{\text{pr}} = \mathbb{R}^2$, enjoys the following symmetries:

\mathbf{T}_1 . Reflection across the base plane: $\phi \rightarrow -\phi$.

\mathbf{T}_2 . Vertical translation: $\phi \rightarrow \phi + \phi_0$, where ϕ_0 is a constant.

T₃. Rotation (isotropy) around a vertical axis centered at *any* point in the base plane (homogeneity): $\mathbf{x} \rightarrow \mathbf{R}\mathbf{x}$ for any $\mathbf{x} \in \mathbb{R}^2$.

T₄. Conformal transformations: $z \rightarrow F(z)$ for any analytic function F and $z \in \mathbb{C} \simeq \mathbb{R}^2$.

The fourth symmetry was neglected in Chapter 3, but we will make use of it here. With the inclusion of particles, the homogeneity condition on **T₃** is necessarily broken as it makes the boundary points unique. Earlier when we considered an isolated circular particle, the rotational symmetry was retained about the particle center, which simplified both the construction of the effective Hamiltonian and the background-response boundary value problem (BVP). For arbitrarily-shaped particles, **T₃** is broken completely (in general). This is where **T₄** comes in. Although the effective Hamiltonian will be more complicated, the BVP can be conformally mapped onto a circular boundary where the solution is straightforward, and then mapped back.

5.1.1 EFT for particles of arbitrary shape

As usual, we will take the characteristic particle sizes to be much smaller than the interparticle separations. This allows for the accommodation of particles into the surface Hamiltonian through a “point-particle”-like derivative expansion evaluated at each particle position, or *worldline*. This adds to the unconstrained Hamiltonian $\mathcal{H}_0[\phi]$ a *worldline* Hamiltonian $\Delta\mathcal{H}[\phi]$ to give an effective Hamiltonian $\mathcal{H}_{\text{eff}} = \mathcal{H}_0 + \Delta\mathcal{H}$. Generically, $\Delta\mathcal{H}$ is constructed out of all possible operators $\mathbf{C}^{(k)} \cdot \mathbf{O}_k[\phi]$ that obey the symmetries (and isometries) of the particle boundaries. The prefactors $\mathbf{C}^{(k)}$ are the usual Wilson coefficients that encode the short-distance information regarding particle-field responses. Since we have taken ϕ to be dimensionless, the dimensions of each operator $\mathbf{O}_k[\phi]$ are carried by derivatives. Here, there are two relevant length scales for a single particle: the characteristic particle size s , and the molecular length scale ℓ_m —defined above—which characterizes the amplitude of vertical fluctuations and is thus associated with ϕ . The particle size s essentially characterizes the length over which gradients in ϕ may be affected (and *vice versa*), and is thus associated with derivatives. Hence, denoting the overall power of ϕ by n_k and the total number of derivatives by d_k , we can write $\beta\Delta\mathcal{H}$ up to some unknown dimensionless (possibly tensor) coefficients $c^{(k)}$,

$$\begin{aligned} \beta\Delta\mathcal{H}[\phi] &= \sum_{\alpha} \sum_k \mathbf{C}_{\alpha}^{(k)} \cdot \mathbf{O}_k[\phi(\mathbf{x}_a)] \\ &= \sum_a \sum_k \ell_m^{n_k-2} s_{\alpha}^{d_k} \mathbf{c}_{\alpha}^{(k)} \cdot \mathbf{O}_k[\phi(\mathbf{x}_a)], \end{aligned} \tag{5.3}$$

where $n_k + d_k - 2 = 0$. This series, although complete, may include redundancy. As exploited multiple times in the preceding chapters, operators containing $\delta\mathcal{H}_0/\delta\phi$ can be removed by appropriate field redefinitions without affecting the physics, so long as we only calculate with on-shell quantities, *i.e.*, with fields ϕ satisfying the bulk Euler-Lagrange equation $\delta\mathcal{H}_0/\delta\phi = 0$. In this case, the condition is $-\nabla^2\phi = 0$, eliminating all terms containing a Laplacian. Terms with $n_k > 2$ correspond to nonlinearities in \mathcal{H}_0 (*cf.* Eq. (5.1)), so in the

small-gradient approximation $n_k \leq 2$, eliminating the dependency on ℓ_m and truncating $\Delta\mathcal{H}$ at quadratic order in ϕ .

Returning to symmetries, we again note that the particle boundary conditions can either respect or break the bulk symmetries. Those that break them require external forces, such as wetting properties of the particle surface to pin the contact line or external mechanisms that fix the particles' vertical positions or orientations. Hence, the terms in $\Delta\mathcal{H}$ can be categorized as symmetry-breaking, and thus couple to external source terms, or symmetry-preserving. Since the presence of particles will always break some symmetry, namely homogeneity, we refine these categories to distinguish between those that source permanent surface deformations or only respond to background deformations. For the flat, free particles we consider, no permanent deformations are imparted and no external mechanism fixes the vertical positions. That is, \mathbf{T}_1 will always hold, and therefore eliminate any terms linear in ϕ . Additionally, for (BC 2) and (BC 3), \mathbf{T}_2 will also hold and therefore impose the restriction that all field instances must carry at least one derivative. For (BC 3) in particular, the freedom to tilt out of the plane eliminates—in the small-gradient approximation—any field instance with one derivative (see the discussion in Section 3.3.1). As mentioned earlier, \mathbf{T}_3 is broken in general. In previous chapters, rotation invariance restricted the Wilson coefficients to be scalars. However, for arbitrary shapes we must construct scalar terms out of tensors, such as $\partial_i \phi C_{ijk} \partial_j \partial_k \phi$, or more generally $\partial_{i_1} \cdots \partial_{i_n} \phi C_{i_1 \cdots i_n j_1 \cdots j_m}^{(n,m)} \partial_{j_1} \cdots \partial_{j_m} \phi \equiv \partial_I^n \phi C_{IJ}^{(n,m)} \partial_J^m \phi$ in multi-index notation.¹ The most general worldline Hamiltonian can therefore be written as

$$\beta \Delta\mathcal{H}[\phi] = \sum_{\alpha} \sum_{n,m} \partial_I^n \phi(\mathbf{x}_a) C_{\alpha, IJ}^{(n,m)} \partial_J^m \phi(\mathbf{x}_a), \quad (5.4)$$

where $n, m \geq 1$ for (BC 2) and $n, m \geq 2$ for (BC 3). It follows from dimensional analysis that the Wilson coefficients scale as $[C_{IJ}^{(n,m)}] \sim s^{n+m}$, and from exchange symmetry that the index sets I and J are (independently) fully symmetric and $C_{IJ}^{(n,m)} = C_{JI}^{(m,n)}$. Although these terms break rotation symmetry, they do not permanently deform the surface. Much like how a conductor polarizes in the presence of an electric external field, these particles respond via *induced* deformations in response to background surface curvature. Just as in previous chapters, we will appropriately interpret and refer to the Wilson coefficients as *polarizabilities*.

The present form for $\Delta\mathcal{H}$ requires significant index manipulation and will result in some rather unwieldy expressions. However, the previous two chapters have demonstrated that a change of variables to complex coordinates $\mathbf{z} = (z, \bar{z})$ with $z = x + iy$ and $\bar{z} = z^*$ tends to simplify matters dramatically. Without attempting to express the relationship with the yet undetermined polarizability tensors above, we may directly reconstruct the worldline Hamiltonian using the Wirtinger derivatives $\partial := (\partial_x - i\partial_y)/2$ and $\bar{\partial} := (\partial_x + i\partial_y)/2$. Since $\nabla^2 \equiv 4\partial\bar{\partial}$, the elimination of redundant terms means each field instance can be acted on by strictly ∂ - or $\bar{\partial}$ -derivatives, but not both. The most general worldline Hamiltonian satisfying

¹For circular particles, the coefficients would reduce to $C_{i_1 \cdots i_n j_1 \cdots j_m}^{(n,m)} \rightarrow C^{(n)} \delta_{nm} \delta_{i_1 j_1} \cdots \delta_{i_n j_n}$.

the symmetries discussed above is therefore simple to write down, and takes the form

$$\beta\Delta\mathcal{H}[\phi] = \sum_{\alpha} \sum_{n,m} \left[C_{\alpha}^{nm} \partial^n \phi \bar{\partial}^m \phi + \frac{1}{2} \chi_{\alpha}^{nm} \partial^n \phi \partial^m \phi + \frac{1}{2} \bar{\chi}_{\alpha}^{nm} \bar{\partial}^n \phi \bar{\partial}^m \phi \right] \Big|_{z=z_{\alpha}}, \quad (5.5)$$

where each term is evaluated at the particle position z_{α} , and again $n, m \geq 1$ for (BC 2) and $n, m \geq 2$ for (BC 3). The polarizabilities all scale like above as $\sim s^{n+m}$. The only remaining restrictions are that C^{nm} is Hermitian and $\bar{\chi}^{nm} = (\chi^{nm})^*$, which follows from the requirement that $\beta\Delta\mathcal{H}$ be real, and that both χ^{nm} and $\bar{\chi}^{nm}$ are symmetric, which follows from the exchange of derivatives. We have included the factors of $1/2$ to account for double counting under an index swap, but it also conveniently places the conventional half in front of each squared field terms $(\partial^n \phi)^2$ and $(\bar{\partial}^n \phi)^2$.

5.2 EFT for elliptical particles

Equation (5.5) is the general form for *any* anisotropic particle. However, just as the permitted rigid-body particle motions put constraints on the $n = 0$ and $n = 1$ terms, additional symmetries associated with the particle boundary conditions or shape may lead to further restrictions (or vanishing) of some terms. For example, in the case of the circular disks considered in Chapter 3, there is complete rotational symmetry for each particle α in isolation. Applying the transformation $(z - z_{\alpha}) \rightarrow e^{i\theta}(z - z_{\alpha})$ with $\theta \in [0, 2\pi)$ to the single-particle version of Eq. (5.5), and enforcing invariance, leads to the conditions $C^{nm} \rightarrow C^{nm} \delta_{nm}$ and $\chi^{nm} = \bar{\chi}^{nm} = 0$, and reproduces the worldline Hamiltonian (3.71) (and (3.80)). Hence, particle anisotropies must be encoded in the χ^{nm} and $\bar{\chi}^{nm}$ tensors as well as the off-diagonal elements of C^{nm} . For ellipses, the primary particle shape considered in this chapter, the symmetry is limited to discrete rotations by an angle π , *i.e.*, $(z - z_{\alpha}) \rightarrow -(z - z_{\alpha})$. Since the worldline Hamiltonian must obey this same symmetry, we find that the polarizabilities for an ellipse are reduced to only those whose indices obey $n + m \in 2\mathbb{N}$; that is, the sum $n + m$ must be even.

To determine the polarizabilities, we must perform an appropriate matching procedure such that the EFT correctly reproduces the physics at large distances. That is, any observable calculated in the EFT must asymptotically match the result obtained by the full BVP. The aim then is to find a convenient set of observables such that their calculation in the full theory is as simple as possible. In line with previous chapters, the obvious choice is to employ the background field method in which we introduce some background surface deformation ϕ_{bg} and compute from the full and effective theories the response $\delta\phi$, such that the total field $\phi = \phi_{\text{bg}} + \delta\phi$ satisfies the boundary conditions, and match the two results. Since each particle can be independently characterized by its response to external fields, we need only compute the response for each particle in isolation.

We first examine the EFT response for a general background. The form of the response will motivate a convenient choice of background field, which we will then apply to the full

theory boundary value problem. We will perform the calculations first for (BC 2), and later discuss the modifications to accommodate (BC 1) and (BC 3).

5.2.1 Effective response

The coupling between the particle and surface generates an effective source, induced by the imposed background ϕ_{bg} . Since we have chosen an on-shell operator basis for $\Delta\mathcal{H}$, we must require any permissible background field to satisfy $(\delta\mathcal{H}_0/\delta\phi)|_{\phi_{\text{bg}}} = 0$, or equivalently $-\nabla^2\phi_{\text{bg}} = 0$. Setting $\phi = \phi_{\text{bg}} + \delta\phi$ in Eq. (5.5) and taking the terms linear in $\delta\phi$ therefore gives the effective source for this background. Without loss of generality, we will take the particle to be positioned at the origin and find the (dimensionless) effective source in the usual way:

$$\begin{aligned} \rho(\mathbf{z} | \phi_{\text{bg}}) &= - \left. \frac{\delta(\beta\Delta\mathcal{H})}{\delta\phi(\mathbf{z})} \right|_{\phi=\phi_{\text{bg}}} \\ &= - \sum_{n,m \geq 1} [C^{nm}(-\partial)^n \delta(\mathbf{z}) \bar{\partial}^m \phi_{\text{bg}}(0) + \chi^{nm}(-\partial)^n \delta(\mathbf{z}) \partial^m \phi_{\text{bg}}(0)] + \text{c.c.}, \end{aligned} \quad (5.6)$$

where c.c. stands for the complex conjugate. The response is given by the convolution

$$\delta\phi_{\text{eff}}(\mathbf{z} | \phi_{\text{bg}}) = \int d^2z' G(\mathbf{z} - \mathbf{z}') \rho(\mathbf{z}' | \phi_{\text{bg}}), \quad (5.7)$$

where

$$G(\mathbf{z} - \mathbf{z}') = -\frac{1}{4\pi} \ln[(z - z')(\bar{z} - \bar{z}')] \quad (5.8)$$

is the Green function for the Laplacian² $-\nabla^2 \equiv -4\partial\bar{\partial}$, and $d^2z' = d(\text{Re } z') d(\text{Im } z')$, resulting in

$$\delta\phi_{\text{eff}}(\mathbf{z} | \phi_{\text{bg}}) = - \sum_{n,m \geq 1} (-\partial)^n G(\mathbf{z}) [C^{nm} \bar{\partial}^m \phi_{\text{bg}}(0) + \chi^{nm} \partial^m \phi_{\text{bg}}(0)] + \text{c.c.} \quad (5.9)$$

The form of both the effective source (5.6) and response (5.9) suggests choosing a general set of background multipole fields

$$\phi_{\text{bg}}^{(n)}(\mathbf{z} | \vartheta) = A^{(n)}(z^n e^{-in\vartheta} + \bar{z}^n e^{in\vartheta}), \quad (5.10)$$

where $A^{(n)} \in \mathbb{R}$ and ϑ is an arbitrary rotation introduced to double the parameters and allow both C^{nm} and χ^{nm} to be matched for each background (otherwise the matching condition would be underdetermined). These multipole backgrounds are particularly desirable since

²Technically, the argument of the Green function should be dimensionless, so it should be divided by some appropriate length scale. However, for the (BC 2) and (BC 3) cases, such a constant will be immaterial since the Green function will always be acted upon by derivatives. In the case of (BC 1), the length scale is significant and must be included (*cf.* Eq. (5.32)).

the derivatives in Eq. (5.9) will independently pick off one multipole order at a time via

$$\partial^m \phi_{\text{bg}}^{(n)}(0) = A^{(n)} n! e^{-in\vartheta} \delta_{nm}. \quad (5.11)$$

Plugging the multipole background into Eq. (5.9) and using

$$(-\partial)^n G(z) = \frac{(n-1)!}{4\pi z^n} \quad (5.12)$$

gives the effective response

$$\delta\phi_{\text{eff}}^{(n)}(z | \vartheta) = -A^{(n)} n! \sum_{k \geq 1} \frac{(k-1)!}{4\pi z^k} \left[C^{kn} e^{in\vartheta} + \chi^{kn} e^{-in\vartheta} \right] + \text{c.c.} \quad (5.13)$$

5.2.2 Full-theory response

The full theory response is a solution to the Laplace boundary value problem $\partial\bar{\partial}\delta\phi = 0$ for the outer domain $z \in \mathbb{R}^2 \setminus \mathcal{A}$, where \mathcal{A} is the area of the ellipse projected onto the base plane, subject to the boundary condition $\phi|_{\partial\mathcal{A}} = (\phi_{\text{bg}} + \delta\phi)|_{\partial\mathcal{A}} = \phi_0$, where ϕ_0 is the dimensionless free parameter of (BC 2) describing the height above the base plane, and $\delta\phi(|z| \rightarrow \infty) \rightarrow 0$. Since global height translations are a symmetry of the (BC 2) theory, ϕ_0 will take on the value of the total background surface height so that the symmetry remains respected. Given this symmetry, we may assume that the particle has already translated to the appropriate vertical position of the surface and, accordingly, we may safely ignore any constants that arise during the following calculations, saving ourselves from an unnecessary technical distraction. We will revisit the constants that may appear when we discuss monopoles.

Conformal mapping

As evident from our analysis in Chapter 3, this Dirichlet problem is simple for a circular boundary of radius R . Indeed, for backgrounds that can be put into a Laurent series

$$\phi_{\text{bg}}(z) = \sum_{k > 0} \left[A_k \left(\frac{z}{R} \right)^k + B_k \left(\frac{R}{z} \right)^k \right] + \text{c.c.}, \quad (5.14)$$

the response is given by

$$\delta\phi(z) = - \sum_{k > 0} \left[(A_k^* + B_k) \left(\frac{R}{z} \right)^k + \text{c.c.} \right], \quad (5.15)$$

as can be seen by plugging in $z = R e^{i\varphi}$. With this in mind, we exploit the conformal symmetry **T**₄ of Laplace's equations and map the ellipse BVP to a circle, solve using the simple replacement above, and map back (see Fig. 5.1).

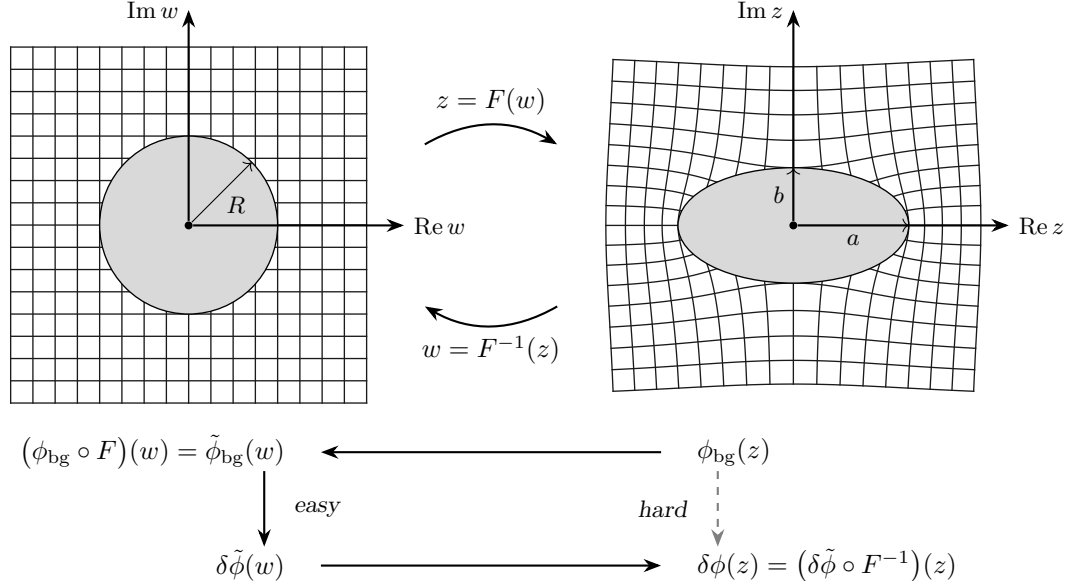


Figure 5.1: Conformal mapping between circle (w -space) and ellipse (z -space) boundaries. The mapping takes a background field $\phi_{\text{bg}}(z)$ imposed on an ellipse to a new field $\tilde{\phi}_{\text{bg}}(w) = (\phi_{\text{bg}} \circ F)(w)$ imposed on a circle, for which calculating the response $\delta \tilde{\phi}(w)$ is easy and follows from Eq. (5.15). Mapping back gives the ellipse response $\delta \phi(z) = (\delta \tilde{\phi} \circ F^{-1})(z)$.

The conformal transformations between an ellipse (z -space) of semi-major axis a and semi-minor axis b , with the major axis aligned along the real axis, and a circle (w -space) of radius R are

$$z = F(w) = \frac{1}{2} \left(s_+ \frac{w}{R} + s_- \frac{R}{w} \right) \quad (5.16)$$

and

$$w = F^{-1}(z) = \frac{R}{s_+} \left(z + \sqrt{z^2 - s_+ s_-} \right), \quad (5.17)$$

where $s_+ := a + b$ and $s_- := a - b$. The quantity $\sqrt{s_+ s_-} = \sqrt{a^2 - b^2} =: f$ is the ellipse *focus*. The expression for $F^{-1}(z)$ results from solving a quadratic equation, where it is necessary to choose the (+) sign so that the ellipse and circle boundaries correspond.³ Since

³To clarify, consider the circular boundary parametrization $w = R e^{i\varphi}$. Applying the map (5.16) produces the boundary parametrization of the ellipse: $z = 1/2(s_+ e^{i\varphi} + s_- e^{-i\varphi}) = a \cos \varphi + ib \sin \varphi$. Conversely, the inverse transformation has a sign ambiguity and, using $z^2 - s_+ s_- = [1/2(s_+ e^{i\varphi} - s_- e^{-i\varphi})]^2$, leads to

$$w_{\pm} = \frac{(1 \pm 1)}{2} R e^{i\varphi} + \frac{s_-}{s_+} \frac{(1 \mp 1)}{2} R e^{-i\varphi}.$$

It is clear then that choosing w_+ gives the correct circle boundary $w_+ = R e^{i\varphi}$.

we are considering points z outside the ellipse, the branch cut for the square root can be conveniently chosen as the interval $(-f, f)$, which lies within the ellipse.⁴

Under this transformation, the background field (5.10) becomes

$$\tilde{\phi}_{\text{bg}}^{(n)}(\mathbf{w} \mid \vartheta) = \frac{A^{(n)}}{2^n} \left[\left(s_+ \frac{w}{R} + s_- \frac{R}{w} \right)^n e^{-in\vartheta} + \left(s_+ \frac{\bar{w}}{R} + s_- \frac{R}{\bar{w}} \right)^n e^{in\vartheta} \right]. \quad (5.18)$$

To solve the circle BVP, we first expand (5.18) as a binomial series using

$$\begin{aligned} \left(s_+ \frac{w}{R} + s_- \frac{R}{w} \right)^n &= \sum_{\ell < n/2} \left\{ \binom{n}{\ell} s_+^{n-\ell} s_-^\ell \left(\frac{w}{R} \right)^{n-2\ell} + \binom{n}{\ell} s_+^\ell s_-^{n-\ell} \left(\frac{R}{w} \right)^{n-2\ell} \right\} \\ &\quad + \binom{n}{n/2} (s_+ s_-)^{n/2}, \end{aligned} \quad (5.19)$$

where the last term only appears when n is even. This extra constant term can be ignored due to the height-translation symmetry of (BC 2); however, we must revisit it later when we discuss (BC 1). The above series now puts Eq. (5.18) in the required form (*cf.* Eq. (5.14)), so the response follows from the appropriate substitutions *à la* Eq. (5.15):

$$\delta \tilde{\phi}^{(n)}(\mathbf{w} \mid \vartheta) = -\frac{A^{(n)}}{2^n} \sum_{\ell < n/2} \left[\left(s_+^{n-\ell} s_-^\ell e^{in\vartheta} + s_+^\ell s_-^{n-\ell} e^{-in\vartheta} \right) \left(\frac{R}{w} \right)^{n-2\ell} + \text{c.c.} \right]. \quad (5.20)$$

To transform back to the ellipse BVP (z -space), we set $w = F^{-1}(z)$ and use the expansion

$$\frac{1}{(1 + \sqrt{1-x})^n} = \frac{n}{2^n} \sum_{k=0}^{\infty} \frac{1}{n+2k} \binom{n+2k}{k} \left(\frac{x}{4} \right)^k \quad (5.21)$$

to produce a proper power series in $1/z$, and thus find the full-theory ellipse response,

$$\delta \phi_{\text{full}}^{(n)}(\mathbf{w} \mid \vartheta) = \sum_{\ell < n/2} \sum_{k=0}^{\infty} \mathcal{C}(n, \ell, k) \frac{1}{z^{n-2\ell+2k}} + \text{c.c.}, \quad (5.22)$$

⁴Choosing the appropriate branch cut depends on whether z is inside or outside the ellipse. In general, we can write $\sqrt{z^2 - f^2} = \sqrt{(z+f)(z-f)} = e^{\frac{1}{2}(\theta_+ + \theta_-)} \sqrt{r_+ r_-}$, where $r_{\pm} = |z \pm f|$ and $\theta_{\pm} = \arg(z \pm f)$. If z is outside the ellipse, the most convenient choice for the branch cut is between the two branch points, $z \in (-f, f)$, corresponding to the principal arguments $\theta_{\pm} \in (-\pi, \pi]$. If instead z is within the ellipse we should choose the branch cuts $z \in (-\infty, -f) \cup (f, \infty)$, corresponding to the principal angles $\theta_+ \in [0, 2\pi)$ and $\theta_- \in (-\pi, \pi]$. Using the conventional definition for the *principal square root*, $\sqrt{z} = e^{\frac{1}{2} \text{Arg } z} \sqrt{|z|}$ where $\text{Arg } z \in (-\pi, \pi]$, we could instead write $\sqrt{z^2 - f^2} \equiv \sqrt{z+f} \sqrt{z-f}$.

where

$$\begin{aligned} \mathcal{C}(n, \ell, k) = & -\frac{A^{(n)}}{2^n} \binom{n}{\ell} \left(s_+^{n-\ell} s_-^\ell e^{in\vartheta} + s_+^\ell s_-^{n-\ell} e^{-in\vartheta} \right) \\ & \times \left(\frac{s_+}{2} \right)^{n-2\ell} \frac{n-2\ell}{n-2\ell+2k} \binom{n-2\ell+2k}{k} \left(\frac{s_+s_-}{4} \right)^k. \end{aligned} \quad (5.23)$$

5.2.3 Matching

To match the polarizabilities, we wish to set $\delta\phi_{\text{eff}}^{(n)} \stackrel{!}{=} \delta\phi_{\text{full}}^{(n)}$. So that we can directly compare coefficients, we first put (5.22) into more convenient form by re-indexing the sums. We omit the details for brevity, but after performing the appropriate index manipulations we obtain

$$\delta\phi_{\text{full}}^{\binom{n \text{ even}}{n \text{ odd}}} = \sum_{k=\begin{cases} \text{even} \\ \text{odd} \end{cases}}^{\infty} \sum_{\ell=\begin{cases} \text{even} \\ \text{odd} \end{cases}}^{\min[n,k]} \mathcal{C}\left(n, \frac{n-\ell}{2}, \frac{k-\ell}{2}\right) \frac{1}{z^k} + \text{c.c.}, \quad (5.24)$$

where both sums are over only positive even (odd) integers when n is even (odd). Comparing the coefficients to that of (5.13) and simplifying finally gives the full set of polarizabilities:

$$\begin{aligned} C^{nm} &= \sum_{\ell=\begin{cases} \text{even} \\ \text{odd} \end{cases}}^{\min[n,m]} \frac{4\pi\ell}{2^{n+m}n!m!} \binom{n}{\frac{n-\ell}{2}} \binom{m}{\frac{m-\ell}{2}} (s_+s_-)^{\frac{n+m}{2}} \left(\frac{s_+}{s_-} \right)^\ell, \\ \chi^{nm} &= \sum_{\ell=\begin{cases} \text{even} \\ \text{odd} \end{cases}}^{\min[n,m]} \frac{4\pi\ell}{2^{n+m}n!m!} \binom{n}{\frac{n-\ell}{2}} \binom{m}{\frac{m-\ell}{2}} (s_+s_-)^{\frac{n+m}{2}} \\ &= \begin{cases} \frac{2\pi nm}{2^{n+m}(n+m)} \frac{(s_+s_-)^{\frac{n+m}{2}}}{[(\frac{n}{2})!]^2[(\frac{m}{2})!]^2}, & n, m \text{ even} \\ \frac{8\pi}{2^{n+m}(n+m)} \frac{(s_+s_-)^{\frac{n+m}{2}}}{[(\frac{n-1}{2})!]^2[(\frac{m-1}{2})!]^2}, & n, m \text{ odd} \end{cases} \end{aligned} \quad (5.25)$$

where again the sums are over ℓ strictly even or odd depending on whether both n and m are even or odd. Recall that if $n+m \notin 2\mathbb{N}$, meaning one is even and the other is odd, then $C^{nm} = \chi^{nm} = 0$.

Rotated ellipse. The conformal map we considered treats the special case in which the ellipse's major principal axis is aligned with the x -axis and, consequently, this matching procedure gives the polarizabilities for a single ellipse in the same configuration. If we instead consider an ellipse rotated an angle θ from the x -axis, we can equivalently rotate the coordinate system by $-\theta$ (*i.e.*, $z \rightarrow e^{i\theta}z$). This has the effect $\partial \rightarrow e^{-i\theta}\partial$ and, applying it to Eq. (5.5) and enforcing coordinate-invariance of the energy, it follows that the polarizabilities

are modified via

$$C^{nm} \rightarrow e^{i(n-m)\theta} C^{nm} \text{ and } \chi^{nm} \rightarrow e^{i(n+m)\theta} \chi^{nm}, \quad (5.27)$$

where the values of C^{nm} and χ^{nm} are unchanged from Eqs. (5.25) and (5.26).

Tilt freedom. For the case of (BC 3), the tilt degree of freedom allows the ellipse to tilt out of the plane without costing energy so as to align with a dipole background field. Dipole backgrounds are linear in z , so this freedom forbids terms with fewer than two derivative. We therefore conclude that $C^{nm} = \chi^{nm} = 0$ if $n = 1$ or $m = 1$. Since the higher-order multipole fields do not impose an overall slope on the surface, it follows that the higher-order matching is unaffected and the remaining polarizabilities are the same as in (BC 3).

Limiting cases: rods and disks

The polarizabilities of thin rods and disks are natural limiting cases of our ellipse model. For a thin rod of length L , the full set of polarizabilities is given by (5.25), (5.26), and (5.44)—with the appropriate subsets vanishing depending on the boundary conditions—with $a \rightarrow L/2$ and $b \rightarrow 0$ (implying $s_{\pm} \rightarrow L/2$), which does not change the overall form of the expressions. However, for a rotationally symmetric disk we expect the anisotropic terms to vanish. Indeed, setting $a, b \rightarrow R$ (implying $s_+ \rightarrow 2R$, $s_- \rightarrow 0$) gives $\chi = \bar{\chi} = 0$. For C^{nm} , the only non-vanishing terms are those for which $\ell = (n+m)/2$. Since $\ell \leq \min[n, m]$, taking $n \geq m$ leads to $(n+m)/2 \leq m \implies n \leq m$, therefore $n = m$. Hence, for disks

$$C^{mm} = \frac{4\pi R^{2n}}{n!(n-1)!} \delta_{nm} \quad (5.28)$$

which agrees with the results of Chapter 3 (see Technical Note 3.1), and Refs. [YRD12] and [Rot12] up to a factor of $\sigma/2^n$ due to the difference in definition.

5.2.4 Monopoles

For the case of (BC 1), the particle constraint breaks the \mathbf{T}_2 vertical translation symmetry, so we must also include in the effective Hamiltonian the $n = 0$ and $m = 0$ terms (along with the $n = 1$ and $m = 1$ terms required for (BC 2)). We will refer to these as *monopole* terms and distinguish them by writing

$$\beta \Delta \mathcal{H}_m[\phi] = \sum_{\alpha} \left[\frac{1}{2} M_{\alpha}^{(0)} \phi^2 + \sum_{\substack{n>0 \\ \text{even}}} \left(M_{\alpha}^{(n)} \phi \partial^n \phi + \bar{M}_{\alpha}^{(n)} \phi \bar{\partial}^n \phi \right) \right] \Big|_{z=z_{\alpha}}, \quad (5.29)$$

where $\bar{M} = M^*$ and the condition that n is even follows from the π -rotation symmetry of each ellipse. The first term is the familiar “charge reservoir” contribution (*cf.* Eq. (1.35) of Chapter 1 and, in particular, Eq. (3.81) of Chapter 3) that accounts for the external work required to freeze the particle’s vertical position, analogous to the work done by a battery to maintain a conductor’s electrostatic potential. The remaining terms account for the

anisotropies of these boundary “charges.” These terms present a particular challenge: the monopole field, proportional to $\ln|\mathbf{x}|$, exhibits a long-distance divergence and is therefore ill-defined as it stands. For a sensible theory, we must regulate the Hamiltonian so as to dampen the long-range correlations.

Regularization can be realized in a physically-motivated way by accounting for the gravitational energy of the surface via Eq. (5.2). In the usual field theory parlance, this is equivalent to adding a small “mass” term into the bulk Hamiltonian:

$$\beta\mathcal{H}_0[\phi] \rightarrow \beta\mathcal{H}_0[\phi] + \beta\mathcal{H}_g[\phi] = \frac{1}{2} \int d^2x [(\nabla\phi)^2 + \ell_c^{-2}\phi^2]. \quad (5.30)$$

This change in the bulk Hamiltonian *does not* alter the form of our effective worldline Hamiltonian $\Delta\mathcal{H}[\phi] + \Delta\mathcal{H}_m[\phi]$. The appearance of $\partial\bar{\partial}\phi$ in any operator can be traded for $\ell_c^{-2}\phi$ by the bulk Euler-Lagrange equation (5.31), and the prefactor can be absorbed into one of the pre-existing terms. This implies, of course, that the polarizabilities will therefore acquire a dependence on ℓ_c . However, the capillary length is assumed large, so that we have the scaling hierarchy $a, b \ll r = |\mathbf{x}| \ll \ell_c$, and we will ultimately take $\ell_c \rightarrow \infty$. Hence, the polarizabilities that are regular in the limit $\ell_c \rightarrow \infty$ should remain unaffected, namely C^{nm} and χ^{nm} , but all $M^{(n \geq 0)}$ should vanish. However, the order of limits matters: Introducing ℓ_c *globally* breaks the bulk vertical translation symmetry, but the limit $\ell_c \rightarrow \infty$ restores it. If ℓ_c is meant to regulate the previously ill-posed monopole problem, ℓ_c must be treated as large but *finite* until the end of a calculation, after which the limit $\ell_c \rightarrow \infty$ may be safely taken. We have seen examples in Chapter 3 in which being cavalier about this technicality can lead to inconsistent results. In this chapter, we will provide brief commentary only when the issue is encountered.

With the regulator in place, the bulk Euler-Lagrange equation becomes

$$\frac{\delta(\beta\mathcal{H}_0)}{\delta\phi} = (-\nabla^2 + \ell_c^{-2})\phi = 0. \quad (5.31)$$

The bulk Green function is then the modified Bessel function of the second kind, which limits to a logarithm for large ℓ_c (see Eq. (3.34)):

$$G(\mathbf{x}) = \frac{1}{2\pi} K_0(r/\ell_c) \xrightarrow{\ell_c \rightarrow \infty} \frac{1}{2\pi} \ln\left(\frac{2\ell_c}{\gamma_e r}\right), \quad (5.32)$$

where $\gamma_e = e^{\gamma_E}$ and γ_E is the Euler-Mascheroni constant.

Effective response

To match the coefficients, we proceed as before by introducing a background field ϕ_{bg} , computing the response $\delta\phi$ in both the effective and full theories, and comparing. Considering only the monopole terms $\Delta\mathcal{H}_m$ for a single particle at the origin, we find the background

induces an effective source

$$\begin{aligned} \rho_{\text{m}}(\mathbf{z} \mid \phi_{\text{bg}}) &= -M^{(0)}\delta(\mathbf{z})\phi_{\text{bg}}(0) \\ &\quad - \sum_{\substack{n>0 \\ \text{even}}} \left\{ M^{(n)}[\delta(\mathbf{z})\partial^n\phi_{\text{bg}}(0) + \phi_{\text{bg}}(0)(-\partial)^n\delta(\mathbf{z})] + \text{c.c.} \right\}. \end{aligned} \quad (5.33)$$

Convolving with the bulk Green function gives effective linear response

$$\begin{aligned} \delta\phi_{\text{m}}(\mathbf{z} \mid \phi_{\text{bg}}) &= -M^{(0)}G(\mathbf{z})\phi_{\text{bg}}(0) \\ &\quad - \sum_{\substack{n>0 \\ \text{even}}} \left\{ M^{(n)}[G(\mathbf{z})\partial^n\phi_{\text{bg}}(0) + (-\partial)^nG(\mathbf{z})\phi_{\text{bg}}(0)] + \text{c.c.} \right\}. \end{aligned} \quad (5.34)$$

Finally, using the asymptotic form of the Green function (5.32) with Eq. (5.12), we obtain the result

$$\begin{aligned} \delta\phi_{\text{m}}(\mathbf{z} \mid \phi_{\text{bg}}) &= -\frac{M^{(0)}}{2\pi} \ln\left(\frac{2\ell_{\text{c}}}{\gamma_{\text{e}}|z|}\right) \phi_{\text{bg}}(0) \\ &\quad - \sum_{\substack{n>0 \\ \text{even}}} \left\{ M^{(n)} \left[\frac{1}{2\pi} \ln\left(\frac{2\ell_{\text{c}}}{\gamma_{\text{e}}|z|}\right) \partial^n\phi_{\text{bg}}(0) + \frac{1}{4\pi} \frac{(n-1)!}{z^n} \phi_{\text{bg}}(0) \right] + \text{c.c.} \right\}. \end{aligned} \quad (5.35)$$

Full-theory response

Since the bulk Hamiltonian with the “mass” term also breaks the \mathbf{T}_4 conformal symmetry, we unfortunately cannot use the mapping trick as before to compute the full-theory response. Instead, based on the geometry of the system, it will prove convenient to work in confocal elliptic coordinates, defined by

$$x = f \cosh \xi \cos \eta \quad (5.36a)$$

$$y = \sinh \xi \sin \eta, \quad (5.36b)$$

where $\xi \in [0, \infty)$, $\eta \in (-\pi, \pi]$, and the focus $f = \sqrt{a^2 - b^2}$. Curves of constant ξ give ellipses, as can be seen by rearranging the defining equations:

$$\left(\frac{x}{f \cosh \xi}\right)^2 + \left(\frac{y}{f \sinh \xi}\right)^2 = \cos^2 \eta + \sin^2 \eta = 1. \quad (5.37)$$

By the appropriately “reverse” argument, curves of constant η are hyperbolas. In the present case, the boundary of our ellipse results from setting $f \cosh \xi_0 = a$ and $f \sinh \xi_0 = b$, which leads to

$$f e^{\pm \xi_0} = a \pm b \implies \xi_0 = \frac{1}{2} \ln \left(\frac{a+b}{a-b} \right). \quad (5.38)$$

In complex variables, the defining relations (5.36) can be written compactly as

$$z = f \cosh(\xi + i\eta). \quad (5.39)$$

To extract ξ we must invert the hyperbolic cosine. From the definition of cosh, we find

$$fe^{\xi+i\eta} = z \pm \sqrt{z^2 - f^2}. \quad (5.40)$$

The sign ambiguity is resolved by defining the branch cuts of the square root as before and requiring the ellipse boundary to be consistent. Just as in Eq. (5.17), we take the (+) sign.⁵

The matching procedure requires an appropriate background field and response solution pair. The complete set of solutions for the full theory—*i.e.*, Eq. (5.31) with boundary conditions—is provided in Appendix C, Section C.2. Using the $n = 0$ background field of Eq. (C.15), for which $\phi_{\text{bg}}^{(0)} = A^{(0)}$ and $\partial^n \phi_{\text{bg}}^{(0)}(0) = 0$, the full-theory response is

$$\delta\phi_{\text{full}}^{(0)}(\xi, \eta) = -A^{(0)} \frac{\ln\left(\frac{fe^{\xi}}{4\ell_c} \gamma_e\right)}{\ln\left(\frac{a+b}{4\ell_c} \gamma_e\right)}. \quad (5.41)$$

Matching

Now, to compare the full and effective responses—respectively Eqs. (5.41) and (5.35) with $\phi_{\text{bg}} = A^{(0)}$ —we must choose to express the results in either complex or elliptic coordinates. Either choice will require an expansion, but the expansion of (5.41) in complex coordinates is somewhat simpler ($\cosh^{-1} z$ versus $1/\cosh^n z$). This is accomplished by first noting that

$$f^2 e^{2\xi} = \left| z + \sqrt{z^2 - f^2} \right|^2, \quad (5.42)$$

which follows from multiplying Eq. (5.40) by its complex conjugate, and then expanding the logarithm of (5.41) for large z :

$$\begin{aligned} \ln\left(\frac{fe^{\xi}}{4\ell_c} \gamma_e\right) &= \frac{1}{2} \ln\left(\left|\frac{z\gamma_e}{4\ell_c}\right|^2 \left|1 + \sqrt{1 - (f/z)^2}\right|^2\right) \\ &= \ln\left(\frac{|z|\gamma_e}{2\ell_c}\right) - \frac{1}{2} \sum_{\substack{n>0 \\ \text{even}}} \frac{(n-1)!}{2^n \left[\left(\frac{n}{2}\right)!\right]^2} \left[\left(\frac{f}{z}\right)^n + \left(\frac{f}{\bar{z}}\right)^n\right]. \end{aligned} \quad (5.43)$$

⁵Consistency is checked by evaluating (5.40) at any point (ξ_0, η) on the boundary, for which the left side gives $fe^{\xi_0+i\eta} = (a+b)e^{i\eta}$. Plugging $z = f \cosh(\xi_0 + i\eta)$ into the right side and choosing (+) (and the appropriate branch cut) recovers the same value.

Plugging this into (5.41) and comparing with (5.35) (with $\phi_{\text{bg}} = A^{(0)}$) yields the monopole polarizabilities

$$M^{(n)} = \frac{2\pi}{2^n \left[\left(\frac{n}{2}\right)!\right]^2} \frac{(a^2 - b^2)^{n/2}}{\ln\left(\frac{4\ell_c}{(a+b)\gamma_e}\right)}. \quad (5.44)$$

For an ellipse rotated an angle θ from the x -axis, the monopole polarizability is modified to $M^{(n)} \rightarrow e^{in\theta} M^{(n)}$, similar to C^{nm} and χ^{nm} in Eq. (5.27).

Higher-order polarizabilities. Since the bulk Hamiltonian has been modified, the question arises as to whether the higher-order polarizabilities will be affected. At first glance, it appears they may be unaltered since the higher order terms respect the conformal symmetry and the associated effective response involves only derivatives of the Green function, which are nonsingular in the $\ell_c \rightarrow \infty$ limit. But, due to the boundary conditions we cannot ignore the constant terms generated in (5.19). However, this term behaves like the constant background field introduced above and, as shown in Section C.3, the monopole terms conspire to *exactly* cancel it, thereby leaving C^{nm} , χ^{nm} , and $\bar{\chi}^{nm}$ with the same values found for (BC 2).

Limiting cases. Just as for C^{nm} and χ^{nm} , the fully anisotropic limit of a thin rod or needle of length L , the form of the expression (5.44) does not change significantly, only the replacements $a \rightarrow L/2$ and $b \rightarrow 0$ (*i.e.*, $s_{\pm} \rightarrow L/2 \implies f \rightarrow L/2$) is required. However, for a rotationally-symmetric disk of radius R (*i.e.*, $a, b \rightarrow R \implies f \rightarrow 0$), the anisotropic pieces $M^{(n \geq 1)}$ all clearly vanish, and the only surviving monopole polarizability is

$$M^{(0)} = \frac{2\pi}{\ln\left(\frac{2\ell_c}{R\gamma_e}\right)}, \quad (5.45)$$

in agreement with Chapter 3, and Ref. [YRD12] up to normalization.

5.3 Entropic interactions: free particles

The particle boundaries locally constrain thermal fluctuations which consequently induce surface-mediated, *entropic* interactions. The interaction potentials appear as differences associated free energy, and depend on the spatial arrangements and orientations of the particles. In particular, we write the interaction energy U as the difference in the free energy with respect to the particle-free surface,

$$\begin{aligned} -\beta U &:= -\beta(\mathcal{F} - \mathcal{F}_0) = \ln(Z/Z_0) \\ &= \sum_{q=0}^{\infty} \frac{1}{q!} \langle (-\beta \Delta \mathcal{H}[\phi])^q \rangle_c, \end{aligned} \quad (5.46)$$

where Z_0 is the particle-free (bulk) partition function, the correlation functions are (Gaussian) averages over the bulk Hamiltonian,

$$\langle \cdots \rangle = \frac{1}{Z_0} \int \mathcal{D}\phi (\cdots) e^{-\beta \mathcal{H}_0[\phi]}, \quad (5.47)$$

and the sum is over all *connected* correlation functions (cumulants). In this section we will first consider the simpler case of particles with the freedom to fluctuate vertically with the surface, applicable to (BC 2) and (BC 3), and treat the case of broken (vertical) translation invariance in the next section.

5.3.1 Diagrammar

By now, our approach for calculating such interactions should be of recent vintage: we reformulate the cumulant expansion as a diagrammatic expansion, thereby taking advantage of the systematics and transparency of the calculational bookkeeping and interpretation. Since the interactions considered here are strictly quadratic and of the entropic variety, we have from Chapter 3 that the interaction energy can be expressed as

$$-\beta U = \sum_{k \geq 1} \text{diagram with } k \text{ vertices labeled } V, \quad (5.48)$$

where the interaction vertices are define by the functional derivatives,

$$\begin{aligned} \text{diagram with one vertex } V \text{ and two legs } z, z' &= - \left[\frac{\delta^2(\beta \Delta \mathcal{H})}{\delta \phi(z) \delta \phi(z')} \right]_{\phi=0} \\ &= - \sum_{\alpha} \sum_{n, m \geq 1} \left[C_{\alpha}^{nm} (-\partial)^n \delta_{\alpha}^z (-\bar{\partial})^m \delta_{\alpha}^{z'} \right. \\ &\quad \left. + \frac{1}{2} \chi_{\alpha}^{nm} (-\partial)^n \delta_{\alpha}^z (-\partial)^m \delta_{\alpha}^{z'} \right. \\ &\quad \left. + \frac{1}{2} \bar{\chi}_{\alpha}^{nm} (-\bar{\partial})^n \delta_{\alpha}^z (-\bar{\partial})^m \delta_{\alpha}^{z'} \right] + (z \leftrightarrow z') \\ &\equiv \text{diagram with one vertex and two legs } z, z' + \text{diagram with one vertex and two legs } z, z' + \text{diagram with one vertex and two legs } z, z' + (z \leftrightarrow z'), \end{aligned} \quad (5.49)$$

and the propagators are given by the harmonic Green function (5.8). In the above expressions, $\delta_{\alpha}^z := \delta(z - z_{\alpha})$, and the sum over particle worldlines and derivative orders is implicit in each diagram vertex. The explicit operators corresponding to these vertices are as follows:

$$z_{\alpha} \cdots \text{diagram with one vertex and two legs } z, z' = -C_{\alpha}^{nm} e^{i(n-m)\theta_{\alpha}} (-\partial)^n \delta_{\alpha}^z (-\bar{\partial})^m \delta_{\alpha}^{z'} \quad (5.50a)$$

$$z_\alpha \cdots \begin{array}{c} \nearrow^n \\ \bullet \\ \searrow^m \end{array} \begin{array}{c} z \\ z' \end{array} = -\frac{1}{2} \chi_\alpha^{nm} e^{i(n+m)\theta_\alpha} (-\partial)^n \delta_\alpha^z (-\partial)^m \delta_\alpha^{z'} \quad (5.50b)$$

$$z_\alpha \cdots \begin{array}{c} \nearrow^n \\ \bullet \\ \searrow^m \end{array} \begin{array}{c} z \\ z' \end{array} = -\frac{1}{2} \bar{\chi}_\alpha^{nm} e^{-i(n+m)\theta_\alpha} (-\bar{\partial})^n \delta_\alpha^z (-\bar{\partial})^m \delta_\alpha^{z'}, \quad (5.50c)$$

where we have also accounted for the particle orientation as per Eq. (5.27). The factors of $1/2$ in front of the χ and $\bar{\chi}$ polarizabilities must be included since we have given the explicit endpoints z and z' and derivative orders n and m ; however, when the sum over derivatives is included, the two legs are symmetric under exchange ($z \leftrightarrow z'$) so the two cases cancel the $1/2$ factor.

The single- and double-line vertex legs are meant to indicate the type of derivatives the vertex places on the propagators, respectively ∂ and $\bar{\partial}$. Moreover, they inform the connectivity of the diagrams in that only single-line legs can connect with each other, and similarly for double-line legs, manifestly enforcing the constraint $\partial \bar{\partial} G(z_\alpha - z_\gamma) = 0$ for two particles α and γ . As we have discussed in previous chapters, the expansion (5.48) formally includes self-interactions, in which propagators begin and end on the same particle worldline. This is of course unfavorable since such self-interactions diverge, but these divergences are an artifact of coarse-graining the particles as infinitesimal points. A similar analysis as done in Appendix A shows that a proper renormalization treatment completely removes these self-interactions with no nontrivial renormalization group flow. That is, there is no physical information contained in the divergences and, furthermore, the unphysical (and *unobservable*) counterterms necessarily introduced in the renormalization procedure will completely remove them. Equivalently, we may simply set all diagrams containing self-interactions to zero.

Calculating the interaction energy therefore consists of expanding the vertices for each diagram of (5.48) according to (5.49), at which point the number of diagrams quickly proliferates. We can group the diagrams by noting that two diagrams are equivalent if they can be reflected or rotated into one another. Under this grouping, each representative diagram then carries an extra factor given by the number of distinct orientations multiplied by a factor of 2 for each χ and $\bar{\chi}$ vertices, due to the exchange symmetry of their indices. As we mentioned earlier, these powers of 2 are canceled by the factors of $1/2$ in (5.49). What remains simplifies to the expected $1/S_\Gamma$, where $S_\Gamma = |\text{Aut } \Gamma|$ is the symmetry factor for the diagram Γ .

The number of expected diagrams with k vertices is equivalent to the standard combinatorial problem of the number of ways to paint a necklace of k beads with only two colors. However, relationships among the diagrams effectively reduce this number; exchanging single lines and double lines gives the complex conjugate of the diagram. Diagrams with equal numbers of single line and double line edges—which can only occur for those with an even number of vertices—give diagrams in the same equivalency class of the original under this exchange (they are related by reflections and rotations) and therefore are their own conjugate; *i.e.*, they are real.

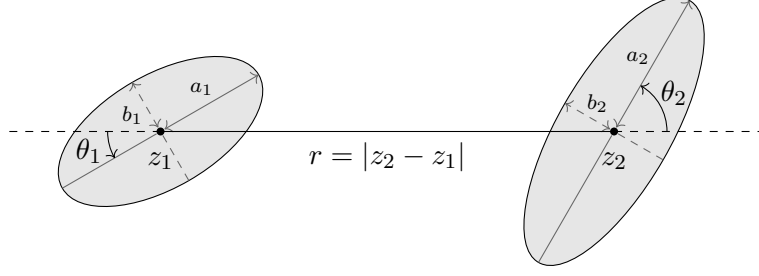


Figure 5.2: Configuration for two ellipses as viewed from above. The orientation angle θ_2 of second ellipse is measured from the line extended from z_1 past z_2 . Similarly, the orientation angle θ_1 is measured (counterclockwise) from the line extended from z_2 past z_1 .

5.3.2 Pair interactions

Consider two ellipses of semi-major axes a_1, a_2 and semi-minor axes b_1, b_2 respectively, positioned and oriented as shown in Fig. 5.2. The interaction energy expansion will only contain diagrams with an even number of vertices to prevent self interactions once the particle assignments are made at each vertex. We provide explicitly the relevant diagrams and their corresponding symmetry factors in Technical Note 5.1 for reference. To order the expansion in powers of the interparticle separation r , we note that each vertex places derivatives on the propagators, and $\partial^n G \sim r^{-n}$ (as per Eq. (5.12)). It follows that each diagram with a set of vertex indices $\{n_i, m_i\}$ will be of order $r^{-\sum_i (n_i + m_i)}$. Determining which diagrams are relevant at $\mathcal{O}(r^{-p})$ is therefore equivalent to the problem of partitioning the integer p into $2k$ integers and distributing them across the index pairs $\{n_i, m_i\}_{i \leq k}$ at each of the k vertices (while satisfying the constraint $n_i + m_i \in 2\mathbb{N}$). The resulting interaction energy can then be written in the form

$$-\beta U = \sum_{\substack{p > 0 \\ \text{even}}} \frac{u^{(p)}}{r^p}. \quad (5.51)$$

The leading order terms come from the diagrams with $k = 2$ vertices. For (BC 2), the polarizabilities begin at $n = m = 1$ and hence the leading order interaction energy is $\mathcal{O}(r^{-4})$. For (BC 3), however, these coefficients vanish and the polarizabilities begin at $n = m = 2$, implying the leading order interaction energy is $\mathcal{O}(r^{-8})$. Following the diagrammatic rules and accounting for the angular dependence using (5.27), we evaluate the diagrams in Technical Note 5.1 and find for (BC 2)

$$u^{(4)} = \frac{1}{16} [(s_1^+ s_2^+)^2 + f_1^2 f_2^2 \cos(2\theta_1 + 2\theta_2)], \quad (5.52a)$$

$$u^{(6)} = \frac{1}{32} \left\{ (s_1^+ s_2^+)^2 [(s_1^+)^2 + 3f_1^2 \cos(2\theta_1)] + 4f_1^4 f_2^2 \cos(4\theta_1 + 2\theta_2) \right\} + (1 \leftrightarrow 2), \quad (5.52b)$$

Technical Note 5.1: Expansion of entropic interaction diagrams

We provide for reference the vertex expansions and symmetry factors for the first few interaction diagrams relevant to particle pairs according to Eq. (5.49):

$$\begin{aligned}
 \text{Diagram 1} &= \text{Diagram 1a} + 2 \text{Re} \left[\text{Diagram 1b} \right] \\
 &\quad S[\Gamma_1^{(2)}]=2 \quad S[\Gamma_2^{(2)}]=4 \quad () \\
 \text{Diagram 2} &= \text{Diagram 2a} + \text{Diagram 2b} + 2 \text{Re} \left[\text{Diagram 2c} + \text{Diagram 2d} \right] \\
 &\quad S[\Gamma_1^{(4)}]=4 \quad S[\Gamma_2^{(4)}]=2 \quad S[\Gamma_3^{(4)}]=8 \quad S[\Gamma_4^{(4)}]=2 \\
 \text{Diagram 3} &= \text{Diagram 3a} + \text{Diagram 3b} + \text{Diagram 3c} \\
 &\quad S[\Gamma_1^{(6)}]=6 \quad S[\Gamma_2^{(6)}]=1 \quad S[\Gamma_3^{(6)}]=2 \\
 &\quad + 2 \text{Re} \left[\text{Diagram 3d} + \text{Diagram 3e} + \text{Diagram 3f} + \text{Diagram 3g} + \text{Diagram 3h} \right] \\
 &\quad S[\Gamma_4^{(6)}]=12 \quad S[\Gamma_5^{(6)}]=2 \quad S[\Gamma_6^{(6)}]=2 \quad S[\Gamma_7^{(6)}]=2 \quad S[\Gamma_8^{(6)}]=4
 \end{aligned}$$

For each diagram $\Gamma_i^{(k)}$ with k vertices, there is a set $\{n_j, m_j\}_{j=1}^k$ of derivative orders that ultimately contribute an overall factor of r^{-p} , where $p = \sum_{j=1}^k (n_j + m_j) \equiv |\mathbf{n} + \mathbf{m}|$. Denoting by I_k the label set of distinct diagrams possessing k vertices, we may express the series in increasing powers of $1/r$ by

$$-\beta U = \sum_{\substack{p>0 \\ \text{even}}} \sum_{k=2}^{p/2} \sum_{i \in I_k} \sum_{\substack{\{n_j, m_j\}_{j=1}^k \\ |\mathbf{n} + \mathbf{m}|=p}} \Gamma_i^{(k)}(\mathbf{n}, \mathbf{m}) \equiv \sum_{\substack{p>0 \\ \text{even}}} \frac{u^{(p)}}{r^p}.$$

$$\begin{aligned}
 u^{(8)} &= \frac{1}{2^{10}} \left\{ 19(s_1^+ s_2^+)^4 + f_1^2 f_2^2 (s_1^+ s_2^+)^2 [36 \cos(2\theta_1 - 2\theta_2) + 124 \cos(2\theta_1 + 2\theta_2)] \right. \\
 &\quad + 271 f_1^4 f_2^4 \cos(4\theta_1 + 4\theta_2) + 12(s_1^+)^6 (s_2^+)^2 + 36 f_1^4 (s_1^+ s_2^+)^2 + 2 f_1^4 (s_2^+)^4 \\
 &\quad + 32(s_1^+ s_2^+)^2 f_1^2 [2(s_1^+)^2 + 3(s_2^+)^2] \cos(2\theta_1) + 80 f_1^4 (s_1^+ s_2^+)^2 \cos(4\theta_1) \\
 &\quad \left. + 192 f_1^6 f_2^2 \cos(6\theta_1 + 2\theta_2) \right\} + (1 \leftrightarrow 2), \quad (5.52c)
 \end{aligned}$$

where $f^2 = s_+ s_-$ as before. Since the expressions become increasingly more lengthy, we have only included the interactions up to and including $\mathcal{O}(r^{-8})$, which only require diagrams with $k = 2$ and $k = 4$ vertices. The $k = 6$ diagrams appear at $\mathcal{O}(r^{-12})$.

For (BC 3) we find

$$u^{(8)} = \frac{9}{256} [(s_1^+ s_2^+)^4 + f_1^4 f_2^4 \cos(4\theta_1 + 4\theta_2)], \quad (5.53a)$$

$$u^{(10)} = \frac{3}{128} \left[(s_1^+)^6 (s_2^+)^4 + 5f_1^2 (s_1^+ s_2^+)^4 \cos(2\theta_1) \right. \\ \left. + 3f_1^4 (s_1^+)^2 (s_2^+)^4 + 9f_1^6 f_2^4 \cos(6\theta_1 + 4\theta_2) \right] + (1 \leftrightarrow 2), \quad (5.53b)$$

$$u^{(12)} = \frac{5}{2^{11}} \left\{ 5(s_1^+ s_2^+)^6 + 5(s_1^+ s_2^+)^2 \left[(s_1^+)^6 (s_2^+)^2 + 6(s_1^+)^4 f_2^4 + 8(s_1^+ s_2^+)^2 f_2^4 \right] \right. \\ + 45(s_1^+ s_2^+)^2 f_1^4 f_2^4 + 396f_1^6 f_2^6 \cos(6\theta_1 + 6\theta_2) + 63(s_1^+ s_2^+)^4 f_1^4 \cos(4\theta_1) \\ + 4(s_1^+ s_2^+)^4 f_1^2 f_2^2 [10 \cos(2\theta_1 - 2\theta_2) + 21 \cos(2\theta_1 + 2\theta_2)] \\ + 12(s_1^+ s_2^+)^2 f_1^2 \cos(2\theta_1) [3(s_1^+)^4 (s_2^+)^2 + 4(s_1^+)^2 (s_2^+)^4 \\ \left. + 6f_1^4 (s_2^+)^2 + 12(s_1^+)^2 f_2^4] + 216f_1^8 f_2^4 \cos(8\theta_1 + 4\theta_2) \right\} + (1 \leftrightarrow 2). \quad (5.53c)$$

To this order, only the diagrams with $k = 2$ vertices contribute. The $k = 4$ diagrams do not contribute until $\mathcal{O}(r^{-16})$.

For identical ellipses, we simply set $s_1^\pm = s_2^\pm$ in the above expressions. The leading order terms then reproduce the results of [NO09] up to powers of 2^p for $\mathcal{O}(r^{-p})$, where the discrepancy is due to differing assignments of a and b ([NO09] refers to the principal axes, which are twice the values of the semi-major and semi-minor axes used here). Setting $s_i^+ = 2R_i$ and $s_i^- = 0$ gives the interaction energy between two disks of radii R_1 and R_2 respectively and reproduce the results of [YRD12] for (BC 2) (compare also with Eqs. (3.208), (3.209), and (3.211)). Since the result for disks obeying (BC 3) appears to be absent from the literature, we provide the first few terms explicitly:

$$\beta U_{\{1,2\}}^{\text{disks}} = -9 \frac{R_1^4 R_2^4}{r^8} - 24 \frac{R_1^6 R_2^4 + R_1^4 R_2^6}{r^{10}} - 50 \frac{R_1^8 R_2^4 + 2R_1^6 R_2^6 + R_1^4 R_2^8}{r^{12}} + \mathcal{O}(r^{-14}), \quad (5.54)$$

which agrees with our earlier leading-order result Eq. (3.213) calculated in Chapter 3. Furthermore, setting $s_i^\pm = L_i/2$ in Eqs. (5.52) and (5.53) gives the interaction energy between rods.

Since we have computed the interaction energies between nonidentical ellipses, we can also consider the limiting cases of disks and rods for each particle independently. Doing so gives new results for the interactions between an ellipse and rod, ellipse and disk, and a rod and disk. Furthermore, since the boundary constraints are contained within the polarizabilities, it is straightforward to compute the interactions between particles with different boundary conditions. For example, the leading order interactions between a bobbing disk (D) and an ellipse (E) free to bob *and* tilt is given by the polarizabilities C_D^{11} and C_E^{22} respectively, yielding⁶

$$\beta U_{D-E} = -4 \frac{C_D^{(11)} C_E^{(22)}}{(4\pi)^2 r^6} + \mathcal{O}(r^{-8}) \\ = -\frac{R^2(a+b)^4}{8r^6} + \mathcal{O}(r^{-8}). \quad (5.55)$$

⁶Unfortunately the published version—Eq. (62) of [HD14]—is off by a factor of two.

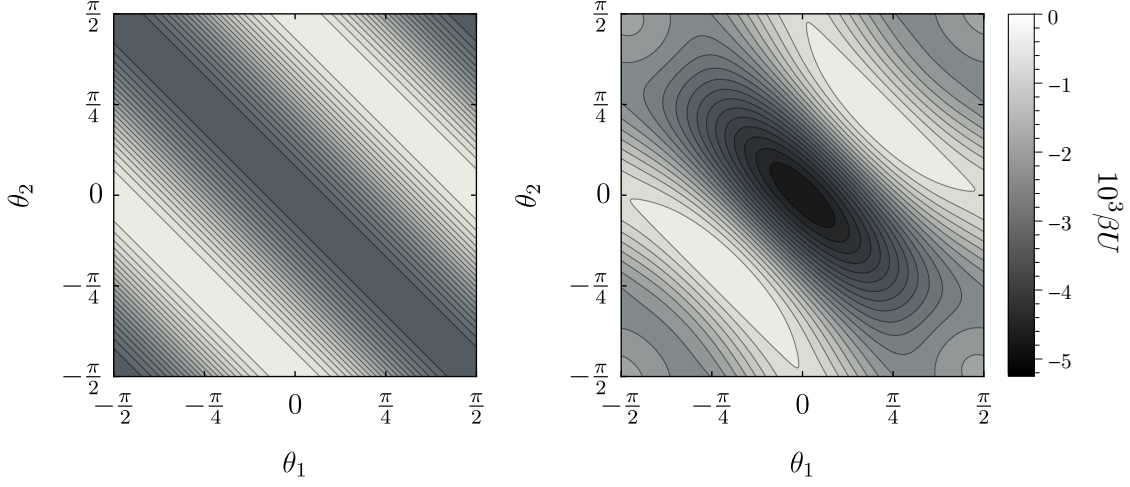


Figure 5.3: Plots of the pair interaction free energy between identical rods of length L separated by a distance $r = 1.25L$. The leading-order $\mathcal{O}(r^{-4})$ result is presented on the left and shows the degeneracy of the minimum energy configurations. The plot on the right includes the $\mathcal{O}(r^{-6})$ correction and demonstrates the breakdown of this degeneracy after leading order.

Oriental dependence

At leading order for (BC 2), the energy is minimized for $\theta_1 + \theta_2 = n\pi$, $n \in \mathbb{Z}$, which is degenerate for a full range of angles. Similarly, there is a degenerate maximum-energy state given by $\theta_1 + \theta_2 = (n + 1/2)\pi$, $n \in \mathbb{Z}$. This degeneracy was noted in Ref. [GGK96a] with the speculation that it should be broken by higher-order terms. Indeed, at the very next order, the angular dependence breaks this symmetry and we find the true minimum-energy configuration occurs for $\theta_1 = \theta_2 = 0$ (up to integer multiples of π) which aligns the major principal axes (tip-to-tip). The energy is maximized for two unique values $\theta_1 = \theta_2 \lesssim \pi/4$ and $\gtrsim 3\pi/4$ which depend on particle size and separation. This symmetry breaking is illustrated in Fig. 5.3 for the limiting case of identical rods. Although the leading-order angular dependence for (BC 3) differs by an additional factor of two from (BC 2), we find similar behavior, but the least-preferred orientations—which depend on particle size and separation—lie within the intervals $(\pi/4, \pi/2)$ and $(\pi/2, 3\pi/4)$. It is interesting to compare the preferred orientations with those observed for ellipsoidal objects in the three-dimensional electromagnetic case [EGJK09]; the preferred orientations are similar, but the least preferred orientations are different.

We can also compare with the ground state angular dependence of two permanent quadrupoles considered in Chapter 3. The leading-order (BC 2) term, Eq. (3.146), appears with the same separation dependence $\sim r^{-4}$ and a similar angular dependence $\sim \cos(2\alpha_1 + 2\alpha_2)$, where α_1 and α_2 are the angles which the principle curvature axes of each particle makes with the interparticle joining line. We discovered that the preferred, maximally attractive configurations occur for all $\alpha_1 + \alpha_2 \equiv 0 \pmod{\pi}$. That is, the

particles tend to align like-curvatures, including the “tip-to-tip” configuration that aligns their principle axes. The primary difference, however, is that the angular degeneracy for permanent quadrupoles persists to all orders (see the discussion on page 115). This is because the anisotropy is due only to the out-of-plane curvature, but the multipole moments in one particle induced by the presence of another inherit the symmetries of the circular in-plane boundary. This contrasts with the elliptical particles of this chapter, for which the anisotropy is due solely to the in-plane boundary shape and contaminates the symmetries associated with the induced multipole moments.

5.3.3 Multibody interactions

In addition to pairwise interactions, the energy also receives contributions from multibody terms. In general, N -body interactions will begin to appear in diagrams with N vertices of lowest multipole order. However, in special cases the symmetry of the particles may lead to the vanishing of some terms. For example, only the C^{mn} polarizabilities are nonzero for axisymmetric particles (disks), and all diagrams with an odd number of vertices vanish. As we discussed in Chapter 3 (see Section 3.6.3), this conclusion becomes obvious in the diagrammatic language since it is impossible to connect an odd number of C -vertices such that each vertex connects to both a single and a double line. This property was first stated in Ref. [YRD12] (with slightly different diagrammatic rules), and is a manifestation of the vanishing of $\partial\bar{\partial}G$. With this symmetry relaxed, however, the χ -vertices allow for nonvanishing diagrams with an odd number of vertices and represent pure anisotropic effects. For brevity, we will restrict our discussion to the (BC 2) case, but the results for (BC 3) follow similarly.

Since the multibody interactions mix the particle coordinates, it is desirable to define a suitable parametrization that relates to the geometry of the particle configuration in a coordinate-free manner. To this aim, we define $z_{ij} := z_j - z_i \equiv r_{ij}e^{i\varphi_{ij}}$ as well as the exterior vertex angle $\varphi_{ik}^j := -\varphi_{ij} + \varphi_{jk}$ as shown in Fig. 5.4. Furthermore, we parametrize the orientation of the particles with respect to the exterior vertex angles via $\theta_{ij}^{(j)} := \theta_j - \varphi_{ij}$, where θ_i is the angle the particle makes from the x -axis. Note that $\varphi_{ji} \equiv \varphi_{ij} \pmod{\pi}$, and therefore under the exchange of indices we can equate $\varphi_{ki}^j = -\varphi_{ik}^j$ and $\theta_{ij}^{(i)} = \theta_{ji}^{(i)}$ up to integer multiples of π .

We first consider the leading-order triplet (three-body) interaction, which comes from the diagrams


(5.56)

and their complex conjugates. Since self-interactions are set to zero, the sum over particle

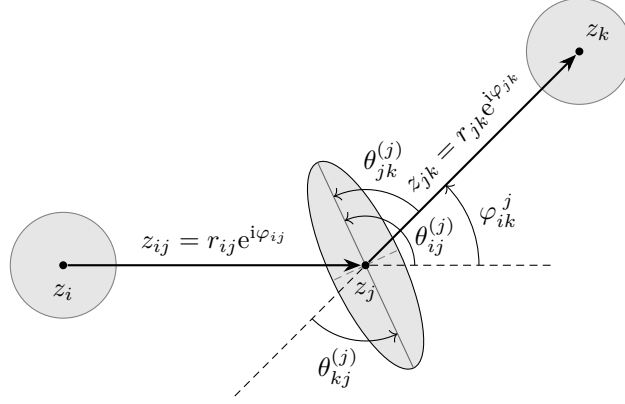


Figure 5.4: Illustration of the parameter and angle definitions for a particle at position z_j . The exterior angle φ_{ik}^j is measured between the two joining lines defined by z_{ij} and z_{jk} . Similarly, $\theta_{ij}^{(j)}$ measure the orientation angle of the particle j with respect to z_{ij} . Alternatively, $\theta_{jk}^{(j)}$ provides the orientation with respect to z_{jk} , which is equivalent to the corresponding (exterior) orientation angle $\theta_{kj}^{(j)}$. These two angles are in agreement with Fig. 5.2 so that $\theta_{ij}^{(j)}$ is appropriate for pairwise comparisons between particles i and j , and $\theta_{kj}^{(j)}$ is appropriate for pairwise comparisons between particles j and k .

labels becomes the sum over permutations of $\{1, 2, 3\}$. Computing the diagrams results in

$$\begin{aligned} \beta U_{\text{tri}}^{(6)} &= -2 \operatorname{Re} \sum_{i,j,k}^{\text{perm. } \{1,2,3\}} \left[\frac{1}{2} \frac{\chi_i^{11} C_j^{11} C_k^{11}}{(4\pi)^3} \frac{e^{2i\theta_i}}{z_{ij}^2 \bar{z}_{jk}^2 z_{ki}^2} + \frac{1}{6} \frac{\chi_i^{11} \chi_j^{11} \chi_k^{11}}{(4\pi)^3} \frac{e^{2i(\theta_i + \theta_j + \theta_k)}}{z_{ij}^2 z_{jk}^2 z_{ki}^2} \right] \\ &= -\frac{1}{64} \sum_{i,j,k}^{\text{perm. } \{1,2,3\}} \frac{1}{r_{ij}^2 r_{jk}^2 r_{ki}^2} \left[f_i^2 (s_j^+ s_k^+)^2 \cos(2\theta_{ki}^{(i)} + 2\varphi_{ik}^j) \right. \\ &\quad \left. + \frac{1}{3} f_i^2 f_j^2 f_k^2 \cos(2\theta_{ki}^{(i)} + 2\theta_{ij}^{(j)} + 2\theta_{jk}^{(k)}) \right]. \end{aligned} \quad (5.57)$$

This expression can be simplified by noting that if the summand is invariant under the exchange of two indices, the sum can be written as twice the sum over cyclic permutations. The second term is seen to be invariant under $j \leftrightarrow k$ by noticing that

$$\begin{aligned} \theta_{ji}^{(i)} + \varphi_{ij}^k &= \theta_i - \varphi_{ji} - \varphi_{ik} + \varphi_{kj} \\ &= \theta_{ki}^{(i)} + \varphi_{ik}^j. \end{aligned} \quad (5.58)$$

Using this same property, we see the second term is also invariant under $j \leftrightarrow k$:

$$\begin{aligned}\theta_{ji}^{(i)} + \theta_{ik}^{(k)} + \theta_{kj}^{(j)} &= \theta_{ki}^{(i)} + \theta_{ij}^{(j)} + \theta_{jk}^{(k)} - \varphi_{ik}^j - \varphi_{ji}^k - \varphi_{kj}^i \\ &= \theta_{ki}^{(i)} + \theta_{ij}^{(j)} + \theta_{jk}^{(k)} - 2\pi,\end{aligned}\tag{5.59}$$

where we have used that the sum over all exterior angles gives 2π . The result finally simplifies to

$$\begin{aligned}\beta U_{\text{tri}}^{(6)} &= -\frac{1}{32} \frac{1}{r_{12}^2 r_{23}^2 r_{31}^2} \left[f_1^2 f_2^2 f_3^2 \cos(2\theta_{31}^{(1)} + 2\theta_{12}^{(2)} + 2\theta_{23}^{(3)}) \right. \\ &\quad \left. + \sum_{i,j,k}^{\text{cyc.}} f_i^2 (s_j^+ s_k^+)^2 \cos(2\theta_{ki}^{(i)} + 2\varphi_{ik}^j) \right].\end{aligned}\tag{5.60}$$

From the above expression, we see that the minimum energy configurations—suggested from the triplet interaction alone—occur for $\theta_{ki}^{(i)} = -\varphi_{ik}^j$, up to integer multiples of π . It is also apparent that the least preferred configurations occur when $\theta_{ki}^{(i)} = \pi/2 - \varphi_{ik}^j$, which maximizes the energy. Note that we can as well rewrite these expressions in terms of the *interior* angles by noting that an interior angle $\alpha_{ik}^j = \pi - \varphi_{ik}^j$, but all expressions are equivalent modulo π . These configurations are illustrated in Fig. 5.5.

Since pair interactions will of course also contribute to the three-body interaction energy, it may be that the preferred angular configuration suggested above could be modified. From the leading-order pair interaction (5.52a), we find⁷

$$\beta U_{\text{p}}^{(4)} = -\frac{1}{16} \sum_{i,j}^{\text{cyc.}} \frac{1}{r_{ij}^4} \left[(s_i^+ s_j^+)^2 + f_i^2 f_j^2 \cos(2\theta_{ji}^{(i)} + 2\theta_{ij}^{(j)}) \right].\tag{5.61}$$

The energy is minimized when $\theta_{ji}^{(i)} + \theta_{ij}^{(j)} \equiv 0 \pmod{\pi}$, which when summed over the three particle labels gives the condition

$$\theta_{31}^{(1)} + \theta_{12}^{(2)} + \theta_{23}^{(3)} \equiv 0 \pmod{\frac{\pi}{2}}.\tag{5.62}$$

From Eq. (5.58) and the condition $\theta_{ji}^{(i)} + \theta_{ij}^{(j)} \equiv 0 \pmod{\pi}$, it also follows that $\theta_{ki}^{(i)} + \theta_{ij}^{(j)} \equiv \varphi_{kj}^i \pmod{\pi}$. This combined with Eq. (5.62) finally gives the preferred-configuration conditions,

$$\theta_{ki}^{(i)} = \pi - \varphi_{ik}^j + \frac{n\pi}{2} = \alpha_{ik}^j + \frac{n\pi}{2}, \quad n \in \mathbb{Z}.\tag{5.63}$$

⁷In Ref. [HD14], the argument of the cosine was written as $2(\theta_{ki}^{(i)} + \theta_{ij}^{(j)} - \varphi_{kj}^i)$. This is also correct and follows from Eq. (5.58) with some rearrangement. I have changed it to the present form so that the energy expression follows more clearly from Eq. (5.52a) in light of the angle definitions in Figures 5.2 and 5.4.

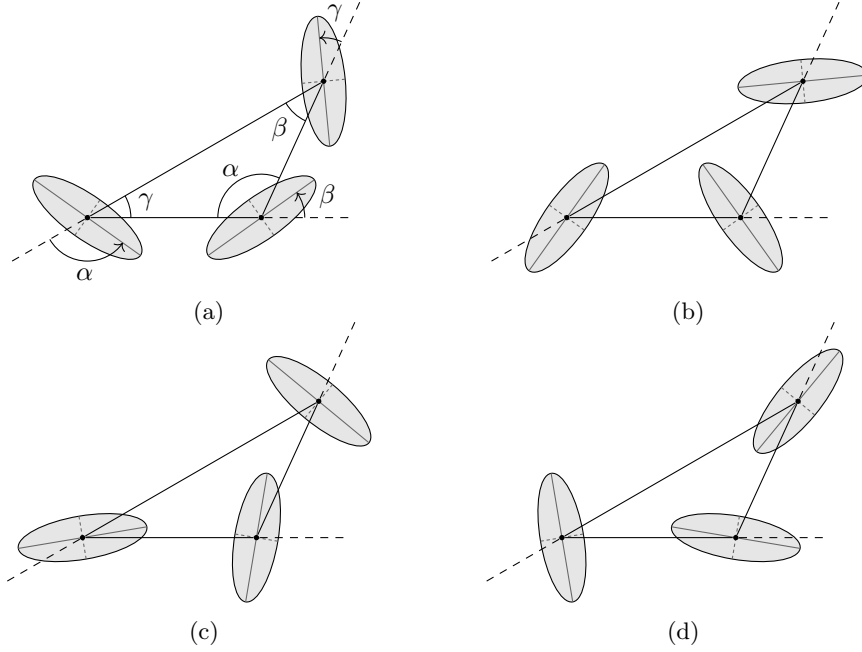


Figure 5.5: Illustration of the various ellipse orientations for an arbitrary three-body particle configuration. The pure triplet interaction suggests configuration (a) is preferred (minimizes the energy), while configuration (b) is preferred the least (maximizes the energy). However, with the inclusion of all the pair interactions up to the same order, this conclusion switches: (b) is actually preferred, while (a) is just a local minimum. The least preferred configurations as suggested by the pair interactions are shown in (c) and (d).

The angular configuration that maximizes the energy is similar, but with $\pi/4$ subtracted from each angle. These configurations again appear in Fig. 5.5.

At leading order, the minimum-energy configuration therefore suffers from a double degeneracy. This degeneracy is broken at the next order with the pair and triplet interactions. To simplify the remainder of our discussion, we can take advantage of the similarity of the solutions—the preferred ellipse orientations all depend similarly on the respective adjacent interior angles of the particle configuration as per Eq. (5.63)—and consider the highly symmetric case of the particles sitting at the vertices of an equilateral triangle with side lengths d . Furthermore, consider the limiting case in which the ellipses become identical rods of length L . This results in reducing the problem to a one dimensional angular subspace in which $\theta_{31}^{(1)} = \theta_{12}^{(2)} = \theta_{23}^{(3)} \equiv \theta$ and $\varphi_{13}^2 = \varphi_{21}^3 = \varphi_{32}^1 = 2\pi/3$. This simplification gives for the pair energies

$$\beta U_{\text{p}}^{(4)} = -\frac{3}{16} \left(\frac{L}{2d} \right)^4 \left\{ 1 + \cos \left[4 \left(\theta - \frac{\pi}{3} \right) \right] \right\}, \quad (5.64)$$

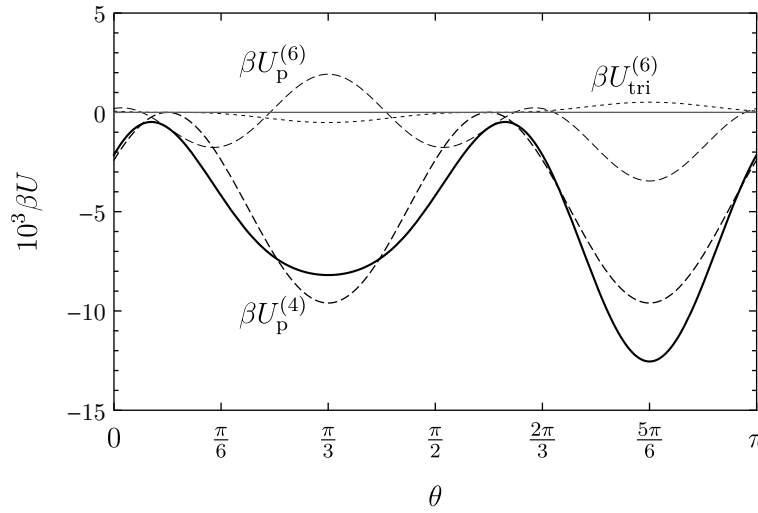


Figure 5.6: Plot of the pair and triplet contributions to the overall interaction free energy for identical rods of length L sitting at the vertices of an equilateral triangle of sides $d = 1.25L$. Notice the competition between the triplet and pair interactions appearing at $O(d^{-6})$. The pair interactions ultimately dominate and we find the preferred orientations occur for $\theta = 5\pi/6$, in which all rods point inwards.

$$\begin{aligned} \beta U_p^{(6)} = & -\frac{3}{32} \left(\frac{L}{2d} \right)^6 \left\{ 2 + 3 \cos \left[2 \left(\theta - \frac{2\pi}{3} \right) \right] + 3 \cos(2\theta) \right. \\ & \left. + 4 \cos \left[2 \left(3\theta - \frac{4\pi}{3} \right) \right] + 4 \cos \left[2 \left(3\theta - \frac{2\pi}{3} \right) \right] \right\}; \end{aligned} \quad (5.65)$$

and for the triplet energy

$$\beta U_{\text{tri}}^{(6)} = -\frac{1}{32} \left(\frac{L}{2d} \right)^6 \left\{ \cos(6\theta) + 3 \cos \left[2 \left(\theta + \frac{2\pi}{3} \right) \right] \right\}. \quad (5.66)$$

The result, which is plotted in Fig. 5.6, is that the degeneracy is broken and the $\theta = 5\pi/6$ configuration preferred. This implies the $\theta_{ki}^{(i)} = \alpha_{ik}^j + \pi/2$ solution from before is the true minimum. Surprisingly, there is competition at $O(d^{-6})$ between the pairs and triplet: the preferred angular configurations are opposite one another, but with the pairs ultimately dominating. That is, the triplet interaction alone suggests the opposite conclusion of the full result, and simply decreases the difference between the two minima.

5.4 Entropic interactions: fixed particles

Let us now consider the interactions between particles with fixed heights. Such particles break the vertical translation symmetry of the surface and are consequently excited by zero-mode fluctuations. For this two-dimensional system, the excitation of zero-modes

is problematic and leads to pathological results. However, with the inclusion of the gravitational potential as a regulator—so that $a, b \ll r \ll \ell_c$ —we found that the divergences are tamed and, moreover, sensible results can still be obtained in the harmonic limit in which $\ell_c \rightarrow \infty$. The key is to be careful and consistent with the use of the regulator, taking the limit only at the end of the calculation of an *observable* (*i.e.*, not a single Feynman diagram), namely

$$U = \lim_{\ell_c \rightarrow \infty} U(\ell_c).$$

In Section 5.2.4, we were successful in capturing the monopole response at finite Bond number, finding that the monopole polarizabilities decay as $\sim 1/\ln \ell_c$ (see Eq. (5.44)). Since the Green function diverges as $\sim \ln \ell_c$, as per Eq. (5.32), interesting limiting behavior should be expected. This is particularly true regarding the “pure” monopoles, characterized by $M^{(0)}$, since their induced interactions are governed by the Green function without derivatives. Moreover, these pure monopoles are accounted for in the effective Hamiltonian by marginal *dimensionless* operators and therefore cannot be dealt with perturbatively; instead, the naïve perturbative expansion must be resummed in its entirety. Luckily, we developed the required resummation principles and mathematical machinery in Chapter 3, namely Sections 3.5.4 and 3.6.4, and we will make liberal use of it here. This section will closely mirror the development of Section 3.6.4.

5.4.1 Leading order

The leading order interactions consist of strictly monopole vertices and is given by the infinite series

$$-\beta U^{(0)} = \sum_{k=1}^{\infty} \text{diagram with } k \text{ vertices}, \quad (5.67)$$

where each vertex has the diagrammatic correspondence

$$z_\alpha \cdots \text{diagram} \cdots z_{\alpha'} = -M_\alpha^{(0)} \delta_\alpha^z \delta_\alpha^{z'}, \quad (5.68)$$

and the dashed-line propagators remind us that no derivatives are placed on the Green function. The diagrammatic rules also dictate that all free positions (*e.g.*, z and z') are integrated over and all particle labels are summed over, but with the stipulation that no two adjacent vertices can simultaneous occur at the same particle position (*i.e.*, no self-interactions). The integrations and summations ultimately contract all spatial variables to the particle positions and therefore the operator algebra reduces to matrix algebra. This is achieved by following the steps leading up to Eq. (3.224), so that the sum is recast as

$$-\beta U^{(0)} = -\frac{1}{2} \ln \det(\mathbf{1} + \mathbf{G} \mathbf{M}), \quad (5.69)$$

where the determinant is taken over the interaction matrix

$$(\mathbf{1} + \mathbf{GM})_j^i = \delta_j^i + \sum_{\alpha} G^{i\alpha} M_{\alpha}^{(0)} \delta_j^{\alpha} (1 - \delta_a^i) = \delta_j^i + G^{ij} M_j^{(0)} (1 - \delta_j^i). \quad (5.70)$$

The indices i and j run over all particle labels, and the factor $(1 - \delta_j^i)$ makes explicit the absence of self-interactions. For a collection of N particles, we see the calculation of the leading-order interaction reduces to taking the determinant of the matrix

$$\mathbf{1} + \mathbf{GM} = \begin{pmatrix} 1 & G^{12} M_2^{(0)} & \cdots & G^{1N} M_N^{(0)} \\ G^{21} M_1^{(0)} & 1 & \cdots & G^{2N} M_N^{(0)} \\ \vdots & \vdots & \ddots & \vdots \\ G^{N1} M_1^{(0)} & G^{N2} M_2^{(0)} & \cdots & 1 \end{pmatrix}, \quad (5.71)$$

and plugging the result into Eq. (5.69). In line with Chapter 3, we will express the results using the notation

$$g_{ij}^2 := G^{ij} M_j^{(0)} G^{ji} M_i^{(0)} = \frac{\ln^2\left(\frac{2\ell_c}{\gamma_e r_{ij}}\right)}{\ln\left(\frac{4\ell_c}{\gamma_e s_i^+}\right) \ln\left(\frac{4\ell_c}{\gamma_e s_j^+}\right)}, \quad (5.72)$$

and furthermore introduce the parameter

$$\Lambda_{ij} := \ln\left(\frac{4\ell_c}{\gamma_e \sqrt{s_i^+ s_j^+}}\right) \quad (5.73)$$

to massage the expression into a form better suited for later expansions:

$$g_{ij} = \frac{\Lambda_{ij} - \ln\left(\frac{2r_{ij}}{\sqrt{s_i^+ s_j^+}}\right)}{(\Lambda_{ij}^2 - \ln^2 \sqrt{s_i^+ s_j^+})^{1/2}} = 1 - \frac{1}{\Lambda_{ij}} \ln\left(\frac{2r_{ij}}{\sqrt{s_i^+ s_j^+}}\right) + \frac{\ln^2 \sqrt{s_i^+ s_j^+}}{2\Lambda_{ij}^2} + \mathcal{O}(\Lambda_{ij}^{-3}). \quad (5.74)$$

Two particles.

For two particles, the determinant is very simple and we quickly find the interaction energy

$$\beta U_{\{1,2\}}^{(0)} = \frac{1}{2} \ln(1 - g_{12}^2). \quad (5.75)$$

With the help of Eq. (5.74), we expand this result in powers of $1/\Lambda$ and find the divergences only appear as an irrelevant (infinite) constant:

$$\beta U_{\{1,2\}}^{(0)} = -\frac{1}{2} \ln \Lambda_{12} + \beta \mathcal{E}_{12} + \mathcal{O}(\Lambda^{-1}), \quad (5.76)$$

where

$$\beta\mathcal{E}_{12} = \frac{1}{2} \ln \left[2 \ln \left(\frac{2r_{12}}{\sqrt{s_1^+ s_2^+}} \right) \right] \quad (5.77)$$

contains the r -dependent terms. The r -dependence, in agreement with [NO09], shows that at this order the interaction is always attractive.

Three particles.

For a three-particle system, we find the complete leading-order interaction energy

$$\beta U_{\{1,2,3\}}^{(0)} = \frac{1}{2} \ln [1 - (g_{12}^2 + g_{23}^2 + g_{31}^2 - 2g_{12}g_{23}g_{31})]. \quad (5.78)$$

This result contains but somewhat obscures the role of both pair and triplet interactions (*i.e.*, two-body versus three-body effects). We may examine each explicitly, however, through the additive decomposition

$$U_{\{1,2,3\}}^{(0)} = U_{\{1,2\}}^{(0)} + U_{\{2,3\}}^{(0)} + U_{\{3,1\}}^{(0)} + U_{\text{tri}}^{(0)}, \quad (5.79)$$

where $U_{\{i,j\}}^{(0)}$ is the pair interaction (5.76) between particles i and j , and $U_{\text{tri}}^{(0)}$ is the triplet interaction,

$$\beta U_{\text{tri}}^{(0)} = \frac{1}{2} \ln \left[\frac{1 - (g_{12}^2 + g_{23}^2 + g_{31}^2 - 2g_{12}g_{23}g_{31})}{(1 - g_{12}^2)(1 - g_{23}^2)(1 - g_{31}^2)} \right]. \quad (5.80)$$

In the limit of circular particles ($s_i^+ = 2R_i$), we recover the result obtained by a scattering approach in Ref. [NWZ13a]⁸ (as well as the results of Chapter 3).

To understand the three-particle behavior at vanishing Bond number, we expand Eq. (5.78) using Eq. (5.74). After some simplification, we find the *total* three-body interaction energy

$$\beta U_{\{1,2,3\}}^{(0)} = -\frac{1}{3} \ln(\Lambda_{12}\Lambda_{23}\Lambda_{31}) + \beta\mathcal{E}_{\text{tot}} + O(\Lambda^{-1}), \quad (5.81)$$

with

$$\beta\mathcal{E}_{\text{tot}} = \frac{1}{2} \ln \left(\sum_{i,j,k}^{\text{cyc.}} \left[2 \ln \left(\frac{2r_{ij}}{\sqrt{s_i^+ s_j^+}} \right) \ln \left(\frac{2r_{jk}}{\sqrt{s_j^+ s_k^+}} \right) - \ln^2 \left(\frac{2r_{ij}}{\sqrt{s_i^+ s_j^+}} \right) \right] \right). \quad (5.82)$$

The triplet (pure three-body) interaction is of course found by subtracting off the pairs:

$$\mathcal{E}_{\text{tri}} = \mathcal{E}_{\text{tot}} - \mathcal{E}_{12} - \mathcal{E}_{23} - \mathcal{E}_{31}. \quad (5.83)$$

Consider now a collection of three identical particles ($s_i^+ = s_+$ for all i) in two different configurations: sitting at the vertices of an equilateral triangle of side lengths d ($r_{12} =$

⁸Note that Ref. [NWZ13a] has a typo in their g^3 term (see footnote 34 on page 146).

$r_{23} = r_{31} = d$), and equally spaced on a line ($r_{12} = r_{23} = r_{31}/2 = d$). For the triangle configuration, Eq. (5.81) reduces to

$$\beta U_{\triangle}^{(0)} = -\ln \Lambda + \frac{1}{2} \ln [3 \ln^2(2d/s_+)] + \mathcal{O}(\Lambda^{-1}), \quad (5.84)$$

which is overall attractive. To see what role the triplet interaction plays, we subtract off the pairs as in Eq. (5.80) and find that the triplet and pair interactions can be expressed with the same d -dependence, but with opposite signs:

$$\begin{aligned} \beta U_{\text{tri},\triangle}^{(0)} &= \frac{1}{2} \ln \Lambda - \frac{1}{2} \ln \left[\frac{8}{3} \ln^2 \left(\frac{2d}{s_+} \right) \right] + \mathcal{O}(\Lambda^{-1}) \\ &= \frac{1}{2} \ln \frac{3\Lambda}{4} - \frac{1}{2} \ln \left[2 \ln^2 \left(\frac{2d}{s_+} \right) \right] + \mathcal{O}(\Lambda^{-1}). \end{aligned} \quad (5.85)$$

This pure three-body interaction is in fact *repulsive*, but not enough so to overcome the attractive pair interactions. For the linear configuration, the total energy is given by

$$\beta U_{\text{lin}}^{(0)} = \frac{1}{2} \ln \left[4 \ln^2 \left(\frac{2d}{s_+} \right) \ln^2 \left(\frac{4d}{s_+} \right) - \ln^2 \left(\frac{4d}{s_+} \right) \right] - \ln \Lambda + \mathcal{O}(\Lambda^{-1}) \quad (5.86)$$

which is also overall attractive. Although it is less obvious than in the triangle configuration, the pure three-body interaction in this case is also repulsive, as can be checked by subtracting off the pairs. Dropping the (infinite) constants, the triplet interaction reads

$$\beta \mathcal{E}_{\text{tri,lin}} = -\frac{1}{2} \ln \left[\frac{8 \ln^2 \left(\frac{2d}{s_+} \right)}{3 \ln^2 \left(\frac{2d}{s_+} \right) - \ln 2} \right]. \quad (5.87)$$

In both the two- and three-body results, Eqs. (5.75) and (5.78) respectively, the interaction energies are isotropic. Indeed, the results agree with Eqs. (3.225) and (3.228) computed for circular disks, but with the replacement $R \rightarrow (a+b)/2$ as the characteristic particle size. Given that the pure monopole polarizability $M^{(0)}$ does not depend on the particle's orientation, this should not be surprising. At higher orders the anisotropic effects begin to appear, particularly those related to $M^{(n \geq 1)}$.

5.4.2 Higher orders

To calculate higher orders, we must again include an infinite number of $M^{(0)}$ -insertions. This has the effect of replacing each propagator with the sum

$$\bullet \cdots \bullet \rightarrow \bullet \cdots \bullet + \bullet \cdots \otimes \bullet + \bullet \cdots \otimes \cdots \otimes \bullet + \bullet \cdots \otimes \cdots \otimes \cdots \otimes \bullet + \cdots \quad (5.88)$$

This infinite series, which we recognize as a type of Dyson equation, is a geometric sum involving powers of $\mathbf{1} + \mathbf{GM}$ and is formally convergent in the sense of matrices. Reorganizing

the inner vertex sum gives

$$\begin{aligned}
 & \succ \text{---} \otimes \text{---} \prec + \succ \text{---} \otimes \text{---} \otimes \text{---} \prec + \succ \text{---} \otimes \text{---} \otimes \text{---} \otimes \text{---} \prec + \dots \\
 &= \succ \text{---} \otimes \text{---} \prec \left(\bullet \text{---} \prec + \bullet \text{---} \otimes \text{---} \prec + \bullet \text{---} \otimes \text{---} \otimes \text{---} \prec + \dots \right) \\
 &= \succ \text{---} \otimes \text{---} \prec \sum_{k=0}^{\infty} \left(\bullet \text{---} \otimes \text{---} \prec \right)^k \\
 &\stackrel{*}{=} \succ \text{---} \otimes \text{---} \prec \left(\bullet \text{---} \prec - \bullet \text{---} \otimes \text{---} \prec \right)^{-1} \\
 &\equiv \succ \text{---} \otimes \text{---} \prec (\mathbf{1} + \mathbf{GM})^{-1}, \tag{5.89}
 \end{aligned}$$

where in the starred equality we completed the geometric sum, and in the last line we recognized the diagrammatic result as the inverse of the matrix $\mathbf{1} + \mathbf{GM}$. As long as the number of particles is not too large, this matrix inverse is relatively straightforward to compute. It follows from the Cayley–Hamilton theorem (see Technical Note 3.2) that for N particles, the inverse will contain an overall factor of $1/\det(\mathbf{1} + \mathbf{GM})$ and up to $N - 1$ powers of \mathbf{GM} and their traces.

The vertex sum contains two possibilities: either the vertices begin and end on the same particle worldlines (diagonal entries), or begin and end on different particle worldlines (off-diagonal entries). This motivates grouping the elements of Eq. (5.89) into the following effective monopole vertices:

$$i \succ \text{---} \otimes \text{---} \prec j = - \sum_{\alpha} M_{\alpha}^{(0)} [(\mathbf{1} + \mathbf{GM})^{-1}]_{\alpha}^{\alpha} \delta_{\alpha}^i \delta_j^{\alpha} \tag{5.90}$$

$$i \succ \text{---} \otimes \text{---} \otimes \text{---} \prec j = - \sum_{\alpha} M_{\alpha}^{(0)} [(\mathbf{1} + \mathbf{GM})^{-1}]_{\gamma}^{\alpha} \delta_{\alpha}^i \delta_j^{\gamma} \tag{5.91}$$

These effective vertices are then incorporated into interaction diagrams through the vertex expansion, and the symmetry factors are determined in the normal way. The interaction energy for (BC 1) is therefore given by the diagrammatic series

$$\begin{aligned}
 -\beta U^{(0)} = & \sum_{k=1}^{\infty} \text{diagram}_k + \sum_{k \geq 1} \text{diagram}_k + \text{diagram}_1 + \text{diagram}_1 \\
 & + \text{diagram}_1 + \text{diagram}_1 + \text{diagram}_1 + \text{diagram}_1 + \text{diagram}_1 + \dots, \tag{5.92}
 \end{aligned}$$

where the \textcircled{V} vertex is taken to also contain the $M^{(n>0)}$ terms and the solid lines represent generic propagators (not necessarily with ∂ -derivatives).

To account for the $M^{(n>0)}$ terms, first observe that for $n \geq m$ the product

$$(M^{(0)})^n (G^{\alpha\gamma})^m \xrightarrow{\ell_c \rightarrow \infty} \delta_{nm}. \quad (5.93)$$

Since $M^{(n)} \propto M^{(0)}$, this suggests that for every $M^{(n>0)}$ vertex in a given diagram, there *must* be a compensating propagator with no derivatives; otherwise the diagram vanishes. To make this apparent in the diagrams, we represent the $M^{(n)}$ and $\bar{M}^{(n)}$ vertices respectively by

$$z_\alpha \cdots \begin{array}{c} \textcircled{(n)} \\ \nearrow^z \\ \searrow_{z'} \end{array} = -M_\alpha^{(n)} e^{in\theta_\alpha} (-\partial)^n \delta_\alpha^z \delta_\alpha^{z'} \quad (5.94a)$$

$$z_\alpha \cdots \begin{array}{c} \textcircled{(n)} \\ \nearrow^z \\ \searrow_{z'} \end{array} = -M_\alpha^{(n)} e^{-in\theta_\alpha} (-\bar{\partial})^n \delta_\alpha^z \delta_\alpha^{z'}, \quad (5.94b)$$

where the dashed line represents (and enforces) a propagator with no derivatives, and the orientation-dependence has been written explicitly so that $M^{(n)}$ is given by Eq. (5.44). To demonstrate, we provide the expansion for the first effective monopole diagram:

$$\textcircled{V} = \textcircled{\bullet} + 2 \text{Re} \left[\textcircled{\circ} + \textcircled{\bullet} \right]. \quad (5.95)$$

Two Particles

For two particles, the (2×2) matrix inverse is given by

$$(\mathbf{1} + \mathbf{G} \mathbf{M})^{-1} = \frac{\mathbf{1} - \mathbf{G} \mathbf{M}}{\det(\mathbf{1} + \mathbf{G} \mathbf{M})} \quad (5.96)$$

and the effective vertices take particularly simple forms in the limit $\ell_c \rightarrow \infty$ (cf. Eqs. (3.175) and (3.240)):

$$i \text{---} \textcircled{\otimes} \text{---} j = - \sum_\alpha 2\pi \delta_\alpha^i \left(\frac{1}{2\varrho_{12}} \right) \delta_j^\alpha \quad (5.97)$$

$$i \text{---} \textcircled{\otimes} \text{---} j = \sum_{\alpha, \gamma} 2\pi \delta_\alpha^i \left(\frac{1 - \delta_\gamma^\alpha}{2\varrho_{12}} \right) \delta_j^\gamma, \quad (5.98)$$

where we have introduced the frequently appearing logarithmic parameter,

$$\varrho_{ij} = \ln \left(\frac{2r_{ij}}{\sqrt{s_i^+ s_j^+}} \right). \quad (5.99)$$

The interaction energy must therefore be a power series in the interparticle separation distance r , augmented by logarithmic corrections. Expanding out the vertices and using

the notation

$$-\beta U_{\text{BC1}} = -\beta U^{(0)} + \sum_{\substack{p>0 \\ \text{even}}} \frac{u^{(p)}(\varrho)}{r^p}$$

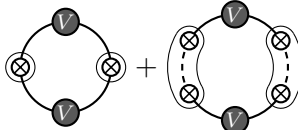
we find the higher order terms

$$u_{\text{BC1}}^{(2)} = \frac{1}{16\varrho_{12}} [(s_1^+)^2 + 3f_1^2 \cos 2\theta_1] + (1 \leftrightarrow 2) \quad (5.100)$$

$$u_{\text{BC1}}^{(4)} = u_{\text{BC2}}^{(4)} + \frac{1}{128\varrho_{12}} \left\{ (s_1^+)^4 + 2(s_1^+ s_2^+)^2 + 4f_1^2 [(s_1^+)^2 + 3(s_2^+)^2] \cos 2\theta_1 \right. \\ \left. + 11f_1^4 \cos 4\theta_1 + 22f_1^2 f_2^2 \cos(2\theta_1 + 2\theta_2) + (1 \leftrightarrow 2) \right\} + \left(u_{\text{BC1}}^{(2)} \right)^2. \quad (5.101)$$

At all orders, the interaction energy contains contributions with logarithmic prefactors in the form of ϱ_{12} , and they do not vanish in the isotropic limit. These terms exist between two particles, *both* of which are frozen in place at fixed heights, and they originate from cross-talk between monopoles and higher-order multipoles. Such contributions were previously claimed to vanish [YRD12], based on the argument that every diagram involving monopoles and higher-order multipoles vanishes in the limit $\ell_c \rightarrow \infty$. However, adding extra monopole insertions to such a diagram does not change its order, hence consistency requires we sum over the complete (infinite) set of insertions, as we have done here. After this resummation, the final result no longer vanishes in the $\ell_c \rightarrow \infty$ limit.

The higher-order terms in Eqs. (5.100) and (5.101) agree with what has been calculated by Noruzifar et al. [NO09] (up to differing definitions of a and b), except for a prefactor in the last term of Eq. (5.101). This term is a consequence of the single and double effective vertices limiting to the same value and results from following diagrammatic argument (valid only for pairs):



$$= \sum_{\alpha \neq \gamma}^2 \left(\frac{2\pi\sigma}{2\varrho_{12}} \right)^2 \left\{ \frac{1}{4} \left(\begin{array}{c} \gamma \quad \alpha \quad \gamma \\ \vdots \quad \vdots \quad \vdots \\ \bullet \quad V \quad \bullet \end{array} \right)^2 + \frac{1}{4} \left(\begin{array}{c} \gamma \quad \alpha \quad \gamma \\ \vdots \quad \vdots \quad \vdots \\ \bullet \quad V \quad \bullet \end{array} \right) \left(\begin{array}{c} \alpha \quad \gamma \quad \alpha \\ \vdots \quad \vdots \quad \vdots \\ \bullet \quad V \quad \bullet \end{array} \right) \right\} \\ = \left[\frac{1}{2} \sum_{\alpha \neq \gamma}^2 \left(\frac{2\pi\sigma}{2\varrho_{12}} \right) \left(\begin{array}{c} \gamma \quad \alpha \quad \gamma \\ \vdots \quad \vdots \quad \vdots \\ \bullet \quad V \quad \bullet \end{array} \right) \right]^2 = \left[\begin{array}{c} V \\ \text{loop with cross} \end{array} \right]^2. \quad (5.102)$$

In Ref. [NO09] it occurs with an extra prefactor of $1/2$, the origin of which is unclear. Equation (5.102) is actually quite special in that the diagrammatic recomposition is independent of any vertex expansion beyond the sum over the two particle worldlines. Just to emphasize, it holds for the present expansion as well as the special case Eq. (3.247)

considered in Section 3.6.4 and, moreover, it holds for the full sum over polarizabilities implied in the vertex. That is, by expanding the square on the right side and collecting similar powers, one may obtain its contribution to each order without additional work.

We can also compare these results to those obtained using conformal field theory techniques in Ref. [BEK13], for which the authors provide expansions for a couple of special cases. For two identical disks of radius R , and using $x = r/R$, our results reduce to

$$\beta U_{\text{BC1}} = \frac{1}{2} \ln(2 \ln x) - \frac{1}{2x^2 \ln x} - \frac{1}{x^4} \left(1 + \frac{3}{4 \ln x} + \frac{1}{4 \ln^2 x} \right) + \dots, \quad (5.103)$$

in agreement with Ref. [BEK13] as well as Eq. (3.250) of Chapter 3. For two identical *aligned* rods ($\theta_1 = \theta_2 = 0$) of length L ($s_+ = L/2$ and $f^2 = L^2/4$), our results reduce to

$$\beta U_{\text{BC1}} = \frac{1}{2} \ln \left(2 \ln \frac{4r}{L} \right) - \frac{1}{2(2r/L)^2 \ln(4r/L)} - \left(\frac{L}{2r} \right)^4 \left(\frac{1}{8} + \frac{13}{16 \ln(4r/L)} + \frac{1}{4 \ln^2(4r/L)} \right) + \dots \quad (5.104)$$

If we calculate the total force $F = -\partial U / \partial r$ and expand in terms of the *tip-to-tip* distance $d = r - L$, we find (with $x = d/(2L)$)

$$2LF = -\frac{1}{2x \ln(8x)} + \frac{1 + \ln(8x)}{4x^2 \ln^2(8x)} + \dots, \quad (5.105)$$

again in agreement with Ref. [BEK13].

Three particles

For three particles, the (3×3) matrix inverse is given by

$$(\mathbf{1} + \mathbf{GM})^{-1} = \frac{[1 - \frac{1}{2} \text{tr}(\mathbf{GM})^2] \mathbf{1} - \mathbf{GM} + (\mathbf{GM})^2}{\det(\mathbf{1} + \mathbf{GM})}. \quad (5.106)$$

The $\ell_c \rightarrow \infty$ limit for the effective vertices follows after a short calculation, ultimately yielding for the effective single vertex (*cf.* Eqs. (3.191) and (3.241))

$$\begin{aligned} i \text{---} \text{---} \text{---} \text{---} \text{---} \text{---} j &= - \sum_{\alpha} 2\pi \delta_{\alpha}^i \frac{2\varrho_{k\ell}}{\sum_{\text{cyc.}} (2\varrho_{ab}\varrho_{bc} - \varrho_{ab}^2)} \delta_j^{\alpha}, \\ &= - \sum_{\alpha} 2\pi \delta_{\alpha}^i e^{-2\beta(\mathcal{E}_{\text{tri}} + \mathcal{E}_{k\alpha} + \mathcal{E}_{\alpha\ell})} \delta_j^{\alpha}, \end{aligned} \quad (5.107)$$

where $\alpha, k, \ell \in \{1, 2, 3\}$ with $\alpha \neq k, \ell$, and $k \neq \ell$ (*i.e.*, (α, k, ℓ) is some permutation of $(1, 2, 3)$). In the second line, we have applied Eqs. (5.77) and (5.99) to put the effective vertex into the “screening form” (*cf.* Eq. (3.261a)) discussed in Chapter 3 (see Section 3.6.4, page 152). This interpretation recognizes the role of the external work required to fix the particles respective heights against vertical fluctuations. The associated external sources

serve to suppress fluctuations near the particle boundaries and consequently screen the interactions between particles, namely those between fluctuation-induced monopole and higher-order multipole moments, according to the pair (5.77) and triplet (5.83) interaction energies. Similarly, the effective double vertex becomes (*cf.* Eqs. (3.192) and (3.241))

$$\begin{aligned}
 i \text{---} \text{---} \text{---} \text{---} \text{---} j &= \sum_{\alpha, \gamma} 2\pi \delta_{\alpha}^i \frac{\varrho_{\alpha k} + \varrho_{k\gamma} - \varrho_{\alpha\gamma}}{\sum_{\text{cyc.}} (2\varrho_{ab}\varrho_{bc} - \varrho_{ab}^2)} \delta_j^{\gamma}, \\
 &= \sum_{\alpha, \gamma} 2\pi \delta_{i\alpha} \frac{1}{2} e^{-2\beta(\mathcal{E}_{\text{tri}} + \mathcal{E}_{\alpha\gamma})} \\
 &\quad \times \left[e^{-2\beta\mathcal{E}_{\alpha k}} + e^{-2\beta\mathcal{E}_{k\gamma}} - e^{-2\beta(\mathcal{E}_{\alpha k} + \mathcal{E}_{k\gamma} - \mathcal{E}_{\alpha\gamma})} \right] \delta_j^{\gamma},
 \end{aligned} \tag{5.108}$$

in which (α, γ, k) is a permutation of $(1, 2, 3)$. Like before, we provide the “screening form” (*cf.* Eq. (3.261b)) in the second line. Note that if there are only two particles, the constraints on α , γ , k , and ℓ in Eqs. (5.107) and (5.108) reduce both three-body effective vertices to the two-body vertices (5.97) and (5.98), which is most clear in the screening form since $\mathcal{E}_{\text{tri}} = \mathcal{E}_{\alpha k} = \mathcal{E}_{k\gamma} = 0$ and $\alpha, \gamma \in \{1, 2\}$. However, as long as the system has three height-constrained particles, the monopole interactions will always be “screened” by the triplet energy, in addition to the pairs.

To demonstrate, we calculate the first subleading correction to the energy of a three-particle configuration, which comes from the diagrams in Eq. (5.95) plus those same diagrams with the double monopole vertex (5.108):

$$\begin{aligned}
 \beta U_{\{1,2,3\}}^{(2)} &= - \sum_{i,j,k}^{\text{cyc.}} \left\{ \frac{\varrho_{ki}(s_i^+)^2 + f_i^2[\varrho_{ki} + (\varrho_{ki} - \varrho_{ij}) + \varrho_{jk}] \cos 2\theta_{ji}^{(i)}}{4r_{ij}^2 \sum_{\text{cyc.}} (2\varrho_{ab}\varrho_{bc} - \varrho_{ab}^2)} \right. \\
 &\quad \left. + \frac{[\varrho_{ki} + (\varrho_{ij} - \varrho_{jk})] \left[(s_i^+)^2 \cos \varphi_{kj}^i + f_i^2 \cos(\theta_{ki}^{(i)} + \theta_{ij}^{(i)}) \right]}{4r_{ki}r_{ij} \sum_{\text{cyc.}} (2\varrho_{ab}\varrho_{bc} - \varrho_{ab}^2)} \right\}.
 \end{aligned} \tag{5.109}$$

The argument of the last cosine is most directly suggested from the evaluation of the diagrams and refers to the angle of particle i measured with respect to both lines $z_i \rightarrow z_j$ and $z_k \rightarrow z_i$. A perhaps better expression derives from the identity $\theta_{ki}^{(i)} = \theta_{ij}^{(i)} + \varphi_{kj}^i$, so that the argument of the last cosine is $2\theta_{ij}^{(i)} + \varphi_{kj}^i$, referring to one representation of the particle orientation plus the exterior angle of the vertex on which the particle sits. The equivalent

“screening form” of the above result may be expressed in the form⁹

$$\begin{aligned}
 \beta U^{(2)} = & - \sum_{i,j,k}^{\text{cyc.}\{1,2,3\}} \frac{e^{-2\beta(\mathcal{E}_{\text{tri}}+\mathcal{E}_{ij})}}{8r_{ij}^2} \left\{ e^{-2\beta\mathcal{E}_{jk}} \left[(s_i^+)^2 + f_i^2 \left(2 + e^{-2\beta(\mathcal{E}_{ki}-\mathcal{E}_{jk})} \right. \right. \right. \\
 & \left. \left. \left. - e^{-2\beta(\mathcal{E}_{ki}-\mathcal{E}_{ij})} \right) \cos 2\theta_{ji}^{(i)} \right] + (i \leftrightarrow j) \right\} \\
 & - \sum_{i,j,k}^{\text{cyc.}\{1,2,3\}} \frac{e^{-2\beta(\mathcal{E}_{\text{tri}}+\mathcal{E}_{jk})}}{8r_{ki}r_{ij}} \left(e^{-2\beta\mathcal{E}_{ij}} + e^{-2\beta\mathcal{E}_{ki}} - e^{-2\beta(\mathcal{E}_{ki}+\mathcal{E}_{ij}-\mathcal{E}_{jk})} \right) \\
 & \times \left[(s_i^+)^2 \cos \varphi_{kj}^i + f_i^2 \cos(\theta_{ki}^{(i)} + \theta_{ij}^{(i)}) \right]
 \end{aligned} \tag{5.110}$$

Observe that the first sum is exponentially suppressed by the leading-order pair energies between one particle and the other two, but amplified by the triplet energy (recall that the triplet energy is repulsive and $\mathcal{E}_{\text{tri}} < 0$). This result differs from simply adding the two-particle result (5.100) pairwise because of this suppression term. However, from the screened version we can again see how the result is consistent with the two-body expression (5.100)—second sum is purely three-body and would vanish in a two-particle system, and setting $\mathcal{E}_{jk} = \mathcal{E}_{ki} = \mathcal{E}_{\text{tri}} = 0$ and $i, j \in \{1, 2\}$ in the first sum reduces the expression to Eq. (5.100). Continuing to even higher orders will follow similarly as straightforward computations of Feynman diagrams, including the proper insertions of the effective monopole vertices.

We conclude by finding the preferred particle orientations of an example three-body arrangement. Taking the ellipses to be identical for convenience ($s_i^+ = a + b$ for all particles i), we consider the three particles situated at the vertices of an equilateral triangle with equal side lengths d . For this arrangement, the above energy contribution reduces to

$$\begin{aligned}
 \beta U^{(2)} = & - \frac{3(a+b)^2}{8d^2 \ln\left(\frac{2d}{a+b}\right)} - \frac{(a^2 - b^2)}{12d^2 \ln\left(\frac{2d}{a+b}\right)} \\
 & \times \sum_{i,j,k}^{\text{cyc.}\{1,2,3\}} \left[\cos\left(2\theta_{ij}^{(i)} + \frac{2\pi}{3}\right) + 2 \cos\left(2\theta_{ij}^{(i)} + \frac{4\pi}{3}\right) + 2 \cos 2\theta_{ij}^{(i)} \right].
 \end{aligned} \tag{5.111}$$

The anisotropic information is contained in the sum and depends on only one particle angle at a time. Hence, we may solve for each particle orientation independently, finding that the solution $\theta_{12}^{(1)} = \theta_{23}^{(2)} = \theta_{31}^{(3)} = \pi/6$ maximizes the summand in square brackets and thus minimizes the energy. The preferred orientations of the three particles therefore consists of

⁹This corrects Eq. (102) of Ref. [HD14], in which the exponentials were improperly distributed through the first term, and the final $\cos(\theta_{ki}^{(i)} + \theta_{ij}^{(i)})$ term is missing.

all ellipses pointing toward a common point at the triangle center, in agreement with the (BC 2) conclusion.

Summary and conclusion

At the end of a long and fruitful journey, it is befitting to reflect upon the adventures experienced and the lessons learned along the way. The guiding philosophy of effective field theory, underpinned by scaling and symmetry principles, has revealed a powerful and elegant framework that can systematically reformulate the conceptually simple yet technically challenging problem of mediated interactions into one that is both physically intuitive and tractable. Moreover, it demonstrates a mathematical universality among a wide class of physical systems, permitting one to exploit decades of field theoretic machinery and experience to tackle novel problems. In this thesis we have explored several applications of the EFT formalism as it pertains to soft matter and, in particular, surface-mediated interactions between adsorbed particles.

We began by considering a familiar problem in electrostatics: the interaction between conducting spheres at fixed potentials or fixed charges. We used this example to both introduce some of the key ideas of EFT as well as serve as a guiding analogy for the later applications. In particular, we highlighted the interplay between the conductors and the scalar field (electric potential): the interaction between conductors is mediated by the electric potential and thus the information transmitted by each is restricted to the boundary data allowable by the field energetics. Such information is encapsulated by each conductor's *polarizabilities* which, although they dictate the conductor's response to an external field, are themselves of geometric origin and field-independent. Throughout the remainder of this thesis, we have retained this intuitive idea to capture field-relevant particle descriptions as a set of generalized polarizabilities, affording us conceptual and computational faculties that come with it.

In the second chapter, we began our foray into the physics of soft-matter surfaces, wherein a general curvature Hamiltonian, quickly specialized to the Helfrich Hamiltonian, was constructed via EFT principles. The effective theory captures the mesoscopic behavior of a fluid surface, wherein the short-scale physics of its constituents are subsumed into a few relevant and marginal phenomenological parameters, namely the surface tension, spontaneous curvature, and the two curvature moduli. We then specialized further to two classes of surfaces: (i) a surface whose energetics are dominated by the surface tension alone—relevant to fluid–fluid interfaces and films—and (ii) a surface whose energetics are dominated by bending rigidity—relevant to fluid lipid membranes. From the associated energy functionals we obtained the permissible boundary data that may be probed and transmitted through the surface.

In the third chapter we fully capitalized on the utility of the EFT formalism by considering the interactions between small particles adsorbed on a tension-dominated, fluid surface. By applying the EFT prescription, we were able to disentangle the constraints imposed by the

particle boundaries to create a *completely equivalent* point particle description. Similar to the electrostatics case, we were able to capture all the finite-size information, as well as the rigid-body degrees of freedom, in a complete set of point-like *polarizabilities*, which were determined by matching the full and effective theory results to a simple linear response boundary value problem. Since the scaling of each term in the resulting derivative expansion is manifestly transparent, it allows for systematic control (and ensured validity) over any desired accuracy. We then introduced the diagrammatic technique to aid in calculating ground state elastic and fluctuation-induced entropic interactions between surface-bound particles. Although a number of the results we obtained had been known before we re-derived them, by revisiting them the EFT prescription proves its merit:

- The formalism captures the key underlying physics in such a way that each term and contribution has an intuitive interpretation.
- Both ground state and fluctuation-induced interactions can be treated within the same framework.
- Calculating the polarizabilities is disentangled from the full problem and only needs to be done once. In complicated situations may they be determined numerically or even experimentally, or left undetermined as a phenomenological theory.
- Since the polarizabilities are independent of the rest of the system, it is straightforward to extend the theory to complicated, multiparticle systems.

Indeed, we demonstrated the versatility of the EFT formalism by pushing the pair interactions to all orders and calculating the three-body interactions to several orders, all for nonidentical particles with various boundary conditions. Furthermore, we elucidated the subtleties of monopole-type interactions, which are problematic since their perturbative contributions are marginal, and showed how to regulate and completely resum their contributions for and recover proper power counting of the resulting interaction energy. At leading order, the elastic interaction energy between two particles with fixed positions is long ranged ($\sim 1/\ln r$) and repulsive. We find that for three particles, the energy is also collectively repulsive but less so than the sum of pairwise energies, indicating that the pure three-body (triplet) effect is in fact attractive. Curiously, at the next order the triplet interaction *does* overcome the pairwise sum *at that order*, thereby reducing the overall repulsion further, suggesting that a pairwise approximation to a multiparticle system is not adequate to properly capture the aggregate behavior. We obtained similar results for entropic interactions, for which the leading-order pair interaction is very long ranged ($\sim \ln \ln r$) and attractive. The pure three-body contribution is again contrarian, collectively repelling the particles, but not enough so that it overcomes the attractive pairwise sum. Interestingly, and in contrast to the elastic case, both the pairwise and triplet contributions reinforce the the leading-order attraction at the next order. Finally, we considered a particular case of semi-relaxed constraints in which the particle position is set by an external

potential (*e.g.*, optical tweezers), and calculated the interparticle forces for both pinned and unpinned contact lines.

Next, we turned our attention to particle interactions mediated by membranes. Although the energetics of a membrane are governed by its bending rigidity rather than tension, many of the same principles apply, but with modified expansion terms and boundary conditions. As before, we were able to calculate the complete set of generalized polarizabilities for flat and curved particles and calculated interactions to many orders. Since the richness of the elastic interaction energy landscape is not adequately represented or discussed in the literature, we examined in detail the minimum energy orientations for two saddle-shaped particles with nonzero mean curvature in both the up-down symmetric and antisymmetric cases. We found that in terms of the scaled separation distance $\chi = r/R$ and the ratio $\eta = S/J$ between the particles' saddle and mean curvatures, there exists a critical line separating the energy in the $\chi\eta$ -plane into two orientational phases with one or two (degenerate) minima respectively. The plane is further subdivided into attractive or repulsive regions showing that, for instance, for sufficiently small η the interaction is always repulsive as suggested by the leading-order interaction energy for $S = 0$, but most of the phase space is dominated by attraction. Additionally, we calculate the fluctuation-induced interactions between two-, three-, and four-body systems.

A class of particle shape anisotropies were considered in Chapters 3 and 4, namely those that curve out of the plane but otherwise remain circular in the projected base plane. Such deformations appeared as permanent sources in the effective Hamiltonian and account for the existence of ground state (elastic) interactions. In Chapter 5 we generalized the EFT of particles on a tension-dominated surface to account for anisotropies in the (projected) boundary shape. The primary complication is that many additional terms originally forbidden by the rotational symmetry of the projected boundary must now be accounted for, including those with tensorial polarizabilities. However, once again we were able to determine the complete set of polarizabilities for particles with elliptical contact lines. We accomplished this by exploiting the conformal invariance of the effective Hamiltonian to map the single-particle boundary value problem required for matching, to the much simpler case of a circular boundary. As a consequence of the Riemann mapping theorem, this trick is readily generalizable to more arbitrary shapes—all one must know to proceed is the Laurent expansion (to a some desired order) of the map to a circular boundary. Just as in Chapter 3, we obtain high-order results for the entropic interactions in two- and three-body systems with varying fluctuation degrees of freedom. We found in particular that elliptical particles will minimize their interaction free energy by aligning tip-to-tip or, in a three-body configuration, align their tips to a common center. Triplet and higher-order interactions become stronger at closer distances, hence they will be especially relevant in dense bulk phases, in which many particles coat a fluid surface. The free energy of such phases can be written as a sum over all pairs, all triplets, and so on. We expect the resulting system to give rise to nontrivial ordered phases; for instance, it is easy to see that a regular triangular lattice would be frustrated, since three close particles tend to point their tips together, but this is a local conformation that cannot be assumed by every close triplet. While the terms

beyond the pair level are only a small correction to the overall free energy, they would shift the location of phase boundaries between such dense phases, but this is beyond the scope of our present work.

Appendix A

Linear response and complete renormalization of polarizabilities

Throughout this thesis, we have claimed that the effective field (EFT) theory reproduces all of the physics of the corresponding full theory. However, in constructing the EFT we were somewhat cavalier about divergences, both in calculating interactions as well as during the matching procedure. Here we will revisit and justify the assertions made in the main text. For simplicity, we will consider a surface dominated by surface tension only. Furthermore, we will work in the Monge gauge and rescale the height function by the length scale $\ell_m = \sqrt{k_B T / \sigma}$ so that the field $\phi = h / \ell_m$ is dimensionless. Then, as per Chapter 3, the effective Hamiltonian for a single, flat, circular particle at the origin is

$$\begin{aligned} S[\phi] &:= \beta \mathcal{H}_{\text{eff}}[\phi] = \frac{1}{2} \int d^2x \, \phi (-\nabla^2 + \ell_c^{-2}) \phi + \left(\frac{1}{2} M^{(0)} \phi^2(0) + \sum_{n \geq 1} C^{(n)} |\partial^n \phi(0)|^2 \right) \\ &= S_0[\phi] + \Delta S[\phi]. \end{aligned} \quad (\text{A.1})$$

The EFT in essence re-expresses the Hamiltonian as a derivative expansion evaluated on the particle worldlines. The couplings, or Wilson coefficients, concomitant to each term in the expansion were interpreted as generalized polarizabilities, which we determined by calculating and matching the field responses to imposed background fields in both the EFT and full theory. However, when calculating these observables in the effective theory, we did so by assuming a linear response and dropping the divergent worldline terms that are independent of the background. The justification was that the full theory boundary value problem is indeed linear in the field, so the EFT response must be as well. We then claimed that the additional divergent terms were of no consequence and were merely an artifact of reducing the particle to a point. Let us now retain those terms and discuss the consequences.

A.1 Linear response

Once a background field ϕ_{bg} is imposed, we express the total field as $\phi = \phi_{\text{bg}} + \varphi$ and expand the functional as

$$S[\phi_{\text{bg}} + \varphi] = S[\phi_{\text{bg}}] + \left. \frac{\delta S}{\delta \phi^x} \right|_{\phi_{\text{bg}}} \varphi^x + \frac{1}{2} \left. \frac{\delta^2 S}{\delta \phi^x \delta \phi^y} \right|_{\phi_{\text{bg}}} \varphi^x \varphi^y, \quad (\text{A.2})$$

where we have used continuous index notation in which $\varphi^x = \varphi(\mathbf{x})$ and repeated “indices” are integrated. As usual, we take the background field to be on-shell; *i.e.*, $(\delta S_0/\delta\phi)|_{\phi_{\text{bg}}} = 0$. The response field must then satisfy

$$\begin{aligned} \frac{\delta S[\phi_{\text{bg}} + \varphi]}{\delta\varphi^x} &= \left. \frac{\delta S}{\delta\phi^x} \right|_{\phi_{\text{bg}}} + \left. \frac{\delta^2 S}{\delta\phi^x \delta\phi^y} \right|_{\phi_{\text{bg}}} \varphi^y \\ &\equiv -J_x + (K_{xy} + M_{xy} + V_{xy})\varphi^y \stackrel{!}{=} 0 \end{aligned} \quad (\text{A.3})$$

where $K(\mathbf{x}, \mathbf{y}) = (-\nabla_x^2 + \ell_c^{-2})\delta(\mathbf{x} - \mathbf{y})$ is the usual bulk kernel function, and the remaining terms in the second line follow from the functional derivatives:

$$M_{xy} = M^{(0)}\delta_x^0\delta_y^0, \quad (\text{A.4})$$

$$V_{xy} = \sum_{n \geq 1} C^{(n)} (\partial^n \delta_x^0 \bar{\partial}^n \delta_y^0 + \text{c.c.}), \quad (\text{A.5})$$

$$J_x = -M^{(0)}\phi_{\text{bg}}(0)\delta_x^0 - \sum_{n \geq 1} C^{(n)} [\partial^n \phi_{\text{bg}}(0) \bar{\partial}^n \delta_x^0]. \quad (\text{A.6})$$

In the above expressions we use the definition $\delta_x^w = \delta(\mathbf{w} - \mathbf{x})$, and the complex derivatives are taken with respect to the whole argument (*e.g.*, $\partial^n \delta_x^0 = (-\partial)^n \delta_0^x$).

In the text, we dropped both M_{xy} and V_{xy} and solved for the effective response via

$$K_{xy}\varphi^y = J_x \implies \varphi^x = G^{xy}J_y, \quad (\text{A.7})$$

where $G^{xy} = K_{xy}^{-1}$ is the bulk Green function given by (in the $\ell_c \rightarrow \infty$ limit)

$$G(\mathbf{x}, \mathbf{y}) = \frac{1}{2\pi} \ln \left(\frac{2\ell_c}{|\mathbf{x} - \mathbf{y}|_{\gamma_e}} \right). \quad (\text{A.8})$$

If M_{xy} and V_{xy} are retained, the problem instead becomes

$$(\mathbf{K} + \mathbf{M} + \mathbf{V}) \boldsymbol{\varphi} = \mathbf{J}, \quad (\text{A.9})$$

where we have used the bold “matrix” notation of Chapter 3. The solution then follows formally by the *full Green function* \mathcal{G} :

$$\boldsymbol{\varphi} = \mathcal{G} \mathbf{J}, \quad \mathcal{G} = (\mathbf{K} + \mathbf{M} + \mathbf{V})^{-1}. \quad (\text{A.10})$$

As discussed in detail in Chapter 3, since $M^{(0)}$ scales the same as the Hamiltonian—in this case it is dimensionless—monopole interactions cannot be treated perturbatively if we wish to have a consistent expansion in powers of inverse distance. Rather all monopole interactions must be summed in their entirety. A particularly economical way to perform

this sum is by first rewriting \mathcal{G} through the following formal manipulations:

$$\begin{aligned}
 \mathcal{G} &= [\mathbf{K}(\mathbf{1} + \mathbf{G}\mathbf{M} + \mathbf{G}\mathbf{V})]^{-1} \\
 &= (\mathbf{1} + \mathbf{G}\mathbf{M} + \mathbf{G}\mathbf{V})^{-1} \mathbf{G} \\
 &= [(\mathbf{1} + \mathbf{G}\mathbf{M})(\mathbf{1} + (\mathbf{1} + \mathbf{G}\mathbf{M})^{-1} \mathbf{G}\mathbf{V})]^{-1} \mathbf{G} \\
 &= [\mathbf{1} + (\mathbf{1} + \mathbf{G}\mathbf{M})^{-1} \mathbf{G}\mathbf{V}]^{-1} (\mathbf{1} + \mathbf{G}\mathbf{M})^{-1} \mathbf{G}.
 \end{aligned} \tag{A.11}$$

Finally, define $\mathcal{M} = \mathbf{1} + \mathbf{G}\mathbf{M}$ and expand the inverse so that

$$\mathcal{G} = (\mathbf{1} + \mathcal{M}^{-1} \mathbf{G}\mathbf{V})^{-1} \mathcal{M}^{-1} \mathbf{G} = \sum_{k \geq 0} (-\mathcal{M}^{-1} \mathbf{G}\mathbf{V})^k \mathcal{M}^{-1} \mathbf{G}. \tag{A.12}$$

A.2 Regularization and resummation

The resummation of the monopole terms results from the inverse of \mathcal{M} . We calculate the inverse in a couple of steps. First, we expand the inverse and perform the corresponding contractions using $G^{xw} M_{wy} = M^{(0)} G^{x0} \delta_y^0$:

$$\begin{aligned}
 (\mathcal{M}^{-1})_y^x &= \delta_y^x + \sum_{\ell \geq 1} [(-\mathbf{G}\mathbf{M})^\ell]_y^x \\
 &= \delta_y^x - M^{(0)} G^{x0} \delta_y^0 + M^{(0)2} G^{x0} \delta_w^0 G^{w0} \delta_y^0 - M^{(0)3} G^{x0} \delta_w^0 G^{w0} \delta_z^0 G^{z0} \delta_y^0 + \dots \\
 &= \delta_y^x - M^{(0)} G^{x0} \delta_y^0 + M^{(0)2} G^{x0} G^{00} \delta_y^0 - M^{(0)3} G^{x0} (G^{00})^2 \delta_y^0 + \dots
 \end{aligned} \tag{A.13}$$

Next, we recognize the expansion as a geometric series in numbers rather than operators. Since this operator always acts on the Green function, we write

$$\begin{aligned}
 (\mathcal{M}^{-1})_w^x G^{wy} &= G^{xy} - M^{(0)} G^{x0} \sum_{\ell \geq 0} (-M^{(0)} G^{00})^\ell G^{0y} \\
 &= G^{xy} - \left(\frac{M^{(0)}}{1 + M^{(0)} G^{00}} \right) G^{x0} G^{0y}.
 \end{aligned} \tag{A.14}$$

According to the first line, a surface excitation impinging on the particle experiences modifications from a series of self-interactions due to the particle's induced monopole polarizability. In the second line, we sum the (Dyson-like) series to give a total effective monopole interaction. Observe that the monopole terms depend on the Green function evaluated at zero which, given Eq. (A.8), is clearly logarithmically divergent. We will return to this in a moment.

With the monopoles resummed, we may begin to look at corrections due to the higher-order polarizabilities. The leading order correction comes from the $k = 1$ term of Eq. (A.12),

and requires the operator

$$\begin{aligned}
 (\mathcal{M}^{-1} \mathbf{G} \mathbf{V})_y^x &= (\mathcal{M}^{-1} \mathbf{G})^{xw} \sum_{n \geq 1} C^{(n)} (\partial^n \delta_w^0 \bar{\partial}^n \delta_y^0 + \text{c.c.}) \\
 &= \sum_{n \geq 1} C^{(n)} \left\{ \left[(-\partial)^n G^{x0} - \left(\frac{M^{(0)}}{1 + M^{(0)} G^{00}} \right) G^{x0} (-\partial)^n G^{00} \right] \bar{\partial}^n \delta_y^0 + \text{c.c.} \right\}
 \end{aligned} \tag{A.15}$$

Notice the appearance of a new type of divergence, $\partial^n G(0)$, which because of the derivatives diverges as $\sim 1/z^n$. We may continue as is, but it is worth making a few comments to simplify the following expressions. Already we have encountered several divergences just by attempting to calculate the full propagator (Green function) for a single particle. This is not too surprising since we have condensed all the physical characteristics of the particle, and hence the uncountably-infinite field degrees of freedom, to a single point, so divergences are expected to result as an artifact. From the perspective of renormalization group theory, we have parametrized the effective theory in a way that is sensitive to such a coarse-graining procedure. The effect is that under coarse-graining, divergences should be expected, but serve only to renormalize the couplings of the naïvely-parametrized theory. To properly parametrize the theory, we must also include unphysical *counterterms* that eliminate the unphysical divergences but otherwise make no appearance in physical observables. However, in doing so we must also keep careful watch over the scaling behavior due to renormalization. For instance, the power-law divergences mentioned above do not pick out a particular scale and the renormalization group flow is trivial; *i.e.*, there is no nontrivial physical information contained within the divergences. Logarithmic divergences, however, can contain information since they necessarily entail a particular renormalization scale. As such, we will retain terms $\propto G(0)$.

Regarding terms $\propto \partial^n G(0)$, we note the following. In any sensible renormalization scheme, the method used to regulate and isolate divergences should respect as many important symmetries as possible. In our case, the bulk Green function G is isotropic, and thus has no preferred directionality. Hence derivatives of G evaluated at the origin, such as $\partial_i \partial_j \partial_k \cdots G(0)$, must also be isotropic and, moreover, fully symmetric in all the indices. Such tensors must therefore be proportional to combinations of Kronecker delta-functions that pair off each of the indices amongst one another, and are zero unless all the derivative indices are (pairwise) contracted. The corresponding statement in complex coordinates is that all ∂ -derivatives must be paired with $\bar{\partial}$ -derivatives such that $\partial^n \bar{\partial}^n G(0) = \delta_{nm} (\partial \bar{\partial})^n G(0)$. The immediate implication is that any terms proportional to $\partial^n G(0)$ (or $\bar{\partial}^n G(0)$) will vanish under a suitable renormalization scheme, most notably the terms proportional to $M^{(0)}$ in Eq. (A.15). That is, we see that the monopole terms decouple from the higher-order corrections of the full propagator. As one final note, due to the definition of the Green function, it follows that $\partial \bar{\partial} G(0) = \ell_c^{-2} G(0)$, so we will retain these terms as well.¹

¹Since we are working in the $\ell_c \rightarrow \infty$ limit, one might wonder whether we should instead apply $-4\partial \bar{\partial} G(0) = \delta(0)$. One could indeed proceed this way, and in dimensional regularization such terms would

Applying these insights, we contract Eq. (A.15) with $\mathcal{M}^{-1} \mathbf{G}$ to give the leading order correction,

$$-(\mathcal{M}^{-1} \mathbf{G} \mathbf{V} \mathcal{M}^{-1} \mathbf{G})^{xy} = - \sum_{n \geq 1} C^{(n)} [(-\partial)^n G^{x0} \bar{\partial}^n G^{0y} + (\text{terms} \propto \bar{\partial}^n G^{00})] + \text{c.c.}, \quad (\text{A.16})$$

where we may drop the terms proportional to $\partial^n G(0)$ and $\bar{\partial}^n G(0)$. Continuing along, the next order correction follows by contracting $\mathcal{M}^{-1} \mathbf{G} \mathbf{V}$ with the above expression. In doing so, we encounter the factor $\partial^n (-\partial)^m G(0)$, which as per the above discussion should be replaced by $\delta_{nm} (-\partial \bar{\partial})^n G(0)$. This has the effect of projecting the second sum onto the same polarizability order so that the correction is proportional to $[C^{(n)}]^2$:

$$[(\mathcal{M}^{-1} \mathbf{G} \mathbf{V})^2 \mathcal{M}^{-1} \mathbf{G}]^{xy} = \sum_{n \geq 1} [C^{(n)}]^2 \left\{ (-\partial)^n G^{x0} (-\partial \bar{\partial})^n G^{00} \bar{\partial}^n G^{0y} + \text{c.c.} \right\}. \quad (\text{A.17})$$

This behavior is seen to generalize to all the higher orders such that

$$\left[(-\mathcal{M}^{-1} \mathbf{G} \mathbf{V})^k \mathcal{M}^{-1} \mathbf{G} \right]^{xy} = \sum_{n \geq 1} [-C^{(n)}]^k \left\{ (-\partial)^n G^{x0} [(-\partial \bar{\partial})^n G^{00}]^{k-1} \bar{\partial}^n G^{0y} + \text{c.c.} \right\}. \quad (\text{A.18})$$

We now recognize the sum over $k \geq 1$ as a geometric series. Combining the sum with Eq. (A.14) into Eq. (A.12), we finally find the full propagator to be

$$\begin{aligned} \mathcal{G}^{xy} &= G^{xy} - G^{x0} \left(\frac{M^{(0)}}{1 + M^{(0)} G^{00}} \right) G^{0y} \\ &\quad - \sum_{n \geq 1} \left\{ (-\partial)^n G^{x0} \left(\frac{C^{(n)}}{1 + C^{(n)} (-\partial \bar{\partial})^n G^{00}} \right) \bar{\partial}^n G^{0y} + \text{c.c.} \right\}. \end{aligned} \quad (\text{A.19})$$

We may also interpret the full propagator graphically. The conditions $\partial^n G(0) = 0$ and $\partial^n \bar{\partial}^m G(0) = \delta_{nm} (\partial \bar{\partial})^n G(0)$ justify the claim that ∂ - and $\bar{\partial}$ -derivatives must be paired at every vertex, even for a self-interaction, and furthermore re-enforce the diagrammatic choice of representing the V_{xy} vertices with single- and double-line legs used in the previous chapters. Furthermore, self-interactions must only connect identical multipole orders. The full propagator is therefore a sum of the free (bulk) propagator plus corrections due to the self-energy corresponding to each polarizability; that is, the particle interacting with its own structure.

all formally vanish. With the long-distance regulator ℓ_c in place, it appears that $G(0)$ cannot diverge more than logarithmically, so the extra inverse powers of ℓ_c will ultimately kill off those terms as well. We will, however, retain all such terms for this demonstration.

A.3 Matching and counterterms

To finish off, we will consider explicitly again the matching procedure. In the full theory (with $\ell_c \rightarrow \infty$), a convenient background field is the linear sum of exterior solutions,

$$\phi_{\text{bg}} = \sum_{n \geq 0} a_n (z^n + \bar{z}^n). \quad (\text{A.20})$$

The full theory response, with the flat-particle boundary conditions $\phi_{\text{bg}}(R) + \varphi(R) = 0$, is easily found (by calculation or a peek at Chapter 3) to be

$$\varphi = -a_0 \frac{\ln\left(\frac{2\ell_c}{r\gamma_e}\right)}{\ln\left(\frac{2\ell_c}{R\gamma_e}\right)} - \sum_{n \geq 1} a_n R^{2n} \left(\frac{1}{z^n} + \frac{1}{\bar{z}^n} \right) \quad (\text{A.21})$$

For convenience, we can re-express the response in terms of derivatives of the Green function via the identity

$$(-\partial)^n G(z, \bar{z}) = \frac{(n-1)!}{4\pi z^n}, \quad (\text{A.22})$$

so that

$$\varphi = -a_0 \frac{2\pi G}{\ln\left(\frac{2\ell_c}{R\gamma_e}\right)} - \sum_{n \geq 1} a_n \frac{4\pi R^{2n}}{(n-1)!} [(-\partial)^n G + \text{c.c.}] \quad (\text{A.23})$$

The effective response follows from the solution $\varphi = \mathcal{G} \mathbf{J}$, where the induced source is given by Eq. (A.6). Using $\partial^n \phi_{\text{bg}}(0) = n! a_n$, we find

$$\varphi^x = -a_0 M^{(0)} \mathcal{G}^{x0} - \sum_{n \geq 1} C^{(n)} n! a_n [(-\partial)^n \mathcal{G}^{x0} + \text{c.c.}] \quad (\text{A.24})$$

Next, we plug in the expansion (A.19) for the full propagator, which requires the contraction

$$\begin{aligned} \mathcal{G}^{xy} \partial^n \delta_y^0 &= \partial_y^n \mathcal{G}^{xy} \delta_0^y \\ &= (-\partial)^n G^{x0} - (-\partial)^n G^{x0} \left(\frac{C^{(n)}}{1 + C^{(n)} (-\partial \bar{\partial})^n G^{00}} \right) (-\partial \bar{\partial})^n G^{00}. \end{aligned} \quad (\text{A.25})$$

To arrive at the above expression, we pay close attention to the derivative variable, apply $\bar{\partial}^m \partial_y^n G^{0y} \delta_y^0 = \delta_{nm} (-\partial \bar{\partial})^n G^{00}$, and drop the terms proportional to $\partial^n G(0)$. Finally, simplifying the terms gives the effective response

$$\varphi^x = -a_0 \left(\frac{M^{(0)}}{1 + M^{(0)} G^{00}} \right) G^{x0} - \sum_{n \geq 1} a_n n! \left(\frac{C^{(n)}}{1 + C^{(n)} (-\partial \bar{\partial})^n G^{00}} \right) [(-\partial)^n G^{x0} + \text{c.c.}] \quad (\text{A.26})$$

Comparing this with the full-theory response (A.23), we obtain the matching conditions,

$$\frac{M^{(0)}}{1 + M^{(0)}G^{00}} \stackrel{!}{=} \frac{2\pi}{\ln\left(\frac{2\ell_c}{R\gamma_e}\right)} =: M_r^{(0)} \quad (\text{A.27})$$

$$\frac{C^{(n)}}{1 + C^{(n)}(-\partial\bar{\partial})^n G^{00}} \stackrel{!}{=} \frac{4\pi R^{2n}}{n!(n-1)!} =: C_r^{(n)}. \quad (\text{A.28})$$

In the above expressions for the polarizabilities, we reproduce the values listed in Technical Note 3.1, but not for the *bare* parameters. As mentioned before, this should be expected since the bare parameters do not necessarily correspond to observables, and may indeed diverge themselves. Instead, what we do measure through observables are the *renormalized* parameters, designated above by $M_r^{(0)}$ and $C_r^{(n)}$. These are the values we obtained in the main text by ignoring the unphysical divergences.

To put things differently, the original effective Hamiltonian (A.1) was naïvely expressed in terms of bare parameters, written now as $M_b^{(0)}$ and $C_b^{(n)}$. If we wish to instead re-express the Hamiltonian in terms of physical renormalized parameters, we may make the replacement $M_b^{(0)} = M_r^{(0)} + (M_b^{(0)} - M_r^{(0)})$ and similarly for $C_b^{(n)}$ so that the functional becomes a sum of the renormalized Hamiltonian and a series of counterterms that exactly cancel off the divergences:

$$S[\phi] = S_r[\phi] + S_{\text{ct}}[\phi], \quad (\text{A.29})$$

where

$$S_{\text{ct}}[\phi] = \frac{1}{2}M_r^{(0)} \left[\frac{M_r^{(0)}G^{00}}{1 - M_r^{(0)}G^{00}} \right] \phi^2(0) + \sum_{n \geq 1} C_r^{(n)} \left[\frac{C_r^{(n)}(-\partial\bar{\partial})^n G^{00}}{1 - C_r^{(n)}(-\partial\bar{\partial})^n G^{00}} \right] |\partial^n \phi(0)|^2. \quad (\text{A.30})$$

We may instead expand the fractions to produce the series

$$S_{\text{ct}}[\phi] = \sum_{k \geq 1} \left\{ \frac{1}{2}M_r^{(0)} \left[M_r^{(0)}G^{00} \right]^k \phi^2(0) + \sum_{n \geq 1} C_r^{(n)} \left[C_r^{(n)}(-\partial\bar{\partial})^n G^{00} \right]^k |\partial^n \phi(0)|^2 \right\}. \quad (\text{A.31})$$

Although we will not prove it here, the benefit of the expanded form of the counterterms is that they can be seen to cancel out *all* self-interactions, order-by-order, in the perturbative expansions for every observable. This generalizes in the obvious way for multiple particles, with an analogous sum of counterterms on each worldline. Since the observables are in essence calculated with the full propagator, all self-interactions will manifest the same form as discussed above, and will be subsequently removed by the appropriate counterterms from Eq. (A.31). This both justifies and assures that it is safe to completely neglect all self-interactions during our calculations. Alternatively, these results can be summed up by a modification of the bulk Green function, $G^{ab} \rightarrow (1 - \delta_{ab})G^{ab}$ (no sum) for particles a and b , which we used liberally throughout the main text.

Appendix B

Soft monopoles and unpinned particles

Throughout this thesis, we have primarily studied particles that are pinned to a surface with a fixed contact line. For such particles, their actual shapes were irrelevant in that only the fixed boundary information (including allowable rigid body motions) could be transmitted through the surface. Here we will consider a different scenario in which the contact line is *not* fixed, but instead governed by three-phase interfacial energy (*i.e.*, between the particle and the two fluids). In this case, the full particle shape matters since the contact line is unpinned and may move about the particle's surface.

In Section 3.7 we added a touch of experimental realism by constraining the particles' vertical positions through the use of external, harmonic trap potentials. When comparing our results to the published literature, namely Ref. [LO07], we found it necessary to also consider the effects due to unpinned contact lines. In this appendix, we construct the effective Hamiltonian for an unpinned spherical particle at a fluid–fluid interface, including trapping effects, and calculate the resulting interactions between particles.

B.1 Particle boundary conditions

Isolated particle

For a single, surface-bound spherical particle, the equilibrium fluid–fluid interface becomes flat and the particle settles at a center of mass height $h_{\text{cm}}^{\text{ref}} = -R \cos \theta$ (see Fig. B.1). The contact line forms a circle of radius $R_0 = R \sin \theta$, where the contact angle obeys Young's Equation [Saf94, Chap. 4], $\cos \theta = (\sigma_{\text{I}} - \sigma_{\text{II}})/\sigma$. The parameter $\sigma_{\text{I(II)}}$ refers to the interfacial energies between the particle and phase I (II) and σ is the surface tension of the fluid–fluid interface. For deviations from this reference configuration, we may parametrize the contact line according to Fig. B.1 such that

$$\tilde{R}(\varphi) = R \sin \vartheta(\varphi), \tag{B.1a}$$

$$h_{\text{cm}} = h(\tilde{R}(\varphi)) - R \cos \vartheta(\varphi), \tag{B.1b}$$

where \tilde{R} and ϑ may in general depend on the azimuthal angle φ such that the above two equations hold.

We now apply the philosophy of Section 3.2 (Conditions for the contact line) to express

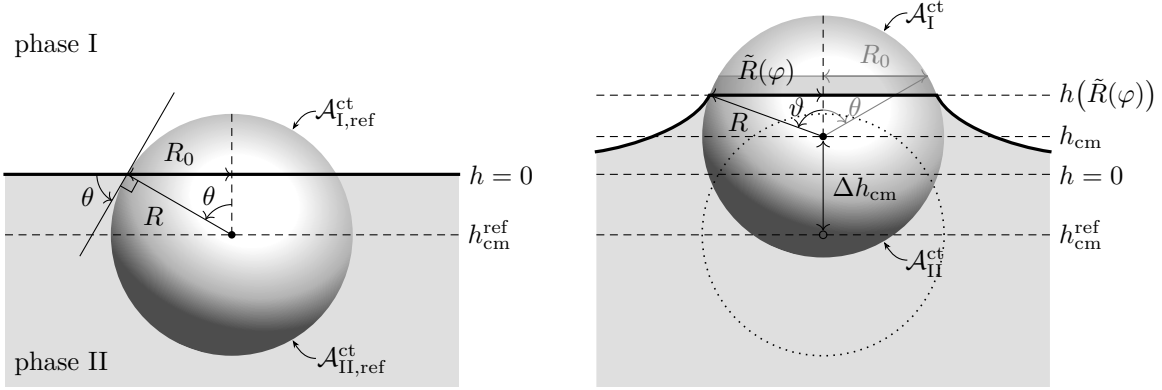


Figure B.1: Parametrizations for an unpinned particle. The left figure illustrates the equilibrium reference configuration in which the position of the three-phase contact line is governed by Young's law. The right figure illustrates a deviation from equilibrium in which the contact line height and position with respect to the particle changes.

the total free-energy difference from the reference configuration as

$$\begin{aligned} \mathcal{H} &= \mathcal{H}_0 + \Delta\mathcal{H}_{\text{ex}} + \Delta\mathcal{H}_{\text{ct}} \\ &= \frac{\sigma}{2} \int_{\mathcal{S}_{\text{pr}}^{\text{ref}}} d^2x [(\nabla h)^2 + \ell_c^{-2} h^2] + \sigma(\mathcal{A}_{\text{ref}} - \mathcal{A}) + (\sigma_{\text{I}} - \sigma_{\text{II}}) \Delta\mathcal{A}_{\text{I}}^{\text{ct}}, \end{aligned} \quad (\text{B.2})$$

where $\mathcal{S}_{\text{pr}}^{\text{ref}} = \mathbb{R}^2 \setminus \mathcal{A}_{\text{ref}}$, \mathcal{A}_{ref} and \mathcal{A} are respectively the projected particle areas in the equilibrium state and an arbitrary state, and $\Delta\mathcal{A}_{\text{I}}^{\text{ct}}$ is the change in contact surface area (not the projection) of the particle with phase I. Following Appendix A of Ref. [ODD05], we expand and rearrange the last term, resulting in¹

$$(\sigma_{\text{I}} - \sigma_{\text{II}}) \Delta\mathcal{A}_{\text{I}}^{\text{ct}} = \frac{\sigma}{2} \int_0^{2\pi} d\varphi [h(R_0(\varphi)) - \Delta h_{\text{cm}}]^2 + \frac{\sigma}{2} \int_0^{2\pi} d\varphi [\tilde{R}^2(\varphi) - R_0^2], \quad (\text{B.3})$$

where $\Delta h_{\text{cm}} = h_{\text{cm}} - h_{\text{cm}}^{\text{ref}}$. Similarly, the second term of Eq. (B.2) becomes

$$\sigma(\mathcal{A}_{\text{ref}} - \mathcal{A}) = \sigma \int_0^{2\pi} d\varphi \int_{\tilde{R}(\varphi)}^{R_0} dr r = \frac{\sigma}{2} \int_0^{2\pi} d\varphi [R_0^2 - \tilde{R}^2(\varphi)], \quad (\text{B.4})$$

¹ To provide a few details: Starting with the contact area integral

$$\mathcal{A}_{\text{I}}^{\text{ct}} = R^2 \int_0^{2\pi} d\varphi \int_0^{\vartheta(\varphi)} d\psi \sin \psi = R^2 \int_0^{2\pi} d\varphi [1 - \cos \vartheta(\varphi)],$$

and using the relationships $\sigma_{\text{I}} - \sigma_{\text{II}} = \sigma \cos \theta$ and $\vartheta_{\text{ref}} \equiv \theta$, one expands out $(\sigma_{\text{I}} - \sigma_{\text{II}}) \Delta\mathcal{A}_{\text{I}}^{\text{ct}}$. After completing the square using the identity $a^2 - ab = \frac{1}{2}(a-b)^2 + \frac{1}{2}(a^2 - b^2)$ and applying the relationships (B.1), one then obtains Eq. (B.3).

which cancels the second term of Eq. (B.3). Finally, assuming the contact profile does not deviate significantly from the reference profile, we may approximate $h(\tilde{R}(\varphi)) \approx h(R_0, \varphi)$, which is certainly valid to monopole-order (corrections are of third order in the boundary multipoles [LO07]). The energy functional therefore takes the form

$$\mathcal{H}[h, \Delta h_{\text{cm}} | \tilde{R}(\varphi)] \approx \mathcal{H}_0[h | \mathcal{S}_{\text{pr}}^{\text{ref}}] + \frac{\sigma}{2} \int_0^{2\pi} d\varphi [h(R_0, \varphi) - \Delta h_{\text{cm}}]^2. \quad (\text{B.5})$$

Note that in this formulation, the functional contains two “dynamical” fields, h and Δh_{cm} . This differs from the functional for a pinned particle, Eq. (3.24), where the force density is instead dynamical and the height constraint enters in linearly (see also Eq. (3.265)).

Particle in a harmonic trap

A particle trap, such as optical tweezers, may be modeled by an external harmonic potential that subjects the particle to a linear restoring force for vertical height deviations from the potential minimum. As we did in Section 3.7, we account for the trapping energy by amending the energy functional (B.5) with

$$V(h_{\text{cm}}) = \frac{1}{2}k(h_{\text{cm}} - h_0)^2 = \frac{1}{2}k(\Delta h_{\text{cm}} - \Delta h_0^{\text{ref}})^2, \quad (\text{B.6})$$

where $\Delta h_0^{\text{ref}} = h_0 - h_{\text{cm}}^{\text{ref}}$ is the height difference between the trap potential minimum and the center of mass height of the particle in the (isolated) equilibrium reference configuration.

The presence of the external trap potential will generally alter the equilibrium configuration. We obtain the conditions for the surface profile h in the usual way by requiring that the energy functional be stationary under small variations of the two dynamical fields h and Δh_{cm} . Taking the linear variations and collecting terms gives

$$\begin{aligned} \delta\mathcal{H} = & \sigma \int_{\mathcal{S}_{\text{pr}}^{\text{ref}}} d^2x (-\nabla^2 + \ell_c^{-2}) h \delta h - \sigma \int_0^{2\pi} d\varphi \left\{ R_0 \frac{\partial h}{\partial r} \Big|_{r=R_0} - [h(R_0, \varphi) - \Delta h_{\text{cm}}] \right\} \delta h \\ & - \sigma \int_0^{2\pi} d\varphi \left[h(R_0, \varphi) - \left(1 + \frac{2\pi\sigma}{k} \right) \Delta h_{\text{cm}} + \frac{k}{2\pi\sigma} \Delta h_0^{\text{ref}} \right] \delta \Delta h_{\text{cm}} \stackrel{!}{=} 0. \end{aligned} \quad (\text{B.7})$$

The first term gives the usual bulk Euler–Lagrange equation. The second term yields the two-field boundary condition

$$\frac{\partial h}{\partial r} \Big|_{r=R_0} = \frac{h(R_0, \varphi) - \Delta h_{\text{cm}}}{R_0}, \quad (\text{B.8})$$

and the third term relates the two fields,

$$\Delta h_{\text{cm}} = \frac{\frac{2\pi\sigma}{k} h(R_0, \varphi) + \Delta h_0^{\text{ref}}}{1 + \frac{2\pi\sigma}{k}}. \quad (\text{B.9})$$

Together, these provide the boundary condition for the surface:

$$\left. \frac{\partial h}{\partial r} \right|_{r=R_0} = \frac{h(R_0, \varphi) - \Delta h_0^{\text{ref}}}{\left(1 + \frac{2\pi\sigma}{k}\right) R_0}. \quad (\text{B.10})$$

Note that this differs from the pinned-particle boundary condition (3.267), most notably by the replacement $2\pi\sigma/k \rightarrow (1 + 2\pi\sigma/k)$.

B.2 Background field and response

Recall that in general, the effective worldline Hamiltonian for a particle is constructed by symmetry considerations and that the particle boundary conditions find their influence only in the polarizabilities and permanent charges. Hence, there is no need to reconstruct the effective Hamiltonian, but only match the coefficients to the modified “full theory.” In particular, only the monopole and permanent charge terms in Eq. (3.270) are relevant here, so we need only match $\tilde{M}^{(0)}$ and $\tilde{Q}^{(0)}$.

As usual, we decompose the height function into the background and response fields as the superposition $h = h_{\text{bg}} + \delta h$. Using $h_{\text{bg}} = A_0 I_0(r/\ell_c)$ and $\delta h = B_0 K_0(r/\ell_c)$, we determine

$$\begin{aligned} B_0 &= \frac{A_0 \left[\frac{R_0}{\ell_c} I_1(R_0/\ell_c) - \frac{I_0(R_0/\ell_c)}{1+2\pi\sigma/k} \right] + \frac{\Delta h_0^{\text{ref}}}{1+2\pi\sigma/k}}{\frac{K_0(R_0/\ell_c)}{1+2\pi\sigma/k} + \frac{R_0}{\ell_c} K_1(R_0/\ell_c)} \\ &\xrightarrow{\ell_c \rightarrow \infty} -\frac{A_0 - \Delta h_0^{\text{ref}}}{1 + \frac{2\pi\sigma}{k} + \ln\left(\frac{2\ell_c}{R_0\gamma_e}\right)}, \end{aligned} \quad (\text{B.11})$$

and thus in the large ℓ_c limit the induced response is

$$\delta h = -\left[\frac{A_0 - \Delta h_0^{\text{ref}}}{1 + \frac{2\pi\sigma}{k} + \ln\left(\frac{2\ell_c}{R_0\gamma_e}\right)} \right] \ln\left(\frac{2\ell_c}{r\gamma_e}\right). \quad (\text{B.12})$$

Comparing with the effective response, Eq. (3.272), yields the modified soft-monopole polarizability and permanent charge,

$$\tilde{M}^{(0)} = \frac{2\pi\sigma}{1 + \frac{2\pi\sigma}{k} + \ln\left(\frac{2\ell_c}{R_0\gamma_e}\right)} \quad (\text{B.13})$$

$$\tilde{Q}^{(0)} = \tilde{M}^{(0)} \Delta h_0^{\text{ref}}. \quad (\text{B.14})$$

B.3 Leading-order interaction energy

We are now in the position to calculate the interaction energy between unpinned particles as promised in Section 3.7.3. Just as before, we need only appropriate the results of Sections 3.5.4 and 3.6.4 using the replacements $M^{(0)} \rightarrow \tilde{M}^{(0)}$ and $Q^{(0)} \rightarrow \tilde{Q}^{(0)}$.

B.3.1 Elastic interactions

The first case we wish to consider is the elastic interaction between identical particles subjected to identical trap potentials so that we may compare with Eqs. (3.278) and (3.280). After simplification, we obtain

$$\begin{aligned} E_{\{1,2\}}^{(0)} &= \frac{2\pi\sigma(\Delta h_0^{\text{ref}})^2 2\pi G^{12}}{(2\pi\sigma/\tilde{M}^{(0)})[(2\pi\sigma/\tilde{M}^{(0)}) + 2\pi G^{12}]} \\ &= -\frac{2\pi\sigma(\Delta h_0^{\text{ref}})^2 \ln\left(\frac{2\ell_c}{r\gamma_e}\right)}{\left[1 + \frac{2\pi\sigma}{k} + \ln\left(\frac{2\ell_c}{R_0\gamma_e}\right)\right] \left[1 + \frac{2\pi\sigma}{k} + \ln\left(\frac{4\ell_c^2}{rR_0\gamma_e^2}\right)\right]}, \end{aligned} \quad (\text{B.15})$$

which vanishes in the $\ell_c \rightarrow \infty$ as expected.

The second case to consider is that between particles with nonidentical trap potentials, for which a nonvanishing contribution is expected to survive the $\ell_c \rightarrow \infty$ limit. In this case we find agreement with Lehle and Oettel's result (up to a factor of two), Eq. (3.281), and generalize to nonidentical particles:

$$E_{\{1,2\}}^{(0)} \xrightarrow{\ell_c \rightarrow \infty} \frac{(\pi\sigma/2)(\Delta h_{0,1}^{\text{ref}} - \Delta h_{0,2}^{\text{ref}})^2}{1 + \pi\sigma(1/k_1 + 1/k_2) + \ln\left(\frac{r}{\sqrt{R_{0,1}R_{0,2}}}\right)}. \quad (\text{B.16})$$

Note that for nonidentical particles, $\Delta h_{0,1}^{\text{ref}} - \Delta h_{0,2}^{\text{ref}} = (h_{0,1} - h_{0,2}) - (h_{\text{cm},1}^{\text{ref}} - h_{\text{cm},2}^{\text{ref}})$, showing that both the trap height differences and particle reference height differences come into play.

B.3.2 Entropic interactions

For completion, we also present the leading-order entropic interaction between unpinned, trapped particles. From Eq. (3.225) with the replacement $M^{(0)} \rightarrow \tilde{M}^{(0)}$, we find

$$\begin{aligned} \beta U_{\{1,2\}}^{(0)} &= \frac{1}{2} \ln(1 - \tilde{g}_{12}^2) \\ &= -\frac{1}{2} \ln \Lambda_{12} + \frac{1}{2} \ln \left[2 + \frac{2\pi\sigma}{k_1} + \frac{2\pi\sigma}{k_2} + 2 \ln \left(\frac{r}{\sqrt{R_{0,1}R_{0,2}}} \right) \right] + \mathcal{O}(\Lambda^{-1}). \end{aligned} \quad (\text{B.17})$$

The corresponding interparticle force in the $\ell_c \rightarrow \infty$ limit is

$$F_{\{1,2\}}^{(0)} = -\frac{\partial U_{\{1,2\}}^{(0)}}{\partial r} = -\frac{k_B T}{2r \left[1 + \pi \sigma (1/k_1 + 1/k_2) + \ln \left(\frac{r}{\sqrt{R_{0,1} R_{0,2}}} \right) \right]} + \mathcal{O}(\Lambda^{-1}), \quad (\text{B.18})$$

which is in agreement with Ref. [LO07] (*cf.* Eqs. (3.283) and (3.285)).

Appendix C

Monopole contributions for the ellipse: asymptotics and matching

In this appendix we present a more detailed discussion of the anisotropic monopole problem, including the mathematical technicalities associated with the $\ell_c \rightarrow \infty$ asymptotics. We begin with a construction of the general solution in elliptic coordinates and find the limiting asymptotic forms. Next, we apply this to the ellipse BVP to generate a convenient background and response solution pair. We conclude by demonstrating the matching independence between the monopole and higher-order polarizabilities.

C.1 Asymptotics in elliptic coordinates

The inclusion of the gravitational potential breaks the bulk conformal symmetry and, hence, the conformal mapping trick used in Section 5.2.2 is no longer applicable. We can instead, however, transform to elliptic coordinates, which are well-suited for the ellipse BVP.

General case

We first recast the partial differential equation (5.31) in elliptic coordinates. Under this change of variables, it becomes

$$\frac{1}{f^2(\sinh^2 \xi + \sin^2 \eta)} \left(\frac{\partial^2 \phi}{\partial \xi^2} + \frac{\partial^2 \phi}{\partial \eta^2} \right) - \frac{1}{\ell_c^2} \phi = 0. \quad (\text{C.1})$$

Now, we separate variables by assuming a solution of the form $\phi(\xi, \eta) = R(\xi)\Phi(\eta)$. Plugging this in gives

$$\frac{R''}{R} + \frac{\Phi''}{\Phi} - \frac{f^2}{\ell_c^2} (\sinh^2 \xi + \sin^2 \eta) = 0. \quad (\text{C.2})$$

The squares can be removed by using the identities $\sinh^2 \xi = (\cosh 2\xi - 1)/2$ and $\sin^2 \eta = (1 - \cos 2\eta)/2$. Letting c be the separation constant, we obtain two ordinary differential equations (ODEs),

$$R'' - \left[\left(c - \frac{f^2}{2\ell_c^2} \right) + \frac{f^2}{2\ell_c^2} \cosh 2\xi \right] R = 0, \quad (\text{C.3a})$$

$$\Phi'' + \left[\left(c - \frac{f^2}{2\ell_c^2} \right) + \frac{f^2}{2\ell_c^2} \cos 2\eta \right] \Phi = 0. \quad (\text{C.3b})$$

Finally, we define $p := c - f^2/2\ell_c^2$ and $q := -f^2/4\ell_c^2$, which puts the ODEs into the forms

$$R'' - (p - 2q \cosh 2\xi)R = 0, \quad (\text{C.4a})$$

$$\Phi'' + (p - 2q \cos 2\eta)\Phi = 0. \quad (\text{C.4b})$$

The angular ODE is recognized as the Mathieu equation. The periodic boundary condition $\Phi(\eta) \equiv \Phi(\eta + 2\pi)$ implies that p depends on a positive integer n (via the separation constant c). The two families of solutions are given by the (even) cosine-elliptic function $\text{ce}_n(q; \eta)$, where $n \in \mathbb{N}_0$, and the (odd) sine-elliptic function $\text{se}_n(q; \eta)$, where $n \in \mathbb{N}$. We will not elaborate on the details here, but these solutions may be obtained by considering Eq. (C.4b) as an eigenvalue problem—more information may be found in Ref. [AW05]. The general solution of $\Phi(\eta)$ is then the linear superposition

$$\Phi_n(\eta) = A_n \text{ce}_n(q; \eta) + B_n \text{se}_n(q; \eta), \quad B_0 = 0. \quad (\text{C.5})$$

With these same eigenvalues p_n , the radial ODE becomes the *modified* Mathieu DE, with solutions given by the even and odd evanescent (since $q < 0$) radial Mathieu functions of the first kind: $\text{Ie}_n(q; \xi)$ and $\text{Io}_n(-q; \xi)$, and second kind: $\text{Ke}_n(-q; \xi)$ and $\text{Ko}_n(-q; \xi)$. The general solution is again a linear superposition

$$\begin{aligned} R_n(\xi) = & a_n \text{Ie}_n(-q; \xi) + b_n \text{Io}_n(-q; \xi) \\ & + c_n \text{Ke}_n(-q; \xi) + d_n \text{Ko}_n(-q; \xi), \end{aligned} \quad (\text{C.6})$$

where $b_0 = d_0 = 0$. The notation highlights the analogy between the modified Mathieu functions from an elliptic geometry with the modified Bessel functions of a circular geometry. Indeed, the behavior of the modified Mathieu functions is analogous to the modified Bessel functions: Both Ke_n and Ko_n decay at infinity, whereas both Ie_n and Io_n diverge at infinity. Finally, the complete general solution is given by

$$\phi(\xi, \eta) = \sum_{n=0}^{\infty} R_n(\xi) \Phi_n(\eta). \quad (\text{C.7})$$

We could continue in this manner and find the explicit solution to our boundary value problem; however, we are only interested in the limiting case of $\ell_c \rightarrow \infty$.

Asymptotics

Since the capillary length ℓ_c is being used as a regulator, we must consider the solution behavior for $q = -f^2/4\ell_c^2 \rightarrow 0$. Although asymptotic series expansions for the Mathieu functions exist in the literature, we can easily get the relevant terms by reconsidering the original ODEs (C.4a) and (C.4b).

The angular ODE for $q \rightarrow 0$ simply reduces to the harmonic oscillator DE with an angular frequency \sqrt{p} , giving $\cos(\sqrt{p}\eta)$ and $\sin(\sqrt{p}\eta)$ as general solutions. Enforcing periodicity

requires $p = n^2$ for some integer n . For the radial solution, we must be a little more careful since $\cosh 2\xi$ is not bounded above. However, since $\xi \in [0, \infty)$, we have for large ξ the asymptotic form

$$2q \cosh 2\xi = q(e^{2\xi} + e^{-2\xi}) \sim q e^{2\xi} \text{ as } q \rightarrow 0. \quad (\text{C.8})$$

Recalling that $q < 0$, this motivates introducing an effective elliptic radius $\rho := \sqrt{-q} e^\xi$. Applying this to Eq. (C.4a) using $d\rho = \rho d\xi$ gives

$$\rho \frac{d}{d\rho} \left(\rho \frac{dR}{d\rho} \right) - \left(p + \rho^2 + \frac{q^2}{\rho^2} \right) R = 0. \quad (\text{C.9})$$

Finally, taking $q \rightarrow 0$ and using $p = n^2$ from before yields the asymptotic ODE

$$\rho \frac{d}{d\rho} \left(\rho \frac{dR}{d\rho} \right) - (n^2 + \rho^2) R = 0. \quad (\text{C.10})$$

This is recognized as the modified Bessel equation, whose solutions $I_n(\rho)$ and $K_n(\rho)$ are the modified Bessel functions of the first and second kind respectively, again reflecting the analogy with the Mathieu functions. Of course, this is exactly what one would expect. Far away from the central ellipse, the coordinate lines approach circles and therefore approach the circular case which, as discussed in Chapter 3, lead to the modified Bessel equation.

C.2 Background field and response

In order to match the monopole polarizabilities, we need a convenient set of background fields as well as their (full-theory) responses. Based on the previous section, we should consider the set of background fields

$$\phi_{\text{bg}}^{(n)}(\rho, \eta | \vartheta) = A^{(n)} \left(\frac{I_n(\rho)}{I_n(\rho_0)} \right) \cos[n(\eta - \vartheta)], \quad (\text{C.11})$$

where we have included a possible phase ϑ that may be useful for matching later on, and $\rho_0 = f e^{\xi_0} / 2\ell_c = (a + b) / 2\ell_c$. The corresponding responses that satisfy $(\phi_{\text{bg}} + \delta\phi)|_{\rho=\rho_0}$ and $\delta\phi(\rho \rightarrow \infty) \rightarrow 0$ are given by

$$\delta\phi_{\text{full}}^{(n)}(\rho, \eta | \vartheta) = -A^{(n)} \left(\frac{K_n(\rho)}{K_n(\rho_0)} \right) \cos[n(\eta - \vartheta)]. \quad (\text{C.12})$$

Since $\rho \sim \ell_c^{-1}$, we can simplify matters by taking the asymptotics further, keeping only the singular terms since the remaining terms will vanish in the $\ell_c \rightarrow \infty$ limit. To make the expressions more transparent in powers of ℓ_c , we set $\rho =: \tilde{\rho} / \ell_c$. The required expansions then become

$$\frac{I_n(\tilde{\rho} / \ell_c)}{I_n(\tilde{\rho}_0 / \ell_c)} = \left(\frac{\tilde{\rho}}{\tilde{\rho}_0} \right)^n + \mathcal{O}(\ell_c^{-2}), \quad (\text{C.13})$$

and

$$\frac{K_n(\tilde{\rho}/\ell_c)}{K_n(\tilde{\rho}_0/\ell_c)} = \begin{cases} \frac{\ln(\frac{2\ell_c}{\gamma_e \tilde{\rho}})}{\ln(\frac{2\ell_c}{\gamma_e \tilde{\rho}_0})} + \mathcal{O}(\ell_c^{-2}), & n = 0 \\ \left(\frac{\tilde{\rho}_0}{\tilde{\rho}}\right)^n + \mathcal{O}(\ell_c^{-2}), & n \geq 1, \end{cases} \quad (\text{C.14})$$

where $\gamma_e = e^{\gamma_E}$ and γ_E is the Euler-Mascheroni constant. Using the definitions of ρ and $\tilde{\rho}$, the background and response fields may finally be expressed as

$$\phi_{\text{bg}}^{(n)}(\xi, \eta | \vartheta) = A^{(n)} e^{n(\xi - \xi_0)} \cos[n(\eta - \vartheta)], \quad (\text{C.15})$$

and

$$\delta\phi_{\text{full}}^{(n)}(\xi, \eta | \vartheta) = \begin{cases} -A^{(n)} \frac{\ln(\frac{f e^\xi}{4\ell_c} \gamma_e)}{\ln(\frac{a+b}{4\ell_c} \gamma_e)}, & n = 0 \\ -A^{(n)} e^{-n(\xi - \xi_0)} \cos[n(\eta - \vartheta)], & n \geq 1. \end{cases} \quad (\text{C.16})$$

C.3 Independence of matching

The conformal transformation of the z -space background field (5.10) to the w -space background field (5.18) in Section 5.2.2 requires the expansion

$$\begin{aligned} \left(s_+ \frac{w}{R} + s_- \frac{R}{w}\right)^n &= \sum_{\ell < n/2} \left\{ \binom{n}{\ell} s_+^{n-\ell} s_-^\ell \left(\frac{w}{R}\right)^{n-2\ell} + \binom{n}{\ell} s_+^\ell s_-^{n-\ell} \left(\frac{R}{w}\right)^{n-2\ell} \right\} \\ &\quad + \binom{n}{n/2} (s_+ s_-)^{n/2}, \end{aligned} \quad (\text{C.17})$$

where the last term only appears when n is even (hence the “ $+$ ” notation). As seen in Eqs. (C.15) and (C.16), a nonzero constant background generates a monopole response. In particular, the response to the full *constant term* in w -space is similar to (C.16) and given by

$$\delta\tilde{\phi}_c^{(n)}(\mathbf{w} | \vartheta) = -\frac{A^{(n)}(s_+ s_-)^{n/2}}{2^n} \binom{n}{n/2} \frac{\ln(\frac{|w|\gamma_e}{2\ell_c})}{\ln(\frac{R\gamma_e}{2\ell_c})} (e^{-in\vartheta} + e^{in\vartheta}). \quad (\text{C.18})$$

Since there is no singular behavior in mapping back to the ellipse via $w \rightarrow w(z)$, we can safely take the limit $\ell_c \rightarrow \infty$, giving

$$\delta\phi_c^{(n)}(\mathbf{z} | \vartheta) = -\frac{A^{(n)}(s_+ s_-)^{n/2}}{2^n} \binom{n}{n/2} (e^{-in\vartheta} + e^{in\vartheta}). \quad (\text{C.19})$$

Now let’s consider the effect of the background field in the monopole EFT response (5.35).

From $\phi_{\text{bg}}^{(n \geq 1)}(0) = 0$ and $\partial^k \phi_{\text{bg}}^{(n \geq 1)}(0) = A^{(n)} n! \delta_{kn} e^{-in\vartheta}$, we obtain the nonvanishing term

$$\begin{aligned}
 \delta\phi_{\text{m}}^{(n)}(z \mid \vartheta) &= \sum_{\substack{k>0 \\ \text{even}}} \frac{M^{(k)}}{2\pi} \ln\left(\frac{|z|\gamma_e}{2\ell_c}\right) \partial^k \phi_{\text{bg}}^{(n)}(0) + \text{c.c.} \\
 &= - \sum_{\substack{k>0 \\ \text{even}}} \frac{\ln\left(\frac{|z|\gamma_e}{2\ell_c}\right)}{\ln\left(\frac{(a+b)\gamma_e}{4\ell_c}\right)} \frac{f^k A^{(n)} n! \delta_{kn} e^{-in\vartheta}}{2^k \left[\left(\frac{k}{2}\right)!\right]^2} + \text{c.c.} \\
 &\xrightarrow{\ell_c \rightarrow \infty} - \frac{f^n A^{(n)} n!}{2^n \left[\left(\frac{n}{2}\right)!\right]^2} \left(e^{-in\vartheta} + e^{in\vartheta}\right) \quad (n \text{ even}). \tag{C.20}
 \end{aligned}$$

Recalling that $f^n = (s_+ s_-)^{n/2}$ and $\binom{n}{n/2} = n! / \left[\left(\frac{n}{2}\right)!\right]^2$, we find (C.20) is precisely equal to (C.19). Therefore, we find that the higher-order polarizabilities can be matched independently of the monopole terms without contamination by simply ignoring the constant term in the binomial expansion of Eq. (C.17).

List of Figures

| | | |
|-----|---|-----|
| 1.1 | Two conducting spheres | 7 |
| 1.2 | Electrostatic forces near contact | 32 |
| 2.1 | Surface parametrization and local coordinate system | 45 |
| 2.2 | Illustration of principal curvatures | 48 |
| 2.3 | Monge gauge representation | 52 |
| 3.1 | Embedded particles with circular footprints | 73 |
| 3.2 | Illustration of the three boundary conditions | 74 |
| 3.3 | Projected domain of a tilted particle | 76 |
| 3.4 | Saddle-shaped particle | 78 |
| 3.5 | Parameter definitions in a multibody configuration | 118 |
| 3.6 | Electrostatics analogy for monopoles at $\ell_c \rightarrow \infty$ | 128 |
| 3.7 | Electrostatics analogy for a trapped particle | 158 |
| 4.1 | Membrane inclusions and representative particles | 165 |
| 4.2 | Rigid body displacements of a particle inclusion | 166 |
| 4.3 | Cap and saddle shapes | 167 |
| 4.4 | Interaction energy landscape | 193 |
| 4.5 | Minimum-energy bifurcation behavior | 196 |
| 4.6 | Phase portraits in the $\chi\eta$ -plane | 200 |
| 4.7 | Parameter definitions in a multibody configuration | 202 |
| 5.1 | Conformal mapping between the circle and ellipse, and associated BVP solution scheme | 217 |
| 5.2 | Configuration for two ellipses as viewed from above | 227 |
| 5.3 | Breakdown of the two-particle preferred-configuration degeneracy after lead- ing order | 230 |
| 5.4 | Parameter definitions in a multibody configuration | 232 |
| 5.5 | Three-body ellipse configurations | 234 |
| 5.6 | Breakdown of the three-particle preferred-configuration degeneracy after leading order | 235 |
| B.1 | Parametrizations for an unpinned particle | 259 |

List of Technical Notes

| | | |
|-----|---|-----|
| 1.1 | Derivatives of the electrostatic Green function | 24 |
| 1.2 | Attraction at close approach | 30 |
| 2.1 | Domain walls in Ginzburg–Landau theory | 42 |
| 2.2 | Covariant and contravariant components | 46 |
| 2.3 | Gauss–Bonnet theorem | 56 |
| 3.1 | The complete EFT for circular particles | 103 |
| 3.2 | The Cayley–Hamilton theorem and matrix inverse | 125 |
| 4.1 | The biharmonic Green function | 170 |
| 4.2 | Membrane point dipoles | 172 |
| 4.3 | Biharmonic solution on an annulus | 176 |
| 4.4 | Derivatives of the biharmonic Green function | 181 |
| 4.5 | Point reflections across a line | 194 |
| 5.1 | Expansion of entropic interaction diagrams | 228 |

Bibliography

- [ABC03] R. Aveyard, B. P. Binks, and J. H. Clint, *Emulsions stabilised solely by colloidal particles*, *Advances in Colloid and Interface Science* **100–102**, 503–546 (2003).
- [AG09] T. Auth and G. Gompper, *Budding and vesiculation induced by conical membrane inclusions*, *Phys. Rev. E* **80**, 031901 (2009).
- [AJL⁺83] B. Alberts, A. Johnson, J. Lewis, M. Raff, K. Roberts, and P. Walter, *Molecular Biology of the Cell*, Garland Science, New York (1983).
- [AJL⁺07] B. Alberts, A. Johnson, J. Lewis, M. Raff, K. Roberts, and P. Walter, *Molecular Biology of the Cell*, 5th ed., Garland Science, New York (2007).
- [App84] J. Applequist, *Fundamental relationships in the theory of electric multipole moments and multipole polarizabilities in static fields*, *Chemical Physics* **85**, 279–290 (1984).
- [App89] J. Applequist, *Traceless cartesian tensor forms for spherical harmonic functions: new theorems and applications to electrostatics of dielectric media*, *Journal of Physics A: Mathematical and General* **22**, 4303 (1989).
- [AW05] G. B. Arfken and H. J. Weber, *Mathematical Methods for Physicists: A Comprehensive Guide*, 6th ed., Academic Press, Oxford (2005).
- [Bai13a] J. Bain, *Effective Field Theories*, in R. Batterman (ed.), *The Oxford Handbook of Philosophy of Physics*, Oxford University Press (2013).
- [Bai13b] J. Bain, *Emergence in effective field theories*, *European Journal for Philosophy of Science* **3**, 257–273 (2013).
- [Bar79] G. I. Barenblatt, *Similarity, Self-similarity, and Intermediate Asymptotics*, Consultants Bureau, New York (1979).
- [Bar96] G. I. Barenblatt, *Scaling, self-similarity, and intermediate asymptotics: dimensional analysis and intermediate asymptotics*, vol. 14, Cambridge University Press (1996).
- [Bat13] R. Batterman, *The Tyranny of Scales*, in R. Batterman (ed.), *The Oxford Handbook of Philosophy of Physics*, Oxford University Press (2013).

- [BB81] E. Burgos and H. Bonadeo, *Electrical multipoles and multipole interactions: compact expressions and a diagrammatic method*, Molecular Physics **44**, 1–15 (1981).
- [BB07] G. Brannigan and F. L. H. Brown, *Contributions of Gaussian curvature and nonconstant lipid volume to protein deformation of lipid bilayers*, Biophysical Journal **92**, 864–876 (2007).
- [BCGW99] N. Bowden, I. S. Choi, B. A. Grzybowski, and G. M. Whitesides, *Mesoscale Self-Assembly of Hexagonal Plates Using Lateral Capillary Forces: Synthesis Using the "Capillary Bond"*, J. Am. Chem. Soc. **121**, 5373–5391 (1999).
- [BDF10] A.-F. Bitbol, P. G. Dommersnes, and J.-B. Fournier, *Fluctuations of the Casimir-like force between two membrane inclusions*, Phys. Rev. E **81**, 050903 (2010).
- [BDFN95] J. J. Binney, N. J. Dowrick, A. J. Fisher, and M. E. J. Newman, *The theory of critical phenomena*, Clarendon Press, Oxford (1995).
- [BEK13] Bimonte, G., Emig, T., and Kardar, M., *Conformal field theory of critical Casimir interactions in 2D*, EPL **104**, 21001 (2013).
- [BF03] D. Bartolo and J.-B. Fournier, *Elastic interaction between “hard” or “soft” pointwise inclusions on biological membranes*, Eur. Phys. J. E **11**, 141–146 (2003).
- [Bin02] B. P. Binks, *Particles as surfactants – similarities and differences*, Current Opinion in Colloid and Interface Science **7**, 21–41 (2002).
- [Bin07] B. P. Binks, *Colloidal particles at liquid interfaces*, Phys. Chem. Chem. Phys. **9**, 6298–6299 (2007).
- [BKS99] M. E. S. Borelli, H. Kleinert, and A. M. Schakel, *Derivative expansion of one-loop effective energy of stiff membranes with tension*, Phys. Lett. A **253**, 239–246 (1999).
- [BKT⁺09] M. A. Bucaro, P. R. Kolodner, J. A. Taylor, A. Sidorenko, J. Aizenberg, and T. N. Krupenkin, *Tunable liquid optics: electrowetting-controlled liquid Mirrors based on self-assembled Janus tiles*, Langmuir **25**, 3876–3879 (2009).
- [BL75] F. Brochard and J. F. Lennon, *Frequency spectrum of the flicker phenomenon in erythrocytes*, Journal de Physique **36**, 1035–1047 (1975).
- [BLDW07] C. Bachas, P. Le Doussal, and K. J. Wiese, *Wetting and minimal surfaces*, Phys. Rev. E **75**, 031601 (2007).

- [BO07] F. Bresme and M. Oettel, *Nanoparticles at fluid interfaces*, Journal of Physics: Condensed Matter **19**, 413101 (2007).
- [Boa12] D. Boal, *Mechanics of the Cell*, Cambridge University Press (2012).
- [BSR00] A. B. D. Brown, C. G. Smith, and A. R. Rennie, *Fabricating colloidal particles with photolithography and their interactions at an air-water interface*, Phys. Rev. E **62**, 951–960 (2000).
- [BTCW97] N. Bowden, A. Terfort, J. Carbeck, and G. M. Whitesides, *Self-Assembly of Mesoscale Objects into Ordered Two-Dimensional Arrays*, Science **276**, 233–235 (1997).
- [Bur07] C. P. Burgess, *An Introduction to Effective Field Theory*, Annual Review of Nuclear and Particle Science **57**, 329–362 (2007).
- [BV06] P. D. Blood and G. A. Voth, *Direct observation of Bin/amphiphysin/Rvs (BAR) domain-induced membrane curvature by means of molecular dynamics simulations*, Proc. Nat. Acad. Sci. (USA) **103**, 15068–15072 (2006).
- [BVS13] D. Boda, M. Valiskó, and I. Szalai, *The origin of the interparticle potential of electrorheological fluids*, Cond. Matt. Phys. **16**, 43002 (2013).
- [BWCW01] N. B. Bowden, M. Weck, I. S. Choi, and G. M. Whitesides, *Molecule-Mimetic Chemistry and Mesoscale Self-Assembly*, Acc. Chem. Res. **34**, 231–238 (2001).
- [BZ15] J. M. Borwein and Q. J. Zhu, *A variational approach to Lagrange multipliers*, Journal of Optimization Theory and Applications 1–30 (2015).
- [Can70] P. B. Canham, *The minimum energy of bending as a possible explanation of the biconcave shape of the human red blood cell*, J. Theoret. Biol. **26**, 61–81 (1970).
- [Cas48] H. B. G. Casimir, *On the attraction between two perfectly conducting plates*, Proc. Kon. Ned. Akad. Wetensch. **51**, 793–795 (1948).
- [CFHQ02] D. J. Campbell, E. R. Freidinger, J. M. Hastings, and M. K. Querns, *Spontaneous assembly of soda straws*, Journal of Chemical Education **79**, 201 (2002).
- [CGS03] R. Capovilla, J. Guven, and J. A. Santiago, *Deformations of the geometry of lipid vesicles*, Journal of Physics A: Mathematical and General **36**, 6281 (2003).
- [Che05] T.-P. Cheng, *Relativity, gravitation and cosmology: A basic introduction*, Oxford University Press, New York (2005).

- [CHJW81] D. Y. C. Chan, J. D. Henry Jr., and L. R. White, *The interaction of colloidal particles collected at fluid interfaces*, J. Coll. Interface Sci. **79**, 410–418 (1981).
- [CKO01] T. Chou, K. S. Kim, and G. Oster, *Statistical Thermodynamics of Membrane Bending-Mediated Protein-Protein Attractions*, Biophys. J. **80**, 1075–1087 (2001).
- [CL95a] W. Cai and T. C. Lubensky, *Hydrodynamics and dynamic fluctuations of fluid membranes*, Phys. Rev. E **52**, 4251–4266 (1995).
- [CL95b] P. M. Chaikin and T. C. Lubensky, *Principles of condensed matter physics*, Cambridge University Press (1995).
- [CLNP94] W. Cai, T. C. Lubensky, P. Nelson, and T. Powers, *Measure factors, tension, and correlations of fluid membranes*, J. Phys. II (France) **4**, 931–949 (1994).
- [Dav] F. David, *Geometry and field theory of random surfaces and membranes*, Chapter 7 of [NPW04].
- [Dav88] F. David, *Conformal field theories coupled to 2-D gravity in the conformal gauge*, Modern Physics Letters A **03**, 1651–1656 (1988).
- [dC76] M. do Carmo, *Differential Geometry of Curves and Surfaces*, 1 ed., Prentice Hall, New Jersey (1976).
- [Del04] B. Delamotte, *A hint of renormalization*, American Journal of Physics **72**, 170–184 (2004).
- [Des] M. Deserno, *Fluid lipid membranes – a primer*, https://www.cmu.edu/biolphys/deserno/pdf/membrane_theory.pdf.
- [Des05] S. Deser, *How special relativity determines the signs of the nonrelativistic Coulomb and Newtonian forces*, American Journal of Physics **73**, 752–755 (2005).
- [Des15] M. Deserno, *Fluid lipid membranes: From differential geometry to curvature stresses*, Chemistry and Physics of Lipids **185**, 11–45, Membrane mechanochemistry: From the molecular to the cellular scale (2015).
- [DF99a] P. G. Dommersnes and J.-B. Fournier, *Casimir and mean-field interactions between membrane inclusions subject to external torques*, Europhys. Lett. **46**, 256–261 (1999).
- [DF99b] P. G. Dommersnes and J.-B. Fournier, *N-body study of anisotropic membrane inclusions: membrane mediated interactions and ordered aggregation*, Eur. Phys. J. E **12**, 9–12 (1999).

- [DF02] P. Dommersnes and J.-B. Fournier, *The Many-Body Problem for Anisotropic Membrane Inclusions and the Self-Assembly of “Saddle” Defects into an “Egg Carton”*, Biophys. J. **83**, 2898–2905 (2002).
- [dGBWQ04] P.-G. de Gennes, F. Brochard-Wyart, and D. Quéré, *Capillarity and wetting phenomena*, Springer, New York (2004).
- [dGT82] P. G. de Gennes and C. Taupin, *Microemulsions and the flexibility of oil/water interfaces*, J. Phys. Chem. **86**, 2294–2304 (1982).
- [DK89] J. Distler and H. Kawai, *Conformal field theory and 2D quantum gravity*, Nuclear Physics B **321**, 509–527 (1989).
- [DK10] K. D. Danov and P. A. Kralchevsky, *Capillary forces between particles at a liquid interface: General theoretical approach and interactions between capillary multipoles*, Advances in Colloid and Interface Science **154**, 91–103 (2010).
- [DKNB05] K. D. Danov, P. A. Kralchevsky, B. N. Naydenov, and G. Brenn, *Interactions between particles with an undulated contact line at a fluid interface: Capillary multipoles of arbitrary order*, Journal of Colloid and Interface Science **287**, 121–134 (2005).
- [DL91] F. David and S. Leibler, *Vanishing tension of fluctuating membranes*, J. Phys. II (France) **1**, 959–976 (1991).
- [DLMF] *NIST Digital Library of Mathematical Functions*, <http://dlmf.nist.gov/>, Release 1.0.10 of 2015-08-07, online companion to [OLBC10].
- [Don03] C. Donolato, *An extension of Thomson’s theorem and its application for determining induced charge densities*, American Journal of Physics **71**, 1232–1236 (2003).
- [Dun08] G. V. Dunne, *Functional determinants in quantum field theory*, J. Phys. A **41**, 304006 (2008).
- [DY06] T. P. Doerr and Y.-K. Yu, *Electrostatics of charged dielectric spheres with application to biological systems*, Phys. Rev. E **73**, 061902 (2006).
- [Eas10] J. Eastoe, *Surfactant aggregation and adsorption at interfaces*, in T. Cosgrove (ed.), *Colloid science: principles, methods and applications*, 2nd ed., Wiley, Great Britain (2010).
- [EGJK07] T. Emig, N. Graham, R. L. Jaffe, and M. Kardar, *Casimir Forces between Arbitrary Compact Objects*, Phys. Rev. Lett. **99**, 170403 (2007).

- [EGJK08] T. Emig, N. Graham, R. L. Jaffe, and M. Kardar, *Casimir forces between compact objects: The scalar case*, Phys. Rev. D **77**, 025005 (2008).
- [EGJK09] T. Emig, N. Graham, R. L. Jaffe, and M. Kardar, *Orientation dependence of Casimir forces*, Phys. Rev. A **79**, 054901 (2009).
- [ETS03] A. R. Evans, M. S. Turner, and P. Sens, *Interactions between proteins bound to biomembranes*, Phys. Rev. E **67**, 041907 (2003).
- [Eva74] E. A. Evans, *Bending Resistance and Chemically Induced Moments in Membrane Bilayers*, Biophys. J. **14**, 923–931 (1974).
- [EW13] M. B. Einhorn and J. Wudka, *The bases of effective field theories*, Nuclear Physics B **876**, 556–574 (2013).
- [FD97] J.-B. Fournier and P. G. Dommersnes, *Comment on “Long-range forces in heterogeneous fluid membranes”*, Europhys. Lett. **39**, 681 (1997).
- [FdG78] M. E. Fisher and P.-G. de Gennes, *Wall Phenomena in a Critical Binary Mixture*, Compt. Rendus Hebd. Seanc. Acad. Sci. **287**, 207–209 (1978).
- [FDP03] J.-B. Fournier, P. G. Dommersnes, and G. P., *Dynamin recruitment by clathrin coats: a physical step?*, Comptes Rendus Biologies **326**, 467–476 (2003).
- [FEPN11] M. C. N. Fiolhais, H. Essen, C. Providencia, and A. B. Nordmark, *Magnetic field and current are zero inside ideal conductors*, Progress In Electromagnetics Research B **27**, 187–212 (2011).
- [FG02] J.-B. Fournier and P. Galatola, *Anisotropic capillary interactions and jamming of colloidal particles trapped at a liquid-fluid interface*, Phys. Rev. E **65**, 031601 (2002).
- [FHP03] J.-C. Faugère, M. Hering, and J. Phan, *The membrane inclusions curvature equations*, Adv. Appl. Math. **31**, 643–658 (2003).
- [FN91] E. Frey and D. R. Nelson, *Dynamics of flat membranes and flickering in red blood cells*, J. Phys. I France **1**, 1715–1757 (1991).
- [För86] D. Förster, *On the scale dependence, due to thermal fluctuations, of the elastic properties of membranes*, Phys. Lett. A **114**, 115–120 (1986).
- [För87] D. Förster, *Tangential Flows in Fluid Membranes and their Effect on the Softening of Curvature Rigidity with Scale*, Europhys. Lett. **4**, 65 (1987).
- [FRT⁺01] K. Farsad, N. Ringstad, K. Takei, S. R. Floyd, K. Rose, and P. De Camilli, *Generation of high curvature membranes mediated by direct endophilin bilayer interactions*, Journal of Cell Biology **155**, 193–200 (2001).

- [Gam09] A. Gambassi, *The Casimir effect: From quantum to critical fluctuations*, Journal of Physics: Conference Series **161**, 012037 (2009).
- [GB08] A. Gramada and P. E. Bourne, *Resolving a distribution of charge into intrinsic multipole moments: A rankwise distributed multipole analysis*, Phys. Rev. E **78**, 066601 (2008).
- [GBA⁺01] B. A. Grzybowski, N. Bowden, F. Arias, H. Yang, and G. M. Whitesides, *Modeling of Menisci and Capillary Forces from the Millimeter to the Micrometer Size Range*, J. Phys. Chem. B **105**, 404–412 (2001).
- [GBP93a] M. Goulian, R. Bruinsma, and P. Pincus, *Long-Range Forces in Heterogeneous Fluid Membranes*, Europhys. Lett. **22**, 145–150 (1993).
- [GBP93b] M. Goulian, R. Bruinsma, and P. Pincus, *Long-Range Forces in Heterogeneous Fluid Membranes: Erratum*, Europhys. Lett. **23**, 155 (1993).
- [Geo93] H. Georgi, *Effective field theory*, Annual review of nuclear and particle science **43**, 209–252 (1993).
- [GFG98] D. P. G., J.-B. Fournier, and P. Galatola, *Long-range elastic forces between membrane inclusions in spherical vesicles*, Europhys. Lett. **42**, 233–238 (1998).
- [GGK96a] R. Golestanian, M. Goulian, and M. Kardar, *Fluctuation-induced interactions between rods on a membrane*, Phys. Rev. E **54**, 6725–6734 (1996).
- [GGK96b] R. Golestanian, M. Goulian, and M. Kardar, *Fluctuation-induced interactions between rods on membranes and interfaces*, Europhys. Lett. **33**, 241–245 (1996).
- [GHV14] J. Guven, G. Huber, and D. M. Valencia, *Terasaki Spiral Ramps in the Rough Endoplasmic Reticulum*, Phys. Rev. Lett. **113**, 188101 (2014).
- [GK96] G. Gompper and D. M. Kroll, *Random Surface Discretizations and the Renormalization of the Bending Rigidity*, J. Phys. I **6**, 1305–1320 (1996).
- [GLR10] C. R. Galley, A. K. Leibovich, and I. Z. Rothstein, *Finite Size Corrections to the Radiation Reaction Force in Classical Electrodynamics*, Phys. Rev. Lett. **105**, 094802 (2010).
- [GMH⁺09] A. Gambassi, A. Maciolek, C. Hertlein, U. Nellen, L. Helden, C. Bechinger, and S. Dietrich, *Critical Casimir effect in classical binary liquid mixtures*, Phys. Rev. E **80**, 061143 (2009).
- [GMO89] N. Goldenfeld, O. Martin, and Y. Oono, *Intermediate asymptotics and renormalization group theory*, Journal of scientific computing **4**, 355–372 (1989).

- [Gol92] N. Goldenfeld, *Lectures on Phase Transitions and the Renormalization Group*, Frontiers in physics, Addison-Wesley, Advanced Book Program (1992).
- [GR06a] W. D. Goldberger and I. Z. Rothstein, *Dissipative effects in the worldline approach to black hole dynamics*, Phys. Rev. D **73**, 104030 (2006).
- [GR06b] W. D. Goldberger and I. Z. Rothstein, *An effective field theory of gravity for extended objects*, Phys. Rev. D **73**, 104029 (2006).
- [GS71] W. A. Gifford and L. E. Scriven, *On the attraction of floating particles*, Chem. Eng. Sci. **26**, 287 (1971).
- [Guv04] J. Guven, *Membrane geometry with auxiliary variables and quadratic constraints*, J. Phys. A: Math Gen **37**, L313 (2004).
- [GYX99] B. Gates, Y. Yin, and Y. Xia, *Fabrication and characterization of porous membranes with highly ordered three-dimensional periodic structures*, Chemistry of Materials **11**, 2827–2836 (1999).
- [Ham09] H. W. Hamber, *Quantum Gravitation: The Feynman Path Integral Approach*, Springer, Berlin (2009).
- [HB05] D. L. Hu and J. W. M. Bush, *Meniscus-climbing insects*, Nature **437**, 733–736 (2005).
- [HBS98] B. T. Holland, C. F. Blanford, and A. Stein, *Synthesis of macroporous minerals with highly ordered three-dimensional arrays of spheroidal voids*, Science **281**, 538–540 (1998).
- [HD14] R. C. Haussman and M. Deserno, *Effective field theory of thermal Casimir interactions between anisotropic particles*, Phys. Rev. E **89**, 062102 (2014).
- [Hel73] W. Helfrich, *Elastic properties of lipid bilayers: theory and possible experiments*, Z. Naturforsch. C **28**, 693–703 (1973).
- [Hel85] W. Helfrich, *Effect of thermal undulations on the rigidity of fluid membranes and interfaces*, J. Phys. France **46**, 1263–1268 (1985).
- [Hel87] W. Helfrich, *Measures of integration in calculating the effective rigidity of fluid surfaces*, J. Phys. France **48**, 285–289 (1987).
- [Hel98] W. Helfrich, *Stiffening of fluid membranes and entropy loss of membrane closure: Two effects of thermal undulations*, Eur. Phys. J. B **1**, 481–489 (1998).
- [HHG⁺08] C. Hertlein, L. Helden, A. Gambassi, S. Dietrich, and C. Bechinger, *Direct measurement of critical Casimir forces*, Nature **451**, 172–175 (2008).

- [Hob57] E. W. Hobson, *A Treatise on Plane and Advanced Trigonometry*, Dover books on elementary and intermediate mathematics, 7th ed., Dover Publications, Mineola, NY (1957).
- [Hoh67] P. C. Hohenberg, *Existence of Long-Range Order in One and Two Dimensions*, Phys. Rev. **158**, 383–386 (1967).
- [HW01] W. Helfrich and T. R. Weikl, *Two direct methods to calculate fluctuation forces between rigid objects embedded in fluid membranes*, Eur. Phys. J. E **5**, 423–439 (2001).
- [IER⁺05] T. Itoh, K. S. Erdmann, A. Roux, B. Habermann, H. Werner, and P. De Camilli, *Dynamin and the Actin Cytoskeleton Cooperatively Regulate Plasma Membrane Invagination by BAR and F-BAR Proteins*, Developmental Cell **9**, 791–804 (2005).
- [IMN76] J. N. Israelachvili, D. J. Mitchell, and B. W. Ninham, *Theory of self-assembly of hydrocarbon amphiphiles into micelles and bilayers*, J. Chem. Soc., Faraday Trans. 2 **72**, 1525–1568 (1976).
- [Ise92] C. Isenberg, *The Science of Soap Films and Soap Bubbles*, Dover, Mineola, NY (1992).
- [Isr11] J. N. Israelachvili, *Intermolecular and surface forces*, 3rd ed., Academic Press, San Diego, CA (2011).
- [IZ05] C. Itzykson and J.-B. Zuber, *Quantum field theory*, Dover (2005).
- [Jas72] J. J. Jasper, *The Surface Tension of Pure Liquid Compounds*, Journal of Physical and Chemical Reference Data **1**, 841–1010 (1972).
- [Kar07] M. Kardar, *Statistical Physics of Fields*, Cambridge University Press (2007).
- [KCR08] K. S. Kim, T. Chou, and J. Rudnick, *Degenerate ground-state lattices of membrane inclusions*, Phys. Rev. E **78**, 011401 (2008).
- [KD01] P. A. Kralchevsky and N. D. Denkov, *Capillary forces and structuring in layers of colloid particles*, Current Opinion in Colloid and Interface Science **6**, 383–401 (2001).
- [KDD01] P. A. Kralchevsky, N. D. Denkov, and K. D. Danov, *Particles with an undulated contact line at a fluid interface: interaction between capillary quadrupoles and rheology of particulate monolayers*, Langmuir **17**, 7694–7705 (2001).

- [Ken12] R. Kenna, *Universal Scaling Relations for Logarithmic-Correction Exponents*, in Y. Holovatch (ed.), *Order, Disorder and Criticality: Advanced Problems of Phase Transition Theory*, vol. III, chap. 1, World Scientific, Amsterdam (2012).
- [KG99] M. Kardar and R. Golestanian, *The “friction” of vacuum, and other fluctuation-induced forces*, Rev. Mod. Phys. **71**, 1233–1245 (1999).
- [Kle86] H. Kleinert, *Thermal softening of curvature elasticity in membranes*, Phys. Lett. A **114**, 263–268 (1986).
- [Kle89] H. Kleinert, *Tangential flow in fluid membranes. Absence of renormalization effects*, J. of Stat. Phys. **56**, 227–232 (1989).
- [KN00] P. A. Kralchevsky and K. Nagayama, *Capillary interactions between particles bound to interfaces, liquid films and biomembranes*, Advances in Colloid and Interface Science **85**, 145–192 (2000).
- [KNO98] K. S. Kim, J. Neu, and G. Oster, *Curvature-Mediated Interactions Between Membrane Proteins*, Biophys. J. **75**, 2274–2291 (1998).
- [KNO99] K. S. Kim, J. C. Neu, and G. F. Oster, *Many-body forces between membrane inclusions: A new pattern-formation mechanism*, Europhys. Lett. **48**, 99–105 (1999).
- [Kok06] D. Koks, *Explorations in mathematical physics: The concepts behind an elegant language*, Springer, New York (2006).
- [Koz07] M. M. Kozlov, *Biophysics – bending over to attract*, Nature **447**, 387–389 (2007).
- [KPD⁺93] P. A. Kralchevsky, V. N. Paunov, N. D. Denkov, I. B. Ivanov, and K. Nagayama, *Energetical and Force Approaches to the Capillary Interactions between Particles Attached to a Liquid-Fluid Interface*, J. Coll. Interface Sci. **155**, 420–437 (1993).
- [KPIN92] P. A. Kralchevsky, V. N. Paunov, I. B. Ivanov, and K. Nagayama, *Capillary meniscus interaction between colloidal particles attached to a liquid-fluid interface*, Journal of Colloid and Interface Science **151**, 79–94 (1992).
- [Kre09] K. Kreutz-Delgado, *The Complex Gradient Operator and the CR-Calculus*, arXiv:0906.4835 [math.OC] (2009).
- [LAZY05] J. C. Loudet, A. M. Alsayed, J. Zhang, and A. G. Yodh, *Capillary Interactions Between Anisotropic Colloidal Particles*, Phys. Rev. Lett. **94**, 018301 (2005).

- [LBT⁺09] E. P. Lewandowski, J. A. Bernate, A. Tseng, P. C. Searson, and K. J. Stebe, *Oriented assembly of anisotropic particles by capillary interactions*, *Soft Matter* **5**, 886–890 (2009).
- [Lek12a] J. Lekner, *Electrostatic calibration of sphere–sphere forces*, *Measurement Science and Technology* **23**, 085007 (2012).
- [Lek12b] J. Lekner, *Electrostatics of two charged conducting spheres*, *Proceedings of the Royal Society A: Mathematical, Physical and Engineering Science* **468**, 2829–2848 (2012).
- [Lek12c] J. Lekner, *Nurturing genius: the childhood and youth of Kelvin and Maxwell*, *New Zealand Science Review* **69**, 8–14 (2012).
- [Lip91] R. Lipowsky, *The conformation of membranes*, *Nature* **349**, 475–481 (1991).
- [Lip13] R. Lipowsky, *Spontaneous tubulation of membranes and vesicles reveals membrane tension generated by spontaneous curvature*, *Faraday Discuss.* **161**, 305–331 (2013).
- [Lip14] R. Lipowsky, *Coupling of bending and stretching deformations in vesicle membranes*, *Advances in Colloid and Interface Science* **208**, 14–24, special issue in honour of Wolfgang Helfrich (2014).
- [LK91] H. Li and M. Kardar, *Fluctuation-induced forces between rough surfaces*, *Phys. Rev. Lett.* **67**, 3275–3278 (1991).
- [LL01] L. D. Landau and E. M. Lifshitz, *Theory of Elasticity*, 3 ed., Butterworth & Heinemann, Oxford (2001).
- [LLP84] L. D. Landau, E. M. Lifshitz, and L. P. Pitaevskii, *Electrodynamics of continuous media; 2nd ed.*, *Course of theoretical physics*, Butterworth, Oxford (1984).
- [LM08] L. Levrel and A. C. Maggs, *Boundary conditions in local electrostatics algorithms*, *The Journal of Chemical Physics* **128**, 214103 (2008).
- [LNO08] H. Lehle, E. Noruzifar, and M. Oettel, *Ellipsoidal particles at fluid interfaces*, *Eur. Phys. J. E* **26**, 151–160 (2008).
- [LO07] H. Lehle and M. Oettel, *Importance of boundary conditions for fluctuation-induced forces between colloids at interfaces*, *Phys. Rev. E* **75**, 011602 (2007).
- [LOD06] H. Lehle, M. Oettel, and S. Dietrich, *Effective forces between colloids at interfaces induced by capillary wavelike fluctuations*, *Europhys. Lett.* **75**, 174 (2006).

- [LS95] R. Lipowsky and E. Sackmann (eds.), *Structure and Dynamics of Membranes: From Cells to Vesicles*, Elsevier, Amsterdam (1995).
- [Luc92] J. Lucassen, *Capillary forces between solid particles in fluid interfaces*, Colloids and Surfaces **65**, 131–137 (1992).
- [LYP06] J. C. Loudet, A. G. Yodh, and B. Pouligny, *Wetting and Contact Lines of Micrometer-Sized Ellipsoids*, Phys. Rev. Lett. **97**, 018304 (2006).
- [LZMP11] H.-K. Lin, R. Zandi, U. Mohideen, and L. P. Pryadko, *Fluctuation-induced forces between inclusions in a fluid membrane under tension*, Phys. Rev. Lett. **107**, 228104 (2011).
- [Mag04] A. C. Maggs, *Auxiliary field Monte Carlo for charged particles*, The Journal of Chemical Physics **120**, 3108–3118 (2004).
- [Mag12] A. C. Maggs, *A minimizing principle for the Poisson-Boltzmann equation*, EPL **98**, 16012 (2012).
- [Max91] J. C. Maxwell, *A treatise on electricity and magnetism*, 3rd ed., Oxford, UK, reprinted by Dover 1954 (1891).
- [MCTS13] B. B. Machta, R. Chachra, M. K. Transtrum, and J. P. Sethna, *Parameter Space Compression Underlies Emergent Theories and Predictive Models*, Science **342**, 604–607 (2013).
- [MG05] H. T. McMahon and J. L. Gallop, *Membrane curvature and mechanisms of dynamic cell membrane remodelling*, Nature **438**, 590–596 (2005).
- [Mil01] K. A. Milton, *The Casimir effect: physical manifestations of zero-point energy*, World Scientific, Singapore (2001).
- [MM02] V. I. Marchenko and C. Misbah, *Elastic interaction of point defects on biological membranes*, Eur. Phys. J. E **8**, 477–484 (2002).
- [MMY⁺12] R. Murakami, H. Moriyama, M. Yamamoto, B. P. Binks, and A. Rocher, *Particle stabilization of oil-in-water-in-air materials: powdered emulsions*, Advanced Materials **24**, 767 (2012).
- [Mül07] M. M. Müller, *Theoretical studies of fluid membrane mechanics*, Ph.D. thesis, Johannes Gutenberg-Universität in Mainz (2007).
- [MW66] N. D. Mermin and H. Wagner, *Absence of Ferromagnetism or Antiferromagnetism in One- or Two-Dimensional Isotropic Heisenberg Models*, Phys. Rev. Lett. **17**, 1133–1136 (1966).

- [Nag13] J. F. Nagle, *Introductory Lecture: Basic quantities in model biomembranes*, Faraday Discuss. **161**, 11–29 (2013).
- [NB15] T. Ngai and S. Bon (eds.), *Particle-Stabilized Emulsions and Colloids*, RSC Soft Matter Series, The Royal Society of Chemistry (2015).
- [Net97] R. R. Netz, *Inclusions in fluctuating membranes: exact results*, J. Phys. I (France) **7**, 833–852 (1997).
- [NHB09] U. Nellen, L. Helden, and C. Bechinger, *Tunability of critical Casimir interactions by boundary conditions*, Europhys. Lett. **88**, 26001 (2009).
- [Nic49] M. M. Nicolson, *The interaction between floating particles*, Proc. Cambridge Philos. Soc. **45**, 288 (1949).
- [Nic14] G. L. Nicolson, *The Fluid–Mosaic Model of Membrane Structure: Still relevant to understanding the structure, function and dynamics of biological membranes after more than 40 years*, Biochimica et Biophysica Acta (BBA) - Biomembranes **1838**, 1451–1466, Membrane Structure and Function: Relevance in the Cell’s Physiology, Pathology and Therapy (2014).
- [NO88] J. W. Negele and H. Orland, *Quantum many-particle systems*, Westview Press (1988).
- [NO09] E. Noruzifar and M. Oettel, *Anisotropies in thermal Casimir interactions: Ellipsoidal colloids trapped at a fluid interface*, Phys. Rev. E **79**, 051401 (2009).
- [NPW04] D. Nelson, T. Piran, and S. Weinberg (eds.), *Statistical Mechanics of Membranes and Surfaces*, Statistical Mechanics of Membranes and Surfaces, 2nd ed., World Scientific Pub. (2004).
- [NWZ13a] E. Noruzifar, J. Wagner, and R. Zandi, *Scattering approach for fluctuation-induced interactions at fluid interfaces*, Phys. Rev. E **88**, 042314 (2013).
- [NWZ13b] E. Noruzifar, J. Wagner, and R. Zandi, *Three-body fluctuation-induced interaction at fluid interfaces: A strong deviation from the pairwise summation*, Phys. Rev. E **87**, 020301 (2013).
- [ODD05] M. Oettel, A. Domínguez, and S. Dietrich, *Effective capillary interaction of spherical particles at fluid interfaces*, Phys. Rev. E **71**, 051401 (2005).
- [OLBC10] F. W. J. Olver, D. W. Lozier, R. F. Boisvert, and C. W. Clark (eds.), *NIST Handbook of Mathematical Functions*, Cambridge University Press, New York, NY, print companion to [DLMF] (2010).

- [OYLXYZ99] Z. C. Ou-Yang, J. X. Liu, Y. Z. Xie, and X. Yu-Zhang, *Geometric Methods in the Elastic Theory of Membranes in Liquid Crystal Phases*, Advanced series on theoretical physical science, World Scientific (1999).
- [Pad10] T. Padmanabhan, *Gravitation: Foundations and frontiers*, Cambridge University Press (2010).
- [PF11] B. J. Park and E. M. Furst, *Attractive interactions between colloids at the oil–water interface*, Soft Matter **7**, 7676–7682 (2011).
- [PH00] H. A. Pinnow and W. Helfrich, *Effect of thermal undulations on the bending elasticity and spontaneous curvature of fluid membranes*, Eur. Phys. J. E **3**, 149–157 (2000).
- [Pic07] S. U. Pickering, *Emulsions*, J. Chem. Soc., Trans. **91**, 2001–2021 (1907).
- [PKDN93] V. N. Paunov, P. A. Kralchevsky, N. D. Denkov, and K. Nagayama, *Lateral Capillary Forces between Floating Submillimeter Particles*, J. Coll. Interface Sci. **157**, 100–112 (1993).
- [PKT09] R. B. Phillips, J. Kondev, and J. Theriot, *Physical Biology of the Cell*, Garland Science, New York (2009).
- [PL85] L. Peliti and S. Leibler, *Effects of Thermal Fluctuations on Systems with Small Surface Tension*, Phys. Rev. Lett. **54**, 1690–1693 (1985).
- [PL96] Park, Jeong-Man and Lubensky, T. C., *Interactions between membrane Inclusions on Fluctuating Membranes*, J. Phys. I France **6**, 1217–1235 (1996).
- [PRR11] R. A. Porto, A. Ross, and I. Z. Rothstein, *Spin induced multipole moments for the gravitational wave flux from binary inspirals to third Post-Newtonian order*, J. Cosmol. Astropart. Phys. **1103**, 009 (2011).
- [PUWS09] R. Phillips, T. Ursell, P. Wiggins, and P. Sens, *Emerging roles for lipids in shaping membrane-protein function*, Nature **459**, 379–385 (2009).
- [Ram03] W. Ramsden, *Separation of solids in the surface-layers of solutions and ‘suspensions’ (Observations on surface-membranes, bubbles, emulsions, and mechanical coagulation) – preliminary account*, Proceedings of the Royal Society of London **72**, 156–164 (1903).
- [REJK08] S. J. Rahi, T. Emig, R. L. Jaffe, and M. Kardar, *Casimir forces between cylinders and plates*, Phys. Rev. A **78**, 012104 (2008).
- [RH11] Y. Rao and V. Haucke, *Membrane shaping by the Bin/amphiphysin/Rvs (BAR) domain protein superfamily*, Cellular and Molecular Life Sciences **68**, 3983–3993 (2011).

- [RIH⁺07] B. J. Reynwar, G. Illya, V. A. Harmandaris, M. M. Müller, K. Kremer, and M. Deserno, *Aggregation and vesiculation of membrane proteins by curvature-mediated interactions*, Nature **447**, 461–464 (2007).
- [Rot04] I. Z. Rothstein, *TASI lectures on effective field theories*, arXiv:hep-ph/0308266v2 (2004).
- [Rot12] I. Z. Rothstein, *Partition functions on the Euclidean plane with compact boundaries in conformal and non-conformal theories*, Nuclear Physics B **862**, 576–585 (2012).
- [RSZ13] H. Rezvantlab and S. Shojaei-Zadeh, *Capillary interactions between spherical Janus particles at liquid-fluid interfaces*, Soft Matter **9**, 3640–3650 (2013).
- [RW02] J. S. Rowlinson and B. Widom, *Molecular theory of capillarity*, Dover, Mineola, NY (2002).
- [Saf94] S. A. Safran, *Statistical thermodynamics of surfaces, interfaces, and membranes*, Perseus, Cambridge (1994).
- [SBO98] J. Sliško and R. A. Brito-Orta, *On approximate formulas for the electrostatic force between two conducting spheres*, American Journal of Physics **66**, 352–355 (1998).
- [SDJ00] D. Stamou, C. Duschl, and Johannsmann, *Long-range attraction between colloidal spheres at the air-water interface: The consequence of an irregular meniscus*, Phys. Rev. E **62**, 5263 (2000).
- [SDJMT98] J. S. Schwinger, L. L. DeRaad Jr., K. A. Milton, and W.-y. Tsai, *Classical electrodynamics*, Perseus, Reading, MA (1998).
- [Sei97] U. Seifert, *Configurations of fluid membranes and vesicles*, Adv. Phys. **46**, 13–137 (1997).
- [SJOdlC13] F. J. Solis, V. Jadhao, and M. Olvera de la Cruz, *Generating true minima in constrained variational formulations via modified Lagrange multipliers*, Phys. Rev. E **88**, 053306 (2013).
- [SN72] S. J. Singer and G. L. Nicolson, *The Fluid Mosaic Model of the Structure of Cell Membranes*, Science **175**, 720–731 (1972).
- [Spi75] M. Spivak, *A Comprehensive Introduction to Differential Geometry*, vol. 3, Publish or Perish, Boston, MA (1975).
- [SS01] A. Stein and R. C. Schroden, *Colloidal crystal templating of three-dimensionally ordered macroporous solids: materials for photonics and beyond*, Current Opinion in Solid State and Materials Science **5**, 553–564 (2001).

- [SVR06] Y. Shibata, G. K. Voeltz, and T. A. Rapoport, *Rough Sheets and Smooth Tubules*, Cell **126**, 435–439 (2006).
- [SZ05] J. A. Santiago and A. Zamora, *The one-loop elastic coefficients for the Helfrich membrane in higher dimensions*, Journal of Physics A: Mathematical and General **38**, 1225 (2005).
- [SZH⁺08] F. Soyka, O. Zvyagolskaya, C. Hertlein, L. Helden, and C. Bechinger, *Critical Casimir Forces in Colloidal Suspensions on Chemically Patterned Surfaces*, Phys. Rev. Lett. **101**, 208301 (2008).
- [TMB⁺15] M. K. Transtrum, B. B. Machta, K. S. Brown, B. C. Daniels, C. R. Myers, and J. P. Sethna, *Perspective: Sloppiness and emergent theories in physics, biology, and beyond*, The Journal of Chemical Physics **143**, 010901 (2015).
- [TSHDC99] K. Takei, V. I. Slepnev, V. Haucke, and P. De Camilli, *Functional partnership between amphiphysin and dynamin in clathrin-mediated endocytosis*, Nature Cell Biology **1**, 33–39 (1999).
- [Vai14] V. Vaidya, *Casimir torque on a cylindrical gear*, Phys. Rev. A **90**, 022105 (2014).
- [Vas04] A. N. Vasil’ev, *The field theoretic renormalization group in critical behavior theory and stochastic dynamics*, CRC press (2004).
- [VM05] D. Vella and L. Mahadevan, *The “Cheerios effect”*, Am. J. Phys. **73**, 817–825 (2005).
- [vNSH05] E. A. van Nierop, M. A. Stijnman, and S. Hilgenfeldt, *Shape-induced capillary interactions of colloidal particles*, Europhys. Lett. **72**, 671–677 (2005).
- [VPS⁺06] G. K. Voeltz, W. A. Prinz, Y. Shibata, J. M. Rist, and T. A. Rapoport, *A Class of Membrane Proteins Shaping the Tubular Endoplasmic Reticulum*, Cell **124**, 573–586 (2006).
- [Vre05] C. Vrejoiu, *A formula for gauge invariant reduction of electromagnetic multipole tensors*, Journal of Physics A: Mathematical and General **38**, L505 (2005).
- [VS06] V. Vogel and M. Sheetz, *Local force and geometry sensing regulate cell functions*, Nat. Rev. Mol. Cell. Biol. **7**, 265–275 (2006).
- [Wei01] T. R. Weikl, *Fluctuation-induced aggregation of rigid membrane inclusions*, Europhys. Lett. **54**, 547–553 (2001).
- [WG02] G. M. Whitesides and B. Grzybowski, *Self-Assembly at All Scales*, Science **295**, 2418–2421 (2002).

- [Wil71a] K. G. Wilson, *Renormalization Group and Critical Phenomena. I. Renormalization Group and the Kadanoff Scaling Picture*, Phys. Rev. B **4**, 3174–3183 (1971).
- [Wil71b] K. G. Wilson, *Renormalization Group and Critical Phenomena. II. Phase-Space Cell Analysis of Critical Behavior*, Phys. Rev. B **4**, 3184–3205 (1971).
- [Wil10] J. Wilson, *Non-reductive Physicalism and Degrees of Freedom*, The British Journal for the Philosophy of Science **61**, 279–311 (2010).
- [WKH98] T. R. Weikl, M. M. Kozlov, and W. Helfrich, *Interaction of conical membrane inclusions: Effect of lateral tension*, Phys. Rev. E **57**, 6988–6995 (1998).
- [YD12] C. Yolcu and M. Deserno, *Membrane-mediated interactions between rigid inclusions: An effective field theory*, Phys. Rev. E **86**, 031906 (2012).
- [YHD14] C. Yolcu, R. C. Haussman, and M. Deserno, *The Effective Field Theory approach towards membrane-mediated interactions between particles*, Advances in Colloid and Interface Science **208**, 89–109, special issue in honour of Wolfgang Helfrich (2014).
- [YRD11] C. Yolcu, I. Z. Rothstein, and M. Deserno, *Effective field theory approach to Casimir interactions on soft matter surfaces*, Europhys. Lett. **96**, 20003 (2011).
- [YRD12] C. Yolcu, I. Z. Rothstein, and M. Deserno, *Effective field theory approach to fluctuation-induced forces between colloids at an interface*, Phys. Rev. E **85**, 011140 (2012).
- [YS07] Y. S. Yang and S. M. Strittmatter, *The reticulons: a family of proteins with diverse functions*, Genome Biology **8**, 234 (2007).
- [Zan13] A. Zangwill, *Modern electrodynamics*, Cambridge Univ. Press, Cambridge (2013).
- [ZcH89] O.-Y. Zhong-can and W. Helfrich, *Bending energy of vesicle membranes: General expressions for the first, second, and third variation of the shape energy and applications to spheres and cylinders*, Phys. Rev. A **39**, 5280–5288 (1989).
- [Zee03] A. Zee, *Quantum field theory in a nutshell*, Princeton University Press, Princeton (2003).
- [ZJ02] J. Zinn-Justin, *Quantum field theory and critical phenomena*, Oxford University Press, New York (2002).

- [ZK06] J. Zimmerberg and M. M. Kozlov, *How proteins produce cellular membrane curvature*, Nat. Rev. Mol. Cell. Biol. **7**, 9–19 (2006).